An Investigation of Glaciological and Meteorological Parameters in the Lambert Glacier Basin Using High Precision GPS Strategies

by

Rachael S. Hurd (Rachael Simone)

B.Surv Hons. (University of Tasmania)

A thesis submitted in fulfilment of the requirements for the degree of
Doctor of Philosophy (Ph.D.)

Centre for Spatial Information Science, University of Tasmania,
Hobart, Australia

May, 2002

DECLARATION

I received assistance from others for some of the work presented in this thesis. The processing of the 1989/90 and 1990/91 GPS data (chapter 4) was performed in collaboration with Matt King. The balance flux program and associated data (chapter 5) were made available by Laurent Testut.

Other than those cases already mentioned, this thesis contains no material that has been accepted for a degree or diploma by the University or any other institution, except by way of background information and duly acknowledged in this thesis. To the best of my knowledge and belief, no material previously published or written by another person, except where due acknowledgment is included in the text of this thesis.

Rachael S. Hurd

AUTHORITY OF ACCESS

This thesis may be made available for loan and limited copying in accordance with the *Copyright Act 1968*.

Rachael S. Hurd

SUPPORTING PUBLICATIONS

Some of the work presented in this thesis appears in published papers. Where substantial parts of these papers are reproduced in this thesis, it is in all cases my own original contribution to those papers that is transposed.

The papers directly related to this thesis are:

Chapter 4 and Section 5.1

Manson, R., M. King and R. Coleman (1998). GPS: Putting it on ice. 39th Australian Surveyors Conference, 8-13th November 1998, Launceston, Tasmania, Australia. pp 31-42.

Chapter 4, Section 5.1 and Section 5.4

Manson, R., R. Coleman, P. Morgan and M. King (2000). Ice Velocities of the Lambert Glacier from Static GPS observations. *Earth, Planets and Space* **52**(11), pp 1031 - 1036.

ABSTRACT

Changes in the Earth's global climate and sea level are two of the most important issues facing scientists today. Antarctica plays a vital role in any consideration of sea level change as the southern polar ice-sheet holds the majority of non-oceanic water on the Earth's surface (IPCC, 1997). Changes in the volume of the Antarctic ice-sheet are intricately linked to global climate change due to the strong interactions between the components of the Earth's system in this region. However, in spite of its potential impact on global climate and sea level change, the mass balance (net gain or loss in volume) of the Antarctic ice sheet is poorly known. Thus, in an effort to understand past and current climate and its susceptibility to change, scientists have embarked upon programs to study and monitor many aspects of the Antarctic environment.

One scientifically important area of the Antarctic ice-sheet is the Lambert Glacier Basin (LGB) in East Antarctica. The LGB is an ice drainage basin that covers approximately 13% of the Antarctic ice cap and transports ice from this region through a small section (approximately 1.7%) of the continental coastline. During the late 1980s, several major Australian glaciology programs focussed on the LGB region, collecting field measurements for mass balance studies. The commencement of these programs coincided with the introduction of reliable, civilian quality Global Positioning System (GPS) units for use in scientific research and this was therefore selected as the primary means of collecting position data for the LGB fieldwork. One glaciology program in particular used GPS instruments to determine repeat site positions along a 2015 km traverse route, approximately following the 2500 m surface contour of the LGB. This series of GPS surveys were undertaken between 1989 and 1995, a period which coincided with major changes in the GPS system, advances in GPS technology, the introduction of permanent GPS networks and extreme variations in the ionospheric cycle.

Using the GAMIT/GLOBK software package (Herring, 1999; King and Bock, 1999), all five seasons of LGB GPS data have been analysed. The primary results of this analysis include determinations of ITRF97 positions for the LGB sites with horizontal uncertainties (1σ) of approximately 3 mm and height uncertainties at the majority of sites within 10 mm. From the repeat occupation of the LGB sites, surface ice velocities with uncertainties (1σ) of approximately 0.01 m/yr were computed.

These high quality position and velocity estimates have been analysed in terms of identifying topographic and ice flux characteristics of the LGB. The GPS derived

results have also been compared with remote sensing (i.e., European Remote-sensing Satellite altimeter Digital Elevation Models) and other available datasets in the LGB region (i.e., GPS derived velocities from other studies). The velocity results from the GPS processing were used to validate the mass balance modelling technique of Testut (2000). This validation process has indicated that the modelling generally produces balance velocities within 20% of the observed values and a flow pattern close to that indicated by the GPS results. These comparisons between modelled and observed values are within the expected error-bounds of the modelling process and indicate that the LGB is close to a state of balance.

The velocity and topography of the LGB are important data for the analysis of ice movement out of the basin, but in terms of mass balance studies, the amount of ice introduced into the system is also vital information. Measuring atmospheric water vapour is one way of obtaining information on the amount of moisture available for addition into the ice systems. It is now well known that the delay of GPS signals by the Earth's troposphere may be interpreted as a measurement of precipitable water (PW) above the GPS site. In this study it was proposed that, in principle, PW estimates for the LGB GPS sites could be determined using the GPS meteorology technique even though expected values would be less than 2 mm.

GPS-meteorology calculations were initially carried out on data from Amundsen-Scott (South Pole), Mawson, Davis and Casey (East Coast of Antarctica) to determine the absolute limits of the technique. The results of this analysis showed constant, site-specific biases of approximately 2 mm for the GPS PW values when compared to those determined from radiosonde observations for the same period (winter 1998 and summer 1999). However, the precision (around the bias) of these GPS PW results was approximately 0.6 mm indicating that signal to noise ratios were at an acceptable level (> 3).

The positive evaluation of the GPS-meteorology technique at the permanent GPS sites allowed the method to be applied to LGB GPS data from 1993/94 and 1994/95. From the LGB PW results, a general decrease in PW over the eastern sector of the traverse route was observed between summer 1993/94 and summer 1994/95. This result is in agreement with the mean PW trends observed for these periods in time-series analysis of 11 years of radiosonde data at Davis and Mawson and strongly suggests that the GPS results are a reflection of actual variation over this time period. An important result from this first-ever observation of PW over the interior LGB is the ability to validate modelling of atmospheric processes over inland Antarctica, where ground-based measurements are incredibly scarce. The GPS PW values determined in this study compare well to National Centre for Environmental Prediction model values at the LGB elevations, with differences of less than 1 mm.

The 11-year analysis of radiosonde data at Mawson and Davis was also an important component in the study of PW over the LGB region as it displayed interesting variations in the water vapour signal over various time-scales. An approximately 6 year cycle observed in the radiosonde PW appears to have a significant correlation with the passage of the Antarctic Circumpolar Wave through the study region.

It is clear that high quality GPS data are now able to provide much more than just positions. In this study, it has been demonstrated that GPS techniques provide a valuable tool for generating a wide-range of information that are important for studying the current state of the Antarctic and global environment. Through re-observation processes, these GPS techniques have also been used to determine parameters and detect changes within the study region at unprecedented levels of precision and provide the foundations for long-term studies of the LGB.

ACKNOWLEDGMENTS

The completion of this thesis would not have been possible without the assistance and support of many people.

First of all I would like to thank my two supervisors, they have always been extremely supportive, understanding and helpful and I could not have got to this point without them. Thankyou Richard for being next-door when I needed to chat and thankyou Peter for flying down whenever a help call was sent out. It has been really great to work with both of you over these past few years.

Other people at the University and Australian Antarctic Division have also been of great assistance to me, especially in digging up the old LGB traverse data and logbooks and delving into their memories for other information that was very much appreciated. Thankyou to Ian Allison for helping to set up this project and for providing access to the GPS and AWS data. To Mike Craven (Duk), thankyou for all the answered emails and for searching for the met data for me. Rob Kiernan was also very helpful when I first started, giving me information on the GPS data collection and his processing methodology. I would also like to thank the remainder of the LGB traverse teams for undertaking the surveys and collecting such a huge amount of data.

The meteorological information used throughout this thesis was provided by Neil Adams and Kieran Jacka from the Australian Bureau of Meteorology and Antarctic CRC and from Doug Shepherd at the Australian Bureau of Meteorology. I would like to thank all of these people for answering all of my requests and for helping me understand these data.

I would also like to thank Laurent Testut for providing me with his balance flux modelling program and associated data. Thanks also to Helen Fricker and Glenn Hyland for providing the CRC-DEM and accumulation datasets.

To the people at the Centre for Spatial Information Science (CenSIS), I would like to say how much I have enjoyed working/studying here, it's been a very friendly and relaxing place to work. In particular, I would like to thank all of the people who have inhabited room 116 with me over these past few years, it's been a pleasure to know you all and I apologise for not being particularly cheerful on Monday mornings. I would especially like to thank Matt King for his support and friendship during our time working together. During my time at CenSIS I also had the pleasure of taking

part in two GPS field campaigns on the Amery Ice Shelf. I would like to thank everyone who made these campaigns possible and all of the people that I met during these trips for allowing me to experience and enjoy such a wonderful place.

I would also like to thank all of my wonderful family and friends who have always been there for me, and have been especially important during this past year when I needed to relax and 'get away' from my thesis. In particular I would like to thank my parents and Sam and Nerida for providing a great family environment to grow up in and for their friendship, love and support. To my 'new' family - the Hurds - thankyou also for all of your encouragement and support during these past four years.

Last but not least, I would like to thank Dave for always being on my side! Thankyou for being there when it got too much for me and for encouraging me when things were going well. I definitely could not have done this without your love and support and I look forward to being able to spend evenings and weekends with you again.

TABLE OF CONTENTS

Chapter 1

INTRODUCTION

Chapter 2

GEODETIC APPLICATIONS OF THE GLOBAL POSITIONING SYSTEM

Chapter 3

GLACIOLOGY, ANTARCTICA AND THE LAMBERT GLACIER BASIN

Chapter 4

GPS Data Processing

Chapter 5

Glaciological Results and Analysis

Chapter 6

GPS Meteorology

Chapter 7

GPS Water Vapour Estimation in Antarctica

Chapter 8

WATER VAPOUR IN THE LAMBERT GLACIER BASIN

Chapter 9

CONCLUSIONS

LIST OF FIGURES

LIST OF TABLES

TABLE OF FREQUENTLY USED ACRONYMS

ACW	**Antarctic Circumpolar Wave**
AIS	**Amery Ice Shelf**
AMISOR	**Amery Ice Shelf Oceanographic Research**
ANARE	**Australian National Antarctic Research Expeditions**
AUSLIG	**Australian Survey and Land Information Group**
AWS	**Automatic Weather Stations**
BoM	**Australian Bureau of Meteorology**
DEM	**Digital Elevation Model**
DORIS	**Doppler Orbitography by Radiopositioning Integrated on Satellite**
DOY	**Day Of Year**
ERP	**Earth Rotation Parameters**
ERS-1	**European Remote-sensing Satellite**
GIG	**GPS, International Earth Rotation Service and Geodynamics Experiment**
GL	**Glaciology Traverse Train**
GLAS	**Geoscience Laser Altimeter System**
GPS	**Global Positioning System**
GRACE	**Gravity Recovery and Climate Experiment**
HZD	**Hydrostatic Zenith Delay**
ICESat	**Ice, Cloud and Land Elevation Satellite**
IGS	**International GPS Service**
IMS	**Ice Movement Stations**
InSAR	**Interferometric Synthetic Aperture Radar**
IPCC	**Intergovernmental Panel on Climate Change**

IR	**Ice-Radar Traverse Train**
ITRF	**International Terrestrial Reference Frame**
IWV	**Integrated Water Vapour**
KAOS	**Kinematic Amery Over-snow Survey**
LEO	**Low Earth Orbiting**
LGB	**Lambert Glacier Drainage Basin**
MSL	**Mean Sea Level**
NCEP	**National Centre for Environmental Prediction**
NPCMs	**Northern Prince Charles Mountains**
PAGEOS	**Passive Geodynamics Satellite**
PSD	**Power Spectral Density**
PW	**Precipitable Water**
SCAR	**Scientific Committee for Antarctic Research**
SOPAC	**Scripps Orbit and Permanent Array Centre**
SPCMs	**Southern Prince Charles Mountains**
TCM	**Total Column Moisture**
TEC	**Total Electron Content**
TIN	**Triangulated Irregular Network**
TZD	**Total Zenith Delay**
UT	**Universal Time**
VCV	**Variance-Covariance**
VLBI	**Very Long Baseline Interferometry**
WVR	**Water Vapour Radiometer**
WZD	**Wet Zenith Delay**

Chapter 1

INTRODUCTION

1.1 Overview

This thesis is concerned with applications of Global Positioning System (GPS) data in East Antarctica for observing and monitoring environmental parameters. The broad reason for undertaking such studies in this region is to assist in measurement and monitoring of Antarctic ice sheets and ice shelves for the further understanding of the effects of global climate change. In particular, this study aims to quantify parameters that are useful in i) determining the current state of the ice sheet in terms of mass balance[1] and ii) monitoring variations in moisture content of the Antarctic atmosphere. The geographical location for the study is the Lambert Glacier Drainage Basin (LGB) in East Antarctica, a region in which a large amount of GPS data have been collected during glaciological field programs over more than a decade.

To address the first question, topographic and dynamic features of the LGB are investigated through the determination of position, ice velocity and surface slope data at seventy-three semi-permanent sites in the interior of the basin. The precise determination of these parameters within a consistent, definable reference coordinate system is achieved through the use of high-level GPS data cleaning and processing strategies. Once determined, these parameters are used for improving our understanding of the movement of mass through the drainage basin and for validation of larger-scale ice sheet balance flux models. Future possible uses of the results from this study include the calibration of remotely sensed data, such as those from Interferometric Synthetic Aperture Radar (InSAR) and the Gravity Recovery and Climate Experiment (GRACE) (e.g., Rignot and MacAyeal (1998) and Wahr *et al* (2000)).

The second part of this study uses the results of the LGB GPS data processing to determine values for precipitable water (PW) above the observed sites. Although the levels of PW in the Antarctic atmosphere are low, they are very important to the global energy cycle and to the mass input of the ice sheet. However, water vapour in

[1] The mass balance of a region is the net difference between mass input (e.g. precipitation) and output (e.g., iceberg calving).

the Antarctic atmosphere is currently not well monitored. The use of GPS to observe this parameter has the potential to greatly increase our understanding of the distribution and transport of PW in the Antarctic interior and to observe the seasonal variation of this variable in relation to large scale climate parameters such as, for example, sea ice distribution and ocean/atmosphere circulations.

1.2 Climate Change

Climate change and its effect on various regions of the Earth has been the focus of much scientific research over the past few decades with many programs designed to analyse current and historic trends and also to understand and predict future changes in the Earth's systems. The Intergovernmental Panel on Climate Change (IPCC) is charged with compiling all of these studies into concise assessments of observed and predicted climate change for the dissemination to governments, business and the global population. The most recent of these reports states that there has been an increase in global average surface temperature (approximately 0.6°C) and in ocean heat content during the 20th century (IPCC, 2001). This increase in temperature and the associated decrease in snow cover and sea-ice extent have contributed to a rise in global average sea level of between 0.1 and 0.2 m during the same period (IPCC, 2001). In regard to the model predictions for future climate change, the IPCC, in the Third Assessment Summary, reports that confidence in the ability of models to project future climate has increased. These models predict that the globally averaged surface temperature, water vapour concentration and precipitation will increase over the next century. It is also predicted that precipitation will increase over Antarctica in winter leading to an initial gain in ice volume (IPCC, 2001). The climate models also show a continued rise in global mean sea level (0.09 to 0.88 m) between 1990 and 2100 due to thermal expansion and loss of land ice (IPCC, 2001).

The IPCC (2001) summary for policy makers concludes by outlining a need for greater observational networks and further research to improve the ability to detect and understand current climate and to predict future changes. The understanding of climate change, its causes, effects and future trends is vital to ensuring optimum management of the Earth's resources and to minimise the impact of human activity on the Earth's systems.

1.3 Antarctica and Global Change

Antarctica is known to be quite sensitive to changes in the global environment due to the intricate links and feedbacks between the atmosphere, ice and oceans in this region (Weller, 1992; King and Turner, 1997; Bromwich and Parish, 1998). Two

important roles of the Antarctic region in the Earth's climate system are as a store of the majority of the Earth's freshwater and as a heat sink in the global energy cycle.

1.3.1 Ice Storage

The Antarctic continent stores approximately 60% of the freshwater and approximately 90% of the ice on the Earth's surface (Meier, 1993) and as such it is an important component of the Earth's climate system and hydrological cycle.

Since the last ice age, global sea level has risen approximately 120 m and it continues to rise at a rate of approximately 1 - 2 mm/yr (Meier, 1983; IPCC, 2001). The most significant potential contribution to future sea level increases is from a reduction in ice volume of the Antarctic ice-sheet (Meier, 1993). However, the current mass balance of this region is not well known and therefore its impact on present-day global sea level is also uncertain (Meier, 1993). Further improvements in our understanding of the Antarctic mass balance are necessary in order to allow monitoring and prediction of future changes in this parameter.

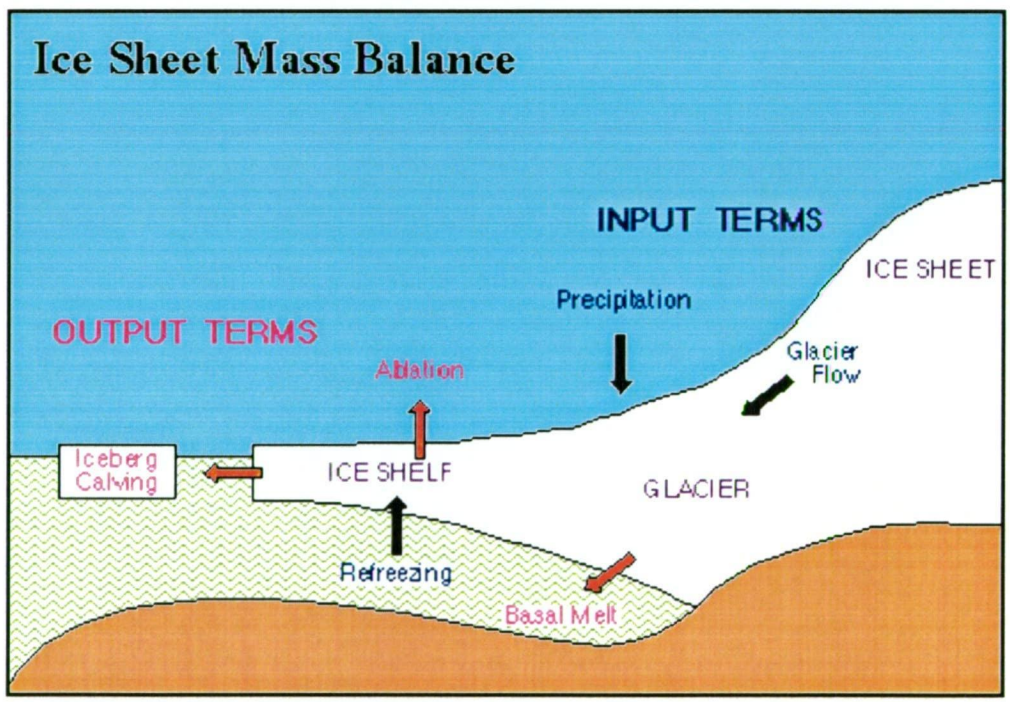

Figure 1.1 - Schematic diagram of ice sheet mass balance components (obtained from http://www.antcrc.utas.edu.au/antcrc).

Most recent mass balance studies have suggested that the Antarctic ice-sheet is in a state of slight imbalance (i.e., a net gain or loss in ice volume - see Figure 1.1). However there is no agreement on the magnitude or sign of this value (e.g., Bentley and Giovinetto (1991), Jacobs *et al* (1992) and Paterson (1993)). Even the most current estimates of the mass balance of the Antarctic ice sheet are inconclusive due to difficulties in obtaining reliable data over such a large, remote and complex ice

mass and also because changes in volume generally occur at long time-scales of 10^4 or 10^5 years (Meier, 1983). Future improvements in the determination of the mass balance of the Antarctic ice-sheet require (Weller, 1992; Meier, 1993):

i) better understanding of iceberg calving, ice-shelf melting, freezing and accretion rates,
ii) improved monitoring of surface elevation and ice velocities and
iii) increased spatial and temporal coverage and accuracy of accumulation datasets.

Currently there are many studies looking into the characteristics of ice-shelf/ocean interactions to further understand mass variations due to the processes mentioned in point i), for example, Doake *et al* (1998), Rignot and MacAyeal (1998), Allison (2001), Foldvik *et al* (2001) and Fricker, Popov *et al* (2001). Surface elevation and velocity (point ii) are now well observed over most of the continent from ground-based and remotely sensed data (e.g., Chapter 5 of this study, Frezzotti *et al* (1998), Hamilton *et al* (1998) and Fricker, Hyland *et al* (2000)). Continued improvements in data collection and processing techniques will strengthen our knowledge of these parameters in the future. At present, most of the uncertainty in studies of the mass balance of the Antarctic ice sheet arise from the lack of information regarding the major input parameter (point iii) of the mass balance equation (Fricker, Warner *et al*, 2000).

The high spatial and temporal variation in accumulation makes it very difficult to observe over large areas. Instead, accumulation datasets generally rely on interpolation of discrete surface measurements and/or estimates of precipitation minus evaporation values from atmospheric data. Precipitation is not well measured in Antarctica due to difficulties in differentiating between blowing and falling snow and observing clear sky precipitation of minute ice crystals in the interior. Therefore it is more common to use atmospheric water vapour as an indicator of potential mass input to the continental ice sheets. However, accurately measuring water vapour over the entire region and over a range of temporal scales is itself difficult. Once these limitations in the Antarctic water vapour/precipitation and accumulation datasets are overcome, it will be possible to obtain a more accurate determination of the ice sheet mass balance.

1.3.2 Energy Balance

In the global atmospheric circulation system, the Antarctic region acts as a 'heat sink' where there is a net loss of energy to the upper atmosphere and the lower atmosphere is cooled (King and Turner, 1997). This cooling effect helps drive the atmospheric circulation of the Southern Hemisphere and is partially controlled by the

amount of water vapour in the atmosphere. Atmospheric water vapour absorbs outgoing radiation, which in turn causes a warming of the air. The low levels of water vapour found in the Antarctic atmosphere cause most of the outgoing radiation to be lost to space. In terms of climate change scenarios, increases in Antarctic temperatures lead to increases in the amount of water vapour that can be held in the atmosphere which in turn lower the amount of cooling that occurs and results in increased temperatures. This feedback mechanism is important in terms of its effect on the global energy cycle and climate patterns. Therefore accurate measurement and monitoring of these two atmospheric parameters and understanding the relationships between them is vital (Bromwich and Parish, 1998).

Temperature has been measured in Antarctica on a regular basis since the middle of the last century and most records indicate a slight rise in temperature over this period (King and Turner, 1997). These records have mostly been surface-based and occur only at manned stations (mostly near the coast) and isolated Automatic Weather Stations (AWS) (Bromwich and Parish, 1998). In more recent times, satellite measurement of surface and atmospheric temperatures have added to the coverage of temperature data over the continent (Weller, 1992). There are also good records of past temperatures from borehole measurements within the ice which allow change over longer time scales to be observed (Weller, 1992; King and Turner, 1997).

Currently, water vapour in Antarctica is primarily measured via radiosonde soundings at occupied stations and more recently, data from Earth observing satellite systems has become available for meteorological studies (King and Turner, 1997; Bromwich and Parish, 1998). The radiosonde observations are typically made in coastal areas and are infrequently sampled (Connolley and King, 1993) indicating a need for improved techniques for monitoring long-term and higher frequency variations and the inclusion of measurements from the vast interior of the continent. Satellite based observations provide a better spatial coverage but do not allow short-term temporal variations to be monitored and additionally, they require validation using ground based observations. These water vapour measurements provide the only input and validation data for current numerical models which are known to show significant differences in the analysed circulation over this region (Connolley and King, 1993). Therefore, in order to obtain a more detailed understanding of the distribution and transport of Antarctic water and improve the model analyses for climate change studies, it can be seen that it is desirable to have more efficient and autonomous water vapour observation techniques operating in this region.

1.4 GPS for Positioning and Water Vapour Measurements

Since its inception, the GPS has proved itself as a high-quality positioning tool for use in a large number of environmental applications (see Chapter 2 of this study, Herring (1999a), Segall and Davis (1997) and Ware *et al* (2000a)). It is now well known that dual-frequency GPS measurements are capable of providing millimetre precision positions and velocities when processed using high-level software (Herring, 1999a). In addition to the high quality of results obtained from GPS measurements, these data also provide the logistical advantage of being able to be undertaken in remote and isolated locations under a range of environmental conditions. It is the combination of these logistical and data-quality characteristics that make the GPS an ideal tool for use in investigations of the ice dynamics of the Antarctic ice sheet (e.g., Motoyama *et al* (1995), Chen *et al* (1996) and Hamilton *et al* (1998))

Recently, GPS observations have been used to detect the amount of water vapour in the troposphere surrounding a GPS antenna with a level of precision similar to that available from other meteorological techniques (e.g., Emardson *et al* (1998), Fang *et al* (1998) and Tregoning, Boers *et al* (1998)). The advantages of using the GPS technique over other methods of water vapour detection are that it does not require constant supervision and is capable of making continuous observations.

GPS has not yet been used for water vapour detection in the Antarctic interior due to the limited amount of data in this region and the expected water vapour amounts being close to the noise level in the GPS results. However, it is highly likely that this technique could prove useful as a tool for monitoring variations in Antarctic water vapour over both coastal and inland areas. The possibility of using the GPS meteorology technique in Antarctica would lead to a great improvement in our understanding of the spatial and temporal distribution of water vapour over this continent, especially in regions that are currently not well sampled (i.e., the interior).

1.5 The Lambert Glacier Drainage Basin

Antarctic field-based research programs generally focus on an individual region of scientific importance. In terms of Australian glaciology programs, one of the major focus regions has been the Lambert Glacier Drainage Basin in East Antarctica (see Figure 1.2). The LGB is the largest drainage system entirely within East Antarctica, draining an area of more than one million square kilometres (Allison, 1991) through an area representing approximately 1.7% of the continental coastline (Budd *et al*,

1967). It is therefore an important region of study in terms of the mass balance of the ice sheet and has been the focus of many glaciological studies since the International Geophysical Year in 1957.

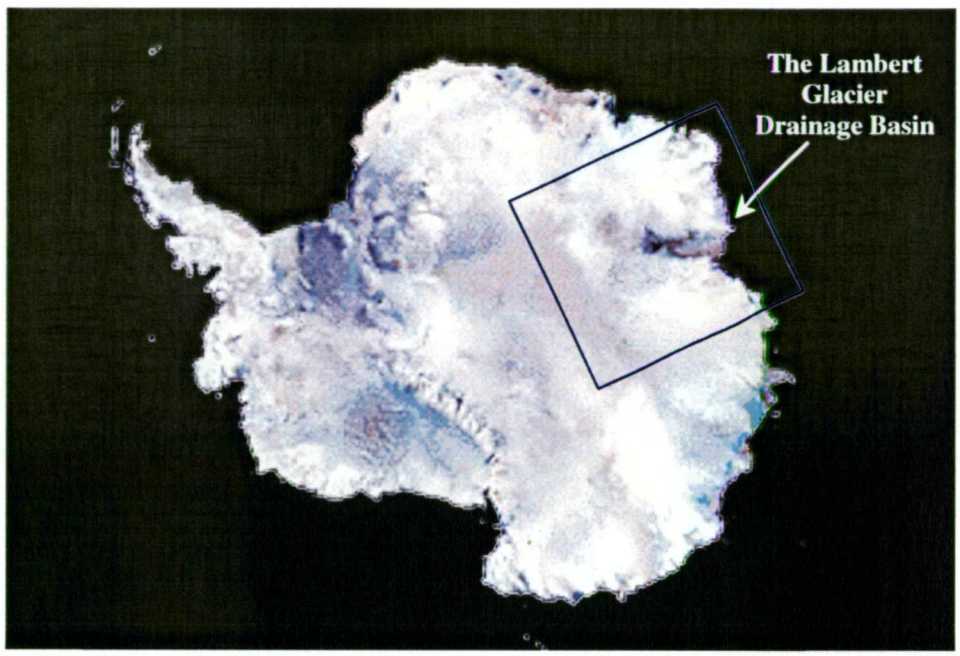

Figure 1.2 - AVHRR colour composite image of the Antarctic continent indicating the approximate location of the study area. (Image obtained from http://terraweb.wr.usgs.gov/TRS/projects/Antarctica/AVHRR.html).

Since 1988, GPS has been used for positioning purposes in glaciological studies of the LGB region. These observations were made to allow determination of the dynamics and state of balance of the basin and to provide a basis from which future change may be monitored. The two regions of focus for these GPS surveys were the ice shelf (ice leaving the system) and the interior of the basin (ice entering the system). In this thesis, the GPS data collected in the interior basin between 1989 and 1995 are analysed to investigate ice sheet surface characteristics (i.e., topography and velocity) and accumulation information (i.e., atmospheric water vapour content) near the 2500 m elevation contour. These studies help define important terms for the determination of ice sheet mass balance in the LGB.

1.6 Thesis Aims and Structure

The broad aims of these studies are to i) use high-level processing techniques to process the full complement of LGB traverse GPS data (of varying quality) and extract optimum position and velocity information ii) use the GPS data to estimate the amount of precipitable water above the LGB sites and iii) apply all of the results from the GPS data processing to investigations of mass balance and meteorological conditions in this region.

This chapter has outlined the major reasons for undertaking the work presented in this thesis. It has also introduced the study region and data that provide the focus for the discussion and analyses in the following chapters.

Chapter 2 provides an overview of GPS observation and processing techniques and also outlines the current uses of this technology for environmental applications. Following from this discussion of global applications, the history of geodetic quality GPS observations for Antarctic studies is presented.

In ***Chapter 3*** the glaciological characteristics of the Antarctic continent are introduced, with a more detailed discussion of the importance and current status of mass balance studies in this region. The focus then moves to the LGB with an introduction to the glaciological and bedrock characteristics of this area. The history and use of geodetic GPS techniques in the determination of glaciological parameters within the LGB is also presented, with an emphasis on the data collected during the traverses around the interior of the LGB.

Chapter 4 outlines the processing methodology used for analysis of the GPS data from the LGB traverses. A brief overview of the GAMIT software (King and Bock, 1999) is given along with full details of the GPS networks, cleaning parameters and solution procedures used to determine site coordinates, velocities, and tropospheric delay at the LGB sites. The cleaning and processing methods used to extract the highest-quality results from the lower-quality LGB GPS data (collected between 1989 and 1993) are given particular attention in this chapter.

The results of the GPS analyses for the determination of ice-dynamics and surface topography along the Lambert Glacier GPS traverse route are presented in ***Chapter 5***. These GPS results are compared to other ground-based results in the study region and are then applied to the validation of altimeter Digital Elevation Models (DEMs) and mass balance studies in the LGB region. Strategies for future field programs using GPS observations for determination of ice sheet velocities are also discussed at the end of this chapter.

The Global Positioning System (GPS) is primarily regarded as an instrument for use in navigation and positioning applications, however, it has now become an extremely useful tool for remote sensing of water vapour in the atmosphere. ***Chapter 6*** provides a thorough discussion of the importance of atmospheric water vapour to the global climate and the methods commonly used for measuring this variable. The theory behind the GPS meteorology technique is then introduced, including a full description of the methods used in this thesis.

There have been many studies undertaken which show the precision of the GPS meteorology technique compared to values obtained from other observation methods.

However, a critical issue is that the absolute error in the GPS values cannot be determined as there are no available 'true' measures of the amount of water vapour above a given site. Antarctica provides a unique location for the study of the absolute error in the GPS technique due to the presence of theoretically zero water vapour at the South Pole. ***Chapter 7*** details the methodology and results of a study using GPS data from a South Pole site and three coastal sites to i) observe the absolute error in the GPS PW results and ii) validate the GPS PW method at sites in East Antarctica. Two of the coastal sites in this study are located in the LGB region, and therefore comparisons between GPS and radiosonde-derived values at these locations in winter provide an indication of the feasibility of using GPS to observe PW at remote sites in the interior. Validation of GPS as a method of measuring water vapour in East Antarctica allows the same strategy to be applied to GPS data from regions where no radiosonde information is available.

The first section of ***Chapter 8*** presents an overview of Antarctic Meteorology. This discussion is followed by an examination of PW in the LGB region through the analysis of an 11-year time-series of radiosonde-derived values. The second section of this chapter details the results of a study using the LGB GPS data processing solutions to determine mean PW values along the traverse route. The GPS results are subsequently used to verify values from the National Centre for Environmental Prediction (NCEP) numerical model analyses and to formulate strategies for future GPS observations to monitor water vapour in the LGB region.

The final chapter, ***Chapter 9***, brings together the findings from each of the analyses described in the previous chapters and summarises the main conclusions from this study.

Chapter 2

GEODETIC APPLICATIONS OF THE GLOBAL POSITIONING SYSTEM

In this chapter, a brief overview of GPS technology for geodetic applications is given. For more detailed information on GPS theory and practice, the reader is referred to Seeber (1993), Leick (1995) and Herring (1999a). For more information on current capabilities/applications of geodetic GPS, the proceedings from 'The International Symposium on GPS - application to Earth sciences and interaction with other space geodetic techniques (GPS99 in Tsukuba)' published in two special editions of *Earth, Planets and Space* (Vol 52 Nos 10 and 11) covers a wide range of projects.

The second section of this chapter concentrates on the application of geodetic techniques in Antarctica. It includes a discussion of the history of geodetic positioning techniques in the region and an overview of modern GPS projects.

2.1 The Global Positioning System

The Navigation Satellite Timing and Ranging (NAVSTAR) Global Positioning System is a global, 24-hour, multi-satellite, all-weather positioning system. It is controlled by the United States Department of Defence and was first implemented in the late 1970's, becoming operational (24 satellites) in December 1993 (Leick, 1995). The GPS is most commonly used for the determination of three-dimensional coordinates at a given site. In order to obtain a reliable, instantaneous stand-alone position, the signals from a minimum of four satellites are required for determination of the three coordinate unknowns plus a system timing error.

GPS satellites transmit signals on two microwave frequencies, L1 (1575.42 MHz) and L2 (1227.6 MHz). These signals are modulated by a navigation message and two coded signals (coarse/acquisition (C/A) and precise (P)). The code information carried in the GPS signals is generally used to determine the time taken for the signal to reach the receiver and convert this value into an approximate range measurement (pseudorange) by multiplying by the speed of travel. These code-based observations have a measurement precision at the sub-metre level but external error sources, such

as clock offsets and ionospheric and tropospheric interference, cause the final precision of point positions to be of a much lower quality.

For users requiring greater precision, the other measurement tool within the GPS signal is the carrier wave. In carrier-based measurements, the difference in phase between the satellite signal (L1 or L2) and a receiver-generated copy of the carrier for each satellite is determined. The range to the satellite can then be calculated by using the measured phase difference plus the number of whole cycles (ambiguity) between the receiver and satellite and the known frequency of the signal. Carrier phase observations have a measurement precision of a few millimetres but are generally not determined at this level due to the presence of errors in the signals.

All GPS observations are affected by many sources of error. These errors (random and systematic) create 'noise' in the collected data and are due to factors within and external to the positioning system. The major sources of error in GPS data are summarised below and depicted in Figure 2.1:

- Satellite and receiver clock errors
- Satellite orbit errors
- Multipath
- Carrier phase ambiguity
- Antenna phase centre variation
- Ionospheric interference
- Tropospheric delay

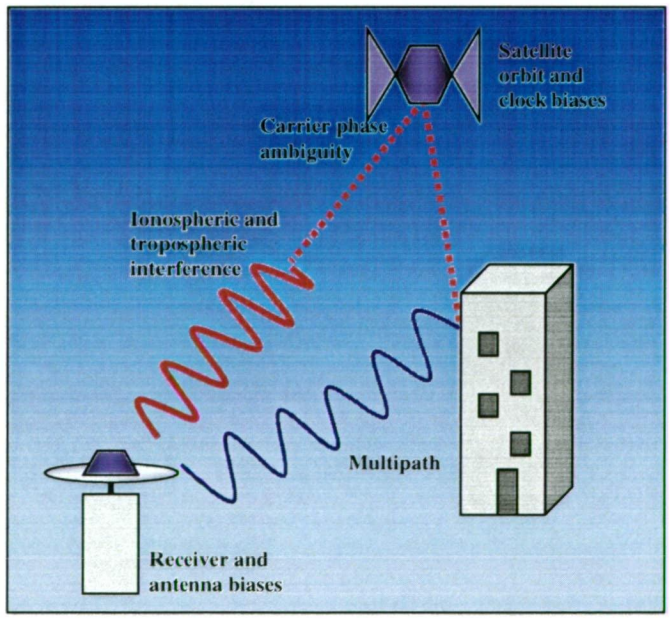

Figure 2.1 - Major errors sources in GPS observations (adapted from http://www.gmat.unsw.edu.au/snap/gps/gps_survey/chap6/621.htm)

It is possible in most cases to remove or reduce the error effects by employing certain data collection and processing techniques or by using reliable error models. For example, one of the major errors in GPS measurements is due to ionospheric

interference on the signals. The effect of this particular error can be minimised by making dual-frequency measurements and exploiting the frequency dependant nature of ionospheric dispersion.

2.1.1 Differential Positioning

Differential or relative positioning provides a means of overcoming many of the biases and errors in the GPS signals. This process requires that near-simultaneous observations to a common set of satellites are made by two receivers at different locations. In theory, over short distances ($\lesssim$ 10-20 km), the receivers will record satellite signals that are affected by approximately the same error sources. For these short baselines, common errors can be cancelled or minimised by differencing the observation equations of the two receivers. However, as the receiver separation distance (baseline length) increases, the errors in the signals become less similar and can not be completely removed using differencing techniques.

For high-precision applications, the carrier phase is the primary observable and can be written as (adapted from Langley (1993)):

$$\Phi_k^p(t) = \rho_k^p + c[dt_k(t) - dt^p(T)] + \lambda N_k^p - I_{k,\varphi}^p + T_k^p + m_{k,\varphi}^p + \varepsilon_\varphi \qquad (2.1)$$

where: t is the signal reception time
T is the time at which the signal was sent
Φ_k^p is the carrier phase observable for station k and satellite p
ρ_k^p is the geometric range
dt^p is the satellite clock error
dt_k is the receiver clock error
c is the speed of light
λ is the signal wavelength
N_k^p is the initial phase ambiguity
$I_{k,\varphi}^p$ is the ionospheric delay
T_k^p is the tropospheric delay
$m_{k,\varphi}^p$ is the multipath effect
ε_φ is the random measurement noise

The differential processing technique is based upon forming differences between GPS observations thereby reducing/removing common mode errors from the equation. There are three levels of GPS difference equations that are generally formed. These are single differences, double differences and triple differences. Single and double difference equations are formed between receivers and satellites and have the effect of removing clock bias terms and minimising all other common biases (i.e., all but the ambiguity, multipath and random error terms) thereby increasing the potential resolution of ambiguities (Langley, 1993). Double difference solutions with integer ambiguity resolution provide the most precise results from

GPS data. Triple differences are formed between epochs and represent the differencing of a pair of double differences. The triple difference equation cancels the ambiguity term when lock is maintained between epochs and therefore displays a jump when there has been a change in ambiguity value (a cycle slip) between epochs. Triple differences have a reduced geometric strength and are generally only used in pre-processing to determine approximate site positions and to correct or flag cycle slips before double difference solutions are undertaken (Leick, 1995).

Another type of equation that is used in dual frequency GPS processing to reduce errors and biases and to provide the most precise solutions by resolving ambiguities are linear combinations of the L1 and L2 observations. Some of the most frequently used linear combinations include the:

Ionosphere-free: ***(L3 or LC)***	removes the effect of the ionospheric path delay but produces an ambiguity term, N_{L3}, which will not necessarily have an integer value [i.e., $N_{L3} = 2.546N_{L1} - 1.984N_{L2}$]. This combination also has noise levels that are significantly higher than those in the raw signals.
Geometry-free: ***(L4 or LG)***	has no range, satellite/receiver clock bias or tropospheric delay terms. Variation in this combination over time will generally be proportional only to changes in the ionosphere and is therefore useful in the detection of cycle slips and tracking of the ionospheric delay.
Wide-lane: ***(L5 or WL)***	has a wavelength of 0.862 m which is much greater than either the L1 (λ = 0.019 m) or L2 (λ = 0.024 m) signals. This increased wavelength provides large integer ambiguity values (which are more easily detected above other noise/errors). The biggest drawbacks with this observable are that ionospheric terms are amplified (especially over long baselines and in areas of high ionospheric activity) and signal noise is high.

2.1.2 GPS Processing

High-level GPS processing is generally carried out using a combination of dual frequency equations, double difference solutions and bias modelling/estimation techniques (e.g., GAMIT (King and Bock, 1999) and Bernese (Beutler *et al*, 1996)). These processing strategies provide the highest quality solutions as they allow the effect of all biases and errors in the data to be minimised or removed and provide

thorough ambiguity resolution where possible. In this thesis GAMIT software is used[1]. This analysis package performs cleaning routines to remove problem data and then carries out a weighted least squares solution of the double difference phase observations to determine parameters such as satellite orbit components, receiver coordinates, ambiguities, tropospheric delays, Earth rotation terms and the solution co-variance matrix (King and Bock, 1999).

Proprietary (commercial) software packages generally do not apply such rigorous solution techniques and commonly rely on individual baseline solutions using double differences, linear combinations, atmospheric models and fixed orbit values to minimise the effects of errors on the solution. The results from this type of software are adequate for most general applications but can not be expected to produce high-precision estimates for data obtained over long baselines, with high-noise levels. In these cases and for reliable, consistent, high-precision results in any application, it is typically necessary to employ the more rigorous processing techniques.

2.2 Current GPS Applications

Over the past decade GPS has become one of the most important tools for scientific studies requiring positional data. Current GPS capabilities include the determination of satellite orbit parameters with centimetre precision and the estimation of three-dimensional site positions with millimetre uncertainty (Segall and Davis, 1997; Herring, 1999a). The following are examples of some current major areas of research using high-precision GPS technology.

2.2.1 Plate Tectonics and Crustal Deformation

One of the largest areas of GPS use for scientific purposes is in the study of plate tectonics and crustal deformation. In particular, GPS has been used extensively in geophysical studies to investigate

> "coseismic, postseismic and interseismic deformation; plate motion and crustal deformation at plate boundaries; volcano deformation; and the deformation associated with glacial isostatic adjustment and its application to sea level studies." (Segall and Davis, 1997, p301).

The measurement of plate tectonics and crustal deformation generally require the determination of very accurate and/or long-term point positions as the movement being measured may range from millimetres per year to well over one-hundred millimetres per year (Herring, 1999a).

[1] For further information on GAMIT processing techniques refer to King and Bock (1999) and Feigl *et al* (1993). Details of the processing techniques used in this thesis are given in Chapter 4.

The International GPS Service (IGS) network of permanent GPS stations provides a strong basis for global (or large regional) studies of crustal dynamics by allowing a time series analysis of the motions at 'stable' sites on multiple continents (e.g., Larson and Freymueller (1995) and Bouin and Vigny (2000)). Long-term data from IGS sites has been used in many studies to determine site velocities with an accuracy of approximately 3 mm/yr and show that movement at sites away from active deformation zones display good comparisons with geological predictions of plate motion (Larson and Freymueller, 1995; Herring, 1999a; Bouin and Vigny, 2000)

Local permanent GPS arrays and campaign-style GPS measurement programs have been deployed in many locations to monitor and understand the dynamics of highly active or otherwise geophysically significant regions of the Earth's crust (e.g., Japan - Vijakumar and Miyashita (2000), California - Feigl *et al* (1993); Dong *et al* (1998), Asia - Tregoning, Lambeck *et al* (1998); Michel *et al* (2000), Europe - Reilinger *et al* (1997); Scherneck *et al* (1998) and Antarctica - Tregoning (2000); http://geodynamics.jpl.nasa.gov/antarctica). GPS campaign observations generally take place over a number of weeks/months and are then reobserved after a period of years. These regional networks have been shown to determine velocities with uncertainties of approximately 3 mm/yr (e.g., Sauber *et al* (1997), Simons *et al* (1999) and Tregoning *et al* (1999)). This level of precision is sufficient to detect the effects of seismic/tectonic motions at a range of distances from the focal points of activity. The accurate determination of these motions increases our understanding of crustal processes and also allows discrimination between various geodynamic models for monitoring and predicting changes.

2.2.2 Reference Frame, Earth Rotation Parameters and Orbit Definition

The IGS global network of more than 200 stations provides data used in the determination of station positions and velocities, GPS orbits, Earth rotation parameters, satellite/receiver clock information, tropospheric delays and ionospheric mapping (Beutler *et al*, 1998).

The main processing of the IGS data is undertaken by analysis centres whose high-precision solutions of the GPS network are combined to form the official IGS products based on the International Terrestrial Reference Frame (ITRF) coordinates and velocities of 47 well-determined sites (Beutler and Kouba, 1998). Within these solutions, satellite orbits and receiver/satellite clock information are determined to their most precise values, and provide valuable data for the correction/processing of other GPS data. The translation and rotation of the global GPS network observed in the combined solutions has provided information on the Earth rotation parameters

(ERP) with a one-day resolution since 1995 (Beutler and Kouba, 1998). The IGS determinations for the values of the ERP represent the longest running and highest resolution time-series available. The combined analyses of IGS network data also produce estimates of precise station locations and velocities in a consistent reference frame (Ferland *et al*, 2000) which are then included in various projects, such as plate tectonic studies and the densification of the ITRF (Beutler and Kouba, 1998).

2.2.3 Meteorology

GPS signals are refracted by the Earth's troposphere. This refraction can be determined as a component of the error signal within the GPS observations (see equation (2.1)) known as the tropospheric delay. It has been shown that this delay can be separated into two sections, the hydrostatic and wet delays. The hydrostatic delay can be well-modelled using ground based pressure and temperature measurements whereas the wet delay (due solely to the presence of water vapour) is highly variable and difficult to model accurately (Langley, 1996). It is known that the wet-delay is approximately inversely proportional to the amount of water vapour along the signal path and therefore can be easily converted into a value of the PW surrounding a GPS site (Bevis *et al*, 1992). Comparisons between GPS PW estimates and measurements made using water vapour radiometers (WVRs) and radiosondes, have shown differences of within 1 - 2 mm of PW (e.g., Emardson *et al* (1998), Tregoning, Boers *et al* (1998) and Fang *et al* (1998)).

This technology has now become one of the major areas of GPS research, with regional GPS networks being used to measure PW over spatial and temporal scales never before realised with other techniques (e.g., Ware *et al* (2000b), Seko *et al* (2000) and Emardson *et al* (1998)). With the latest improvements in the precision of IGS rapid products and the introduction of slant-path water vapour determination, highly accurate, near real-time water vapour monitoring is now possible providing valuable information to meteorological forecasters and analysts (e.g., Rocken, Van Hove *et al* (1997) and (Smith *et al* (2000)).

The use of this GPS water vapour measurement technique in East Antarctica forms the basis of the second section of this thesis and is therefore discussed in more detail in Chapters 6,7 and 8.

2.2.4 Ionosphere

Data from the IGS global GPS network are now regularly used to produce two-hourly maps of vertically averaged total electron content (TEC) in the ionosphere (Ware, Fulker *et al*, 2000b). These maps are obtained through the conversion of ionospheric delay estimated using dual frequency GPS observations into a TEC value

(Beutler and Kouba, 1998). The IGS TEC data are used to validate and update global ionospheric models for correction of single frequency GPS data and to provide a better understanding of ionospheric activity through the monitoring of geomagnetic disturbances (Komjathy and Langley, 1996). Other smaller projects have used regional GPS data to observe TEC patterns in auroral zones. For example, Zarraoa and Sardon (1996) used sites in Scandinavia to continuously monitor local TEC values and observe the effects of geomagnetic activity with an accuracy of approximately 1 - 3 TEC units.

2.2.5 Glaciology

GPS has been used extensively by glaciologists to monitor ice movement and map the surface features of Antarctica and Greenland with centimetre level precision (e.g., Chapter 5 of this study, King *et al* (2000) and Hulbe and Whillans (1993)). These data are useful in providing information for direct use in mass balance studies (see Chapter 3) and/or for validation of the more spatially extensive remote sensing data.

The application of high-level GPS techniques in Antarctic glaciological studies forms the focus of the first half of this thesis and will be discussed in greater detail in the following section and in Chapters 3, 4 and 5.

2.3 GPS in Antarctic Applications

The introduction of GPS technology into Antarctic science has broadened the possibilities for geodesy and surveying in this region. Traditionally, optical surveys (i.e., theodolite, electronic distance measurement and levelling observations) had not been simple or quick to perform under Antarctic conditions. The difficulties experienced in these surveys were due to the impact of the environmental conditions on personnel and equipment, the remoteness and extent of study areas and in some regions, the lack of static features on which to place control stations or use as reference sites. Because of these environmental, technological and logistical obstacles, many important Antarctic scientific measurements had been almost impossible to obtain prior to the development of satellite technologies.

The use of GPS survey methods (in conjunction with new logistical capabilities) has allowed most of the previous survey limitations to be overcome, enabling the collection of large amounts of accurate data over extensive areas and short time frames. In addition to the advantages for regional scientific applications, the use of GPS in Antarctica has also provided reliable geodetic connections between this continent and the global reference frame.

2.3.1 History and Development of Geodetic Techniques in Antarctica

Major scientific programs in Antarctica commenced in the middle of the twentieth century with a major expansion of activity after the International Geophysical Year in 1957/58 (Manning *et al*, 1992). Prior to 1957/58, geodetic positioning in Antarctic and connections to other continents had relied on positional astronomy and local trigonometric and barometric surveys (Manning, 2000). In the early 1960's electronic distance measurement technology was introduced which enabled the extension of local control networks and provided geodetic connections between fixed points across the continent (Watson, 1998).

Table 2.1 - History of positioning techniques in Antarctic geodesy and glaciology

Prior to 1961	Astrofixes and barometric levelling (Murphy *et al*, 1990).
1961 - 1975	Traditional surveying using theodolites, levels and electronic distance measuring equipment (Murphy *et al*, 1990; Watson, 1998).
1969 - 1990	Artificial satellite Doppler measurements (e.g., the Passive Geodynamics Satellite (PAGEOS), and Transit systems) (Young, N. W., 1979b; Murphy *et al*, 1990; Manning *et al*, 1992).
1988 - 1993	Low-level GPS surveys (early model receivers, incomplete satellite constellation, small global network) and Very Long Baseline Interferometry (VLBI) connections.
1993 - 2001	High-precision GPS surveys, permanent GPS sites, VLBI, Doppler Orbitography by Radiopositioning Integrated on Satellite (DORIS).

The first space geodesy measurements were made in Antarctica in 1969 when sites on the continent and surrounding islands were included in the PAGEOS network (Murphy *et al*, 1990). The early 1970's saw the introduction of satellite microwave technology into Antarctic surveying with Transit Doppler measurements being recorded at many Antarctic sites for glaciological and geodetic purposes (Murphy *et al*, 1990; Allison, 1993). The precision from the Transit system was related to the precision of the orbits used in processing and the number of observations made at a given site. In general, it was found that at least two days of observations were required to obtain point measurements with an accuracy of better than 2 m (Allison, 1993).

The space-based reference of the Doppler technique (i.e., the satellites) allowed the first-ever geodetic quality measurements in remote regions of the ice sheet to be made. Previously, position measurements for glaciological studies had been confined to regions near to the fixed control networks (e.g., Allison (1979) and Budd *et al* (1967)) and therefore the introduction of satellite positioning techniques signalled the

commencement of an intensive period of programs for the determination of ice-dynamics. In particular, extensive glaciology studies using Doppler satellite systems were undertaken in the Ross ice streams (e.g., Shabtaie *et al* (1988), McDonald and Whillans (1992) and Whillans and van der Veen (1993)), near the Ronne-Filchner Ice Shelf (e.g., Hinze and Seeber (1988)) and as part of the International Antarctic Glaciological Project study of the East Antarctic Ice Sheet (e.g., Morgan and Jacka (1979), Young (1979) and Hamley *et al* (1985)).

In terms of geodetic connections, Doppler measurements obtained at some fixed Antarctic sites were used to determine positions in the NWL-9D reference system with an uncertainty of approximately 2 m (Anderle, 1977). However, these results were not of sufficient quality for use in inter-continental baseline connections and the understanding of regional plate tectonics (Murphy *et al*, 1990; Manning, 2000). The Doppler positioning technique did however allow local terrestrial networks to be controlled more precisely although individual countries continued to maintain their own control networks (Manning, 2000).

The GPS was introduced to civilian users in the early 1980's as a new method of space-based positioning providing centimetre accuracy. Shortly after, in the late 1980s, GPS technology was introduced into Antarctic glaciology projects for the precise determination of positions and surface velocities in remote locations (e.g., 1984-1987 - Hinze and Seeber (1988), 1988/89 - Allison (1993) and 1988/89 - Whillans *et al* (1990)). Following from the success of the glaciological programs, GPS technology was introduced into Antarctic geodetic campaigns in the early 1990's. These observations provided the first high-quality GPS determinations of inter-continental baselines, connections to a global reference frame and monitoring of crustal motion in Antarctica (e.g., Morgan and Tiesler (1991) and Morgan *et al* (1992). The introduction of geodetic GPS observations in Antarctica was also important for connecting the various control networks across the continent and providing better determinations of site coordinates within these local networks (Manning, 2000).

Permanent GPS sites were established in Antarctica during the mid 1990's which extended the connections between Antarctica and the global network and initiated the inclusion of Antarctic data into global solutions of satellite orbits and Earth rotation parameters (e.g., Mader *et al* (1994) and Rothacher *et al* (1994)). These permanent sites also provide a large-scale regional fiducial network for use in the processing of data collected during scientific field campaigns. Currently there are more than twenty permanent GPS sites operating on the continent and surrounding islands (see Figure 2.2).

Figure 2.2 - Locations of permanent GPS sites in Antarctica (obtained from http://www.scar-ggi.org.au/geodesy/perm_ob/gps/gps.htm). Red dots indicate sites where data are available via satellite connection, blue dots indicate sites requiring manual download.

Over the past decade, other types of geodetic observations have also been collected at permanent or short-term sites across the Antarctic continent (mostly near the coast) (Manning, 2000). Examples of other Antarctic geodetic observations include:

- VLBI (2 sites)
- DORIS (4 sites)
- Absolute Gravity (8 sites)
- Tide Gauges (17 sites)

The measurements from these sites provide vital additional connections between the Antarctic and global networks and allow the inclusion of important Antarctic information in global geodetic datasets (Manning, 2000).

Since its widespread acceptance in the early part of the 1990s, GPS has continued to provide the basis for most high-precision glaciological and geodetic programs in Antarctica (see sections 2.3.2 and 3.3). As the system has developed over time, the level of precision able to be obtained from GPS measurements has improved dramatically thereby enabling the use of GPS in a wider range of applications for the advancement of our understanding of the Antarctic continent.

2.3.2 Applications of High-Level GPS in Antarctica

Geodetic GPS has been used as the primary positioning tool for Antarctic science programs since the late 1980's. The first projects to use this technology were impeded by high levels of ionospheric disturbance, long baseline lengths, receiver inefficiencies and the reliance on a system that had not yet reached full operational capability[2].

The benefits provided by the use of GPS technology to positioning studies have been especially important to geodesists and glaciologists working on remote projects in Antarctica. These groups of scientists have used the GPS extensively since its introduction to the continent in order to obtain positioning data at locations, scales and precisions that were not previously achievable. The following are some examples of the major uses of precise GPS techniques in Antarctica.

2.3.2.1 Global reference frame and plate tectonics

The Scientific Committee for Antarctic Research (SCAR) GPS campaigns commenced in 1989/90 and were undertaken to provide geodetic information from the southern hemisphere including ITRF connections, tectonic motion of the Antarctic plate and data for use in Earth rotation parameter estimation (Morgan *et al*, 1992; Bouin and Vigny, 2000; Dietrich *et al*, 2001)

The broad aim of the pilot SCAR GPS campaign undertaken in 1989/90 was to determine the capabilities of GPS techniques in the hostile Antarctic environment. This campaign also included mid-latitude sites located in Australia and New Zealand (see Figure 2.3) and the results obtained from network processing of these data indicated that solutions with a precision of 1 part in 100 million were obtainable (Morgan and Tiesler, 1991). In the following season (1990/91), GPS observations were made at eighteen mid and high latitude Southern Hemisphere sites, some of which were already collecting data as part of the GIG'91[3] campaign (see Figure 2.3) (Morgan *et al*, 1992). The results from the SCAR '90/91 GPS campaign provided the first reliable connections between Antarctic stations and those in the Southern Hemisphere mid-latitude belt (Morgan, 1994).

The major SCAR GPS campaign was undertaken in the austral summer of 1991/92 and benefited considerably from the lessons learned in the previous years in regard to receiver quality, data collection and data processing requirements. In this campaign, GPS data were collected at twenty-eight Southern Hemisphere stations, half of which were located in Antarctica (see Figure 2.3). This campaign was also a success and

[2] These problems will be discussed further with particular reference to the LGB surveys in Chapter 3
[3] the GPS IERS and Geodynamics Experiment (Melbourne *et al*, 1991).

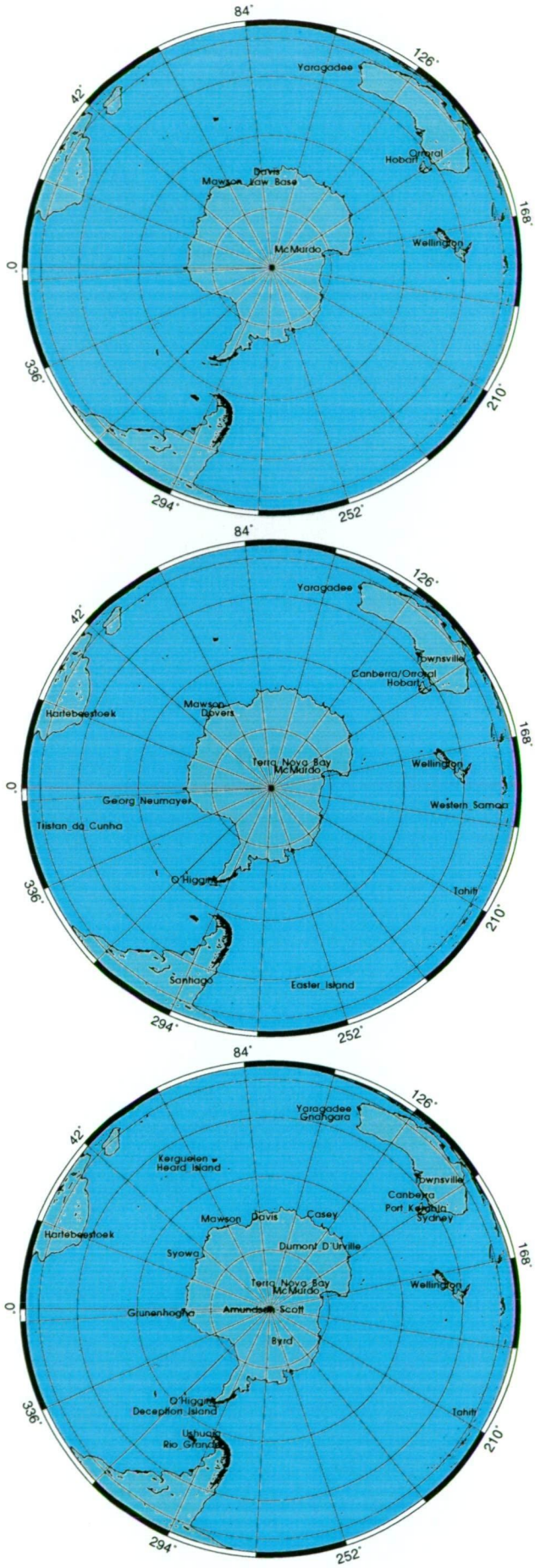

Figure 2.3 - Stations participating in the SCAR 1989/90 (top), 1990/91 (centre) and 1991/92 (bottom) GPS campaigns.

provided new, precise connections between Antarctica and the global reference frame and allowed strengthening of the connections between local Antarctic geodetic networks.

At the conclusion of the 1991/92 SCAR GPS project, it was decided, for logistical reasons, that concentrated observation campaigns would not be undertaken over the next few field seasons (Manning, 2000). However, it was important to continue the geodetic ties between Antarctica and the global network and therefore, in 1993 and 1994, a series of permanent GPS sites were established in and around Antarctica at McMurdo, Mawson, Amundsen-Scott, Casey, Davis, Macquarie Island, O'Higgins, Syowa and Kerguelen stations. The installation of permanent GPS stations at these sites has provided time-series position information across the continent and allowed the continued inclusion of Antarctic data in IGS global network solutions (Beutler and Kouba, 1998). The establishment of permanent sites on the Antarctic continent has also been important in providing fiducial connections for Antarctic scientific programs (Manning, 2000).

From 1995 onwards, the Antarctic Peninsula has been the focus region for a new series of SCAR GPS campaigns (Dietrich *et al*, 2001; http://www.tu-dresden.de/ipg/SCARGPS/database.html). These campaigns have concentrated on studying the geodynamics of the peninsula region and the densification of the ITRF in Antarctica but have also provided information on the effects of ocean loading and water vapour on GPS solutions in this region (Dach and Dietrich, 2000, 2001; Dietrich *et al* (2001)). During this time, new permanent sites have also been installed on the continent and on surrounding islands (see Figure 2.2) providing further strength to Antarctic and global GPS solutions (Manning, 2000).

2.3.2.2 Antarctic geodynamics

Another use of geodetic-quality GPS in Antarctica is to monitor crustal movement due to glacial retreat and tectonic deformation. These measurements are important in determining the isostatic component of sea-level variation and in identifying historical changes in the volume of ice covering the continent (Tregoning, 2000).

There are several research groups using GPS data to study crustal dynamics on the Antarctic continent (e.g., Bouin and Vigny (2000), Dietrich *et al* (2001), http://geodynamics.jpl.nasa.gov/antarctica and Tregoning, 2000). For example, in West Antarctica, autonomous GPS systems have been installed in Marie Byrd Land and the Transantarctic Mountains to provide data for the determination of the rates and causes of tectonic strain and uplift within and across these regions (http://geodynamics.jpl.nasa.gov/antarctica). These GPS systems are designed to run continuously for four to five years, potentially providing sufficient data to estimate

crustal motion with a horizontal and vertical uncertainty of 1 mm and 2 mm respectively (http://geodynamics.jpl.nasa.gov/antarctica). On the other side of the continent, GPS observations are being used to detect post-glacial rebound in the Lambert Glacier region of East Antarctica (Tregoning, 2000). The main aims of this project are to measure the relative vertical motion of the bedrock at the GPS sites (between -7 to +7 mm/yr) and from these observations, identify the most appropriate model for deglaciation in this region (Zwartz *et al*, 1999; Tregoning, 2000). In this study, a network of autonomous GPS stations have been installed on exposed rock at one coastal site and at other sites approximately 200 - 450 km further inland on either side of the Lambert Glacier/Amery Ice Shelf system (Tregoning, 2000). These sites are expected to run for several years and collect sufficient data to determine movements of less than 1 mm (Zwartz *et al*, 1999). However, on-going system modifications and malfunctions have delayed the determination of conclusive results from these sites (Tregoning, 2000).

2.3.2.3 Glaciology

The glaciology community were one of the first groups of Antarctic scientists to embrace the GPS as a precise positioning tool and have undertaken numerous static and kinematic GPS programs to measure ice flow, ice topography, glacier dynamics, ice shelf motion and other characteristics of the Antarctic ice. The results of many of these GPS projects have subsequently been used for the determination of mass balance parameters, modelling of ice-sheets/shelves and ground truthing of remotely sensed data.

An example of the growing reliance of glaciologists on GPS technology are the Australian programs in the LGB region of East Antarctica which have used the GPS for measurement and navigation purposes over more than a decade. These GPS surveys have been useful in defining many characteristics of the region, including ice velocities, surface strain rates, vertical motion and surface elevations (see Table 3.1 in section 3.3.1) The use of GPS in the LGB region represents the main focus of this thesis and therefore, these GPS programs will be discussed in greater detail in section 3.3.

GPS techniques have also been used extensively by other glaciological programs in various regions of East Antarctica. For example, Italian scientists have used kinematic and static GPS techniques in the Terra Nova Bay region to determine glacier velocities, vertical motion on a floating ice tongue and elevation profiles for comparison to DEM values (e.g., Gandolfi *et al* (1997) and Frezzotti *et al* (1998)). The Japanese Antarctic glaciological program has also been using GPS in East Antarctica since 1988 to determine ice-velocities and elevation along a traverse line near the eastern edge of the Shirase glacier and Dome Fuji (e.g., Toh and Shibuya

(1992), Motoyama *et al* (1995)) and more recently to monitor sea-level variation near Syowa station (Aoki *et al*, 2000). From the GPS study described in Frezzotti *et al* (1998), surface velocities of between 70 - 560 m/yr were observed for the David, Priestley and Reeves glaciers and found to compare well to values determined from feature tracking on Landsat imagery (generally GPS and Landsat velocities compared within ±15 - 20 m/yr and ~10°). Motoyama *et al* (1995) and Toh and Shibuya (1992) were able to measure much slower velocities of between 4 and 22 m/yr and thinning rates of approximately 0.55m/yr (validated by gravity measurements) using GPS and Doppler measurements over fourteen years. These surveys provided results with increasing precision due to the advances in system technology over the survey period (Motoyama *et al*, 1995).

In West Antarctica, most glaciological analysis using GPS has been carried out by scientists from the U.S., German and British Antarctic expeditions, with most projects concentrated around the Ross and Ronne-Filchner Ice Shelves (e.g., Hinze and Seeber (1988), Whillans *et al* (1990), Whillans (1992), Hulbe and Whillans (1993, 1994a, 1994b), Vaughan (1994) and Hamilton *et al* (1998)).

The first GPS operations in West Antarctica were carried out on the Ronne-Filchner (1986/87) and Ekstrom Ice Shelf (1987) (Hinze and Seeber, 1988). Positions on the fast moving ice at the front of the Ronne-Filchner Ice-Shelf (1000+ m/yr) and on the Ekstrom Ice Shelf (~170 m/yr) were combined with previous Doppler results to determine velocities over a multi-year period (Hinze and Seeber, 1988). Since this period, it has been the U.S. glaciology program that has made the most use of GPS technologies for studying ice dynamics in West Antarctica.

The main focus for GPS fieldwork by U.S. glaciologists has been in the Ross Ice Shelf and Siple coast region. These programs were mostly undertaken to observe strain and velocity (vertical and horizontal) of the ice streams in this area (e.g., Whillans (1992), Hulbe and Whillans (1993), Chen *et al* (1996) and Hamilton *et al* (1998)). The first GPS positions for velocity/strain studies on the Ross ice streams were observed in 1988/89 as part of a test season to investigate the performance of this new technology in Antarctica and compare it to Doppler methods and results (Whillans *et al*, 1990). Following the success of this trial program, the first major GPS campaign in this region was conducted in 1991/92 and 1992/93 where strain grids and velocity markers on two ice streams were positioned using stop-go, short baseline GPS techniques (Hulbe and Whillans, 1993). From this project, horizontal strain rates accurate to 1% and relative vertical velocities accurate to 20 mm/yr were determined.

In 1994, Hulbe and Whillans (1994b) first discussed the potential use of GPS in determining point ice-thickness change (i.e., point mass balance). In this method, a

series of poles (or wires) are attached to cans (to prevent settling) and placed in covered shafts drilled into the ice sheet (Hulbe and Whillans, 1994b; Hamilton *et al*, 1998). The height of the tops of these poles/wires are then determined relative to a local reference by means of a stop-go GPS survey (Hulbe and Whillans, 1994b; Hamilton *et al*, 1998). The thinning rate at each site can then be determined from the difference between long-term accumulation rates and the vertical velocity measurements with minor corrections for surface slope and firn settling (Hamilton *et al*, 1998). Initial results at two sites have shown that this technique is capable of detecting thinning rates of 0.004 to 0.096 m/yr with uncertainties of 0.02 - 0.04 m/yr (Hamilton *et al*, 1998).

2.4 Chapter Summary

Current GPS technology is capable of providing high-precision site coordinates that are useful for many scientific applications. The most efficient method of processing GPS data collected under adverse conditions and/or for the determination of precise coordinates in a consistent reference frame is to use high-level GPS processing software incorporating the most rigorous cleaning and solution procedures.

GPS has been used extensively in Antarctic science programs since the late 1980's to provide vital information connecting this continent to the global network and for the determination of high-precision geodetic and glaciological parameters in this region.

Chapter 3

GLACIOLOGY, ANTARCTICA AND THE LAMBERT GLACIER BASIN

In simple terms, glaciology is the study of the physical and chemical properties of snow and ice. It involves the collection and analysis of information regarding the structure, composition, accumulation, chemistry, movement, strain, physics and topography of ice in all its forms on the Earth.

The Antarctic ice-sheet has been a focus of glaciological interest since its existence was first confirmed in 1820 (Radok, 1985). However, it was not until the beginning of the International Geophysical Year (in 1957) that the first surface elevation measurements were made on the continent and the first maps produced (Radok, 1985). Since then, Antarctica has been the focus of many glaciological projects, some involving extensive field measurements and others employing satellite remote sensing techniques. Regardless of the methods used, all of these projects have the same broad incentive, which is, to discover new information regarding the glaciology of the Antarctic ice-sheet. The information obtained from these studies can then be used to understand, monitor and predict the effects of climate change in this region and the global implications of these changes.

This chapter and the following chapters, 4 and 5, are concerned with the use of GPS data in studying the surface characteristics, dynamics and mass balance of the Lambert Glacier Basin.

3.1 Antarctic Glaciology

The Antarctic ice cap is not static, it is a dynamic surface with a range of mechanisms involved in assisting the gravitational flow of ice from the high interior to the coast. The major ice features of the continent are the slow moving (0 - 25 m/yr) ice-sheets which cover 98% of the land area (http://www.glacier.rice.edu). These ice sheets also contain regions where large volumes of ice are more rapidly transported coastward in the form of ice streams and outlet glaciers. Upon reaching the coast, the various ice transport mechanisms either form abrupt boundaries of sheer ice-cliffs or continue to flow over the ocean to form ice-shelves and glacier

tongues. At the coast, sections of ice break away from the continent and form icebergs that may be transported northwards by ocean currents where they eventually succumb to the warmer ocean temperatures.

3.1.1 Major Antarctic Glaciological Characteristics

Antarctica can be divided broadly into three sections, East Antarctica, West Antarctica and the Antarctic Peninsula (see Figure 3.1). Each of these sections has its own set of characteristics which makes whole-continent studies of parameters such as accumulation, ice flow and mass balance difficult to execute accurately. It is due to these spatial variations in character that Antarctic studies commonly concentrate on only one of these major regions or individual features within the regions.

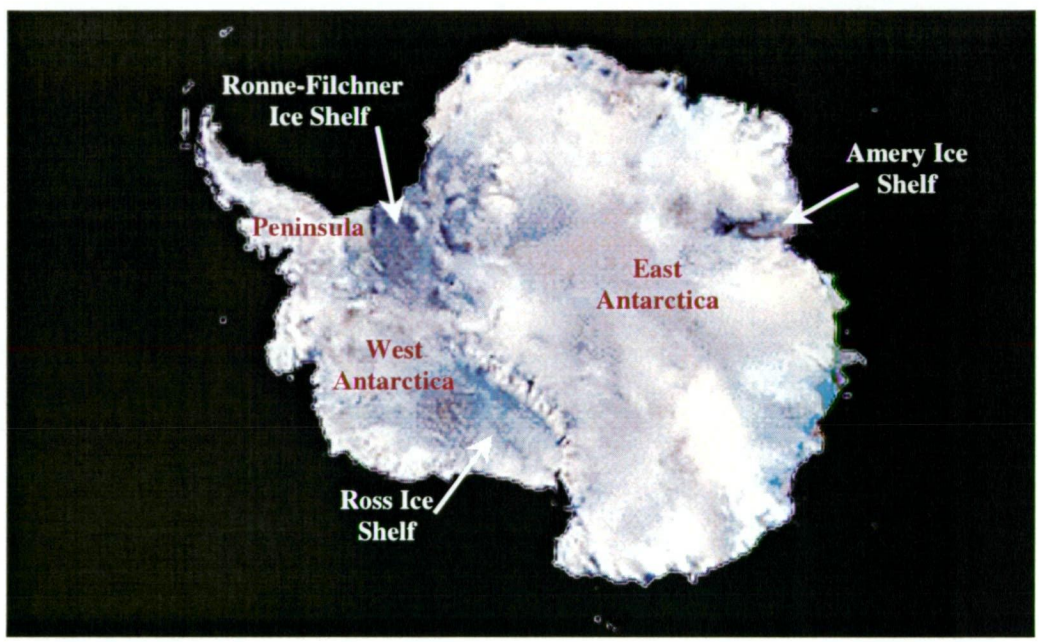

Figure 3.1 - AVHRR colour composite image of the Antarctic continent (obtained from http://terraweb.wr.usgs.gov/TRS/projects/Antarctica/AVHRR.html). The two major ice sheets and three major ice shelves are indicated in the figure.

3.1.1.1 Ice sheets

The Antarctic ice-sheet is generally divided into two sections, the East Antarctic Ice Sheet (approximately 10 million square kilometres) and the West Antarctic Ice Sheet (approximately 2 million square kilometres) (http://www.glacier.rice.edu).

The West Antarctic Ice Sheet is dominated by the massive Ross and Ronne-Filchner ice shelves (see Figure 3.1), the ice-streams and glaciers that flow into them and the Transantarctic Mountains. Approximately 50% of this ice sheet is grounded on bedrock that is below sea level and it is therefore referred to as a marine ice sheet (Whillans and Van Der Veen, 1993; Bentley, 1997). Two of the most defining surface features of the West Antarctic Ice Sheet are its concave profile and the fast

flowing ice-streams inland of the ice shelves. In particular, the region inland of the Ross Ice Shelf is characterised by a series of ice streams with speeds of approximately 800 m/yr (see Figure 3.2) (Whillans and Van Der Veen, 1993). In terms of climate change response, the West Antarctic Ice Sheet is theoretically capable of relatively rapid variations due to its marine characteristics. However, according to current data, the likelihood of a sudden collapse of this ice sheet due to global warming is low (Bentley, 1997; IPCC, 2001).

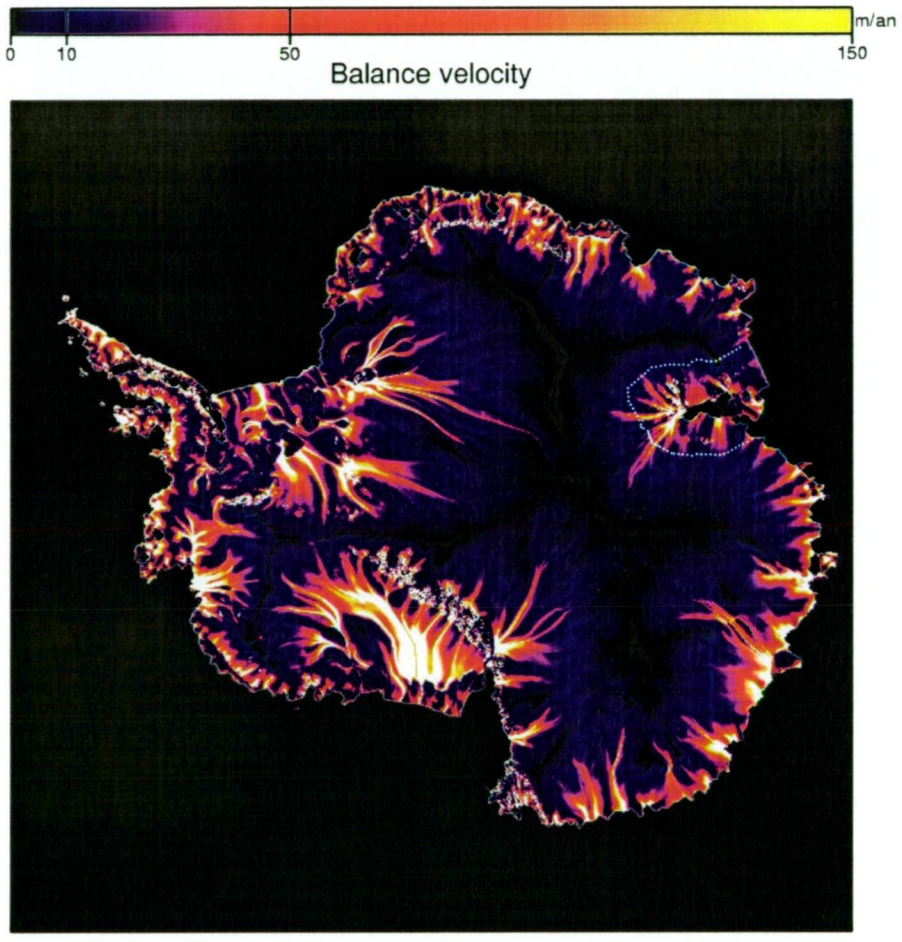

Figure 3.2 - Modelled Antarctic Ice Flow (from Testut, 2000). Yellow, red and white areas indicate high velocity ice flow.

The East Antarctic Ice Sheet is much larger, thicker and generally higher than the West Antarctic ice sheet and represents the majority of ice covering the continent (see Figure 3.1). The major glacier/ice shelf system in this region is the Lambert Glacier/Amery Ice Shelf system (see Figures 3.1 and 3.3). The remainder of the East Antarctic Ice Sheet is characterised by large areas of sheet flow and smaller ice stream/glacier systems (see Figure 3.2). These features of the East Antarctic Ice Sheet and the fact that the bedrock below it is generally above sea level cause it to be relatively stable, with a generally slow response to climate change (http//www.glacier.rice.edu).

The flow of ice within the ice sheets is relatively slow (< 50 m/yr) and occurs through internal deformation due to the gravitational force on the ice mass (Morgan *et al*, 1982). Variations in the speed of ice-sheet flow are caused by variations in the driving stress, τ_d (from Bentley, 1987):

$$\tau_d = \rho_i g h \sin\alpha \qquad (3.1)$$

where: ρ_i = density of ice
g = gravitational acceleration
h = ice thickness
α = surface slope

which is primarily controlled by the ice thickness (h) and surface slope (α). In regions of ice-sheet flow, the driving stresses are minimal and the surface topography is therefore relatively flat and smooth (Morgan *et al*, 1982).

In recent projects, ice thickness measurements have been made over wide areas of the continent using land-based, airborne or satellite radar systems, while in the past, gravity and seismic data were also used to obtain this information (Radok, 1985; Lythe and Vaughan, 2001). Accurate models of Antarctic surface topography have also recently been determined using ice sheet surface elevation measurements from satellite altimeters and ground-based surveys (Bamber and Bindschadler, 1997; Remy *et al*, 1999; Fricker, Hyland *et al*, 2000). These new and extensive datasets of surface slope and ice thickness spanning the entire continent have allowed large-scale models of the ice dynamics to be developed and used in detailed analyses of flow patterns and ice sheet mass balance (see Figure 3.2) (e.g., Fricker, Warner *et al* (2000) and Testut (2000)).

3.1.1.2 Drainage basins

Gravity is the primary force that causes the Antarctic ice to flow in various directions away from the high points of the ice-sheets. The drainage pattern of the continental ice can be divided into several distinct regions based on the direction of the ice flow. Giovinetto and Bentley (1985) defined six large drainage systems of the Antarctic ice sheet (see Figure 3.3). Three of these drainage basins are characterised by ice-flow within substantial glacial systems discharging into the three major ice-shelves (i.e., the Ronne-Filchner, Ross and Amery) (see Figure 3.3). It is these three systems that drain most of the ice from the deep interior of the continent (Giovinetto and Bentley, 1985).

The most significant drainage basin in East Antarctica is the LGB (see Figure 3.3). The LGB, located between the two Australian bases of Mawson and Davis, has been the subject of many glaciological studies since the 1960s and is the region of interest for this thesis.

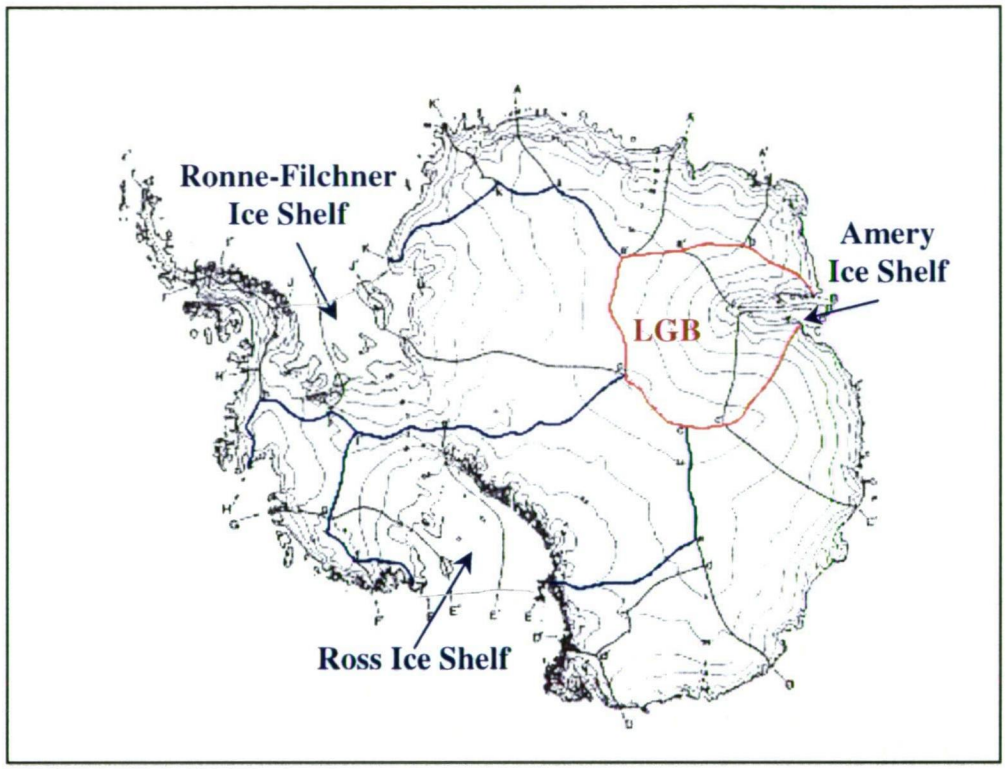

Figure 3.3 - Antarctic drainage basins as defined by Giovinetto and Bentley (1985). The three major drainage basin/ice shelf systems are identified in blue (Ross and Ronne-Filchner) and red (Amery) - referred to here as the LGB.

3.1.1.3 Ice streams and outlet glaciers

An ice stream is "a part of an inland ice-sheet that flows rapidly through the surrounding ice" (Bentley, 1987, p8843). Outlet glaciers are similar to ice streams but are bounded (at least partially) by exposed rock rather than slower ice (Bentley, 1987). Outlet glaciers are usually aligned with deep bedrock depressions, surface depressions and regions of high internal stress (Morgan *et al*, 1982; Bentley, 1987). Figure 3.2 shows the results of an ice flow model derived from the most recent elevation, ice thickness and accumulation datasets (Testut, 2000). Within this figure, the major Antarctic outlet glaciers and ice streams can be easily identified.

Ice stream and outlet glacier flow is controlled by internal deformation, basal sliding and/or bed deformation resulting in flow rates up to and greater than 1 km/yr (Bentley, 1987). These regions of the ice sheet generally have high surface slopes related to the increased driving stresses, and often, the bedrock topography beneath them is reflected in the surface profile (Herzfeld *et al*, 1993).

Of all the Antarctic ice streams and outlet glaciers, the ice streams flowing into the Ross Ice Shelf are unique. This series of ice streams differ from other regions of fast moving ice, due to their lower surface and bedrock gradients and a driving stress profile that is low and increases towards the heads of the streams (Bentley, 1987; Whillans and Van Der Veen, 1993).

3.1.1.4 Ice shelves

Ice shelves are large floating extensions of the grounded ice sheets and are generally fed by one or more fast flowing ice streams/outlet glaciers (http//www.glacier.rice .edu). More than 80% of the Antarctic ice shelf regions are in West Antarctica, the largest being the Ronne-Filchner and Ross ice shelves (see Figure 3.1) (Jacobs, Helmer *et al*, 1992). The points at which the land-based ice begins to float are known as grounding lines and it is at these points that the ice attains a thickness allowing it to be in hydrostatic equilibrium with the ocean (Jacobs *et al*, 1992). The major functions of ice-shelves are as the main region of mass loss from the Antarctic continent and to act as buttresses, slowing the motion of ice from the polar cap (Jacobs *et al*, 1992).

The primary mechanisms of mass output from the ice-shelves are iceberg calving and basal melting (see Figure 3.4). Increases in ocean temperature will enhance these processes, thus reducing the size and extent of the ice-shelves. As such, the Antarctic ice shelves are highly susceptible to global warming (Doake *et al*, 1998). The reduction in volume of the ice-shelves is not directly related to sea level rise as the ice has already made its contribution to sea level once it crosses the grounding line. However, the disintegration of some or all of an ice-shelf is expected to impact on the dynamics and discharge across the coastal margins of the continental ice systems (i.e., removal of the blocking function), and therefore cause variation in the mass balance of the ice sheet (Jacobs *et al*, 1992).

3.1.2 Antarctic Mass Balance

The volume of ice stored on the Antarctic continent is constantly changing due to the accumulation and discharge of ice through various natural processes (see Figure 3.4). In order to balance the mass inputs and outputs, there is a continual movement of ice toward the edge of the continent. However, under different environmental conditions, there may or may not be agreement between the amount of material gained and lost, leading to a state of mass imbalance.

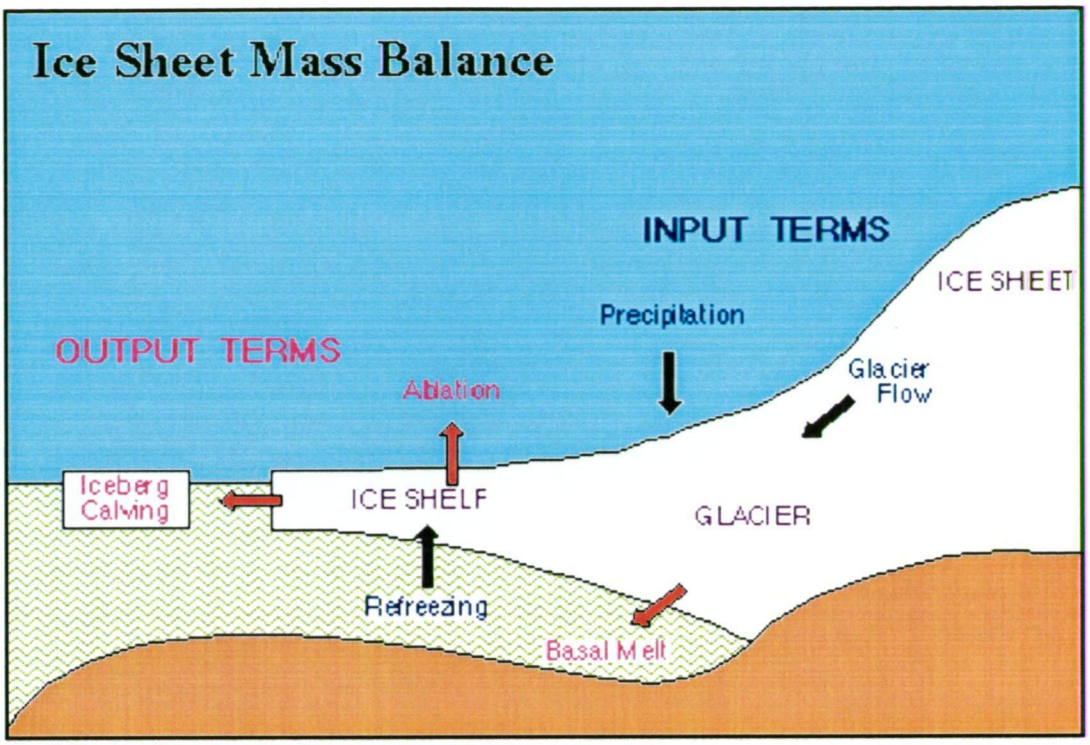

Figure 3.4 - Schematic diagram of ice sheet mass balance components (obtained from http://www.antcrc.utas.edu.au/antcrc)

A positive imbalance infers that more ice is being incorporated into the system than is being lost, resulting in a thickening of the ice-sheet and the removal of water from the oceans. A negative imbalance will have the opposite effect, with ice being lost to the oceans and contributing to a rise in sea level. The accurate determination of the state of mass balance of Antarctica is therefore an important component of climate change research (see section 1.3.1).

There are two methods by which the mass balance of an area of ice may be calculated (Craven *et al*, 1995). One is to directly measure a change in volume (i.e., a change in surface elevation) usually via satellite altimetry (e.g., Lingle *et al*, 1994), or by performing repeated field measurements (e.g., Hamilton and Whillans, 2000). The other method is to measure the physical parameters that influence the patterns of ice accumulation and discharge (e.g., Bentley and Giovinetto, 1991). This thesis will concentrate on the second method as that is the technique for which the LGB traverse data (see section 3.4) were collected.

The determination of the mass balance of the Antarctic ice-sheet is not a simple task due to the large uncertainties in some of the major components of mass balance calculations (e.g., accumulation, basal melting and iceberg calving) (Fricker, Warner *et al*, 2000). Accumulation rates are the most difficult component to determine and represent one of the largest gaps remaining in modern mass balance research (Fricker, Warner *et al*, 2000). The difficulties in determining accumulation rates stem from the limited number of available measurements and the lack of accurate wide-

scale data. Most accumulation models are based on interpolated point-measurement data or information (precipitation - evaporation) from atmospheric models neither of which are reliable at the continental scale (Fricker, Warner *et al*, 2000). The removal of mass from the Antarctic ice-systems to the ocean is another parameter that is difficult to quantify due to a lack of wide-scale information on basal melting rates and iceberg calving processes (Jacobs *et al*, 1992).

Of the other major mass balance variables, the rate of mass discharge between regions is one of the best determined, although there is still some uncertainty in these values over large areas due to errors in interpolation from point measurements, the accuracy of remotely sensed data and the uncertainty in the ratio of surface velocity to the column-averaged value (Fricker, Warner *et al*, 2000). The rate of discharge can be determined in two ways, either from ice thickness and surface slope values (see equation (3.1)) or from direct measurement of surface velocities. It is possible to measure these properties of the ice sheet over large areas using remote sensing (e.g., Lythe and Vaughan (2001), (Bindschadler *et al* (1996) and Fricker, Hyland *et al* (2000)) or for smaller areas, using ground based techniques (e.g., section 5.1.2 of this study and Chen *et al*, (1996)). Errors in point velocity measurements are now minimal (i.e., centimetre level - see section 5.1.2) while uncertainty in elevation and thickness data may be as high as tens of metres (Fricker, Hyland *et al*, 2000).

The various regions of the Antarctic ice-sheet are expected to have differing mass balance states due to regional variations in ice accumulation and discharge (Drewry and Morris, 1992). Bentley and Giovinetto (1991) therefore calculated a value (+180 Gta^{-1}) for the current mass balance of the Antarctic ice-sheet (minus the peninsula region) in terms of the contribution from each of the six drainage basins. However, this method of calculation, neglecting the feedback from variation in the volume of the ice shelves, is not useful for detecting change in the mass budget (Drewry and Morris, 1992). Jacobs *et al* (1992) determined a negative balance for the Antarctic ice-sheet (-468 Gta^{-1}) using a variation of the Bentley and Giovinetto (1991) analysis that included the peninsula region and the effect of mass loss from the ice shelves. However, they do suggest that the uncertainties in the values used for these calculations result in the mass balance estimate not being significantly different to equilibrium (Jacobs *et al*, 1992). Jacobs *et al* (1992) also discuss the fact that their analysis does not give direct evidence as to the reason behind the imbalance, i.e., it may be due to changes in either the ice-shelf (melt) or ice-sheet volume (discharge).

Many studies have also been carried out in smaller regions of the Antarctic continent in order to provide better understanding of the mass balance of individual systems. Regions that have been the focus of these localised mass balance studies include the Lambert Glacier Basin (e.g., Allison (1979) and Fricker, Warner *et al* (2000), sections of the East Antarctic Ice sheet (e.g., Morgan *et al* (1982), Hamley *et al* (1985) and Shimizu *et al* (1978)) and the Ross Ice Streams (e.g., Bindschadler *et al* (1996) and Shabtaie *et al* (1988)).

Model predictions of the future effects of climate change on the mass balance of the Antarctic ice-sheet indicate that there will be an initial thickening as warmer temperatures increase precipitation over the poles followed by a thinning due to increased melting of the ice shelves by the warmer ocean temperatures (Budd and Simmonds, 1991).

3.2 The Lambert Glacier Drainage Basin

The LGB is one of the three major drainage basins moving ice from the interior of the continent and, as such, is an important component of Antarctic mass balance calculations (Giovinetto and Bentley, 1985). At present, using information from ground-based surveys and satellite data, the LGB is estimated to have a slightly positive mass imbalance (Fricker, Warner *et al*, 2000).

Australian National Antarctic Research Expeditions (ANARE) undertaking fieldwork in the LGB commenced in 1964, with exploratory traverses from Mawson station onto the Amery Ice Shelf (AIS) (Budd *et al*, 1967), and have continued to the present-day. The wide spatial coverage of the various LGB expeditions and research programs has allowed scientists to compile information on the topography, structure, dynamics and meteorological characteristics of the LGB and its major components. The primary goals of this body of research have been to obtain an understanding of the present mass balance, the ice-sheet/ocean/atmosphere interactions and the dominant factors that control change within the basin. The collection of this information provides a basis from which the region can be monitored and assists in the predicting future changes through better definition of modelling parameters.

3.2.1 Characteristics of the Lambert Glacier Basin

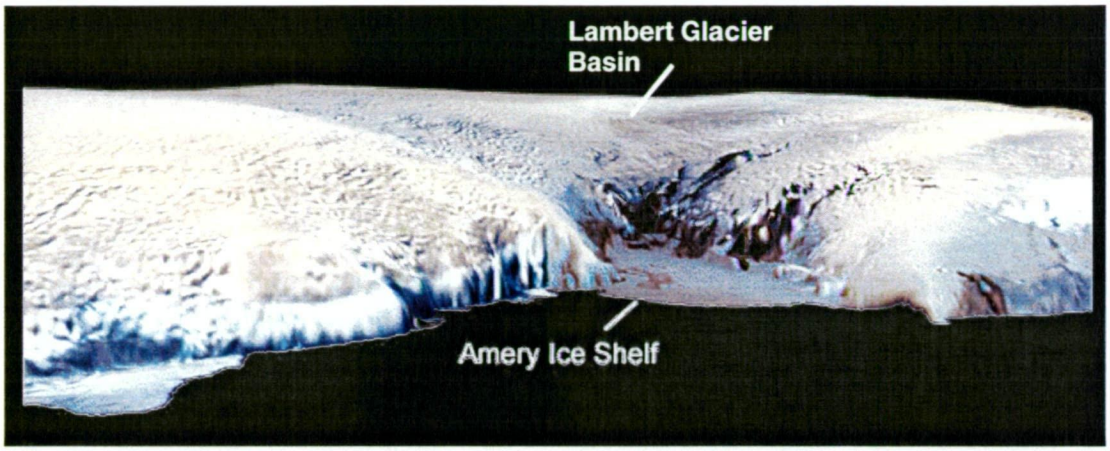

Figure 3.5 - AVHRR[1] image overlain on a DEM to provide a perspective view of the LGB region (image obtained from http://TerraWeb.wr.usgs.gov/projects/Antarctica/color/nuvu/amery.html)

The Lambert Glacier Basin is the largest drainage basin entirely within East Antarctica and also contains the largest glacier-ice shelf system (the Lambert Glacier-Amery Ice Shelf system) in this region. The area of ice that is drained through the LGB is around 1.550 million square kilometres or approximately 16% of the grounded East Antarctic ice sheet (Fricker, Warner *et al*, 2000). The outlet of the LGB is located in Prydz Bay where the ice is channelled into the AIS through a section of coastline that represents only 1.7% of the perimeter of the entire continent (Budd *et al*, 1967).

3.2.1.1 Ice flow characteristics

The LGB has its southern boundary around 81°S or 3500 - 4000m elevation and extends longitudinally between 40° - 90°E (Fricker, Hyland *et al*, 2000). At the interior boundaries of the basin, the ice moves slowly (10 - 20 km/yr) as ice sheet flow and gradually focuses into the major ice streams and outlet glaciers of the region (see Figure 3.6).

The majority of ice flowing into the LGB is channelled through the Lambert Glacier or one of the other major glaciers in the region, such as the Fisher and Mellor Glaciers (Allison, 1991c) (see Figure 3.6). The Lambert Glacier is the largest outlet glacier in the LGB, being approximately 200 km long, more than 40 km wide (Allison, 1979) and up to 2500 m thick at the grounding line (Morgan and Budd, 1975). Surface velocities of up to 60 m/yr near the 2500 m elevation (see section 5.1.2), increasing to over 200 m/yr near the 1500 m elevation (Allison, 1979) have been observed on the main trunk of this glacier.

[1] Advanced Very High Resolution Radiometer (AVHRR)

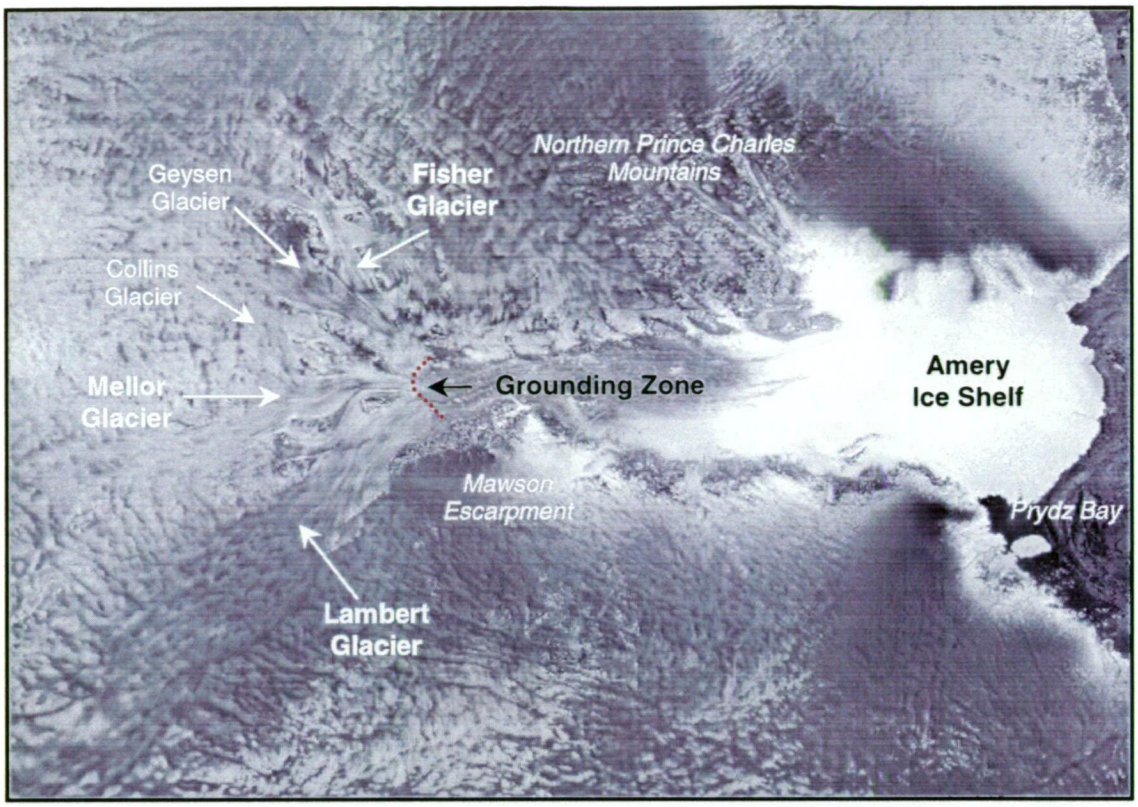

Figure 3.6 - RADARSAT (1997) mosaic image of the LGB (900 x 675 km) (obtained from http://www.jpl.nasa.gov/images/earth/antarctica)

At approximately 73.20° - 73.32°S the glacier ice has a thickness which allows it to float at the point where it encounters sea water (Fricker, Allison *et al*, 2001). This region of the system is termed the grounding zone and represents the transition in flow from glacier to ice shelf. Once the ice crosses the grounding zone and is fully floating, it is referred to as an ice shelf (the AIS) and begins to move much more rapidly due to the removal of the restraints on its basal flow in the change of base from bedrock to sea water (Allison, 1991a).

The AIS extends approximately 500 km north to around 68.5°S. At the front of the shelf, the ice reaches speeds of approximately 1500 m/yr and eventually is discharged via melting processes or as icebergs (Allison, 1991a). There has not been a major iceberg calving event in the LGB since 1963 when approximately 9600 km^2 (or 40 years of growth) broke away from the ice shelf (Budd *et al*, 1967). Predictions for future AIS calving events are in the range of the next 10 - 20 years (Fricker, Young *et al*, 2001).

3.2.1.2 Bedrock topography

Ground and air-based radio-echo sounding surveys of the northern LGB were undertaken by ANARE scientists during the austral summers of 1959/60, 1971/72 and 1973/74. The major results from these measurements were summarised by Morgan and Budd (1975) and included observations regarding the ice-thickness,

surface topography and bedrock structure of the LGB. From the radio-echo soundings, Morgan and Budd (1975) identified bedrock elevations within the northern LGB ranging from –2000 m to +3000 m (average of -800 m) with respect to sea level. The features observed in the bedrock data indicate the presence of a sub-glacial valley system with deep valleys and high mountain peaks mostly hidden below the ice (Morgan and Budd, 1975). The deepest valley, the Lambert Graben, was found to be aligned with the Lambert Glacier and reached its lowest point near the confluence of the three main glacier streams (approximately 73°S) (Morgan and Budd, 1975).

As part of the LGB traverses (see section 3.4), ice radar data were collected near to the 2500 m surface elevation, along the traverse route. The ice radar measurements were collected every 8 - 16 m but for analysis purposes were averaged over 1 km intervals (Higham *et al*, 1995). The analysis of these data clearly shows the extension of the sub-glacial topography noted in Morgan and Budd (1975) as well as the continuation of many of the major bedrock features that are visible above the snow surface (Higham *et al*, 1995). The bedrock in the traverse region was found to be mainly above sea level with a mean elevation of 560 m and the lowest value (1150 m below sea level) was observed in the region of the Lambert and Mellor Glaciers (i.e., a southward extension of the Lambert Graben) (Higham *et al*, 1995).

3.2.1.3 Ice thickness

The radio-echo sounding results presented by Morgan and Budd (1975) also depict the thickness of ice in the LGB region. The maximum thickness of ice, approximately 2500 m, determined from these results is observed in the area of deepest bedrock elevation, i.e., the confluence zone of the Fisher, Mellor and Lambert Glaciers (Morgan and Budd, 1975). Other regions of high thickness (approximately 2000 m) were also identified by Morgan and Budd (1975) along the centrelines of the three major glaciers and in the western ice-sheet above the glacial system. After the grounding zone[2], Morgan and Budd (1975) found that the AIS thins gradually from approximately 1000 m to just 200 m at the front of the shelf.

3.2.1.4 Surface topography

Surface elevation measurements from the radio-echo sounding surveys of the northern LGB indicate a large scale pattern of a slightly convex plateau, with gradually increasing slope up to the zone of steepest slope at 2000 m - 1000 m elevation (Morgan and Budd, 1975). The surface then assumes a gentler slope from

[2] Approximately 73.2°S (Fricker, Allison *et al*, 2001).

approximately 500 m elevation up to the front of the ice shelf (Morgan and Budd, 1975; Phillips, 1999).

Satellite DEMs, such as those of Fricker, Hyland *et al* (2000) and (Remy *et al*, 1999), give a clear picture of the topography of the entire basin and indicate an overall 'bowl' type structure with surface ridges and valleys consistent with the bedrock topography and ice-stream locations. These DEMs have a spatial resolution of 5x5 km and approximately 3.5x1km respectively and an accuracy (compared to field measurements) of approximately 1-12 m, depending on ground topography and DEM grid size (Fricker, Hyland *et al*, 2000). From the DEM information it can be seen that in the eastern sector of the basin, the surface slopes are on average 50% steeper than those of the same elevation in the west, a factor which has a major effect on the meteorology and accumulation in the LGB (Allison, 1998).

3.2.1.5 Accumulation

The accumulation regime of the LGB region is not well sampled by observational data and is one of the key parameters with the greatest uncertainty in current mass balance estimates (Fricker, Warner *et al*, 2000). Many researchers have attempted to define accumulation rates for Antarctica, and the LGB in particular, using the sparse observational data or results from atmospheric modelling (Fricker, Warner *et al*, 2000). For the LGB, the most recent observationally-derived distributions have been published by Higham *et al* (1997) (see Figure 3.7) and (Vaughan *et al*, 1999). Atmospheric model-derived (i.e., precipitation minus evaporation) distributions are also available with some recent examples being those of (Smith *et al*, 1998) and (Budd *et al*, 1995).

The largest series of accumulation observations in the region were made between 1989 and 1995, approximately along the 2500 m contour of the LGB as part of the LGB traverse program (see section 3.4). The results of these measurements were presented by Higham *et al* (1997) and are discussed in more detail in section 8.2.5. In summary, Higham *et al* (1997) found that the interior basin could be divided into three distinct accumulation regimes. Highest accumulation rates (94 $kgm^{-2}a^{-1}$) were identified in the western region, while the southern section of the traverse (corresponding to the major ice streams) was found to experience very low accumulation rates (56 $kgm^{-2}a^{-1}$). Strong easterly winds and the structure of the local topography caused the accumulation rates in the eastern basin (70 $kgm^{-2}a^{-1}$) to be lower than those observed at similar elevations in the west (Higham *et al*, 1997). Higham *et al* (1997) concluded that the accumulation distribution of the interior basin is largely controlled by local topographic features (and prevailing winds) and that elevation and continental effects are evident in the western and southern sectors. This compilation indicates very low accumulation rates (approximately 0 - 50 kgm^{-}

$^{2}a^{-1}$) over the northern end of the major glacial streams and the southern region of the ice shelf, and rates of between 50 - 100 $kgm^{-2}a^{-1}$ elsewhere in the basin (see Figure 3.7). Highest accumulation rates are observed at the northern end of the AIS (see Figure 3.7).

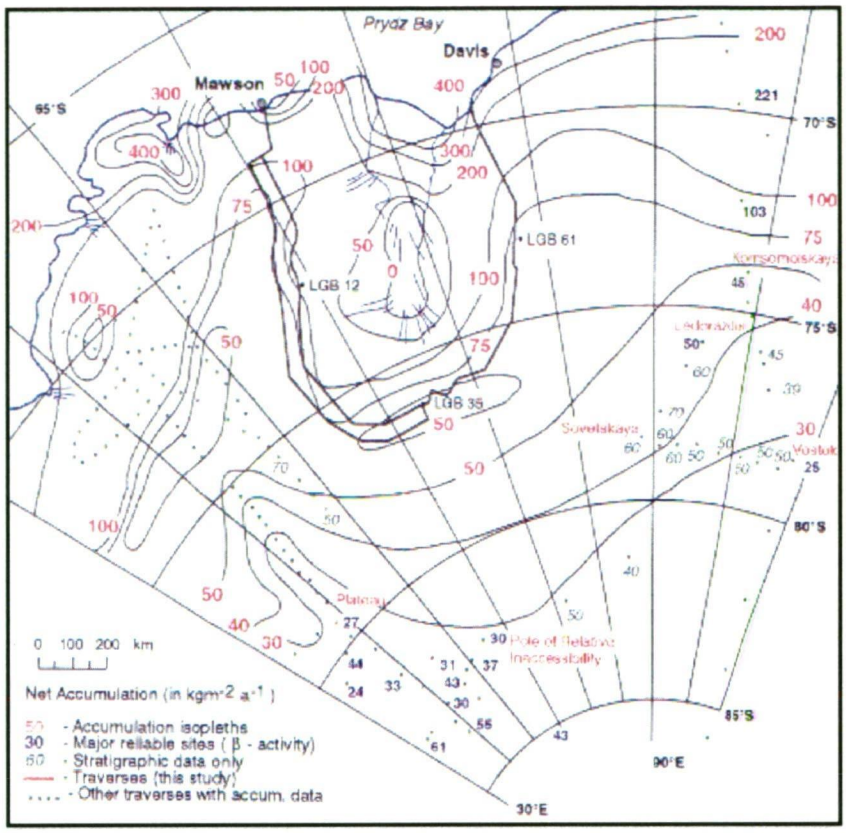

Figure 3.7 - Accumulation distribution for the LGB and surrounding area (from Higham and Craven (1997))

3.2.2 Mass Balance of the LGB

Over the past three decades, several authors have calculated estimates of the current state of balance of the LGB using increasingly sophisticated techniques and accurate datasets (e.g., Budd *et al* (1967), Allison (1979), McIntyre (1985) and Fricker, Warner *et al* (2000)). Each of these mass balance studies has produced results that indicate a slightly positive state of balance although the error margins, even in the most recent studies, are very high and encompass the possibilities of a zero or negative balance state.

Allison (1979) was the first author to provide a detailed mass balance estimation relying on a large set of field measurements. For the Allison (1979) study, velocity and accumulation data were available at a series of markers in the region of the major ice streams (1000-2000 m elevation) and also across the southern end of the Amery

Ice Shelf[3]. Ice thickness data for the mass balance calculations were available from the radio-echo sounding results of Morgan and Budd (1975).

Using the location of the velocity markers as boundary lines, Allison (1979) divided the LGB into two regions a) the Lambert Glacier System - "the area between the southern end of the Amery Ice Shelf and a perimeter through a number of ice movement stations around the Prince Charles Mountains" and b) the Interior Basin - "that inland accumulation area which drains into the Lambert Glacier system". Allison (1979) then went on to estimate a total mass gain of 60 Gta^{-1} for the Interior Basin and an outflux into the Lambert Glacier System of 29.7 Gta^{-1} (the greatest contribution to this flux being in the Lambert Glacier), giving a positive mass balance for the Interior Basin of approximately +30 Gta^{-1}. The Lambert Glacier System was also found by Allison (1979) to have a slightly positive balance of +12 Gta^{-1}. Velocity and ice thickness measurements across the ice shelf suggested a mass flux into the Amery from the Lambert Glacier system of 11 Gta^{-1}, while other losses within the region were estimated at -7 Gta^{-1} (Allison, 1979). The total mass budget for the glacier streams and interior drainage basin from the study by Allison (1979) was therefore estimated at +42Gta^{-1} (with limits of +9 to +89 Gta^{-1}).

The most recent estimation of the LGB mass balance has been published by Fricker, Warner *et al* (2000). In this study, Fricker, Warner *et al* (2000) have re-evaluated the balance flux across the southern sites of the Allison (1979) study and introduced flux measurements from the LGB traverse data near the 2500 m surface elevation contour (see section 3.4). Fricker, Warner *et al* (2000) used a DEM derived from European Remote-sensing Satellite (ERS-1) altimeter data and six different accumulation distributions as input to the balance flux model of Budd and Warner (1996) and produced a series of balance flux[4] estimates within the LGB (see section 5.3.2.2). These balance fluxes were then compared to the observed fluxes across the lines defined by the surveyed sites to determine six independent estimates of the current state of balance.

The main conclusion from the Fricker, Warner *et al* (2000) study is that each of the accumulation definitions produced a wide range of flux values across both transects (i.e., -23.8 to +19.9% for the LGB traverse line and -17.7 to +70.2% for the Allison (1979) line). The results of this study indicate that the LGB is likely to be in a state

[3] At the time of Allison's (1979) paper, the southern extent of the Amery Ice Shelf was defined at a location approximately 150 km north of the currently accepted position (Fricker, Allison *et al*, 2001).
[4] "the balance flux distribution of a glacier system is the hypothetical distribution of mass flux that would exist if the system were in 'steady state'." (Fricker, Warner *et al*, 2000, p562).

of positive imbalance (Fricker, Warner *et al*, 2000). However, Fricker, Warner *et al* (2000) also state that current accumulation data are not adequate for these types of mass-balance studies and until better data become available, accurate mass balance estimates (using this 'gate' technique) are not possible.

3.3 GPS in Glaciological Studies of the LGB Region

Over the last four decades, ANARE programs have collected large amounts of positional and topographic data in the LGB. In the early years (1962 - 1974), this information was collected using traditional surveying techniques, such as tellurometer and levelling traverses (Budd *et al*, 1967) and was confined to the northern LGB in areas close to reference sites on exposed rock. With the introduction of GPS measurement techniques in the 1980s, it became possible to collect high-precision survey data over larger and more remote regions of the LGB (see Table 3.1 and Figure 3.8).

3.3.1 1988 - 1993

3.3.1.1 Amery Ice Shelf GPS surveys (1988/89, 1989/90 & 1990/91)

GPS was first used in the LGB region in 1988-89 as part of a glaciology program investigating the dynamics, mass flux and grounding zone characteristics of the lower Lambert Glacier[5] and AIS (Allison, 1991b). The GPS units used for this initial survey were single frequency Wild Magnavox WM101s. The results obtained from the data collected with these instruments were highly degraded due mainly to the long-baselines and ionospheric disturbances encountered during the survey (Allison, 1991b).

During the 1988/89 survey, a total of twenty-nine marker poles within the grounding zone[6] region, at the confluence of the Charybdis Glacier and upstream on the Charybdis and Scylla Glaciers were located using GPS (Allison, 1991a) (see Figure 3.8). GPS reference stations were operated at Dovers in the Northern Prince Charles Mountains (see Figure 3.8) or at one of a number of exposed rock sites in closer proximity to the ice shelf units. The horizontal error in the positions of the marker poles determined from these GPS observations was approximately 10m, too high for use in calculating velocities at the required accuracy (Allison, 1991b).

[5] Now known to be the southern Amery Ice Shelf.
[6] in the 1988 - 1993 surveys, the term 'grounding zone' refers to the previously defined location, just south of Beaver Lake.

In the following season (1989-90), fifteen of the sites established in 1988/89 were reoccupied using dual frequency GPS receivers (Wild Magnavox WM102s) (Allison, 1991a). Although theoretically these instruments should have provided high-quality results, the GPS data obtained in this season were greatly affected by the high ionospheric activity (see section 4.3.1.1) and horizontal position estimates were again of a very poor quality (approximately 5 m) (Craven *et al*, 1995; Kiernan, 2001).

The survey team returned in 1990/91 and successfully re-observed all twenty-nine marker poles on the ice shelf and glaciers using the dual frequency GPS instruments (WM102s). During this field campaign, eight new ice movement sites were established near the grounding zone and reoccupied after a period of four weeks (see Figure 3.8). Two marker poles left by the 1968 optical survey program (Budd *et al*, 1967) were also discovered by the survey team and were occupied with GPS to allow the determination of long term velocity estimates (Allison, 1991b). GPS receivers at Mawson, Dovers and other rock sites in the vicinity of the ice shelf were operating as reference sites during this field campaign. The data collected in this campaign produced horizontal positions for the velocity markers with precisions of approximately 1 m (Kiernan, 2001).

Horizontal positions and consequently, velocities for each of the ice-marker poles were originally determined using commercial GPS processing software (PoPs). The data from the fourteen sites occupied between 1989/90 and 1990/91 have recently been re-analysed by King (2001) to provide updated (higher accuracy and precision) estimates of the site parameters. The new velocities determined at the AIS velocity markers range from 200 - 400 m/yr, while for sites on the northern glaciers, slower rates of 40 to 110 m/yr have been observed (King, 2001).

3.3.1.2 LGB traverses (1989/90, 1990/91 & 1992/93)

The 1989/90 summer field season was also the time at which the LGB traverses commenced. This series of surveys was designed to observe the characteristics of ice flowing into the basin across approximately the 2500 m elevation contour. The GPS data collected during these traverses forms the basis of the remainder of this thesis and will be discussed in detail in section 3.4.

In 1989/90 the first LGB traverse collected data at twenty sites in the western LGB. The next two traverses, 1990/91 and 1992/93 reoccupied these first twenty sites and also extended the traverse line further south (see Figure 3.10 and sections 3.4.1.1 - 3.4.1.3).

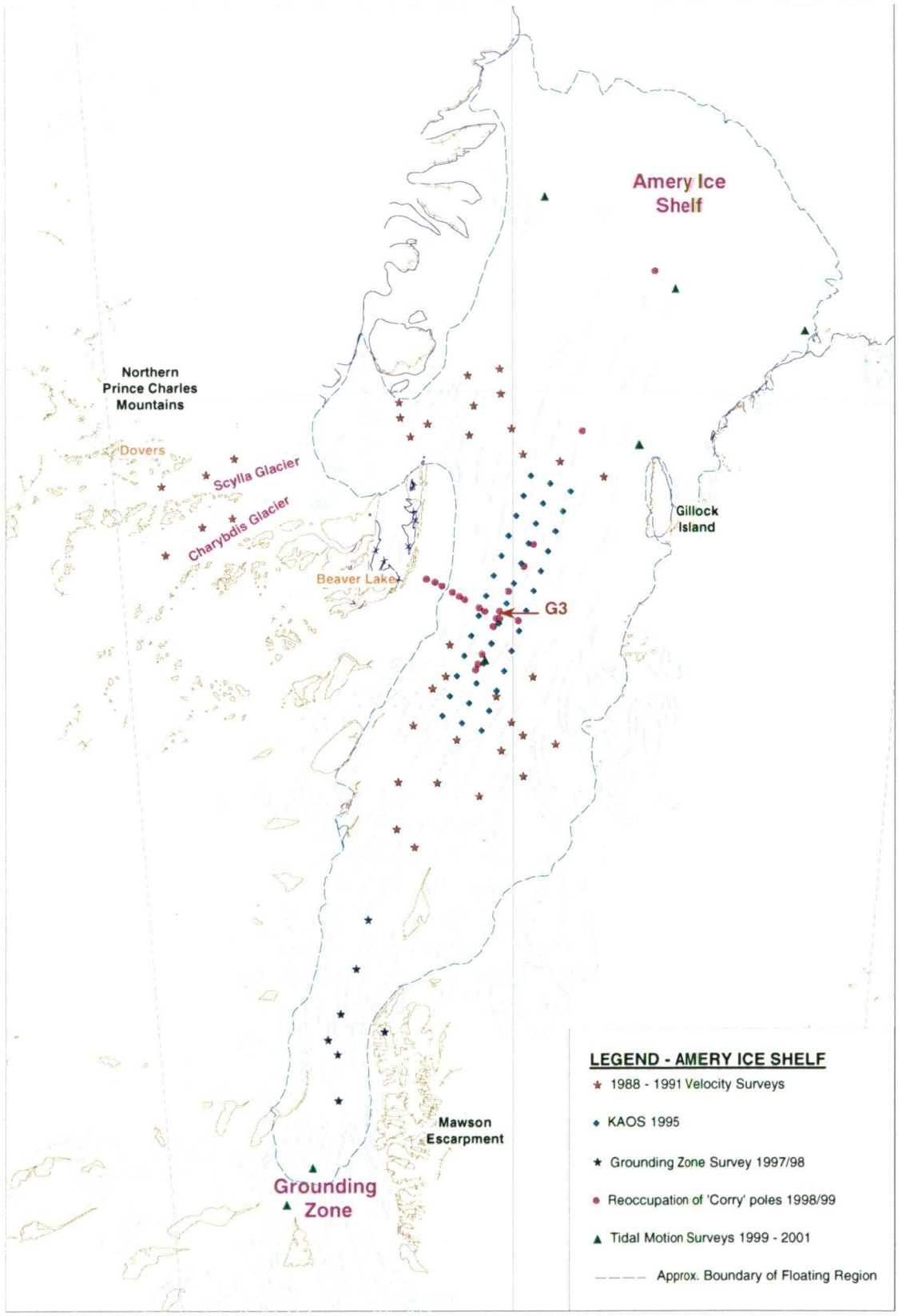

Figure 3.8- Map of GPS survey locations on the AIS

Table 3.1 - Summary of glaciological GPS projects in the LGB region 1988-2001

Season	Location	GPS Equipment	Purpose
1988/89	Amery Ice Shelf	Wild Magnavox WM101	Surface ice velocity
1989/90	Amery Ice Shelf	Wild Magnavox WM102	Surface ice velocity
	LGB traverse	Wild Magnavox WM102	Surface ice velocity Surface elevation/slope
1990/91	Amery Ice Shelf	Wild Magnavox WM102	Surface ice velocity
	LGB traverse	Wild Magnavox WM102	Surface ice velocity Surface elevation/slope
1992/93	LGB traverse	Wild Magnavox WM102	Surface ice velocity Surface elevation/slope
1993/94	LGB traverse	Leica SR299	Surface ice velocity Surface elevation/slope
1994/95	LGB traverse	Leica SR299	Surface ice velocity Surface elevation/slope
1995/96	Amery Ice Shelf	Leica SR299	Altimeter validation Re-survey old traverse route Surface ice velocity Tidal motion Surface profile
1997/98	Grounding Zone	Leica SR9500	Grounding zone location Surface ice velocity Tidal motion
1998/99	Amery Ice Shelf	Leica SR9500 Ashtech Z12	Re-survey old markers/routes Surface ice velocity Surface strain Tidal motion Surface profile
1999/2000	Amery Ice Shelf and Grounding Zone	Leica CRS1000	Tidal motion Re-survey old markers
2000/01	Amery Ice Shelf and Grounding Zone	Leica CRS1000 Leica SR9500	Grounding zone location Surface ice velocity Tidal motion Altimeter validation Surface profile

3.3.2 1993 - 1995

3.3.2.1 LGB traverses (1993/94 & 1994/95)

During the austral summers of 1993/94 and 1994/95, the second phase of the LGB traverses was completed. These two campaigns employed more sophisticated GPS equipment for data collection and completed the entire route from one side of the basin to the other and return. These surveys are discussed in more detail in section 3.4.1.4.

3.3.3 1995 - 2001

3.3.3.1 KAOS survey (1995/96)

During the summer field season of 1995/96, the KAOS (Kinematic Amery Over-snow Survey) GPS campaign collected data over a 120 x 20 km grid in the centre of the Amery Ice Shelf (see Figures 3.8 and 3.9). The primary goals of this survey were to a) provide elevation data for comparison to ERS-1 satellite altimetry measurements and b) remeasure surface height and velocity along a survey line initially established in a 1968-1970 traverse of the ice shelf (Allison, 1995).

The KAOS survey used Leica SR299 receivers in static mode to collect velocity and tidal information at 6 'camp' sites (C2, C4, C6, C8, C10 and C12) and used the same style of receiver for a kinematic survey of the ice shelf topography along the gridlines (see Figure 3.9). From the static data, the first-ever GPS measurements of the AIS tidal signal were obtained by splitting the GPS files into two hour segments (to provide data periods where station movement was within the noise levels of the processing) and estimating multiple positions for each site using GAMIT software (Phillips *et al*, 1996). The vertical motion detected in the GPS results for the camp sites has been shown to closely fit a tidal model for the region to within 10 – 50 mm (Phillips *et al*, 1996; King *et al*, 2000).

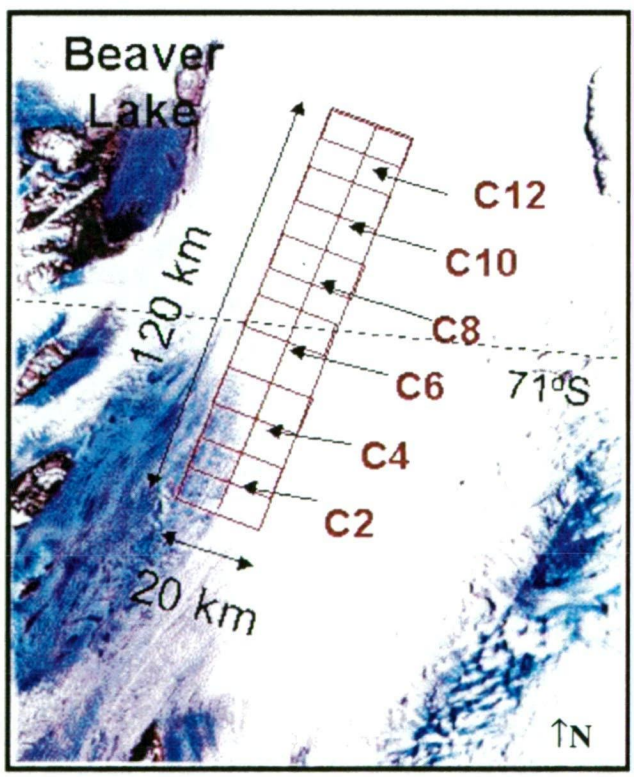

Figure 3.9 - The KAOS survey grid (pers. com., H. Phillips, 1996). Static GPS observations made at C2 - C12. Kinematic GPS observations made along the boundaries of each grid cell.

The use of a segmented processing scheme for the static GPS data also allowed the determination of surface velocities at the 'camp' sites over the short occupation periods (Phillips *et al*, 1996; Phillips *et al*, 1998). The magnitude of the velocities at these sites was found to be approximately 340 - 390 m/yr, values that are within the error margins of the original 1968-70 velocity results. This result indicates that no significant variation in flow had occurred in this area during the 30 years between velocity estimates. Statistical testing of results using terrestrial and GPS data by King (2001) confirms this finding.

Leica proprietary software (SKi v2.0) was used to process the kinematic data over two baselines 1) from the 100km distant, fixed GPS station at Beaver Lake and 2) from the nearest, moving 'camp' site (approximately 0-10 km) (Phillips, 1999). The resulting surface profile of the survey region was found by Phillips *et al* (1998) to closely match (1.7 m rms) the DEM values determined from ERS-1 altimetry.

3.3.3.2 Grounding zone survey (1997/98)

Phillips *et al* (1996) confirmed (using altimeter measurements and hydrostatic calculations) that the grounding zone of the Amery Ice Shelf was located at approximately 72.6°S, 150 km south of the previously designated position. This revised grounding zone location was investigated by collecting GPS data at six AIS sites during the summer of 1997/98 (see Figure 3.8). The primary goal of this study was to detect and observe the horizontal and vertical motion of the ice shelf near to its grounding zone. Initial investigations showed that the vertical movement of the ice shelf at these locations is closely following the full tidal signal (pers. com. A. Ruddell, 1998). A full analysis of the motion at two of these sites (V3 and V5) has been carried out by King *et al* (2000) using both segmented and sequential GPS processing techniques. King *et al* (2000) showed that the GPS vertical signal at this location is comparable to the tidal signal for the AIS region, but has a slight variation in phase and amplitude.

3.3.3.3 Reoccupation of the 1968 - 1970 AIS traverse sites (1998/99)

During the 1990/91 Amery Ice Shelf GPS survey and again during the KAOS program, it was found that several of the original marker poles ('Corry' poles) from the 1968 - 1970 terrestrial surveys (Budd *et al*, 1967) were still visible above the snow surface. Following on from this discovery, a project to resurvey the 1968 - 1970 traverse lines using GPS techniques was undertaken in the 1998/99 field season.

In the 1998/99 ice shelf survey, a GPS base station was operated continuously at the base camp (near G3, Figure 3.8) for the duration of the survey (thirteen days). Twenty-two of the original 'Corry' marker poles were found during this campaign and occupied with Leica SR399 and Ashtech Z12 equipment (see Figure 3.8). The processing of these data was undertaken by King (2001) using GAMIT (King and Bock, 1999) and then FONDA (Dong *et al*, 1998) software to combine the GPS results with the original terrestrial survey data and compute 30-year velocities at each of the relocated poles. The 1998/99 GPS data have also been used to observe a 13-day tidal signal at the continuous 'static' GPS site (G3) and calculate new velocities for several of the KAOS sites which were also re-occupied during this survey program (King *et al*, 2000).

3.3.3.4 Hot water drill GPS site (1999/2000)

During the 1999/2000 field season, a hot water drilling program was initiated as part of the Amery Ice Shelf Oceanographic Research (AMISOR) project. The drilling site was set up in the northeastern corner of the AIS (see Figure 3.8) and a Leica CRS1000 GPS receiver was installed at the camp. This GPS site collected 31 days of near continuous data. These data have formed part of a study into the ocean circulation and tidal motion of the ice shelf with results from this site comparing closely to tidal models for the region (pers. com. M. King, 2001).

Also during the 1999/2000 summer, a field party was able to locate and reoccupy five of the 1997/98 grounding zone sites, allowing more precise calculation of the surface velocity at these locations.

3.3.3.5 Altimeter validation and tidal motion project (2000/01 - continuing)

King *et al* (2000) observed a phase shift and amplitude variation in the GPS-derived tidal constituents of the ice shelf along an approximately north-south profile near the centre of the AIS. In order to further examine the tidal effects across all regions of the shelf and to observe the oceanic circulation pattern under the AIS, static GPS observations were made during the 2000/01 field season at six locations across and along the ice shelf from the front to the grounding zone (Coleman, Allison *et al*, 2000; Coleman, Morgan *et al*, 2000) (see Figure 3.8).

Data from only three of these sites have been recovered at the time of writing and therefore complete results of this survey are not available. Preliminary results show that the tidal signal has been well sampled by the GPS observations over a period of more than one month thereby allowing determination of the tidal constituents at these sites (pers. com. M. King, 2001).

The locations of some of the static sites on the ice shelf were also selected to act as ground-truthing data for the Ice, Cloud and Land Elevation Satellite (ICESat) (carrying the Geoscience Laser Altimeter System - GLAS) verification phase. In addition to these static sites, some kinematic GPS profiles were also completed during the 2000/01 season for use in validation of the altimeter data (Coleman, Allison *et al*, 2000).

3.4 The Lambert Glacier Basin Traverses[7]

The LGB traverses were completed as part of the Lambert Amery Regional Glaciology Experiment project undertaken by ANARE and the Australian Antarctic Division Glaciology section between 1989 and 1995 (Higham *et al*, 1997). The LGB traverse program was comprised of a series of five surveys approximately following the 2500 m surface elevation contour and covering some 2015 km in the region between the Australian bases at Mawson and Davis (see Figure 3.10). During these traverses, seventy-three permanent ice movement stations (IMS) (fibreglass poles) were established at approximately 30 km intervals along the traverse route (see Figure 3.10). Each of these IMS was occupied at least twice during the course of the traverse program in order to obtain information regarding the surface velocity and elevation at these locations.

The primary purpose of the LGB surveys was to collect information regarding the ice characteristics and dynamics of the interior LGB for use in glaciological studies, including mass balance calculations, of the region (Craven *et al*, 1995). In order to obtain this information, the traverses collected field measurements of surface velocities, surface elevation, surface slope, ice thickness, gravity, meteorology, accumulation, snow stratigraphy, snow density, firn temperature and snow surface characteristics (Kiernan, 2001) (see Table 3.2).

3.4.1 The LGB GPS Campaigns

3.4.1.1 1989 - 1990 (13th January - 7th February)

The 1989/90 LGB traverse covered approximately 600 km along the western side of the basin, collecting GPS measurements at each IMS between LG00 and LG20 (see Figure 3.10). During this survey, the traverse team had access to four WM102 dual frequency receivers, two serving as base stations at Dovers and Mawson (Wombat) and two at the traverse sites. These GPS systems had been used in the previous season on the Amery Ice Shelf (see section 3.3.1.1) and produced sub-standard results, largely attributed to the high levels of ionospheric activity, poor receiver

[7] The LGB traverses are described in full detail in Kiernan (2001) and Higham and Craven (1997).

Table 3.2 - Measurements made during the LGB traverses

Ice Thickness -	The ANARE 100 MHz ice radar was mounted on a tractor van and hauled along the traverse route providing continuous digital information on the bedrock topography below the ice (Higham *et al*, 1995).
Surface Slope -	In 1992/93 and 1994/95, a 50 km offset line was surveyed using static GPS observations parallel to the Western traverse route (see section 5.1.4). In the Eastern sector, slope was determined by a series of five kinematic GPS surveys, running perpendicular to the main route and covering approximately 5km either side of the selected IMS (Craven *et al*, 1995) (see section 5.1.4 of this study).
Surface Strain -	Cane grids spanning a number of kilometres were established at various locations along the traverse route. The movement of the grid markers between seasons was then determined by repeat rapid-static GPS surveys (Craven *et al*, 1995).
Surface Velocity -	IMS were established at intervals of 30 km for the majority of the traverse and approximately 15 km intervals for the region of the major ice streams. Each of these poles was occupied with GPS equipment on at least two occasions during the traverses. Surface ice velocities were determined from the change in position between occupations (section 5.1.2 of this study; Kiernan, 2001).
Elevation -	The heights of the IMS were determined using GPS techniques (see section 5.1.3). Between IMS, the surface elevation was measured continuously using barometric levelling (Craven *et al*, 1995).
Accumulation -	Canes were placed approximately every 2 km along the traverse route and at seven cane farms located at the AWS sites and LG68. Height above the surface was measured to markers on these canes in each season to observe change in the surface height (Higham and Craven, 1997).
Sub-surface -	1-metre ice cores were collected at each accumulation cane, 2-metre cores and 10-metre firn temperatures were collected at each IMS and 10 to 60 m cores were collected at fifteen IMS (Higham and Craven, 1997).
Gravity -	Gravity was measured at each accumulation cane (i.e., every 2 km) (Craven *et al*, 1995).
Meteorology -	Six AWS were deployed approximately every 10 IMS (~300km) at LG00, LG10, LG20, LG35, LG46, LG59 (see Figure 3.10). Throughout the traverses, continuous digital meteorological readings were collected (Craven *et al*, 1995).

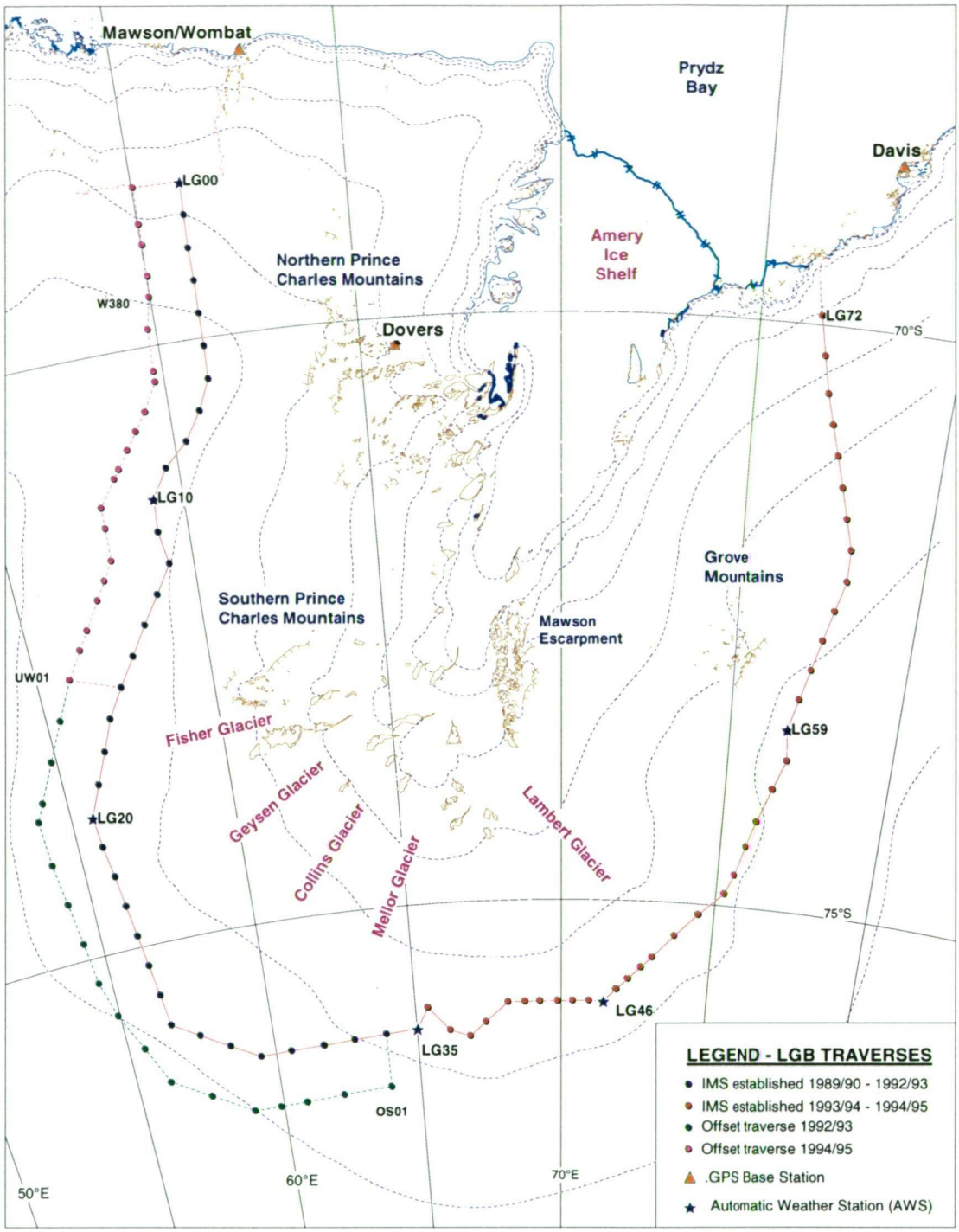

Figure 3.10 - Map of the LGB traverse IMS locations

satellite tracking techniques and the limited satellite constellation available at this time. In order to minimise the impact of these factors on the quality of results, the LGB GPS survey program was designed to incorporate a significant amount of redundant observations (Kiernan, 2001). These redundancies included the use of two reference stations and the simultaneous observation of consecutive IMS. To give added strength to the final network adjustment of the GPS results, Precise Ephemeris Transit observations were obtained at every fifth IMS (Kiernan, 2001).

The survey team set out in three parties, one dedicated to glaciology work, another carrying the ice radar and the third transporting fuel (Kiernan, 2001). Figure 3.11 shows the three parties stopped at an IMS. The initial survey plan was for the two scientific parties (ice radar and glaciology) to carry one set of GPS equipment each and travel separately, at a spacing of approximately 30 km, stopping 'overnight' to record GPS observations at two neighbouring IMS. In this manner, each observation session would include simultaneous GPS measurements at consecutive IMS.

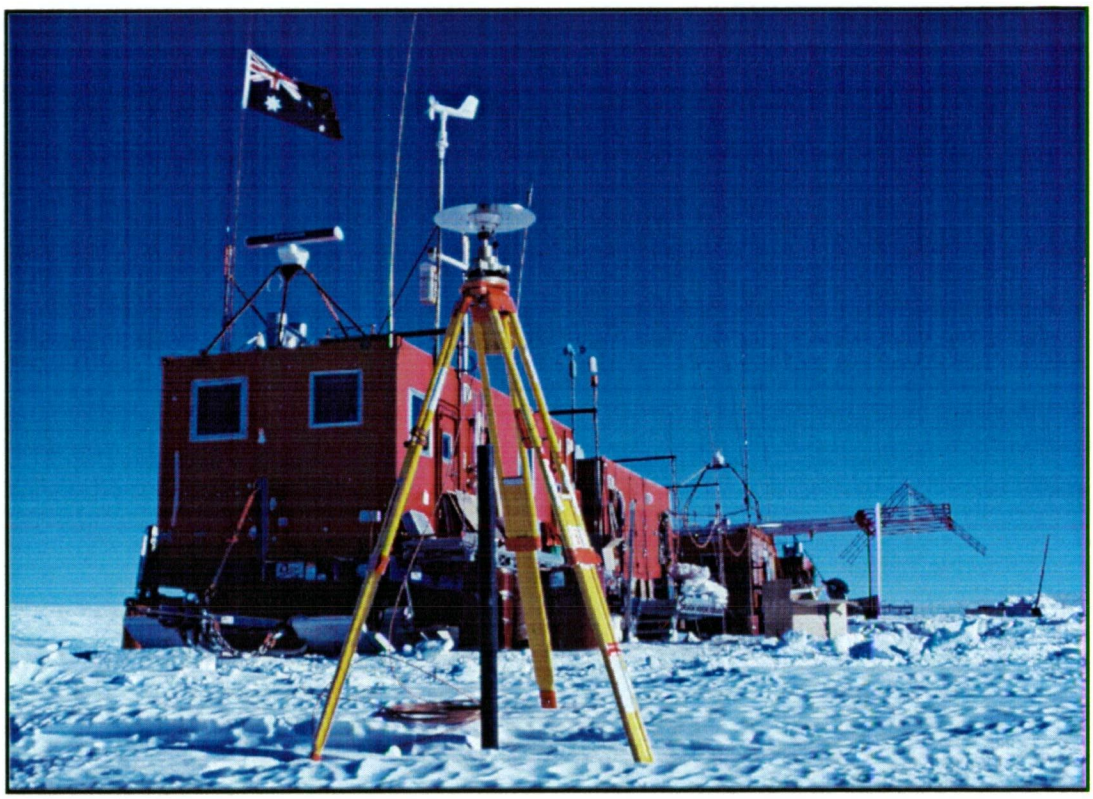

Figure 3.11 - LGB traverse vans stopped at an IMS. (Note: the GPS antenna in this photo was set up as a base station for a kinematic survey, not to record ice movement.) Photo courtesy of M. Craven.

Unfortunately, early in the survey, one of the traverse vehicles broke down and remained stationed at LG10 while the other parties continued to LG20 and then returned (Kiernan, 1990). GPS observations in this season could therefore only be made once at each of the IMS between LG20 and LG11 during which time, GPS data were also continuously recorded at LG10. Repairs on the vehicle at LG10 were completed during this observation period and the survey was therefore able to proceed as originally planned between LG10 and LG00 (Kiernan, 2001).

3.4.1.2 1990 - 1991 (30th December - 18th February)

In the 1990/91 austral summer the LGB traverse route was extended further around the western side of the basin, covering approximately 1200 km from LG00 to LG35 (see Figure 3.10). This survey made use of the same WM102 GPS equipment and IMS observation strategy as the 1989/90 survey except that in this season, only one base station was available, either at Wombat (Mawson) or Dovers. During this survey, no significant incidents were reported and GPS data were collected using simultaneous measurements at consecutive IMS, providing two sets of observations at each IMS between LG00 and LG35.

3.4.1.3 1992 - 1993 (20th December - 5th February)

In the 1992/93 summer field season, the major aims of the traverse were altered slightly from the previous seasons to focus on the collection of ice core data and the determination of surface gradients near the western LGB traverse route (Kiernan, 2001).

For this survey, GPS observations were again made with the WM102 receivers and used a fixed reference station located at Mawson (Wombat). GPS observations were completed at all IMS between LG00 and LG16 using the same methodology as in the 1990/91 traverse. The northward leg of the 1992/93 LGB traverse was undertaken along a line parallel to the main traverse and offset by 50 km to the west (Higham, 1993) (see Figure 3.10). Along this survey route, GPS data were recorded every 30 km or so to provide elevation data and therefore slope information for the region between the offset and main traverse lines. This was the final season in which the WM102 receivers were used and the last in which a base station was erected on Wombat Hut at Mawson station.

3.4.1.4 1993 - 1994 and 1994 -1995 (26th November - 15th February and 14th November - 13th February)

In November 1993, a traverse team set out from Mawson to collect glaciological, topographical, meteorological and GPS information approximately along the 2500 m contour of the entire LGB. In this survey the traverse route around the LGB was completed, with the establishment of IMS between LG36 and LG72 (see Figure 3.10). In the section of the traverse route spanning the major glacial streams, the IMS were established approximately every 15 km (LG40 - LG50) so that a better indication of the velocity pattern could be obtained (see Figure 3.10). In this region of the traverse, every second site was observed only once for a period of approximately two hours due to time limitations and the expectation of higher flow rates in this region. Also, as the first seventeen IMS in the western sector (LG00 to

LG16) had already been occupied in three previous seasons, only a selection of these sites were re-observed in 1993/94.

During March and April 1994, the traverse team returned to the LGB route and re-occupied sites between LG72 and LG65. These observations were made to provide an estimation of the accuracy of results obtained over a re-occupation period of only a few weeks. Results from this short survey are presented in section 5.4.

The traverse team returned to the LGB region in November 1994 and re-occupied most of the IMS established during the previous seasons. During the course of this survey, the western offset line was extended southwards to provide surface gradient information for the entire western sector. In the eastern sector, kinematic GPS profiles were recorded at five sites to determine local slope information for this region (see Figure 3.12). As in the previous season, the 1994/95 traverse only observed the odd-numbered IMS in the glacial section of the traverse route for a 1-2 hour period and also recorded GPS data for only a small selection of IMS between LG16 and LG00.

Figure 3.12 - Initialising the roving antenna for a kinematic survey next to the reference IMS. Photo courtesy of M. Craven.

For the 1993 - 1995 LGB traverses, GPS data were observed at IMS sites in the same manner as for the previous surveys, i.e., with simultaneous measurements made at each set of consecutive IMS. These traverses employed Leica SR299E dual frequency GPS receivers and benefited from the presence of an almost complete satellite constellation and reduced ionospheric activity. The fixed base stations used

in the 1993 - 1995 surveys were Rogue SNR-8100 receivers located at Davis and Mawson, some 150 to 1000 km from the LGB traverse route (see Figure 3.10). These permanent sites had been established in November 1993 by the Australian Survey and Land Information Group (AUSLIG) as part of the Australian Regional GPS Network and the IGS network (Kiernan, 2001).

3.5 Chapter Summary

Antarctica is an important region for studies of global climate change and sea level monitoring. Each region of the Antarctic continent has its own characteristics and role in the overall accumulation, transport and discharge of ice from the interior to the ocean. Studies investigating the movement of ice and variation between the mass input and output of the Antarctic ice sheet are termed mass balance studies. At present, these studies cannot provide definitive information regarding the balance state of the ice sheet due to uncertainties in the calculation variables (Weller, 1992; Fricker, Warner *et al*, 2000). Therefore the contribution from the Antarctic ice sheet remains one of the major unknowns in sea level budget calculations (Meier, 1993; Bromwich and Parish, 1998).

The LGB is one of the major Antarctic drainage basins through which ice from a large portion of the East Antarctic ice sheet is discharged. It is located between two Australian Antarctic bases and therefore has been the focus of many scientific expeditions since the 1960s. After 1988, GPS technology was introduced as the preferred positioning method for studies in the LGB region. Since this time many surveys using GPS methods have been completed on the ice shelf, the glaciers and the interior basin in order to monitor ice flow, ice thickness and accumulation and improve our knowledge of the mass balance of this region.

The LGB traverses were a series of five GPS surveys (undertaken in conjunction with other glaciological and meteorology projects) approximately along the 2500 m contour of the LGB. These surveys produced positional data of varying quality due to receiver, ionosphere and GPS system improvements between 1989 and 1995, the period of the traverse program.

The following chapters (4 and 5) discuss the 're-computing' of the position and velocity results from the LGB traverses using high-level GPS processing techniques. This re-analysis is being undertaken in order to improve the results obtained from these GPS data, especially for the three earliest campaigns in which the data contained a significant amount of noise. The use of high-level processing techniques should provide a more accurate set of velocity and position results (Manson, 1995) and therefore reduce the uncertainty in mass flux calculations at the LGB IMS.

Chapter 4

GPS DATA PROCESSING

4.1 Introduction

The LGB data were collected during two very different periods in the development of GPS technology. The first surveys (1989/90 - 1992/93), covering the western sector of the traverse route, were undertaken when GPS was in its infancy as a scientific tool. This period was also one of high ionospheric activity (see section 4.3.1.1), which compounded the problems encountered with the available technology. The second phase of the surveys (1993/94 - 1994/95) was completed using modern GPS receivers and a full satellite constellation at a time of relatively normal ionospheric conditions.

Initial results from the LGB GPS data were obtained from baselines solutions using commercial software (PoPs and SKi) (Kiernan, 2001). The surface ice velocities determined for the IMS sites from these solutions were within the original specifications for the survey (±10%) at most of the traverse sites (see Kiernan (2001) for full details of these initial results). Prior to the data from the final traverse being thoroughly analysed, high level GPS processing software (GAMIT) was introduced at the University of Tasmania. Access to this software suggested that improvements in the LGB results should be possible especially in the determination of surface height and ice flow direction. Manson (1995) carried out a comparative study on a small section of the 1993/94 and 1994/95 data to determine the benefits gained by processing the LGB data with this new software. The results of this honours thesis indicated that higher precision results could indeed be obtained by employing the new, more sophisticated processing techniques.

The work presented here extends the Manson (1995) study to include the entire traverse route and data from all LGB survey periods. In this chapter, the processing software is introduced followed by a full description of the methodology used in obtaining position and velocity estimates from the LGB GPS data.

4.2 Overview of the Processing Software

4.2.1 GAMIT

[For further details regarding GAMIT software, refer to King and Bock (1999)]

GAMIT is a GPS analysis package that is based on a least-squares process for the estimation of the three-dimensional coordinates of a series of GPS stations and the satellite orbital parameters of the GPS constellation (King and Bock, 1999). The software is designed to be run as a series of modules, which are executed sequentially to provide a final solution (see Figure 4.1). The modules

> "...perform the functions of preparing the data for processing, generating reference orbits for the satellites, computing residual observations (O-C) and partial derivatives from a geometrical model, detecting outliers or breaks in the data and executing a least squares analysis" (King and Bock (1999), p1-1).

The sequence of processing modules, their input files and analysis options are listed in a batch file created prior to the least-squares solution. The major modules required for standard GAMIT solution are (King and Bock, 1999):

ARC - uses a file of orbital initial conditions and parameter values to generate a binary satellite ephemeris file including partial derivatives.

MODEL - computes the prefit residuals and partial derivatives from the input observation data and writes them (with the observation data) to new binary files (*c-files*).

AUTCLN - reads in *c-files* and identifies cycle slips and outliers in the pre-fit one-way and double-difference residuals. Creates new *c-files* with flagged and corrected residuals and phase observations.

CFMRG - sets up the input for the least-squares process indicating the files to be used and the parameters in the adjustment.

SOLVE - the least-squares solution process for determining ambiguity values and solving for station, orbit and Earth orientation parameters.

Within the *SOLVE* module, a series of intermediate solutions for the ionosphere-free, wide-lane and narrow-lane observables using varying degrees of constraint are undertaken in order to resolve ambiguities and determine the parameter estimates and their covariance matrix (Feigl *et al*, 1993). The output information (parameters and variance-covariance (VCV) matrix) is stored in an ascii-format *h-file*, which may then be used in further analysis.

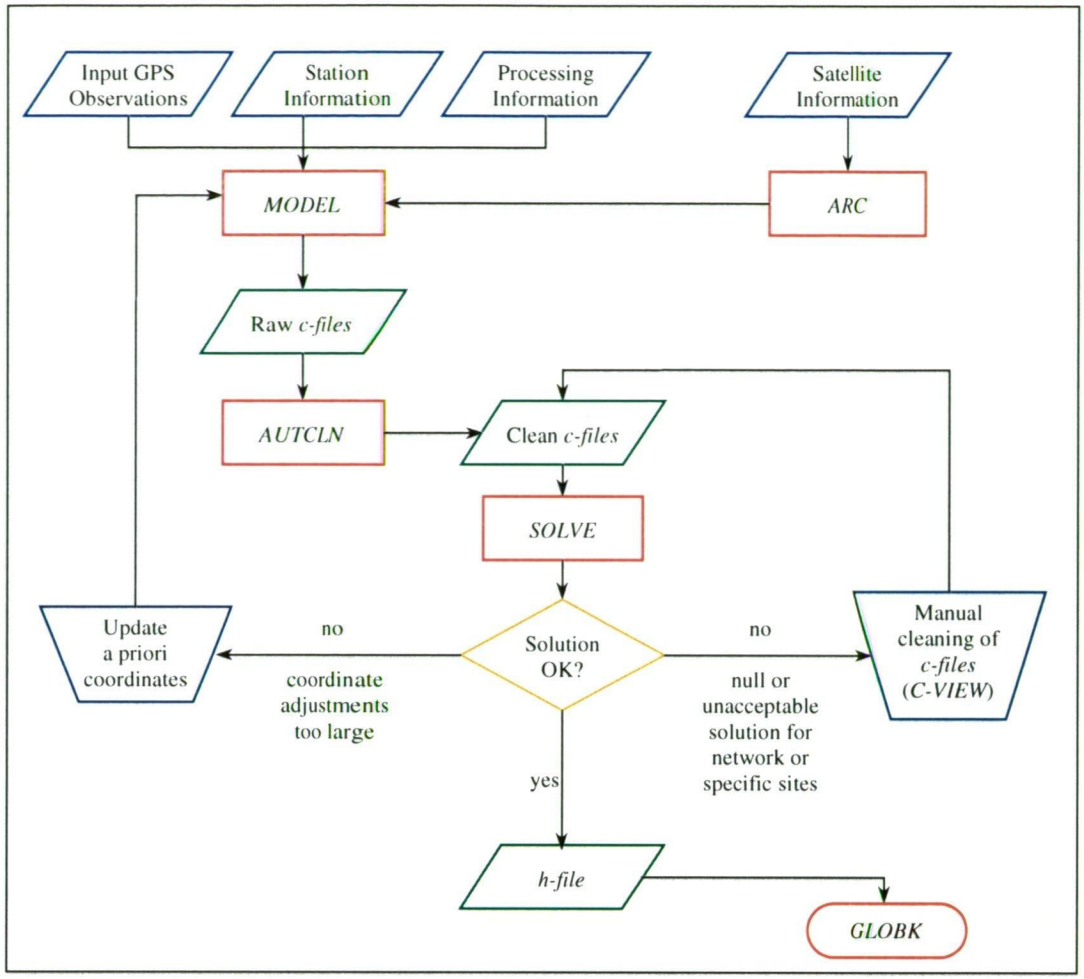

Figure 4.1 - Flowchart of basic GAMIT solution procedure

4.2.2 Global Kalman Filter (GLOBK)

[For further details regarding GLOBK/GLORG methods and procedures, refer to Appendix A.1 of this thesis, Herring (1999b) and Dong *et al* (1998)]

> "*GLOBK* is a Kalman filter whose primary purpose is to combine solutions from the processing of primary data from space-geodetic or terrestrial observations. It accepts as data, or "quasi-observations" the estimates and associated covariance matrices for station coordinates, Earth rotation parameters, orbital parameters, and source positions generated from analyses of the primary observations" (Herring (1999b), p1).

The primary output from GLOBK solutions are station coordinates and velocities in a consistent reference frame. The software is most commonly used for estimating averaged station coordinates over multiple days, station velocities from multiple occupations and coordinate repeatability (precision assessment) over time (Herring, 1999b).

The advantages of GLOBK are that it allows large amounts of data to be easily and efficiently handled, stored and combined. Also, the software provides a basis for determining geodetic results when there is variation in the configuration of the tracking network and allows these data to be combined and analysed in a consistent manner (Feigl *et al*, 1993).

The input for these GLOBK solutions, in regard to GPS data, is usually the GAMIT output *h-files* from loosely constrained (fixed or free ambiguity) least squares solutions. Using these data allows constraints to be applied uniformly in the combined solution (Herring, 1999b) and a consistent reference frame to be imposed on the solution after combination (Dong *et al*, 1998). The quasi-observations from the *h-files* have four major sources of systematic errors:

> "inadequately modelled non-gravitational perturbations in the motions of the satellites; inadequately modelled atmospheric corrections; oscillations in phase due to multipathing; unmodelled offsets and variations in the effective phase-centres of the receiving antennas" (Dong *et al* (1998), p208.)

These systematic errors have been shown to contribute to short-term scatter (several days) of position estimates with a $\left(\chi^2/f\right)^{1/2}$ value (where χ^2 is the chi-squared statistic and f is the number of degrees of freedom) of approximately 0.8 to 1.5 and long-term $\left(\chi^2/f\right)^{1/2}$ values of approximately 2.0 (Feigl *et al*, 1993). These findings suggest that there is a need to adjust the quasi-observation VCV information in multi-campaign processing in order to allow for the long-term scatter in the GPS results (Feigl *et al*, 1993). In practice, this is usually accomplished by scaling the formal values of the final results of each campaign by a factor which is representative of the noise in that experiment (e.g., Feigl *et al* (1993) and Dong *et al* (1998)).

Generally, the GLOBK solutions are computed using 'loose' constraints on all site coordinates and satellite orbit parameters, thereby providing results in a consistent but undefined reference frame. Once the final GLOBK solution has been determined the network may then be translated, rotated and scaled onto a specified reference frame (usually ITRF). This is accomplished via the GLORG program, which fixes the origin of the solution by minimising the deviations from a priori coordinates at a number of well-defined sites (Herring, 1999b).

4.3 The GPS Data

The GAMIT processing of the LGB GPS data involved the use of all available observations from 1989 to 1995. As mentioned in section 3.4.1, these surveys were carried out over a period of changing technological and atmospheric conditions, which resulted in a tremendous variation in the quality and volume of data collected. Therefore, in this and following sections, the LGB GPS data will be discussed in terms of the two distinct traverse periods (i.e., 1989 - 1993 and 1993 - 1995).

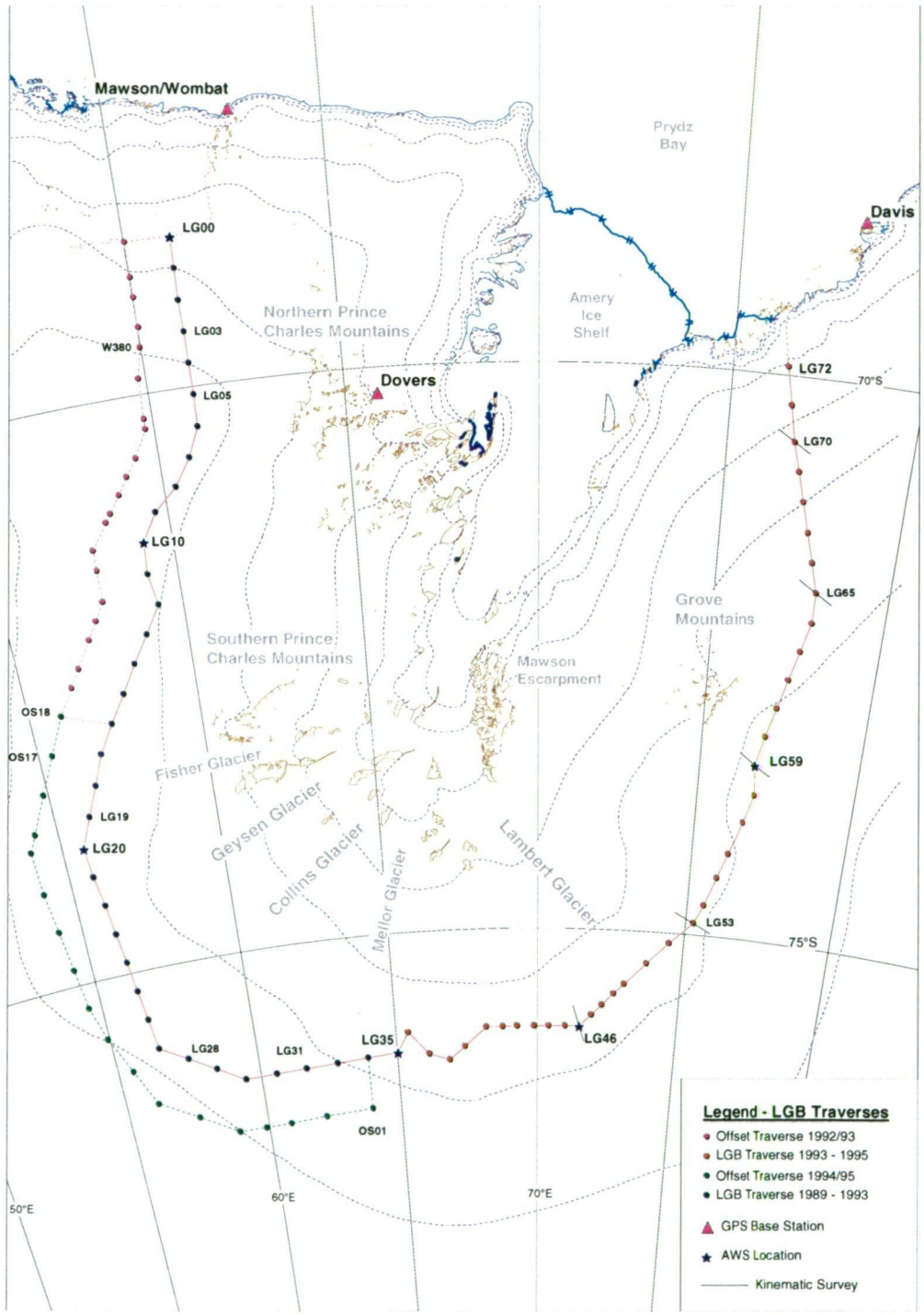

Figure 4.2 - The LGB traverses 1989 - 1995

4.3.1 1989 - 1993

The 1989/90 - 1992/93 LGB traverses observed GPS data (using WM102 receivers - see sections 3.4.1.1 and 4.3.1.1) at the LGB IMS between LG00 and LG35 (see Figure 4.2). The design of these surveys resulted in many days where a given IMS was observed in the morning and evening of the same day using two different sets of equipment (see section 3.4.1). For processing purposes, data files that related to the same IMS and UT day were joined, creating one RINEX file per IMS for each day of occupation.

As discussed in section 3.4.1.1, the local base stations for these LGB surveys were situated at Mawson (GPS station referred to as Wombat) and/or sites in the Northern Prince Charles Mountains (e.g., Dovers) (see Figure 4.2). These GPS sites were occupied with WM102 receivers and operated throughout the traverse periods.

The global GPS sites operating during the period of the early LGB surveys were very sparsely distributed. In particular, there were very few sites located in the Southern Hemisphere prior to 1992/93 (see Table 4.1 and Figures 4.3 and 4.4). Fortunately, the GIG'91 (Melbourne *et al*, 1991) and SCAR'91 (Morgan *et al*, 1992) GPS campaigns were undertaken during the austral summer of 1990/91 and provided

Table 4.1 - GPS sites (Global and LGB) 1989 - 1993
(# Sth indicates the number of sites in the Southern Hemisphere)

Period	1989/90	1990/91 (001 - 021)	1990/91 GIG/SCAR (022 - 044)	1990/91 (045 - 049)	1992/93
LGB Sites	Lg00 - Lg20	Lg33 - Lg19	Lg18 - Lg03	Lg03 - Lg00	Lg00 - Lg16 UW01 - W380
Global Network	Davi Trom Koke Tsul Moj1 Well Onsa Wes1 Orrx Wtz1 Ric1 Yar1 Tas1 Ykn1	Jplm Sio1 Koke Tas1 Ds10 Town Ds40 Tsu1 Ds60 Well Moj1 Wes1 Pin1 Wtz1 Ric1 Yell	Algo Mcm0 Town Ds10 Moj1 Trom Ds40 Nyll Tsu1 Ds60 Ohig Usug Eis1 Orro Well Fair Pin1 Wes1 Hart Pgc0 Wetb Hone Ric1 Wsam Jplm Sang Yar1 Kokb Sio1 Yell Kosg Tas1 Matg Tnob	Ankt Sio1 Ds10 Tas1 Ds40 Town Ds60 Tsu1 Fair Usud Hone Well Kokb Wes1 Moj1 Wtz1 Pin1 Yar1 Pgc0 Yell Ric1	Albh Kosg Sio2 Algo Kour Stjo Darw Masp Taiw Ds10 Mate Tas1 Ds42 Mcmu Trom Ds60 Mets Usud Drao More Wett Fair Onsa Yar1 Hart Pama Yell Hob1 Rcm2 Kokb Sant
# Sth	5	4	13	5	9

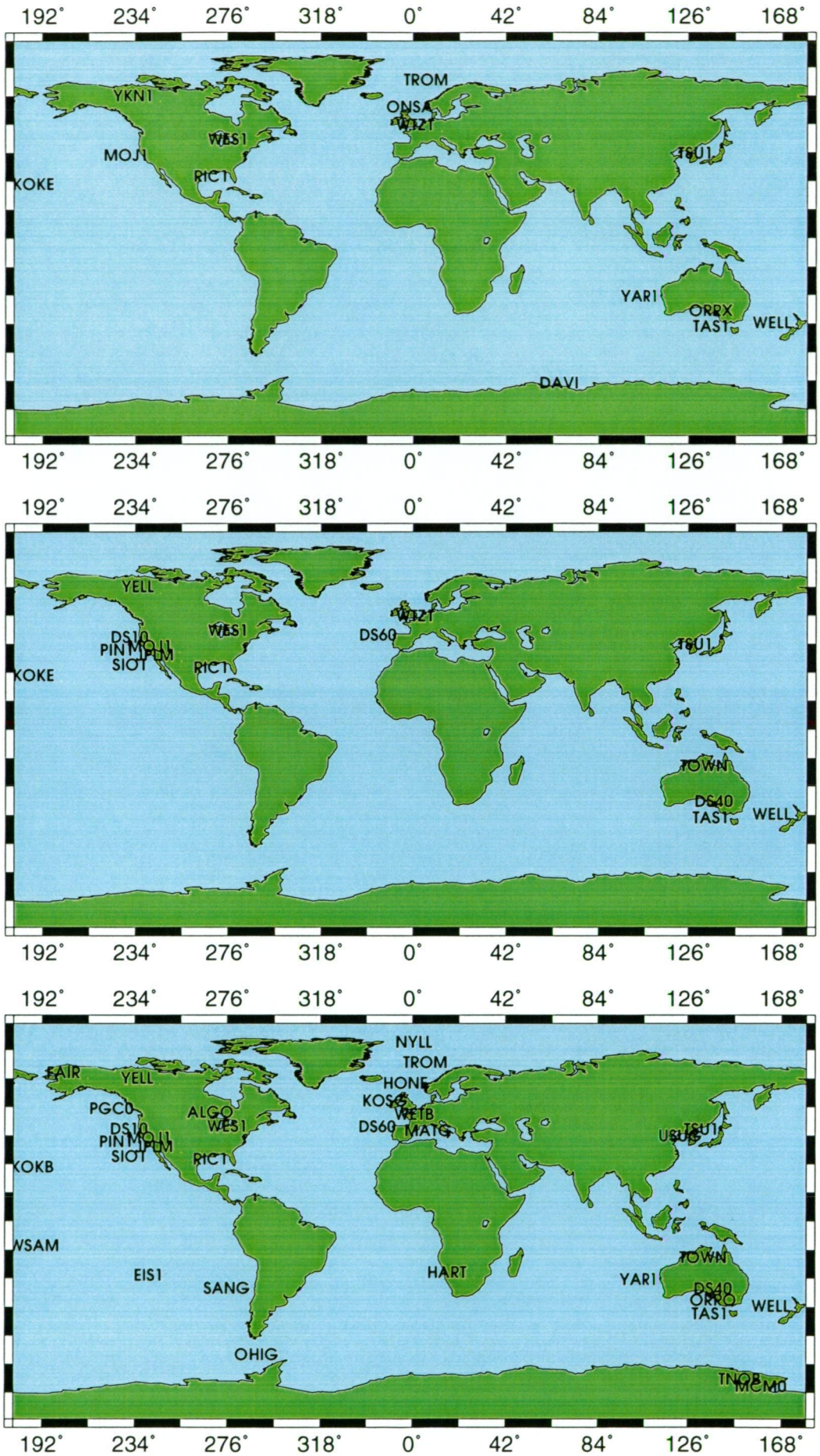

Figure 4.3 - The global processing network a) 1989/90, b) 1990/91-preGIG, c) 1990/91-GIG

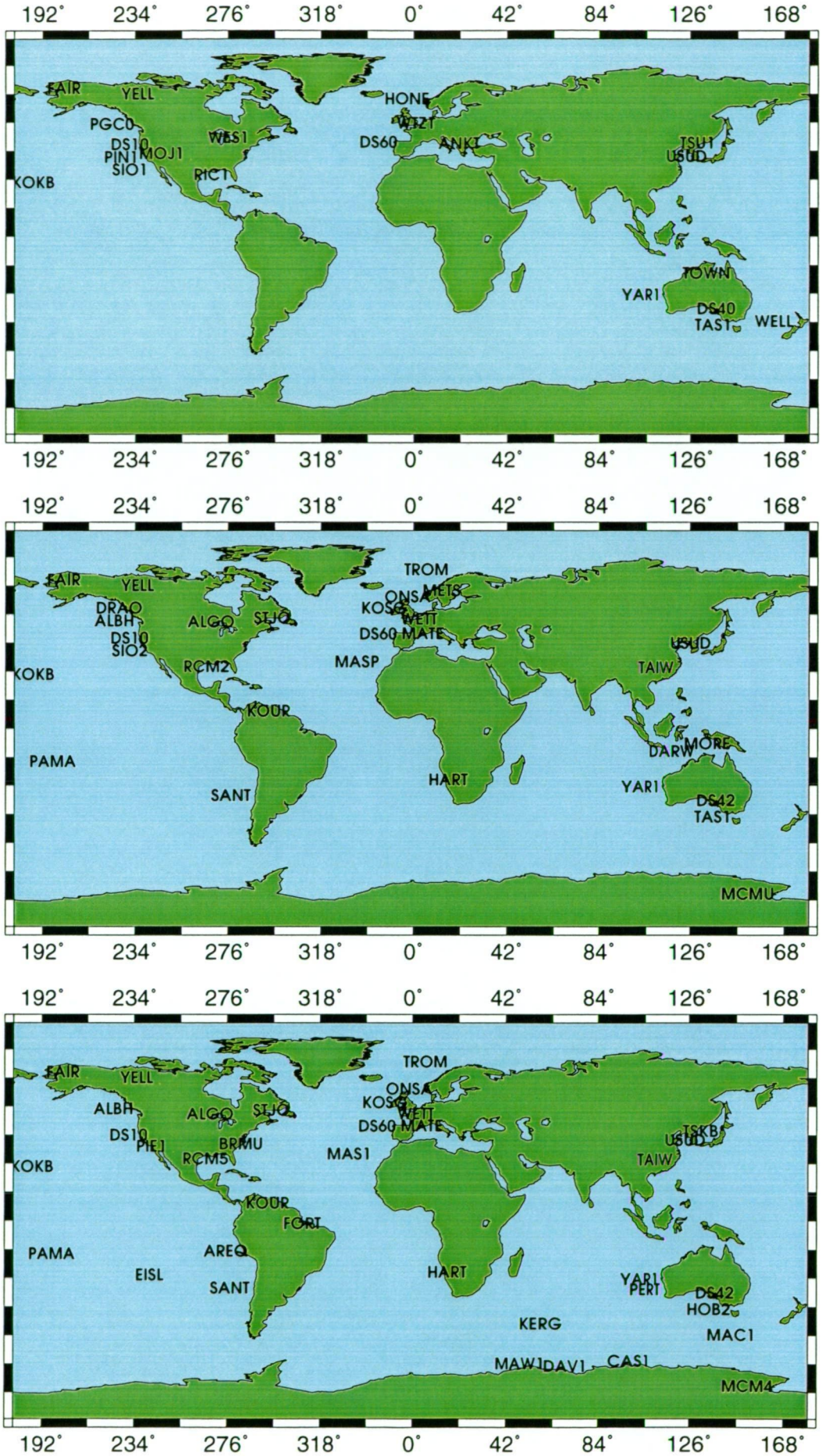

Figure 4.4 - The global processing network a) 1990/91-postGIG, b) 1992/93, c) 1993/94 & 1994/95

invaluable global network data (especially in the Southern Hemisphere) for inclusion in the processing of most of the 1990/91 LGB GPS data (see Figure 4.3c). The SCAR sites in particular, provided vital additional data on the Antarctic continent, allowing relatively short baselines between these stations and the LGB sites to be computed in the network solution. Prior to the GIG '91 campaign, the only available global GPS data had been from sites within the CIGNET network (Chin, 1988) and from selected experimental sites in Northern America (see Table 4.1 and Figures 4.3a and 4.3b). At the conclusion of the official GIG'91 observation period, many of the campaign sites continued operating, but very few remained in the Southern Hemisphere (see Table 4.1 and Figure 4.4a).

4.3.1.1 LGB GPS data quality

Initial testing carried out on sections of the 1989 - 1993 LGB data prior to the major processing exercise revealed that the GPS data collected during these surveys were of a consistently poor quality with very high noise levels and frequent L2 signal dropouts. Several factors were found to contribute to the degradation of this early data, the most significant being:

Satellites:

The GPS constellation at the start of this survey period consisted of only ten satellites, increasing to twenty-one by the end of the 1992/93 survey. Also, at the latitudes of the LGB traverse (67°S to 76°S) the inclination of the orbital plane causes satellites to be observable only for short periods and at low elevation angles (< 70°). The combination of these factors resulted in daily observation windows of two to four hours with only four to six available satellites during these periods.

Ionosphere:

The ionosphere is the electrically active layer of the Earth's atmosphere and varies in strength on both spatial and temporal scales. In a spatial sense, the most active ionospheric conditions are observed in the polar latitudes, especially in and around the auroral zones (Allison, 1991) where the Earth's magnetic field interacts with the solar wind (Craven *et al*, 1995). Temporally, the level of ionospheric activity is closely related to variations in solar activity, which is known to have an 11-year cycle (see Figure 4.5). Periods of high ionospheric fluctuation, as observed during peaks in solar activity and in the auroral region generally, may cause the strength of GPS signals to fade in and out (scintillation) or even completely prevent signal tracking by the receiver resulting in high numbers of cycle slips being present in the data (Langley, 1996).

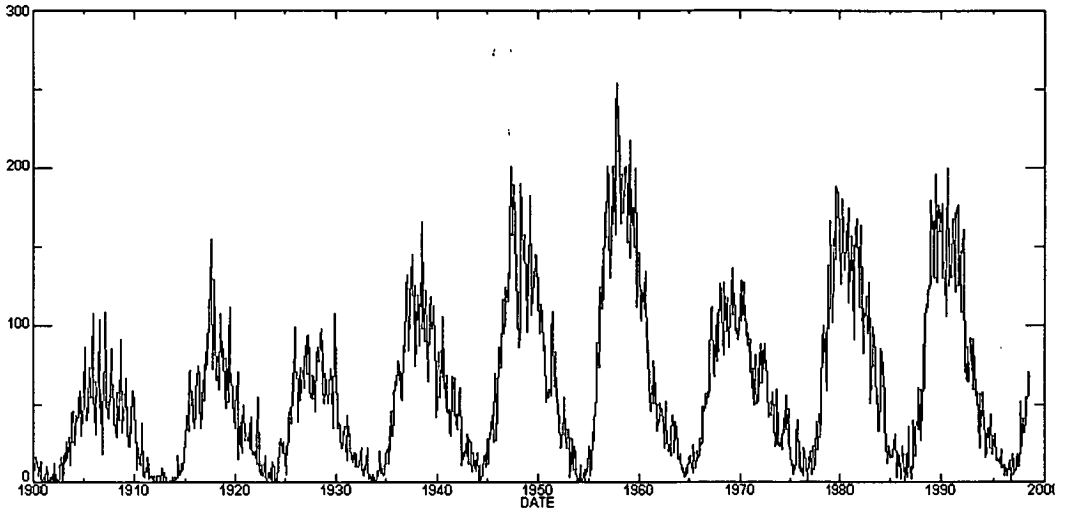

Figure 4.5 - Sunspot numbers observed from 1900 - 2000 (from http://www.sunspotcycle.com/images). From these data, the 11-year cycle of solar activity can be clearly identified.

The combination of a peak in the solar cycle (see Figure 4.5) and a geographic location near to the southern auroral zone resulted in extremely high levels of ionospheric interference in the 1989 - 1993 LGB GPS data. Figure 4.6 shows a plot (using the GAMIT *C-VIEW* utility) of raw one-way data observed at site LG32 to satellite PRN21. The panels give the time history (over approximately three hours) of the L1 and L2 carrier phases and the linear combination observables of LC (L3) and LG (L4). The fluctuations in the level of ionospheric interference can be observed in the LG panel.

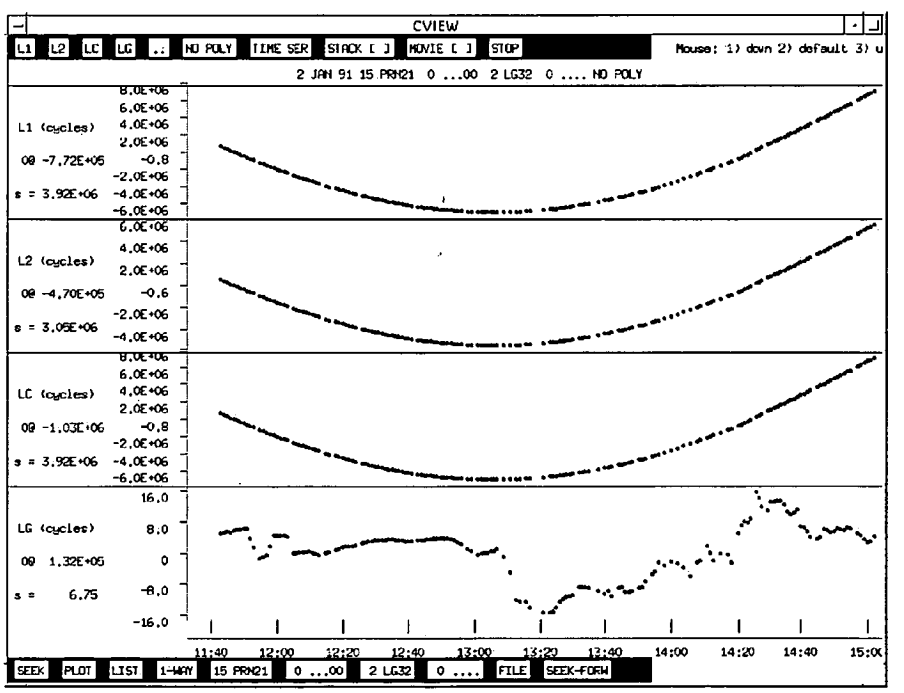

Figure 4.6 - Raw GPS data collected at LG32 (DOY002 1991). The variable ionosphere and data dropouts can be clearly seen in the LG panel.

Instrumentation:

The WM102 receivers used during the 1989 -1993 LGB campaigns employed an eight-channel tracking mechanism with six channels dedicated to the L1 frequency and only one for the L2 data (Piechocinska and Sjoberg, 1990). The L2 channels operate by employing a sequencing technique to alternately track data from multiple satellites (Magnavox, 1988). This multiplexing function of the L2 channel did not operate well in the presence of high noise levels and often resulted in frequent loss of lock on the L2 signals (Morgan and Tiesler, 1991).

The very high ionospheric activity encountered during the early LGB surveys heightened the inadequacies in the L2 tracking of the WM102 receivers and resulted in extensive loss of data on this frequency. However, the 1989 - 1993 LGB GPS data were not completely degraded by the ionospheric effects and significant epochs of useful dual frequency data were available for processing. These useable data were characterised by short, sometimes highly noisy, data segments separated by large gaps (see Figure 4.7).

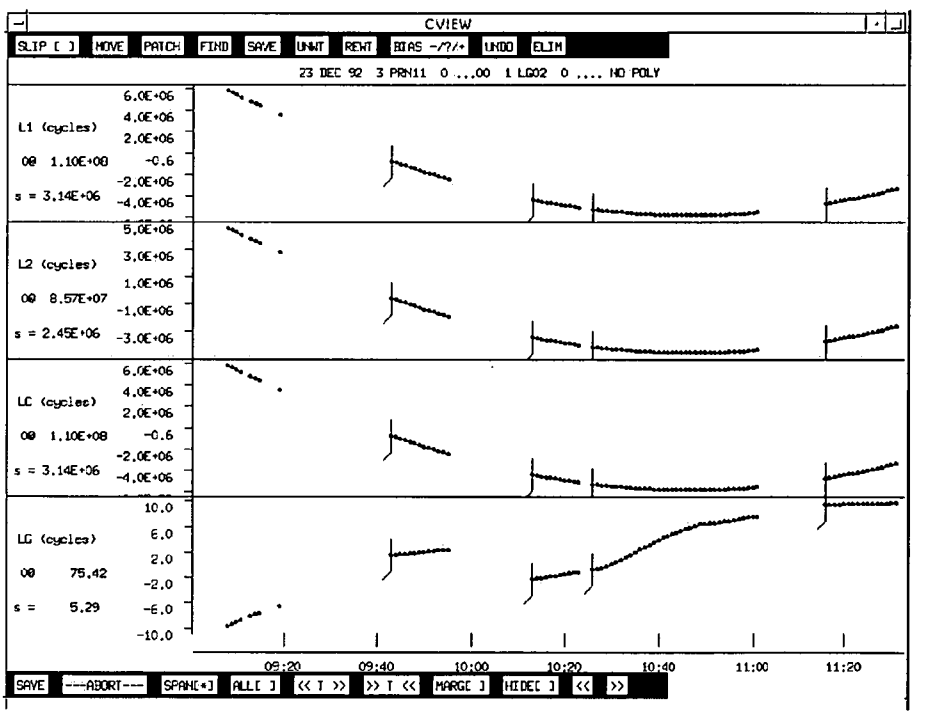

Figure 4.7 - Cleaned GPS data collected at LG02 (DOY358 1992). The short data spans and large gaps are evident in all panels. The vertical lines at the start of the data segments represent bias flags.

4.3.2 1993 - 1995

The final LGB surveys took measurements along the entire traverse route from LG00 to LG72 and return (see Figure 4.2). These 1993/94 and 1994/95 data were collected using new generation receivers (Leica SR299), which had superior performance capabilities and improved design features compared to the WM102 equipment. These receivers simultaneously track L1 and L2 on nine channels with the L2 signal tracked using a squaring technique in times of Anti-Spoofing activation. This improved receiver architecture allowed data from up to nine satellites to be collected continuously on both carrier wavelengths and therefore had minimal impact on the signal to noise ratios and maintenance of signal lock in the observations.

As with the earlier traverses, the observation technique employed in these campaigns resulted in two occupations (with different equipment) at each site on most days. For processing purposes, the data relating to an individual IMS on a given day were concatenated into a single, daily RINEX file.

In 1993, the first permanent GPS stations were installed on fixed rock sites in Antarctica (Manning, 2000). As part of this program, permanent sites were established at Davis and Mawson that provided local reference data for the 1993/94 and 1994/95 LGB surveys. At this same time, the global GPS tracking network had increased markedly in size and global coverage due mainly to the implementation of an initial 'trial' IGS network during 1992 (Beutler and Kouba, 1998). For processing purposes, the number of GPS sites was limited to 40 stations (including the LGB sites) per day and therefore a subset of the available global data was selected (see Figure 4.4c and Table 4.2). The processing network was selected on the basis of obtaining a balanced global distribution with emphasis on the inclusion of sufficient Southern Hemisphere data to maintain strong connections to the Antarctic sites.

Table 4.2 - GPS sites (Global and LGB) 1993 - 1995
(# Sth indicates the number of sites in the Southern Hemisphere)

Period	1993/94				1994/95			
LGB Sites	LG00 - LG72				LG72 - LG00 OS01 - OS18			
Global Network	Albh	Eisl	Mac1	Stjo	Albh	Eisl	Mac1	Rcm5
	Algo	Fair	Masp	Taiw	Algo	Fair	Mas1	Sant
	Areq	Fort	Mate	Trom	Areq	Fort	Mate	Stjo
	Brmu	Hart	Mcm1	Tskb	Brmu	Hart	Maw1	Taiw
	Cas1	Hob1	Onsa	Usud	Cas1	Hob2	Mcm4	Trom
	Dav1	Kokb	Pama	Wett	Dav1	Kerg	Onsa	Tskb
	Ds10	Kosg	Pert	Yar1	Ds10	Kokb	Pama	Wett
	Ds42	Kour	Rcm5	Yell	Ds42	Kosg	Pert	Yar1
	Ds60	Maw1	Sant		Ds60	Kour	Pie1	Yell
# Sth	13				14			

4.3.2.1 LGB GPS data quality

The factors affecting data quality in the initial LGB survey period had generally been overcome prior to the commencement of the 1993 - 1995 traverses resulting in the collection of high-quality data throughout these campaigns. The improvements in receiver technology and the creation of global and Antarctic permanent GPS networks have already been discussed. In regard to the GPS constellation, the Initial Operational Capability phase commenced during 1993 (declared on the 8/12/93 - Leick, (1995)) and consequently the number of satellites had increased to a minimum of 24. In the region of the LGB surveys, satellite data were still only available below 70° elevation, however 24-hour observation windows were available and six or more satellites could be tracked at any given epoch. The other significant factor in the improvement in data quality after 1993 was that the solar cycle and therefore ionospheric activity was at a minimum during this period. However, due to the proximity of the LGB to the southern auroral belt, there was still some significant ionospheric effect on the LGB GPS data that required consideration during cleaning and processing.

4.4 Data Processing (1989 - 1993)

4.4.1 Set-up

Prior to processing of the LGB data, the GAMIT input file containing station information was edited to include the logbook information (e.g., antenna height, antenna type, start and stop times/dates) for the LGB and other Antarctic sites (e.g., Figure 4.8). To account for the dual occupations of the LGB sites on most days, each occupation session was entered explicitly within the station information file thereby allowing antenna heights (potentially different between sessions) to be entered accurately. In these instances, the station name was maintained between observation sessions to ensure that all data on the relevant day were used to determine the coordinates for the IMS.

TRCK	SITE	Name	AntHt	AntN	AntE	Rcvr	AntCod	HtCod	Ver	Yr	Doy	Start	Stop
LG00	LG00	LG00	3.560	0.00	0.00	WM-102	WM-102	DHPAB	0.0	91	047	00 00 00	24 00 00
LG01	LG01	IR01	3.555	0.00	0.00	WM-102	WM-102	DHPAB	0.0	91	046	00 00 00	11 48 00
LG01	LG01	LG01	3.560	0.00	0.00	WM-102	WM-102	DHPAB	0.0	91	046	20 07 00	24 00 00
LG01	LG01	LG01	3.560	0.00	0.00	WM-102	WM-102	DHPAB	0.0	91	047	00 00 00	24 00 00
LG02	LG02	IR02	3.555	0.00	0.00	WM-102	WM-102	DHPAB	0.0	91	045	00 00 00	11 48 00
LG02	LG02	LG02	3.560	0.00	0.00	WM-102	WM-102	DHPAB	0.0	91	045	20 09 00	24 00 00
LG02	LG02	LG02	3.560	0.00	0.00	WM-102	WM-102	DHPAB	0.0	91	046	00 00 00	24 00 00

Figure 4.8 - Excerpt from a LGB experiment GAMIT station information file (1990/91).

Two other GAMIT input files (*sittbl. and l-file*) were also edited to set the site specific constraints, modelling parameters and a priori coordinates for the LGB IMS and other Antarctic sites. In the site constraint file, each IMS (and other LGB/AIS campaign sites) was allocated loose coordinate constraints (500m for lat, lon and geocentric radius), a 15° satellite elevation angle cut-off and default GAMIT clock and meteorological settings.

4.4.2 Satellite and Station Data

Prior to November 1993, IGS precise ephemeris files were not available and therefore, for the initial LGB surveys, broadcast navigation files (global) were used to acquire a priori satellite position information.

The input GPS data for GAMIT is required in a software specific (*x-file*) format. For each site on each day, one *x-file* is created (from the RINEX information) containing all of the necessary information and data for the given observation session at a selected processing interval. During the *x-file* creation process, the raw data is also scanned to remove incomplete or erroneous observations. For the processing of the LGB surveys between 1989 and 1993, careful selection of the *x-file* observation interval was necessary to ensure that the optimum data were retained for the solution of the GPS network in each season:

- In 1989/90 and pre-GIG 1990/91, the data at most of the global sites were collected at 30 second intervals (2 or 3 sites collected at 120 second epochs) while the Antarctic data were collected at intervals of 15, 30 (at the LGB IMS) and 60 seconds. It was decided that the most appropriate *x-file* interval for these data was 30 seconds thereby including all of the global data and ensuring adequate network control and orbit definition. This interval selection resulted in some of the Antarctic sites having a 'gap' at every second epoch of data but it was assumed that this frequency of data gaps could be handled effectively by the automatic cleaning process.
- In the 1990/91GIG and post-GIG periods, the global data were collected at 120 second intervals while the Antarctic data were collected at 15, 30 (at the LGB IMS) or 60 seconds. Therefore a decision was required between either a) creating 30 second data files to retain most of the Antarctic data but create gaps in the global files or b) using a 120 second interval and losing at least half of the Antarctic data but maintaining continuity at the global sites. The second option was selected to ensure adequate network control and orbit definition.
- During the 1992/93 LGB survey, all global sites were collecting data at 30 second intervals while the LGB data in this traverse were collected at 60 seconds. For this campaign, a 60 second *x-file* interval was selected to ensure the

maximum amount of data were included at the LGB sites and to minimise the number of gaps in the already extremely noisy data. During the construction of the LGB IMS and Wombat *x-files*, it was typical to find a data rejection rate of close to 50%, mainly due to dropouts on the L2 frequency.

4.4.3 Solution Design

Prior to running a GAMIT batch solution, it is necessary to specify the desired processing parameters. The processing methodology used for the 1989 - 1993 LGB data (indicated by the parameters given in Appendix A.3) is a single least-squares solution using the ionosphere-free observable (LC), solving for floating ambiguities and outputting station, satellite and earth-orientation parameters. Tropospheric estimation was carried out at two-hour intervals using standard methods (see sections 6.3.4.1 and 8.4.2.1). Standard (GAMIT v9.6) Earth orientation constraints and orbit definitions were also used. Standard (GAMIT v9.6) tide (Earth and frequency dependent), and Earth (UT1 and pole) models were applied during processing. At the time of the LGB data processing, no WM102 antenna model was available and therefore antenna phase centre modelling was not used in the processing of these data[1].

4.4.4 Data Cleaning (*AUTCLN* module)

After running several 'test' solutions using data from the 1990/91 campaign, it was found that insufficient LGB data (in some cases, no data) were being maintained after cleaning using a default *AUTCLN* command file. The command file was therefore edited using an iterative process on the test data. This involved running GAMIT solutions using edited *AUTCLN* command settings, followed by inspection of the output *AUTCLN* summary files to identify the cause of extreme data rejection within the data cleaning operation. The result of this iterative process was a series of *AUTCLN* commands that would allow sufficient LGB data to progress into the least-squares solution without degrading the estimated station coordinates. A description of the final version of the *AUTCLN* command file used for the 1989 - 1993 data processing is given in Appendix A.2.

4.4.5 Data Processing and Solution Summary.

Once the optimum settings for the cleaning and processing procedures had been resolved, the final solutions for the LGB GPS data were completed. To evaluate the quality of each solution, two sections of the output were scrutinised. These were (i)

[1] As the height of the LGB GPS antennas were not precisely measured, and the general quality of the GPS observations were so poor, it can be assumed that the use of antenna phase modelling would have a negligible effect on the LGB results.

the postfit nrms value for the constrained solution[2] and (ii) the station/satellite parameter adjustments and formal uncertainties. In terms of the postfit nrms, values of 0.35[3] or less were considered acceptable as final solutions. For the 1989 - 1993 LGB data processing, almost every solution required editing and multiple iterations before obtaining an acceptable nrms value and producing high quality estimates of the site/satellite parameters. In particular, extensive manual editing was required throughout the processing of the 1989 - 1993 traverse GPS data in order to determine acceptable coordinate solutions at the IMS and nrms values for the constrained solutions of < 0.35.

On those occasions where solutions were unacceptable due to poor station results (at either ice or rock sites), it was often the case that the a priori coordinate information was incorrect or too approximate. These problems generally arose when there were undocumented changes at a site, confusion as to the correct name of a particular site or poorly determined initial site coordinates. These problems were mostly easy to detect and amendments were made prior to re-running the GAMIT solution. For solutions with high post-fit nrms values in which one or more satellites showed significant variations from the broadcast orbit and displayed high uncertainty values, the satellite(s) in question was generally removed and the solution re-run. Once a reasonable nrms had been obtained (using the broadcast ephemeris information), solutions were re-run using the updated (solution) *g-file* of orbital conditions to provide the best determination of the network.

The most common problems encountered in the initial GAMIT solutions were LGB (and other Antarctic) site coordinates with very high formal uncertainties or, in many cases, a complete failure in estimation of the site parameters at one (or more) of the Antarctic sites. These problems were generally a result of high data rejection rates in the cleaning of the data from these sites. For these failed solutions, it became necessary to manually edit the input *c-files* (using the *C-VIEW* module) in order to reinstate the 'best' sections of data at the problem site(s). Identification of a 'reasonable' data section was based mainly on the length of the segment, the 'flatness' of the LC signal and the absence of large gaps and/or jumps in the data. During the manual editing process, efforts were made to reinstate data from multiple satellites within similar epoch ranges to allow the formation of sufficient double differences to provide the strongest possible solutions at the site(s) of interest.

It was very common for poor nrms values (> 0.35) to be obtained (for the constrained solution) even when all station, satellite and cleaning problems had been amended. These high values were generally due to cycle slips remaining in the data or, in the

[2] the nrms provides an indication of the fit of the data to the model.
[3] a value determined from previous experience with solutions using data of this vintage. Higher values indicate data modelling or cleaning problems.

case where manual editing of the *c-files* had occurred, the inclusion of 'bad' data points. In these instances, manual patching or removal of cycle slips in the *c-files* was carried out. On some occasions, even when all potential cycle slips had been removed, the nrms values were found to be above 0.35. In these instances, a utility program was used to identify poorly performing satellites and/or stations which were then removed from further solutions.

4.4.5.1 1989/90 processing methodology

The 1989/90 LGB data (and 1990/91) were processed in collaboration with Matt King, a post-graduate student who was analysing GPS data that had been collected on the AIS during the same period - see King (2001) for discussion of the AIS results.

The 1989/90 GPS data were required to be processed in a different fashion to the other LGB data due to the small number of global GPS sites operating at this time (see Figure 4.3) and therefore, a lack of sufficient baselines to connect the Antarctic sites to the global network. The initial strategy used for processing these data was to carry out a network solution including all CIGNET and Antarctic sites (see Table 4.1). However, on some days, coordinate solutions for the Antarctic sites were not able to be determined in this fashion. On these occasions, an updated orbit was computed using the CIGNET sites and these new orbits were then used to perform baseline solutions (from DOVE) for the AIS/LGB data. After day 034 1990, there were no global data available and therefore these days were solved using only loosely constrained broadcast orbits and baseline solutions with tight constraints on the coordinates at DOVE in order to extract the minimum available information from these occupations.

4.4.5.2 1990/91 processing methodology

At the time that these data were processed, information in the *station.info* file was not complete or, in some cases, not accurate. Therefore, during processing of the 1990/91 LGB data, many large errors were found in station position estimates for various sites due to renaming, relocation or a priori coordinate inaccuracies. The inaccuracies in the fieldbook (and consequently *station.info*) entries was especially troublesome at the WOMB and DOVE base stations.

The pre-GIG period of 1990/91 had a slightly larger global network than the one available in 1989/90, although the pre-GIG network actually had fewer stations in the Southern Hemisphere (see Table 4.1). This slightly larger global network assisted in obtaining good quality solutions although the Antarctic data were contaminated by high noise levels and therefore much manual editing was still required. It was very

common during the processing of these data for the initial solution on a given day to have a high postfit nrms value. These high nrms values were generally found to be caused by the loose, customised cleaning commands allowing cycle slips to be retained in the data. The initial solutions therefore generally required significant manual editing in order to repair undetected jumps and gaps. Also on many occasions it was necessary to manually reinstate data in the Antarctic *c-files* after the first processing solution had failed to determine a coordinate solution at these sites.

The GIG and post-GIG periods of 1990/91 contained sufficient global GPS data to allow acceptable solutions to be obtained with more ease than for previous processing. However, data from these periods still required significant manual editing to remove cycle slips and re-instate epochs at the Antarctic sites before satisfactory coordinate estimates and nrms values were obtained.

4.4.5.3 1992/93 processing methodology

At the time of processing the 1992/93 data, most of the global and Antarctic site naming inconsistencies had been amended, which reduced the number of solution problems caused by the network data. However, the LGB data collected in this traverse were particularly bad, with large amounts of observations being rejected during *x-file* formation due to the very short observation periods (2 to 3 hours) and a lack of observations on the L2 frequency (between 19 and 80% (mean 44%) of observations in each session were rejected due to lack of L2 data). For example, on day 006 1993, LG12 had 429 observations rejected and 494 retained while LG13 had 399 observations rejected and 416 retained on the same day. In this example, both sites were able to have positions determined after manually reinstating data removed during the automated cleaning process. Typically, this type of manual editing was required on most days for the majority of the Antarctic sites in order to obtain acceptable coordinate solutions and nrms values.

4.5 Data Processing (1993 - 1995)

The 1993-1995 LGB data were collected during a much more advanced phase of GPS technology (see section 4.3.2). As such, standard GAMIT processing techniques were used to solve for the LGB positions in these campaigns.

The general set-up and processing methodology were as for the earlier data. However, in these later survey periods, very little manual data editing was required (only occasionally to mend undetected cycle slips) and the processing and cleaning parameters were generally set to standard values.

4.5.1 Set-up

The 1993/94 and 1994/95 LGB occupation information was added to the station information file. In these campaigns, no antenna heights had been recorded in the logbooks, although a height offset value of 0.6 m was included in the RINEX header information. This value was confirmed by the field surveyor as the approximate offset from nominal L1 phase centre to the bottom of the antenna sleeve and the only available measurement for these data (pers. com. R. Kiernan, 1997).

4.5.2 Satellite and Station Data

IGS precise orbits[4] were obtained from the IGS Central Bureau ftp site[5] and used in the processing of the 1993 - 1995 LGB data.

All of the GPS data at the global and LGB sites in 1993/94 and 1994/95 were collected with a 30 second observation interval. Therefore the *x-files* created from these data were also compiled at 30 seconds. Very little data rejection occurred during the conversion due to the improved L2 tracking in the Leica receivers and lower levels of ionospheric interference at these times.

4.5.3 Data Processing and Solution Summary

The least-squares solutions for station, satellite, tropospheric (2-hourly) and Earth orientation parameters were performed using the LC observable. These solutions computed floating ambiguities and employed default Earth and tide models (see Appendix A.4). No antenna modelling was used for these solutions, as the Leica AT202 antenna models had not been defined at the time of processing.

4.5.3.1 1993/94

Generally, most solutions for this campaign solved on the first attempt. Post-fit nrms values of 0.32 or less were obtained for most of these solutions without the need for editing and iteration. On occasions where the nrms was high (> 0.35), the cause was usually identified as a poorly performing station, satellite or station/satellite combination. A less common cause of high nrms was the presence of large unflagged cycle slips in the solution that were easily detected in the data. Removing poorly performing satellites or global stations was generally acceptable for these solutions due to the high number of available satellites and the globally distributed, densely populated station network.

[4] SIO precise orbits were used for days 316 and 317 1993 as IGS products were not available prior to day 319 1993.
[5] ftp://igscb.jpl.nasa.gov

4.5.3.2 1994/95

All solutions in this campaign were completed with nrms values below 0.3. Generally, this was achieved after the first solution for each day. Again, there were some days where the initial solution's post-fit nrms value was too high due to unflagged cycle slips or poor satellite, station or station/satellite combinations. However, for this campaign, these occasions were very rare.

4.6 GLOBK Method

4.6.1 Individual Campaigns (coordinate estimation)

For each of the five campaigns, the loosely constrained, ambiguity free *h-files* (solution output files) from the daily GAMIT solutions were extracted and converted to binary format in preparation for use in GLOBK analysis.

A table of ITRF96 coordinates and velocities from an University of Canberra GLOBK solution including the CIGNET, SCAR and GIG GPS sites and the official ITRF97 coordinates and velocities for the IGS GPS sites (Boucher *et al*) were obtained for use as a priori information in the GLOBK solutions. A priori coordinate information for the LGB and other sites not included in the ITRF files were taken directly from the GAMIT output (*h-files*).

A GLOBK command file was written for each campaign[6] (after 1990/91, command files were the same for each campaign) to loosely constrain the solution and produce a campaign output file (*h-file*) for use in the combined solution. For each campaign, a GLORG rotation/translation defined by selected global sites (i.e., the IGS core sites for 1992/93 - 1994/95 and three CIGNET sites prior to 1992/93) was also completed to produce coordinate solutions in the ITRF97 reference frame. The basic command structure of these files was the same in each campaign except for the level of coordinate constraint and the selection of constrained parameters. The 1990/91 campaign in particular, required special treatment (velocity estimation and addition of extra noise to the local vertical coordinate) to account for the tidal motion and high velocity of the sites located on the Amery Ice Shelf (for further details refer to King (2001)).

[6] As with the GAMIT processing, these GLOBK analyses were also completed in collaboration with Matt King. Sections of the command files for 1989/90 and 1990/91 that pertained directly to the solution of the AIS sites (i.e., accounting for tidal motion) were developed in King (2001).

4.6.1.1 1989/90

In the 89/90 GLOBK solution, Earth wobble and UT1 parameters were given realistic constraints of 10 mas and 1 mas/yr to provide some consistency in the orientation of the network due to the poor global distribution of the GPS sites and low quality of the satellite orbits. These polar motion parameters were also allowed to vary from day to day by approximately ±1 mas using a random walk process. Local coordinates (N, E and U) at the GPS sites were constrained to 99 m and station velocities were generally not estimated. Some of the more well-defined, fixed sites were subsequently more heavily constrained to 2.5, 2.5 and 10 m (N, E and Up) to provide additional consistency to the network and prevent singularity problems within the solution process. Satellite constraints were set to default, loose values (i.e., 100 m and 10 mm/sec for the initial satellite position and velocity conditions, 100% for the direct and y-bias sigmas and 2% for the remaining parameters).

Only three sites (MOJ1, YELL and TROM) were available for reference frame definition in the GLORG solution of 1989/90 data (other possible sites being discarded due to poor agreement between solution and ITRF coordinates). The postfit rms for the reference frame definition was 26.2 mm and the χ^2 value for the GLOBK solution was 1.053, indicating that a statistically acceptable result had been obtained for this survey period.

As mentioned in section 4.4.5.1, there were several days during the 1989/90 LGB campaign where no global sites were available and therefore baseline solutions between Dovers and the LGB sites were estimated using broadcast orbits. For these days, it was necessary to perform a separate GLOBK solution with a reference frame defined by applying tight constraints to the Earth orientation and satellite parameters. The LGB sites included in these solutions were LG00, LG01, LG02 and LG03.

4.6.1.2 1990/91

In the solution of the 1990/91 network, the same a priori polar motion, coordinate and earthquake files were used as for the 1989/90 analysis. However, in the 1990/91 analysis, weak constraints were imposed on the polar motion and satellite orbit parameters with the Earth wobble and UT1 parameters also allowed to vary as a random walk process. Site constraints were generally set at 99 m for all coordinates except at a) four of the more consistent CIGNET sites (TAS1, MOJ1, WELL, KOKE) which were constrained at 5 m and b) nine GIG sites (that later became IGS 'core' sites) which were constrained at 2.5 m.

The reference frame for the final GLOBK/GLORG solution of the 1990/91 LGB campaign was defined by eight global sites (MADR, ALGO, YELL, GOLD, FAIR, YAR1, TROM and KOSG). While this group contains only one Southern

Hemisphere site, YAR1, it satisfies several of the conditions in Morgan *et al* (1996). These conditions include a) ALGO, TROM and FAIR are in a rough circle for the control of UT1 and b) movement at ALGO and YAR1 will show opposite signs for the control of polar motion. The selection of this group of control sites resulted in a rotation and translation onto the ITRF97 reference frame with a rms of 29.5 mm. The prefit χ^2 of the GLOBK solution was 1.366, indicating a statistically acceptable result.

4.6.1.3 1992/93 - 1994/95

The GLOBK/GLORG solutions for the 1992/93, 1993/94 and 1994/95 LGB traverses were carried out using standard command and a priori files. Generally, the solution commands were similar to those used in the previous campaigns except that tighter coordinate constraints were only applied to the thirteen IGS core sites (2.5, 2.5 and 5 m for N, E and Up respectively). All other site coordinates were constrained to 99 m and no velocities were estimated.

For the GLORG solutions, a reference frame was defined by the ITRF97 coordinates at the thirteen IGS core sites. The postfit rms of the GLORG definitions were < 7 mm and the χ^2 value for the GLOBK solutions were < 1.35, indicating statistically acceptable results for each of these campaigns.

4.6.2 Combined Solution (velocity estimation)

The combined *h-files* from each of the campaign GLOBK solutions formed the basis of a full multi-year (1989 - 1995) solution (see Appendix A.1 for details of the methodology of a GLOBK solution). These *h-files* contain all of the vital station coordinate and covariance information resulting from the initial, campaign-by-campaign solutions and allow it to be easily introduced into a multi-year analysis.

The a priori coordinate files used in the multi-year solution were the tables used previously in the campaign solutions along with the output coordinate estimates for all sites from the GLORG solutions. These files were ordered so that the most reliable were read last, i.e., the ITRF97 coordinates took precedent over any coordinates for the same site in a different table.

The GLOBK commands used in the multi-year solution were similar to those in the campaign solutions. The main difference in the multi-year solution was the application of loose constraints to the velocity values for all sites observed in more than one campaign (i.e., 10 m/yr for fixed sites and 50 m/yr for ice sites). A new *earthquake file* (containing station adjustments - mainly used for selected site re-naming or height adjustment) was written and used to overcome station naming disparities between solutions and to ensure that each set of site coordinates were

identified by only one name throughout the entire analysis period. The coordinates and velocities at the 13 core IGS sites (YAR1, HART, TIDB, SANT, TROM, MADR, GOLD, ALGO, FAIR, WETT, KOKB, KOSG and YELL) were more tightly constrained (2.5 m and 0.5 m/yr for position and velocity respectively) to impose a consistent but relatively loose network orientation (see Appendix A.5).

During initial runs of the multi-year solution, many site inconsistencies were discovered and amended by renaming the sites in question or by changing the site names in the a priori tables. These initial solutions also identified problems with the 1989 - 1993 solutions for some western LGB sites that were causing high inter-campaign χ^2 values. The solutions for sites LG00, LG16, LG19 and LG26 in 1990/91 were identified as the major cause of the poor fit between 1990/91 and other campaigns. Therefore, in the multi-year solution, these sites were re-named (for the 1990/91 period) and were not used in the determination of the final coordinate and velocity results at the respective LGB IMS.

In the multi-year GLOBK solution, the campaign *h-files* were reweighted according to their relative reliability. This is standard practice when combining data over a long period. Feigl *et al* (1993) show that long-term systematic errors and scatter are apparent in the position estimates over time and can be represented in the GLOBK solution by reweighting the input covariance matrices. In this study, the most realistic uncertainties for the solution coordinate estimates were obtained using the values given in Table 4.3. These scale factors were selected based on the observed quality of each solution and were determined after initial solutions of the multi-year data. The final scale values appear to be appropriate for the known relative quality of the individual solutions, however, it is not known why the 1992/93 campaign is significantly less cohesive than the earlier campaigns[7]. Many avenues have been pursued in an attempt to determine the cause of this poor fit, such as the removal of potentially 'bad' stations, checking the Earth orientation adjustments and reanalysis of the campaign solution but no obvious causes or improvements have been found.

Table 4.3 - Multi-year solution reweighting and χ^2 values

Name	Scale	Forward χ^2
LAMB_9495.GLX	2.000	0.000
LAMB_9394.GLX	2.000	0.008
LAMB_9293.GLX	6.000	3.564
LAMB_9091.GLX	4.000	2.047
LAMB_8990brdc.GLX	4.000	0.211
LAMB_8990.GLX	4.000	1.162

[7] This anomaly is not due to problems in the Antarctic data, as the fit is also poor when Antarctic data are excluded. Additionally, all sites have been cleared of inconsistencies between the 1992/93 and other seasons.

The multi-year GLOBK solution was run backwards in time so that the strength of the network in the later years was utilised in combining data from the earlier, weakly defined, small global network solutions. The χ^2 increment per degree of freedom for each campaign file in the combined solution is shown in Table 4.3. The values given in this table indicate that the constraints and reweighting used in this solution are reasonable and adequately reflect the variation in data quality from pre-1993/94 to post 1993/94.

The GLORG solution of the multi-year data was completed using the thirteen IGS core sites for network stabilisation. The final rms of the fit to the ITRF97 reference frame (at epoch 1997.0) after four iterations was 14.9 mm and 3.7 mm/yr for position and velocity respectively. The summary information from the GLORG output file and the GLOBK command file are given in Appendix A.5. The final χ^2 value for the multi-year solution using the reweighting shown in Table 4.3 was 1.147.

4.7 Kinematic Data Processing

During the 1994/95 LGB traverse, slope information was collected up- and down-slope of five IMS in the eastern sector of the traverse using a kinematic GPS technique (see section 3.4.1.4 and Figure 4.2). At the time of data processing, there was no kinematic module available in GAMIT and therefore, the LGB kinematic data were processed using SKi (v2.3) software.

SKi processing is done in baseline mode and therefore the local IMS GPS (GLOBK coordinates) were used as local reference stations for the kinematic data. The data were processed using an IGS precise ephemeris (final product) and default SKi kinematic solution parameters.

The SKi baseline processing resulted in integer ambiguities being resolved for the majority of data in the continuous kinematic profiles. At points where integer ambiguities were not determined, a maximum (1σ) uncertainty of 0.1 m was selected as the cut-off value for retaining the point positions in the profile solution. This selection strategy enabled a sufficient level of data retention and precision for estimation of local surface slope at the IMS. At LG70 and LG59, the kinematic data were interrupted and although re-initialisation was carried out, it was not successful. Therefore, the quality of these solutions after the re-initialisation epochs was very poor and only partial profiles are available at these sites (see section 5.1.4.2).

4.8 Chapter Summary

This chapter has described the successful processing of the LGB traverse GPS data (1989 - 1995) using GAMIT/GLOBK software for the determination of coordinates and velocities (in the ITRF97 reference frame) at the LGB IMS.

The 1989/90 - 1992/93 LGB GPS data were of a very poor quality due to a combination of factors, namely:

- the multiplexing L2 channel in the WM102 receivers.
- the very high ionospheric activity caused by the location of the sites (near the auroral zone) and a peak in the solar cycle.
- the low number of satellites in the constellation.
- short observation windows and low elevation angles for GPS observations.

The 1993/94 and 1994/95 LGB GPS data were of a much higher quality due to improvements in all of the above factors. However, ionospheric interference was still an important consideration due to the location of the survey being near to the auroral zone.

During the period of the 1989/90 - 1992/93 LGB campaigns, there were only a small number of permanent GPS sites operating (an exception being the period of the GIG'91 and SCAR'91 campaigns) and therefore, there was only a limited amount of data available for the formation of a processing network. Most significantly, there was only a very small number (< 9) of Southern Hemisphere sites available for baseline connections to the Antarctic sites. At the time of the 1993/94 and 1994/95 LGB traverses, there had been major expansion of the permanent GPS network and therefore the processing network used for these data was large and well distributed globally.

In GAMIT processing, it was necessary to develop customised cleaning and processing options in order to overcome the poor data quality and network configuration and achieve acceptable IMS coordinate solutions for the early LGB campaigns. The major variations to standard processing options were the acceptance of higher ionospheric noise levels and the retention of smaller data segments during data cleaning and the reduction in orbital and ionospheric constraints during data processing. However, the use of these customised options did not guarantee a successful solution and in most cases it was necessary to perform significant amounts of manual editing before acceptable coordinates were determined for the LGB IMS.

For the 1993/94 and 1994/95 LGB surveys, standard GAMIT cleaning and processing options were able to be employed due to the improvements in data and

network quality. For these campaigns, the determination of coordinates at the LGB IMS was typically successful on the first attempt and very little manual intervention was required in these solutions.

GLOBK/GLORG software was used to combine the daily solutions for each LGB campaign and subsequently, combine all of the LGB campaign solutions to produce coordinate and velocity results in a consistent reference frame (ITRF97 at epoch 1997.0).

The kinematic GPS data from the 1994/95 LGB traverse were successfully processed using commercial software (SKi 2.3). The results of this processing are surface elevation profiles at five of the LGB IMS.

These analyses represent the best and most complete study of the LGB GPS data and have used customised, high-level processing techniques in order to extract the optimum results from the entire series of LGB GPS surveys. The complete results of the LGB GAMIT/GLOBK processing are presented and discussed in the following chapter (Chapter 5).

Chapter 5

GLACIOLOGICAL RESULTS AND ANALYSIS

High quality position and velocity estimates, such as those obtained from the LGB GPS data provide vital ground truth information for many areas of glaciological study. For example, the validation of current DEMs created from satellite altimeter data requires accurate height and slope information (e.g., Fricker, Hyland *et al* (2000)), while for ice sheet balance flux models, accurate ice flow (magnitude and direction) information is vital in confirming that the models represent real values and discriminating between solutions (e.g., Testut (2000) and section 5.3 of this study). Future satellite missions such as ICESat are anticipated to provide elevation data over Antarctica with centimetre precisions (Brenner *et al*, 2000), and therefore validation of these data will require highly accurate ground truth information. To be of most benefit to these and other glaciological applications, it is essential that the parameters determined from GPS field measurements be obtained with the highest possible precision/accuracy and in a consistent, reproducible reference system.

For future GPS surveys at remote locations such as the LGB, it should be possible, given the advances in both receiver and processing technology, to employ a more efficient means of obtaining high precision ice velocity measurements. In section 5.4 of this chapter, short-term GPS occupations of sites in the northeastern section of the LGB traverse have been analysed using varying re-occupation periods to define optimum survey methodologies for both helicopter and land-based programs. This case study includes the consideration of other factors, such as baseline lengths and time constraints that are likely to be encountered when planning field operations in Antarctica.

The main focus of this chapter is to present the topographical and glaciological results obtained from the LGB data processing and compare these results to other available ground and remote sensing data for the region. The significance of these comparisons and identification of major glaciological features within the LGB GPS results are also discussed.

5.1 LGB GPS Results

5.1.1 Position

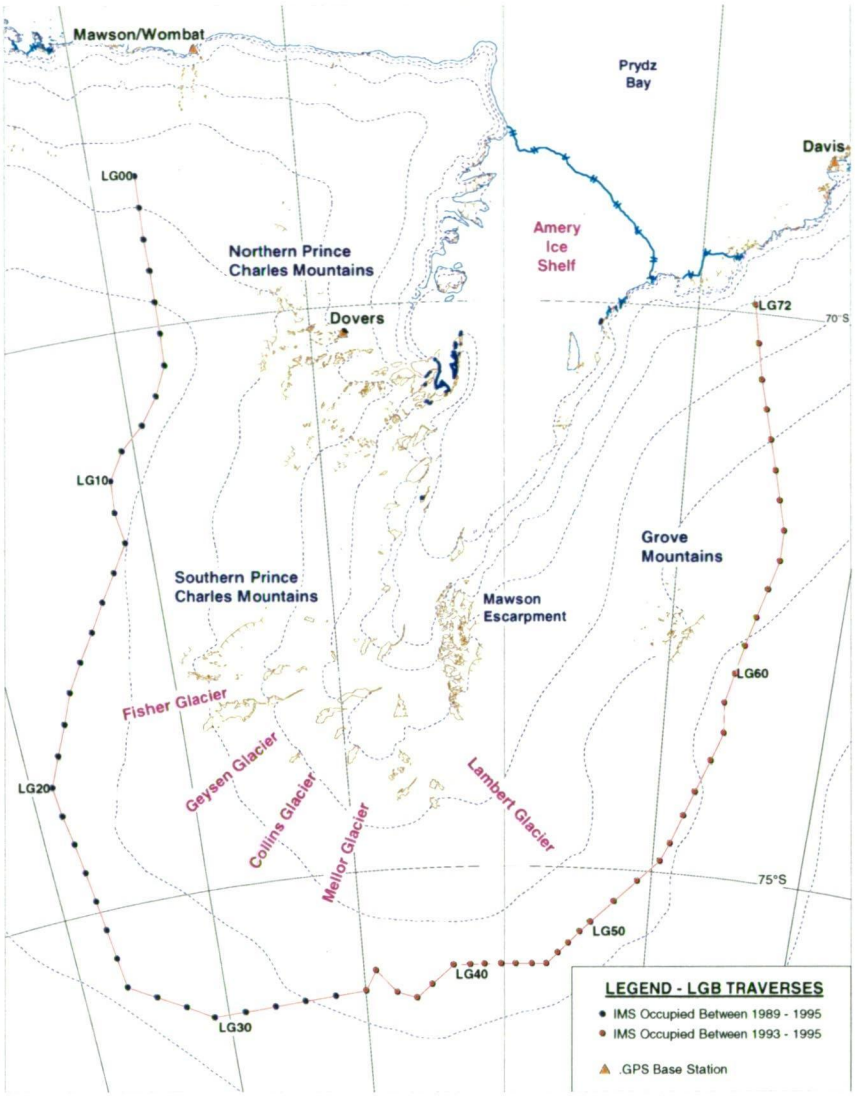

Figure 5.1 - Locations of the LGB traverse ice movement stations (IMS)

Table 5.1 contains the horizontal coordinates[1] for the LGB IMS (see Figure 5.1) with respect to the ITRF97 reference frame at the mean epoch of the 1994/95 traverse (1995.122). This epoch was selected to provide positions corresponding to the surface height calculations given in section 5.1.3. The majority of the values given in Table 5.1 were extracted from the multi-year GLOBK solution described in section 4.6.2. For the LGB sites that were only observed in the early survey periods (indicated in Appendix B - Table B.1), the values in Table 5.1 (indicated by ^) have been extracted from the 1990/91 GLOBK solution. The 1991.1 epoch coordinates are presented for these sites, as extrapolating to the 1995.122 epoch was considered unreliable due to the uncertainty of these velocities.

[1] vertical coordinates (height) are discussed later in section 5.1.3

Table 5.1 - ITRF97 positions for the LGB sites (GRS80 ellipsoid, epoch 1995.122)

Site	Latitude (° ' ")			Longitude (° ' ")		
LG00	-68	39	15.469	61	7	12.442
LG01	-68	56	16.096	61	6	32.062
LG02	-69	13	22.364	61	5	43.543
LG03^	-69	30	14.090	61	7	14.210
LG04	-69	47	9.250	61	7	28.955
LG05	-70	4	2.334	61	8	0.489
LG06	-70	21	8.118	61	7	15.572
LG07	-70	36	43.555	60	47	1.173
LG08^	-70	51	0.210	60	18	36.130
LG09^	-71	2	38.230	59	39	43.680
LG10	-71	17	10.454	59	12	28.892
LG11^	-71	34	15.280	59	9	43.250
LG12^	-71	51	3.000	59	18	31.650
LG13	-72	5	29.494	58	50	4.652
LG14^	-72	19	40.940	58	19	46.270
LG15^	-72	34	11.250	57	50	47.220
LG16	-72	48	30.195	57	20	6.612
LG17	-73	3	4.757	56	50	18.385
LG18	-73	18	53.346	56	27	59.527
LG19	-73	34	21.908	56	4	12.562
LG20	-73	49	54.680	55	40	10.759
LG21	-74	5	53.162	55	47	20.445
LG22	-74	21	53.757	55	54	37.303
LG23	-74	37	54.972	56	2	23.788
LG24	-74	53	54.762	56	10	19.540
LG25	-75	9	51.815	56	18	32.128
LG26	-75	25	49.239	56	27	0.349
LG27	-75	41	49.876	56	35	47.128
LG28	-75	50	16.865	57	31	40.628
LG29	-75	58	29.125	58	28	36.846
LG30	-76	6	29.022	59	26	37.849
LG31	-76	6	19.973	60	33	44.111
LG32	-76	5	52.753	61	40	51.347
LG33	-76	5	5.000	62	47	44.477
LG34	-76	3	57.970	63	54	49.952
LG35	-76	2	35.619	65	1	25.844
LG36	-75	52	24.794	65	25	47.564
LG37	-76	4	34.817	66	8	55.612
LG38	-76	8	10.531	66	51	10.564
LG39	-76	1	23.441	67	24	50.612
LG40	-75	51	36.674	68	12	5.828
LG41	-75	51	37.852	68	47	23.200
LG42	-75	51	27.987	69	17	50.036
LG43	-75	51	24.831	69	53	16.534
LG44	-75	51	18.347	70	23	59.758
LG45	-75	51	14.159	70	59	9.595
LG46	-75	51	8.832	71	29	56.116
LG47	-75	45	6.207	71	54	44.055
LG48	-75	39	41.624	72	16	5.477
LG49	-75	33	31.757	72	40	16.890
LG50	-75	28	14.285	73	1	45.501
LG51	-75	16	43.079	73	46	38.452
LG52	-75	5	14.459	74	30	54.047
LG53	-74	53	47.056	75	14	43.440
LG54	-74	43	57.764	75	31	57.778
LG55	-74	28	45.464	75	52	31.937
LG56	-74	15	34.332	76	10	6.980
LG57	-73	58	19.595	76	32	44.300
LG58	-73	43	9.381	76	52	22.684
LG59	-73	27	7.017	76	47	15.618
LG60	-73	11	29.009	77	1	36.377
LG61	-72	55	52.281	77	15	47.021
LG62	-72	40	16.276	77	29	36.481
LG63	-72	24	38.152	77	43	22.615
LG64	-72	9	1.694	77	56	57.197
LG65	-71	52	50.672	77	57	2.929
LG66	-71	37	13.742	77	43	49.257
LG67	-71	21	38.301	77	30	40.071
LG68	-71	5	43.298	77	17	18.818
LG69	-70	50	6.574	77	4	40.139
LG70	-70	34	32.359	76	51	58.770
LG71	-70	15	31.132	76	40	58.332
LG72	-69	55	14.962	76	29	35.001

^ ITRF97 positions at epoch 1991.1

For the results extracted from the combined GLOBK solution, the mean uncertainty in the horizontal position estimates is 3 mm. For the odd numbered IMS between LG41 and LG49, the coordinates are of a higher uncertainty (21 mm) due to the short duration of the occupations at these sites (approximately 2 hours).

The coordinate results of the GLOBK solution for each campaign contribute to the final position and velocity values in the combined solution. To assess the reliability of the results from each campaign, the variation in the horizontal precisions over the series of LGB traverses is investigated. Table 5.2 shows the mean coordinate precisions obtained from each GLOBK solution.

Table 5.2 - Coordinate 1σ precision (mm) from GLOBK solutions

Survey Period	Lat	Lon	H
Combined (1989 - 1995)	3	3	8
1994/95	3	2	8
1993/94	3	3	9
1992/93	250	250	500
1990/91 (GIG and post-GIG)	40	40	90
1990/91 (pre-GIG)	430	550	960
1989/90	2500	2200	2600

As can be seen from the data in this table, the 1993/94 and 1994/95 campaigns are far superior to the other traverses. Of the early campaigns, the 1990/91 GIG and post-GIG periods perform an order of magnitude better than the others. This result is expected due to improvements in the size and quality of the global network and the increased number of Antarctic and Southern Hemisphere stations observed during this period.

The 1992/93 LGB traverse had the highest level of GPS data rejection (due to ionospheric interference and the WM102 receivers) and required the most manual data-editing of all the LGB solutions. It is this poor quality survey data (plus the reduction in number of available Antarctic GPS sites) which has caused the inferior coordinate results obtained from this campaign, even though the global network was comparable to that of the GIG period (see Table 4.1).

The level of precision obtained for the IMS positions derived from the 1993 - 1995 campaigns and the multi-year GLOBK solution is useful for many applications in the LGB region. In particular, future remote sensing studies (e.g., ICESat (Brenner *et al*, 2000)) will require information of this quality for validation of their products. Currently, surface data of a lower precision are required for most glaciological studies of the region. For example, present studies of the mass-balance of the LGB are affected by poor definition of the major physical parameters, such as surface topography (accuracy approximately 10 m) and accumulation rates (poorly sampled, low accuracy) (Fricker, Warner *et al*, 2000). The coordinates obtained for the LGB IMS (Table 5.1) are therefore more than adequate for use in positioning ground truth data, the determination of surface velocities and the validation of glaciological analyses.

5.1.2 Velocity

Flow rates in the east (E_{rate}) and north (N_{rate}) components were determined for each IMS within the final combined GLOBK solution (refer to section 4.6.2). These rates and their 1σ uncertainties were extracted from the GLOBK solution and combined to determine a horizontal rate (Hor_{rate}) and azimuth (given in Table 5.3) using the standard equations:

$$Hor_{rate} = \sqrt{E_{rate}^2 + N_{rate}^2} \tag{5.1}$$

and

$$Azimuth = atan\left(\frac{E_{rate}}{N_{rate}}\right) \tag{5.2}$$

The (1σ) uncertainties in the east and north rates were propagated to obtain an estimate of the uncertainty in the horizontal rate. These uncertainties need to be regarded with caution as, for many sites, there are only two observations and therefore the velocity result has no redundancy. That is, for sites with only two observations, the uncertainties given in Table 5.3 are merely a reflection of the quality of the coordinates used to determine the velocity.

Table 5.3 - Surface velocities at the LGB IMS (1989/90 - 1994/95)
(Highlighted sections indicate regions of highest and lowest velocities.)

Site	Nº Obs	E_{rate} (m/yr)	σE_{rate} (mm/yr)	N_{rate} (m/yr)	σN_{rate} (mm/yr)	Hor_{rate} (m/yr)	σHor_{rate} (mm/yr)	Azimuth (°)	σAzimuth (°)
LG00	3	2.24	13	19.40	15	**19.52**	15	**6.5902**	0.0007
LG01	4	2.69	15	12.35	10	**12.64**	10	**12.2697**	0.0011
LG02	4	4.80	30	7.57	22	**8.97**	24	**32.3812**	0.0031
LG03	3	2.13	114	4.45	164	**4.93**	156	**25.5850**	0.0253
LG04	4	0.56	39	1.84	31	**1.93**	32	**16.8990**	0.0199
LG05	4	0.21	35	0.39	34	**0.44**	34	**29.1391**	0.0793
LG06	4	1.89	27	-1.83	19	**2.64**	24	**134.1144**	0.0089
LG07	5	5.62	18	-4.10	17	**6.96**	17	**126.0655**	0.0024
LG08	3	7.67	501	-4.29	566	**8.78**	517	**119.2306**	0.0627
LG09	3	7.24	106	-3.65	110	**8.11**	107	**116.7250**	0.0135
LG10	4	7.21	10	-4.06	9	**8.27**	9	**119.3729**	0.0011
LG11	2	9.00	731	-3.46	769	**9.65**	736	**111.0486**	0.0792
LG12	3	13.42	430	-5.20	444	**14.40**	432	**111.1741**	0.0307
LG13	4	12.30	10	-0.66	8	**12.32**	10	**93.0637**	0.0007
LG14	3	8.29	331	-0.19	312	**8.30**	331	**88.6793**	0.0376
LG15	3	6.54	419	-2.55	415	**7.02**	418	**111.3292**	0.0592
LG16	2	7.53	5	-2.89	4	**8.07**	5	**110.9685**	0.0005
LG17	4	8.91	6	-3.39	5	**9.53**	6	**110.8330**	0.0005
LG18	4	10.98	5	-3.59	4	**11.56**	5	**108.1141**	0.0004
LG19	3	10.38	6	-2.70	5	**10.72**	6	**104.6115**	0.0005
LG20	3	11.85	7	-1.89	5	**12.00**	7	**99.0600**	0.0004
LG21	2	9.94	7	0.95	5	**9.98**	7	**84.5323**	0.0005
LG22	3	12.69	19	0.43	10	**12.69**	18	**88.0607**	0.0008
LG23	3	11.84	6	2.06	5	**12.01**	6	**80.1472**	0.0004
LG24	3	9.45	7	4.07	5	**10.29**	6	**66.6940**	0.0005
LG25	3	13.07	7	10.97	8	**17.06**	8	**49.9803**	0.0004
LG26	2	8.63	8	7.48	6	**11.42**	7	**49.0820**	0.0006
LG27	2	7.40	6	7.28	5	**10.38**	5	**45.4831**	0.0005
LG28	3	7.87	10	5.88	8	**9.82**	9	**53.2505**	0.0009
LG29	3	8.14	6	9.64	5	**12.62**	5	**40.1882**	0.0004
LG30	3	6.58	4	6.62	4	**9.34**	4	**44.8394**	0.0004
LG31	3	5.48	8	2.97	7	**6.23**	8	**61.5970**	0.0012
LG32	2	6.75	429	8.00	490	**10.47**	465	**40.1241**	0.0435
LG33	2	12.96	285	19.05	485	**23.04**	432	**34.2304**	0.0157
LG34	2	22.91	5	39.83	5	**45.95**	5	**29.9115**	0.0001
LG35	2	14.47	4	40.22	3	**42.75**	3	**19.7910**	0.0001
LG36	2	9.05	5	48.22	5	**49.06**	5	**10.6265**	0.0001

Site	Nº Obs	E_{rate} (m/yr)	σE_{rate} (mm/yr)	N_{rate} (m/yr)	σN_{rate} (mm/yr)	Hor_{rate} (m/yr)	σHor_{rate} (mm/yr)	Azimuth (°)	σAzimuth (°)
LG37	2	-4.17	4	19.18	4	**19.63**	4	**347.7379**	0.0002
LG38	2	4.34	4	12.21	3	**12.96**	3	**19.5546**	0.0003
LG39	2	7.06	5	17.23	4	**18.62**	4	**22.2692**	0.0002
LG40	2	0.23	5	12.71	4	**12.71**	4	**1.0586**	0.0004
LG41	2	-8.22	112	16.00	118	**17.99**	117	**332.8070**	0.0063
LG42	2	-11.90	4	20.78	4	**23.94**	4	**330.2013**	0.0002
LG43	2	-15.95	39	26.46	44	**30.90**	43	**328.9175**	0.0013
LG44	2	-18.67	4	32.85	4	**37.78**	4	**330.3951**	0.0001
LG45	2	-19.90	46	29.41	46	**35.50**	46	**325.9163**	0.0013
LG46	2	-18.62	4	27.97	3	**33.60**	3	**326.3510**	0.0001
LG47	2	-20.61	41	30.17	38	**36.54**	39	**325.6647**	0.0011
LG48	2	-27.00	5	41.28	4	**49.33**	4	**326.8129**	0.0001
LG49	2	-35.86	45	47.29	32	**59.34**	37	**322.8258**	0.0007
LG50	2	-20.65	5	27.24	4	**34.18**	4	**322.8359**	0.0001
LG51	2	-21.41	5	23.44	4	**31.75**	4	**317.5937**	0.0001
LG52	2	-22.97	5	7.42	4	**24.14**	5	**287.8906**	0.0002
LG53	2	-9.86	4	0.71	3	**9.88**	4	**274.1476**	0.0003
LG54	2	-7.27	5	3.36	4	**8.01**	4	**294.8310**	0.0005
LG55	2	-17.85	5	6.91	4	**19.14**	5	**291.1773**	0.0002
LG56	2	-21.34	5	1.31	4	**21.38**	5	**273.5204**	0.0002
LG57	2	-20.37	5	2.15	5	**20.48**	5	**276.0351**	0.0002
LG58	2	-14.15	6	3.21	5	**14.51**	6	**282.7815**	0.0004
LG59	2	-10.48	4	1.44	3	**10.58**	4	**277.8386**	0.0003
LG60	2	-7.63	5	-0.38	4	**7.64**	5	**267.1696**	0.0005
LG61	2	-6.51	4	5.55	4	**8.55**	4	**310.4640**	0.0005
LG62	2	-17.11	4	12.65	3	**21.28**	4	**306.4716**	0.0002
LG63	2	-17.31	4	11.96	4	**21.04**	4	**304.6433**	0.0002
LG64	2	-21.48	6	11.12	5	**24.19**	6	**297.3806**	0.0002
LG65	2	-20.36	5	9.59	4	**22.51**	5	**295.2235**	0.0002
LG66	2	-20.91	7	8.52	6	**22.58**	7	**292.1573**	0.0003
LG67	2	-14.06	6	4.57	5	**14.79**	6	**287.9923**	0.0003
LG68	2	-10.59	5	9.24	3	**14.05**	4	**311.1258**	0.0003
LG69	2	-10.26	8	14.37	6	**17.66**	6	**324.4702**	0.0004
LG70	2	-11.98	6	22.46	5	**25.45**	5	**331.9102**	0.0002
LG71	2	-42.02	8	46.46	5	**62.65**	7	**317.8727**	0.0001
LG72	2	-42.89	10	30.98	6	**52.91**	9	**305.8391**	0.0001

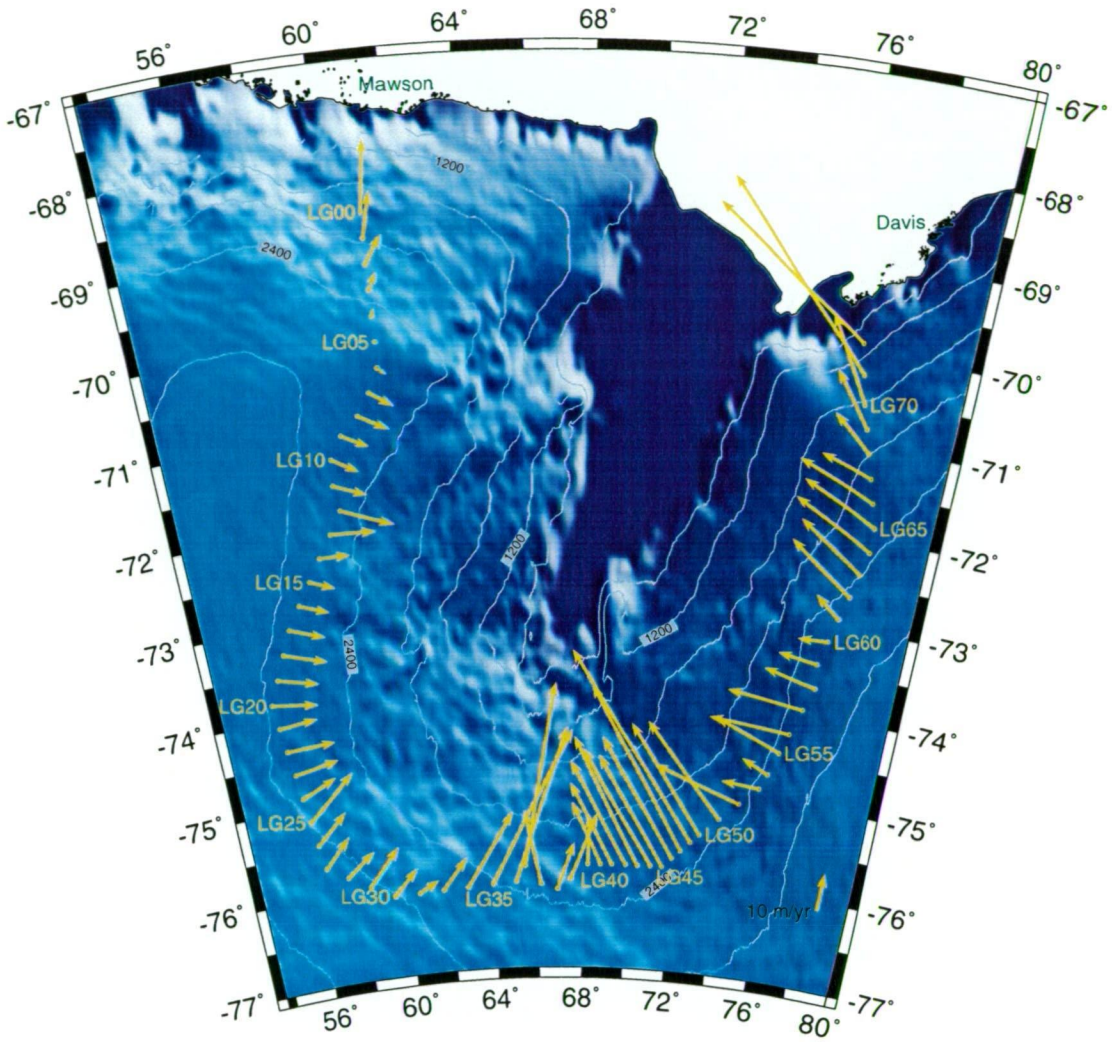

Figure 5.2 - LGB IMS velocities overlaid on DEM and contour data obtained from Fricker, Hyland *et al* (2000)

From the results given in Figure 5.2 and Table 5.3, it can be seen that the velocities at the LGB sites range from 0.5 to 63 m/yr, the magnitude being dependent upon location within the basin. The fastest speeds (> 30m/yr, highlighted in Table 5.3) are observed at the far eastern coastal sites (LG71 and LG72) and in the southern section of the traverse spanning the region of the Mellor and Lambert Glaciers (LG33 to LG37 and LG43 to LG52 respectively). The mean flow rate within the region feeding the major glaciers is 37 m/yr while average speeds for sites representing the eastern coastal ice-sheet are 58 m/yr. The slowest speeds (< 8 m/yr, highlighted in Table 5.3) are noted in the western ice-sheet between LG03 and LG07 (see Figure 5.3). This slow region is located on a flat ridge in the topography (identified in the DEM shown in Figures 5.2 and 5.3) which would be expected to create this zone of

low speeds and variation in flow direction. The majority of the remaining sites represent regions of ice-sheet flow with observed rates of approximately 8 to 25 m/yr. These sites indicate significant variation in the flow rates between the eastern and western regions of the traverse line. The flow rates at sites on the western side of the basin are generally around 10 m/yr, while in the east the mean flow is 17 m/yr, reflecting the greater slopes in the eastern basin (section 5.1.4 and Allison, 1998). Further comparisons between these GPS derived velocities and the results of other studies investigating ice flow within the basin are discussed in section 5.3.3.

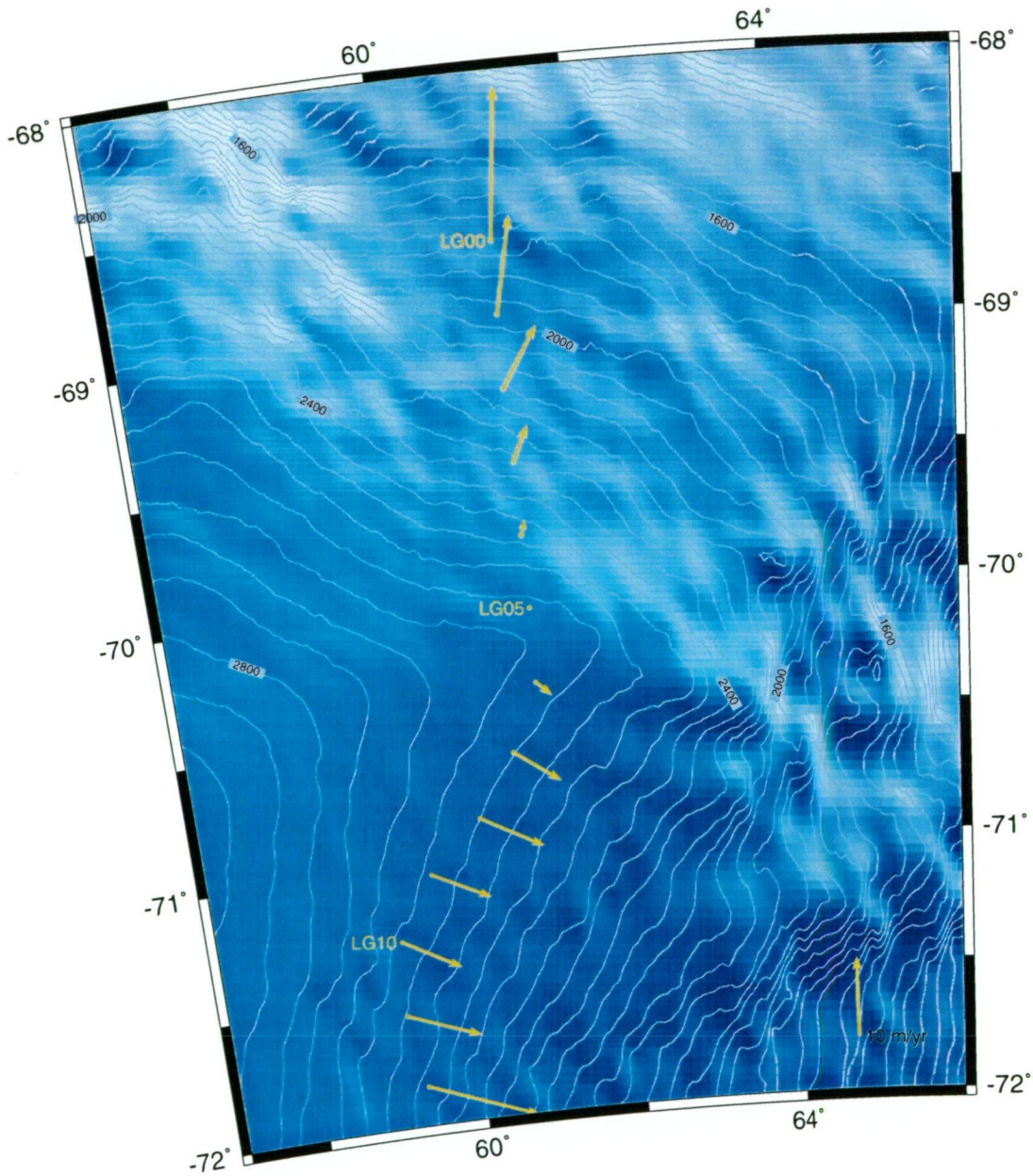

Figure 5.3 - Enlargement of Figure 5.2 in the region of LG05.

The high (and well-defined) precision of these velocity results is a significant outcome from the application of high level processing methods to the LGB GPS data. The mean uncertainty of all the calculated LGB flow rates is 0.06 m/yr (1σ). However, due to the inconsistent nature of the IMS occupations, it is more appropriate to review the uncertainties of the results using two subsets of IMS (refer to Appendix B - Table B.1). The first subset (LGBa) contains velocities observed during two or more campaigns between 1989/90 and 1994/95 (i.e., the western sites, LG00 to LG33) and the second subset (LGBb[2]) includes sites occupied only during the 1993/94 and 1994/95 surveys (i.e., the LGBb group represents the southern and eastern basin, LG34 to LG73). This division of the data gives a mean (1σ) velocity precision of 0.114 m/yr for the LGBa sites and 0.005 m/yr for the LGBb sites. Note that the uncertainties at all LGBb sites have no redundancy and are merely reflections of the coordinate errors.

The revised uncertainty value given for the LGBa sites is relatively large and not indicative of the majority of results. Upon closer inspection (see Appendix B - Table B.1), seven sites (LG03, LG05, LG06, LG08, LG09, LG11, LG12) were found to have been only observed during the poor quality 1989/90 to 1992/93 surveys. Accordingly, velocities at these sites have larger uncertainties (1σ of approximately 0.3 m/yr) compared to the other LGBa sites. Sites LG32 and LG33 were also found to have similarly large uncertainties due to the extremely small amount of data used in the 1990/91 coordinate solutions at these sites. Therefore, excluding these nine sites, the mean 1σ uncertainty for the remaining LGBa velocities becomes 0.012 m/yr, a comparable value to that of the LGBb group (0.005 m/yr).

5.1.3 Surface Height

Figure 5.4 depicts the typical GPS occupation configurations for the two traverse periods. Prior to 1993/94, the GPS antennas (Wild Magnavox WM102) were affixed to a 'sleeve' that fitted over the top of an extension pole that then could be fitted and secured to the IMS pole. GPS antenna height measurements from the antenna reference point (base of the antenna) to the snow surface, bottom of the sleeve and top of IMS pole ('join') had been recorded for each site occupation during the 1989 - 1993 surveys. These measurements allowed the vertical coordinate estimates in the GPS processing to be automatically reduced to represent the location of the join (Figure 5.4 and Table 5.4) in each survey thus maintaining a consistent reference point. For the 1993 - 1995 surveys, the only available antenna (Leica AT202) height information was an offset value (0.6 m) recorded in the RINEX header information.

[2] Note, the LGBb group does not include sites LG41, LG43, LG45, LG47 and LG49 as these were intermediate sites and only occupied for 1 to 1.5 hours in each traverse, therefore they are not of a similar class to the other sites which were occupied for several hours on each occasion.

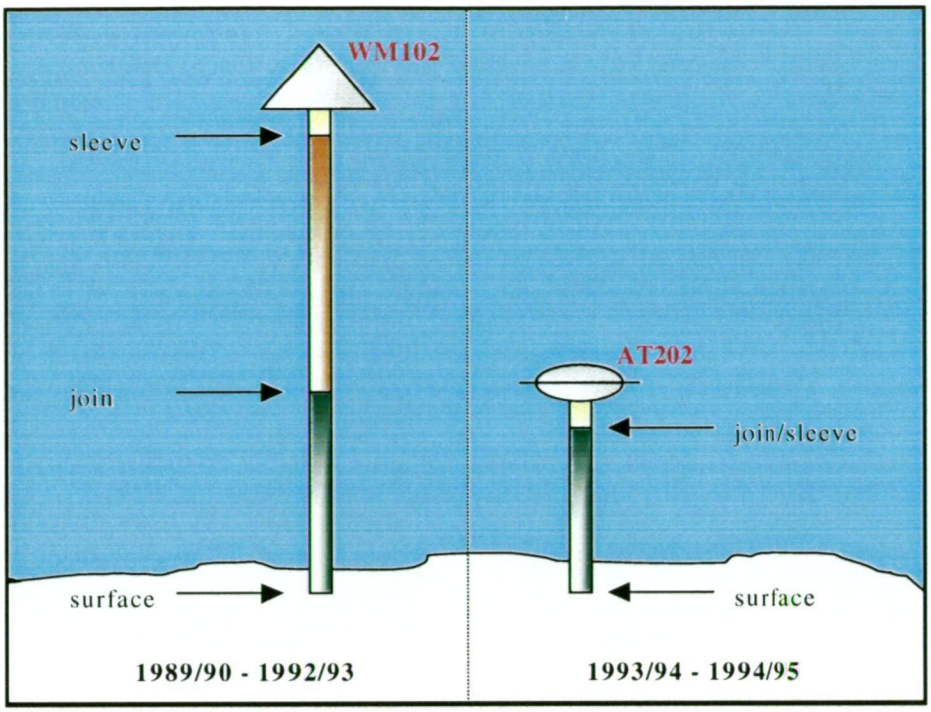

Figure 5.4 - LGB IMS GPS occupation reference points

This value represented an approximate measurement from the nominal L1 phase centre to the bottom of antenna sleeve (pers. com. R. Kiernan, 1995) and therefore allowed the vertical coordinates for these occupations to be estimated at the same point (join) as those of the previous traverses (see Figure 5.4).

Measurements of the distance between the join and snow surface were made for the new IMS poles (LG36 to LG72) in 1994/95, however no such measurements were available for the 1993/94 survey or for LG00 to LG35 in 1994/95 (pers. com. Kiernan 1997). It was therefore necessary to estimate values for the surface-join distance at sites with no direct measurement. This was achieved by using the surface-join measurement made in 1992/93 (LG00 to LG15) or 1991/92 (LG16 to LG35) and adjusting this by the height of snow accumulation between the GPS occupations as given in Higham and Craven (1997) (see Appendix B - Table B.2). In using these adjustments, it is assumed that other changes in the distance between join and surface (i.e., melt/sinking of pole and compaction) were small. In 1994/95, there were also five sites (LG00, LG01, LG10, LG19, LG20) whose GLOBK height value for the join was too high by approximately 3 m when compared to the heights for other campaigns and the observed height trend for the join point. For these sites, it was assumed that one of the 3.05 m extension poles had been used during the site occupation and had not been recorded in the field notes.

The surface height at each of the LGB IMS varies between campaigns due primarily to the down-slope movement of the IMS and accumulation of snow (also other smaller contributions from snow compaction and melt/sinking of the pole). In order

to account for these variations, it was necessary to determine a separate set of surface height values for each survey period. The WGS84[3] height values for the join at each IMS (at the mean epoch for each survey) were therefore determined from the results of the campaign GLOBK solutions. These height data were adjusted for the distance between the join and snow surface, and for the local geoid-ellipsoid[4] separation value to provide orthometric heights of the snow surface at the IMS observed in each traverse. The height values from the 1994/95[5] traverse (the most recent, precise and complete set of IMS values) are given in Table 5.4, while the values obtained for the remaining campaigns are given in Appendix B, Tables B.3 - B.6. The column headings in each of these tables refer to the following parameters (refer also to Figure 5.4):

h sleeve	ellipsoidal height (WGS84) of the base of the antenna sleeve (value determined from the GLOBK solution for the 1993 - 1995 results).
σh	1σ uncertainty in the GLOBK ellipsoidal height value.
sleeve - join	length of extension pole between the base of the antenna sleeve and the top of the IMS pole.
h join	ellipsoidal height (WGS84) of the top of the IMS pole determined from the campaign GLOBK solution (equal to h sleeve for the majority of 1993 - 1995 results).
join - surface	height of the top of the IMS pole above the snow surface.
h surface	WGS84 ellipsoidal height of the snow surface at the given epoch.
N	the geoid-ellipsoid (EGM96) separation value.
H surface	the orthometric height of the snow surface at the given epoch.

The precision of the GPS (join) height results varies from 1989/90 to 1994/95 (1σ approximately 2.6 m to 0.01 m respectively; refer to Table 5.2) according to the reliability of the survey data and processing method/network used. However, the accuracy of these join height values will be reduced due to inaccuracies (centimetre level) in the offset measurements. The quality of the height data obtained from this study is required for validation of future remote sensing missions (e.g., ICESat elevation precision estimated at < 10 cm (Brenner *et al*, 2000)) and is more than acceptable for current applications (e.g., for ERS-1 altimeter heights, accuracy over the LGB traverse is approximately 12 m (Fricker, Hyland *et al*, 2000)).

[3] The WGS84 reference ellipsoid was used to be consistent with values given in (Kiernan, 2001) and the reference frame used for the generation of the Fricker, Hyland *et al* (2000) DEM.
[4] EGM96 (Lemoine *et al*, 1997)
[5] Some of the Western IMS were not occupied in 1994/95 (indicated in Table 5.4).

Table 5.4 - Heights for the LGB IMS at epoch 1995.122
(h values refer to WGS84 ellipsoid; N values represent EGM96 separations.)

LGB Traverse 1994/95								
Site	**h sleeve (m)** (GLOBK)	**σh (m)** (GLOBK)	**sleeve-join (m)**	**h join (m)**	**join-surface (m)**	**h surface (m)**	**N (m)**	**H surface (m)**
LG00	**1860.47**	0.007	3.05	1857.42	-0.14	**1857.56**	28.352	**1829.21**
LG01	**2025.54**	0.009	3.05	2022.49	0.29	**2022.20**	28.190	**1994.01**
LG02⁺	**2205.29**	0.028		2205.29	1.62	**2203.68**	28.275	**2175.40**
LG03^	**2354.42**	0.090		2354.42	1.60	**2352.82**	28.157	**2324.66**
LG04	**2526.23**	0.008		2526.23	1.51	**2524.73**	27.634	**2497.09**
LG05⁺	**2652.34**	0.028		2652.34	0.86	**2651.48**	26.746	**2624.73**
LG06⁺	**2635.49**	0.028		2635.49	0.67	**2634.82**	25.743	**2609.08**
LG07	**2603.70**	0.009		2603.70	0.24	**2603.46**	25.153	**2578.31**
LG08^	**2600.77**	0.085		2600.77	1.50	**2599.27**	24.514	**2574.76**
LG09^	**2636.76**	0.054		2636.76	1.47	**2635.29**	23.792	**2611.50**
LG10	**2644.19**	0.005	3.05	2641.14	0.55	**2640.59**	22.692	**2617.90**
LG11^	**2608.34**	0.200		2608.34	1.38	**2606.96**	21.754	**2585.20**
LG12^	**2529.00**	0.045		2529.00	1.16	**2527.84**	21.335	**2506.50**
LG13	**2581.14**	0.012		2581.14	0.82	**2580.33**	21.324	**2559.00**
LG14^	**2636.38**	0.046		2636.38	1.42	**2634.96**	21.043	**2613.92**
LG15^	**2719.95**	0.042		2719.95	1.10	**2718.85**	20.688	**2698.16**
LG16	**2712.89**	0.005		2712.89	0.48	**2712.41**	20.488	**2691.93**
LG17	**2755.25**	0.009		2755.25	0.58	**2754.68**	20.387	**2734.29**
LG18	**2749.47**	0.007		2749.47	1.07	**2748.40**	20.105	**2728.30**
LG19	**2769.07**	0.008	3.05	2766.02	0.12	**2765.91**	19.525	**2746.38**
LG20	**2761.88**	0.010	3.05	2758.83	0.14	**2758.69**	18.821	**2739.87**
LG21	**2724.84**	0.009		2724.84	0.81	**2724.03**	18.153	**2705.87**
LG22	**2680.68**	0.017		2680.68	0.57	**2680.11**	17.636	**2662.47**
LG23	**2699.56**	0.010		2699.56	0.09	**2699.47**	17.061	**2682.41**
LG24	**2721.97**	0.010		2721.97	0.34	**2721.63**	16.231	**2705.40**
LG25	**2788.46**	0.014		2788.46	2.09	**2786.37**	15.309	**2771.06**
LG26	**2877.00**	0.011		2877.00	1.18	**2875.81**	14.617	**2861.20**
LG27	**2940.66**	0.009		2940.66	1.68	**2938.98**	14.138	**2924.85**
LG28	**2903.48**	0.014		2903.48	1.79	**2901.69**	13.287	**2888.40**
LG29	**2848.30**	0.009		2848.30	1.27	**2847.03**	12.641	**2834.39**
LG30	**2857.28**	0.006		2857.28	1.43	**2855.86**	12.071	**2843.78**
LG31	**2760.73**	0.011		2760.73	1.19	**2759.53**	12.032	**2747.50**
LG32⁺	**2599.91**	0.009		2599.91	1.34	**2598.57**	12.294	**2586.27**
LG33⁺	**2522.59**	0.008		2522.59	1.11	**2521.48**	12.507	**2508.97**
LG34	**2442.51**	0.007		2442.51	1.22	**2441.29**	12.291	**2429.00**
LG35	**2354.73**	0.006		2354.73	1.24	**2353.49**	11.608	**2341.88**
LG36	**2266.70**	0.008		2266.70	1.70	**2265.00**	12.243	**2252.76**

LGB Traverse 1994/95								
Site	**h sleeve (m)** (GLOBK)	**σh (m)** (GLOBK)	**sleeve-join (m)**	**h join (m)**	**join-surface (m)**	**h surface (m)**	**N (m)**	**H surface (m)**
LG37	**2366.39**	0.006		2366.39	1.70	**2364.69**	10.258	**2354.43**
LG38	**2362.37**	0.006		2362.37	1.70	**2360.67**	9.218	**2351.45**
LG39	**2275.04**	0.007		2275.04	1.90	**2273.14**	9.294	**2263.85**
LG40	**2179.86**	0.007		2179.86	1.80	**2178.06**	9.269	**2168.79**
LG41	**2228.77**	0.038		2228.77	1.60	**2227.17**	8.856	**2218.31**
LG42	**2236.20**	0.006		2236.20	1.20	**2235.00**	8.637	**2226.37**
LG43	**2259.85**	0.041		2259.85	1.80	**2258.05**	8.458	**2249.60**
LG44	**2302.31**	0.006		2302.31	1.70	**2300.61**	8.309	**2292.30**
LG45	**2350.01**	0.045		2350.01	1.50	**2348.51**	8.082	**2340.43**
LG46	**2363.19**	0.006		2363.19	1.40	**2361.79**	7.833	**2353.96**
LG47	**2358.16**	0.045		2358.16	2.00	**2356.16**	7.926	**2348.24**
LG48	**2358.99**	0.006		2358.99	1.60	**2357.39**	7.916	**2349.48**
LG49	**2329.12**	0.029		2329.12	1.30	**2327.82**	7.827	**2320.00**
LG50	**2370.30**	0.006		2370.30	1.80	**2368.51**	7.747	**2360.76**
LG51	**2311.83**	0.007		2311.83	1.60	**2310.23**	7.924	**2302.30**
LG52	**2341.24**	0.008		2341.24	1.60	**2339.64**	8.646	**2331.00**
LG53	**2475.05**	0.006		2475.05	1.60	**2473.46**	9.423	**2464.03**
LG54	**2492.98**	0.006		2492.98	1.50	**2491.49**	9.806	**2481.68**
LG55	**2480.02**	0.006		2480.02	2.00	**2478.02**	10.361	**2467.66**
LG56	**2488.12**	0.006		2488.12	1.80	**2486.32**	11.379	**2474.94**
LG57	**2566.17**	0.007		2566.17	1.80	**2564.37**	13.284	**2551.09**
LG58	**2606.13**	0.007		2606.13	1.30	**2604.83**	14.299	**2590.53**
LG59	**2548.97**	0.006		2548.97	1.20	**2547.77**	15.182	**2532.59**
LG60	**2594.21**	0.007		2594.21	2.00	**2592.21**	15.111	**2577.10**
LG61	**2524.61**	0.006		2524.61	1.60	**2523.01**	15.563	**2507.44**
LG62	**2482.50**	0.006		2482.50	1.60	**2480.90**	16.151	**2464.75**
LG63	**2438.29**	0.007		2438.29	1.40	**2436.89**	16.213	**2420.68**
LG64	**2366.14**	0.007		2366.14	1.20	**2364.94**	15.971	**2348.97**
LG65	**2340.85**	0.005		2340.85	1.40	**2339.45**	15.948	**2323.50**
LG66	**2229.83**	0.007		2229.83	1.40	**2228.43**	16.130	**2212.30**
LG67	**2151.51**	0.007		2151.51	1.20	**2150.31**	16.326	**2133.98**
LG68	**2012.25**	0.006		2012.25	1.00	**2011.25**	16.400	**1994.85**
LG69	**1870.78**	0.006		1870.78	1.30	**1869.48**	16.402	**1853.08**
LG70	**1668.39**	0.004		1668.39	1.30	**1667.09**	16.441	**1650.65**
LG71	**1405.14**	0.009		1405.14	1.20	**1403.94**	16.577	**1387.37**
LG72	**1055.62**	0.010		1055.62	1.00	**1054.62**	16.779	**1037.84**

^ heights from 1990/91 solution (epoch 1994.281)
+ heights from 1993/94 solution (epoch 1994.133)

In regard to the accuracy of the surface height results, the errors from the other contributing measurements will have a far more significant impact on this value than the uncertainties in the GPS measurements. Inaccuracies in the measurement of pole lengths and variation in the snow level at the base of the IMS pole may be expected to cause errors in the ellipsoidal surface height value in the order of several centimetres. The use of calculated accumulation values to determine the heights in 1993/94 and 1994/95 will introduce centimetre/decimetre level errors in the surface height results. For the orthometric heights, inadequacies in the geoid definition (Lemoine *et al*, 1997) suggest that these values will have only been determined with an absolute accuracy of a few decimetres/metres. However, orthometric height differences between sites are likely to have centimetre level precisions as they are primarily affected by the GPS processing and antenna offset measurement errors.

Figure 5.5 depicts the surface height variation around the traverse. From this plot, significant topographical features of the LGB at approximately 2500 m elevation can be identified and related to information in the Fricker, Hyland *et al* (2000) DEM (see Figure 5.2).

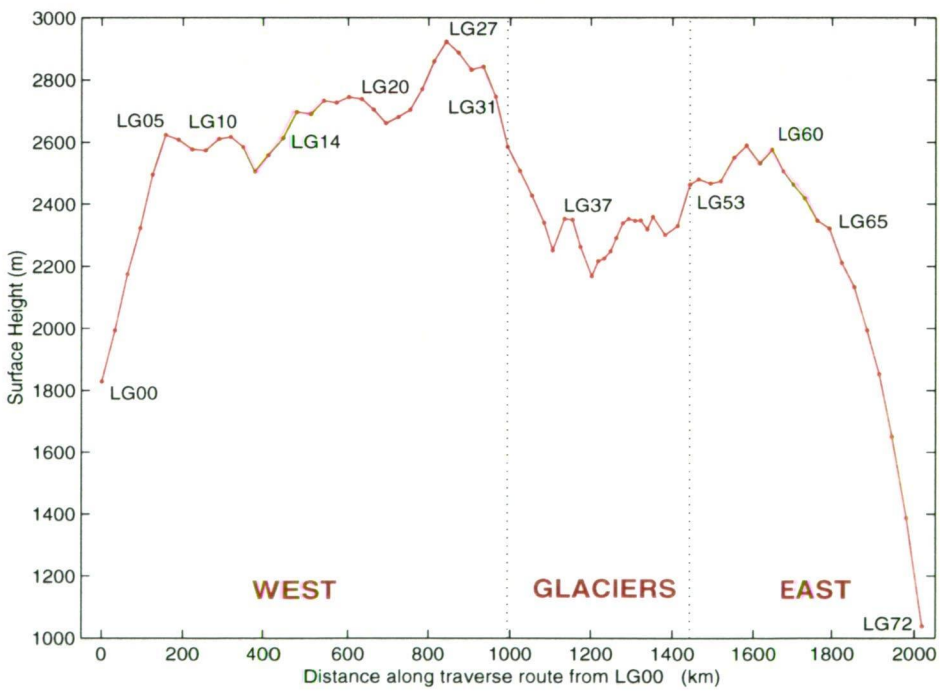

Figure 5.5 - Surface height (H) profile obtained from GPS measurements at the LGB IMS.

The most obvious features in Figure 5.5 are the surface 'valleys' which relate to regions of major ice flow (see Figure 5.2). For example:

- *LG10 - LG14* represent flow between the Northern and Southern Prince Charles Mountains (NPCMs and SPCMs),
- *LG20 - LG27* relate to flow into the Collins and Geysen Glaciers,

- *LG31 - LG37* is the region where ice is directed into the Mellor Glacier and
- *LG38 - LG53* represent ice flowing into Lambert Glacier.

The surface depression between LG31 and LG46 also coincides with the rift valley representing the southern extension of the Lambert Graben identified in the bedrock topography of Higham *et al* (1995).

Ridges in the surface topography are also significant with the two most obvious being those at LG05 and LG58/LG60. The ridge at LG05 has previously been observed in the velocity results and is a dominant topographic surface feature of the western sector of the traverse. This ridge, represents the bedrock extension of the NPCMs (Higham *et al*, 1995) and the transition of flow from the basin to the coastal ice-sheet. The ridge observed in the surface profile at LG58/LG60 is related to the presence of the near-by Grove mountains indicating a local rise in the bedrock topography (also observed in Higham *et al* (1995)). The steep grades between LG00 - LG05 and LG65 - LG72 represent the traverse path crossing the surface contours as the course turned toward the coast and the terminals of the survey route.

5.1.4 Surface Slope

Surface slope was measured at several locations during the 1992/93 and 1994/95 surveys. For the western sector of the traverse (near LG00 to LG35) an offset traverse line was observed with static GPS, while on the eastern side of the basin kinematic profiles approximately 5 km either side of selected IMS were measured (see Figure 5.6 and sections 3.4.1.3 and 3.4.1.4)

5.1.4.1 Western LGB

The static GPS data collected in the 1992/93 and 1994/95 offset traverses were processed in the same manner as the main traverse data from these campaigns. The positions determined from the data at these offset sites are given in Table 5.5 and 5.6. Orthometric heights (H) were determined using EGM96 geoid-ellipsoid separation values at each site and represent the height of the snow surface.

As with the main traverse data, the 1992/93 offset GPS observations were badly contaminated by L2 signal dropouts caused by the WM102 receiver hardware and the poor ionospheric conditions at the time. Coupled with short observation times (< 3 hours), these poor quality data resulted in several of the offset site positions not being resolved (due to complete data rejection during cleaning) and relatively high coordinate uncertainties for sites at which a solution was determined. The 1σ uncertainties for the 1992/93 offset sites range from approximately 0.5 - 1 m in horizontal position and 0.5 - 3 m in height with mean (1σ) precisions of 0.6 m in the horizontal and 1.3 m in the vertical coordinates.

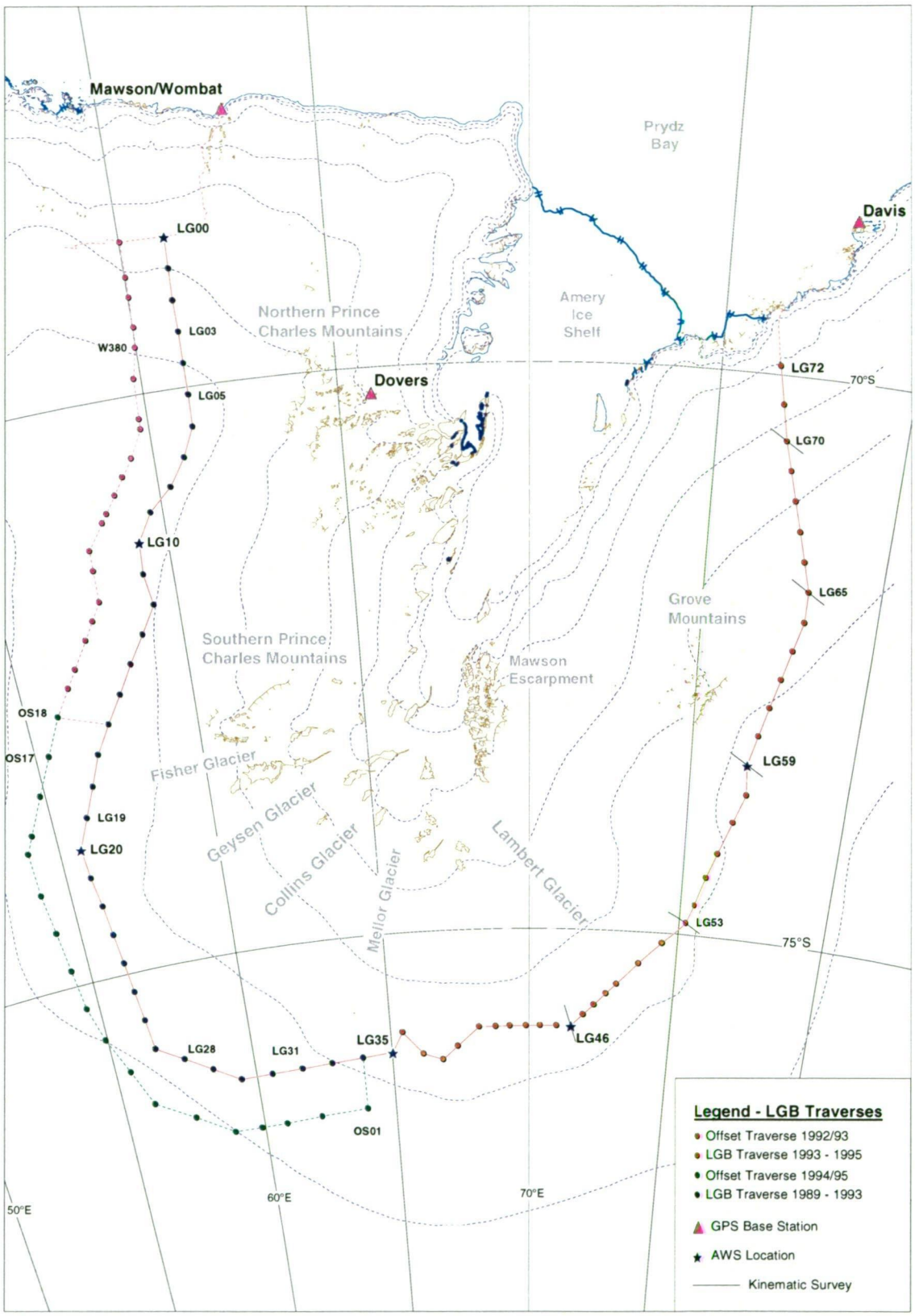

Figure 5.6 - Map of the LGB traverse routes, indicating the locations of the offset traverse points and kinematic GPS profiles.

Table 5.5 - 1992/93 offset traverse WGS84 positions (epoch 1993.097)

Site	Latitude (° ' ")	Longitude (° ' ")	h (m)	N (m)	H (m)
W030	-72 25 27.66	56 24 33.81	2888.18	20.94	2867.23
W120	-71 44 19.03	57 47 30.28	2769.32	21.90	2747.42
W125	-71 41 6.33	57 47 59.94	2760.45	21.97	2738.48
W170	-71 16 49.32	57 48 46.53	2837.78	22.97	2814.82
W210	-70 59 16.59	58 27 25.87	2792.69	23.94	2768.76
W230	-70 50 27.54	58 46 15.73	2757.66	24.54	2733.13
W270	-70 32 46.21	59 23 14.15	2731.82	25.71	2706.11
W310	-70 12 55.69	59 46 28.54	2728.62	26.55	2702.08
W350	-69 51 27.44	59 48 35.62	2616.47	27.13	2589.34
W380	-69 35 10.88	59 58 32.23	2494.76	27.62	2467.14

The 1994/95 GPS data were collected using Leica SR299 receivers, had longer occupation times (4 to 8 hours) and were observed in a period of reduced ionospheric noise levels. These data were therefore more easily processed and generally produced higher precision coordinate estimates than the 1992/93 campaign. The mean precision (1σ) for the 1994/95 offset traverse coordinates are 0.01 m and 0.06 m for the horizontal and vertical coordinates respectively (maximum uncertainties were approximately 0.1 m in horizontal position and 0.4 m in height at three sites).

Table 5.6 - 1994/95 offset traverse WGS84 positions (epoch 1995.122)

Site	Latitude (° ' ")	Longitude (° ' ")	h (m)	N (m)	H (m)
OS01	-76 30 54.83	63 54 35.44	2604.56	12.03	2592.53
OS02	-76 32 13.07	62 10 56.92	2673.28	12.90	2660.38
OS03	-76 33 19.62	60 50 17.34	2804.57	11.91	2792.66
OS04	-76 33 30.68	59 52 23.38	2940.83	11.34	2929.49
OS05	-76 33 14.37	58 53 22.43	2998.55	11.33	2987.22
OS06	-76 20 56.99	57 24 33.99	3039.40	12.32	3027.08
OS07	-76 10 16.06	56 8 51.67	3070.04	13.42	3056.62
OS08	-75 50 44.36	55 31 49.12	3037.49	14.70	3022.79
OS09	-75 31 11.12	54 55 19.69	3012.30	15.78	2996.52
OS10	-75 12 41.64	54 34 6.55	3024.17	16.35	3007.81
OS11	-74 51 22.93	54 23 56.17	2944.13	17.18	2926.96
OS12	-74 30 3.72	54 14 13.44	2896.61	18.21	2878.40
OS13	-74 8 41.78	54 4 33.09	2929.67	18.81	2910.86
OS14	-73 45 37.61	54 1 47.11	2972.42	19.22	2953.20
OS15	-73 36 50.75	54 17 29.42	2923.77	19.43	2904.34
OS16	-73 17 35.14	54 50 53.93	2895.80	20.05	2875.76
OS17	-72 58 15.39	55 23 39.13	2881.59	20.36	2861.24
OS18	-72 39 2.95	55 55 44.58	2878.77	20.58	2858.19

The reason for making the offset traverse GPS measurements was to determine the surface slope between the offset and the main traverse lines. The first stage in determining these slope values was to perform a Delaunay triangulation to create a Triangulated Irregular Network (TIN) surface representation of contiguous, non-overlapping triangles (planes) between the IMS and offset sites. Planar geometry was then used to determine the maximum slope (direction and magnitude) for each triangle in the TIN. The resultant slope vectors for the surface between the LGB and offset traverses are given in Appendix B - Table B.7 and are depicted graphically in Figure 5.7.

The slope vectors from the TIN representation have been plotted against contours created from the LAS-DEM data (Fricker, Hyland *et al*, 2000) to compare the results of the two techniques (see Figure 5.7). Figure 5.7a displays the results of the slope calculations using the 1992/93 data, with one data point removed due to an error in the slope vector at this location. Figure 5.7b shows the slope results from the 1994/95 GPS occupations. Again, two slope vectors in this region were rejected due to gross errors in the slope calculation. Figure 5.7 clearly shows that the contour information from the DEM data corresponds very closely to the slope vectors determined from the GPS observations.

In general, this analysis of the LGB traverse and offset GPS data in the western basin has found that the surface slope between LG35, LG03, OS01 and W380 varies from 2 - 8 m/km with a mean value of 4 m/km. Several notable patterns can also be detected in the slope vectors. For example, the region between LG19 and LG28 appears to show strongly converging slopes, a pattern which can also be seen in the flow directions of the GPS velocities (Figure 5.2). This sector of the traverse is known to represent the upstream flow region into the Geysen and Collins Glaciers (Fricker, Warner *et al* (2000) and Testut (2000)) and therefore converging slopes are expected in this area. The other notable features observed in the western LGB slope vectors are the presence of divergent slopes between LG05 and LG08 and near LG31. The LG05 - LG08 ridge has been previously noted in the GPS velocity and elevation results (see sections 5.1.2 and 5.1.3). The divergence near LG31 appears to correspond to a ridge line defining the boundary of ice-flow into the Mellor Glacier and the Fisher, Geysen and Collins Glaciers (refer to Figure 5.6 for glacier locations).

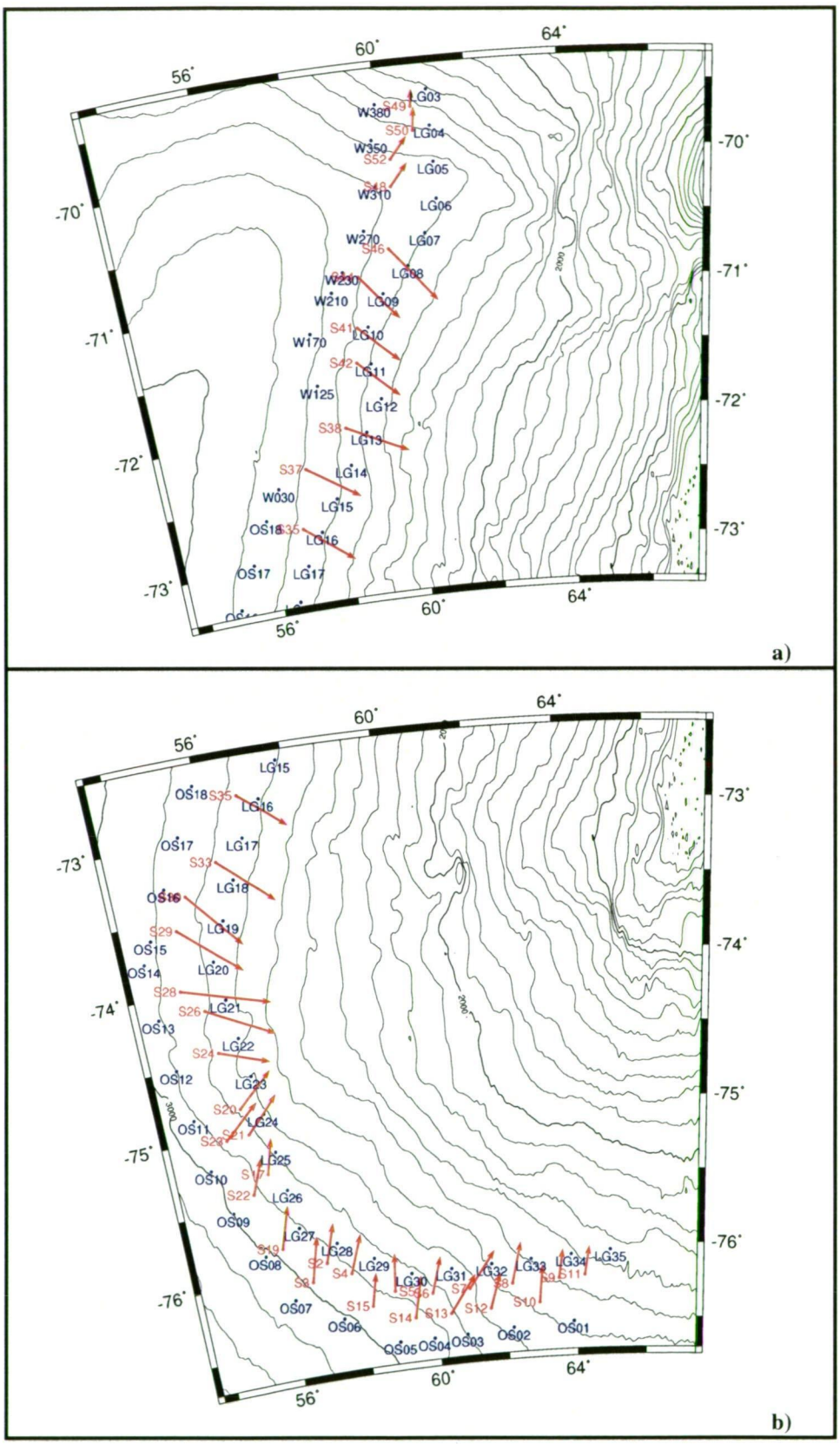

Figure 5.7 - Surface slope direction for the western LGB.
a) sites occupied in 1992/93 and b) sites occupied in 1994/95

5.1.4.2 Eastern LGB

In 1994/95, kinematic GPS profiles were measured approximately 5 km up- and down-slope from the IMS at LG46, LG53, LG59, LG65 and LG70 (see Figure 5.6). These data have been processed using proprietary SKi (v2.3) software with satisfactory results (see section 4.7).

The kinematic profiles determined at each of the IMS are displayed in Figure 5.8. These five profiles have each been analysed to determine mean slope values by performing a least squares fit to the data between specified points along the profile (see Table 5.7 and Figure 5.8). For the profiles at LG46 and LG59, only one slope calculation was necessary due to the relatively uniform inclination of the surface.

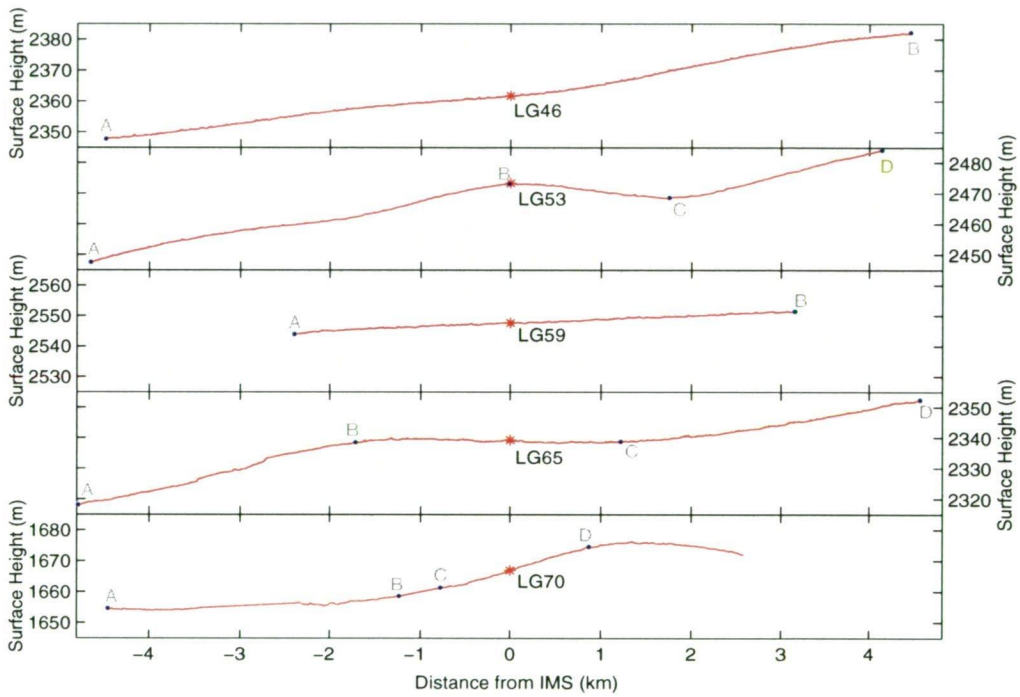

Figure 5.8 - Eastern LGB surface profiles from kinematic GPS observations

Table 5.7 - 1994/95 LGB kinematic profiles
(* indicates mean slope from inward and outward tracks)

Site	Profile Length (km)	Point 1	Point 2	Slope (m/km)
LG46	9	**A)** -75.814°, 71.446°, 2347.7m	**B)** -75.890°, 71.560°, 2382.2m	4*
LG53	8.8	**A)** -74.925°, 75.127°, 2445.7m	**B)** -74.896°, 75.244°, 2471.1m	7*
		C) -74.886°, 75.289°, 2466.6m	**D)** -74.871°, 75.349°, 2482.2m	10*
LG59	5.5	**A)** -73.466°, 76.730°, 2544.1m	**B)** -73.434°, 76.863°, 2551.6m	2
LG65	9.6	**A)** -71.897°, 77.822°, 2318.2m	**B)** -71.886°, 77.904°, 2340.7m	20*
		C) -71.877°, 77.984°, 2338.9m	**D)** -71.867°, 78.070°, 2351.9m	12
LG70	7	**A)** -70.587°, 76.750°, 1654.7m	**B)** -70.579°, 76.834°, 1658.7m	4
		C) -70.578°, 76.846°, 1661.4m	**D)** -70.573°, 76.889°, 1674.6m	30

At the other sites it was necessary to estimate two slope values due to variations between different regions of the surface profile. In general, outward and inward bound kinematic profiles were collected along the same vehicle track. Therefore, for four of the profiles (indicated in Table 5.7), two estimates of the slope value were computed. For all cases where two corresponding profiles exist, the calculated slopes agreed to within 0.5 m/km.

These kinematic profiles do not provide extensive information regarding the general slope of the eastern LGB due to their localised (< 10 km length) nature. However, there are some major features that can be clearly observed within the kinematic profiles. These features include regions of relatively high slope at LG70 and below LG65 (in the coastal ice-sheet). Another observation from these 5-10 km profiles is the presence of significant surface undulations (of several kilometres) at these locations.

Surface slope values at LG53 and LG46 have been calculated from the LAS-DEM data (pers. com. H. Phillips, 1997) as 6.3 and 4.5 m/km respectively. These values are very close to the GPS kinematic measurements (Table 5.7), indicating that the LAS-DEM in these areas gives a good representation of the true surface slope.

5.2 Comparison to Previous Analyses

Upon the completion of each of the LGB traverses, the observed GPS data were processed using proprietary Wild Leica software (SKi) (Kiernan, 2001). The noise in the data (especially the L2 drop-outs), the long baseline lengths and the limited capabilities of the processing package meant that SKi solutions were not easily performed and the processing of these data required significant manual input and editing in order to achieve acceptable results (Kiernan, 2001). Once satisfactory baseline solutions had been obtained, the solutions from each traverse were adjusted campaign-by-campaign using commercial software (GEOLAB) to determine site coordinates via a least-squares solution. The coordinate results and precisions from these adjustments are presented in Kiernan (2001). During this processing, Kiernan (2001) found that the 1992/93 results were of a very poor quality and therefore he generally excluded them when computing the final velocity estimations. IMS positions for the remaining traverses were determined with varying levels of precision, both horizontal and vertical coordinates having uncertainties ranging from 0.1 m to greater than 10 m. For the major 1993/94 and 1994/95 surveys, the IMS positions were determined with precisions generally in the range of 0.1 - 0.3 m but on many occasions, this solution quality was not achieved (Kiernan, 2001).

The major results given in Kiernan (2001) are the surface velocities at the LGB IMS. To obtain these velocity values, Kiernan (2001) used simplified (flat Earth) formulae to compute the easterly and northerly displacement between all available pairs of coordinate solutions for a given IMS and then applied standard velocity formulae (equations (5.1) and (5.2)). Kiernan (2001) was not able to compute precisions for the calculated velocities; instead, a comparative error index was determined from the spatial displacement and error ellipse dimensions of the relevant site coordinate solutions. These error indices were then scaled (by an arbitrary value of 39.1, of unknown origin) to provide approximations of the percentage errors in the velocity results (Kiernan, 2001). At many sites, only two observations were made and therefore the velocity determined from these values was accepted as the final result (Kiernan, 2001). Other sites were occupied multiple times and therefore had multiple velocity calculations over various time intervals. In these instances, Kiernan (2001) selected the velocity calculation with the lowest error index as the final result for the given site.

For sites LG00 to LG15, the best error index of the available solutions was generally above the desired value of 10^6. The index values at these sites ranged from 4.2 to 72.7 and had a mean value of 24.3. Between LG16 and LG35, the best error indices were generally found to be those relating to velocities calculated between 1990/91 and 1993/94 or 1994/95. The error indices for these velocities were all less than 10 with a mean value of 6.4. After LG35, the IMS were only occupied in the final traverses and therefore had only one velocity calculation. The error indices at these sites ranged from 3.4 to 17.6, with a mean value of 6.7. The entire set of selected velocity results from Kiernan (2001) therefore had error indices ranging from 3.4 to 72.7 with a mean value of 10.5.

Given that both this current study and that of Kiernan (2001) used the same raw LGB GPS datasets, it is important to review the differences between the results obtained from these two different processing strategies. The differences between the two solutions will indicate the extent of the benefits obtained from using extensive, high level processing compared to proprietary 'black box' techniques. Some idea of the benefits of the high level processing have already been described in Manson (1995) where improvements in velocity estimates (over periods of approximately 50 days) of up to 2 m/yr were found between GAMIT and SKi solutions for LG65 to LG72. The comparisons between the results of the current study (RH) and those of Kiernan (2001) (RK) for speed, azimuth and join height at the LGB IMS are given in Table 5.8.

[6] An error index of 10 being approximately equivalent to an error in velocity of 10% according to Kiernan (2001).

Table 5.8 - Differences (Diff) between this study (RH) and those of Kiernan (2001) (RK) (Height results were extracted from the 1994/95 traverse solutions.)

Site	Speed (m/yr)			Azimuth (°)			h Join (m)		
	RH	RK	Diff	RH	RK	Diff	RH	RK	Diff
LG00	19.52	19.3	0.22	6.59	7	-0.41	1860.47	1860.80	-0.33
LG01	12.64	12.4	0.24	12.27	13	-0.73	2025.54	2025.94	-0.40
LG02^	8.97	9.1	-0.13	32.38	48	-15.62	2209.47	2211.48	-2.01
LG03^	4.93	9.5	-4.57	25.59	43	-17.41	2357.47	2359.16	-1.69
LG04	1.93	1.9	0.03	16.90	24	-7.10	2526.23	2526.67	-0.44
LG05^	0.44	0.6	-0.16	29.14	314	75.14	2656.44	2657.94	-1.50
LG06^	2.64	3.5	-0.86	134.11	209	-74.89	2639.99	2641.40	-1.41
LG07	6.96	7.1	-0.14	126.07	126	0.07	2603.70	2604.12	-0.42
LG08^	8.78	8.6	0.18	119.23	123	-3.77	2603.82	2602.34	1.48
LG09^	8.11	9.2	-1.09	116.72	115	1.72	2639.81	2637.45	2.36
LG10	8.27	8.4	-0.13	119.37	119	0.37	2644.19	2644.83	-0.64
LG11^	9.65	7.8	1.85	111.05	106	5.05	2611.39	2608.44	2.95
LG12^	14.40	18.1	-3.70	111.17	108	3.17	2532.05	2529.54	2.51
LG13	12.32	12.3	0.02	93.06	93	0.06	2581.14	2581.57	-0.43
LG14^	8.30	9.8	-1.50	88.68	96	-7.32	2639.43	2637.40	2.03
LG15^	7.02	9.2	-2.18	111.33	110	1.33	2723.00	2720.89	2.11
LG16	8.07	8.1	-0.03	110.97	112	-1.03	2712.89	2713.20	-0.31
LG17	9.53	9.5	0.03	110.83	111	-0.17	2755.25	2756.04	-0.79
LG18	11.56	11.5	0.06	108.11	108	0.11	2749.47	2749.70	-0.23
LG19	10.72	10.8	-0.08	104.61	105	-0.39	2769.07	2769.16	-0.09
LG20	12.00	11.9	0.10	99.06	100	-0.94	2761.88	2761.94	-0.06
LG21	9.98	10	-0.02	84.53	85	-0.47	2724.84	2725.09	-0.25
LG22	12.69	12.6	0.09	88.06	89	-0.94	2680.68	2681.25	-0.57
LG23	12.01	12	0.01	80.15	80	0.15	2699.56	2699.72	-0.16
LG24	10.29	10.3	-0.01	66.69	68	-1.31	2721.97	2722.38	-0.41
LG25	17.06	16.9	0.16	49.98	50	-0.02	2788.46	2789.10	-0.64
LG26	11.42	11.3	0.12	49.08	50	-0.92	2877.00	2878.06	-1.06
LG27	10.38	10.4	-0.02	45.48	47	-1.52	2940.67	2940.88	-0.21
LG28	9.82	9.8	0.02	53.25	54	-0.75	2903.48	2902.94	0.54
LG29	12.62	12.5	0.12	40.19	41	-0.81	2848.30	2848.08	0.22
LG30	9.34	9.3	0.04	44.84	46	-1.16	2857.28	2856.92	0.36
LG31	6.23	6.8	-0.57	61.60	61	0.60	2760.73	2760.12	0.61
LG32+	10.47	9.1	1.37	40.12	53	-12.88	2599.91	2600.73	-0.82
LG33+	23.04	22	1.04	34.23	38	-3.77	2522.59	2523.50	-0.91
LG34	45.95	45.5	0.45	29.91	30	-0.09	2442.51	2442.77	-0.26
LG35	42.75	42.1	0.65	19.79	20	-0.21	2354.73	2354.96	-0.23
LG36	49.06	47.6	1.46	10.63	11	-0.37	2266.70	2266.88	-0.18

Site	Speed (m/yr)			Azimuth (°)			h Join (m)		
	RH	RK	Diff	RH	RK	Diff	RH	RK	Diff
LG37	19.63	18	1.63	347.74	346	1.74	2366.39	2366.32	0.07
LG38	12.96	11.3	1.66	19.55	22	-2.45	2362.37	2362.34	0.03
LG39	18.62	17.1	1.52	22.27	24	-1.73	2275.04	2275.02	0.02
LG40	12.71	11.1	1.61	1.06	2	-0.94	2179.86	2179.85	0.01
LG41	17.99	16.4	1.59	332.81	331	1.81	2228.77	2228.65	0.12
LG42	23.94	22.2	1.74	330.20	328	2.20	2236.20	2236.20	0.00
LG43	30.90	29.2	1.70	328.92	328	0.92	2259.85	2259.84	0.01
LG44	37.78	36.1	1.68	330.40	329	1.40	2302.31	2302.28	0.03
LG45	35.50	34	1.50	325.92	325	0.92	2350.01	2349.98	0.03
LG46	33.60	32.5	1.10	326.35	325	1.35	2363.19	2363.19	0.00
LG47	36.54	35.9	0.64	325.66	324	1.66	2358.16	2358.09	0.07
LG48	49.33	48.6	0.73	326.81	326	0.81	2358.99	2359.06	-0.07
LG49	59.34	58.7	0.64	322.83	318	4.83	2329.12	2329.17	-0.05
LG50	34.18	33.8	0.38	322.84	322	0.84	2370.31	2370.35	-0.04
LG51	31.75	31.6	0.15	317.59	316	1.59	2311.83	2311.88	-0.05
LG52	24.14	24.3	-0.16	287.89	286	1.89	2341.24	2341.24	0.00
LG53	9.88	10.3	-0.42	274.15	271	3.15	2475.06	2475.08	-0.02
LG54	8.01	8.2	-0.19	294.83	290	4.83	2492.99	2493.00	-0.01
LG55	19.14	19.4	-0.26	291.18	289	2.18	2480.02	2480.05	-0.03
LG56	21.38	21.8	-0.42	273.52	272	1.52	2488.12	2488.23	-0.11
LG57	20.48	20.9	-0.42	276.04	275	1.04	2566.17	2566.51	-0.34
LG58	14.51	14.9	-0.39	282.78	282	0.78	2606.13	2606.54	-0.41
LG59	10.58	10.2	0.38	277.84	276	1.84	2548.97	2549.35	-0.38
LG60	7.64	7.4	0.24	267.17	265	2.17	2594.21	2594.52	-0.31
LG61	8.55	8.2	0.35	310.46	310	0.46	2524.61	2524.95	-0.34
LG62	21.28	20.9	0.38	306.47	306	0.47	2482.50	2482.86	-0.36
LG63	21.04	20.9	0.14	304.64	304	0.64	2438.29	2438.62	-0.33
LG64	24.19	24	0.19	297.38	297	0.38	2366.14	2366.54	-0.40
LG65	22.51	22.5	0.01	295.22	295	0.22	2340.85	2341.22	-0.37
LG66	22.58	22.7	-0.12	292.16	292	0.16	2229.83	2230.17	-0.34
LG67	14.79	14.9	-0.11	287.99	287	0.99	2151.51	2151.83	-0.32
LG68	14.05	14	0.05	311.13	310	1.13	2012.25	2012.67	-0.42
LG69	17.66	17.4	0.26	324.47	323	1.47	1870.78	1871.14	-0.36
LG70	25.45	25.3	0.15	331.91	331	0.91	1668.39	1668.83	-0.44
LG71	62.65	61.9	0.75	317.87	318	-0.13	1405.14	1405.63	-0.49
LG72	52.91	52.5	0.41	305.84	306	-0.16	1055.62	1056.26	-0.64

^ height results from 1990/91 traverse
+ height results from 1993/94 traverse

For the magnitude of the ice flow, the two sets of results are very similar with a mean variation of ±0.7 m/yr (equal to a mean percentage change of ±5 %). The biggest differences are found between LG32 and LG46 (approximately 1 - 1.5 m/yr) and for sites between LG00 and LG16 that were only occupied in the early surveys (e.g., LG03). LG32 and LG33 were only occupied in 1990/91 and 1993/94 with the initial traverse having only a small amount of data. Therefore it can be assumed that the change in velocity at LG32 and LG33 is indicative of the improvement in the coordinate solutions at these sites. It is not certain why the IMS between LG36 to LG46 have such large velocity differences between the two studies. Odd numbered IMS between LG40 and LG50 were occupied for less than two hours in each traverse and these sites are therefore expected to have better velocities in the results of this thesis due to the improved coordinate solutions obtained from the high-level processing techniques. For the other sites, no explanation has been determined for the large differences.

The ice-flow directions from the two studies have more significant variation than the rates, with azimuth differences of ±0.02° to ±75° (mean difference of approximately ±4°). The most important changes for the azimuth results are in the region between LG02 and LG08 where flow lines from this study run in a direction which is down-slope when plotted in relation to the surface contours (see Figure 5.2). The results of Kiernan (2001), at these same sites, have flow directions that are not consistent with the known topography. At slow flowing sites such as these, the errors in the ΔE and ΔN values become dominant and therefore cause significant variation in the determination of azimuth at these sites. The improved flow directions for LG02 - LG08 indicate that this study has minimised these errors and provided improved results for these sites. Another important result from the azimuth comparisons is that the azimuths in the eastern ('good data') sector also have significant differences, similar to those observed for some sites in the western region. This suggests that even small improvements in site position can have a significant impact on the determination of flow direction.

As an indication of the improvement in height results from the new processing strategy, the differences in ellipsoidal heights for the join points of the IMS are given in Table 5.8. These results show that the high level processing has produced height values for the 1994/95 data that differ to Kiernan (2001) by a mean amount of 0.3 m (differences range from -0.6 to +1.0 m). This level of improvement is not significant in terms of the usefulness of the data for validation of current DEMs but provides more accurate information for future studies. The 1990/91 height data given for LG03, LG08, LG09, LG11, LG12, LG14, LG15 show a mean difference of 2 m in ellipsoidal height between the two processing strategies (the range of differences for the 1990/91 sites, given in Table 5.8, is -2 to +3 m). These comparisons indicate that

the high-level processing technique has produced a significant improvement in the determination of height at the IMS for the early traverses, which will be of use to on-going accumulation studies.

The orthometric surface height comparisons between the two sets of results (given in Appendix B - Table B.8) show significant differences along the entire traverse (differences range from -4.1 to +5.8 m). However, much of these differences are due to the change in the geoid/ellipsoid separation model used in each of the studies. The geoid-ellipsoid separations (N) in Kiernan (2001) were scaled from an AUSLIG Geoid Map (OSU89A, 1:20,000,000 edition 2, 1990) while for this study, N values were calculated using the EGM96 geopotential coefficients. The differences between the N values obtained for the LGB IMS using the OSU89A and EGM96 models range from -5.3 to +3.7 m, with a mean difference of ±2.3 m.

Other variations in the published final results for surface height between the two studies are that this study has presented (where possible) the 1994/95 surface height whereas Kiernan (2001) presented the 1990/91 heights for LG00 to LG35 due, presumably, to the lack of surface-to-sleeve measurements at these sites in the later surveys. In this study, the surface-to-sleeve distances have been inferred by subtracting the accumulation at the given site over the re-occupation interval between GPS measurements. Therefore the surface height values given for 1993/94 and 1994/95 in this study include uncertainty due to the accumulation measurements used for sites LG00 to LG35. This uncertainty is expected to be less than 0.5 m and therefore the surface heights presented here represent an improvement in the quality of the LG00 - LG35 results[7] and maintain a temporal consistency for the value given at each IMS.

The comparisons to previous analysis and the decrease in parameter uncertainty obtained from the high-level GPS processing show that this study has produced improved results for the LGB IMS. The most significant variation between the two LGB GPS studies has been observed in the determination of ice flow azimuths. For this parameter, the mean change for all IMS was found to be around 4°, however, the most significant flow direction result was the determination of realistic values at the very slow IMS. The ellipsoidal heights of the surface along the traverse were also improved by this study, especially for the heights determined at the IMS locations prior to 1993/94.

[7] LG00 - LG35 join heights for 1990/91 in Kiernan (2001) have uncertainties (from the GPS processing) of approximately 1 m. The mean difference between the 1990/91 ellipsoidal join heights from Kiernan (2001) and this study is 2 m.

5.3 Comparison to Remote Sensing and Balance Flux Modelling Studies

5.3.1 LGB DEMs

Satellite remote sensing data provides large-scale information over regions of Antarctica that otherwise would be poorly sampled. One such remote sensing tool is the satellite radar altimeter. Radar altimeters collect range data by timing the return pulse of a transmitted signal reflected from the Earth's surface. After applying filters and corrections to the raw data, the altimeter range information is then commonly used to calculate surface height measurements given the known location of the satellite orbit (e.g., Phillips (1999) and Bamber (1994a)). This surface elevation data can then be used in the construction of precise land-surface topography maps, commonly referred to as DEMs.

Between 1991 and 2000, the altimeter onboard the ERS-1 collected data between latitudes 82°N and 82°S (Fricker, Hyland *et al*, 2000). The ERS-1 mission was designed to collect data in two modes of operation, ocean-mode and ice-mode, with the ice-mode intended to provide more continuous data (by sacrificing some range accuracy) over the rougher and steeper ice surfaces of Antarctica (Bamber, 1994b). During 1994/1995, ERS-1 was put into a 168-day repeat orbit, referred to as the ERS-1 geodetic-phase (Remy *et al*, 1999). During the geodetic-phase, the ERS-1 altimeter collected ice-mode data over Antarctica at approximately 2 km by 0.35 km horizontal resolution with height precisions of approximately 1-2 m (Remy *et al*, 1999). The geodetic phase ERS-1 data have been used by several authors (e.g., Bamber and Bindschadler (1997), Remy *et al* (1999) and Fricker, Hyland *et al* (2000)) to produce surface DEMs of Antarctica which have then been used in glaciological analyses of the ice-sheet (e.g., (Remy and Minster (1997), Legresy and Remy (1997), Fricker, Hyland *et al* (2000) and Testut (2000)). The following discussion focuses on results from two recent mass balance modelling studies using altimeter DEM information: Fricker, Warner *et al* (2000) and Testut (2000).

5.3.2 ERS-1 DEMs and balance flux modelling

The mass balance of the Antarctic ice-sheet is an important parameter used for monitoring changes in the ice volume of the entire continent or a specific region. Two methods incorporating ERS-1 DEM information have recently been presented that investigate the balance flux[8] of the Antarctic ice sheets and make use of ground-

[8] "The 'balance-flux' distribution of a glacier system is the hypothetical distribution of mass flux that would exist if the system were in 'steady-state' " (Fricker, Warner *et al*, 2000, p561).

based data in the LGB for validation purposes. These two investigations use differing techniques to calculate the balance fluxes within the LGB using a selection of topography, ice thickness and accumulation datasets.

5.3.2.1 Testut (2000)

The DEM used in the ice-flow and balance flux study of Testut (2000) is based on that presented in Remy *et al* (1999) and hereafter will be referred to as the CNES-DEM[9]. This DEM was created using ERS-1 geodetic-phase, ice-mode, waveform data that had undergone editing using retracking algorithms, precise orbits, geophysical/environmental corrections, cross-over analysis, interpolation and slope error corrections (for further details refer to Remy *et al* (1999)).

Testut (2000) developed a mass flux model (referred to here as the Testut-model) which integrates accumulation values at points along surface flowlines to calculate the balance flux within a given region. For this method, information regarding the ice thickness, accumulation and surface slope of the study area are required as input.

In the Testut-model, the balance flux calculations commence by defining an initial location at some elevation and two points at an equal distance to either side of the selected point. Each of these three points is then followed (at a given step size) back up the path of steepest slope and the balance flux calculated at each step using an equation of the form:

$$U \cdot E \cdot l_0 = \int b(x) \cdot l(x) \cdot dx \qquad (5.3)$$

where: U is the balance velocity
E is the local ice thickness
l_0 is the divergence of the flowline at the initial point
b is the net accumulation rate
l is the divergence of the flowline at the up-slope 'step' point
x is the curvilinear distance from the flow source

until the flowlines either converge at a crest in the topography or widely diverge. Using this modelling technique, the balance flux calculation is carried out independently at each point and is therefore not constrained by the grid spacing or affected by the calculations for preceding points. However it does mean that adjoining points can define overlapping or non-unique flowlines resulting in over-estimation of balance fluxes.

[9] For latitudes south of 82°, the Remy *et al* (1999) DEM was augmented by data from the Drewry Surface Elevation Map (Drewry, 1983) to form the Centre National d'Etudes Spatiales Digital Elevation Model (CNES-DEM).

5.3.2.2 Fricker, Warner and Allison (2000)

The DEM used in Fricker, Warner *et al* (2000) (the LAS-DEM) was developed by Fricker, Hyland *et al* (2000) using ERS-1 geodetic-phase waveform data. This DEM was constructed after first applying the most precise Delft University of Technology orbits (Scharroo and Visser, 1998) and an accurate set of corrections to the altimeter data and then transferring these data onto a 5km grid using averaging techniques. The smoothing radius used to filter the small-scale topography of the LAS-DEM was 35 km which was found to provide the most coherent results (Phillips, 1999).

The balance flux calculation method used by Fricker, Warner *et al* (2000) is based on the one introduced in Budd and Warner (1996). In this model, the first step is to determine surface slope using the smoothed surface height information. The ice flow into each 5 km grid cell (starting at the highest elevation and working to lowest elevation) is then determined from the slope information, ice flux out of higher cells and the relevant accumulation information. The outflow from each cell is then distributed, in a manner proportional to the elevation differences, to the downstream neighbouring cells. The equations used to perform these calculations are (Fricker, Warner *et al*, 2000):

$$\Psi_{B_{i,j}} = \frac{\Psi^{out}_{i,j}}{\ell\left(|\cos\theta| + |\sin\theta|\right)} \tag{5.4}$$

where: $\Psi_{B_{i,j}}$ is the flux magnitude

ℓ is the cell size

θ is the angle of flow direction relative to grid orientation

$\Psi^{out}_{i,j} = a_{i,j}l^2 + \Psi^{in}_{i,j}$

is the outflow for cell (i,j)

where: a is the net surface accumulation and

$$\Psi^{in}_{i,j} = \frac{h_{x,y} - h_{i,j}}{N}\Psi^{out}_{x,y}$$

is the inflow to cell (i,j) for each neighbouring cell

(i.e., x,y = i-1,j; i+1,j; i,j-1; i,j+1)

where: h is the surface elevation of the cell

N is a normalisation factor

5.3.2.3 Discussion

These two balance flux modelling techniques have been compared by Testut (2000). In these comparisons, Testut (2000) found that the two sets of results produce very similar flux distributions and both successfully identify the major features in the continental ice flow. The differences between the techniques were mainly seen in the

small scale where the Testut-model produced results that gave a better resolution of flow structures. The limitations of the Budd and Warner (1996) method at the small scale occur when 'hollows' in the topography are encountered (i.e., no down-slope for outflow distribution) and are also related to the restrictions placed on the calculations due to the grid size. Errors in the Testut-model are primarily due to the non-conservation of mass inherent in the method. This error is characterised by the potential for different flowlines to pass over the same point (i.e., these points contribute to more than one integration process). The presence of crossed flowlines in the model was found to cause a significant increase (10%) in the calculated balance flux over the whole ice-sheet.

Errors in both modelling techniques are also caused by deficiencies in the input accumulation data (and thickness data for the Testut-model) and by the smoothing used on the DEM data. In the Testut-model, the maximum precision of the calculated balance velocities is expected to be approximately 10% due to these input data uncertainties. In Fricker, Warner *et al* (2000), the accuracy of the balance flux method was investigated by obtaining solutions using six different accumulation distributions. The results of these comparisons are discussed in detail in Fricker, Warner *et al* (2000) and Phillips (1999). In general, the four acceptable accumulation distributions resulted in mass imbalances across the LGB traverse line (compared to the observed flux) of -16.8% to +19.9% (Fricker, Warner *et al*, 2000). These results suggest that accumulation rates are not currently known well enough to provide accurate assessments of the mass balance using these types of modelling strategies (Fricker, Warner *et al*, 2000).

5.3.3 Comparison of GPS Velocities to Modelled Balance Velocities

The velocity results from this analysis of the LGB GPS data (section 5.1.2) have been used by Testut (2000) for validation of the solutions from his balance flux model (equation (5.3)). These observed[10] versus modelled velocity comparisons are mentioned briefly in Testut (2000) and are discussed here in more detail.

The input datasets used for the Testut (2000) balance velocity solution were the CNES-DEM (with 50 km smoothing), the Vaughan *et al* (1999) accumulation values (referred to from here as the Vaughan (VGH) accumulation) and the BEDMAP ice thickness data (Lythe and Vaughan, 2001).

[10] converted to depth-averaged column velocities by multiplying by a factor of 0.87 (Budd and Warner, 1996). The true conversion value is dependant on the ice rheology, ice temperature profiles and possible basal sliding (Fricker, Warner *et al*, 2000). The value used here is an approximate figure, acceptable for use in this region (Fricker, Warner *et al*, 2000).

Figures 5.9 and 5.10 indicate that the flow rates determined for the LGB traverse points in the balance flux calculations of Testut (2000) compare very well to the GPS derived values. Most of the flow rate comparisons for the LGB IMS are better than 20%. The largest differences (of approximately 50%) are found in the regions with high velocities or with significant topographic features (e.g., the major glaciers, the ridge near LG05 and the flow behind the Grove Mountains near LG60).

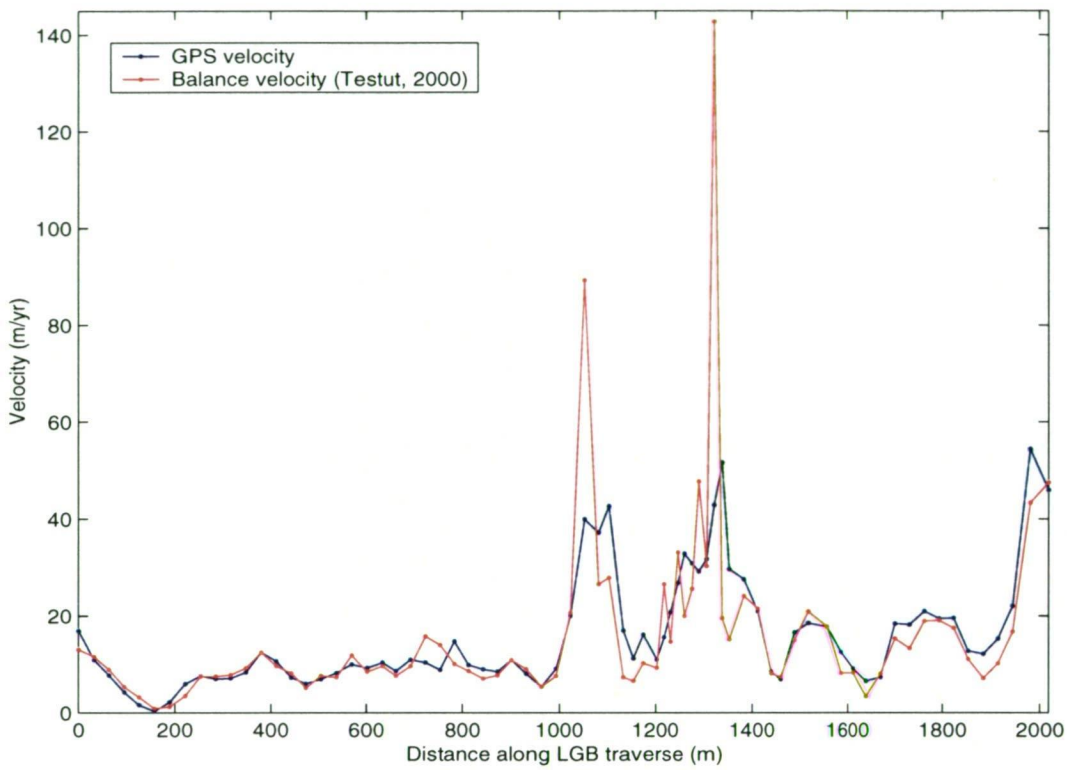

Figure 5.9 - Comparison between the modelled balance velocities from Testut (2000) and the GPS derived velocities at the LGB IMS

Figure 5.10 shows that the flow distribution pattern of the Testut (2000) balance velocities is closely related to magnitude and direction of the GPS derived results along the traverse line. This overlay suggests that the Testut-model is determining a good indication of the direction of flow in this region and of relative flow rates although the absolute velocity magnitudes are not accurate at many locations. These observations indicate that the topographic information is adequate (controlling the geometry of the flowlines) while errors in the accumulation and/or thickness data are likely to be affecting the flow rates.

The main features of Figure 5.10 are the overlap of the GPS and modelled flows into the Mellor and Lambert Glaciers (LG33 - LG37 and LG41 - LG51), in the steep coastal zone near LG70 and the low velocity zone near LG05 which is known to be the top of a ridge line (see 5.1.3). In all other regions, there are more subtle similarities between the GPS and model velocities that indicate that the model is

'seeing' the real physical distribution of ice flow. For example, the existence of flowlines at LG41 and LG43, the direction of flow into the Collins and Geysen Glaciers (around LG22-LG25) and the higher flow rates on the northern side of the Grove Mountains (near LG62 - LG66) are clearly observed in the model data.

These comparisons between modelled and GPS derived velocity are currently being assessed in collaboration with Testut (2000) (see section 5.3.4), especially in terms of examining the overestimations in the model results for the fast-flowing regions of the basin.

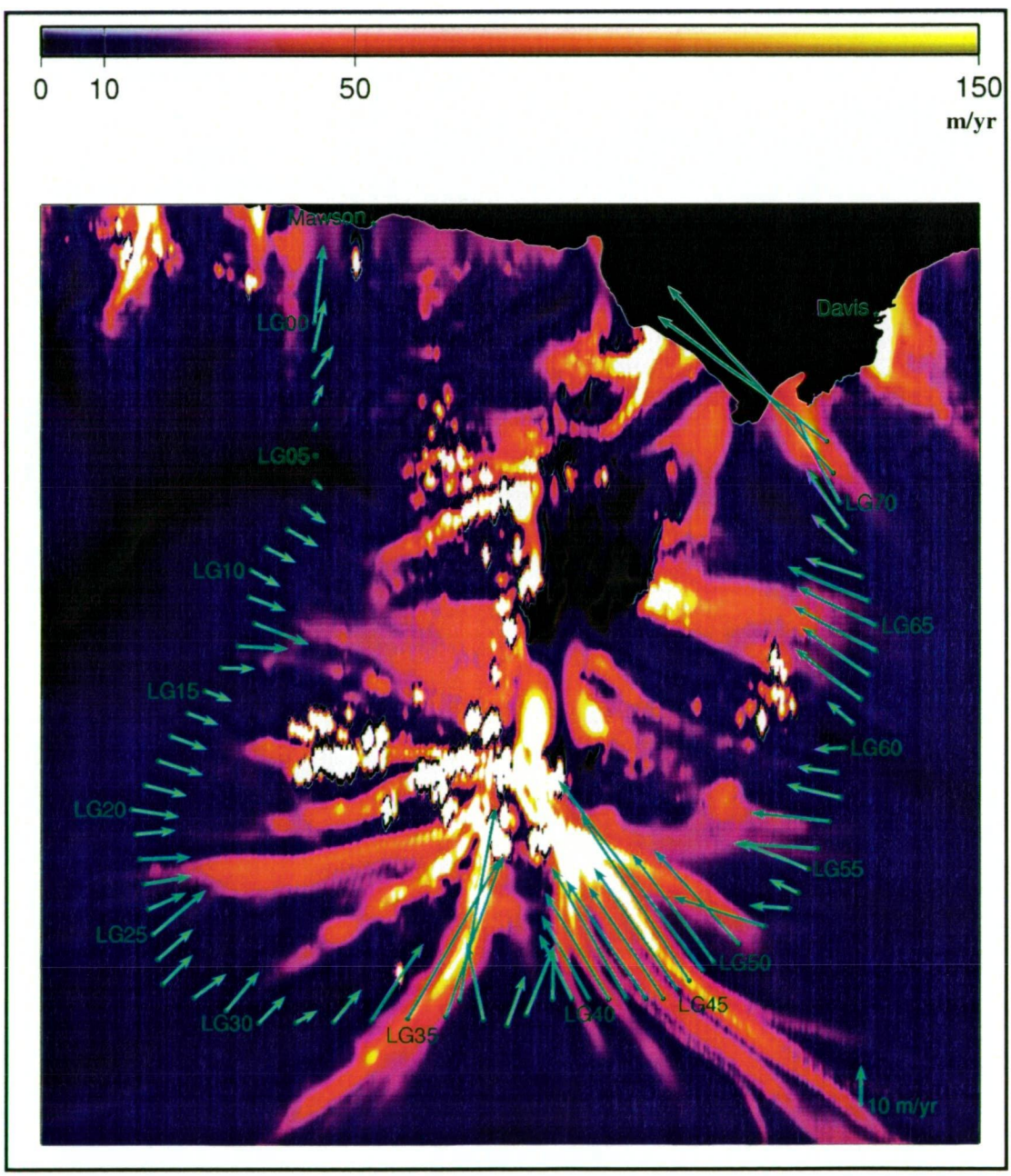

Figure 5.10 - LGB IMS (column) velocities overlaid on the modelled balance velocities of Testut (2000).

5.3.4 Analysis of the Testut Balance Flux Method

The finding of significant variation between the Testut (2000) balance velocities and GPS derived values at several important locations (in terms of mass balance) within the LGB, suggested that further examination of the reasons behind these differences was necessary. The most likely cause of large errors in the modelling results are the uncertainties in the input data. Therefore, in order to quantify the sensitivity of the modelling to the primary input data (i.e., elevation and surface accumulation) a series of test solutions have been produced using alternative accumulation datasets and DEM models.

5.3.4.1 DEM testing

An extended, continental version of the DEM used in Fricker, Warner *et al* (2000) was obtained from the Antarctic CRC, University of Tasmania (pers. com. G. Hyland, 2001) and transformed onto the Testut (2000) grid system. This DEM will be referred to as the CRC-DEM. The CRC-DEM does not include data south of -82° (the limit of ERS-1 altimeter information) and is smoothed at 35 km resolution. The CNES-DEM also uses altimeter data but includes height values extracted from the Glaciology Atlas (Drewry, 1983) for the region south of -82° and is smoothed at 50 km resolution. These two altimeter DEMs were constructed using slightly different waveform data editing and processing techniques and therefore will not be identical (see Remy *et al* (1999) and Fricker, Hyland *et al* (2000) for details of the DEM construction process).

The Testut-model was run using the CRC-DEM, the Vaughan accumulation dataset (Vaughan *et al*, 1999) and the BEDMAP ice thickness information (Lythe and Vaughan, 2001) to produce new estimates of the balance velocities at the LGB IMS for comparison to the Testut (2000) results (given in Figure 5.9).

Figure 5.11 shows the comparison between the GPS flow rates, the Testut (2000) balance velocities and the corresponding values obtained using the CRC-DEM. Figure 5.12 displays the difference between each of these sets of values. These results indicate small variations in the magnitude and pattern of velocity differences for the CNES-DEM and CRC-DEM solutions in the glacier and eastern sectors of the traverse route. However, in general, neither set of model velocities appears to be more outstanding than the other in terms of comparison to the GPS values.

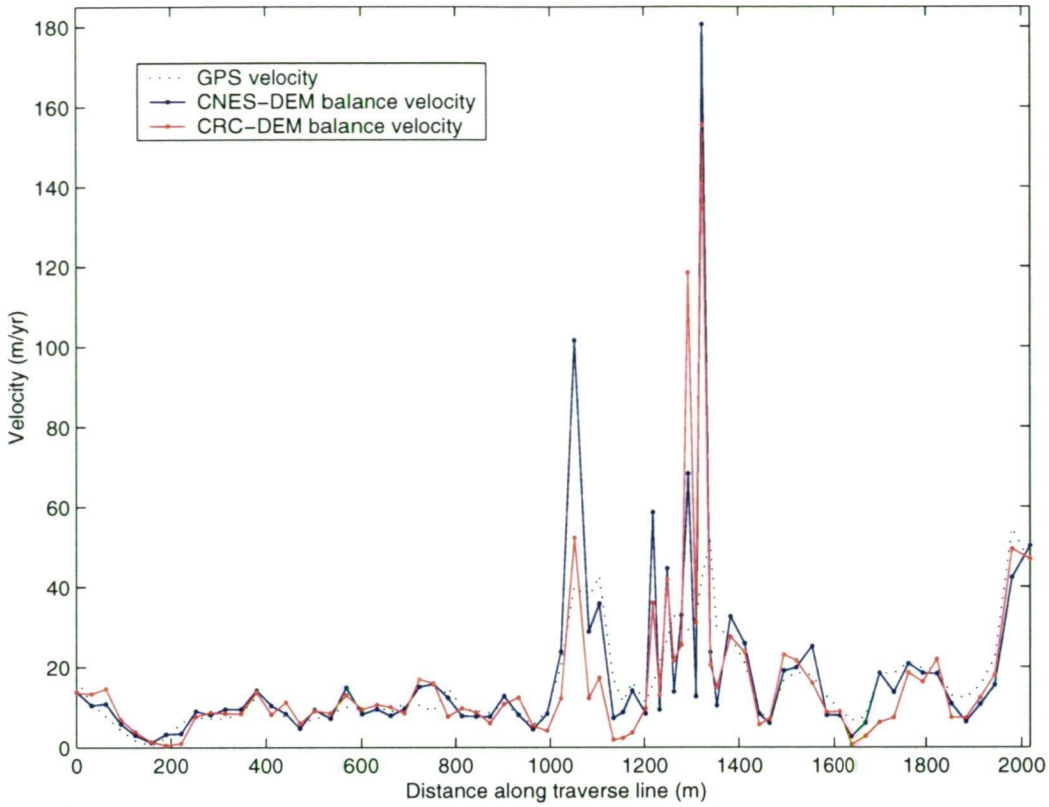

Figure 5.11 - Comparison of balance velocity results using the CNES and CRC DEMs in the Testut-model

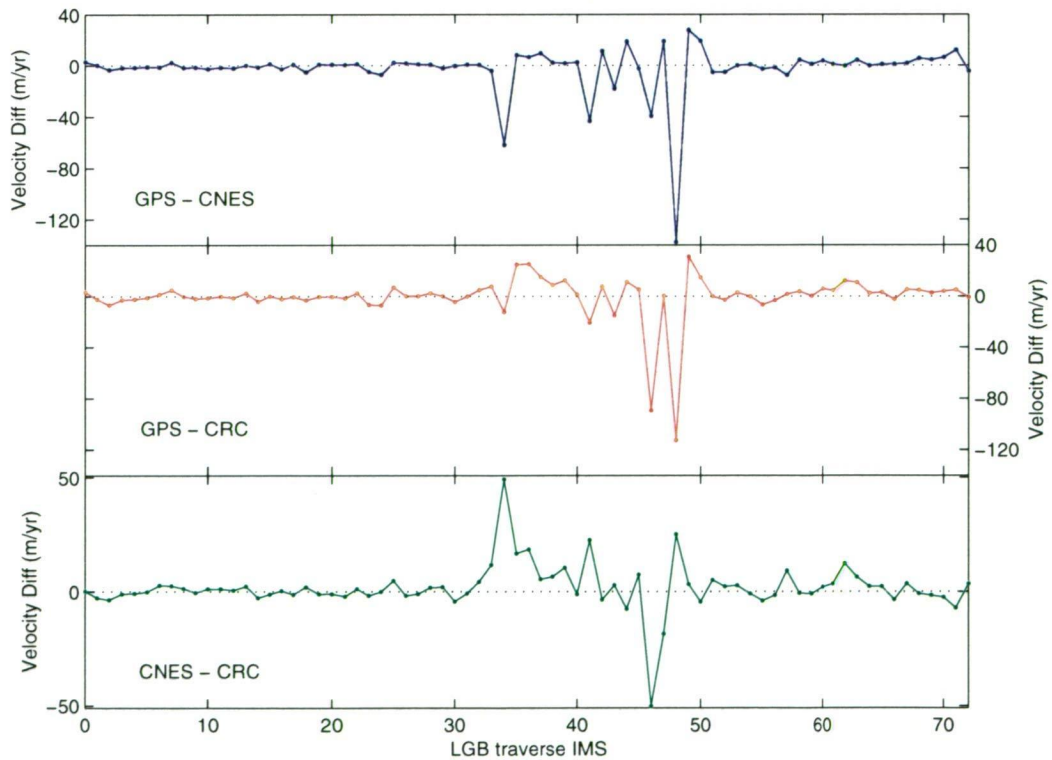

Figure 5.12 - Differences between the GPS, CNES-DEM and CRC-DEM velocity results.

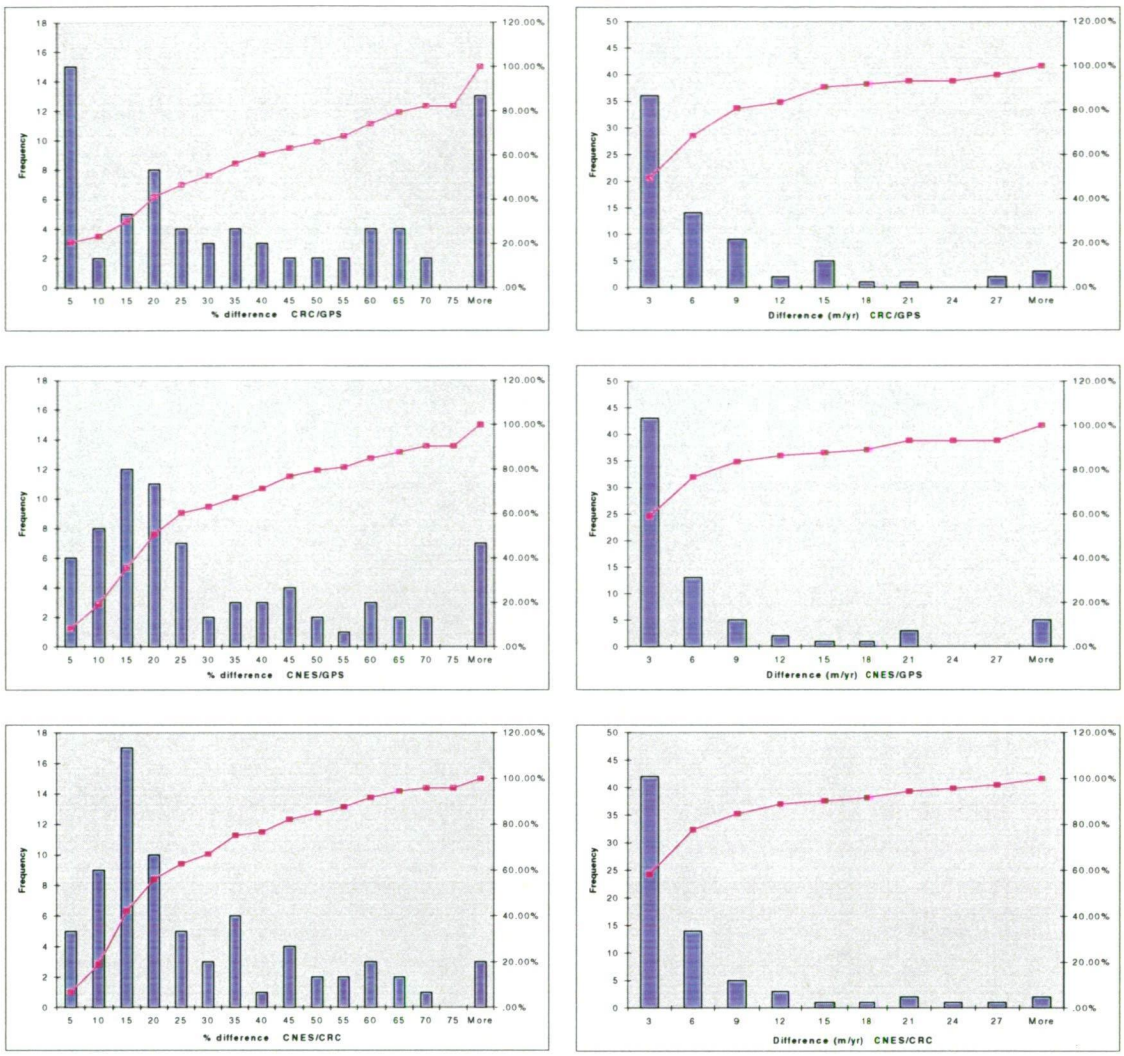

Figure 5.13 - Histograms of the differences given in Figure 5.12. Column (a) represents the absolute differences as a percentage of the GPS velocity while column (b) gives the absolute difference (m/yr) between solutions. The cumulative percentage is indicated by the magenta line.

The differences in the flow rates (shown in Figure 5.12) between both model solutions and the GPS values range between -120 and +40 m/yr with most differences being less than ±3-6 m/yr (see Figure 5.13). For the CRC-DEM balance velocity results, the percentage difference from the GPS value are mostly within ±35% (see Figure 5.13). These small m/yr differences and the generally small percentage differences indicate that most differences between the CRC-DEM and GPS results are in the fast-flowing ice stream regions. However, there is also a peak in the percentage differences at 'greater-than-75%' (see Figure 5.13) indicating that there are also significant differences between model and GPS values at some of the slower IMS (i.e., in the eastern sector - see Figure 5.12). In comparison, the percentage differences between the CNES-DEM results and GPS are generally within ±25%. In this case, the majority of results are concentrated toward the lower end of the graph in Figure 5.13, indicating that the greatest differences are at the faster sites as expected from previous observations.

The differences in velocity results obtained from the CRC-DEM and CNES-DEM balance flux solutions (see Figures 5.12 and 5.13) range between ±50 m/yr with the majority of values within ±3 m/yr. In terms of percentage differences, it can be seen (Figure 5.13) that the average difference between these solutions is ±15-20% and again these results indicate greatest variation is in the glacier region.

These comparisons suggest that the selection of input topography has not consistently increased or decreased the difference between GPS and model velocities along the LGB traverse route. The level of comparison between the modelled velocities indicates that these two DEMs are very similar and it is likely that the slight variation in smoothing radius[11] has made the most significant contribution to the differences seen here. It has previously been observed that the choice of surface smoothing has a large impact on the flowline definition and therefore the determination of velocity estimates (pers. com. Testut, June 2001).

5.3.4.2 Accumulation distribution testing

The second series of tests on the (Testut, 2000) balance flux model were designed to determine the effect of changing the input accumulation data. The four 'best' performing accumulation datasets identified by Fricker, Warner *et al* (2000)[12] were selected for this purpose. These datasets are:

- CRC - Budd and Smith (1982)
- GASP - Budd *et al* (1995)
- CSIRO - Smith *et al* (1998)
- Vaughan (VGH) - Vaughan *et al* (1999)

The CRC and Vaughan datasets are based on field observations while the GASP and CSIRO dataset were determined from atmospheric models (i.e., precipitation minus evaporation) (Fricker, Warner *et al*, 2000). These accumulation datasets were obtained from the Antarctic CRC (pers. com. G. Hyland, 2001) and required transformation onto the Testut (2000) grid system. The CNES-DEM and BEDMAP thicknesses were then used in conjunction with the accumulation datasets to determine four balance velocity solutions.

Figure 5.14 shows the balance velocity flow rates calculated for the four different accumulation data compared to the GPS values. From Figure 5.14, it can be noted that the Vaughan and CRC results are very similar for all regions of the traverse and are close to the GPS values. The GASP and CSIRO data do not produce values of a similar comparison to the GPS results and are especially poor in the coastal and eastern regions of the traverse line.

[11] DEMs were not available with the same spatial smoothing (CRC-DEM 35km, CNES-DEM 50km).
[12] See Fricker, Warner *et al* (2000) for details of the accumulation datasets.

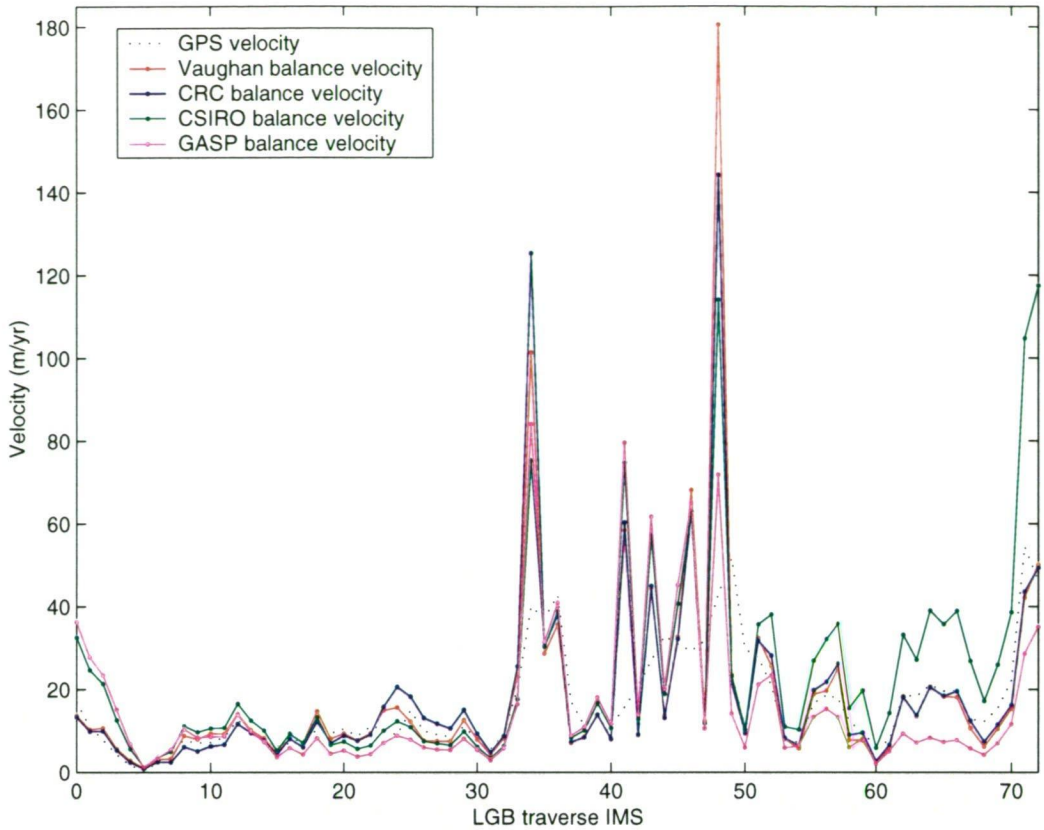

Figure 5.14 - Comparison between balance velocity results using different accumulation datasets as input for the Testut-model.

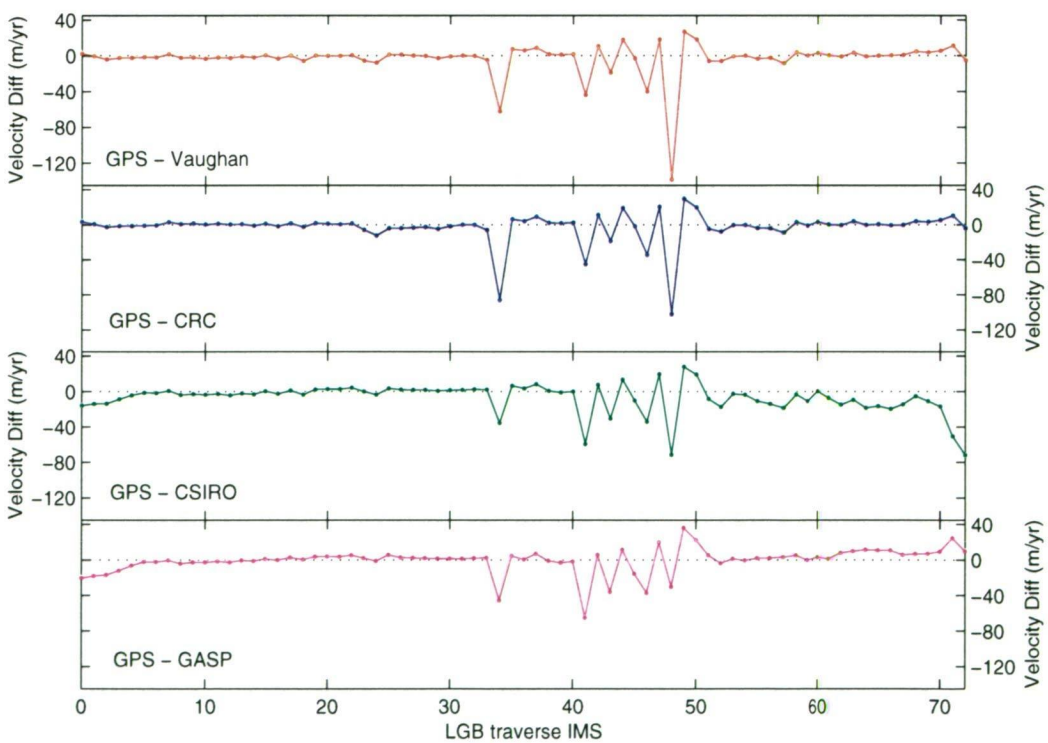

Figure 5.15 - Differences between the GPS velocity values and the balance velocity estimates.

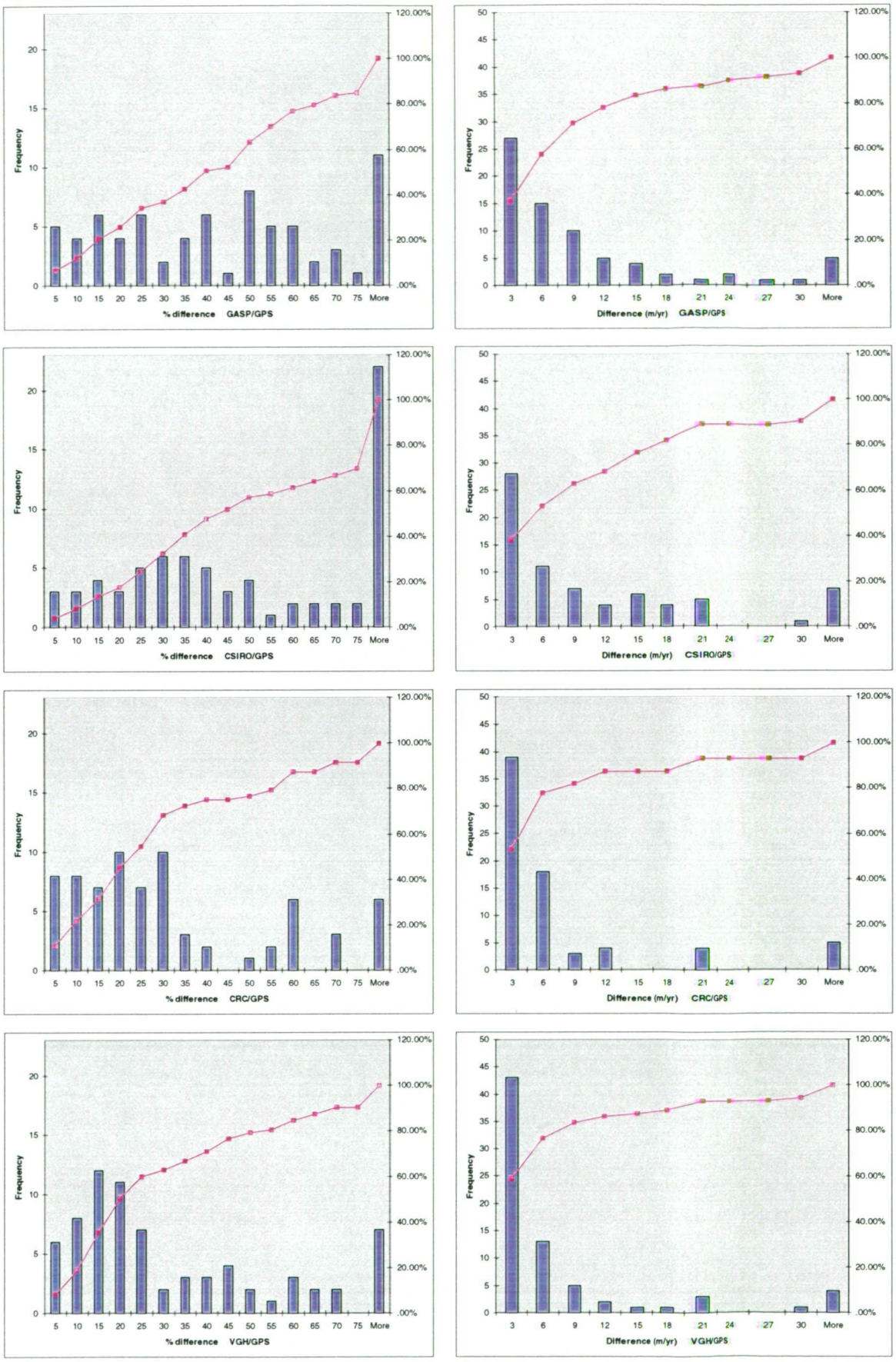

Figure 5.16 - Histograms of the differences given in Figure 5.15. Column (a) represents the absolute differences as a percentage of the GPS velocity while column (b) gives the absolute difference (m/yr) between solutions. The cumulative percentage is indicated by the magenta line.

Differences between the various modelled balance flow rates and the GPS derived columnar flow rates are shown in Figure 5.15. The largest deviations in each of these plots are for the glacial regions and additionally in the coastal regions of the CSIRO and GASP results. The CSIRO and GASP distributions indicate less consistency with the GPS measurements throughout the traverse. For the Vaughan and CRC solutions, differences to the GPS velocities are small except in the major glacial region. In the glacial regions, the differences from the GPS values display a similar pattern for all solutions while the GASP and CSIRO models produce results that are most similar to the GPS.

Histograms of the absolute differences between the modelled and GPS velocity values are given in Figure 5.16. From Figure 5.16 it can be seen that for the GASP and CSIRO data, differences between the model and GPS values range from ±3 m/yr to more than ±30 m/yr with most near to ±3 - 6 m/yr. In percentage terms, most differences are within 50 - 55% of the GPS value, however in the CSIRO results there are also a very large number of sites where the percentage difference is greater than 75%. The structure of the percentage difference distribution indicates significant departures between model and GPS values across all sites and particularly poor comparisons for the CSIRO solution at the slower sites. The CRC and Vaughan (VGH) histograms show that both sets of results differ from GPS by between ±3 m/yr with little data in the higher ranges. The percentage differences are also similar with maximum values in the lower region of the graph indicating the majority of significant differences are at the faster sites. For the CRC and Vaughan solutions, the mean percentage difference from the GPS values is 25 - 30%.

Comparisons between the balance velocity results obtained when using i) the CRC and VGH and ii) the GASP and VGH accumulation values as input data are given in Figure 5.17. These comparisons show very little difference between solutions determined using observational accumulation data (i.e., CRC versus VGH), indicating the similarity of these datasets (see Figure 5.17). Differences between these two sets of modelled velocities are generally within ±10% of the GPS velocity value. On the other hand, the comparisons between the VGH and GASP (i.e., observational versus modelled accumulation datasets) show velocity differences ranging from +/-3 - 18 m/yr (see Figure 5.17). The differences between these velocity solutions are generally within 30% of the GPS velocities and therefore most of the variation is seen in the faster regions. However, there are also many larger percentage errors indicating that there are also significant differences at the slower sites. The differences observed between these two sets of modelled velocities are indicative of the level of variation between the accumulation distributions. From these observations it can be clearly seen that the choice of observation-based versus modelled accumulation dataset has a significant effect on the balance flux results.

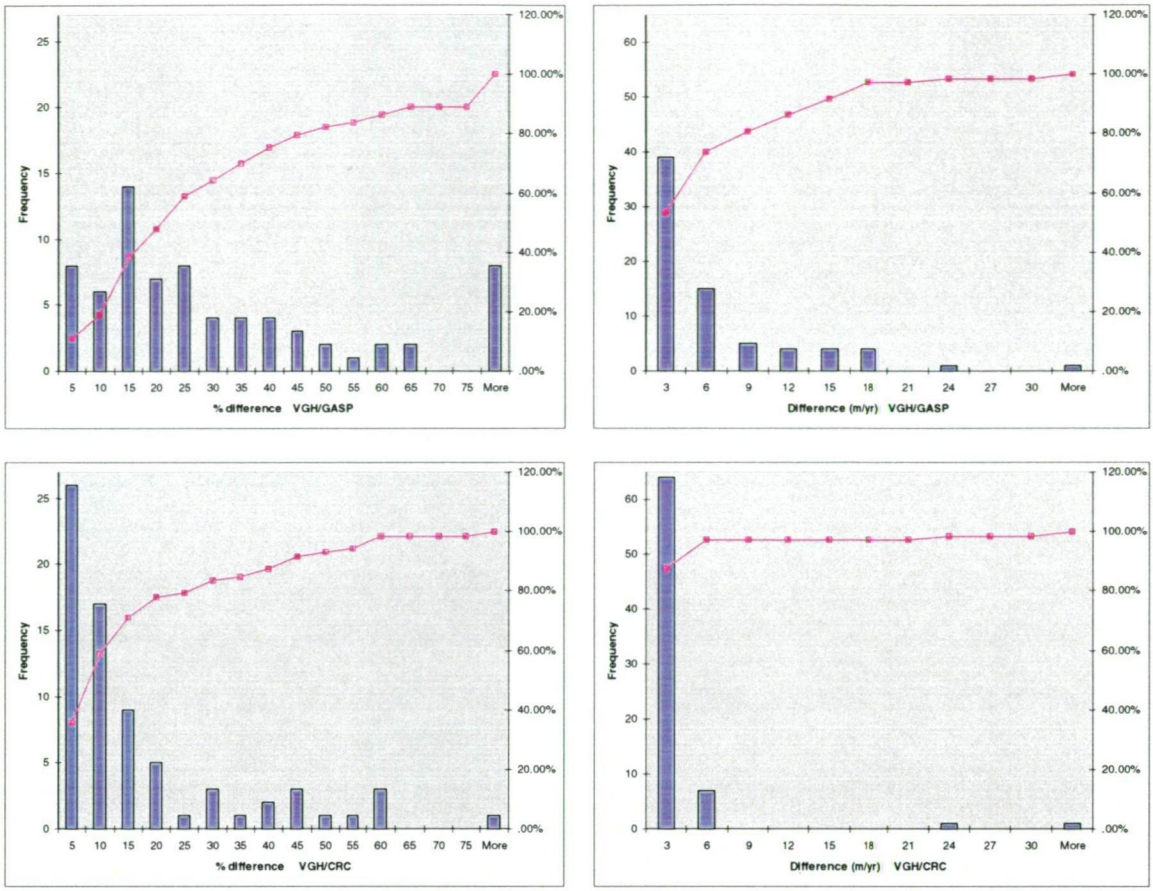

Figure 5.17 - Histograms of the differences between balance flux results using different accumulation datasets. Column (a) represents the absolute differences as a percentage of the GPS velocity while column (b) gives the absolute difference (m/yr) between solutions. The cumulative percentage is indicated by the magenta line.

5.3.4.3 Summary

The balance velocity solutions obtained by varying the DEM input data were generally 25 - 35% different to the GPS values. The choice of accumulation input data caused the resultant velocities to vary from the GPS values by 25 - 55%. These findings indicate that the choice of input accumulation data has had a greater effect on the magnitude of the balance velocity results than the choice of input elevation data.

Differences in the balance velocity results from the CRC-DEM and CNES-DEM were on average ±20% of the GPS value. This result indicates that either of these elevation datasets may be used to provide results within the same error limits (i.e., ±20%) of the GPS data.

Varying the accumulation data between datasets created from observational information has also been shown to make no significant difference to the balance velocity results (less than ±10%). However, using accumulation data from an atmospheric model as opposed to an observational dataset produces velocity

differences of around ±30%, with significantly higher percentage differences at a number of sites. From these findings it can be seen that the choice between observational or model accumulation datasets does have a significant impact on the velocity results obtained in all regions of the LGB traverse.

It should also be noted that varying either the accumulation or DEM input data has not significantly bettered the balance velocity results within the fast-flowing region. It is this region where the modelled velocities in both tests show the largest differences to GPS-derived values. The findings of these tests confirm those of Testut (2000) and suggest the presence of flowline definition problems in this region that need to be overcome either within the balance flux algorithm or through better quality input information.

5.4 Ice Sheet Velocity Measurement: A Case Study

The earliest LGB surveys were carried out over a decade ago (see section 3.4) and in the ensuing time, GPS technology and survey procedures have advanced considerably. Consequently, more efficient methods of collecting GPS data for velocity determination at remote, inland sites are now possible. The major benefits of increasing the efficiency of remote GPS surveys in Antarctica are the considerable lowering of project costs (up to 50% (Craven *et al*, 1995)) and the ability to extract reliable initial results in a shorter time frame.

In recent years, ice-sheet velocity values have been determined from GPS observations in Wilhelm II Land (East Antarctica) between 1000 - 2000 m elevations (pers. com. A. Ruddell). These GPS surveys were carried out at sites with velocities ranging from 12 to 75 m/yr and used helicopters to transport personnel and equipment to the survey area. Each site in the Wilhelm II Land surveys was occupied for a minimum of 2-hours (the maximum shutdown time for the helicopters) in each field-season, with approximately 1-year epochs between site occupations. From these data, horizontal velocities at the ice movement sites were determined with a mean uncertainty of 0.050 m/yr.

The case study described in the following sections was undertaken prior to the Wilhelm II Land surveys. The aim of the case study was to determine the minimum achievable velocity results from GPS data of the same quality as the 1993/94 LGB survey. The testing procedures used in the case-study (i.e., long baselines and short occupations) were designed to reflect the conditions likely to be encountered under the logistical constraints of inland, remote, helicopter-based surveys of the East Antarctic ice-sheet (e.g., helicopter shut-down times, flight availability, flight duration, weather delays, base-station failure, etc.).

From the findings of this case study and our current knowledge of GPS capabilities, a set of recommended survey and processing techniques for future land-based ice-sheet traverse programs has also been included in this section.

5.4.1 Data

Six of the LGB sites that were occupied during both the main 1993/94 traverse and the short autumn 1994 traverse were selected for this case study. These sites have well-determined velocities (see section 5.1.2) ranging from 14 m/yr to 62 m/yr and GPS re-occupation intervals of between 10 and 58 days.

The data from the selected GPS observation periods were cut into smaller files of 1, 2 and 4-hour intervals (with 30-second data epochs) for testing purposes. Base station data were available at the Davis (160 - 370 km baselines) and Mawson (600 - 750 km baselines) permanent GPS stations.

5.4.2 Processing

The case study was carried out under the assumption that many glaciological investigators/institutions do not have access to high-level, network processing capabilities. Therefore, to investigate the minimum achievable results from the selected GPS data, site positions were estimated using standard baseline processing procedures (i.e., similar to strategies available in commercial software).

GAMIT baseline solutions were carried out using fixed IGS orbits, one fixed reference station and minimal settings for all cleaning and processing parameters (e.g., L3 solutions, no ambiguity resolution, no tropospheric delay estimation, no tide models or Earth rotation parameters, etc). In modifying the solution parameters in this fashion, it was assumed that the standard of processing would be similar to using commercial software.

For each day the 1-, 2- and 4-hour data were processed in separate solutions using Davis as the reference site (see Figure 5.18). These daily solutions were then re-processed, on this occasion using Mawson as the reference site. This processing strategy resulted in six independent coordinate estimates for each study site on each day (see Figure 5.18). A series of velocities (1, 2 and 4-hour estimates) were then calculated at each LGB site, from both reference stations and over all available reoccupation intervals (see Figure 5.18).

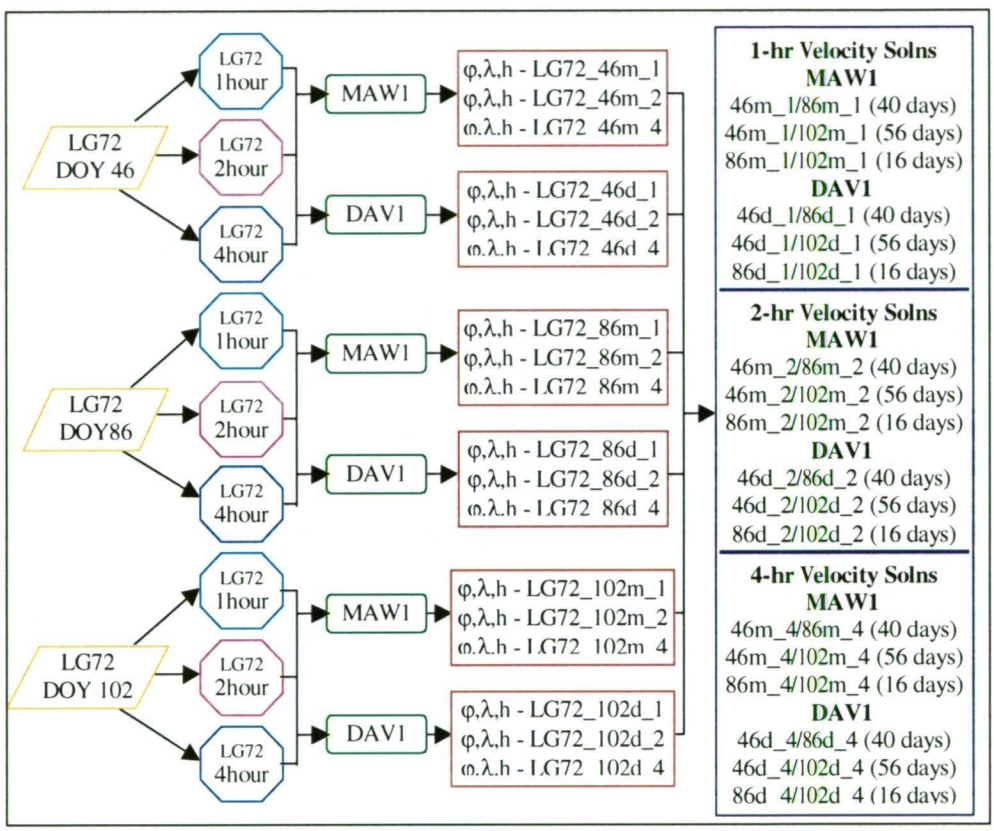

Figure 5.18 - Case study processing strategy (e.g., site LG72)

5.4.3 Results

5.4.3.1 LG69 and LG72

The results for LG69 and LG72 (using Davis as the base-station) are given in Table 5.9 and Figure 5.19. These sites were selected as examples of velocity results from the slower (<20 m/yr) and faster (>40 m/yr) study sites respectively.

Table 5.9 and Figure 5.19a show that the velocity residuals (multi-year minus case-study rate) in all solutions are of a similar magnitude, ranging between ±1 m/yr. However, except for the LG72 16day solutions, the LG72 residuals are smaller than those of LG69 and are centred around an approximately zero-mean (see Figure 5.19). In terms of flow direction, the results at LG69 are significantly poorer than those for

LG72 (mean residuals of -2.0° and -0.1° respectively). The inferior results at LG69 can be mostly attributed to the small variation in position (0.05 m/day) compared to LG72 (0.15 m/day). However, there also appears to be a significant and relatively constant bias in the LG69 residuals, likely due to the use of a longer (254 km) baseline.

At both sites, there is a general improvement in the reliability of all results as the duration of occupation increases from 1- to 4-hours. At LG72, all flow rates are estimated to within 2% of long-term values and flow directions are within ± 0.5° (except for the 1hr/16day solution). At LG69, the 10-day reoccupation interval produces inconsistent results over all observation durations, especially in terms of flow direction. In terms of percentage error in the flow rate, all solutions at LG69 are within 4% (2 and 4-hour estimates within 3%) of the multi-year value. The flow direction estimates at this site for the 47- and 57-day solutions have residuals of less than 1.2°.

Table 5.9 - Case study results: Davis baseline solutions for LG69 (254 km baseline, 17.66 ± 0.01 m/yr, 324.3189 ± 0.0004 °) and LG72 (161 km baseline, 52.92 ± 0.01 m/yr, 305.7864 ± 0.0001°). Highlighted rows indicate solutions over < 40 days.

Site	Duration (hrs)	Interval (days)	Case-study Rate (m/yr)	Residual (m/yr)	%	Case-study Direction (°)	Residual (°)
69	1	57	16.97	0.69	3.9	325.8058	-1.49
69	1	47	16.96	0.70	4.0	324.6272	-0.31
69	1	10	17.13	0.53	3.0	331.2976	-6.98
69	2	57	17.31	0.35	2.0	325.4334	-1.12
69	2	47	17.13	0.53	3.0	325.2611	-0.94
69	2	10	18.13	-0.47	2.7	326.1986	-1.88
69	4	57	17.30	0.36	2.0	325.2901	-0.97
69	4	47	17.22	0.44	2.5	324.6030	-0.28
69	4	10	17.73	-0.07	0.4	328.4275	-4.11
72	1	56	52.84	0.08	0.2	306.1375	-0.35
72	1	40	52.65	0.27	0.5	305.6148	0.17
72	1	16	53.31	-0.39	0.7	307.4284	-1.64
72	2	56	53.07	-0.15	0.3	305.6165	0.17
72	2	40	52.74	0.18	0.3	305.6535	0.13
72	2	16	53.87	-0.95	1.8	305.5259	0.26
72	4	56	53.12	-0.20	0.4	305.7136	0.07
72	4	40	52.81	0.11	0.2	305.8438	-0.06
72	4	16	53.87	-0.95	1.8	305.3946	0.39

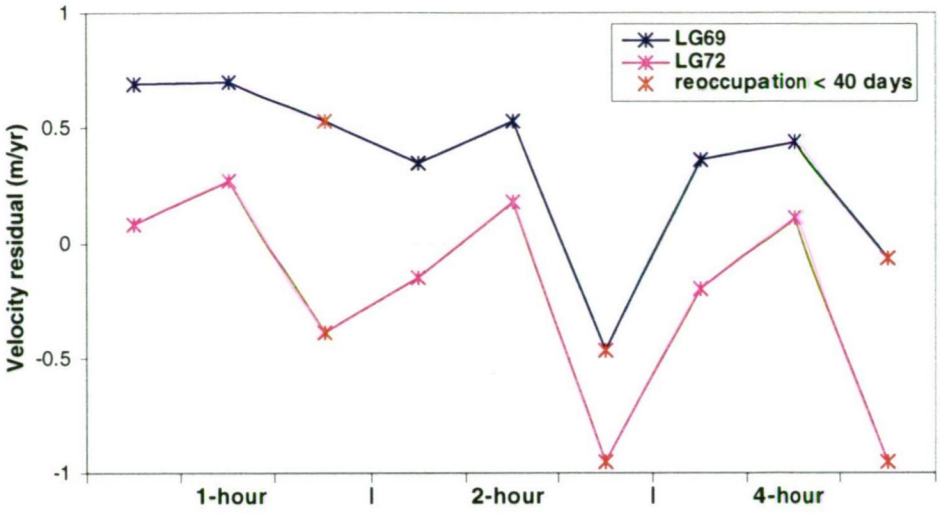

(a

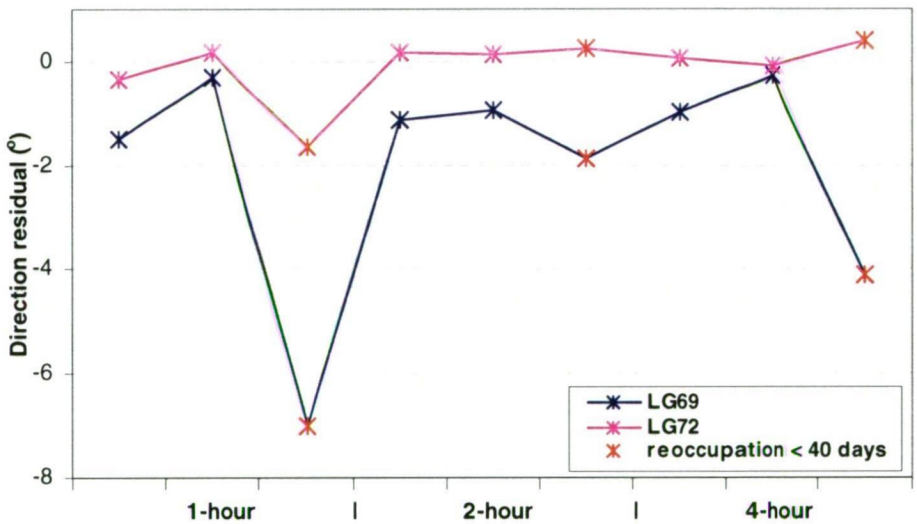

(b

Figure 5.19 - Velocity residuals (multi-year - case study) for LG69 and LG72. The upper panel (a) gives the velocity magnitude residual and the lower panel (b) shows the direction residual. Solutions for reoccupation intervals < 40 days are identified by a ✳.

5.4.3.2 All sites

The 1-hour flow rates at *all* sites and over *all* baselines were estimated to within *9%* of the long-term value and had flow directions that differed by up to *14°*. In general, the 1-hour velocities over all baselines, reoccupation intervals and for all flow rates gave inconsistent and unreliable values. The conclusion reached from these results is that 1-hour occupations are not recommended for surveys with similar observing conditions to those examined in this case study.

Differences between the velocity results from *all* of the 2- and 4-hour occupation solutions and the long-term values are summarised in Table 5.10.

Table 5.10 - Percentage of all 2- and 4-hour case study velocity solutions (i.e., 10 to 63 day re-occupations) within the given error margins of the long-term estimates.

Base Station	Obs	Rate			Direction		
		±1%	±2%	±3%	±0.5°	±1°	±2°
Davis (160-370 km)	2-hr	46%	80%	100%	60%	80%	100%
	4-hr	55%	98%	100%	80%	100%	100%
Mawson (600-750 km)	2-hr	40%	65%	100%	13%	62%	100%
	4-hr	46%	75%	100%	50%	75%	100%

Using the Davis baselines (*160-370 km*), results for the LGB sites, with velocities between *14* and *25 m/yr,* were found to be within *3%* and *1.5°* of the long-term estimates for *2-hour* site occupations (*2%* and *1°* for *4-hour* occupations) separated by at least *40 days*. The faster, coastal sites (*53 - 63 m/yr*) produced results of a similar standard over a shorter reoccupation interval (*16 days*). For the Mawson baseline solutions (*600-750 km*), *all* sites required *2 to 4-hour* occupations with a minimum *40-day* reoccupation to achieve velocities within *3%* and *1.6°* of the long-term values. From the results summarised in Table 5.10, it can be seen that as expected, the shorter baselines from Davis have resulted in smaller percentage errors than those determined from Mawson.

In terms of the measurement uncertainty of the velocity values, improvement with increasing occupation length and reoccupation period is observed, again as expected. Figure 5.20 shows the exponential decrease in velocity uncertainty (1σ) from a 10-day to a 60-day interval over all observation periods. Figure 5.20 also clearly illustrates the superior reliability of the 4-hour and >40-day solutions.

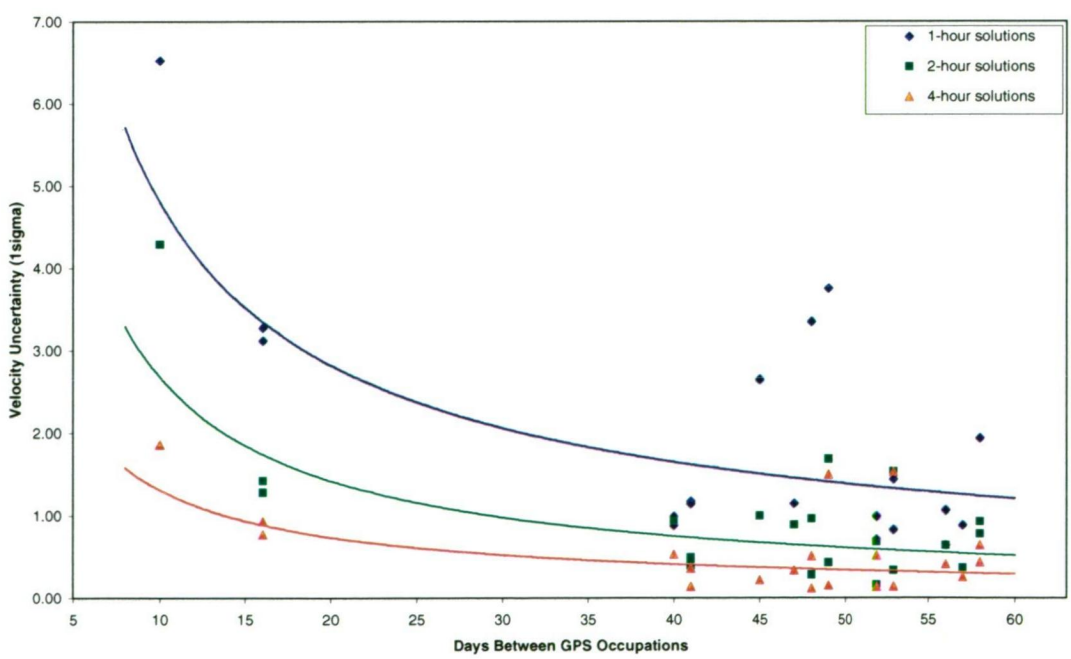

Figure 5.20 - Velocity uncertainty (m/yr) vs reoccupation interval for increasing observation periods.

For mass-balance calculations, surface velocities are required with an error margin of ±5-10% (Craven *et al*, 1995; Kiernan, 2001). This accuracy requirement is due to the fact that other parameters, such as the accumulation rate, have much higher uncertainties and therefore a greater effect on the overall result (Fricker, Warner *et al*, 2000). Another application for GPS derived surface velocities is the discrimination between various mass balance or flow models (see section 5.3). In this application, the level of uncertainty in the velocity result is critical.

This case study has shown that short (2 to 4-hour), single-season GPS surveys using basic processing techniques are capable, at a minimum, of providing ice-sheet velocities (with uncertainties of approximately 1 m/yr) that are within 3% of long-term values for sites with velocities of 14 to 65 m/yr and are therefore adequate for use in many applications.

5.4.4 Recommendations for Land-Based Traverses

For data collection in field-based traverses, as opposed to surveys relying on helicopter support, the time restrictions investigated in this case study are less likely to apply. In these instances, multi-vehicle traverse trains would allow longer GPS occupations, and therefore shorter re-occupation intervals, to determine reliable velocities (i.e., better than 3%) from a single field season.

During the LGB surveys, the method of GPS data collection was designed to provide ice velocity estimates with an accuracy of between 5 and 10% (Craven *et al*, 1995; Kiernan, 2001) and the data obtained were therefore not optimal for higher-level studies. However, this thesis has indicated that high-precision velocity/height estimates (see section 5.1) were able to be obtained using the LGB GPS data. It has also been shown, in section 5.4.3, that reliable velocity results can be determined from GPS data collected during a single field season. Therefore, with a slight variation in the survey methodology, future glaciological programs should be able to determine reliable surface velocities without the need for multiple-season GPS surveys.

For example, ice-sheet movement is known to be approximately 5-20 m/yr near the 2000 to 2500 m surface elevation (Craven *et al*, 1995). Over 14 days, a site with a velocity of 15 m/yr (0.04 m/day) will have moved approximately 0.6 m. Given 24 hours of observations at a site, high-level, network processing techniques are capable of providing site position with an uncertainty of less than 0.010 m. Using these figures, it can be observed that a 2% velocity estimate would be achievable with a reoccupation interval of 14 days for this example site.

Therefore, for future land-based traverses (assuming a travelling speed of 5km/hr, site velocities of around 15 m/yr and access to three vehicles and three GPS units) a survey methodology similar to the following is suggested (see Figure 5.21):

(a) *Vehicle-1* sets up *GPS-1* at *site-1*.

(b) *Vehicle-2* moves to *site-1* and upon arrival, transfers *GPS-2* to *Vehicle-1*. *Vehicle-1* then departs *site-1*. *Vehicle-2* remains at *site-1* until 24 hours of observations with *GPS-1* are complete (i.e., 12 hours after arrival).

(c) *Vehicle-1* arrives at site-2 and sets up *GPS-2*. *Vehicle-1* then remains at *site-2* for 12 hours.

(d) Steps (b) and (c) are repeated for the length of the traverse, giving 24 hours of uninterrupted GPS observation at each site.

(e) *Vehicle-3* commences 14 days behind *Vehicle-1*, collecting 18 hours of data with *GPS-3* at each site and then moving on. This length of occupation/re-occupation should be sufficient to determine velocities, using high-level processing techniques, with an accuracy of 2%.

(f) Assuming that each van travels approximately 30 km per day, all vehicles will reach the end of a 2250 km line after 3 months.

Other scientific data may be collected (i) throughout the duration of the traverse (e.g., atmospheric pressure, air temperature and wind direction/strength), (ii) while moving between sites (e.g., ice-thickness) or (iii) while stationary at the GPS sites (e.g., accumulation, ice cores and snow pits). The length of time spent at each site could also be increased so long as the reoccupation interval remained equal to or greater than 14 days. Also, while stationary, the GPS receiver should be operating continuously regardless of the duration of each site occupation so that the most precise site coordinates can be estimated and to allow other parameters, such as the amount of precipitable water passing over the site (see Chapter 8) to be determined.

The above recommendations are based purely around GPS observation requirements and do not take into account down-time due to weather and unforeseen incidents or observation requirements for other scientific studies. Any increase in time spent at or between sites due to these factors will simply result in a shorter traverse length or longer survey duration.

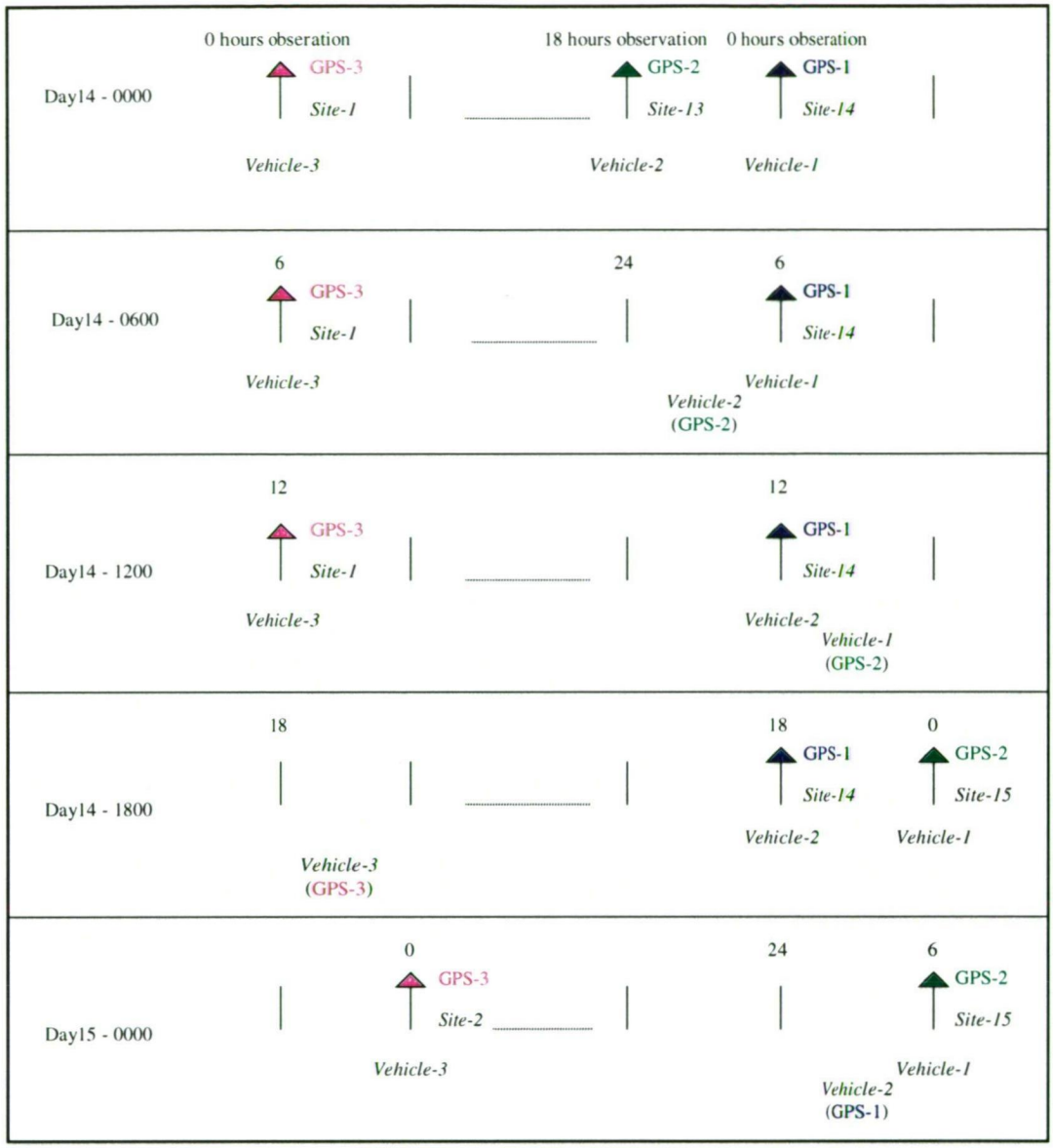

Figure 5.21 - Suggested GPS traverse method for surface velocities (greater than 15 m/yr) with an accuracy of 2%

5.5 Chapter Summary

The most complete, accurate and precise set of position, height, slope and ice velocity results arising from the entire series of LGB traverse GPS data have been determined in this study.

A significant outcome from this analysis of the LGB GPS data is the high level of precision (relative to the data quality) obtained for the LGB IMS position estimates in each year of the traverses. The biggest improvement in the position results has been in the determination of surface heights. The orthometric surface heights obtained in this study, as shown in Table 5.8, are between ±6 m different to those of Kiernan (2001). However, most of this difference is due to the variation in geoid

separation values. In terms of ellipsoidal heights (solved directly from processing), the mean difference between this study and those of Kiernan (2001) for the 1994/95 traverse is 0.3 m while for earlier years, the differences are consistently 1 - 2 m (see Appendix B - Table B.8).

This analysis of the LGB traverse GPS data has also determined accurate surface velocities for all of the LGB IMS with most results having a mean 1σ precision of around 0.01 m/yr. For nine sites between LG00 and LG33, data were only collected during the 1989-1993 period and as such, the mean velocity uncertainty at these sites is approximately 0.4 m/yr. These LGB velocity values have been well determined by using high-level processing techniques and are of a much higher quality than anticipated at the commencement of the traverse program. When compared to the velocities obtained using commercial GPS processing software (Kiernan, 2001), the values obtained in this study generally demonstrate differences of less than 1.5 m/yr. Higher variations were observed for many IMS between LG00 and LG15 while for most sites east of LG16, the difference in flow rate between the two studies is less than 0.5 m/yr. In terms of flow direction, significant improvements have been made when compared to known flow lines and topography, this is especially so in the western LGB region. In general, differences in flow direction of 0.1° to 4° are noted in all regions of the traverse. These differences in flow directions are important due to their influence on the determination of balance flux information.

Detailed analysis of slope measurements from the LGB traverses have been presented here for the first time. These slope calculations were based on static data collected along a 50 km offset line parallel to the main traverse line in the western basin and kinematic data collected approximately 5 km up- and down-slope from 5 sites in the eastern basin. In the west, a mean slope value of 4 m/km was observed over the entire sector (values range from 2 to 8 m/km in this region). In the east, local surface profiles showed a variation in surface gradients, within 10 km of the selected IMS, of 2 to 30 m/km with a mean value of less than 10 m/km. The slope values determined from the GPS data were compared to information from the LAS-DEM (Fricker, Hyland *et al*, 2000) and showed that the DEM appears to give a good representation of the surface gradients in these regions.

These new results from the LGB data have recently been used as validation for remote sensing studies of balance velocities (Testut, 2000) and DEM values (Fricker, Hyland *et al*, 2000) and will form an integral part of future mass balance studies of the region using GLAS (Brenner *et al*, 2000) and GRACE (Wahr *et al*, 2000) satellite data.

Comparisons between the GPS-derived velocities at the LGB IMS and balance values obtained from various solutions using the Testut-model have been studied to

observe the effect of varying the input data for the Testut-model. These tests have revealed that regardless of which (reliable) topographic or accumulation dataset is used as input, the largest errors in the modelled flow rates occur for the ice flowing into the major glaciers. In these regions, the modelling tends to overestimate the flow rates by approximately 50% although the distribution of the flows compares well to the GPS results. In other regions of the LGB traverse route, the comparisons between the model and GPS velocities indicate that the modelling provides an excellent representation of the flow distribution and flow rate estimates that are within 20% of the ground-based measurements.

The final section of this chapter has investigated the level of precision achievable using multiple short-term GPS occupations within a single field season. From these studies, it was found that 2 - 4 hour occupations, re-observed after approximately 40 days were adequate to provide velocities at the 97% confidence level (for sites moving between 14 and 63 m/yr). The precision of the velocity results improved, as expected, with increased occupation times and reoccupation intervals. A strategy for providing accurate ice velocity determination from single-season, traverse-based GPS programs has also been recommended.

Chapter 6

GPS METEOROLOGY

6.1 Introduction

Water vapour plays a vital role in the Earth's atmospheric processes, as it is the principal mechanism for the transport of latent heat and moisture around the planet. It is an extremely variable parameter that acts over a wide range of temporal and spatial scales, from global circulation patterns to micrometeorology. Water vapour is also one of the most important atmospheric components driving the Earth's greenhouse mechanism due to its control over the radiative properties of the atmosphere (Elliott *et al*, 1995). In terms of climate change, warmer air can hold a greater amount of water vapour, which in turn causes more warming and in this regard, water vapour provides a very important climate change indicator (Elliott *et al*, 1995). It is therefore important that worldwide, accurate, short and long-term water vapour monitoring studies are undertaken so that the roles that water vapour plays in changing or modifying climate and weather patterns can be better understood.

The Antarctic region is especially sensitive to changes in atmospheric water vapour from both a hydrological and energy balance perspective. Changes in atmospheric water vapour directly affect the potential amount of precipitation and accumulation occurring over the Antarctic continent and therefore contribute to alteration of the mass budget of the polar ice sheet (Weller, 1992). In the global energy cycle, the polar ice-cap acts as a "heat sink" which drives the Earth's circulation patterns, a process that is partially controlled by the amount of water vapour present in the atmosphere over the continent (King and Turner, 1997). These two climate processes are highly sensitive to variations in water vapour and therefore measuring and monitoring water vapour in the atmosphere is an important part of Antarctic meteorology studies and global climate change research (Weller, 1992). Currently water vapour in Antarctica is measured via radiosonde soundings at the occupied bases and more recently, data from Earth Observing satellite systems have also become available for meteorological studies (King and Turner, 1997). There is still however, a great need for better, automated systems for measuring water vapour

more regularly in coastal areas and for providing a better coverage of information in the remote regions of Antarctica (Connolley and King, 1993).

GPS meteorology is a relatively new and potentially very useful method for improving global water vapour measurements especially in remote locations (e.g. Bevis *et al* (1992), Duan *et al* (1996) and Emardson *et al* (1998)). All GPS observations are affected by the refractivity of the atmosphere, which is partially caused by the presence of water vapour along the signal path. Many studies over the past decade have investigated using the refractivity errors in the GPS data as an indirect measurement of the amount of water vapour in the atmosphere. Results from these GPS studies have shown that the values estimated using this method compare well against more traditional techniques with the respective amounts differing by approximately 1-2 mm of equivalent precipitable water (e.g. Rocken, Van Hove *et al* (1995), Duan *et al* (1996), Tregoning, Boers *et al* (1998) and Emardson *et al* (2000)). The main advantages of using GPS meteorology are that it provides an accurate, automatic, low cost, low maintenance, all weather and continuous method of monitoring the long and short term temporal variation in water vapour at a given location (Rocken, Van Hove *et al*, 1997; Bar-Sever *et al*, 1998). GPS meteorology has many applications in meteorological studies including forecasting, observation of significant weather events and climate monitoring. The technique is most useful when data from a network of receivers are analysed, thus providing both spatial and temporal information on the movement of water vapour (e.g., Elosegui *et al* (1999) and Rocken, Van Hove *et al* (1997)).

In this chapter the importance of water vapour in both a global and Antarctic context is summarised. Some of the most common methods used for measuring water vapour in the atmosphere are then outlined followed by a discussion of the theory of GPS meteorology and the errors encountered when using this technique.

6.2 Water Vapour

6.2.1 Global Water Vapour

> "Water vapour is one of the meteorological variables needed to fully define the state of the atmosphere. It is an important source of heat driving circulations and acts to modify atmospheric radiative properties through direct absorption of infrared radiation and by the formation of clouds.

Water vapour figures prominently in the Earth's hydrological cycle through its role as a storage term giving rise to precipitation, and its variation with height is a prime factor in determining convective stability " (Melfi *et al*, 1989).

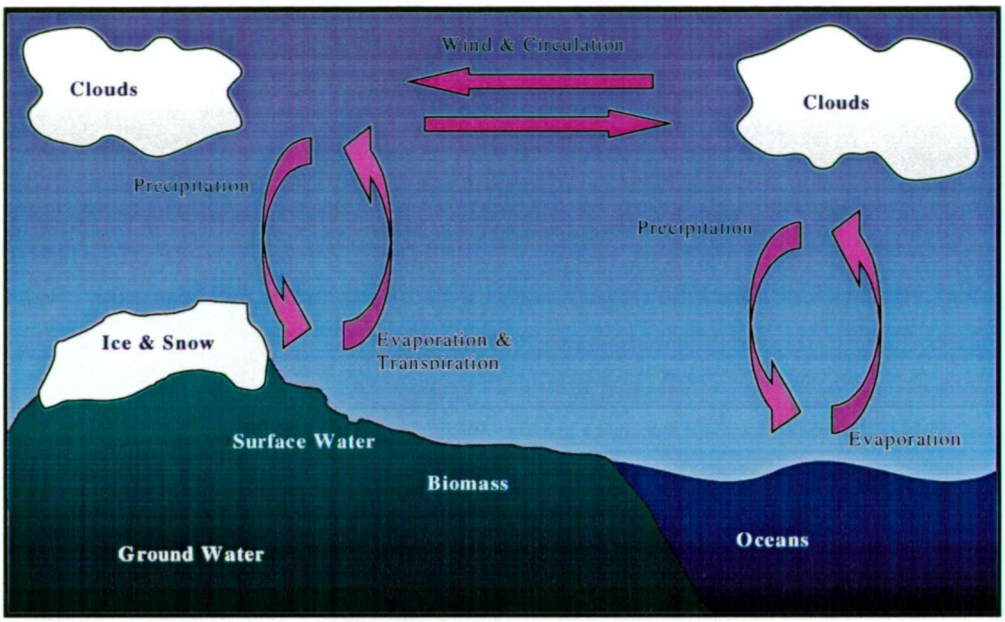

Figure 6.1 - Schematic diagram of the hydrological cycle (adapted from Elliot *et al* 1995)

6.2.1.1 Water vapour in the hydrological cycle

Water vapour plays a fundamental role in the energy and hydrological cycles that control the weather and climate of the Earth. The hydrological cycle (see Figure 6.1) is driven by the movement of water in its three phases between the atmosphere, oceans and continents and the subsequent transfer of energy between the atmosphere and Earth and between low and high latitudes (Elliott *et al*, 1995). At one point in the cycle, water is evaporated or transpirated/respirated into the atmosphere from oceans, land and biological sources. Once inside the atmosphere, water vapour is transported and dispersed via temperature gradients, winds and global circulation systems that cause it to be distributed globally in both a vertical and horizontal manner. At some time after entering the atmosphere, water vapour will condense into either the solid or liquid phase and fall back to the Earth's surface to complete the cycle (see Figure 6.1). The major mechanisms of this hydrological cycle are well known, however some of the smaller details and dynamics are poorly understood mostly due to our incomplete knowledge of the temporal and spatial variability and distribution of water vapour (Elliott *et al*, 1995).

The water vapour component of the hydrological cycle has a dual purpose. The process of evaporation, transportation and condensation requires an initial input of energy (mainly from the sun) which is stored within the water vapour molecules as latent heat. This initial energy is then redistributed throughout the atmosphere via the movement of the water vapour and is released as sensible heat when the water vapour condenses. The release of sensible heat warms the atmosphere which then contributes to the formation of atmospheric circulation systems and is therefore an important factor in the development of climate and weather patterns (Elliott *et al*, 1995).

The spatial distribution of water vapour around the Earth is linked to the distribution of surface temperature, i.e., it decreases from the equator towards the poles, but this pattern can vary in localised areas especially the desert and ocean regions (Elliott *et al*, 1995). In a temporal sense, water vapour varies at a given location on time scales from minutes to seasons and decades. The seasonal and decadal patterns are generally linked to changes in temperature and atmospheric circulation while local short-term variations are dependent on weather patterns, location and local topography.

6.2.1.2 Water vapour as a greenhouse gas

Water vapour is the most important and abundant greenhouse gas in the atmosphere and as such, the atmospheric component of the hydrological cycle is a significant concern in climate change studies (IPCC, 1992).

Greenhouse gases allow incoming short-wave solar radiation to penetrate the Earth's atmosphere but block outgoing long-wave radiation from escaping thus keeping the Earth and its atmosphere warm. Water vapour in its role as a greenhouse gas is involved in an important climate change feedback loop. For example, an increase in air temperature should produce an increase in evaporation leading to a greater concentration of water vapour in the atmosphere. This extra water vapour will then act to absorb more of the outgoing radiation thus causing further atmospheric warming. This water vapour feedback process and its effect on future climate change are not fully understood due, in part, to a lack of extensive water vapour data to accurately represent current and past conditions which would provide a sound basis for testing of the modelling theory (Elliott *et al*, 1995).

Variation in atmospheric water vapour is widely acknowledged as a key indicator of climate change due to the role of water vapour in the greenhouse process and its sensitivity to changes in other greenhouse gases. Monitoring water vapour is therefore important for understanding current conditions and detecting significant changes over time as well as for providing input into predictive studies of the Earth's atmosphere and climate (Elliott *et al*, 1995).

6.2.2 Antarctic Water Vapour

As discussed in section 1.3, Antarctica plays a central role in the Earth's hydrological cycle and circulation systems and is widely recognised as a region that is sensitive to global climate change. The study of Antarctic meteorology is therefore an essential component of investigations related to these topics (Bromwich and Parish, 1998).

The most important characteristic of Antarctic water vapour in terms of significance to the global hydrological cycle is that it is the source of all ice residing in the continental ice sheets (King and Turner, 1997). The transport of water vapour into and out of the Antarctic atmosphere is therefore a crucial element in terms of monitoring change in the mass balance of the ice sheets and the effect of this change on sea level (King and Turner, 1997).

In the global circulation system, the Antarctic ice cap acts as an atmospheric heat sink where there is a net loss of energy to space and the atmosphere is cooled (King and Turner, 1997). This phenomenon is caused by a lack of significant incoming heat from solar radiation, high levels of out-going radiation due to the albedo of the snow/ice surface and the lack of absorption of this outgoing energy because of the low water vapour content of the Antarctic atmosphere (King, and Turner, 1997). The Antarctic's role as a heat sink is extremely important in a global sense as it controls and drives the circulation patterns for the rest of the Southern Hemisphere (King and Turner, 1997).

The immense size and hostile environment of Antarctica makes it a difficult place to perform ground-based meteorological studies that provide adequate coverage over the entire continent. The measurements which are currently made from ground based observations at populated stations (i.e., radiosonde soundings) are affected by accuracy problems due to the limitations of the sensing equipment in cold temperatures. Connolley and King (1993) studied variations in total column moisture (TCM) results caused by the introduction of a temperature error of 0.5 K and a relative humidity error of 10% into Antarctic radiosonde soundings. From this experiment, they concluded that Antarctic TCM estimations may potentially be in error by up to 20%.

If effective observation methods were available, variations in atmospheric water vapour may be easier to detect than changes in air temperature or ice-sheet mass balance due to the high sensitivity of water vapour content in response to climate change (Reid, 2000). Improvements in predictions, current understanding and monitoring of Antarctic water vapour require the collection of greater amounts of and more spatially distributed data. Satellite technology will be very useful in this sense but ground-based observations are also important.

6.2.3 Measuring Water Vapour

There are many methods for measuring water vapour in the atmosphere. Each method has its advantages and disadvantages regarding cost, accuracy, efficiency, spatial coverage and temporal resolution. Some of the most commonly used methods in climate and weather studies are shown in Figure 6.2 and described in the following paragraphs.

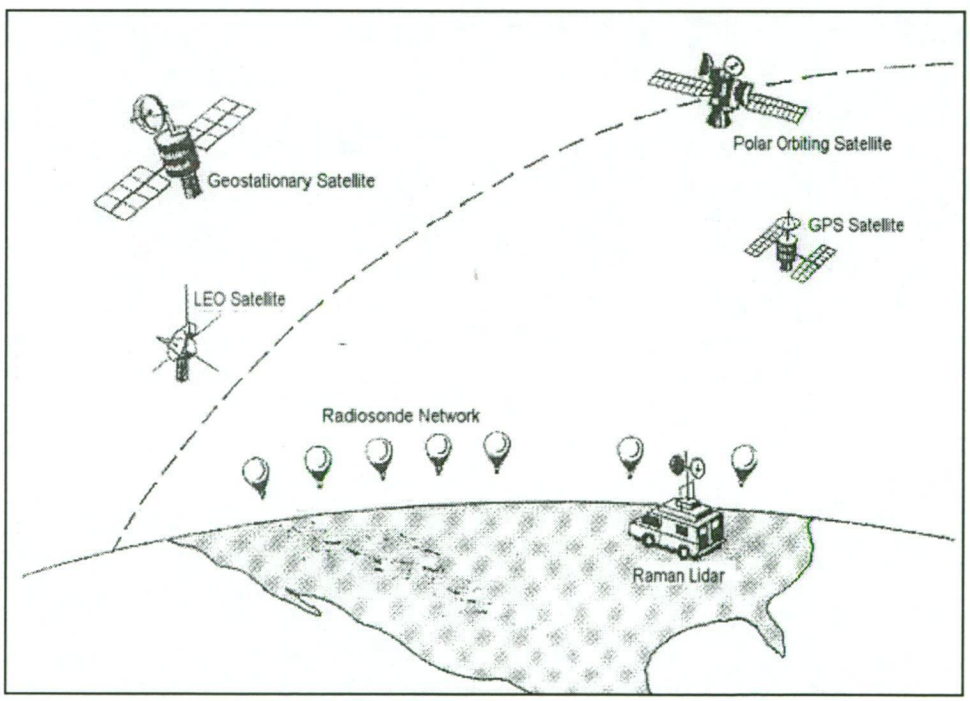

Figure 6.2 - Examples of water vapour measurement systems (adapted from Elliott *et al*, 1995)

6.2.3.1 Radiosondes

Radiosondes are the most commonly used method for water vapour measurement in forecasting and general meteorological applications. These devices consist of a hydrogen filled balloon with an attached sensor array that detects temperature, humidity, and pressure as the balloon rises through the layers of the atmosphere. Radiosondes are reasonably costly to run long-term and require trained observers to

fill, release and track the balloons. Therefore, they are only released at a limited number of locations once or twice a day thus providing a poor spatial and temporal coverage of global atmospheric water vapour (Bevis *et al*, 1992). Each ascent of a radiosonde provides data at a number of levels through the atmospheric profile. In order to measure the amount of total water vapour observed in the sounding, the mixing ratio at each level is determined and then integrated along the sonde trajectory (Stull, 1995).

Radiosondes are not perfect, their instruments have calibration errors and it has been shown that most humidity and temperature sensors do not perform as well in cold and dry atmospheres (Elliott and Gaffen, 1991; Connolley and King, 1993). In addition, due to the wind profile of the atmosphere, the path of the balloon will not be directly above the release point or go in the same direction for each release which results in variation of the actual sampling path between soundings.

Currently in Antarctica, most occupied stations launch one or two radiosondes per day (Connolley and King, 1993). Most of these sites are located on the coast with very few radiosonde measurements collected in the interior. Although many of these sites have a long (20+ yr.) history of measurements and therefore a good long-term time-series, they lack information on the short-term variability and more importantly, the spatial distribution of this important meteorological variable (Connolley and King, 1993).

6.2.3.2 Water Vapour Radiometer (WVR)

WVRs radiate signals at microwave frequencies and measure the atmospheric emissions (brightness temperature) caused by the amount of water vapour and liquid water present in the atmosphere in the direction of the signal path (Sierk *et al*, 1997; Tregoning, Boers *et al*, 1998). The brightness temperature is converted to a measure of PW using an equation that requires knowledge of retrieval coefficients which are site and seasonally dependant. In each experiment, these coefficients must be calculated for the study site using an independent method, such as local radiosonde soundings (Bevis *et al*, 1992). Additionally, in order to determine the relationship between the incoming signal and the measured brightness temperature, a set of calibration constants for the WVR must be determined. This is usually carried out by using a tipping curve calibration technique (Sierk *et al*, 1997; Tregoning, Boers *et al*, 1998).

The WVR antenna has the capability of making PW measurements quickly and in multiple directions. Using this technique, atmospheric water vapour is sampled frequently and thoroughly, thus providing good horizontal, vertical and temporal measurements of the water vapour variations in the vicinity of the WVR.

Unfortunately, the WVR equipment is large and costly and requires the frequent attention of operators for calibration (Wolfe and Gutman, 2000). These factors mean that WVRs are generally not used for day to day meteorological observations and forecasting purposes. There are not many of these systems operating around the world and therefore the spatial coverage of the observations is limited to the local area of the WVR. The other major disadvantage of this system is that it does not perform well in times of heavy cloud and it provides almost no useful information during precipitation events (Bevis *et al*, 1992).

6.2.3.3 LIDAR

Raman LIDAR systems are essentially laser systems that can sample various constituents and characteristics of the atmosphere by measuring backscatter. The instrument consists of a vertically pointed laser, aligned parallel to the optical axis of a telescope (Melfi *et al*, 1989). The laser is fired and the telescope collects the backscattered light as the laser propagates through the atmosphere and splits this light into three channels sensitive to scattering by water vapour, nitrogen and aerosols respectively (Melfi *et al*, 1989). The ratio of the measured scattering by water vapour and nitrogen is proportional to the atmospheric mixing ratio, from which a determination of PW can be obtained (Melfi *et al*, 1989).

One of the benefits of the LIDAR system is that the vertical profile above the instrument can be sampled once every two minutes thus providing excellent temporal information on the passage of water vapour (Melfi *et al*, 1989). The major limitations of LIDAR systems are their cost, size and poor spatial sampling capabilities (i.e., vertical only) which prevent them from being useful as a general meteorological tool.

6.2.3.4 Satellites

Some of the environmental/Earth observing satellites carry infrared and microwave radiometers that measure brightness temperature in the nadir direction (e.g. GOES, TOVS, SSM/I) against the background of a relatively warm Earth surface (Bevis *et al*, 1992; UCAR, 1999). These sensors provide very good spatial coverage of global water vapour content which is especially important over the oceanic and polar regions. This extensive spatial information is extremely valuable to global meteorological studies as many regions of the Earth are not generally well sampled using ground based techniques (UCAR, 1999).

These satellite based sensors are not as efficient/accurate as they potentially could be because the variability in the heat of the continental areas complicates the water vapour measurement (Bevis *et al*, 1992). Clouds also cause problems with many space-based measurements of water vapour (especially with the infrared sensors) due to the measurement background changing from the relatively hot Earth surface to the cool surface of the cloud tops (Bevis *et al*, 1992).

In general, space-based infrared sensors collect their most useful water vapour data over oceanic and polar regions but these measurements are not at all reliable in the presence of clouds (Elliott *et al*, 1995). Data from satellite microwave sensors are less influenced by cloud cover but are limited to measurements over ice-free oceanic regions (Elliott *et al*, 1995). Therefore it can be said that satellite-based measurements of water vapour are capable of providing reasonable spatial but poor temporal information on the global content of water vapour in the atmosphere.

6.2.3.5 Low Earth Orbiting (LEO) GPS receiver

The GPS occultation method stemmed from a technique that was originally designed to sample the atmospheres of other planets. The basis of this technique is that a GPS receiver on a LEO satellite makes phase measurements of GPS signals as they occlude the Earth's atmosphere and are refracted (see Figure 6.3). The GPS satellite and the LEO satellite have known orbits and therefore errors in the distance between the two are due to tropospheric and ionospheric refraction (Bevis *et al*, 1992; Yuan *et al*, 1993). Using similar techniques as for ground-based GPS measurements (see section 2.1.1), the ionospheric delay may be estimated and removed, thus leaving the signal from the neutral atmosphere which can then be used to acquire information on the temperature and humidity of the sampled region.

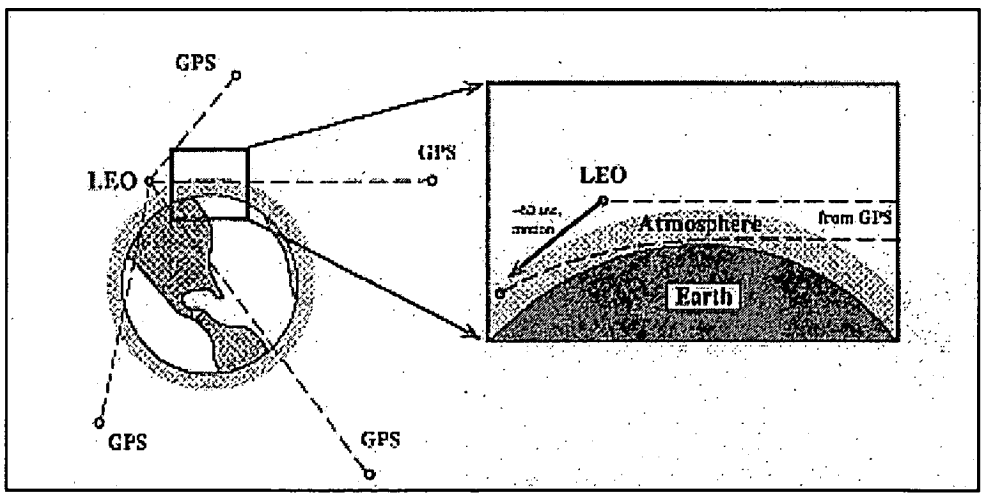

Figure 6.3 - The LEO GPS occultation method (from Bevis *et al* (1992) after Hardy *et al* (1992))

Occultation occurs at a LEO satellite when a GPS satellite rises and sets with respect to the apparent horizon. Bevis *et al* (1992) state that this will occur roughly 600 times per day for a single LEO satellite. They also conclude that a typical occultation measurement will sample a region of the atmosphere 200km long and 1km in vertical extent. There are hundreds of LEO satellites orbiting the Earth at altitudes of up to around 1000km (Bevis *et al*, 1992). Most of these satellites are primarily launched for communications and Earth observing purposes and in order for them to be useful to GPS sensing of the atmosphere all they need do is carry a GPS antenna/receiver. With the large number of potentially available satellites and the predicted number of occultations per satellite, this system could theoretically provide an extraordinary amount of temporal and spatial information on the Earth's atmosphere (Bevis *et al*, 1992).

A demonstration LEO GPS system (GPS/MET) was established by the University Corporation for Atmospheric Research and launched aboard MicroLab-1 in 1995 (Rocken, Anthes *et al*, 1997). Rocken, Anthes *et al* (1997) report that due to system deficiencies in this experiment, the GPS/MET instrument was only able to collect at most 150 soundings per day. This experiment was however highly successful and retrieved vertical profiles of ray bending angle and refractivity which were then used to extract data on the ionospheric electron density, neutral atmospheric density, pressure, temperature and moisture profiles (Rocken, Anthes *et al*, 1997). Following on from the success of this 'proof of concept' experiment, a new LEO GPS system of eight satellites is being planned for launch in 2004 (Anthes *et al*, 2000). This new system, termed COSMIC (Constellation Observing System for Meteorology, Ionosphere and Climate), will provide global coverage of the atmosphere with an expected 4000 soundings per day (Anthes *et al*, 2000). Anthes *et al* (2000) show that a significant number of soundings will be made over the poles (see Figure 6.4) providing valuable new information to many polar science and meteorology programs.

The LEO occultation method of water vapour observation is now recognised as a valuable, relatively simple and inexpensive means of collecting large amounts of global atmospheric measurements for the use of weather, climate and global change research (Rocken, Anthes *et al*, 1997; Anthes *et al*, 2000).

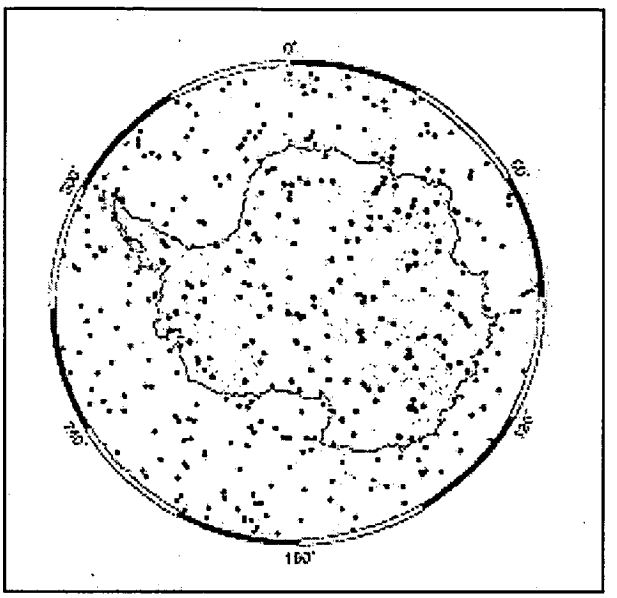

Figure 6.4 - Projected COSMIC soundings in the antarctic region (from Anthes *et al* (2000))

6.2.3.6 Ground-based GPS

Data collected at ground based GPS receivers allow the indirect measurement of water vapour by conversion of the error in the received signal due to refractivity of the atmosphere caused by the presence of water vapour.

The GPS meteorology technique's main advantages are that it provides an accurate, automatic, low-cost, low maintenance, all weather and continuous method of monitoring the long and short term temporal variation in water vapour at a given location (Rocken, Van Hove *et al*, 1997; Bar-Sever *et al*, 1998). GPS meteorology therefore has many applications in meteorological studies including forecasting, observation of significant weather events and climate monitoring. The technique is most useful when data from a network of receivers are analysed, thus providing both spatial and temporal information on the movement of water vapour (Elosegui *et al*, 1999).

This GPS-based technique is the focus of the remainder of this chapter and will be discussed in more detail, together with its associated limitations and error sources, in the following sections.

6.3 Estimating the Tropospheric Delay in GPS Observations.

6.3.1 The Troposphere

The neutral section of the Earth's atmosphere encompasses the regions known as the troposphere and stratosphere. The tropospheric layer is not a constant thickness, it varies depending on location and season and its upper limit ranges in altitude from approximately 9km at the poles to approximately 16km at the equator (Brunner and Welsch, 1993). Most of the Earth's 'weather' (including water vapour) is contained within this section of the atmosphere and within this zone, temperature will generally decrease with altitude (Langley, 1996). The stratosphere extends the neutral atmosphere to a height of approximately 50km but the bulk of the neutral atmosphere is contained within the tropospheric layer (Brunner and Welsch, 1993). These two layers of the atmosphere contain many neutral atoms and molecules which affect the propagation of the GPS signals and cause an error in the measured distance (Langley, 1996). These effects are predominantly caused by the constituents of the air in the tropospheric layer, and therefore from this point forward, the term *troposphere* will be used to refer to the entire neutral section of the atmosphere (i.e., the layer between 0 and 50 km altitude).

6.3.2 Tropospheric Delay

The tropospheric constituents affect the GPS signal causing both a bending (compared to the straight line assumed when travelling through a vacuum) and a delay due to the refractivity of this section of the atmosphere (see Figure 6.5). In the equation for the tropospheric range error (or *tropospheric delay*, TD) given below, the two components of the effect on the GPS signal, slowing and bending, are represented by the first and second terms on the right hand side of the equation (Langley, 1996)

$$TD = \int_{r_s}^{r_a} [n(r) - 1] \operatorname{cosec} \theta(r) dr + \left[\int_{r_s}^{r_a} \operatorname{cosec} \theta(r) dr - \int_{rs}^{r_a} \operatorname{cosec} \varepsilon(r) dr \right] \qquad (6.1)$$

where: n = refractive index

r = geocentric radius

θ = refracted satellite elevation angle

ε = non-refracted satellite elevation angle

r_s = geocentric radius of the earth's surface

r_a = geocentric radius of the top of the neutral atmosphere

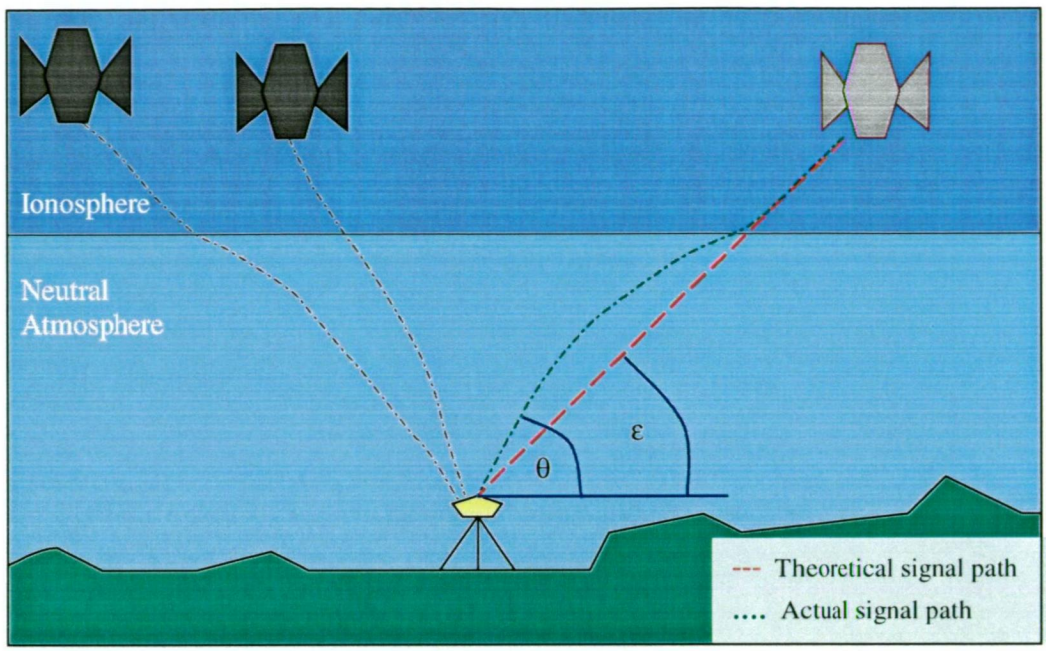

Figure 6.5 - The effect of the neutral atmosphere on the GPS signals

When examining the path of a signal coming from the zenith (total zenith delay, TZD), the bending term becomes zero giving:

$$TZD = \int_{rs}^{ra} [n(r) - 1] dr = 10^{-6} \int_{rs}^{ra} N dr \tag{6.2}$$

where N is the refractivity of the troposphere, which is related to the temperature (T) and the partial pressures of the dry gases (P_d) and of water vapour (e). Refractivity can generally be expressed as (Thayer, 1974):

$$N = k_1 \left(\frac{P_d}{T} \right) Z_d^{-1} + \left[k_2 \left(\frac{e}{T} \right) + k_3 \left(\frac{e}{T^2} \right) \right] Z_w^{-1} \tag{6.3}$$

where k_1, k_2, k_3 are empirically determined refractivity constants (discussed in section 6.4.2) and Z_d, Z_w are compressibility factors for dry air and water vapour respectively and are close to unity (Langley, 1996). Equation (6.3) indicates that N is independent of frequency and therefore the tropospheric delay can not be removed using a dual frequency technique as used to remove the effects of the ionospheric delay from the GPS signal (see section 2.1.1).

Davis *et al* (1985) showed that the refractivity equation may be redefined so that the first term is only dependant upon the total moist air density (ρ), where:

$$N = k_1 R_d \rho + \left[k_2' \left(\frac{e}{T} \right) + k_3 \left(\frac{e}{T^2} \right) \right] Z_w^{-1} \tag{6.4}$$

and R_d is the gas constant for dry air. In the above equation, the first term represents the induced dipole moment of the atmosphere (associated with both dry air components and water vapour) and is usually termed the *hydrostatic* component of the total delay. The bracketed expression represents only the effect of the permanent dipole moment of water vapour, commonly referred to as the *wet* component of the total delay.

The hydrostatic effect accounts for approximately 90% of the total delay and may be determined to within a few millimetres from surface pressure measurements and assuming hydrostatic equilibrium (Langley, 1996). The wet delay however, varies greatly with respect to location and time and can not be predicted accurately from surface meteorological information due to the random and dispersive nature of water vapour in the atmosphere (Bevis *et al*, 1992; Langley, 1996). Hydrometeors (e.g., fog, rain, hail, snow and ice) also have some impact on the refractivity along the signal path if they are present in the atmosphere. Solheim *et al* (1999) concluded that the delays caused by these particles are highly variable and are less than 3% of the largest total delay. The unknown size and spatial distribution of the hydrometeors makes it virtually impossible to model delays which are caused by their presence in the atmosphere (Solheim *et al*, 1999).

6.3.3 Tropospheric Models and Mapping Functions

The equation of the tropospheric delay for a GPS signal arriving from the zenith direction was introduced in section 6.3.2 (equation (6.2)). In reality, signals arrive at GPS antennas from many directions and therefore mapping functions that relate the observed delay to the zenith delay are required in order to accurately reflect the passage of the signals through the atmosphere.

Many such mapping functions have been developed over the past few decades for use in various geodetic and radio applications. These mapping functions have been adopted by GPS users who have also assisted in developing new ones.

Most mapping functions for tropospheric delay take the form (Langley, 1996):

$$TD = d_h^z m_h(\varepsilon_s) + d_w^z m_w(\varepsilon_s) \tag{6.5}$$

where:

d_h^z = zenith delay due to hydrostatic components
d_w^z = zenith delay due to water vapour
m_h = hydrostatic mapping function
m_w = wet mapping function
ε_s = non-refracted elevation angle

This equation requires models of the hydrostatic and wet zenith delays to be constructed and then corrected using a mapping function to account for the elevation angle of the signal. There are only a few commonly used models for the hydrostatic delay. These are generally based on well-known atmospheric properties and are therefore very accurate. Wet delay models are harder to construct so that they are sufficiently accurate for all places and times. Many wet delay models have been developed over the past three decades but all have expected accuracies of only a few centimetres of delay (Mendes and Langley, 1995).

6.3.3.1 Hydrostatic delay models

It has been widely demonstrated that the hydrostatic component of the tropospheric zenith delay may be estimated to a good degree of accuracy from knowledge of surface pressure and an assumption that the atmosphere is in hydrostatic equilibrium. The most commonly used model for the hydrostatic zenith delay (HZD) is that of Saastamoinen (1972) which follows from equation (6.4) and is here written in the terms of Davis *et al* (1985):

$$HZD = 10^{-6} k_1 R_d \frac{P_s}{g_m}$$

or (6.6)

$$HZD = (0.0022768 \pm 0.0000005) \times \frac{P_s}{f(\varphi, h)}$$

where: k_1 = refractivity constant (77.60 Kmbar^{-1})

R_d = gas constant for dry air (0.287053 kPaK^{-1}m^{3}kg^{-1})

g_m = gravitational acceleration $(9.784 \cdot f(\varphi, h)\ \mathrm{ms}^{-2})$

P_s = pressure at GPS antenna (hPa)

$f(\varphi, h) = (1 - 0.0026\cos 2\varphi - 0.00028h)$

φ = geocentric latitude of GPS site

h = height of GPS site above ellipsoid (km)

The other hydrostatic zenith delay model that is commonly used in conjunction with tropospheric mapping functions is the Hopfield (1969) model. This model is based on a single-layer polytropic model, with the atmosphere ranging between the surface and 40 km and parameter values (H_1, H_2 and μ) determined by fitting to one year's radiosonde data at fourteen western hemisphere sites (Janes *et al*, 1991).

The Hopfield model calculates the refractivity effect on the dry (and wet) zenith delay using (Janes *et al*, 1991):

$$N_i(h) = N_{is}\left(\frac{H_i - h}{H_i}\right)\mu \tag{6.7}$$

where: N_i = the refractivity
$i = 1$ (for the dry component)
$i = 2$ (for the wet component)
s = surface
h = height above the tracking station (m)
μ = a constant (= 4)
H_1 = dry term scale height $(40136m + 148.72m/°C \times T_c)$
T_c = mean column temperature (°C)
H_2 = wet term scale height $(11000m)$

and then solves for the total zenith delay:

$$TZD = \frac{10^{-6}}{5}[N_{1s}H_1 + N_{2s}H_2] \tag{6.8}$$

6.3.3.2 Wet delay models

Many attempts have been made at modelling the wet zenith delay, most of which either assume an atmospheric water vapour profile based on surface measurements (some in conjunction with site location) or are formulated from analysis of radiosonde soundings. Most of these models are based on surface measurements of one or more of the following parameters - temperature, humidity and surface pressure. Some models also require the estimation of the water vapour mixing ratio and/or the temperature lapse rate of the atmosphere.

An example of a commonly used model of the first type is the Saastamoinen (1973) wet zenith delay model which is based on the assumption that water vapour decreases with height. The Saastamoinen (1973) equation for the wet zenith delay (WZD) is:

$$WZD = 0.0022768\frac{\left(\frac{1255}{T_s} + 0.05\right)e_s}{f(\varphi, h)} \tag{6.9}$$

where:
T_s = surface temperature
e_s = surface partial pressure of water vapour
$f(\varphi, h)$ = as in equation 6.6

Hopfield's model (equations (6.7) and (6.8)) is a commonly used model of the second type as is the global model developed by Ifadis (1986). Ifadis (1986) created a series of models for the wet zenith delay (global, seasonal and climate dependent) using regression analysis of radiosonde data. From this analysis, a weak link between zenith wet delay and atmospheric temperature, pressure and water vapour pressure was uncovered and the following equation (6.10) was developed (Mendes and Langley, 1995).

$$WZD = 0.00554 - 0.880^{-4}(P - 1000) + 0.272^{-4}e + 2.771\left(\frac{e}{T}\right) \qquad (6.10)$$

Testing of the accuracy of these and other wet zenith models by Janes *et al* (1991) and Mendes and Langley (1995) was carried out by comparing model results to standard atmosphere ray traces[1] and radiosonde profiles respectively. Both of these studies concluded that accurate wet zenith delays (better than a few centimetres) could not be predicted using any of the global models and that the Saastamoinen and Ifadis models were recommended for use from those models tested. The Janes *et al* (1991) study found that the Hopfield and Saastamoinen models had the lowest sensitivity to the water vapour content of the atmosphere, with the Hopfield model producing the best results (compared to standard atmosphere) for low to middle latitudes and the Saastamoinen model performing better for middle to high latitudes.

6.3.3.3 Mapping functions

A large number[2] of hydrostatic and wet mapping functions have been developed by many authors over the past few decades in order to map modelled zenith delays to the true microwave signal paths. The majority of these mapping functions can be divided into two groups i) those based on the Hopfield (1969) model and ii) those based on the Marini (1972) model. Currently, the most commonly used functions in GPS processing are those devised by Niell (1996) (Niell), Davis *et al* (1985) (CfA-2.2), Lanyi (1984) (Lanyi) and Herring (1992) (MTT).

The Hopfield-type mapping functions are based on his single layer polytropic model and are generally arrived at by using a series expansion of Snell's law (equation (6.11)) assuming a spherical atmosphere of uniform refractivity and neglecting the effects of path curvature on the signal propagation (Janes *et al*, 1991).

[1] Ray-tracing involves following a path at a given elevation angle through the radiosonde humidity and temperature profiles to determine the size of the wet and hydrostatic delays.
[2] Refer to the papers by Janes *et al* (1991), Mendes and Langley (1994), Langley (1996) and Niell (1996) for original citations and evaluation of most of the widely used mapping functions over the past three decades.

$$\sec\theta(r) \cong \sec\varepsilon(r) = \left(1 - \left(\frac{r_s^2}{r^2}\right)\sin^2\varepsilon_s\right)^{-\frac{1}{2}} \tag{6.11}$$

where:

θ = the refracted elevation angle

ε = the true satellite elevation angle

ε_s = the true satellite elevation angle at the ground station

r = the geocentric radius

r_s = the geocentric radius of the earth's surface

The Marini-type functions are based on the continued fraction formula of Marini (1972) which can generally be written as:

$$m(\varepsilon) = \cfrac{1}{\sin(\varepsilon) + \cfrac{a}{\sin(\varepsilon) + \cfrac{b}{\sin(\varepsilon) + \cfrac{c}{\sin(\varepsilon) + \ldots}}}} \tag{6.12}$$

where the coefficients a, b, c...etc. are constants or linear functions determined from the methodology used by the individual authors. The Niell, CfA-2.2 and MTT mapping functions belong to this continued fraction category.

Researchers from the Geodetic Research Laboratory at the University of New Brunswick have carried out several studies (in collaboration with researchers from other centres) evaluating the merits of the most common mapping functions (e.g. Janes *et al* (1991), Mendes and Langley (1994) and Santerre *et al* (1995)). In the first two of the cited studies, the researchers compared the tropospheric delays obtained from each of the mapping functions to the values obtained via ray tracing through standard or actual atmospheres and rated each function accordingly. The Mendes and Langley (1994) study evaluated the performance of the mapping functions by examining the differences in the station height results obtained from each determination of the tropospheric delay.

Mendes and Langley (1994) concluded that:

a) for elevation angles above 30°, nearly all functions produced height errors of less than 5 mm with MTT, Ifadis, Lanyi, Niell and Baby (Baby *et al*, 1988) providing sub-millimetre results.

b) for the 10° elevation angle tests, the mapping functions broke into distinct groups. The least accurate results were found when using the Hopfield based mapping functions. This poor result was attributed to neglect of the bending term in the refractivity equation. The best performing functions were those based on the Marini model plus the Baby, Lanyi and CfA2.2 functions.

In their summary, Mendes and Langley (1994) noted that the Niell, Ifadis and MTT models performed outstandingly well at all elevation angles, even when below 10°. They also remarked that the Niell mapping function produced slightly poorer results at the high latitude sites compared to other locations. Their final recommendation was that for high precision applications, the MTT, Ifadis or Niell functions should be used.

Santerre *et al* (1995) studied the effect of different mapping functions on the GPS estimates of site coordinates and concurred with Mendes and Langley (1994) that the Hopfield based functions produced poorer results than the others. They recommended that the same three functions (MTT, Ifadis, and Niell) be used for geodetic research.

In this thesis, the Niell hydrostatic and wet mapping functions have been used in conjunction with Saastamoinen modelling of the wet and hydrostatic delay. These procedures have been selected according to the available a priori meteorological data for the study region/period and the recommendations of the major studies (e.g., Mendes and Langley (1994), Santerre *et al* (1995) and Janes *et al* (1991)). The Saastamoinen models have been discussed previously in sections 6.3.3.1 and 6.3.3.2; the following is a discussion of the Niell mapping functions.

Niell mapping function

Niell (1996), devised continued fraction representations of the hydrostatic and wet mapping functions, and determined coefficients for these fractions which are dependent only on the latitude, height above sea level and day of the year[3]. The most significant characteristics of the Niell (1996) mapping functions are that they require no a priori meteorological information in order to produce very accurate results and they can be used reliably down to an elevation angle of 3°.

[3] Note that the wet mapping function constants are only dependant on the latitude of the site of interest.

Niell's mapping functions are based on the continued fraction mapping function normalised to unity at the zenith as per Herring (1992):

$$m(\varepsilon) = \frac{\left[\dfrac{1}{1+\dfrac{a}{1+\dfrac{b}{1+c}}}\right]}{\left[\dfrac{1}{\sin(\varepsilon)+\dfrac{a}{\sin(\varepsilon)+\dfrac{b}{\sin(\varepsilon)+c}}}\right]} \tag{6.13}$$

where:

a, b, c = function coefficients

ε = satellite elevation angle

Niell used ray-tracing through temperature and relative humidity profiles of the US standard atmospheres for January and July at latitudes 15°N, 30°N, 45°N, 60°N and 75°N to determine the average value at each latitude for the coefficients a, b and c of the hydrostatic and wet forms of his mapping function. To determine the change in the value of the hydrostatic coefficients with respect to time, Niell modelled a, b and c at all latitudes (assuming zonal symmetry) as a sinusoid with a 365.25 day period and estimated a value for the amplitude of each model (a constant phase was adopted for all of the models). The values resulting from these analyses are tabulated in Niell (1996).

To determine the values of the wet coefficients for the observation site, a linear interpolation between the values at the nearest study latitudes is required. The hydrostatic coefficients for a given site on a given day are found by interpolating between the time dependant values (see equation (6.14)) of the coefficient at the nearest study latitudes. For regions between 0° - 15° N/S and 75° - 90° N/S, no interpolation is available and the values for the hydrostatic and wet coefficients at 15°N/S and 75°N/S are assumed to apply.

$$x(\varphi_i, t) = x_{avg}(\varphi_i) + x_{amp}(\varphi_i)\cos\left[2\pi\left(\frac{t-T_0}{365.25}\right)\right] \tag{6.14}$$

where: φ_i = study latitude

t = time (UT) since beginning of year

x_{avg} = average value of coefficient (a,b or c)

a_{amp} = amplitude of coefficient (a,b or c)

T_0 = phase of the signal (DOY28 is the adopted value from experimental results)

The hydrostatic mapping function also requires a correction due to the elevation of the given site. Niell determined three height correction coefficients a_{ht}, b_{ht} and c_{ht} which are the input parameters for the equation of the correction to the mapping function (6.15).

$$\Delta m(\varepsilon) = \frac{dm(\varepsilon)}{dh} H \tag{6.15}$$

where:

H = height above sea level

$$\frac{dm(\varepsilon)}{dh} = \frac{1}{\sin(\varepsilon)} - f\left(\varepsilon, a_{ht}, b_{ht}, c_{ht}\right)$$

As mentioned previously (section 6.3.3.3), the Niell mapping functions are amongst the top performing methods in all mapping function studies. In Niell (1996), he compares his functions to those of Herring, Ifadis and Lanyi at a 5° elevation angle. The results of this comparison show that the Niell function has a lower bias in the hydrostatic delay and has similar values for the wet delay (with less a priori information required) than the other functions when compared to ray tracing of radiosonde soundings. In terms of GPS baseline calculations, Niell (1996) showed that the use of his functions improves results at low elevation angles.

6.3.4 Modelling Tropospheric Delay in GPS Processing

In most high level GPS processing software, the tropospheric delay is modelled as a stochastic parameter and estimated at given time intervals using a filtering analysis (e.g., Kalman filter). The use of stochastic estimation allows the value of the delay to change over time thus allowing the temporal nature of the fluctuations to be considered (Tralli and Lichten, 1990; Shardlow, 1994). The parameters are also correlated between time intervals which accounts for the spatial trends in the water vapour distribution (Tralli and Lichten, 1990; Shardlow, 1994).

Within this stochastic process there are usually two parameters which are solved for, either the entire tropospheric delay or a residual to a measured/estimated a priori value of the delay. It is typically not necessary to input accurate measurements of surface meteorology or actual water vapour content of the atmosphere into the solution as the strength of the GPS data should allow solution of the delay parameter without any additional information (Shardlow, 1994). Generally in high precision GPS processing, surface meteorology data, either estimated or measured, are used to determine the a priori tropospheric delay using selected models and mapping functions. The stochastic process can then estimate corrections to these a priori values using the information from the GPS observations (Tralli *et al*, 1988).

Many of the widely used, high precision GPS processing packages (e.g. GIPSY and GAMIT) model residual tropospheric delay as a first-order Gauss-Markov or random walk stochastic process and employ a filtering technique to estimate changes in this parameter.

The first-order Gauss-Markov process may be described using the following equation (Tralli *et al*, 1988):

$$\frac{dp}{dt} = -\frac{p(t)}{\tau_p} + w(t) \tag{6.16}$$

where: p = model parameter corresponding to the zenith delay

τ_p = correlation time of the process

$w(t)$ = zero-mean, white noise random variable of variance σ_w^2 given by the ensemble average of its square:

$$\langle w(t)\, w(t') \rangle = \sigma_w^2 \delta(t - t') \tag{6.17}$$

where $\langle\ \rangle$ denotes the expectation value operator

and $\delta(t - t')$ = the Dirac delta function for times t and t'

A random walk process, where adjacent measurements are uncorrelated occurs when τ_p approaches infinity or becomes very large compared to the time between observations. Equation (6.16) then becomes (Tralli and Lichten, 1990):

$$\frac{dp}{dt} = w(t) \tag{6.18}$$

The discrete solution to the Gauss-Markov equation (6.16) is (Tralli and Lichten, 1990):

$$p(t + \Delta t) = m \cdot p(t) + \left(1 - m^2\right)^{\frac{1}{2}} w(t) \tag{6.19}$$

where:

$m = e^{\left(-\Delta t / \tau_p\right)}$

= a measure of the time correlation between adjacent measurements

Δt = time between adjacent measurements

For a random walk process, this becomes (Tralli and Lichten, 1990):

$$p(t+\Delta t) = m \cdot p(t) + w\sqrt{\Delta t} \tag{6.20}$$

Tralli and Lichten (1990) compared random walk and Gauss-Markov solutions for the tropospheric delay and found no significant differences in the values obtained for either method. Their study found that estimation of the tropospheric delay using these stochastic methods resulted in baseline repeatabilities of a few parts in 10^8 and suggested that GPS data alone are sufficient to determine tropospheric path delays and that a priori calibration with measured WVR or surface meteorology data is not necessary for geodetic quality solutions.

6.3.4.1 GAMIT TZD estimation

The GAMIT software used in this thesis solves for corrections to the a priori zenith delay in a least squares solution where the partial derivative with respect to the tropospheric delay is simply the wet mapping function (King and Bock, 1999). The zenith delay may be solved for as one parameter per site per day or may be divided into a series of delay values at given time intervals and solved for using Gauss-Markov constraints and a piecewise linear function (King and Bock, 1999).

Before processing, the user must specify the a priori meteorological data that they wish to use. That is, either:

1) standard surface meteorological data and modelled delays,
2) measured surface meteorological data and modelled delays,
3) measured WVR readings and pressure data.

The user must also select the atmospheric models and mapping functions to be used to model the tropospheric delay.

As shown in Figure 6.6, the GAMIT solution firstly models the total delay using the input information for the sites, satellites and meteorological parameters with the given models and mapping functions. From this modelling process, an a priori value for the total delay at each observation epoch and a partial derivative (the wet mapping function) for use in the least squares solution of the GPS data are obtained.

Prior to least-squares processing, the user must decide on the number of tabular points to be used in the piecewise function (thus setting the window size for each tropospheric delay estimate), the a priori zenith delay constraint to be applied and the parameters for the stochastic estimation process (correlation time (τ) and point to point variation). If τ is set long compared to the observation span, then a random walk process will occur (see equation (6.18)). If τ is set comparatively short, then a

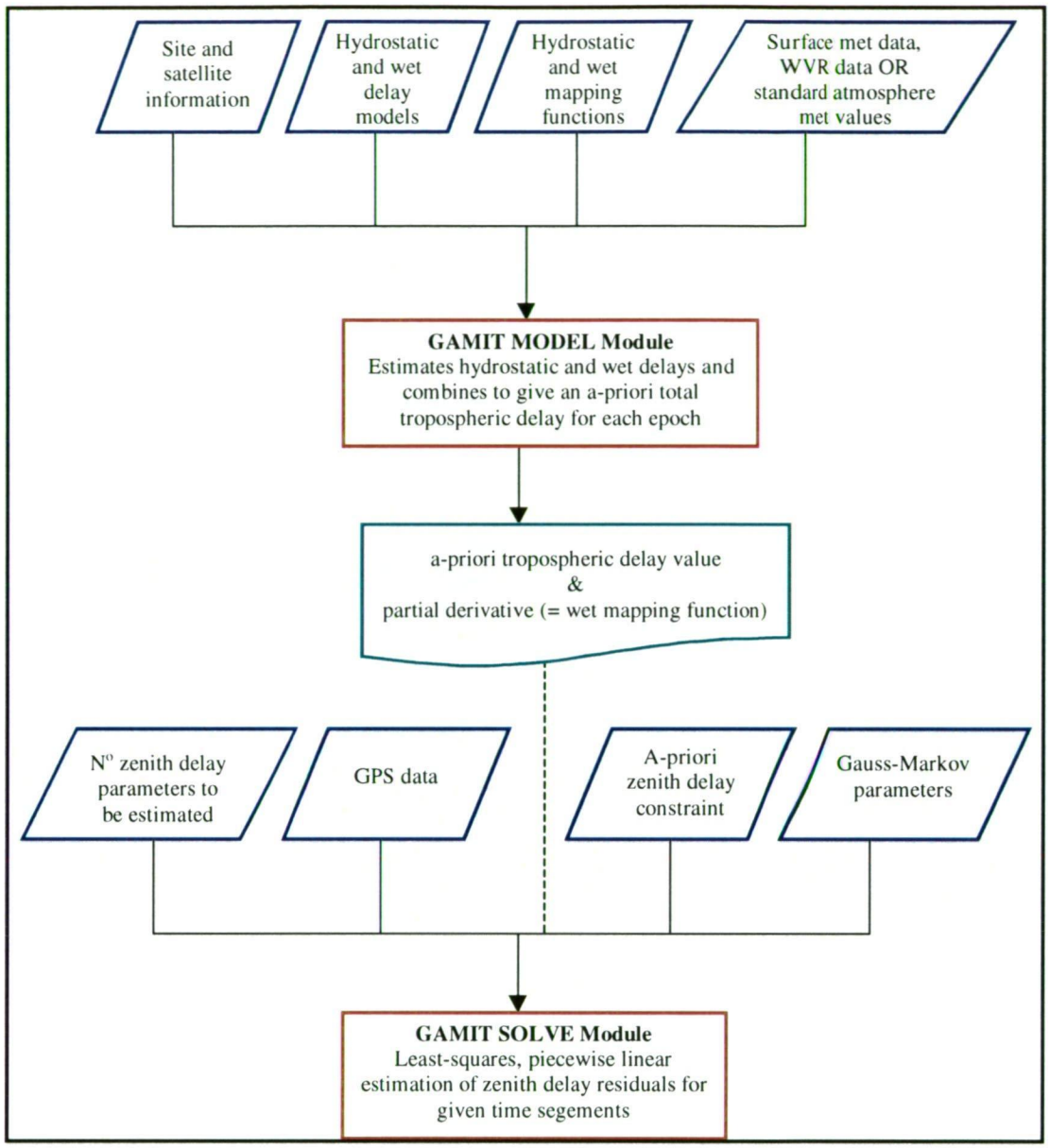

Figure 6.6 - Flowchart of the GAMIT tropospheric zenith delay estimation process.

Gauss-Markov white noise process will occur and the values of subsequent tabular points will depend on the model used and not be based on information from the previous tabular point (King and Bock, 1999).

During the least-squares solution, the piecewise linear solution of tropospheric parameters occurs at each of the tabular points. The contribution from all observations within each zenith delay window is included in the estimate of residual delay for that period.

The results from the GAMIT analysis are the residual tropospheric zenith delay estimates at each tabular point and their 1σ uncertainties. Depending on the input information, the residual delay may represent either the wet delay (i.e., the a priori pressure is correct and therefore the hydrostatic component is 'correct'), the total

delay (i.e., the hydrostatic and wet delay are both given a priori path lengths of 0 mm) or a correction to the estimated total delay (i.e., standard meteorology values or measured pressure and/or WVR data are used in a priori modelling).

6.3.5 GPS Processing Errors in TZD Estimates

The modelling and processing techniques discussed in the preceding sections provide the best possible estimates of the tropospheric zenith delay as observed by the GPS signals. However, in every stage of the estimation process, errors from assumptions and/or adopted parameter values can influence the uncertainty of the final result.

Errors in the tropospheric zenith delay estimation will have a great effect on subsequent PW calculations and importantly, for geodetic purposes, they will also have a large effect on the simultaneously determined station height due to the high correlation between these two parameters (Rothacher and Beutler, 1998). Emardson *et al* (1998) extensively reviewed the errors in PW determination and found that GPS processing generally introduced typical and maximum errors of 0.6 mm and 5.9 mm respectively in the PW estimates over their study area (i.e., Sweden and Finland).

The following sections describe the most significant errors encountered in the estimation of tropospheric zenith delay using GPS techniques.

6.3.5.1 Mapping function errors

There are two major sources of error in most of the commonly used tropospheric delay mapping functions, 1) the assumption of azimuthal asymmetry and 2) the dependence of most functions on at least one type of surface meteorological observation.

Azimuthal asymmetry and horizontal stratification are assumed in the mapping functions discussed previously[4]. At most locations, this assumption will not be representative of the true atmospheric conditions especially at times of passing fronts and large pressure, temperature and humidity gradients (Dodson *et al*, 1996; Collins and Langley, 1998; Elosegui *et al*, 1999). It is widely recognised that by not accounting for these atmospheric gradients in tropospheric mapping functions, errors of several millimetres in coordinates and up to several centimetres of delay may be introduced especially when using a low (<10°) elevation angle cut-off (Ware *et al*, 1993; MacMillan, 1995; Chen and Herring, 1997; Ware *et al*, 1997; Bar-Sever *et al*, 1998; Elosegui *et al*, 1999).

[4] In most GPS processing packages, gradients in the zenith delay can now be solved for using techniques such as those described in MacMillan (1995), Chen and Herring (1997) and Bar-Sever, Kroger and Borjesson (1998).

Many of the tropospheric mapping functions (e.g., CfA-2.2, MTT, Ifadis and Lanyi) use surface pressure, temperature and/or humidity as a basis for defining theoretical profiles through the atmosphere. In reality, these surface measurements are not always relevant to the behaviour of the upper layers due to boundary layer effects. Niell (1996), in his comments on the deficiencies of the current mapping functions, discusses several problems in using surface temperature as an input parameter for mapping functions, all of which occur due to the presence of significant temperature variability in the boundary layer (0 - 2000m) and its non-relationship to the upper atmospheric levels.

In regards to the magnitude of the errors in mapping functions, it has been demonstrated that, for elevation angles above 30°, most mapping functions produce a total delay error of 0 - 5 mm when compared to values from atmospheric ray traces (Mendes and Langley, 1994). At 10° elevations, many mapping functions become very unreliable. The best performing functions (Niell, MTT and Ifadis) have demonstrated accuracies at low elevations (≤10°) of better than 4 mm except at high latitudes where some have shown errors of up to 7.1 mm of the total delay (Mendes and Langley, 1994).

Errors in the wet mapping function are especially significant to the final estimate of the tropospheric delay. It is now common practice to use lower elevation cut-off angles in GPS processing (see section 6.3.5.3) which, as discussed above, increases the effect of atmospheric gradients on the results and reduces the validity of many of the mapping functions.

6.3.5.2 Surface meteorology errors

Errors from the measurement/estimation of surface meteorology data at a GPS site are not significant in terms of their use in estimating a priori tropospheric delay values. However, errors in these values are important when estimating tropospheric delay with a mapping function that relies on input meteorological data to calculate the value of the model coefficients. The Niell function is the only one that is not at all dependent on surface meteorological data and therefore is not sensitive to errors in the input values for these parameters.

6.3.5.3 GPS processing errors

Elevation cut-off

Recently there has been a move in the GPS community to include lower elevation data into GPS processing in order to improve the repeatability of the vertical position, reduce the correlation between this parameter and the tropospheric delay and improve ambiguity resolution (e.g., Mendes and Langley (1994) and Bar-Sever

et al (1998)). Low elevation data have also been shown to improve horizontal coordinate precision when used in conjunction with atmospheric gradient estimation (Bar-Sever *et al*, 1998). The problems with using these data are that at low elevations many of the mapping functions degrade, multipath increases, signal noise increases and antenna phase centre movement increases, thus increasing potential error sources in the TZD results (Bar-Sever *et al*, 1998; Fang *et al*, 1998; Tregoning, Boers *et al*, 1998).

In the paper by Tregoning, Boers *et al* (1998), they found that including lower elevation observations in the GPS analysis produced better wet zenith delay results than the solutions using higher elevation angle cut-offs. They deduced that 12° elevation was optimal for their experiment as lower cut-off angles are likely to introduce extra multipath and phase centre effects and also degrade results if atmospheric gradients are present and/or the mapping function reliability below 12° is questionable. Similar results have been shown in many other studies including MacMillan (1995), Chen and Herring (1997), Wolfe and Gutman (2000) and Bar-Sever *et al* (1998) and it is now suggested that a 7-10° elevation cut-off with gradient estimation will provide the most accurate zenith delay results.

Fang *et al* (1998) performed tests designed to find the best processing method to eliminate elevation dependant systematic errors from GPS TZD estimates. They found that using the Niell mapping function with IGS antenna phase models reduces the dependence on elevation cut-off so that it becomes an almost negligible factor (e.g., a difference of 0.12 mm in TZD between 7° and 15° solutions).

Multipath

As discussed above, it is desirable to use low elevation data in GPS processing in order to decorrelate the zenith delay and height parameters (Santerre *et al*, 1995). However, when including low elevation data, multipath becomes an issue and may introduce more noise into the solution than if the low elevation data had been not included depending on the site and its surroundings. Rocken, Solheim *et al* (1995) calculated that multipath errors at two of their sites (with identical set-ups) had caused errors in the zenith delay of approximately 2 mm but this effect will change depending on the site and antenna of interest.

Satellite orbits

Kruse *et al* (1999) and Dodson and Baker (1998) have studied near-real-time estimation of the tropospheric delay for PW estimation and conclude that using broadcast orbits in the solutions produces unsatisfactory results (bias of 6.5 mm compared to WVR (Kruse *et al*, 1999)) and that using 1 - 2 day predicted orbits typically produces results which are still a factor of two worse than those performed

with precise IGS values. The use of rapid orbits (12 - 24 hr delay) in these studies compared well with the IGS orbit results with differences of approximately 1 mm.

Tregoning, Boers *et al* (1998) studied 3 hour IGS orbit overlaps at day boundaries and observed orbit discontinuities of 0.1 to 0.2 m during these periods. They found that these discontinuities in the orbits contributed to discontinuities of up to 2 mm in PW estimation at these epochs. Rocken, Solheim *et al* (1995) estimated that for a 1 km baseline and 10 cm orbits, the error introduced into TZD by the orbit error is 1.3 mm which would increase given less accurate orbits and/or longer baselines.

Antenna phase centre

The location of the antenna phase centre for each observation changes depending on the direction of the incoming signal. Since the phase centre is the point at which the GPS measurements are made, the effect of the movement of the phase centre is to move the apparent height of the antenna and therefore change the length of the estimated tropospheric delay (Mader and MacKay, 1997). It has been shown by Fang *et al* (1998) that solutions using IGS antenna phase centre models (Mader and MacKay, 1997) produce a significant reduction of the elevation dependant errors in the estimation of tropospheric delay.

Radomes

There are many different antenna covers (radomes) in use to protect the GPS antennas from the weather and environment. The material, shape and mounting position of the radome over the antenna cause delays and alters the direction of the incoming GPS signals (Jaldehag *et al*, 1996). This effect is elevation dependant and significant at the centimetre level for cone-shaped radomes, while hemispherical domes have been shown to have a reduced elevation dependence and a lesser effect on the antenna height (approximately 2 mm) (Johansson *et al*, 1998). As the vertical coordinate and tropospheric delay are highly correlated, the errors caused by the radomes will most likely also propagate into the tropospheric delay estimate. The changes in the apparent height of the antenna phase centre and refraction of the incoming signal may also cause additional errors in the tropospheric delay, as these parameters will affect the validity of the phase centre model and tropospheric mapping function used.

Ocean and pressure loading

Heights and tropospheric zenith delay are known to be highly correlated. Therefore factors which affect the true height of the GPS at the observation time will affect the tropospheric delay estimation.

The effect of ocean loading at a site is defined by a correction term that is applied to GPS data to account for the effects of the ocean movement on the Earth's crust which leads to periodic variation in station heights. (Dach and Dietrich, 2000) performed a model and real life study on the effect of ignoring ocean loading on zenith delay estimates and concluded that the resulting relative difference in zenith delay was approximately 20% of the relative ocean loading difference when no other errors were included. In another ocean loading study by (Dragert *et al*, 2000), they found that the neglect of ocean loading corrections (0.08 to 0.12 m peak to peak) in GPS processing (24-hour solutions) created significant biases (10 mm) in the (1-hour) TZD estimates. However, (Dragert *et al*, 2000) also suggest that estimates obtained from 24-hour solutions are not strongly biased by neglecting ocean loading variation due to the diurnal/semi-diurnal nature of the most significant components of the loading.

Changes in the atmospheric pressure loading are also known to cause variation in the height of GPS stations over time. These pressure fluctuations have been shown to cause vertical displacements of 10mm or larger depending on the location and synoptic conditions of the site (van Dam and Wahr, 1998). Correcting for these atmospheric loading variations is known to improve the scatter of the GPS height estimates by approximately 24% (van Dam *et al*, 1994). The correlation between height and TZD estimates in GPS processing implies that these significant and unaccounted for variations in the true height of the GPS antenna will be at least partially incorporated into TZD estimates and contribute to errors in this parameter (Emardson *et al*, 1998).

Site coordinate constraints

Estimations of zenith delay are very sensitive to coordinate errors and constraints, especially for the vertical component at the site of interest, due to the manner in which errors are distributed during processing. Tregoning, Boers *et al* (1998) found that the uncertainty of WZD estimates varied depending on the number of constraints applied to site coordinates. They found that best results were gained by tightly constraining the coordinates at two reference sites plus the height of the site of interest. They also showed that tightly constraining additional sites did not further benefit the results. Rocken, Solheim *et al* (1995) assumed a 10 mm vertical coordinate error and claim that however caused, the presence of this error would contribute approximately 3 mm to the error in the zenith delay.

Residual ionospheric delay

In GPS processing, the standard technique for removing the effects of the ionosphere from the GPS signals is to form a linear combination of the L1 and L2 signals (see

section 2.1.1). This technique assumes that the refractive index of the ionosphere is dependant on the frequency squared and the electron density (Emardson *et al*, 1998). Although most of the delay is removed by the linear combination, there is some residual delay (several centimetres during peak ionospheric activity (Brunner and Gu, 1991)) remaining in the solution due to the breakdown of these assumptions. This error will therefore be distributed between the estimated parameters, including the TZD.

6.4 Converting Tropospheric Delay to Precipitable Water

It is now well known and documented (e.g., Rocken *et al* (1993), Coster *et al* (1996), Emardson *et al* (1998) and Tregoning, Boers *et al* (1998)) that measurements of tropospheric delay can be converted into a measure of integrated water vapour (IWV) or PW[5] with an accuracy of 1 - 2 mm when compared to WVR and radiosonde measurements. This technique (known as GPS meteorology) combines the TZD estimates with surface meteorology measurements and refractivity relationships to provide an estimate of the amount of water vapour present in the atmosphere above the GPS antenna.

Bevis *et al* (1992) were the first to detail the potential for using tropospheric delay values estimated during GPS processing to extract information on the amount of water vapour surrounding the GPS site. Since then, many authors have written papers outlining the methodologies, accuracies and error sources of GPS meteorology projects (e.g., Rocken *et al* (1993), Bevis *et al* (1994), Coster *et al* (1996), Duan *et al* (1996), Emardson *et al* (1998) and Tregoning, Boers *et al* (1998)). There have also been many GPS networks studied worldwide to investigate the use of the technique for climatology and meteorology applications, including near real time and continuous observation of atmospheric water vapour and the monitoring of weather features such as frontal systems (e.g., Elgered *et al* (1997), Rocken, Van Hove *et al* (1997), Gregorius and Blewitt (1998), Naito *et al* (1998) and Wolfe and Gutman, (2000)).

[5] IWV is defined by Bevis *et al* (1992) as the mass of vapour per unit area (units: g/m^2), PW refers to the height of an equivalent column of water (units: mm). The conversion between the two parameters is $PW = IWV/\rho$ where ρ is the density of liquid water.

6.4.1 TZD to PW Conversion

Most GPS meteorology procedures use a similar technique to arrive at a value for the PW at a given site/epoch. The following series of equations, variables, measurements and constants follow from the work of Bevis *et al* (1992). This methodology, the most commonly employed for this GPS PW estimation, is used in the experiments carried out in this thesis.

The hydrostatic zenith delay is usually estimated using Saastamoinen's equation (6.6) based on measured pressure at the GPS antenna and assuming hydrostatic equilibrium. This delay is then subtracted from the TZD in order to acquire a value for the WZD:

$$WZD = TZD - HZD \qquad (6.21)$$

In order to convert the WZD value into precipitable water, a value for the conversion factor K is required. K is a function of the atmospheric refractivity constants and the mean temperature of the atmosphere (Askne and Nordius, 1987; Bevis *et al*, 1994):

$$K = \frac{10^6}{\rho R_v \left(\frac{k_3}{T_m} + k_2' \right)} \qquad (6.22)$$

where: ρ = density of liquid water

R_v = water vapor gas constant

T_m = mean atmospheric temperature (K)

$\cong 70.2 + 0.72 T_s$ (from Bevis et al., 1992; T_s = surface temperature (K))

k_1, k_2, k_3 = atmospheric refractivity constants (from Bevis et al., 1994)

$$\begin{pmatrix} k_1 = 77.60 \pm 0.05 \left(Kmb^{-1} \right) \\ k_2 = 70.4 \pm 2.2 \left(Kmb^{-1} \right) \\ k_3 = 3.739 \times 10^5 \pm 0.012 \times 10^5 \left(K^2 mb^{-1} \right) \end{pmatrix}$$

$k_2' = k_2 - m k_1$ (m = ratio of the molar masses of water vapour and dry air)

$= 22.1 \pm 2.2 \left(Kmb^{-1} \right)$

Once a value for K is obtained, it is then simple to determine the PW for the air column using:

$$PW = K \times WZD \qquad (6.23)$$

6.4.2 Errors in TZD to PW Conversion

Significant sources of error in the TZD to PW analysis include most of the input data and several of the experimental constants used in equations (6.6) and (6.21) to (6.23). The largest source of error in these computations is the uncertainty in the GPS TZD estimates (see section 6.3.5). Other variables that are likely to have an important but less significant effect on the accuracy of the final results are the pressure and temperature data, site coordinates, refractivity constants and the height difference between the GPS and pressure sensor.

The Saastamoinen hydrostatic zenith delay model (equation (6.6)) is generally considered approximately error free with tested accuracies at the millimetre level (Janes *et al*, 1991) and according to Davis *et al* (1985), only in extreme events will the assumption of hydrostatic equilibrium cause significant uncertainty in the HZD value.

In calculating the hydrostatic zenith delay, the major error contribution comes from errors in the pressure measurement. The f(φ,h) term in equation (6.6) models the effect of the latitude and height above the ellipsoid on the acceleration due to gravity at the site (Elgered *et al*, 1991). Error analysis of the f(φ,h) term shows that this variable is not highly sensitive to errors in station latitude and height. From equation (6.24) and as noted by Elgered *et al* (1991), it can be seen that the error in the hydrostatic delay due to errors in the surface pressure is approximately 0.003 times the pressure error (i.e., a 1 hPa error in pressure results in approximately 2.3 mm error in the hydrostatic delay).

$$\sigma_{HZD} \approx 0.0022678\sigma_p \qquad (6.24)$$

As the wet zenith delay is merely the remainder from the subtraction of the hydrostatic delay from the total delay, it carries the error effects from both of these variables into the water vapour calculations. The error in the WZD is therefore determined from the errors in the GPS processing and the measurement or calculation of pressure at the GPS antenna.

In the final calculation of the PW value (equation (6.23)), the only error sources are the two variables, WZD and K. The error in WZD has been discussed above and is generally in the order of a few millimetres while the error budget for K has been thoroughly analysed previously in papers by Bevis *et al* (1992) and Bevis *et al* (1994), which are summarised below.

Bevis *et al* (1992) presented an experimental result for the relationship between surface temperature and mean atmospheric temperature, a parameter required in equation (6.22). By analysing 8718 radiosonde soundings (over North America[6]), they showed that mean atmospheric temperature can be closely approximated by the equation $T_m = 70.2 + 0.72T_s$. They deduced that relative rms error in K introduced by using this equation to determine T_m is approximately 2%, and in the worst cases, the T_m error could cause errors in PW of a maximum of 4%.

In Bevis *et al* (1994), the authors discussed the effects of errors in the remaining parameters used in determining the value of K (equation (6.23)) for the conversion from WZD to PW. In this discussion, Bevis *et al* (1994) state that "The values of the constants ρ, R_v, m are well determined, and their experimental uncertainties have no potential impact on the parameter K". The main sources of error in K are therefore the mean atmospheric temperature, T_m, and the refractivity constants k_1, k_2 and k_3.

Values for the atmospheric refractivity constants have been published several times since 1953. The most widely used values are those of Thayer (1974), but both Bevis *et al* (1994) and Hill *et al* (1982) dispute his methods used to obtain a value for k_2. Bevis *et al* (1994) chose to reanalyse the experimental data and determine their own robust results with conservative uncertainties and produced values comparable to the earlier analysis of the same data by Hasegawa and Stokesbury (1975).

Bevis *et al* (1994) plot the relationship between the relative error in T_m versus the relative error in K. The results showed that only when the error in T_m is less than 1%, do the errors in the refractivity constants become significant. This magnitude of error in T_m is generally found in most GPS PW studies unless radiosonde or numerical model values are available for measurement of the true mean atmospheric temperature.

Bevis *et al* (1994) conclude that the greatest source of error in GPS PW estimation and the area in which improvements need to be concentrated is in the determination of WZD in GPS processing. They state that it should currently be possible to estimate PW from GPS data with a rms error of less than 2 mm $\pm$ 1% with a long-term bias of less than 2%.

[6] the T_m equation was developed using data from North America but is widely used for PW studies in other regions of the Earth and, theoretically, should be tested for applicability before use.

6.5 Current Capabilities of the GPS Meteorology Technique

The main requirements for obtaining optimum GPS PW results are that IGS antenna phase centre models, precise orbits, slant path corrections, ocean and atmospheric loading corrections, proven mapping functions (e.g. Niell and MTT) and models (e.g. Saastamoinen), ionospheric corrections, 7° - 12° elevation cut-offs, realistic/tight coordinate constraints and at least one baseline over 2000 km are used in processing. Additionally, it is very important that multipath and radome effects are minimised at the data collection stage to minimise signal noise and allow effective implementation of the processing/modelling strategies. High quality meteorological data at the site of interest are also essential for the determination of the highest quality PW estimates from GPS signals. The most recent published studies have shown that if a maximum amount of care is taken in data collection and processing, then GPS PW estimates are comparable to WVR and radiosonde measurements at the 1-2 mm level (e.g., Rocken, VanHove *et al* (1995), Duan *et al* (1996), Emardson *et al* (1998), Fang *et al* (1998), Tregoning, Boers *et al* (1998) and Shoji *et al* (2000)).

The ability to obtain high quality PW estimates over various time scales has led to many GPS meteorology campaigns being undertaken in various regions of the world. One region in which GPS PW has not been investigated is Antarctica. The Antarctic continent is the driest continent on Earth with mean annual PW values obtained from assimilation models ranging from 2 - 6 mm on the peninsula and 2 - 0 mm from the coast to the South Pole (Reid, 2000). There have been many permanent and temporary (field campaign) GPS sites occupied in Antarctica over the past decade (see sections 2.3.2 and 3.3) which have the potential to provide much useful information regarding the water vapour over regions of this continent. The following chapters describe two studies using permanent (Chapter 7) and field campaign (Chapter 8) GPS data to examine the validity and possible applications of using the GPS Meteorology technique in Antarctica.

6.6 Chapter Summary

Water vapour is one of the most important atmospheric variables due to its major role in the transporting latent heat and moisture around the Earth and its control over the radiative properties of the atmosphere. For these reasons, the study of water vapour in the Earth's system is a vital component in the monitoring of climate change and its global effects.

In Antarctica, atmospheric water vapour is not well observed due to the inhospitable environment and the extent of the region. However in this region, variations in the amount and distribution of water vapour are important climate change indicators. Most importantly, changes in amount of water vapour in the Antarctic atmosphere will lead to changes in the mass input of the ice sheets and also in the amount of cooling of the atmosphere. These changes in the Antarctic climate and hydrology have feedback effects on global climate and sea level. It is therefore of major scientific importance to improve the amount and quality of water vapour observations in this region.

The GPS meteorology technique involves estimation of the tropospheric delay within the GPS signals and using surface meteorological observations and theoretical models to convert this into a measure of PW. Many previous studies have shown this technique to be very useful and accurate (i.e., a 1 - 2 mm bias compared to radiosonde and WVR data) in the observation of temporal and spatial patterns of the PW distribution around the observing sites. In this chapter, a complete overview of the GPS meteorology technique has been given. Included in this overview was a thorough discussion of the major error sources encountered when determining PW from GPS data.

Chapter 7

GPS WATER VAPOUR ESTIMATION IN ANTARCTICA

7.1 Introduction to the Study

GPS meteorology is now being used worldwide as a method of water vapour detection for weather and climate studies. Most of the areas where this technique has previously been used have had a temperate, moist atmosphere and experience frequent frontal events (e.g., Coster *et al* (1996), Duan *et al* (1996), Elgered *et al* (1997), Davies and Watson (1998) and Naito *et al* (1998)). One location where GPS meteorology has not yet been used is East Antarctica where water vapour is very low (generally < 10mm) and becomes more so as the distance from the coast increases.

Studies in northern America have shown GPS meteorology to be capable of accurately detecting very low amounts of water vapour (< 2.5 mm) (Gutman *et al*, 1994). It therefore should be possible to use the GPS meteorology technique for measuring and/or monitoring water vapour in Antarctica. However, detecting a statistically valid measurement of water vapour in an arid region, such as inland Antarctica, may be difficult due to the magnitude of the PW values being of a similar size to the expected error signal in the data.

Many authors have shown that it is not possible to achieve absolute PW results with an accuracy of better than 1.2 - 1.5 mm due to the TZD estimation process (e.g., Rocken, VanHove *et al* (1995), Duan *et al* (1996), Elgered *et al* (1997) and Tregoning, Boers *et al* (1998)). The usual practice for calibrating GPS results is to compare them to WVR or radiosonde values at the same site. However, differences between GPS, radiosonde and WVR PW estimates are generally between 1 - 2 mm. It is now widely agreed that each of these methods has a bias of around 1 mm (Fang *et al*, 1998). However, the exact bias value for each of these techniques cannot be determined directly because, in general, the true amount of water vapour is never known.

At the South Pole, the amount of water vapour is known to be effectively zero, therefore providing a unique location for testing GPS PW accuracy against a known benchmark. At this site, any PW detected from the processing of GPS data will not be a true measurement of the tropospheric conditions but instead will represent an error signal originating from mis-modelling and error distribution within the GPS processing.

The estimation of TZD is a least-squares process and is solved for along with an estimation of the precision of the value attained. Many primary parameters (e.g., station position, satellite orbits) and models affect the correct estimation of secondary parameters, such as TZD. This chapter deals with tests that attempt to define the errors in some of the primary parameters and show their effect on estimation of TZD values at a given site. This analysis is carried out with the aim of identifying the correctness of the estimation process used to determine TZD and hence PW using GPS data.

In summary, this chapter aims to address four questions:

1. *What effect do elevation cut-off angles and coordinate constraints have on the TZD/PW estimates at Antarctic sites?*
2. *Are non-zero PW values observed at the South Pole and if so, what is causing them and do they represent the absolute magnitude of GPS PW precision for current processing strategies?*
3. *Are negative PW values ever obtained at sites with low atmospheric water vapour content and if so, what is causing them? Are these effects caused by observational, model or processing deficiencies?*
4. *How do PW values obtained using GPS techniques compare with radiosonde values for data from East Antarctica?*

7.2 Study Sites

Four Antarctic GPS stations were selected for use in this study based on data availability and site location. Three of the test sites are located on the East Antarctic coast (at the Australian Bases, Davis [DAV1], Mawson [MAW1] and Casey [CAS1]) while the fourth (Amundsen-Scott [AMUN]) is located inland near the South Geographic Pole (refer to Figure 7.1). The South Pole site is the primary focus of this investigation into absolute GPS PW errors while the other sites are important in the validation of GPS PW methods in East Antarctica (including the LGB region) and for comparison with the findings from the South Pole.

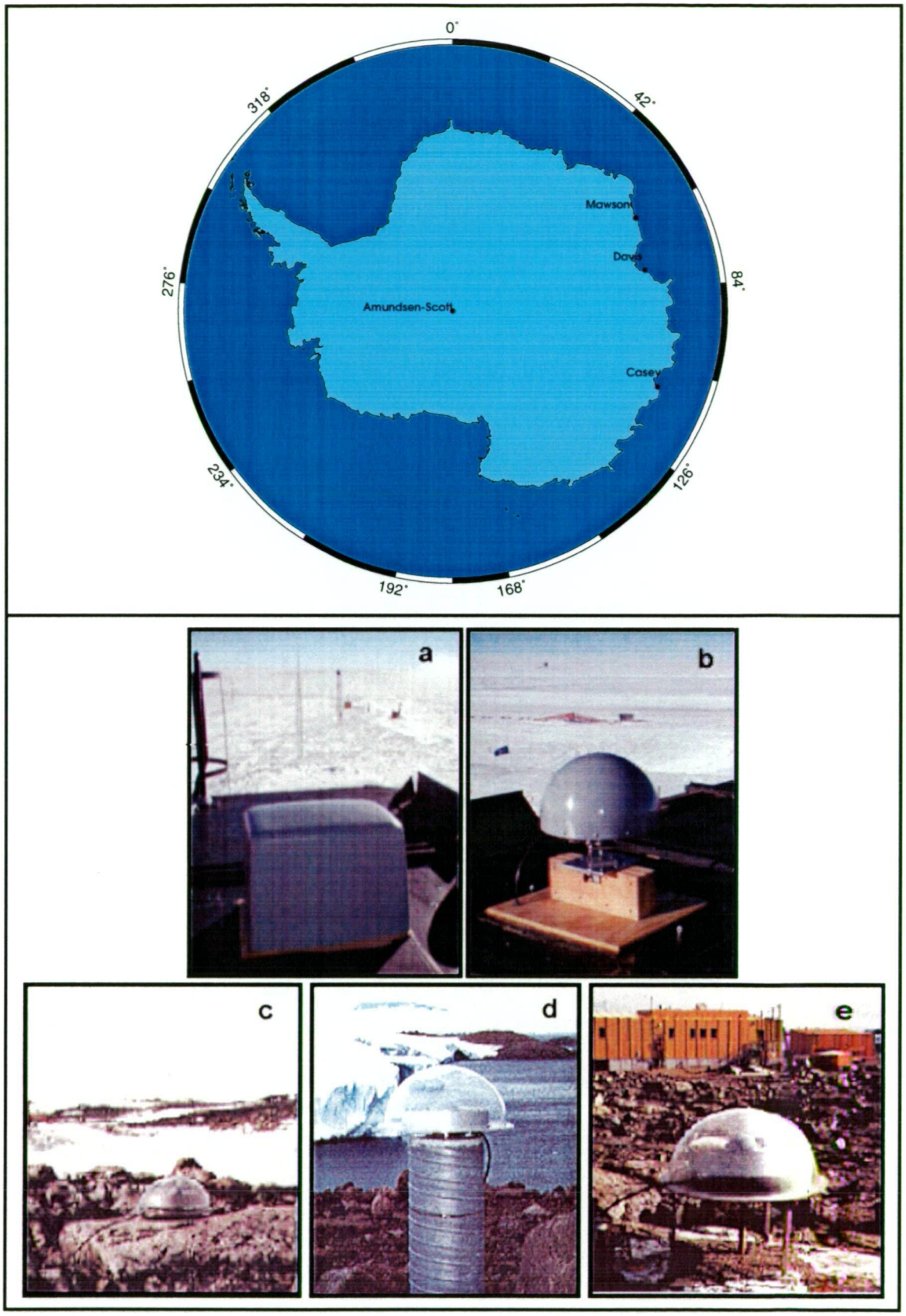

Figure 7.1 - The top panel shows the locations of the Antarctic GPS sites used in this study. The bottom panel contains images of the GPS installations: *a)* AMUN rounded-rectangular dome (1998)[1], *b)* AMUN SCIGN hemispherical dome (1999)[1], *c)* CAS1[2], *d)* MAW1[2], *e)* DAV1[2]

[1] Image from http://www-socal.wr.usgs.gov/scign/group/dome/album/AMUN/
[2] Image from http://www.auslig.gov.au/geodesy/argn/images/

Analyses of 11 years of radiosonde data (discussed later in section 8.3) indicated that tropospheric water vapour levels of approximately 0 - 5 mm during winter and 0 - 10 mm during summer could be expected at the three coastal sites. The South Pole was expected to have approximately zero millimetres of water vapour present in the atmosphere due to the very high elevation, cold air temperature and distance from the coast. This expectation of zero water vapour was confirmed by the analysis of a number of radiosonde soundings (summer and winter) from the South Pole, which showed PW values of less than 0.5 mm (e.g., Tables 7.2 and 7.3). The approximately constant zero value of PW at this site serves as a unique benchmark for identifying absolute error in the GPS PW estimation.

The station configuration at the coastal sites is identical in terms of the GPS equipment used (Table 7.1) although, as shown in Figure 7.1 and Table 7.1, the antenna mounting and satellite elevation range varies between sites. In winter 1998, the AMUN site consisted of an Ashtech choke-ring antenna and a rounded rectangular protective enclosure (Figure 7.1a). This configuration was changed in January 1999 at which time a standard Southern California Integrated GPS Network (SCIGN) short dome[3] was placed over the original antenna (Figure 7.1b).

Table 7.1 - Station descriptions for the GPS study sites.

	AMUN_98	AMUN_99	DAV1	MAW1	CAS1
Antenna	AshDMG	AshDMG	TrbRog-DMT	TrbRog-DMT	TrbRog-DMT
Dome	Kearney Powerglass (rounded-rectangular cover)	SCIGN short dome	Custom-made acrylic hemispherical	Custom-made acrylic hemispherical	Custom-made acrylic hemispherical
Receiver	Ashtech Z12	Ashtech Z12	TurboRogue AOA ICS-4000Z	TurboRogue AOA ICS-4000Z	TurboRogue AOA ICS-4000Z
Location (ITRF97)	S 89° 59' E 139° 14'	S 89° 59' E 139° 14'	S 68° 34' E 77° 58'	S 67° 36' E 62° 52'	S 66° 17' E 110° 31'
Height (MSL)	~ 2845 m	~ 2845 m	28 m	32.5 m	41 m
Maximum Satellite Elevation	50°	50°	75°	75°	80°
Minimum Satellite Elevation	10°	10°	15°	15°	10°
Mounting	Metal bracket and wooden block on flat roof	Metal bracket and wooden block on flat roof	0.29 m high metal bracket bolted to rock.	1.4 m high (0.3 m diameter) concrete pillar	Bolted to rock

[3] http://www-socal.wr.usgs.gov/scign/group/dome/album/album.html

The Mean Sea Level (MSL) heights of the antennas at MAW1, DAV1 and CAS1 have been determined via third order levelling connections to permanent tide gauges (http://www.auslig.gov.au/geodesy/antarc) and are accurate to around 10 mm. The orthometric height of AMUN has been derived using its WGS84 ellipsoidal height and an EGM96 geoid value and therefore may only be accurate to a few metres.

The range of satellite elevation angles at which GPS data are collected varies between the four sites. The maximum observed elevations are determined by a combination of the latitude of the site and the inclination of the satellite orbital planes. Minimum elevations are controlled within the individual receiver settings and are usually selected to avoid multipath interference and obstructions surrounding the antenna.

7.3 Study Periods

7.3.1 Winter 1998

The first section of this study investigated the results of GPS PW calculations at the study sites during the austral winter/spring of 1998. A series of days within this period were selected such that all sites would have minimal amounts of PW. The selection of these study days was based on available information from the meteorological records and GPS data archives.

The main criterion for selecting the potential study days was that they have a very low amount of water vapour at most of the sites so that the performance of GPS PW estimation in a very dry environment could be observed. The meteorological records from Davis and Mawson were used to compile a list of days that had been recorded as being cold, clear and with no precipitation. The GPS data archives at the Scripps Orbit and Permanent Array Centre (SOPAC) and Crustal Dynamics Data Information System were then accessed to determine which of the listed days had data available at all four study sites. At this time it was found that AMUN GPS data were only available after day 202 1998 which set the earliest limit for the study. Eventually three periods were found that satisfied the data availability and meteorological criteria, each period separated from the next by approximately one month:

Winter 1998			
Day of Year:	202 - 205	237 - 239	273 - 275

Surface meteorological and radiosonde data were then also obtained for Casey and Amundsen-Scott stations on the selected days. The radiosonde information at all sites was processed (see to section 7.5) to obtain the measure of atmospheric PW from each available sounding. These radiosonde PW values verified that very low amounts of water vapour were present at all sites on the selected days (Table 7.2). Casey was found to have slightly higher water vapour content on days 202 - 205 and 239 while Amundsen-Scott, as expected, had approximately zero water vapour on all days.

Table 7.2 - Atmospheric precipitable water (PW) from radiosonde soundings - Winter 1998

Day of year	Davis 1998 PW (mm)	Mawson 1998 PW (mm)	Casey 1998 PW (mm)	Amun.-Scott 1998 PW (mm)
202.0	0.93	0.58	4.25	0.14
202.5	1.42	0.54	3.83	
203.0	1.63	0.30	2.94	0.22
203.5	1.21	0.32	3.79	
204.0	1.45	0.83	4.06	0.18
204.5	1.06	1.88	3.65	
205.0	0.95	1.60	3.27	0.08
205.5	0.94	1.46	1.83	
237.0	0.79	0.50	0.83	0.14
237.5	0.90	0.67	0.87	
238.0	0.91	0.41	1.30	0.01
238.5	0.82	0.40	1.26	
239.0	0.61	0.45	1.09	0.09
239.5	1.79	0.42	4.88	
273.0	0.57	2.41	0.97	0.38
273.5	0.77	1.50	1.00	
274.0	0.60	0.72	1.54	0.20
274.5	0.47	0.72	1.40	
275.0	0.86	3.26	1.24	0.07
275.5	2.13	1.69	1.28	

7.3.2 Summer 1999

After processing the Winter 1998 GPS data, the extreme effect of the rectangular shaped cover over the AMUN antenna on the PW results became apparent. A decision was made to perform the same tests using data from a period after the cover had been changed so that the hypotheses could be tested using a more typical (less corrupted) data set. It was also decided that this second round of processing should use data from summer months so that any seasonal differences in the results could be observed. During the summer, the PW observed using radiosonde soundings (Table 7.3) at the South Pole remains very close to zero (less than 0.5 mm) but there is a greater, although still relatively low amount, at the coastal sites (generally 1 - 7 mm).

Table 7.3 - Atmospheric precipitable water (PW) from radiosonde soundings - Summer 1999

Day of year	Davis 1999 PW (mm)	Mawson 1999 PW (mm)	Casey 1999 PW (mm)	Amun.-Scott 1999 PW (mm)
001.0	4.10	3.08	6.46	0.35
001.5	3.61	6.75	5.21	0.21
002.0	4.06	6.41	4.87	0.34
002.5	3.98	6.29	5.25	0.31
032.0	2.85	3.75	4.96	0.41
032.5	3.81	3.43	3.75	0.43
033.0	4.76	4.36	6.69	0.47
033.5	4.20	3.87	6.69	0.22
045.0	2.63	3.04	3.38	0.44
045.5	3.33	2.90	5.00	0.11
060.0	5.49	5.74	7.17	0.28
060.5	4.83	6.45	11.69	-
061.0	3.92	4.48	7.30	0.27
061.5	6.80	3.71	9.08	-
078.0	2.08	1.09	-	0.12
078.5	1.70	0.66	-	-

In this second study, GPS PW values were determined using data collected during the 1999 austral summer/autumn (January - March). On this occasion, the days were selected such that i) there were cold and clear meteorological conditions at most sites, ii) the day was prior to the autumnal equinox (i.e., still significant sunlight), iii) the new dome had been installed at AMUN and iv) GPS and meteorological data were available at all four sites. The use of these criteria resulted in the following days being selected for the study:

	Summer 1999				
Day of Year:	001 - 002	032 - 033	045	060 - 061	078

7.4 Processing Methodology

7.4.1 Input Data

7.4.1.1 GPS data

The GPS data for all sites (global and Antarctic) were accessed via ftp from the SOPAC database[4]. From this site, files containing information on the antennas, receivers, a priori coordinates and coordinate constraints (i.e., GAMIT files: station.info, sittbl. and l-file) were also downloaded for use in processing of the

[4] ftp://lox.ucsd.edu

global network. Although it was intended that all of the study sites would be available on the days selected for the study, this was not always possible and resulted in CAS1 not being included for one day in each study period.

7.4.1.2 Coordinate Information

The ITRF97 Cartesian coordinates (at epoch 1999.0) for the IGS sites (and MAW1) were converted to geodetic coordinates for use as a priori values in the GPS data processing. Significant errors in the a priori site coordinates will have an effect on the results of the GPS processing in tightly constrained solutions. The ITRF97 values for DAV1, MAW1, CAS1 and the global sites are acceptable for use as a priori values due to the relatively small annual movement at these locations. However, at AMUN, the high site velocity[5] makes it necessary to estimate precise coordinates (within a few centimetres) for the site prior to running the final GAMIT solution for determination of TZD values. For the purpose of determining reliable daily a priori coordinates at AMUN, initial regional GAMIT solutions were carried out for each day with the resulting coordinate estimates having formal errors of less than 0.01 m in the horizontal and 0.03 m in the vertical component.

The program used to convert GPS TZD estimates to PW values requires one set of coordinates per site for each season (refer to section 7.4.3). For this purpose, the coordinates do not need to be as precise as for the GPS processing. The ITRF97 coordinates for DAV1 and CAS1 have long-term uncertainties of around 0.01 m while the position of MAW1 is known to approximately 0.1 m. These coordinates are therefore acceptable for the PW estimation process. As the position of AMUN changes more rapidly over time, it was necessary to compute seasonal mean coordinates at this site using GLOBK software (see section 4.2.2). The movement at AMUN over each study period may result in the horizontal coordinates used in the TZD conversion (on a given day) being in error by up to 2 m. The ellipsoidal height values at AMUN may also contain errors of up to 0.01 m for the same reason. These error levels are acceptable for using these coordinate data in the TZD to PW conversion program and will have no significant effect on the estimate of HZD or the final PW values (refer to PW conversion error analysis in section 6.4.2).

7.4.1.3 Meteorological Data

Surface meteorological data were obtained for Davis, Mawson and Casey from the Australian Bureau of Meteorology (BoM), Tasmania and Antarctica Regional Office, while the data for Amundsen-Scott were obtained from the United States National

[5] AMUN is the only study site that is not fixed to bedrock. The building upon which the antenna is mounted is built on the ice cap and is moving horizontally at approximately 9.9 m/yr and vertically at approximately 0.2 m/yr.

Oceanic and Atmospheric Administration Climate Monitoring and Diagnostic Laboratory (CMDL) via their ftp site[6]. These data were recorded as three hourly observations at the Australian stations and hourly observations for the South Pole site which were then converted into daily mean values[7] to be used as input for the TZD to PW conversion (see section 7.4.3).

The pressure readings at the Australian sites have a calibrated precision of 0.1 hPa while the South Pole data are rated to approximately 0.3 hPa (pers. com. Doug Shepherd (BoM), 2000 and Tom Mefford (CMDL), 2000). At all sites the temperature readings are calibrated to 0.1° C (pers. com. Doug Shepherd (BoM), 2000 and Tom Mefford (CMDL), 2000). As the pressure measurements were not made at the exact locations of the GPS antennas, these values needed to be adjusted with respect to the height difference between the barometer and GPS antenna. As shown in Appendix C.2, height differences accurate to better than 4 m are required so that this adjustment does not introduce an uncertainty of more than 0.3 hPa into the adjusted pressures. Unfortunately no direct height connection has been made between the pressure sensor and the GPS antenna at any of the study sites. However, the MSL heights of the pressure sensors at all sites have been determined by topographic surveys (pers. com. D. Shepherd (BoM), 2000 and Tom Mefford (CMDL), 2000) and have an assumed minimum precision of 0.1 m. As discussed in section 7.2, the heights of GPS antennas at DAV1, MAW1 and CAS1 have expected precisions of better than 0.01 m while at AMUN, the uncertainty in orthometric height is around 1 - 3 m. Height differences at all sites may therefore be determined to a sufficient accuracy such that the adjusted pressure does not introduce an error of greater than 0.7 mm in the calculated HZD (see Appendix C.2).

7.4.2 GPS Processing

The GPS data were processed using a global network of 45 stations (Figure 7.2) in 24-hour solutions using default GAMIT (version 9.92) solution parameters[8], files and procedures. A standard set of global input files (e.g., UT1 table, polar motion, coordinate input and station information) were used for all solutions. The site control file was manipulated between solutions to alter the station coordinate constraints and elevation cut-off angle.

A global network was used to give strength to the solution but more importantly, to allow orbits to be constrained rather than fixed, thereby allowing orbit uncertainties to be allocated to the estimated orbit values rather than distributed into other

[6] ftp://ftp.cmdl.noaa.gov
[7] daily mean values were used to reflect the method to be used in the major study of GPS PW in the LGB (Chapter 8).
[8] solution parameters used for all solutions are detailed in Appendix C.1

parameters (i.e., TZD). The processing strategy performed combined (baseline and orbit) solutions on the GPS data using an observation interval of 30 seconds and employed default ('tight') constraints on the orbits and IGS station coordinates (see Appendix C.1). The least squares solution of the double differenced LC observations resulted in estimates for the corrections to the a priori Earth orientation parameters, station coordinates, orbit parameters and tropospheric zenith delay values. The LC observable was used so that the major effects of the ionosphere were removed. Ambiguity resolution was not attempted due to the long lengths of most baselines (300 - 13,000 km). Elevation dependent IGS antenna models were used to correct for movement of the phase centres of the antennas. Earth rotation and tide models were applied during the solution but ocean tides were not modelled in this analysis[9]. It is expected that neglecting this correction will not significantly alter the PW results from this study due to the relatively small ocean loading effect in the Davis/Mawson and Casey regions and the negligible effect (to a first-order approximation) at Amundsen-Scott. Also, the following analyses are based on mean daily PW values which suggests that the effect of ocean loading biases will be minimised in these data due to the diurnal/semi-diurnal nature of the strongest ocean loading components (Dragert *et al*, 2000).

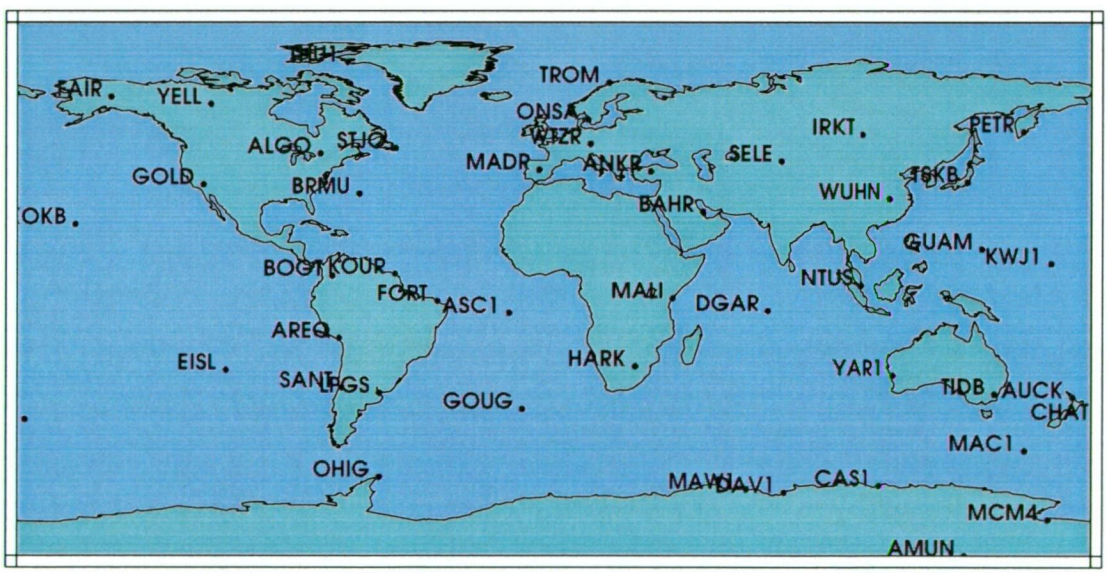

Figure 7.2 - IGS and Antarctic sites used in GPS processing.

The controls for modelling and estimation of the tropospheric zenith delay parameters were identical for all solutions. Saastamoinen wet and dry delay models, in conjunction with the Niell mapping functions, were used to model the tropospheric delay using standard sea level meteorological values corrected for elevation as the a

[9] It is now widely recognised that significant unmodelled ocean loading effects can typically introduce PW errors of 1 - 2 mm over baselines greater than 150 km (e.g., Dach and Dietrich (2000), (Dragert *et al*, 2000)).

priori data. These models were selected because the Saastamoinen model has been shown to perform effectively at high latitudes (refer to section 6.3.3.1) and the Niell functions have been shown to perform well in all circumstances, especially where actual surface meteorological data are not available (Niell, 1996). For each site, thirteen residual TZD parameters were estimated (i.e., 2-hour segments) using a Gauss-Markov piecewise linear process with a 0.5 m zenith delay constraint. Correlation time and between-point variation in the Gauss Markov model were set to the default values of 100 hours and 0.02 m/$\sqrt{}$hr respectively, thereby resulting in a random walk process being used to model the time dependent delay. No atmospheric gradients were estimated in these solutions.

To identify the elevation angle and coordinate constraint dependency of the TZD estimates at the study sites, the following three solutions were run on each day:

- **10t**: tight coordinate constraints (e.g., Table 7.4) were used at all IGS sites (including DAV1 and CAS1). The cut-off elevation angle was set to 10° at the study sites.
- **15t**: tight coordinate constraints (e.g., Table 7.4) were used at all IGS sites (including DAV1 and CAS1). The cut-off elevation angle at all sites was set to 15°.
- **15l**: set loose coordinate constraints at the study sites while tightly constraining the IGS network to their ITRF97 values (e.g., Table 7.4). The cut-off elevation angle at all sites was set to 15°.

Table 7.4 - Example of SOPAC coordinate constraints for Southern Hemisphere sites that form baselines with the study sites.

Site	Latitude (mm)	Longitude (mm)	Radius (mm)
DAV1	3	3	10
CAS1	10	10	50
YAR1	3	3	10
PERT	3	3	10
MCM4	10	10	50
MAC1	3	3	10
KERG	10	10	50
OHIG	3	3	10
GOUG	50	50	100
HARK	3	3	10

As the intention of this processing was to derive TZD/WZD values, tight, realistic coordinate constraints were required for sites in the global network. Therefore, SOPAC constraints were applied at all IGS stations including CAS1 and DAV1 (MAW1 and AMUN were not classified as IGS sites) for the 15t and 10t solutions. For the 15l solution, DAV1 and CAS1 had their constraints relaxed to: 100 mm, 100

mm, 500 mm (latitude, longitude, radius), the level of uncertainty already assigned to AMUN and MAW1, while the IGS sites remained tightly constrained.

The local coordinates for each study site on each day and for each solution type were then extracted after first using GLOBK/GLORG (refer to section 4.2) to bring the daily estimates into a consistent reference frame. Three separate GLOBK/GLORG solutions were initiated such that the 15t, 15l and 10t GAMIT solutions were only combined with other solutions of the same type. This resulted in three sets of daily coordinate estimates (i.e., 15t, 15l and 10t). A mean value for each coordinate component at DAV1, MAW1 and CAS1 was determined and the residuals from these mean values plotted to show changes in the coordinates over time and differences between the three solution types (see Appendix C.4 and C.5). At AMUN, a linear fit to each of the coordinate components was required to account for the high velocity at this site. The linear models were then removed from the estimated coordinates and the residual values analysed for differences between solutions (see Appendix C.4 and C.5).

At this stage in the processing, it became apparent that the GPS antenna cover at AMUN had not been changed in December 1998 as suggested in the available information (http://www-socal.wr.usgs.gov/scign/group/dome/album/ album.html). From the AMUN coordinate plots, it could be clearly seen that a change had occurred at this site between days 002 and 032 (see Figure 7.3). Therefore for the purposes of this study, the January 1999 AMUN results are treated separately from the other days in 1999.

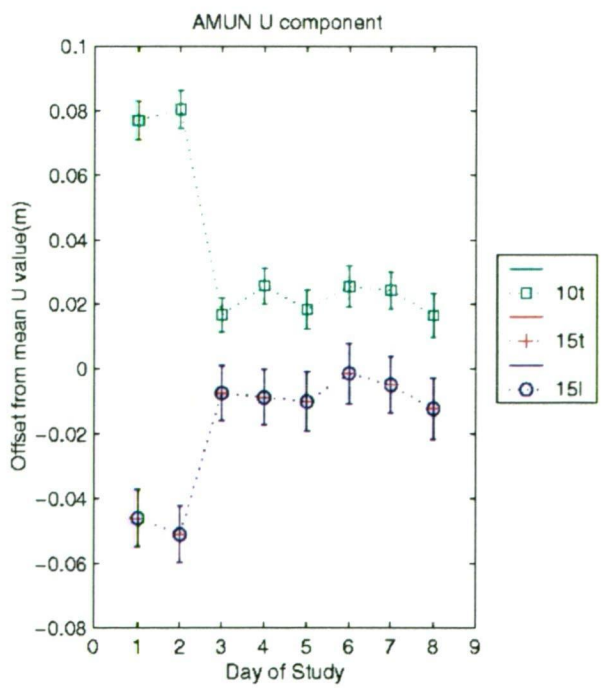

Figure 7.3 - AMUN Up coordinate results 1999. The x-axis represents the study days (see Table 7.2) in chronological order, i.e., '2' is DOY 002 while '3' is DOY 032.

7.4.3 GPS TZD to PW Conversion

[Note: this section provides an overview of the general GPS TZD to PW conversion method employed in the studies described in this and the following chapter (Chapter 8)]

7.4.3.1 Extraction of TZD Values

The GAMIT solutions for the TZD parameter at each study site and for each time interval are output to the standard solution summary file (q-file), an example of which is given in Figure 7.4.

	Label				A priori	Adjust(m)	Formal	Fract	Postfit
DAV1	ATMZEN	m	1	1	2.4059110650	-0.1260	0.0048	-26.4	2.27994702
DAV1	ATMZEN	m	2	1	2.4059110650	-0.1281	0.0054	-23.7	2.27776160
DAV1	ATMZEN	m	3	1	2.4059110650	-0.1183	0.0061	-19.3	2.28756141
DAV1	ATMZEN	m	4	1	2.4059110650	-0.1260	0.0051	-24.7	2.27987854
DAV1	ATMZEN	m	5	1	2.4059110650	-0.1156	0.0059	-19.7	2.29028185
DAV1	ATMZEN	m	6	1	2.4059110650	-0.1254	0.0050	-25.3	2.28046466
DAV1	ATMZEN	m	7	1	2.4059110650	-0.1274	0.0051	-25.0	2.27853819
DAV1	ATMZEN	m	8	1	2.4059110650	-0.1276	0.0045	-28.1	2.27826817
DAV1	ATMZEN	m	9	1	2.4059110650	-0.1274	0.0041	-30.8	2.27847782
DAV1	ATMZEN	m	10	1	2.4059110650	-0.1346	0.0054	-24.8	2.27134351
DAV1	ATMZEN	m	11	1	2.4059110650	-0.1291	0.0053	-24.3	2.27683147
DAV1	ATMZEN	m	12	1	2.4059110650	-0.1192	0.0052	-22.8	2.28668676
DAV1	ATMZEN	m	13	1	2.4059110650	-0.0972	0.0087	-11.2	2.30868948

Figure 7.4 - GAMIT q-file: TZD solution adjustments and estimates

In Figure 7.4 the column headings refer to:

Label gives the station name, parameter name, parameter units and estimate number. In this case, the results for the DAV1 TZD (m) at 13 (2-hourly) intervals are displayed.

A priori is the a priori estimate of the TZD determined from the input meteorological values and selected model and mapping function.

Adjust is the adjustment determined from the least-squares solution for the TZD parameter.

Formal is the formal uncertainty of the adjusted value

Fract is the ratio of the adjustment to the formal uncertainty

Postfit is the final estimate for the total TZD (a priori + adjustment)

A Fortran program (extract_gps_delay.f) was written to automatically extract the TZD estimates (*postfit*) and their formal errors into summary files for each site of interest for subsequent use in the PW conversion routines.

7.4.3.2 Input Data

Several sources of input data are required before the conversion from TZD to PW (equations (6.6) and (6.21) to (6.23)) can be undertaken. Figure 7.5 shows the set-up file for the TZD to PW conversion program used in these studies and indicates the various input data required during the conversion. The file is organised with one line per site, per day and each of the input files uses the Site and/or DOY values as an index to the relevant data.

Site	Yr	DOY	GPS File	Meteorology File	Coordinate File	ΔHeight File
100	98	237	DAV1_237.meteorology	d98surf.txt	IGS.llh	press_ht_IGS.txt
200	98	237	MAW1_237.meteorology	m98surf.txt	IGS.llh	press_ht_IGS.txt
300	98	237	CAS1_237.meteorology	c98surf.txt	IGS.llh	press_ht_IGS.txt
400	98	237	AMUN_237.meteorology	a98surf.txt	IGS.llh	press_ht_IGS.txt
⋮	⋮	⋮	⋮	⋮	⋮	⋮

Figure 7.5 - Section of a set-up file for the GPS PW program

The input files indicated in the header line of Figure 7.5 contain the following information:

GPS File *[TZD σTZD]*
: entries in this column refer to the files containing the GPS (2-hourly) TZD values from GAMIT analysis at the given site and DOY. There will be one of these files for each site observed on a given day.

Meteorology File *[DOY P T]*
: meteorological information (temperature (T) and pressure (P)) pertaining to the time and location of the TZD data are stored in the files indicated in this column. The meteorology files (one for each site for each campaign) are indexed by the DOY.

Coordinate File *[Site_N° Lat Lon H]*
: the file referenced in this column contains the ITRF97 geodetic (φ, λ) coordinates and the MSL height (H) for each site in the study.

ΔHeight File *[Site_N° ΔH]*
: these data are necessary, as surface meteorology measurements are typically not recorded at the exact GPS antenna elevation. In these cases, the pressure values need to be adjusted relative to the orthometric height difference between the GPS antenna and meteorological sensor (see Appendix C.2). The ΔHeight file contains the values of the height difference between pressure and GPS sensor and is indexed by site.

As discussed in section 6.4.2 and Appendix C.2, the accuracy of these input data will have an effect on the error level of the TZD to PW conversion results. Table 7.5 below indicates the precision of the observations collected at the sites in the Antarctic PW studies.

Table 7.5 - Precisions of PW conversion input parameters used in the Antarctic PW studies (information refers to parameters from the studies described in chapters 7 and 8)

Measurement	Location	Precision
Pressure	Davis, Mawson, Casey	0.1 hPa
Pressure	Amundsen	0.3 hPa
Pressure	Lambert traverse	≤ 1 hPa
Pressure Sensor Height	Davis, Mawson, Casey, Amundsen	~ 0.1 m
Pressure Sensor Height	Lambert traverse	~ 1 m
Surface Temperature	Davis, Mawson, Casey, Amundsen	0.1 °C
Surface Temperature	Lambert traverse	~ 5 °C
Latitude	All	centimetres
Height (H)	Davis, Mawson, Casey	centimetres
Height (H)	Amundsen/LGB	1 - 2 m (geoid uncertainty)

The level of uncertainty for most of the input data (Table 7.5) will not have a significant impact on the determination of parameters within the conversion equations or on the final error budget of the PW results (refer to 6.4.2 and Appendix C.2). In this studies, it is the uncertainty in the pressure values (up to 1 hPa) in conjunction with the processing uncertainty of the TZD values, that will have the greatest contribution to the final error level in the PW results (1 hPa pressure error ≈ 0.35 mm error in PW).

7.4.4 Conversion

The conversion from GPS TZD to precipitable water is a relatively simple process performed here using the series of equations outlined by (Bevis *et al*, 1992) and described fully in section 6.4.1 (see Figure 7.6).

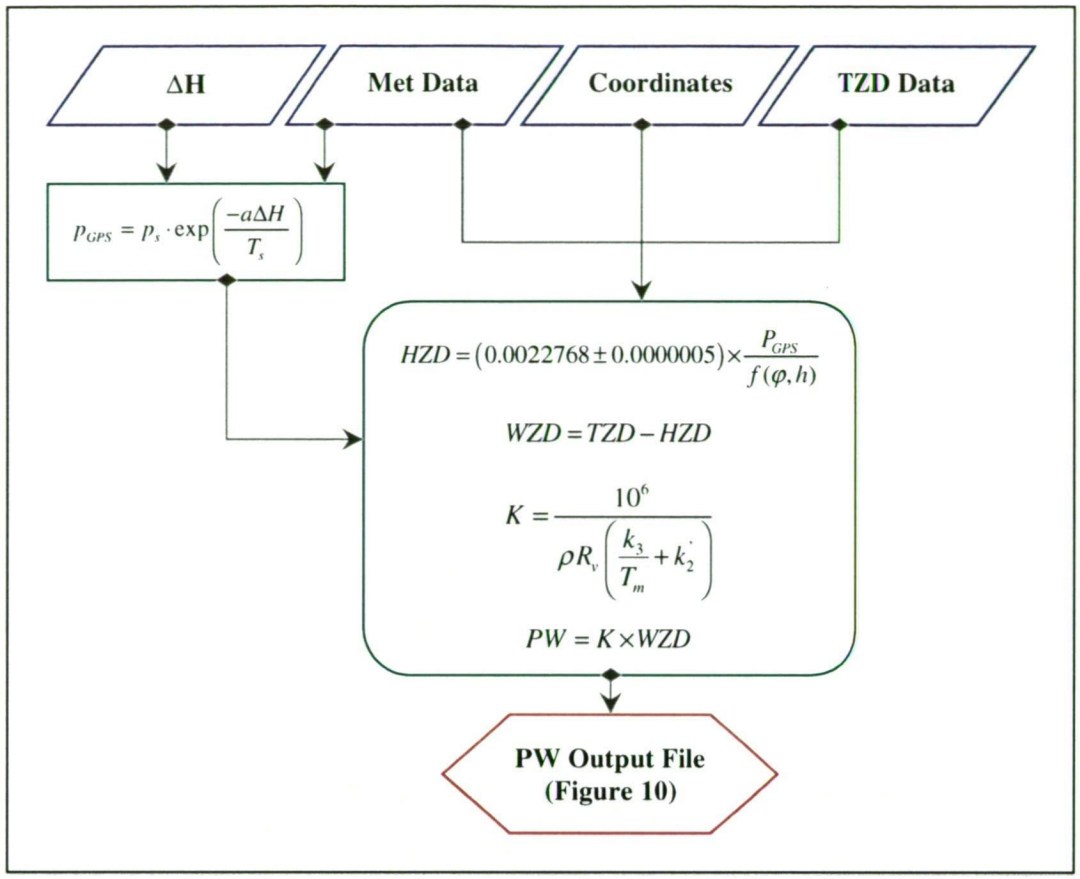

Figure 7.6 - Flowchart of the TZD to PW conversion process

A Matlab program (gps_PW.m), given in Appendix C.3, reads the data from the set-up file and outputs the mean PW value for each site occupation. Inside the Matlab program, the TZD values are cleaned (if necessary) to remove outliers (values greater than 3σ from the mean, generally found at day boundaries) and then the mean daily TZD, GPS antenna pressure, HZD, WZD, K and PW values and their mean uncertainties are determined using the values from the input files, the adopted constants[10] and equations (C.1), (C.2), (6.6) and (6.21) to (6.24).

The output from the conversion program is a file (of which Figure 7.7 is an example) containing values estimated during the various stages of the conversion, the input data values and the final mean PW value. The 1σ uncertainties for the major output parameters are also included in the output.

[10] Refractivity constants used in this program are taken from Bevis *et al* (1994) and are shown in equation (6.22).

```
[set-up file => igs98input.txt  ]          [processed  => 17-Jan-2001 12:32:44 ]
-------------------------------------------------------------------------------
Precipitable Water Results Using TZD Values From GAMIT Processing
-------------------------------------------------------------------------------
Cut-off GAMIT sigma => 0.0065
col 1  Site No
       100 = Davis
       200 = Mawson
       300 = Casey
       400 = Amundsen
col 2  Year
col 3  Day of Year
col 4  Total Zenith Delay (TZD) in mm from GAMIT q-file
col 5  TZD (1σ) uncertainty in mm from GAMIT q-file
col 6  Hydrostatic zenith delay (HZD) in mm
col 7  HZD (1σ) uncertainty in mm
col 8  Wet Zenith Delay (WZD) in mm (TZD - HZD)
col 9  WZD (1σ) uncertainty in mm
col 10 Precipitable Water (PW) in mm
col 11 PW (1σ) uncertainty in mm
col 12 Pressure at GPS (hPa)
col 13 Ground temperature at met station (degC)
col 14 GPS Latitude (geodetic, decimal degrees)
col 15 GPS Height(H) (km)
-------------------------------------------------------------------------------
100,1998,202,2230.212,1.655,2204.983,0.682,25.234,1.790,3.6,0.2,970.2,-20,-68,0.03
100,1998,203,2257.408,1.258,2234.168,0.681,23.239,1.431,3.3,0.2,983.1,-20,-68,0.03
100,1998,204,2270.109,1.734,2254.938,0.681,15.170,1.864,2.1,0.2,992.2,-21,-68,0.03
100,1998,205,2287.711,1.550,2270.014,0.681,17.697,1.693,2.5,0.2,998.8,-22,-68,0.03
100,1998,237,2252.201,1.206,2232.230,0.681,19.970,1.385,2.8,0.2,982.2,-21,-68,0.03
:
```

Figure 7.7 - Section of an output file from the GPS TZD to PW conversion

7.4.5 Conversion method employed for the Winter 1998 and Summer 1999 studies

The three GPS processing solutions, 15l, 15t and 10t, were carried out on each of the study days using the options defined in section 7.4.2. From each of these solutions, thirteen TZD estimates and their least-squares uncertainties were extracted at each of the study sites. These data were cleaned to remove outlier TZD estimates (generally located at the UT day boundaries) and a mean daily TZD value was then calculated for each processing solution, on each day, at each site. Finally, the mean daily TZD values were converted to PW estimates using the program *gps_PW.m* (see Appendix C.3) as discussed in section 7.4.4.

Mean daily PW was selected as the parameter of interest for this study in order to validate the proposed method for PW determination using the LGB GPS data (see Chapter 8). As there is generally very little variation[11] in PW at these Antarctic sites (i.e., daily PW range of 0 - 3 mm from radiosonde data and 0 - 5 mm from the GPS estimates) the use of this technique is assumed to be appropriate for these studies. To determine the likely error introduced by using daily average values for these studies, the 2-hourly GPS TZD estimates (on several different days) were converted to

[11] variation is of a similar magnitude to the noise in the GPS estimates.

individual PW values and compared to the radiosonde soundings at the corresponding epochs. This short test-study showed that the differences calculated between radiosonde and GPS PW at these epochs was generally within 1 mm of the value determined for the difference in between mean radiosonde and mean GPS on the given day.

7.5 Analysis of Radiosonde Soundings

Radiosonde data were made available for this study by the BoM and the Antarctic Meteorological Research Centre[12] and consisted of twice daily soundings (0000 and 1200 UTC) at each of the study sites (see Tables 7.2 and 7.3). Atmospheric column water vapour measurements derived from these radiosonde soundings are used in this study to verify the existence of close-to-zero water vapour at AMUN and as a comparison for the GPS derived PW results at the coastal sites.

Radiosondes collect information on the air temperature, dew point temperature and atmospheric pressure at various levels in the atmosphere. In order to convert this information into a measurement of the water vapour within the atmospheric column, several secondary parameters need to be determined and then integrated over the sounding. Firstly, the partial pressure of water vapour at adjacent integration levels is calculated (using the Clausius-Clapeyron equation (Stull, 1995)) and converted to values for the mixing ratio at each level as shown in Figure 7.8. The mixing ratio is then averaged between the two levels before being transformed into a value of PW within the given atmospheric layer. The methodology and equations that have been used in this thesis to calculate column water vapour from radiosonde measurements generally follow those of Connolley and King (1993) and an extract from the integration program is given below in Figure 7.8.

```
C  Compute the partial pressure of water vapour, the mixing ratio,
C  integrated water vapour and total water vapour for a layer between two
C  atmospheric levels, a and b.

C  Gravity (9.82 ms-1), Dew point temperature (td){K}, Pressure {kPa},
C  Partial pressure of water vapour (e) {kPa},
C  Mixing ratio (r) {g(water)/g(air)}, Precipitable Water (PW) {mm}

      ea = 0.611 * exp(6139.0 * (0.003661 - 1.0d0/(273.16 + tda)))
      eb = 0.611 * exp(6139.0 * (0.003661 - 1.0d0/(273.16 + tdb)))

      ra = 0.622*ea/(pressurea)
      rb = 0.622*eb/(pressureb)
      rm = (ra+rb)/2.0d0

      pw = 1000.0d0*(rm*pressureb - rm*pressurea)/Gravity
      total_water = total_water + pw
```

Figure 7.8 - Extract from radiosonde integration program (tcm_extract_rs)

[12] Research group at the University of Wisconsin, USA.

The number of pressure levels recorded in the radiosonde soundings limits the step size of the integration process and may cause some degradation of the accuracy of the final PW results. The assumptions and constants employed in the integration equations will also introduce errors into the radiosonde-derived PW values but these are likely to be minimal compared to the errors from the actual radiosonde measurements in such cold, dry atmospheres. Connolley and King (1993) state that there are two types of humidity sensors commonly used in modern radiosondes, both of which have been shown to estimate the relative humidity with significant errors (up to 30%) when deployed in regions of low temperature and humidity. Their study concluded that Antarctic radiosonde-derived PW may contain errors of up to 20% (assuming a temperature error of approximately 0.5°C and a relative humidity error of 10%). Therefore, using this assumption and from the expected amounts of PW at the study sites, it can be said that the radiosonde results in this study may potentially be affected by errors of approximately 0.5 to 2 mm depending on the location and time of year.

However, it can be seen from the radiosonde precipitable water measurements at Amundsen-Scott (Tables 7.2 and 7.3) that the difference from an assumed zero value at this site is less than 0.5 mm. This observation indicates that the radiosonde errors in this study are unlikely to be as high as suggested using the above assumptions.

7.6 Results And Discussion

7.6.1 Elevation Dependent Summary

Many researchers (e.g., Fang *et al* (1998) and Tregoning, Boers *et al* (1998)) have shown that varying the cut-off angle used in processing the GPS data and then investigating the variation of elevation-related parameters is an appropriate method of determining site-specific noise sources such as multipath, signal scattering and antenna phase centre errors.

Tables 7.6 and 7.7 and Figure 7.9 show the mean differences between the 15° and 10° elevation cut-off solutions for TZD, WZD, PW, East, North and Up parameters at AMUN and CAS1. The TZD ranges represent the results from the 2 hourly solutions, while for all other parameters the results relate to daily mean values[13]. Elevation dependent results were not obtained at MAW1 and DAV1 as data from these sites were not recorded below 15°.

[13] The daily mean WZD range is a direct reflection of the daily mean TZD range as the same HZD correction is applied to both the 10° and 15° solutions.

Table 7.6 - Winter 1998 elevation dependent results summary

Parameter	Winter 1998 - Mean difference (mm) between solutions (15° - 10°)	
	AMUN (rectangular dome)	CAS1
2hr-TZD	30	0
Daily WZD	30.5	-0.4
Daily PW	3.9	-0.1
East	0.6	1.7
North	-2	0.6
Up	-124	-2.7

Table 7.7 - Summer 1999 elevation dependent results summary

Parameter	Summer 1999 - Mean difference (mm) between solutions (15° - 10°)		
	AMUN (rectangular dome)	AMUN (SCIGN dome)	CAS1
2hr-TZD	32.5	8	0
Daily WZD	31.2	7.7	3
Daily PW	4.4	1.0	0.5
East	1.3	-0.6	-2
North	-1.9	0.3	0
Up	-127	-29	-3

The mean differences between the 15° and 10° elevation angle cut-off solutions are given in Tables 7.6 and 7.7 and indicate the extent of elevation dependency of the parameter estimates at each site. These values clearly show that at Casey, in both seasons, the results are only minimally affected by the change in elevation angle cut-off applied to the solution. In the summer season, there is slightly greater difference observed in the water vapour parameters, however this is not reflected in the Up component, as all coordinate differences remain approximately the same between seasons. For the results at AMUN, the effect of changing the radome is clearly seen in the values given in Table 7.7 where the mean difference drops to more acceptable values for the water vapour parameters and height after the deployment of the SCIGN dome. The East and North coordinates are also improved but to a much lesser degree reflecting the lack of elevation dependence observed in these parameters with the original rectangular dome. Comparing the AMUN 1999 differences to those of CAS1, there is still a clear indication of elevation dependent effects at this site, most significantly in the Up, WZD and PW parameters.

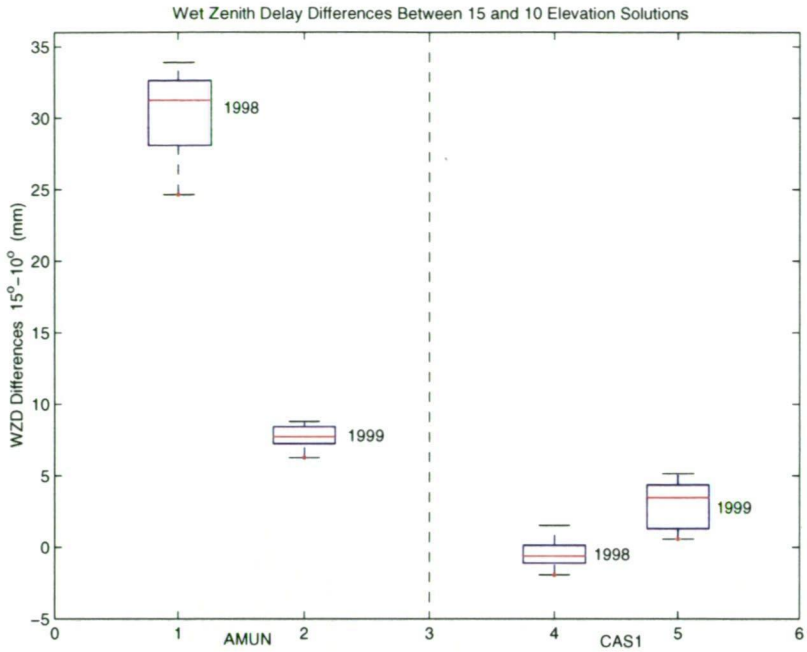

Figure 7.9 - Box and whiskers plot of the distribution of (15° - 10°) differences in WZD at AMUN and CAS1 for Winter 1998 and Summer 1999.

Figure 7.9 clearly shows that the WZD parameter has a significant elevation dependent component in both seasons at AMUN and that these effects are greatly reduced in the presence of the SCIGN dome. It can also be noted from Figure 7.9 that there is a very small elevation dependent effect in the WZD estimates at CAS1 for the 1999 results, while the 1998 values are unaffected by such a dependency. The mean effect on the WZD estimates at CAS1 due to variation of the elevation cut-off angle is 3mm, translating to a variation in PW of less than 0.5 mm.

The rectangular radome at AMUN has introduced significant phase centre modelling errors which is reflected in the biases observed in all parameters related to the vertical attributes of the site (TZD, daily WZD, daily PW, Up). However, it is not understood why smaller but significant biases remain in the AMUN data when the antenna is changed to the well-known SCIGN type in 1999. It is possible that the roof-mounted environment of the AMUN antenna is less favourable than the ground environment of CAS1 or that the mapping function is not well defined at this location. However neither of these possibilities can be confirmed using the information from this study.

From the results of this testing, it is clear that all daily WZD results at AMUN are contaminated by elevation dependent errors that vary in magnitude depending on the radome used. This contamination prevents the completion of the proposed study of the absolute precision of GPS PW determination under zero water vapour conditions, as the elevation dependencies are far greater than the expected PW signal. In particular, *question 2* of section 7.1 cannot be fully resolved.

It is also clear that the results at CAS1 in both periods have a similar, low dependency on the selected elevation angle cut-off. The characteristics of repeatability and small dispersion between the results for the different elevation solutions suggest that at CAS1, there is no significant elevation dependent component.

7.6.2 Coordinate Constraint Effects

In the study by Tregoning, Boers *et al* (1998), constraints on coordinates were shown to influence the ability to recover optimum PW estimates. They concluded that tight constraints should be applied to the three-dimensional coordinates of at least two well-known sites (e.g., IGS) and to the height of the site of interest. They also emphasised that it is critical that heights are constrained to their correct values. Other studies into GPS PW use different constraint methods. For example, Fang *et al* (1998) constrain four IGS sites to their ITRF94 values (using GAMIT), while Elgered *et al* (1997) and Johansson *et al* (1998) allowed all of their sites to be have loose a priori constraints (i.e., minimum constraint of 10m for IGS sites) during processing with GIPSY software. In this study, the differences between tight and loosely constrained solutions with a 15° elevation angle cut-off at DAV1 and CAS1 were observed to determine the effects of the constraints on the PW solution. The results of these analyses are shown in Tables 7.8 and 7.9.

Table 7.8 - Winter 1998 coordinate constraint results summary.

Parameter	Winter 1998 - Difference (mm) between 15° solutions (tight - loose)			
	DAV1		CAS1	
	min	max	min	max
2-hr TZD	-8.0	13.0	-3.0	2.0
Daily WZD	0.7	4.8	-0.3	0.5
Daily PW	0.1	0.7	0.0	0.1

Table 7.9 - Summer 1999 coordinate constraint results summary.

Parameter	Summer 1999 - Difference (mm) between 15° solutions (tight - loose)			
	DAV1		CAS1	
	min	max	min	max
TZD	-8.0	12.0	-3.0	6.0
Daily WZD	-0.5	6.0	-0.6	2.6
Daily PW	-0.1	0.9	-0.1	0.4

In Table 7.8, the range between minimum and maximum differences are less for the more weakly constrained CAS1 site than for the more heavily constrained DAV1 site. This pattern is repeated in the 1999 results (Table 7.9) where PW differences of up to 0.9 mm are observed at DAV1. Table 7.9 also shows slightly higher maximum differences between tight and loose solutions at CAS1 in 1999 than in 1998, however, these maximum differences are much less (50%) than those observed for the DAV1 estimates.

The most likely explanation for the differences between solutions at DAV1 is that overly tight constraints have been used. Long-term time series analyses (from the Scripps Institute of Oceanography global analysis centre) of GPS data from DAV1 and CAS1 between 1998 and 1999 show relatively noisy Up statistics (see Figure 7.10). The weighted rms values given in Figure 7.10 for the Up component at CAS1 and DAV1 over the period of this study are 9.4mm and 8.4 mm respectively. These values suggest that, for the tight solutions in this study, the Up component at DAV1 is overly constrained (10 mm) while for CAS1 the 50 mm constraint is adequate.

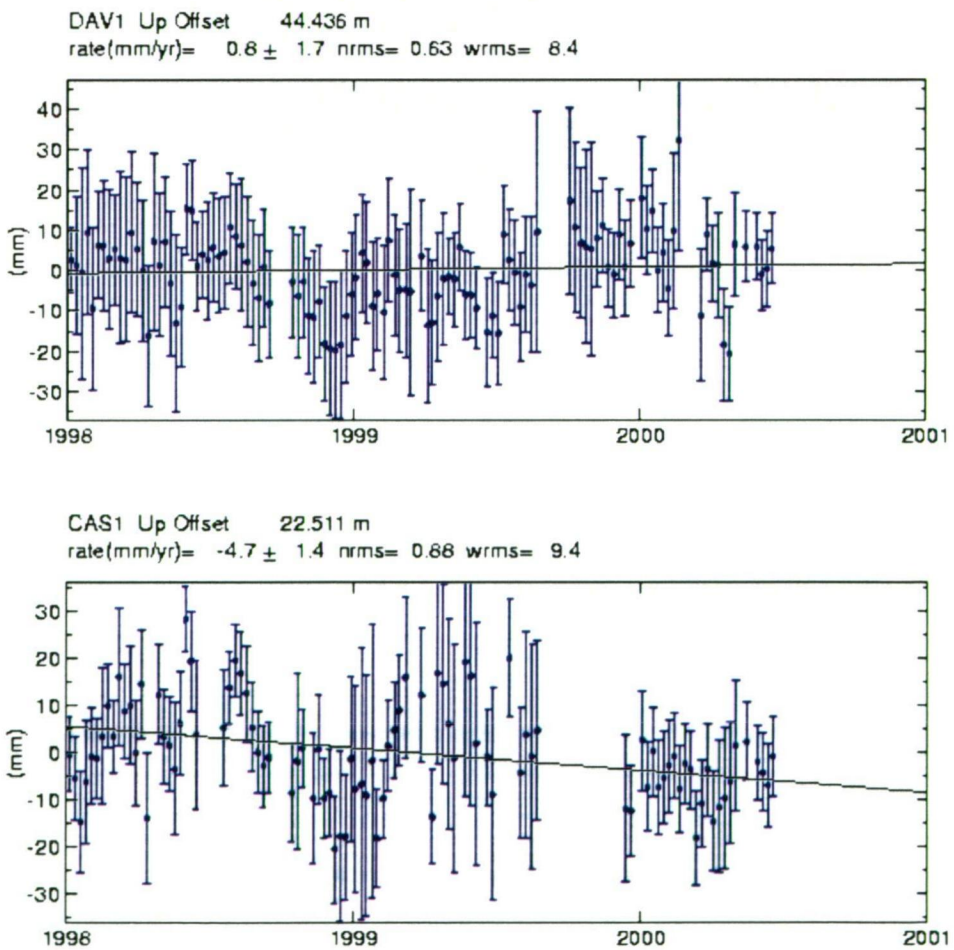

Figure 7.10 - DAV1 and CAS1 time series of Up coordinates from 1998-2001, Scripps Institute of Oceanography weekly-averaged SINEX files. Plots generated using the MIT global time series web page (http://bowie.mit.edu/~fresh/index2.html)

The small magnitude of the difference between these constraint solutions might ordinarily be overlooked and incorporated into systematic biases for PW estimation in temperate regions. However this amount of PW represents a significant percentage (23 - 67% depending on season) of the signal when there is only a few millimetres of PW to observe.

7.6.3 Amundsen Zero Comparison and Site Results

As mentioned in section 7.6.1, AMUN PW values derived from GPS data are unreliable when the rectangular cover (pre-February 1999) was installed due to the effect it has on the incoming signals and the lack of a model to correct for the variation of the electrical phase centre when such a dome is in place. The results of section 7.6.1 also indicate that when the hemispherical SCIGN cover was installed, the GPS PW values improved to a similar standard as the results from CAS1 but continued to display a significant elevation dependant bias. The elevation dependency of the GPS PW estimates with the SCIGN dome (i.e., after day032) is clearly seen in Figure 7.11 which illustrates the approximately 1 mm bias between the 15° and 10° solutions.

AMUN - Summer 1999				
DOY	**Radiosonde PW (mm)**	**GPS PW 10t (mm)**	**GPS PW 15t (mm)**	**GPS PW 15l (mm)**
001	0.28	-0.56 ± 0.11	3.63 ± 0.16	3.62 ± 0.16
002	0.33	-0.09 ± 0.12	4.50 ± 0.18	4.51 ± 0.18
032	0.42	1.95 ± 0.13	2.96 ± 0.17	2.96 ± 0.17
033	0.35	1.85 ± 0.12	3.08 ± 0.16	3.02 ± 0.16
045	0.28	2.75 ± 0.13	3.75 ± 0.17	3.78 ± 0.17
060	0.28	1.34 ± 0.12	2.17 ± 0.16	2.16 ± 0.16
061	0.27	1.62 ± 0.12	2.68 ± 0.16	2.67 ± 0.16
078	0.12	3.43 ± 0.15	4.51 ± 0.19	4.52 ± 0.19
Weighted Mean Bias (mm)		**1.77**	**2.82**	**2.81**
Wrms (mm)		**0.72**	**0.59**	**0.61**

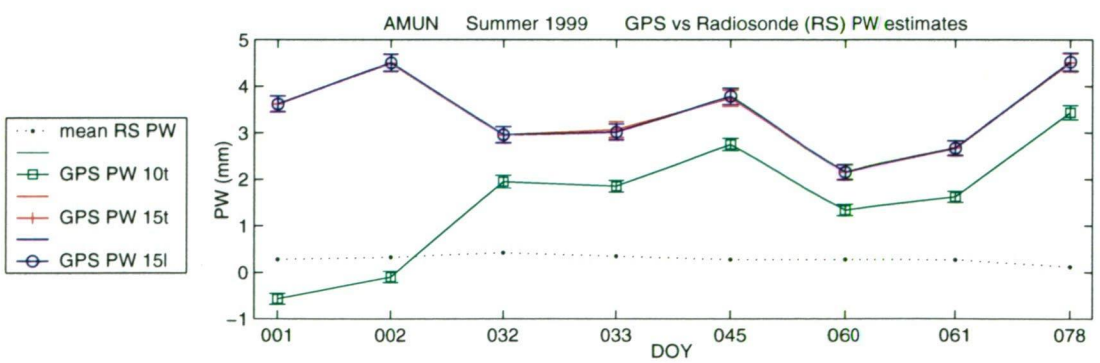

Figure 7.11 - AMUN PW estimates from GPS and radiosonde (Summer 1999)

The rectangular dome consistently produced negative PW for the AMUN 10° solutions (see days 001 and 002 in Figure 7.11), however, no negative GPS daily PW values were observed at AMUN once the SCIGN dome was in place.

GPS estimates of PW at AMUN after January 1999 have a bias of 2 - 4 mm, significantly different to the near-zero radiosonde estimates (given in column 2 of the table in Figure 7.11). The magnitude of these biases at AMUN makes it impossible to observe the small-scale errors introduced into the PW results by the TZD estimation process as originally intended. There are several factors that may be contributing to the biases, however most may be discounted for the reasons given below:

Surface Pressure: A 1 hPa error in pressure will translate into approximately a 2.3 mm error in the hydrostatic zenith delay (HZD) (see section 6.4.2). Therefore a constant error in the pressure measurements of up to 10 hPa is required to create PW biases of the magnitude found in this study. This scenario is not likely given that pressure measurements at this site are calibrated to 0.3 hPa.

Another source of error in the pressure value is the use of the hypsometric equation to adjust measured pressure to a value corresponding to the height of the GPS antenna (see Appendix C.2). The height uncertainty at AMUN (< 4 m) will not introduce an error of more than 0.3 hPa into the adjusted GPS pressure and therefore this is not the cause of the large bias in PW at this site.

HZD: Possible error sources in this parameter include uncertainty in the equation constant (see equation 6.6), the GPS latitude and GPS height. As discussed in section 6.4.2, uncertainties in latitude and height of the magnitude found in this study would not make a significant contribution to the PW bias observed at AMUN. Emardson *et al* (1998) discuss the uncertainty of the constant in the HZD equation (equation 6.6) and suggest that it could be responsible for errors in PW of 0.35 mm, again this error estimate is not large enough to explain the AMUN bias.

TZD: As mentioned in section 6.4.2, the processing of the GPS data is recognised as the greatest contributor to errors in TZD/PW estimates. In this study, orbital errors have been minimised by using IGS precise orbits and a global network solution. Unmodelled multipath, atmospheric pressure and ocean loading

effects have been reduced by calculation of mean daily values for TZD. Residual ionospheric effects would not provide a constant error of the magnitude observed in the data over the three-month period.

Section 7.6.1 discusses the elevation dependence of the results at AMUN, which indicate that site specific, elevation dependent effects are introducing errors into the GPS processing and contaminating the PW (see Figure 7.11) and height estimates (see Figure 7.3). It is possible that inadequacies in the mapping function definition at this latitude are contributing to the TZD error. However, the results of other studies (e.g., Mendes and Langley (1994)) suggest that mapping function errors at this latitude should not exceed 10 mm of the total delay. Therefore this is not likely to be the major error source affecting the AMUN results.

A third possible source of error in the AMUN results is interference in the GPS signals. The antenna dome, an external electrical interference source (e.g., a radio antenna), the metal roof or substructure may be affecting the signal and contributing to the biases observed at this site. This would seem the most likely source of error in the PW and height results due to the elevation dependent and constant nature of the biases in these parameters.

In summary, the biases observed in the height (30 - 40 mm) and PW (2 - 4 mm) estimates at AMUN indicate the likely presence of antenna phase centre definition errors potentially due to mis-modelling of the phase centre variation or the tropospheric delay. The size of these biases makes it impossible to determine the absolute error in the GPS technique from these data as the smaller errors in the PW estimates cannot be observed.

7.6.4 PW at DAV1, CAS1 and MAW1

Sections 7.6.1 to 7.6.3 have shown that:

- elevation modelling is generally correct and consistent at CAS1,
- coordinate constraints do affect results but as long as the constraints and a priori coordinates have realistic values their effect on the PW solution is small,
- negative estimates of PW are unlikely to occur,
- the antenna dome configuration can have a significant impact on the PW values,
- site specific effects and processing uncertainties are the most likely cause of constant biases in the PW solutions.

In the following sections, the GPS PW values for DAV1, CAS1 and MAW1 are compared to radiosonde measurements as an indication of the accuracy and precision

of the GPS results. Figures 7.12 to 7.14 include tables of the radiosonde and GPS mean daily PW results and uncertainties, the weighted mean bias of the GPS estimates from the radiosonde values and the wrms[14] values around this bias for the 15l, 15t and 10t processing solutions.

Figures 7.12 to 7.14 also show plots of the GPS mean daily PW solutions against the radiosonde mean daily values. In examining these results, it should be remembered that the radiosonde values may potentially contain errors, due to equipment malfunction in cold temperatures, of up to 2 mm although results at AMUN suggest that this error is much less (i.e., approx 0.5 mm). The GPS and radiosonde PW data at DAV1, CAS1 and MAW1 show similar patterns over time with small, site dependent biases and wrms values that are relatively consistent (around 0.5 - 0.8 mm) for all solutions.

In Figures 7.12 and 7.13, the constraint and elevation dependent effects noted in sections 7.6.2 and 7.6.1 can be observed in the smaller biases for the 15l solutions at DAV1 and the 10t PW solutions at CAS1 (1999) respectively.

7.6.4.1 DAV1

Figure 7.12 shows that the GPS daily PW values at DAV1 closely follow the pattern of the radiosonde measurements with a 2 - 3 mm bias between the two datasets.

At DAV1, in both seasons, the lowest biases between the GPS and radiosonde values are found in the 15l data, which is consistent with previous findings regarding constraint effects (section 7.6.2).

Comparing the bias values in Figures 7.12a and 7.12b, there is a strong seasonal variation of approximately 0.9 mm, suggesting that either the GPS over-estimates or the radiosonde under-estimates the PW on a seasonal basis. Since the heights at DAV1 are known to be quite variable with a quasi-cyclical pattern (Figure 7.10), there is a strong likelihood that seasonal station height variations are influencing the PW determination and hence the bias. Radiosonde readings are also known to have significant errors especially when low temperatures are coupled with low relative humidity. This will alter their accuracy between seasons and therefore represents another potential source of bias.

The wrms value for the DAV1 solutions have an absolute magnitude that is consistent with the seasonal nature of the bias. The wrms value is not dependent on the elevation mask or coordinate constraints, which suggests the presence of small residual errors in either the GPS or radiosonde processes, or both.

[14] weighted root-mean-square

DAV1 - Winter 1998				
DOY	**Radiosonde PW (mm)**	**GPS PW 10t (mm)**	**GPS PW 15t (mm)**	**GPS PW 15l (mm)**
202	1.18	3.63 ± 0.27	3.52 ± 0.27	3.04 ± 0.28
203	1.42	3.37 ± 0.22	3.28 ± 0.23	3.15 ± 0.23
204	1.25	2.24 ± 0.26	2.23 ± 0.26	1.57 ± 0.27
205	0.95	2.52 ± 0.25	2.45 ± 0.25	2.34 ± 0.26
237	0.85	2.86 ± 0.21	2.95 ± 0.21	2.73 ± 0.21
238	0.87	2.86 ± 0.30	2.83 ± 0.30	2.14 ± 0.30
239	1.20	4.91 ± 0.33	5.02 ± 0.34	4.41 ± 0.35
273	0.67	2.81 ± 0.21	2.75 ± 0.21	2.32 ± 0.22
274	0.54	2.27 ± 0.24	2.21 ± 0.24	1.95 ± 0.26
275	1.50	4.65 ± 0.27	4.56 ± 0.27	4.33 ± 0.27
Weighted Mean Bias (mm)		**2.08**	**2.04**	**1.71**
Wrms (mm)		**0.64**	**0.65**	**0.67**

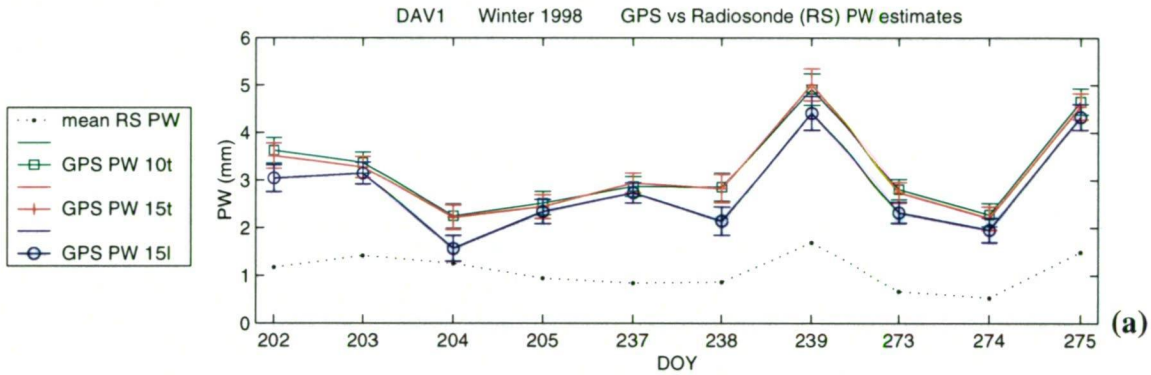

(a)

DAV1 - Summer 1999				
DOY	**Radiosonde PW (mm)**	**GPS PW 10t (mm)**	**GPS PW 15t (mm)**	**GPS PW 15l (mm)**
001	3.86	6.74 ± 0.29	6.61 ± 0.29	6.68 ± 0.31
002	4.02	7.25 ± 0.30	7.14 ± 0.30	7.12 ± 0.31
032	3.33	6.05 ± 0.26	6.10 ± 0.26	5.70 ± 0.27
033	4.48	7.04 ± 0.27	7.01 ± 0.27	6.48 ± 0.28
045	2.98	7.39 ± 0.28	7.39 ± 0.28	6.80 ± 0.29
060	5.16	9.15 ± 0.30	9.14 ± 0.30	8.55 ± 0.31
061	5.36	6.91 ± 0.29	6.91 ± 0.29	6.09 ± 0.29
078	1.89	4.81 ± 0.28	4.81 ± 0.28	3.95 ± 0.29
Weighted Mean Bias (mm)		**3.02**	**2.99**	**2.50**
Wrms (mm)		**0.81**	**0.81**	**0.91**

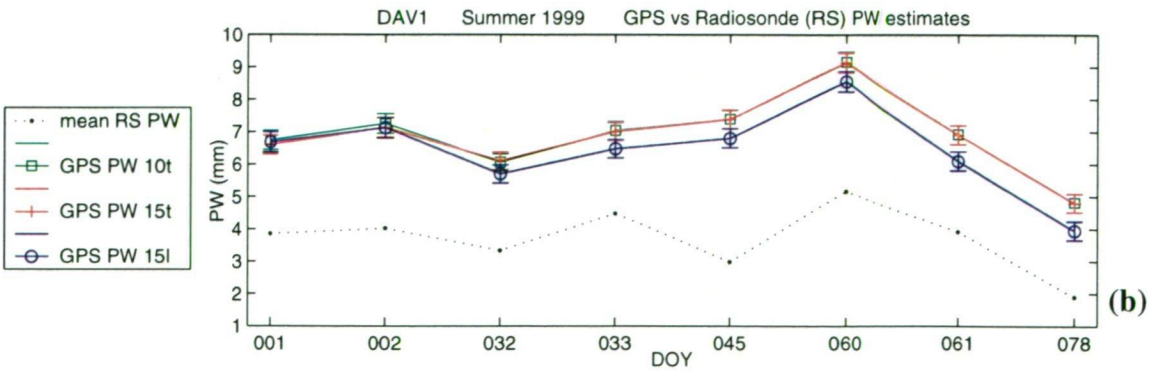

(b)

Figure 7.12 - DAV1 PW estimates from GPS and radiosonde (a) Winter 1998, (b) Summer 1999

7.6.4.2 CAS1

Figure 7.13 displays the comparison between radiosonde and GPS daily PW results at CAS1. As with the DAV1 results, these datasets are seen to compare very well in terms of the pattern of PW over the study period. However, at CAS1 there is no significant bias[15] observed between the GPS and radiosonde mean daily PW values in the Winter 1998 results. The wrms around the bias for the 1998 solutions is approximately 0.7 mm, a similar value to the DAV1 results (0.6 mm). The Summer 1999 GPS PW results at CAS1 do show a small bias (0.45 - 0.79 mm depending on the solution) when compared to the radiosonde values. This is consistent with the increased summer bias observed at DAV1. The change in bias between seasons at CAS1 may therefore be a reflection of seasonal influences on the station height (see Figure 7.10) or seasonal errors in the radiosonde soundings as discussed for DAV1 (see section 7.6.4.1).

A small elevation dependency has been observed in the PW estimates at CAS1 for summer 1999, which is reflected in the results shown in Figure 7.9. The elevation dependency is very limited at CAS1, with differences between the 15t and 10t bias values of less than 0.35 mm. This difference is consistent with the elevation dependent results from the best performing stations in the GPS PW error study of Fang *et al* (1998). In their study, they showed that using the Niell mapping functions and the IGS antenna phase centre model, the median offset between 7° and 15° elevation solutions for Turbo-Rogue antennas was generally less than 1 mm. This slight elevation dependency is not observed in the winter 1998 CAS1 results.

7.6.4.3 MAW1

The MAW1 PW results (Figure 7.14) show no significant variation due to the fact that in all solutions, the coordinate constraint and elevation angle parameters at MAW1 do not change.

In Figure 7.14, the radiosonde and GPS daily PW values follow very similar patterns over the study periods. This close comparison between the GPS and radiosonde PW values indicates that at MAW1, PW can be estimated with a bias of 0.8 to 1.5 mm, depending on the season. The PW results for MAW1 also show the same seasonal pattern as CAS1 and DAV1, with the Summer 1999 bias being significantly and consistently higher than the Winter 1998 results. Again this is possibly related to seasonal errors in the radiosonde soundings (see section 7.6.4.1) or variations in the height solution at MAW1.

[15] the Winter 1998 mean bias is statistically zero within one standard deviation, $\sigma_{\text{weighted mean}} = 0.08\text{mm}$

CAS1 - Winter 1998				
DOY	**Radiosonde PW (mm)**	**GPS PW 10t (mm)**	**GPS PW 15t (mm)**	**GPS PW 15l (mm)**
202	4.04	4.52 ± 0.20	4.57 ± 0.26	4.56 ± 0.26
203	3.37	4.19 ± 0.18	4.10 ± 0.22	4.09 ± 0.22
204	3.86	3.62 ± 0.18	3.47 ± 0.22	3.44 ± 0.22
205	2.55	1.84 ± 0.15	1.56 ± 0.20	1.56 ± 0.20
237	0.85	0.41 ± 0.14	0.40 ± 0.18	0.43 ± 0.18
239	2.99	4.55 ± 0.23	4.77 ± 0.28	4.73 ± 0.28
274	1.47	1.94 ± 0.19	1.85 ± 0.24	1.78 ± 0.24
275	1.26	1.36 ± 0.20	1.18 ± 0.25	1.16 ± 0.25
Weighted Mean Bias (mm)		**0.08**	**0.03**	**0.01**
Wrms (mm)		**0.66**	**0.76**	**0.75**

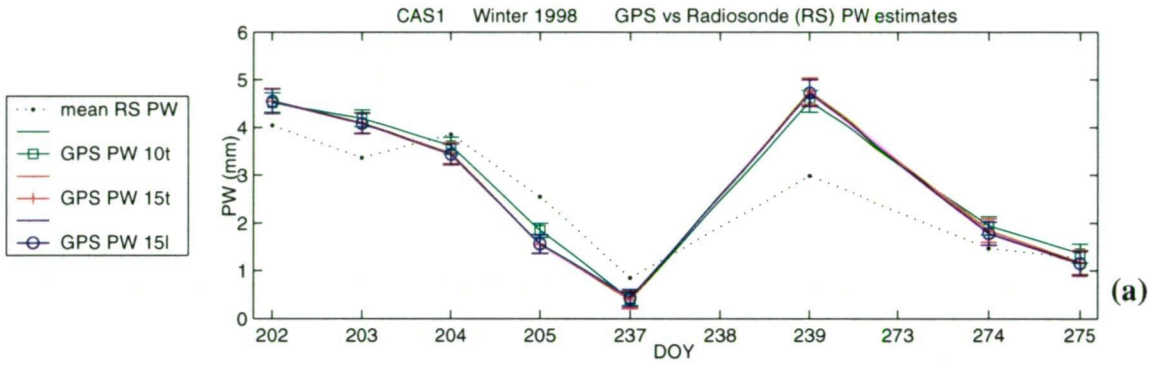

CAS1 - Summer 1999				
DOY	**Radiosonde PW (mm)**	**GPS PW 10t (mm)**	**GPS PW 15t (mm)**	**GPS PW 15l (mm)**
001	5.84	6.23 ± 0.56	6.32 ± 0.75	5.64 ± 0.94
002	5.06	6.63 ± 0.47	7.32 ± 0.59	7.40 ± 0.61
032	4.36	4.40 ± 0.17	4.97 ± 0.20	4.98 ± 0.20
033	6.69	7.01 ± 0.20	7.36 ± 0.23	7.36 ± 0.23
045	4.19	5.33 ± 0.40	5.86 ± 0.50	5.46 ± 0.51
060	9.43	8.77 ± 0.35	9.54 ± 0.44	9.29 ± 0.44
061	8.19	9.23 ± 0.31	9.37 ± 0.36	9.39 ± 0.37
Weighted Mean Bias (mm)		**0.45**	**0.79**	**0.74**
Wrms (mm)		**0.55**	**0.46**	**0.48**

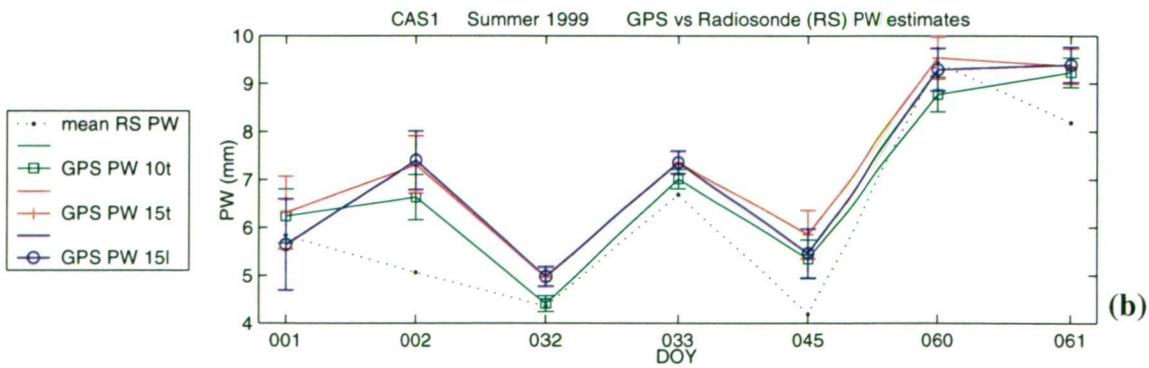

Figure 7.13 - CAS1 PW estimates from GPS and radiosonde (a) Winter 1998, (b) Summer 1999

MAW1 - Winter 1998				
DOY	**Radiosonde PW (mm)**	**GPS PW 10t (mm)**	**GPS PW 15t (mm)**	**GPS PW 15l (mm)**
202	0.56	1.30 ± 0.25	1.25 ± 0.25	1.23 ± 0.25
203	0.31	1.47 ± 0.21	1.32 ± 0.21	1.27 ± 0.21
204	1.36	2.13 ± 0.27	2.12 ± 0.27	2.03 ± 0.27
205	1.53	1.79 ± 0.23	1.76 ± 0.23	1.72 ± 0.23
237	0.59	1.53 ± 0.21	1.48 ± 0.21	1.51 ± 0.21
238	0.41	1.54 ± 0.30	1.61 ± 0.30	1.55 ± 0.30
239	0.43	0.40 ± 0.30	0.33 ± 0.31	0.32 ± 0.31
273	1.95	2.65 ± 0.23	2.58 ± 0.23	2.57 ± 0.23
274	0.72	2.24 ± 0.24	1.95 ± 0.24	1.98 ± 0.24
275	2.48	3.51 ± 0.24	3.45 ± 0.24	3.48 ± 0.24
Weighted Mean Bias (mm)		**0.85**	**0.78**	**0.76**
Wrms (mm)		**0.40**	**0.36**	**0.37**

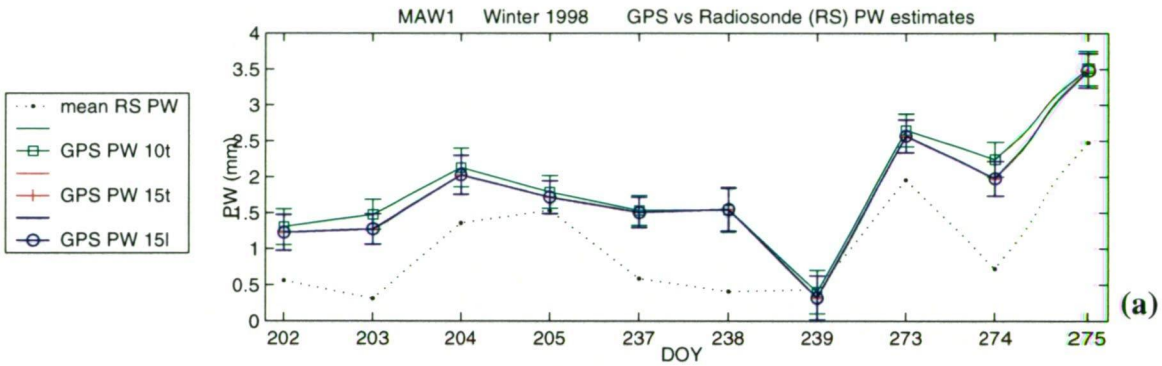

(a)

MAW1 - Summer 1999				
DOY	**Radiosonde PW (mm)**	**GPS PW 10t (mm)**	**GPS PW 15t (mm)**	**GPS PW 15l (mm)**
001	4.92	5.87 ± 0.25	5.58 ± 0.25	5.67 ± 0.25
002	6.35	9.16 ± 0.29	9.08 ± 0.29	9.18 ± 0.29
032	3.59	5.34 ± 0.24	5.29 ± 0.25	5.26 ± 0.25
033	4.12	5.42 ± 0.24	5.27 ± 0.24	5.23 ± 0.24
045	2.97	5.24 ± 0.27	5.18 ± 0.27	5.16 ± 0.27
060	6.10	7.25 ± 0.34	7.31 ± 0.34	7.32 ± 0.34
061	4.10	4.90 ± 0.26	4.96 ± 0.26	4.87 ± 0.26
078	0.88	1.71 ± 0.28	1.64 ± 0.29	1.73 ± 0.29
Weighted Mean Bias (mm)		**1.47**	**1.38**	**1.39**
Wrms (mm)		**0.66**	**0.68**	**0.69**

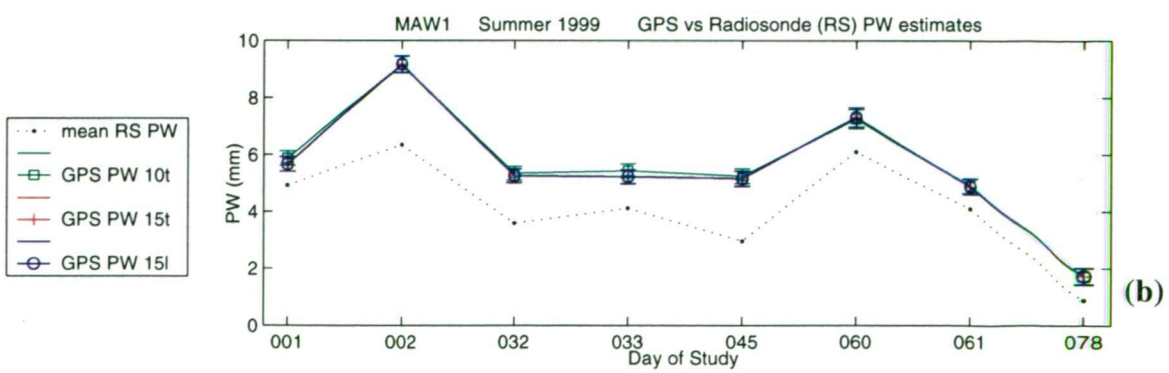

(b)

Figure 7.14 - MAW1 PW estimates from GPS and radiosonde (a) Winter 1998, (b) Summer 1999

7.7 Study Conclusions

In section 7.1 four questions were posed:

1. *What effect do elevation cut-off angles and coordinate constraints have on the TZD/PW estimates at Antarctic sites?*

The analysis of TZD/PW estimates at DAV1, CAS1 and AMUN clearly indicate that the quality of the GPS installation is a major factor affecting the impact of elevation angle cut-off and coordinate constraints. At 'well behaved' and well modelled sites (e.g., CAS1), the effect of varying the elevation mask generally has no significant impact on the TZD/PW parameter. However at a site with non-standard equipment configuration or a poor signal environment (e.g., AMUN), varying the elevation mask has a significant effect on the determination of TZD/PW.

The variation of the level of coordinate constraint imposed on the DAV1 and CAS1 sites resulted in generally consistent and significant variations in the DAV1 PW but had very little effect on the CAS1 results. From the DAV1 GPS and radiosonde PW comparisons, the 'loose' (500 mm) GPS values were found to have a lower bias than the 'tight' (10 mm) results. Inspection of the long-term variations in height at these two sites indicated a wrms scatter of approximately 10 mm. It was concluded that the 10 mm height constraint at DAV1 was therefore too tight given the potential for variation in this parameter. The residual error due to the overly tight constraint on the height component was then distributed to the PW estimates. The low amount of variation found in the CAS1 results indicates that the use of either moderately tight or loose constraints on well-known site coordinates does not significantly affect the final PW value.

The determination of TZD/PW at Antarctic sites has therefore been shown to be relatively robust when the antenna is operated in a good environment with a well-determined elevation model for the antenna phase centre and realistic constraints (i.e., greater than 1σ of the weekly variability) on the a priori Up coordinate.

2. *Are non-zero PW values observed at the South Pole and if so, what is causing them and do they represent the absolute magnitude of GPS PW precision for current processing strategies?*

GPS processing errors could not be studied in detail at AMUN due to site specific, elevation dependant factors dominating the PW estimates.

The PW results for most of the tests carried out on the AMUN data were consistently ±2 - 4 mm from the near-zero predicted value at this site. However, the PW values

were not stable when the elevation mask was varied indicating that the PW estimates at AMUN are significantly affected by the choice of processing parameters.

It is known from this study and those of other researchers (e.g., Emardson *et al*, 1998; Fang *et al*, 1998; Tregoning, Boers *et al*, 1998) that small biases exist for all GPS observations of PW. The fact that biases from a near-zero benchmark at AMUN are relatively large and elevation dependent strongly suggests that the GPS PW values are incorrect and hence no inference can be made on the presence or magnitude of smaller PW error sources as was the original intent of this study.

Thus firm, reliable answers to the absolute magnitude of GPS PW precision cannot be made from the results of this study. It is partially resolved that an upper limit of approximately 4 mm exists but this value contains known elevation dependence and therefore is in error and does not provide an indication of the true capabilities of the GPS PW method.

3. *Are negative PW values ever obtained at sites with low atmospheric water vapour content and if so, what is causing them? Are these effects caused by observational, model or processing deficiencies?*

The strict answer to this question is that negative values do occur. However, in all cases, negative mean daily PW values were found to exist only at AMUN when an inappropriate elevation dependent phase centre model was applied to the data. These negative values were a result of variable path effects caused by the shape of the rectangular radome. Thus, in this case, the detection of negative PW is indicative of a breakdown in system specification and not in the modelling and assumptions used in the determination and reduction of TZD/PW.

4. *How do PW values obtained using GPS techniques compare with radiosonde values for data from East Antarctica?*

The GPS determined values of TZD/PW mimic the radiosonde determined values with seasonal biases of less than +2 - +3 mm and a daily scatter about the bias of less than 1 mm (1σ). These values are consistent with results from other studies (e.g., Emardson *et al* (1998), Fang *et al* (1998) and Tregoning, Boers *et al* (1998)) and therefore indicate that standard GPS PW processing and conversion techniques are valid at Antarctic sites.

The results of this study show that the GPS almost always estimates higher PW values than the radiosonde, it is not known how much of the bias is attributable to GPS errors or radiosonde deficiencies. Given that the radiosonde values of PW at AMUN (Tables 7.2 and 7.3), are close to the expected 0 mm, the radiosonde PW

error is likely to be less than 1 mm. Therefore for the data in this study, the GPS results represent upper limits of the true PW values.

The results in section 7.6.4 also indicate that the bias between the GPS and radiosonde results appears to vary seasonally, a characteristic that is most probably linked in some way to variations in the radiosonde errors and/or station height fluctuations.

The bias between radiosonde and GPS estimates at DAV1, CAS1 and MAW1 is not consistent between sites, indicating the presence of site-specific effects in the GPS data. The bias is highest at Davis (approximately 3 mm) and lowest at CAS1 (0 - 1 mm). These sites have the same GPS equipment configuration, are located at similar latitudes and use the same radiosonde equipment in similar climates. Therefore, the expectation would be that they produce similar PW biases. The only significant difference between the sites is the mounting and local environment of the antennas (refer to Table 7.1 and Figure 7.1). A recent study of antenna characteristics by Johnston (2000) suggests that antennas mounted directly on the ground produce less noisy results than those at 1.5 m above the surface. Johnston (2000) also found that noisiest results occurred for sites with antenna heights close to 0.5 m above the ground or pillar. These findings agree with the between site variations in the PW bias noted in this study (i.e., height at DAV1 = 0.3 m and DAV1 has highest bias level; height at CAS1 $\approx$ 0 and CAS1 has lowest bias level) and may partially explain some of the site dependency observed in the PW results.

Figure 7.15 - DAV1 Antenna and dome (photo courtesy of AUSLIG Geodesy, Feb. 2001)

It has been noted during the course of this study that the custom-built hemispherical domes over the DAV1, CAS1 and MAW1 antennas are not mounted such that the antenna phase centre is located close to the centre of a defined sphere (refer to

Figures 7.1 and 7.15). This non-standard mounting would be expected to contribute to the elevation dependent errors in the GPS derived parameters at these sites. However, in this study, no significant elevation dependency was observed in the CAS1 results and elevation dependencies were not investigated at DAV1 and MAW1. Therefore, any errors due to this non-standard antenna/radome configuration have not been identified in these analyses. Although not detected in this study, it is likely that the PW values at these sites are contaminated in some way by the positioning of the radome and this may be contributing in part to the observed biases. More detailed testing of the GPS data at these sites is recommended in order to fully assess the impact of the radome installation on the site parameters.

Chapter 8

WATER VAPOUR IN THE LAMBERT GLACIER BASIN

In Chapters 1 and 6, the importance of water vapour as a climate change indicator in global and Antarctic studies was introduced. In his thesis, Reid (2000), using numerical model predictions for tripled carbon dioxide levels, showed a more uniform spatial increase in Antarctic TCM than surface temperature, but while temperature increased consistently over the whole year, the TCM increased more during the warm months. These findings and the known exponential nature of the saturation vapour relation[1] suggest that, if measured accurately and frequently, changes in Antarctic water vapour are likely to provide a more sensitive indicator to climate change in this region than other parameters, such as atmospheric temperature.

Atmospheric moisture is also important in Antarctic mass balance studies in that it is the source of all mass input for the ice sheets. If the amount of available water vapour can be monitored accurately in long term studies, then it will provide important information regarding the input parameter in mass balance studies. Connolley and King (1993) used PW information from radiosondes to calculate the flux of water vapour at 16 Antarctic sites. The data from the sites in East Antarctica were then used to calculate a moisture budget and infer an accumulation rate for this region. Connolley and King (1993) concluded that their water vapour budget was not very reliable and had high uncertainties, mainly due to the sparseness of radiosonde locations.

The nature of the GPS meteorology technique suggests that it could be used to overcome some of the temporal and spatial deficiencies in Antarctic water vapour studies. GPS meteorology could provide a useful tool for continuous monitoring of water vapour at Antarctic coastal sites and potentially could also be used for collecting water vapour information in more remote locations. In Chapter 7, initial studies were carried out to determine the feasibility of using this method at sites in East Antarctica. The results from these studies showed that GPS PW values could be obtained such that the GPS values agreed with radiosonde measurements made at

[1] approximately 10% increase in PW per 1°C of temperature increase (Reid, 2000)

these sites after identification and removal of site-dependent, constant biases from the GPS values. In this chapter, the GPS PW estimation method is applied to data collected on the Antarctic plateau, during the LGB traverses, as a case study for remote applications.

The LGB perimeter extends approximately 900 km inland and therefore data collection of any description in this area is difficult and infrequent. Currently, meteorological data in the LGB region is restricted to permanent, manned sites on the coast at Mawson and Davis and eight Automatic Weather Stations (AWS), six[2] on the traverse line and two on the ice shelf (see Figure 8.1). The AWS deployed along the traverse route do not record humidity data and therefore water vapour is essentially not monitored in this region from ground-based equipment.

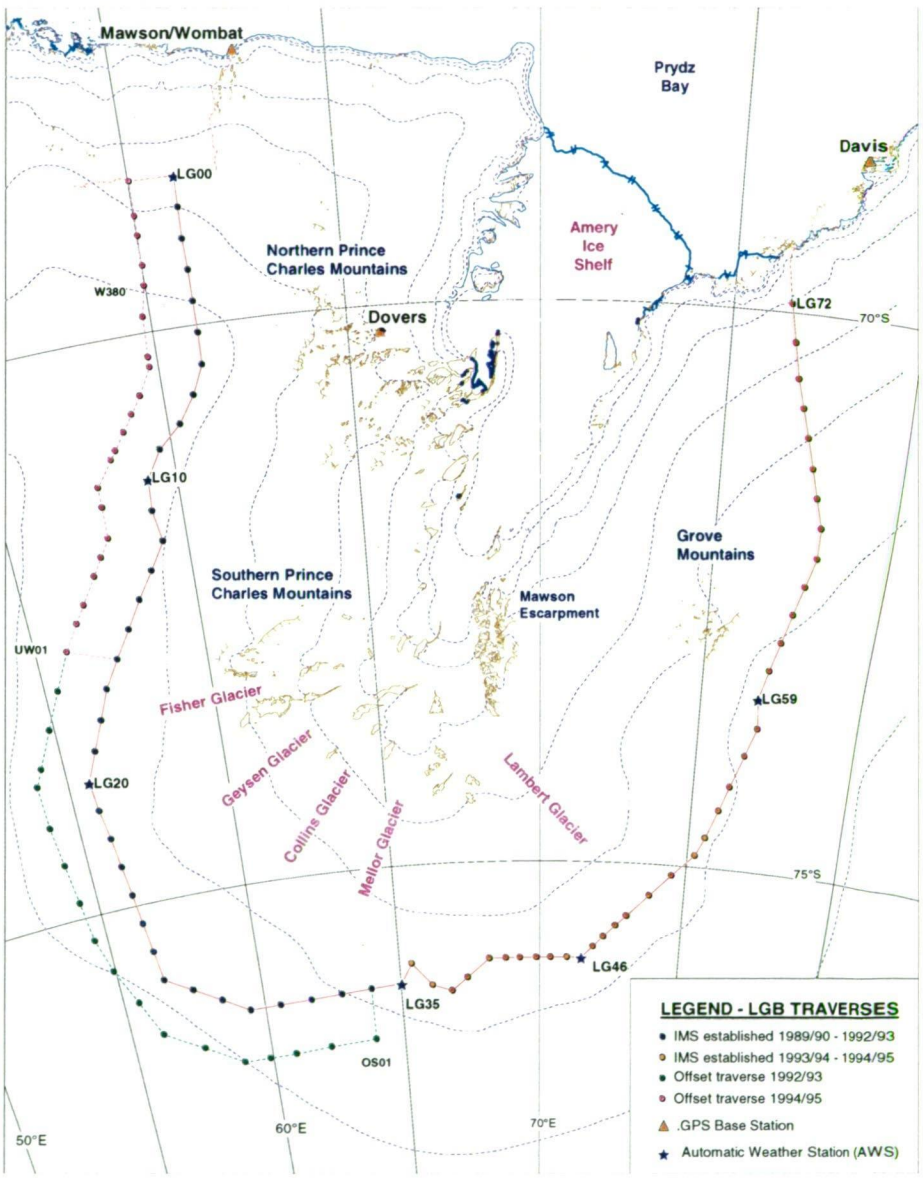

Figure 8.1 - The Lambert Glacier Basin traverses.

[2] Since May 1997 only five of the LGB traverse AWS are functioning, the equipment at LG46 has ceased to collect data.

The GPS PW estimation method would be a useful addition to meteorology measurements in regions like the LGB and, if shown to be effective, should be incorporated into future GPS campaigns. Permanent glacial rebound sites would also be ideal as long term PW monitoring sites and this adaptation has already been considered by researchers in this field (pers. com., P. Tregoning, 2000).

In this chapter, water vapour estimates in the Lambert Glacier region from radiosonde and GPS data are investigated. Firstly, 11 years of radiosonde soundings at Davis and Mawson are studied to understand the dynamics and temporal characteristics of water vapour in this region. The TZD values determined from the LGB GPS data are then converted into PW values at the traverse sites and used in an investigation of the summer distribution of water vapour along the traverse route. Results from this analysis are compared to NCEP model values and discussed in relation to the current understanding of the accumulation and meteorology patterns in the region. Finally, conclusions as to the effectiveness of GPS meteorology in remote Antarctic areas and potential future uses of this technique are discussed.

8.1 Antarctic Meteorology

Before discussing the potential use of GPS in Antarctic PW studies, it is important to have an understanding of the meteorological processes at work in this region. The following is a general overview of the most significant features of Antarctic weather and climate. Unless otherwise stated, the information in the following paragraphs has been sourced from King and Turner (1997).

8.1.1 Pressure

The mean atmospheric circulation of the Earth includes a high pressure region over Antarctica with a band of low pressure at approximately 60 - 70° S known as the circumpolar trough. This large-scale circulation system is created by warm air being transported southward from the tropics over the Antarctic continent and then cooled. This cooling, and the topography of the ice surface causes the air to flow outward from the centre of the continent towards the Southern Ocean. This mean circulation pattern determines the general energy/heat/moisture transport over the high interior of the continent. The coastal region of Antarctica is affected by this circulation but is also influenced by synoptic-scale processes such as cyclones, ridges and frontal systems that generally do not penetrate far inland.

Annual pressure measurements in Antarctica exhibit a very strong semi-annual oscillation with maximum pressures recorded during the solstices and minima at the equinoxes (Bromwich and Parish, 1998) (Figure 8.2). This semi-annual signal is

reflected in the latitudinal variation in the location of the circumpolar trough, which is at its most northerly extent in summer and winter. These significant changes in the mean pressure field are a reflection of large-scale effects resulting from readjustments in the temperature and wind dynamics (air mass transport) due to relatively rapid variations in the amount of incoming solar radiation at these times (Bromwich and Parish, 1998). The largest semi-annual pressure changes are reported in the interior of the continent and decrease in magnitude toward the north (Bromwich and Parish, 1998). An example of this trend is also seen in Figure 8.2 where the variation in mean monthly pressure at LG20 is notably larger than at Mawson and Davis.

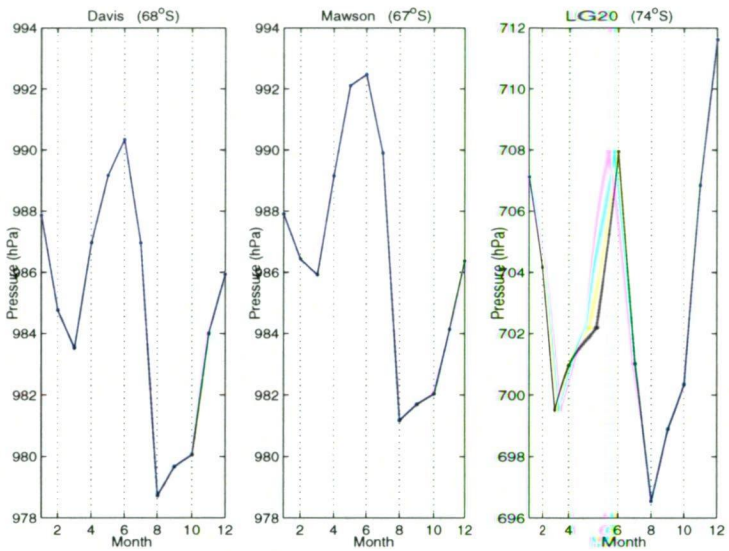

Figure 8.2 - Annual pressure signal (mean monthly values) at Davis, Mawson and LG20 (1990 - 1994)

8.1.2 Surface Inversion

One of the most remarkable features of the lower atmosphere over the Antarctic continent is the presence of a very strong and generally stable surface inversion. This inversion is a product of net radiative cooling of the atmospheric layer directly above the surface and is maintained by the subsidence of warmer, upper air. The inversion is strongest in the continental interior and in winter months, however inversions are observed year round in all locations. The depth of the inversion (i.e., vertical scale) can range from one hundred to several hundred metres and varies depending on the site and time of year.

8.1.3 Temperature

Mean surface temperature in Antarctica is found to generally decrease with altitude and latitude. However the rate of temperature decrease with respect to elevation has

been observed to vary significantly, depending on the surface slope in the region of interest and the distance from the coast.

Annual temperature cycles at Antarctic sites generally show a maximum during the summer months but do not have a corresponding distinct minimum during the winter. The general temperature trend for Antarctic sites displays rapid cooling associated with the decrease in incoming solar radiation in autumn followed by relatively constant values over the winter months and then warming again after September. This phenomenon is well known and referred to as a "coreless" winter. The variation in annual temperatures is largely controlled by continental proximity effects that lead to the greatest range in temperatures being observed at plateau sites (e.g., LG20 in Figure 8.3) (Bromwich and Parish, 1998; Allison *et al*, 1993).

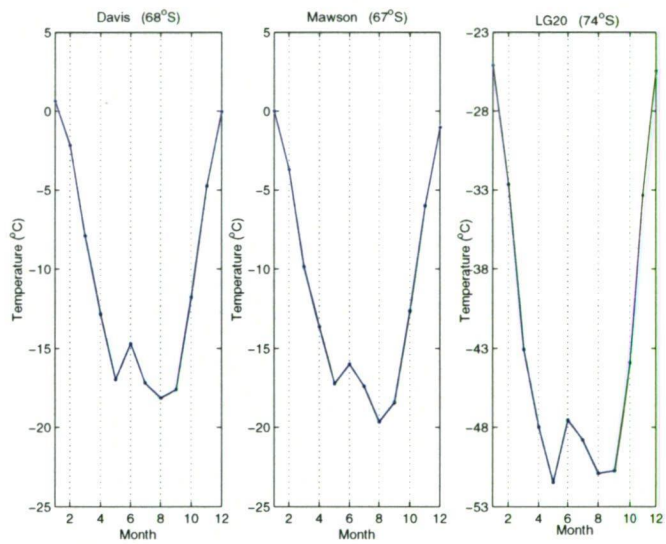

Figure 8.3 - Annual temperature signal (mean monthly values) at Davis, Mawson and LG20 (1990 - 1994)

Antarctic winter temperatures are more variable than summer (Allison, 1998) and this may partially explain the presence of the small winter peaks seen in Figure 8.3. During winter, many inland Antarctic sites have observed frequent warm events which are thought to be related to the stronger meridional (N - S) temperature gradients bringing warmer air over the continent during this period (Allison *et al*, 1993; Allison, 1998) and/or the breakdown of the surface inversion layer by subsiding warm air or turbulent mixing by the high winds observed during winter (Allison, 1998). At coastal sites the same causes of increased winter temperature are applicable but there is also the possibility of warm maritime air being transported by synoptic scale events over these regions during winter (Streten, 1990).

8.1.4 Surface Wind

Surface winds over the ice sheet are predominantly katabatic in nature. They are caused by the gravitational flow of cold, dense air in the boundary (inversion) layer from high to lower elevations. The effect of the Coriolis force turns the gravitational (southerly) flow of the air from the continental interior to the left. At the coast the katabatic winds join with the polar easterlies which are characteristic of the presence of the low pressure band in the Southern Ocean. Therefore the mean near-surface winds tend to range from southerly to easterly in direction (depending on topography and latitude) and consist mainly of colder air being transported from the interior.

Surface winds in the interior generally have a remarkably constant direction, which is closely related to the surface topography. This feature indicates that winds in this region are dominated by the katabatic forcing with little influence from synoptic events. At the coast, there is much greater variation in direction of the air flow, reflecting the considerably greater influence of synoptic events in this region.

Variation in wind speed changes depending on surface slope, location and the annual pressure and temperature cycles. Coastal sites tend to have more variation in wind speed due to synoptic forcing and seasonal variations in the katabatic flow. Wind speeds at sites on steep slopes away from the coastal influences generally vary in relation to seasonal changes in the strength of the temperature inversion. Highest wind speeds are observed on the plateau at sites where a) the topography acts to channel the katabatic flow and/or b) where the katabatic flow and geostrophic forces are aligned.

8.1.5 Upper Level Wind

Connolley and King (1993) produced average upper air wind vectors for the radiosonde sites used in their study. From their information at the 850 hPa level it can be seen that generally the winds follow the anticyclonic pattern seen at the surface. However, at this level the katabatic effects are much weaker and the winds tend slightly more easterly than those at the surface. At 850 hPa the wind direction at Davis tends to flow towards the LGB with a highly variable direction and more strength than the surface flow. For Mawson, the 850 hPa winds appear to be more easterly than at the surface but have a similar speed and tend to have a low variability in direction.

The average annual wind data from the study by Connolley and King (1993) at the 500 hPa level indicates a generally much weaker flow which tends more westerly in direction. This change in direction creates a general inward flow of air at 500 hPa, compensating for the drainage flow observed in the lower atmosphere (Connolley and King, 1993). At Mawson, the mean wind characteristics show an outflow of air

in the form of a weak and relatively constant westerly wind. The air flow at 500 hPa above Davis is also weak and flows generally towards the south but the direction varies significantly around the mean.

At 300 hPa the wind direction at most of the sites studied by Connolley and King (1993) is westerly and stronger than at the 500 hPa level, while at 100 hPa the winds are also westerly and display the strongest and most consistent mean flow in the atmospheric column.

8.1.6 Water Vapour

Atmospheric water vapour is the source of all ice in the continental ice sheets; therefore it is vital in the study of mass balance of the region. Moisture in the Antarctic atmosphere is input via the upper atmosphere circulation or, in coastal areas, by synoptic systems carrying moist maritime air.

The relationship between temperature and saturation is reflected in the similarities of the annual variation in the atmospheric water vapour and temperature (e.g., Figure 8.4). The temperature saturation relation also provides insight into the likely vertical distribution of water vapour in the atmospheric column. It is expected that, in times of little vertical mixing, the air directly above the inversion (i.e., the warmest layer) will hold the most moisture. For most of the year, the cold temperatures of the surface air will cause it to be close to saturation or even supersaturated. During summer months the slight warming of the inversion surface layer may lead to increases in evaporation rates.

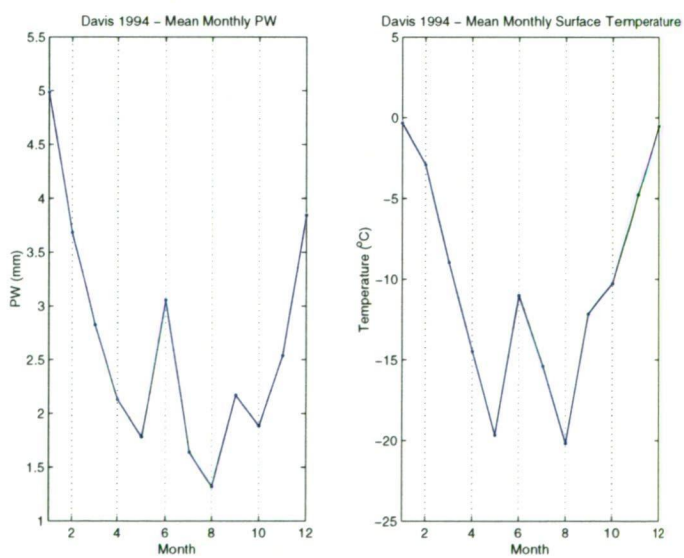

Figure 8.4 - Davis 1994 comparison between PW and temperature

Day to day variation in TCM is greater at coastal sites than those in the interior due to the influence of changing synoptic scale weather systems (Connolley and King, 1993) making the exact amount available at any time/location difficult to predict. Water vapour in the interior of the continent is generally transported there via the mean circulation or by the easterly winds and tends to decrease with increasing elevation.

8.1.7 Precipitation

The general pattern of precipitation over Antarctica shows decreasing precipitation from the coast to the elevated interior and a higher precipitation rate in West Antarctica compared to East Antarctica (Bromwich and Parish, 1998).

Near the coast most precipitation is created by episodic synoptic processes. In this region the most important precipitation mechanism is the adiabatic cooling of moist maritime air as it moves inland, an event usually associated with the eastern side of a low pressure system which provides sufficient energy to lift the air onto the coastal plateau. Precipitation in the interior is mostly from 'clear skies' whereby ice crystals semi-continuously fall without the presence of visible clouds. This type of precipitation is thought to be maintained by the lifting of maritime air and by the radiative cooling of the boundary layer (Bromwich, 1988). Depression systems have been observed several times a year on the high plateau (e.g., at Vostok) and these events also contribute to precipitation but they are not the norm.

On a seasonal basis, it has been observed that more precipitation occurs at coastal sites in autumn and spring than summer and winter, that is, there is more precipitation in periods of low pressure. This is indicative of the role of cyclone activity in the occurrence of precipitation events.

8.2 Meteorology of the LGB

During the LGB traverses, six Automatic Weather stations were deployed along the traverse route (see Figure 8.1). These AWS have been extremely important in understanding the local climate and weather patterns in this region. The dominant katabatic winds and the influence of local topography (refer to Figure 5.2) are major factors influencing the climate of the LGB.

8.2.1 Surface Winds

Allison (1998) presented the results of analysis of the LGB AWS data from 1994 - 1996. In this report, high wind speeds and katabatic flow were observed for all stations. As shown in Figure 8.5, the strongest mean winds in the LGB are observed

at LG00 (due to the steep coastal slope), at LG59 in the east (high surface slope and easterly flow aligned with the geostrophic forces) and LG35 (funnelled flow due to its location in the glacier valley). Winds are also reported to be stronger at these sites during winter as a consequence of the stronger surface inversion and increased katabatic flow.

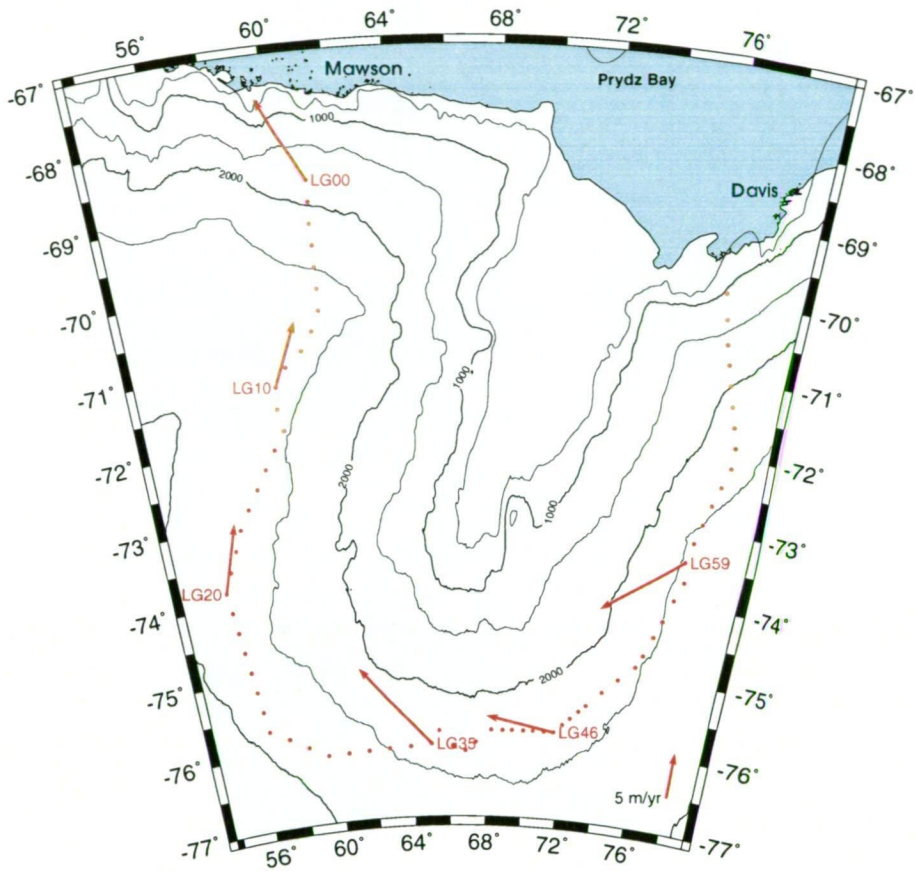

Figure 8.5 - Annual mean surface wind (1994-96) at the LGB AWS (wind data from Allison (1998))

At all of the LGB AWS, the mean wind direction is generally within 30° of the fall line (Allison, 1998). However in the east, the deviations from the mean slope direction are smaller due to the correlation between the slope and mean geostrophic wind direction (Allison, 1998). In the eastern sector, the dominant surface wind flow is from the north-east due to geostrophic and katabatic effects, the southern sites are influenced by south-easterly winds while in the west the winds tend more southerly before returning to south-easterly near the coastal escarpment (Figure 8.5).

At the coastal margins of the LGB the wind patterns are very different to each other. The annual average surface winds at Mawson are observed to have high speed and a relatively constant south-easterly direction (Connolley and King, 1993). At Davis the winds tend to be much weaker and generally flow toward the LGB (Connolley and King, 1993). This wind pattern is assisted by the frequent presence of low pressure systems within Prydz Bay (Budd, 1986).

8.2.2 Temperature

Allison (1998) noted that the AWS at LG59 observed annual average temperatures that were 4.5°C warmer than sites at similar elevations in the western sector of the basin. This feature is confirmed by the values reported in Higham *et al* (1997) for 10 m firn temps around the LGB. Higham *et al* (1997) suggest that the temperature difference between the sectors is due to the transport of cooler air from the interior to the west by the dominant southerly winds. However, Allison (1998) proposes that the temperature difference is caused by adiabatic heating in the East due to the presence of stronger, more easterly katabatic winds. Both of these explanations are plausible.

As shown in Figure 8.3, the pattern of annual variation in temperature at the LGB sites is similar to that observed at Davis and Mawson and generally exhibits the typical Antarctic "coreless" structure. Allison (1998) observed that during winter, the AWS temperature data recorded increases of 20°C or more over 2 - 3 day periods during high pressure/high wind events which may account for some of the slight rise in temperatures seen during mid-winter.

8.2.3 Pressure

Pressure at the AWS has a semi-annual signal, as noted at other Antarctic sites, with maxima observed in July and December (see section 8.1.1 and Figure 8.2). Allison (1998) observed that all of the LGB AWS sites displayed an increase in pressure during winter at approximately the same time.

8.2.4 Water Vapour

The study of radiosonde soundings by Connolley and King (1993) included observations on the average water vapour fluxes through the troposphere at Davis and Mawson. The results of their study indicate that generally, the majority of water vapour enters the LGB from the Davis/Wilhelm II Land region at all atmospheric levels below approximately 100 hPa (see section 8.1.5).

In the LGB, the circulation patterns observed within the lower layers of the atmosphere (i.e., the region expected to contain the majority of water vapour) suggest that the amount of water vapour is likely to be higher in the eastern region of the LGB traverse line and is distributed to southern, western and lower elevation areas via the dominant air flows.

8.2.5 Accumulation

Extensive accumulation measurements were made during the LGB traverses, the results of which are presented in Higham *et al* (1997) and Higham and Craven (1997).

In summary, Higham *et al* (1997) reveal that the western and southern accumulation patterns are somewhat affected by continentality and elevation influences while in the east, accumulation is regulated by the topography and strong winds. They note that spatial accumulation rates along the LGB traverse route are lower than at the same elevation elsewhere in East Antarctica and that accumulation in this region is highly variable due to the redistribution of snow by the dominant winds.

In their report Higham *et al* (1997) identified three distinct accumulation regions within the basin:

i) western sector (LG06 to 29), mean accumulation (1994) = 94 $kgm^{-2}a^{-1}$ (σ = 74)[3]

ii) southern sector (LG29 to 50), mean accumulation (1994) = 56 $kgm^{-2}a^{-1}$ (σ = 72)

iii)eastern sector (LG50 to 67), mean accumulation (1994) = 70 $kgm^{-2}a^{-1}$ (σ = 71)

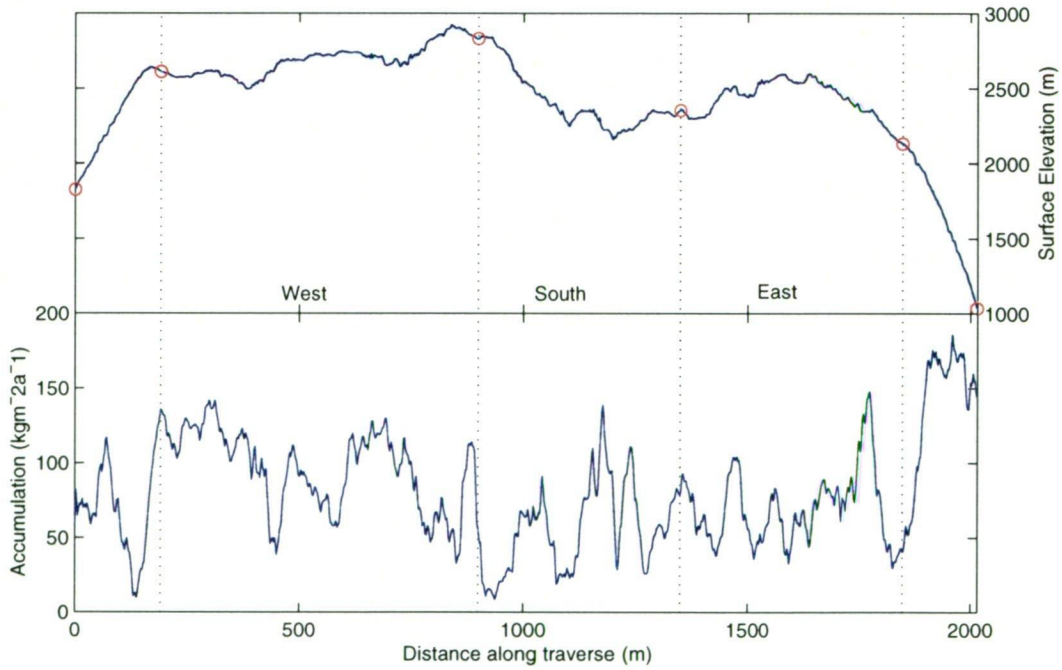

Figure 8.6 - Smoothed (30 km) annual accumulation values (1994) for the LGB traverse route. (Data made available by the Australian Antarctic Division Glaciology Section and presented previously in Higham *et al* (1997))

[3] σ represents the contribution of the average surface microrelief to the variability (Higham *et al*, 1997)

The eastern LGB is in the rain-shadow of prevailing upper level winds and therefore accumulation at a given elevation in this area may be up to 50% less than in the west (Allison, 1998). In regards to accumulation in the eastern sector, Higham *et al* (1997) observe that surface features and slopes are more important factors than elevation in controlling the accumulation rate. The lower value for accumulation at the southern LGB sites appears to be related to continentality and elevation effects (Higham *et al*, 1997).

On an annual basis, there is very little systematic variation in surface net accumulation for Antarctic regions at the elevations of the LGB sites (Budd *et al*, 1995). In terms of interannual variability, Higham *et al* (1997) observe large differences in the accumulation rate along the traverse route over the period of the five traverses. The most significant variation was observed for the western LGB sites in 1993 where very low accumulation rates were measured (Higham *et al*, 1997).

8.3 Water Vapour Characteristics in the LGB Region

8.3.1 Davis and Mawson PW Analysis

Davis and Mawson stations represent the extremes of the LGB region at the coast and therefore are important sites for observing the transport of PW into and out of the basin. In theory, the mean temporal pattern of PW at the inland sites should mimic the signal found in the coastal data as the majority of moisture is carried inland by the movement of air from the coast in the Davis region and via the mean north - south upper air circulation.

Eleven years (1989 - 99) of radiosonde soundings at Davis and Mawson were obtained from the BoM. These files contain measurements of air temperature, dew point temperature, geopotential height, and pressure at specified levels within the atmosphere up to 200 hPa. Generally two soundings per day (approximately 0000UT and 1200UT) were available at both sites. These soundings were integrated to obtain values of PW using the method described in section 7.5.

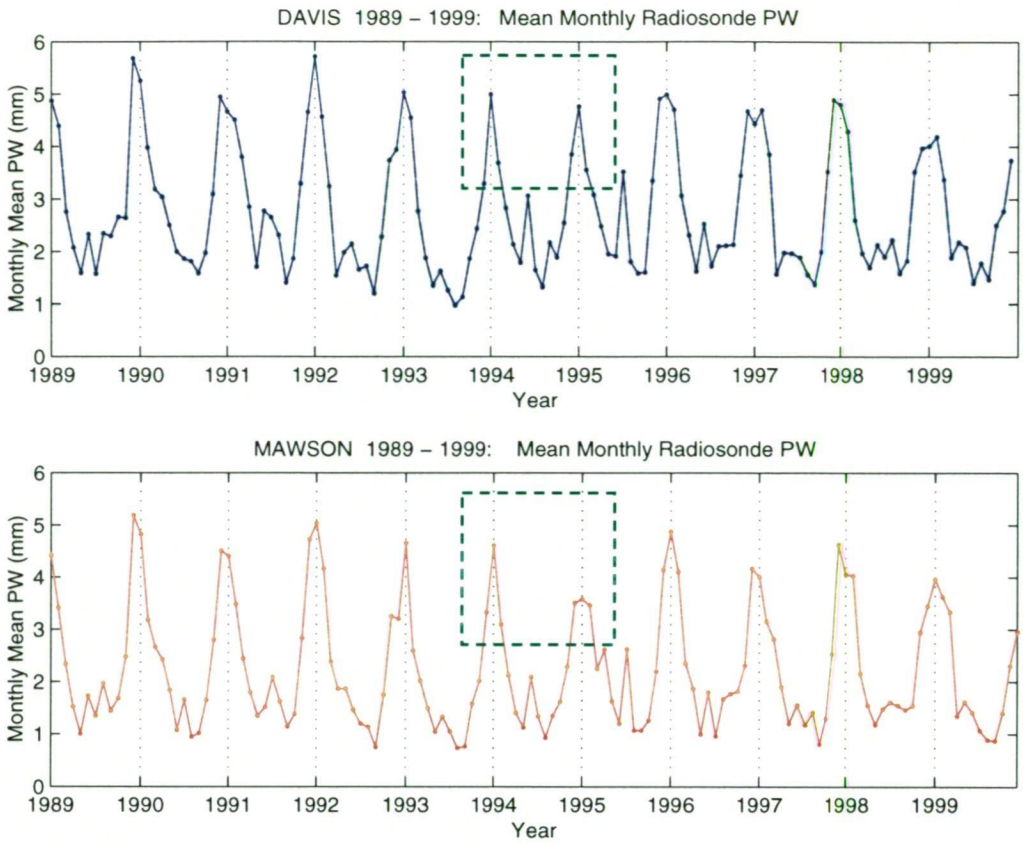

Figure 8.7 - 11-year time series of radiosonde derived precipitable water (green boxes indicate period of LGB GPS PW observations)

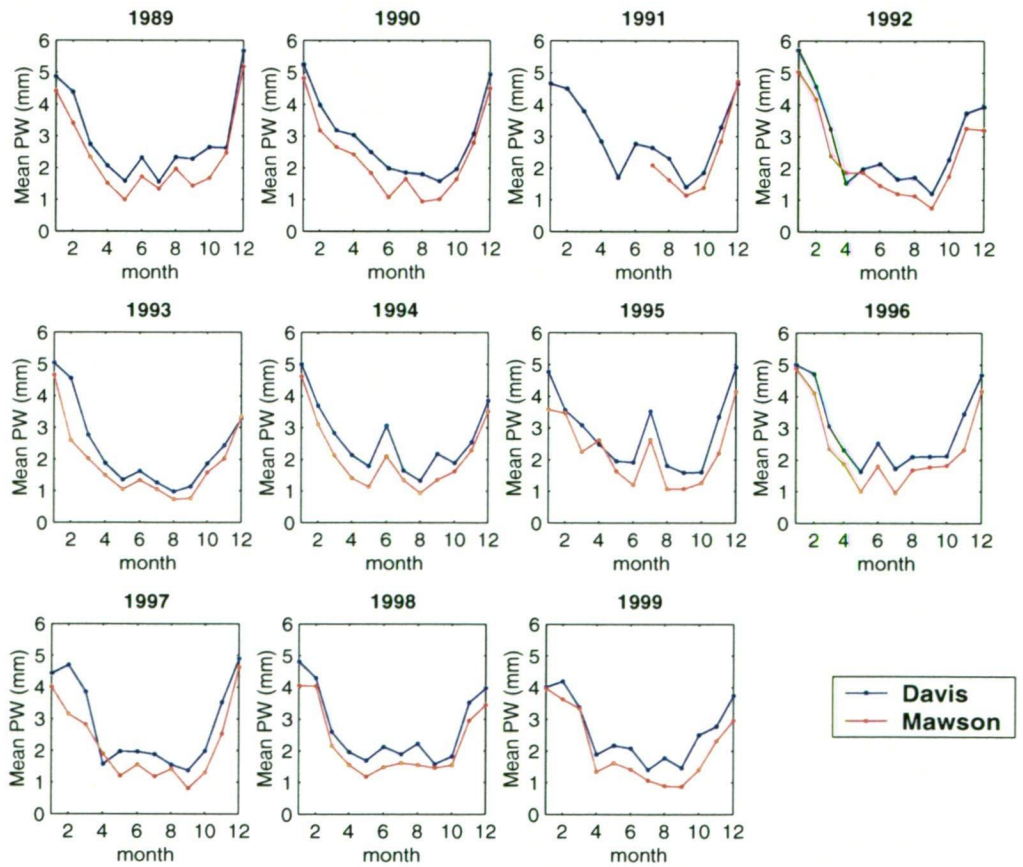

Figure 8.8 - 11 years of radiosonde derived mean monthly PW

8.3.1.1 Time series analysis

The radiosonde PW values were averaged for each month in each year to obtain mean monthly PW estimates at each site. From Figures 8.7 and 8.8, it can be seen that at both sites, the mean monthly PW value follows a similar pattern over time with Davis generally having a higher value than Mawson. In every year, the mean PW reaches a maximum value during the summer months, usually in January but occasionally in December or February. During the winter period, most years display a distinct secondary peak either in June or July. The magnitude of this peak varies between years and is strongest in July 1995.

Figure 8.7 shows the mean monthly PW data as a time-series allowing the identification of variations over the 11-year period. The highest summer PW values were observed in December 1989 and January 1992 at both sites. The lowest summer PW occurred at Davis in February 1999 whilst at Mawson it was in January 1995. The most prominent winter peaks (at both sites) are found in July 1995, June 1994 and June 1991 in descending magnitude. In Figure 8.7, a slight decreasing trend in the maximum annual (i.e., summer) PW can also be seen at both sites while the annual minimum (i.e., winter) values have no significant trend.

From Figure 8.8, it is clear that, in general, the two sites display similar characteristics with PW being greater at Davis. Significant anomalies occur in the 1997, 1998 and 1999 winter months which show peaks in the data that do not correspond between stations. In 1995, the summer/autumn PW values at Mawson show a slightly erratic behaviour when compared to Davis in the same year and the general trend in other years. Other small variations between both years and sites can be seen in Figure 8.8 which do not appear to be of major importance here but may have interesting phenomena driving them which could be looked at in a further study.

8.3.1.2 Frequency analysis

Standard Matlab programs were used to carry out frequency and spectral analyses on the 11-year mean PW signal in order to confirm and investigate the features and trends identified in Figures 8.7 and 8.8. The results of these analyses for Davis and Mawson are shown in Figures 8.9 and 8.10 respectively.

The power spectral density (PSD) plots in Figures 8.9a and 8.10a reveal the strong annual signal and the less energetic, semi annual signal already noted in section 8.3.1.1. The most significant new finding from these PSD analyses is the remarkable similarity between the PW signal at Davis and Mawson. This is especially notable in the frequency band of 0.5 to 2.5 cycles per year where the PSD power, highly smoothed by overlapping Hanning windows of size 32 (equivalent to 2.6 years), is

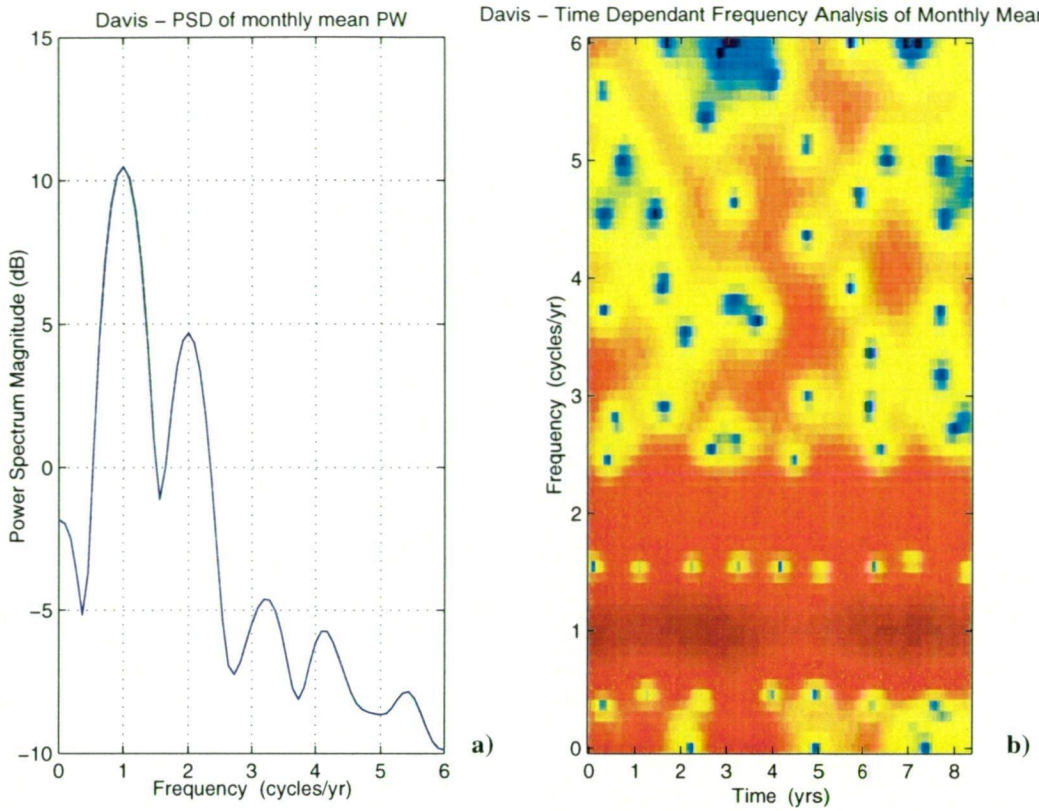

Figure 8.9 - a) Davis Power Spectral Density (PSD) and b) time dependent frequency analysis of mean monthly PW data.

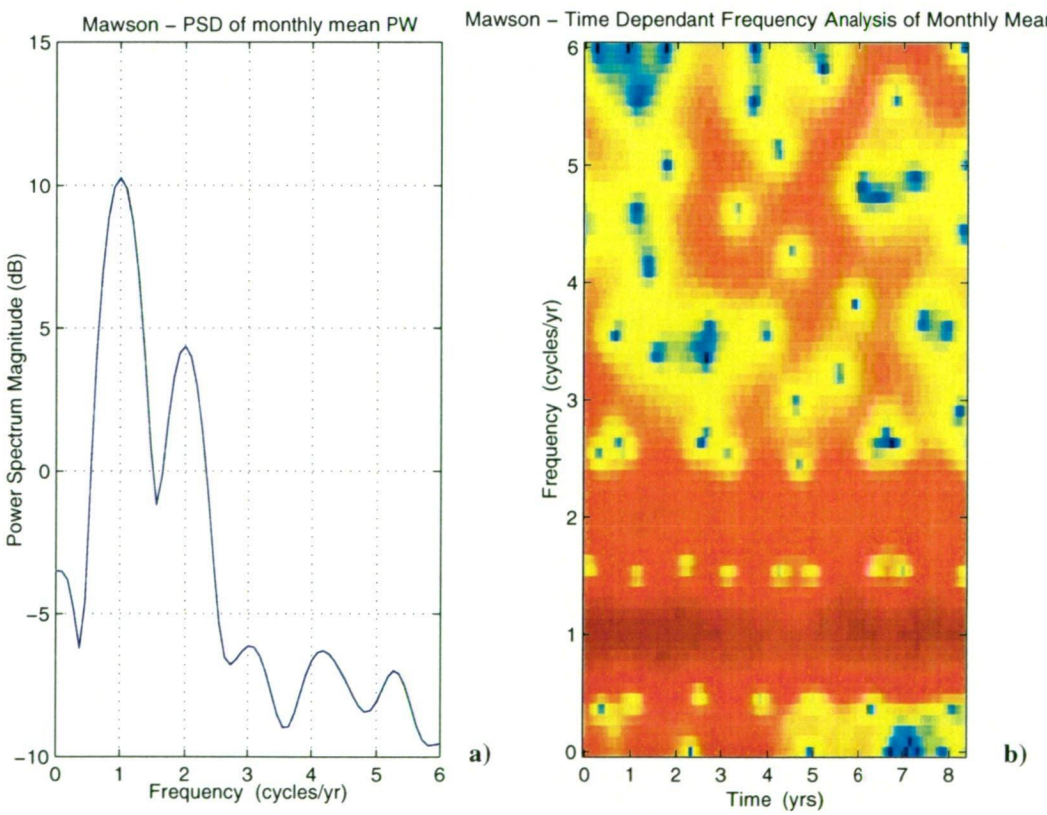

Figure 8.10 - a) Mawson Power Spectral Density (PSD) and b) time dependent frequency analysis of mean monthly PW data.

identical. This finding is a little unexpected due to the very different nature of the air flow at these two sites (discussed in sections 8.1.5 and 8.2.1) and indicates that the larger-scale meteorological processes rather than local effects are driving the dominant PW cycle at these sites.

The differences between the PW signals at the two sites are in the low and high frequency bands where Davis has more energy than Mawson. This is consistent with the larger PW amplitudes observed at Davis in the time series plots (Figures 8.7 and 8.8) and reflects the local meteorological variations.

The strong similarity between these two sites in the PSD plots is repeated in the time dependent plots (Figures 8.9b and 8.10b) especially in regard to the annual and semi-annual signals. The pattern of the power distribution at both sites is generally similar with many regions of the plots showing consistency in timing and frequency of the signals. The differences between the sites are mainly in the power magnitude of the higher frequency and low frequency data, which indicate that the energy density at the sites is not constant and that strong local factors are influencing the amount of available PW. Another feature of these plots is the strong power increase in the high frequency region between 4 - 8 years at both sites indicating the presence of long-period variations in the PW signal.

8.3.1.3 Wavelet decomposition

Wavelet decomposition of the mean monthly PW data was carried out (Figures 8.11 and 8.12) so that further clarification of the various signals indicated in the previous analyses could be made. This was achieved using the Matlab Wavelet Toolbox. A Daubechies wavelet (db6) was used to perform approximations of the PW signals with 6 levels of decomposition. It was found that this methodology produced the smoothest approximation of the input signals and extracted the most meaningful information from within the signal structures.

The decomposition levels shown in Figures 8.11 and 8.12 represent:

d1. High frequency noise
d2. Semi-annual signal
d3. Annual signal
d4. Quasi bi-annual wave
d5. Long period waves
d6. Long period waves
s. Original signal

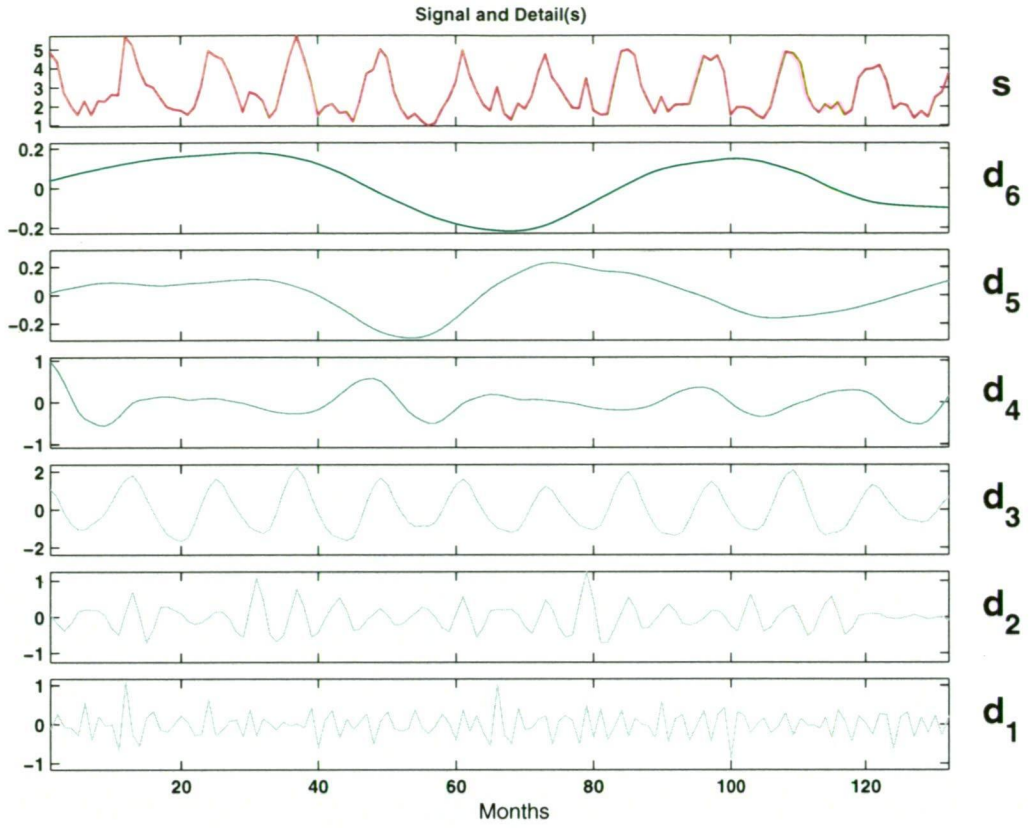

Figure 8.11 - Daubechies (db6) wavelet decomposition of the 11-year PW signal at Davis (1989 - 1999)

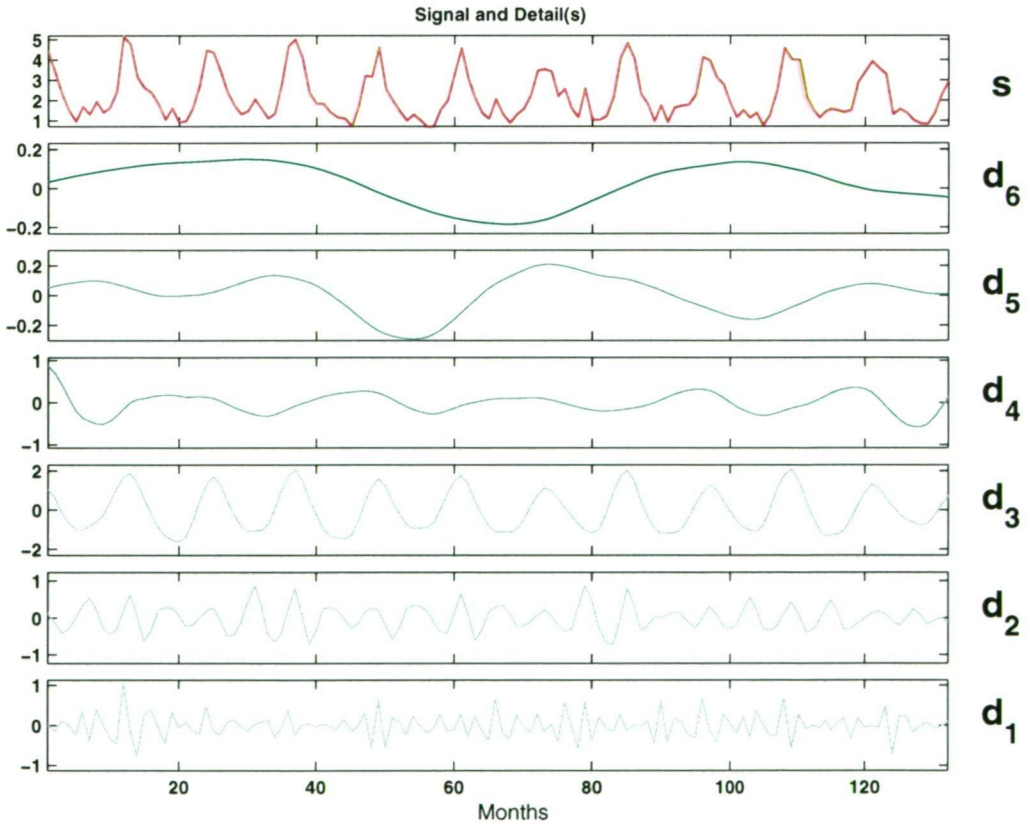

Figure 8.12 - Daubechies (db6) wavelet decomposition of the 11-year PW signal at Mawson (1989 - 1999)

The dominant annual and semi-annual signals observed in the time-series and frequency analyses are readily identified within decomposition layers d2 and d3, as is the variable amount of energy in these bands. The signal in the d4 decomposition level is approximately bi-annual and this appears to have a more constant pattern at Mawson than at Davis.

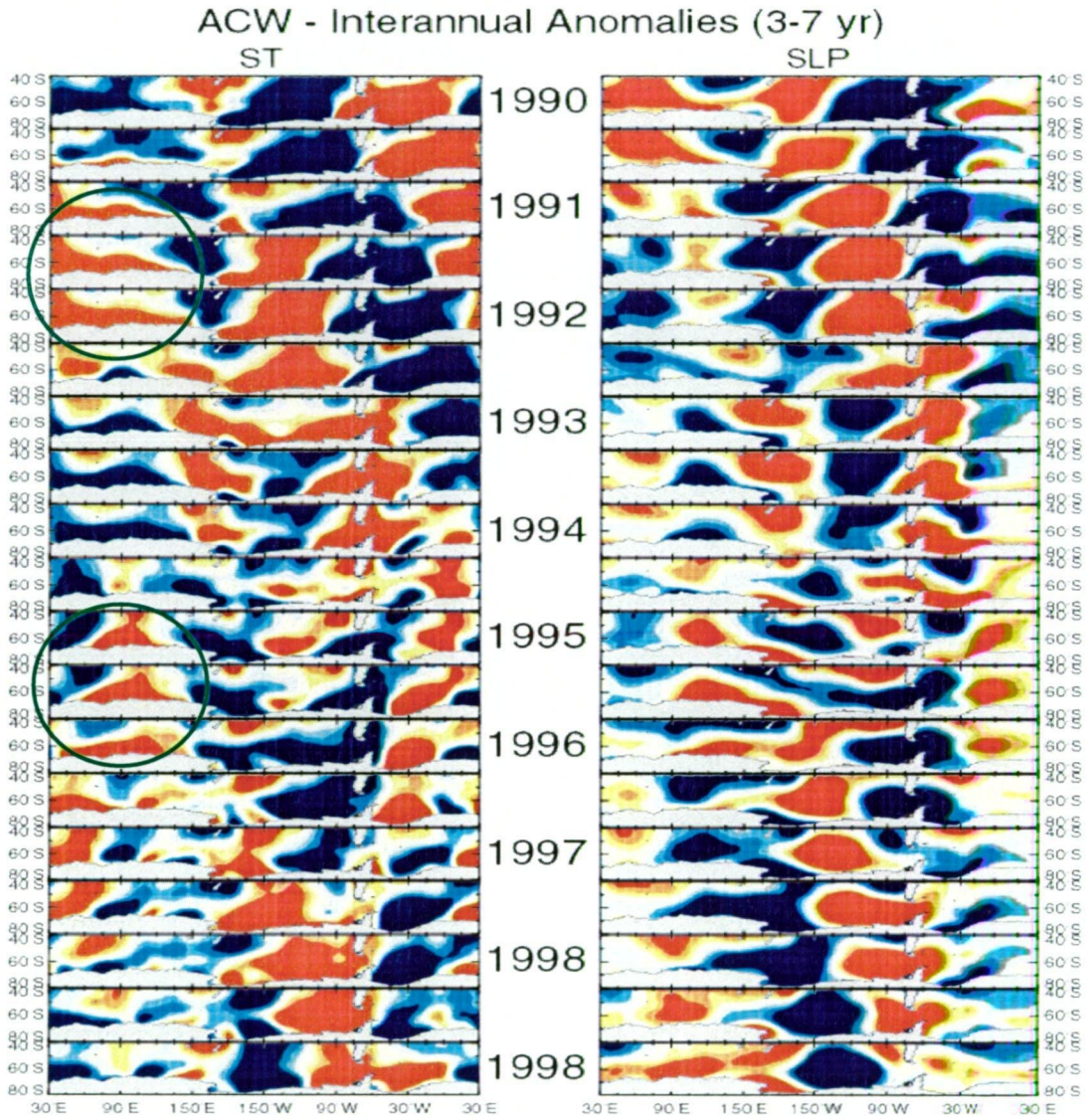

Figure 8.13 - ACW interannual anomalies (obtained from www.acw.ucsd.edu/ACW/index_evolution.html). Green circles indicate periods corresponding to maxima in the d5 wavelet decomposition. (Note: ST = surface pressure, SLP = sea level pressure)

A 4 - 6 year signal is apparent in the level 5 and 6 decompositions, which again agrees well with variations seen in the time dependent frequency analysis. The d5 signals have maxima at approximately Jan 1991 - Jan 1992 and near Jan 1995 while the d6 maxima are at Jun 1991 and Jun 1997. These variations are generally consistent with the movement of the eastward flowing Antarctic Circumpolar Wave (ACW) (White and Peterson, 1996; http://www.acw.ucsd.edu/ACW) in this region, during this period (see Figure 8.13). However, the strength of the ACW is known to

be quite variable (White and Peterson, 1996) and it is therefore likely that the long-term d5/d6 PW signals contain time varying information that cannot be further analysed here as multiple cycles within the 11-year time-series are not available (i.e., it is too short for definitive conclusions).

8.3.1.4 Summary of analyses

A very strong annual and a weaker semi-annual signal were found from visual inspection, frequency analysis and wavelet decomposition of the 11-year mean monthly PW data sets at Davis and Mawson. These analyses clearly show a summer peak in PW followed by a trough beginning at approximately the time of the autumn equinox. In many years there is also a mid-winter peak in the amount of PW, this winter peak is strongest in 1994 and 1995 at both sites. The semi-annual oscillation mirrors that observed in the pressure signal in Antarctica (refer section 8.1) and is also seen in the mean temperature signal at these sites.

The PW signals at Mawson and Davis show remarkable similarity in all analyses reflecting the influence of large-scale meteorological processes on the cycle of PW in the region. The small differences in the timing of minimum/maximum energy levels between the two sites indicate the variable influence of local weather patterns and long-term climatic effects on the general PW signal. Generally, Davis experiences more PW than Mawson as is expected due to the general circulation pattern described in section 8.2.

Long-term variations in the PW signal at the two sites are very similar and relatively stable over the available (11-year) period of data. The most significant of these variations are the approximately bi-annual signal, more clearly defined at Mawson but apparent at both sites, and the 4 - 6 year signal which is strong at both locations with slight phase and amplitude differences between the two sites. The phase difference is due to the distance between the sites.

The 4 - 6 year signal observed in the wavelet decomposition is approximately aligned with the observed progression of the ACW during the 1989 to 1999 period (Figure 8.13). This apparent relationship between the ACW and PW is not unexpected due to the known variations in sea surface temperature and sea-ice extent that are characteristic of the ACW (White and Peterson, 1996). These variables will have a significant influence on the synoptic systems in the Davis/Mawson area as well as the amount of evaporation occurring over the ocean surface and consequently on the water vapour transported over the coast. It is also possible that the ACW and the variation in PW are related to Earth Rotation cycles which are significantly influenced by atmosphere and oceanic processes and are also known to have a main oscillation with a mean period of 5.8 years (Liao and Greiner-Mai, 1999).

In the wavelet analyses, it has also been observed that the removal of regular, almost identical, semi-annual and annual components at each site provides residuals that contains trend information which appears to be cyclical at periods of 2 - 8 years (i.e., subplots d4 to d6 in Figures 8.11 and 8.12). For PW measurements to be useful in understanding climate processes, long-term analysis of signals at a number of permanent sites are required so that these trends can be fully modelled and accounted for.

8.3.2 Vertical Characteristics of PW at Davis and Mawson.

In the previous section, 11-years of radiosonde soundings at Davis and Mawson were used to identify temporal variations in PW at these sites. These radiosonde data are also useful for observing spatial trends in PW, i.e., the vertical distribution of PW through the atmosphere. This information is useful in terms of understanding the seasonal variations in the air moving over a site and the potential for precipitation.

In order to investigate the vertical characteristics of the air entering/leaving the LGB region, the data in the radiosonde soundings at Davis and Mawson were re-integrated using a modified version of the program described in section 7.5. This modified program allowed two PW values to be extracted from each sounding, one with respect to the surface (approximately 985 hPa) and the other with respect to the 700 hPa level. The 700 hPa level was selected for this analysis as i) it is generally expected that above this level there will be very little PW and ii) it is the approximate height of the LGB traverse line (refer to Tables 8.3 and 8.4) and therefore should be useful in indicating the approximate amount of PW to be expected at the IMS.

8.3.2.1 PW above surface versus PW above 700 hPa

Linear Regression Analysis

Linear regression analysis was carried out between the 11-year surface and 700 hPa radiosonde PW data at Mawson and Davis. The results of these analyses are displayed in the panels on the left side of Figures 8.14 and 8.15 with the best-fit lines defined by the slope and y-intercept values and the r values indicating the correlation coefficients.

The panels on the right in Figures 8.14 and 8.15 represent quantile plots of the PW data. These plots were created by sorting the PW values in each data set in order of magnitude and then plotting these values sequentially against each other. A line joining the 1st and 3rd quartiles of the data was then calculated and plotted to indicate the 'normal' distribution of the data. This slope will be different to that calculated in the linear regression plot, as it is determined only from the middle 50% of the PW datasets. The information in these quantile plots indicates whether the surface and

700 hPa PW data sets come from the same probability distribution with deviations from the 'normal' line representing data from a different population to the mean.

Figure 8.14 depicts the results for the annual PW data while Figure 8.15 separates these data into their seasonal components. The information in these plots show that:

(a) The correlation between the surface and 700 hPa PW is at the 80% level and the ratio of 700 hPa to surface PW is around 0.1 to 0.5.

(b) The slope values at Mawson are higher than those at Davis (especially for the winter data) and indicate the presence of less surface moisture at this site.

(c) The PW data for the surface and 700 hPa atmospheric levels are normally distributed below the 90^{th} percentile. Deviations from this relationship appear to be primarily due to the upper level having excess PW (or the lower atmosphere having too little PW). These quantile plots also indicate very different distributions for i) the summer and winter data at both sites and ii) the winter data at Davis and Mawson.

(d) Seasonal values of PW fall into distinct regions of the plots. Autumn, winter and spring data (o, o and + in Figure 8.14) have a significant number of occurrences above the regression line (i.e., a high ratio between 700 hPa and surface values) but the majority of data from these seasons are located near to the line and in the lower left quadrant of the graph. Summer values (+) fall on either side (and near to) the mean regression line and dominate the region of high surface PW values.

(e) The summer distributions are different to all other months and are quite similar for Davis and Mawson, although there is more scatter in the Mawson data.

(f) At Davis, the autumn, winter and spring PW data have approximately the same distributions with only a slight difference between the amount of surface moisture available in each season (i.e., autumn has the least surface PW and spring has the most). All of these seasons have a positive deviation from the normal above the 90^{th} percentile.

(g) At Mawson, the autumn, winter and spring PW data have significantly different distributions above the 90^{th} percentile, and a large difference in the amount of surface PW available in autumn (least) and spring (most). The shape of the winter qq-plot above the 90^{th} percentile is opposite to those of the autumn and spring data at this site and to the autumn, winter and spring data at Davis.

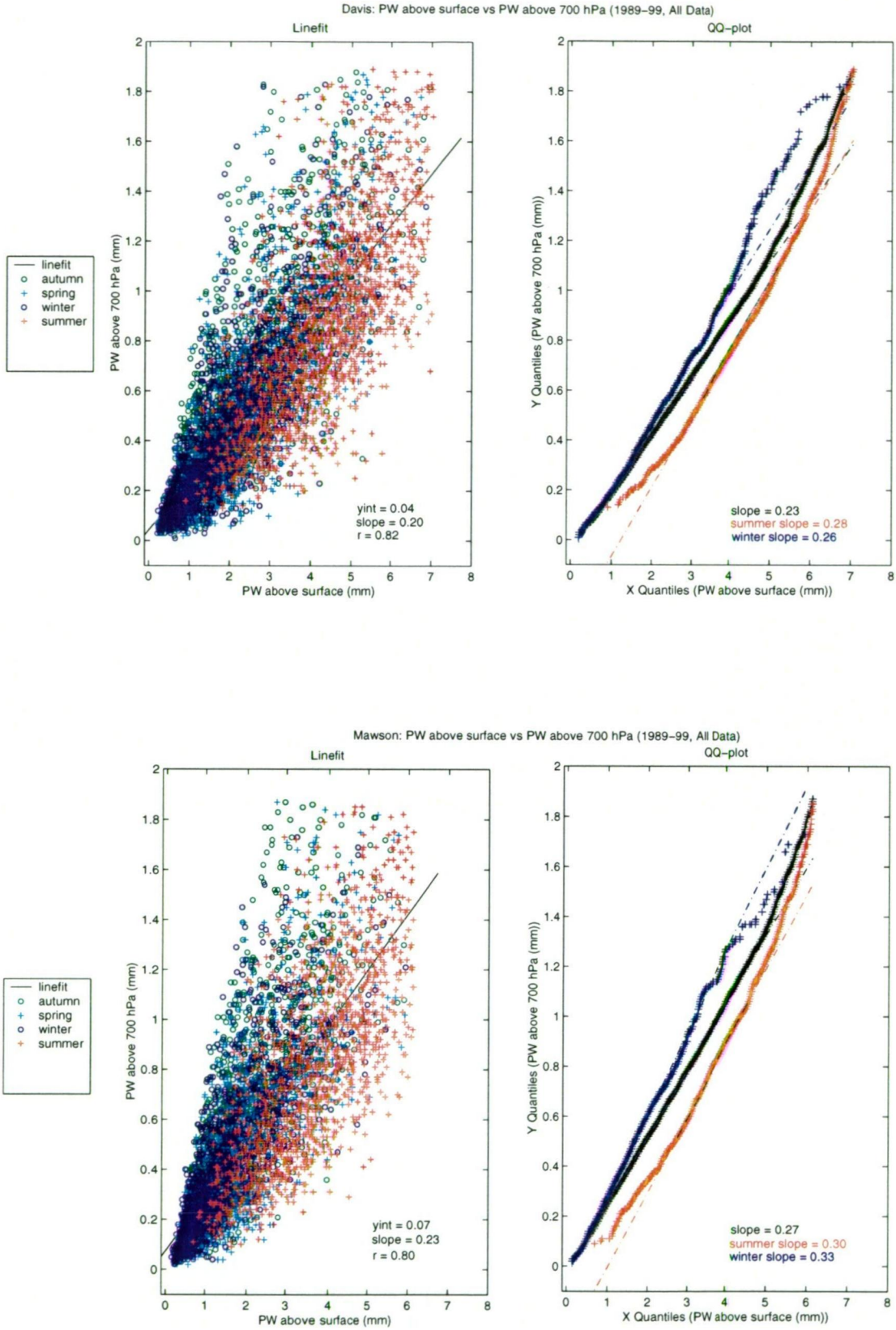

Figure 8.14 - Linear regression analysis of surface vs 700 hPa PW from 11 years of radiosonde data at Davis and Mawson.

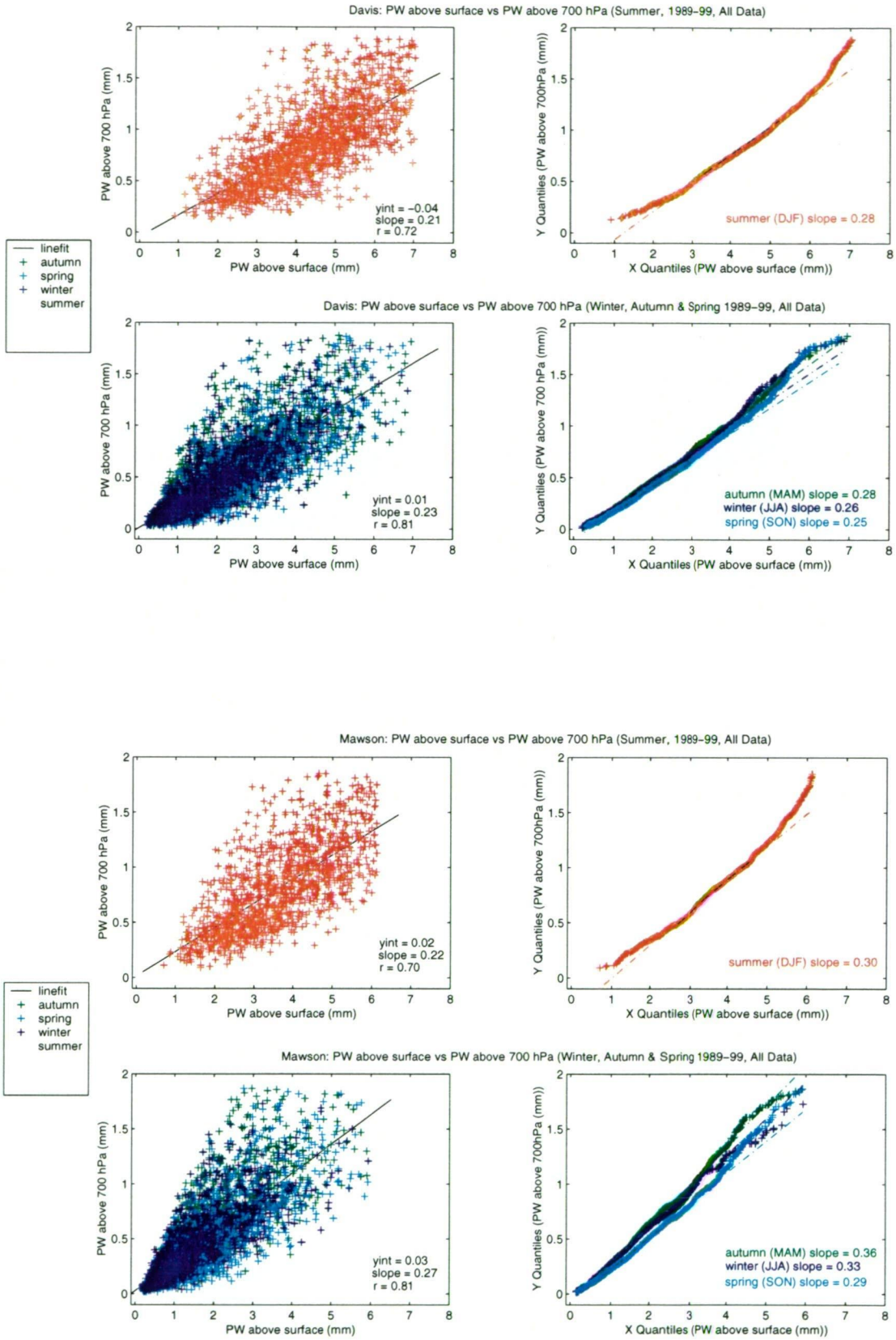

Figure 8.15 - Seasonal analysis of surface vs 700 hPa PW from 11 years of radiosonde data at Davis and Mawson.

In the above findings, most of the variation between Davis and Mawson can be explained by the different mean surface flow patterns at these sites. That is, the lower amount of surface PW found in the Mawson data is reflective of the general out-flowing, drier air in the surface layer at this station.

The variations observed at both sites between summer PW and the PW in other seasons is a factor of the increased temperatures and greater influence of maritime weather systems on the surface layer in this season. Variation in the dominant weather patterns can also explain the slight differences noted between the three colder seasons. The deviations above the normal line for the autumn, winter and spring data represent higher than expected PW above the 700 hPa level and therefore these occasions could result in precipitation if this air was sufficiently raised/cooled as it moved past the site.

Temperature vs Pressure (T vs P) Analysis

The linear approximations of the radiosonde PW data provide an average model of the relationship between the surface and 700 hPa. To define the general characteristics of regions above and below this line in various sectors of the data distribution, a series of days were selected and the atmospheric profile of the corresponding radiosonde soundings (T vs P diagram - e.g., Figure 8.16) plotted and analysed (see Appendix D.1).

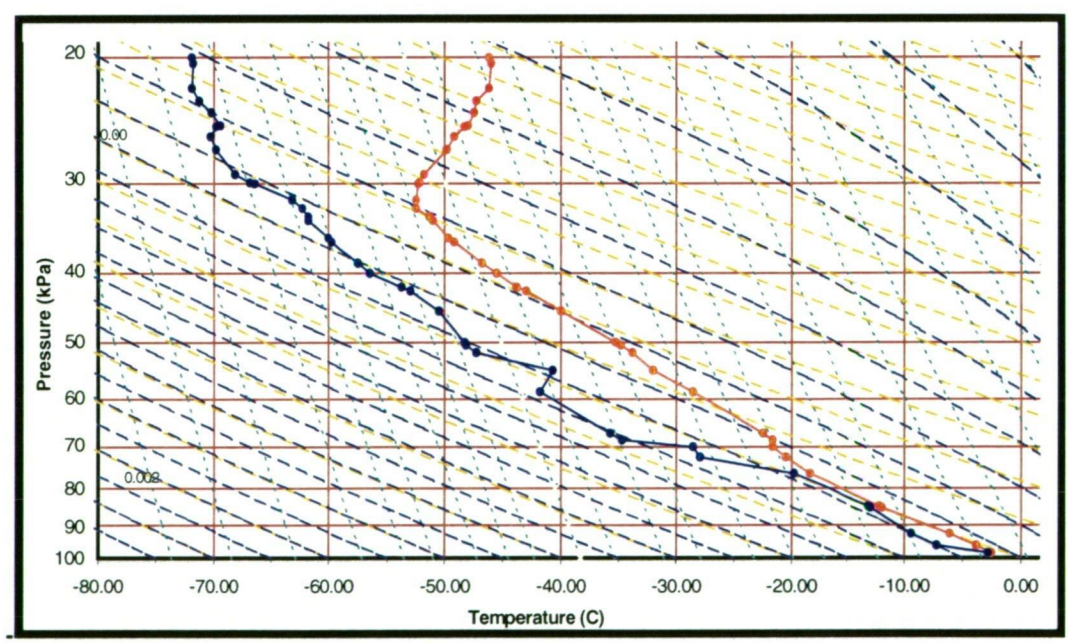

Figure 8.16 - Thermodynamic diagram (T vs P) from radiosonde data collected at Davis (1/1/1995 00:00UT, sounding C in Appendix D.1). The blue and red lines represent the saturated and non-saturated atmospheric profiles respectively. For a full description of the T vs P plot refer to (Stull, 1995).

Analysis of the selected radiosonde soundings indicated that high surface PW values are usually associated with low moist air advecting from the ocean to inland (elevated) areas, therefore experiencing cooling and a decrease in pressure; favourable conditions for saturation and hence precipitation. Days with higher than expected upper level PW showed the presence of a frontal inversion with warmer, dry air in the surface layers and a moist upper atmospheric layer indicating PW being transported by the mean circulation rather than local cyclonic activity. The soundings representing the mean surface-700 hPa relationships displayed well mixed, relatively dry, stable air columns with low level surface inversions, indicating that this is the normal situation at these sites. Figure 8.17 summarises these observations from the T vs P plots and gives a generalisation of the seasonal relationships between surface and 700 hPa at Davis and Mawson.

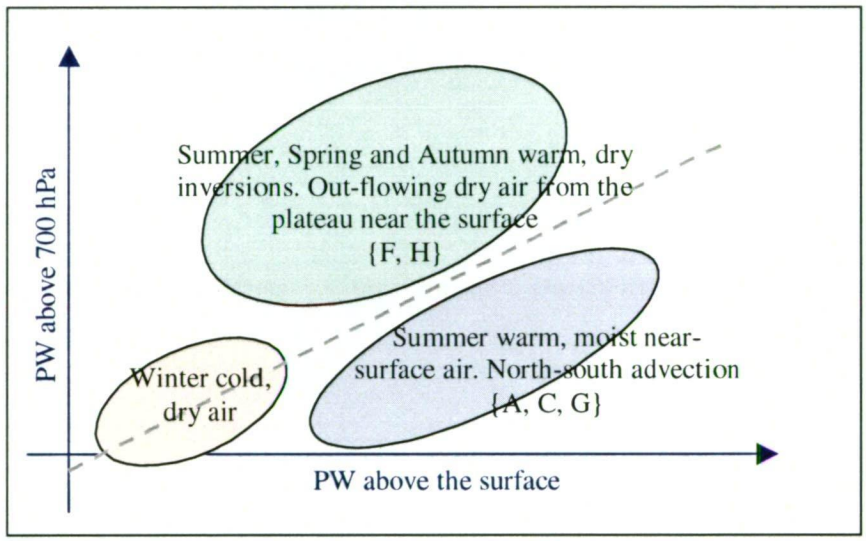

Figure 8.17 - Schematic diagram representing the regions of the surface vs 700 hPa model. Letters inside the {} indicate the example soundings (see Appendix D.1) which fall within each category.

8.3.2.2 Summary of analyses

The analysis of the structure of the air column at Davis and Mawson has shown that a relationship exists between the upper and lower atmospheric PW. This analysis has indicated that these sites experience reasonably constant weather patterns over the available 11-year period with distinct seasonal variations. The results discussed here clearly show that, the atmosphere above Davis contains more water vapour than Mawson and, as expected, the highest amounts of total PW are observed at both stations during summer.

The seasonal analysis suggests that it is possible for winter PW values to be of a similar magnitude to summer ones but these events are less frequent and the PW in all layers of the atmosphere is generally low in winter. Autumn, winter and spring

have the highest ratio of upper air PW to total PW, indicating increased dominance of the mean circulation over smaller scale processes after the incoming radiation is reduced. These cold, moist seasons at Davis are most likely to facilitate precipitation near the coast as the air rises onto the plateau. The quantile plots of the seasonal data also indicate that there is greater variability between seasons in the vertical distribution of PW at Mawson than at Davis.

These findings agree with those of Reid (2000) whose numerical model values indicated that the maximum PW over all of Antarctica is found in summer while the accumulation rates are seen to be higher in winter. Most of this modelled accumulation occurs at the coast and does not generally reach the plateau where accumulation is observed to be relatively constant with a slight peak in the middle of summer (Budd *et al*, 1995).

In general, these analyses have shown that although the pattern and magnitude of PW at Mawson and Davis is similar over time, the vertical PW distribution of the air flowing over these sites can be quite variable and is related to the general air flow over the site as well as the influence of seasonal weather patterns.

8.3.3 LGB PW from NCEP Reanalysis Data

Mean monthly atmospheric data from the NCEP 40-year reanalysis project was downloaded from the NCEP web-site (http://wesley.wwb.noaa.gov/ reanalysis.html) for 1993/94 and 1994/95 so that the modelled large-scale PW distribution over the region during the final LGB traverses could be studied.

The NCEP atmospheric data are produced via a global assimilation model with horizontal resolution of approximately 210 km and containing 28 vertical levels (Kalnay *et al*, 1996). The input for this model includes all available meteorological and climate data from 1957 to 1996. The output from the NCEP reanalysis are classified into four classes indicating the reliability of the parameter. This classification is dependent upon the relative influence of the observational data compared to the model processes (Kalnay *et al*, 1996). For the purposes of this study, data from the top two categories, i.e., a) strongly observational (e.g., atmospheric temperature) and b) observational and model influences (e.g., relative humidity) were used to determine PW in the LGB region.

The NCEP monthly data files were cropped to the LGB region (65°S-77°S, 52°E-80°E) and then converted to NetCDF format by Neil Adams from the BoM. PW values above 700 hPa (the approximate surface pressure at the LGB IMS) were then calculated by integrating the specific humidity data between 700 to 100 hPa at each grid point. The resulting gridded NCEP 700 hPa PW values for the LGB region from

November to February 1993/94 and 1994/95 are shown in Figure 8.18 with the LGB IMS locations overlaid.

In the 1993/94 NCEP PW plot (Figure 8.18a), the November 1993 and February 1994 data appear to represent unusual patterns of mean PW over the LGB. The November 1993 NCEP 700 hPa PW values are much higher than expected. However, these high values are confirmed by synoptic data for this month which describe a broadscale west-southwest airflow over the region carrying moist air from western coastal areas (pers. com. N. Adams, June 2001). For February 1994, the NCEP PW data shows unexpectedly low levels of PW. Upon inspection of the synoptic data for this region and period, it can be seen that there was a strong airflow away from the continental interior representing the presence of very dry air (pers. com. N. Adams, June 2001). Therefore, in this month it can also be said that the NCEP data do reflect a real situation observed in the LGB region at this time. December 1993 and January 1994 appear to follow the general pattern expected from the known meteorology and topography of the basin (see section 8.2) with slightly higher values found over the eastern interior and the highest values seen at the coast. However, the December 1993 synoptic data indicate that relative humidities in the western sector for this month were greater than those observed in November in the same region (pers. com. N. Adams, June 2001), a situation not reflected in Figure 8.18a. It should also be noted that the unusual trend in the magnitude of the PW value observed in these four months of NCEP data is not reflected in the mean monthly radiosonde PW time-series for Davis and Mawson (see Figures 8.7 and 8.8). From this collection of information, it appears that extreme events during November and February may have overshadowed the more general meteorological conditions during these months.

The NCEP data, shown in Figure 8.18b (1994/95), display a temporal variation in 700 hPa PW which is consistent with the Mawson and Davis radiosonde analysis (see Figures 8.7 and 8.8). That is, the coastal region displays a PW maximum in January, decreasing slightly in December and February with the lowest values present in the November data. At the southern-most traverse sites, it appears that the peak in PW occurs in December, decreasing over January and February. The spatial patterns of PW displayed in the plots of Figure 8.18b are in agreement with the expected distribution (see section 8.2), with decreasing PW away from the coast and slightly higher values over the eastern interior.

This NCEP data gives a good regional indication of the observed water vapour patterns over the LGB area and the variation in the mean monthly pattern due to local synoptic situations. These values provide the best indications of expected PW

patterns over the LGB region but have not been verified with ground-based data in the inland areas. At the coast, the radiosonde data at Mawson and Davis provides some ground truthing with average monthly values above 700 hPa being of the same magnitude as the corresponding NCEP grid results (i.e., approx 1 mm).

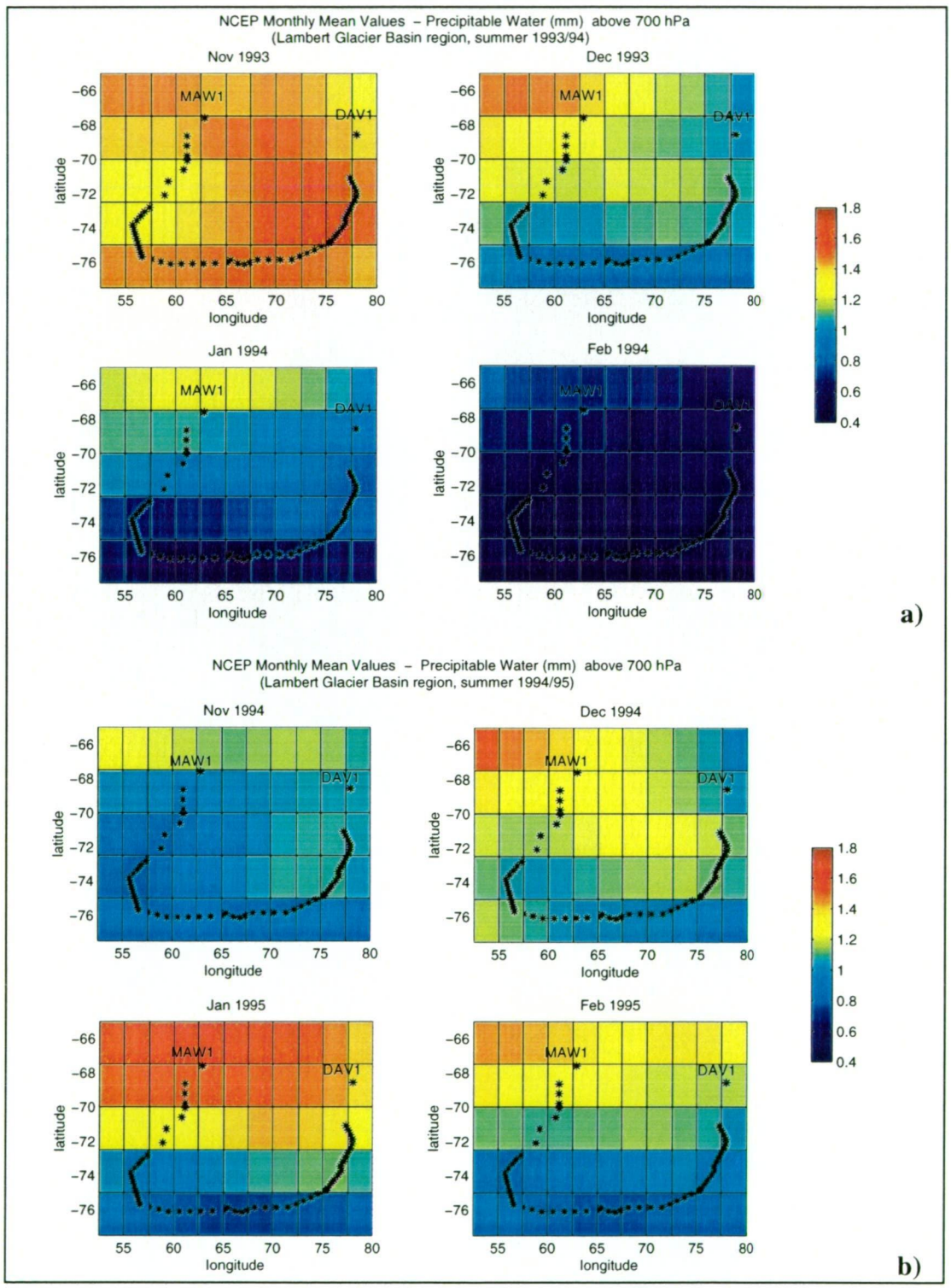

Figure 8.18 - a) 1993/94 NCEP PW above 700 hPa, b) 1994/95 NCEP PW above 700 hPa

8.4 LGB PW Analysis

The major aim of this section of work was to map PW around the LGB traverse line using data from the GPS surveys and available surface meteorological information. Within this analysis it was hoped that information regarding some of the spatial and temporal characteristics of the PW distribution in the region might be obtained.

As discussed previously (section 6.2.3.1), radiosondes are an effective method of sampling the atmospheric profile at a given point in time. However, the frequency of these measurements is governed by logistics, cost and personnel issues and therefore they are generally only carried out once or twice per day at a limited number of global sites. These data provide important daily forecasting information and over long time periods can be used to study climate patterns (see section 8.3.1) but are not useful for monitoring small scale spatial and temporal variations in atmospheric water vapour.

GPS has been shown (e.g., Elgered *et al* (1997), Rocken, Van Hove *et al* (1997) and Rocken, VanHove *et al*, (1995)) to be an effective tool for continuously monitoring the water vapour at a given location in near real-time if required and without the need for constant supervision or great cost. To produce optimum results and maximise the benefits of using GPS meteorology, it is necessary to have high-level data processing capabilities. This level of processing is required so that the non-tropospheric errors in the GPS signal (refer to section 2.1) can be minimised, modelled or removed, thereby allowing more accurate estimation of the tropospheric delay. In Antarctica, this is especially important as the magnitude of noise in the GPS signal is similar to that of the water vapour parameter being extracted.

In Chapter 7 it was shown that GPS data could be used to measure low amounts of PW (0.5 - 5 mm) at coastal GPS sites with a small but constant bias (0 - 3 mm) when compared to the values determined from radiosonde soundings. The results of this case study suggest that the GPS meteorology technique can be used to accurately measure the relative PW at the LGB traverse IMS.

8.4.1 Davis and Mawson GPS PW

The permanent installations at DAV1 and MAW1 were included in the global GPS network used to process the 1993/94 and 1994/95 LGB GPS data (see Table 4.2) and therefore TZD values are available for these sites during these periods. These TZD estimates were converted to mean daily PW values and compared to radiosonde measurements in the same manner as discussed in Chapters 6 and 7 (see sections 6.6

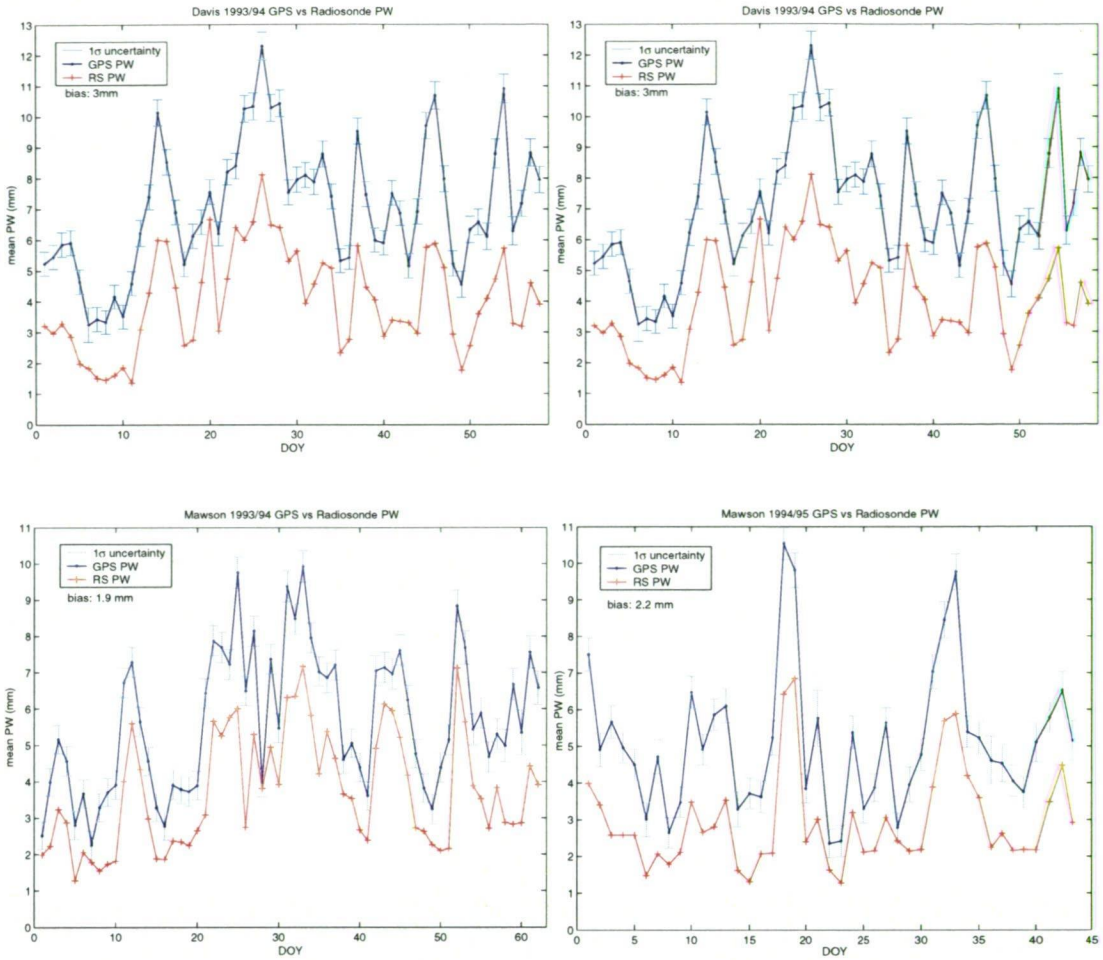

Figure 8.19 - DAV1 and MAW1 GPS mean daily PW estimates plotted against radiosonde (RS) mean daily PW observations

and 7.6.4). These comparisons confirm that over the 1993 to 1995 LGB traverse period, the GPS PW estimates at DAV1 and MAW1 had a similar bias and wrms values as found in Chapter 7[4] (see Figure 8.19). The similarity between the biases and wrms shown in Figure 8.19 and those given in section 7.6.4 confirm that the conclusions reached in Chapter 7 regarding the applicability of the GPS meteorology method in East Antarctica and the effect of major processing errors on the data are valid for this region and period.

8.4.2 Data

8.4.2.1 LGB TZD estimates

The GPS data from the LGB traverses form the basis for this PW study. As described in section 3.4, these surveys were designed for glaciological purposes and therefore data were not collected in an ideal manner for use in estimating PW. However the

[4] Small differences in processing software and modelling (e.g., antenna models, station constraints) (i.e., changes to the GAMIT software) are likely to slightly alter the GPS vs radiosonde PW bias observed in 1993 - 1995 compared to the values given for 1998 - 1999 in section 7.6.4.

data do cover a vast area of the LGB and as no other water vapour measurements have been made at these locations, any reliable information which can be retrieved may prove useful for further understanding of the meteorology of the region.

Section 3.4 describes the LGB GPS surveys that were completed during the Austral summers of 1989/90, 1990/91, 1992/93, 1993/94 and 1994/95. As PW estimation requires high quality a priori orbit information[5] and because the early campaigns collected GPS data with poor quality and very short occupation periods, data from only the 1993/94 and 1994/95 traverses were used for this study. These summers were also the only years that the traverse covered the entire route approximately along the 2500 m contour of the basin between Mawson and Davis.

During the LGB surveys there were two tractor trains, one dedicated to ice-radar work and the other to glaciological measurements. Both trains collected GPS data using their own Leica SR299 GPS receiver (for the remainder of this chapter, the ice-radar train will be denoted as IR and the glaciology train as GL). GPS data were usually collected over a period of 9 to 15 hours for each occupation of the seventy-three ice movement stations located approximately around the 2500 m elevation contour of the basin (refer to Chapter 3 and Figure 8.1). Unfortunately, traverse logistics dictated that these observations be made overnight (UT) and therefore required the observation span to be split into two (minimum of 3 hour) sections during GAMIT processing. The leapfrog style of the survey also resulted in two different instruments occupying the same site at different times on the same day. For example, the GL GPS antenna would be set up on an IMS to collect data overnight, creating an evening observation session on day one and a morning observation session on day two. Upon arrival of the ice-radar train in the morning on day two, the glaciology train would move on and the IR GPS antenna set up on the vacated IMS. During GPS data processing, morning and evening observation sessions on the same day were processed as one site in the 24-hr GAMIT solution even though the antenna had been changed between sessions (see section 4.5).

The 1993/94 and 1994/95 LGB GPS data were processed using standard GAMIT v9.6 session parameters (refer to section 4.5 and Appendix A.4) with residual TZD estimates computed over 2 hour intervals (i.e., thirteen estimates per day). A global network of approximately 32 'loosely' constrained sites in conjunction with IGS precise orbits constrained to their predicted uncertainties provided strength to the solution and allowed the Antarctic sites to be solved within a global reference frame. The LC (ionosphere-free) observable was used in the least-squares solutions. No ambiguity resolution was attempted due to the very long baselines (mostly > 1000 km) involved in the solution. The tropospheric delay was modelled down to satellite

[5] IGS orbits were not available prior to 14th November 1993

elevation angles of 15° using the Saastamoinen models and Niell mapping functions. Parameters for the tropospheric delay estimation procedure were set to 0.5 m for the TZD constraint and 0.02 m/√hr and 100 secs for the Gauss Markov variation and correlation time respectively. Earth rotation and tide models were applied but no ocean loading or antenna phase centre models were available for the region or antennas (AT202) involved in this study until after the processing had been completed. The effect of the exclusion of ocean loading and antenna phase centre models from the data processing has been examined by reprocessing a number of days with these models activated and observing no significant change in the PW results.

The dual antenna/leap-frog style of the survey resulted in many of the LGB occupations having sections of GPS data at either end of the UT day separated by several hours without data (see Figure 8.20). This distribution of data within the daily files and the nature of the TZD estimation process (refer to section 6.3.4) resulted in poor quality results for some intervals. It has previously been shown (Tregoning, Boers *et al*, 1998) that the first and last points in a 24 hr TZD estimation are likely to be of lower accuracy (up to a discontinuity of 13 cm in TZD) due to uncertainties in the orbits at these epochs. The lack of zenith delay information on one side of the tabular points at the ends of a TZD time series is also known to be a major contributor to increased weakness in the piecewise linear estimates at day and observation session boundaries. The large gap in the 24 hour data span at the LGB sites effectively creates four of these weak data points[6], which on some days represents a significant proportion of the total number of TZD estimates.

For example, on day 342 of 1994, the GL GPS antenna occupied IMS LG57 between 0000 and 0820 UT and the IR antenna occupied the same site between 1558 and 2400 UT. Figure 8.20 shows the GAMIT TZD estimates for LG57 on this day, including the values determined for the epochs where no GPS data were available. The effect of the data gap and estimation strategy on the TZD estimates at the session boundaries is clearly visible in Figure 8.20 where the first and last values in each observation session have higher uncertainties and values which do not agree with those estimated at other times during the observation period. In the evening session of Figure 8.20, the gap in the data causes the estimation process to have an unrealistic initial expectation of the first TZD value and the process takes some time to incorporate the information from the new GPS data and adjust the estimates closer to the true value of the TZD.

[6] Due mainly to the lack of GPS data on one side of the first and last tabular point in each section of data.

LG57	1994-342		
Time	TZD	1σ	
0000	1.6179	0.0065	
0200	1.6302	0.0031	
0400	1.6319	0.0032	
0600	1.6309	0.0037	
0800	1.6487	0.0067	
1000	1.6592	0.0231	} NO
1200	1.6537	0.0282	} LG57
1400	1.6482	0.0252	} DATA
1600	1.6426	0.0072	
1800	1.6211	0.0036	
2000	1.6211	0.0039	
2200	1.6090	0.0038	
2400	1.6033	0.0066	

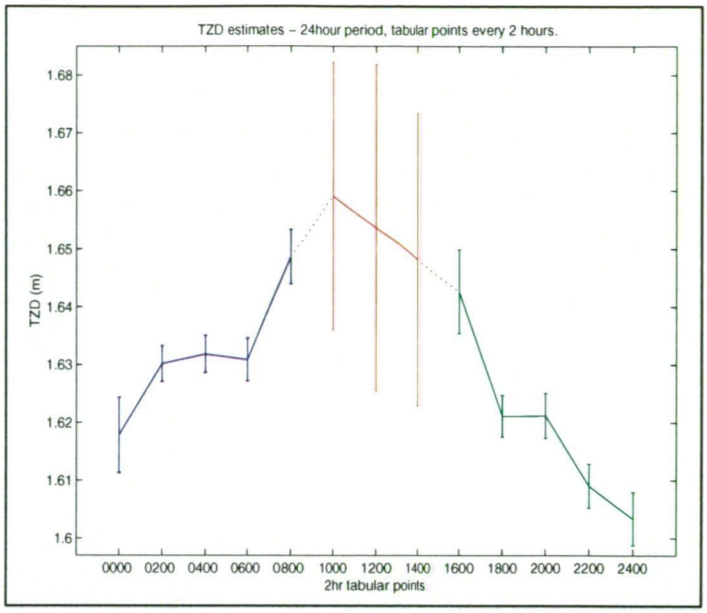

Figure 8.20 - LG57 2-hourly GAMIT TZD estimates for day 342 1994 at LG57 (0000 - 0800 UT occupied by GL, 1800 - 2400 UT occupied by IR).

This study is aimed at achieving a characterisation of the mean summer PW in the LGB region, an outcome that does not require 2 hourly PW values due to the expected lack of extreme daily variation in PW in this region. The mean TZD over each observation session therefore provides sufficient information for the purposes of this study[7]. Also, by removing outlier data points and taking a mean of the remaining two-hourly values, the errors due to the boundary effects and differences between morning and evening observation sessions can be minimised.

Monte Carlo simulations were used to test the 1σ standard deviations of the GPS TZD solutions. These tests revealed that the erroneous boundary values generally had processing uncertainties of greater than 6.5 mm. It was also discovered that removing these high uncertainty data points had little effect on the mean TZD value for the majority of observation sessions. It was concluded that two-hourly TZD estimates with a 1σ uncertainty of greater than 6.5 mm could be discarded without compromising the integrity of the results. This data editing removed the majority of poor boundary values and allowed most observation sessions to retain at least three estimates of TZD. Observation sessions with less than three valid, two-hourly TZD estimates were not included in the final PW analysis.

8.4.2.2 Surface meteorological data

As discussed in section 6.4, PW estimation from GPS TZD values requires simultaneous pressure and temperature data at the GPS antenna. During the LGB

[7] It is also necessary for this study to use mean values due to a lack of continuous meteorological data at the LGB sites.

traverses, digital surface meteorological data were collected continuously using Paroscientific Digiquartz equipment with sensors located on the roof of the traverse van (see Figure 3.12). These digital files have been archived by the Australian Antarctic Division - Glaciology Section but most could not be located when requested for use in this thesis. Eventually one of the meteorological data files was located and fortunately this file contained data from the second half of the 1993/94 LGB traverse (IMS 38 to 72). However, it was still necessary to locate alternative records of surface pressure and temperature relating to the first half of the 1993/94 and the entire 1994/95 traverses in order to complete this PW study.

The only other source of digital pressure data collected during both traverses was found within the header lines of the ice-radar data. These pressure measurements were recorded using a high precision (Paroscientific Digiquartz) barometer and transmitted to the ice radar computer (Higham *et al*, 1995). Unfortunately, the ice-radar collected data only during times when the vehicles were moving between IMS, which obviously did not correspond to the GPS occupation periods. To overcome this timing disparity, start/stop positions and times from the ice-radar header lines were compared to the known GPS locations and observation sessions. From these comparisons, observation sessions where the ice-radar stopped recording within 30 minutes of the commencement of the GPS occupation and within 100 m of the IMS location[8] could be identified. In these instances, pressure values could be obtained for the start and end of the GPS observation session and therefore an approximate mean pressure during the GPS occupation could be calculated. In this fashion, the pressure data from the ice radar files provided adequate information for conversion of mean TZD to mean PW for most IR occupations.

Another record of surface meteorological data from the traverses was discovered in the GL logbooks for 1994/95[9]. During this survey, the scientists kept a regular, manually observed record of the pressure and temperature measured by the digital equipment on the roof of the glaciology van. These observations were generally recorded every three to six hours and/or when the vehicles commenced and ceased moving between sites. The logbook therefore contained important, accurate information on the surface meteorology at the start, end and usually several times during most GL observation periods. This provided an additional, independent source of valuable surface meteorological data that could be used in conjunction with the ice radar header information and digital meteorology files to convert TZD to PW.

[8] The positions recorded in the ice radar files are navigation (uncorrected single frequency) spot coordinates and therefore reliable only to within 100m.
[9] The log book meteorological entries have been extracted into a new document which is included in Appendix D.2.

For all available GPS TZD information to be included in the PW estimation, surface meteorology values were required for both the IR and GL trains throughout the traverses. At times when data at only one site was available, the hypsometric equation (Appendix C.2) and known difference in elevation were used to calculate the expected pressure at the concurrent site. For several sessions in each traverse, simultaneous information was available at both sites due to the existence of the three meteorology data sources. This situation allowed a check to be made on the validity of the hypsometric calculations and on the consistency between the various meteorological data sources and collection methods. For 82% of cases, the comparisons between a calculated and measured mean pressure at a given site/observation session varied by less than 1 hPa with a mean difference of 0.6 hPa. On days where the pressure difference between the log book or digital value and that derived from the ice radar data varied by more than 1 hPa, the log book/digital value was used and the ice radar information discarded. These tests indicate that the mean pressure values, either measured or calculated, for the LGB sites are sufficiently precise (approximately within 1 hPa $\approx$ 0.3 mm of PW) for use in the TZD to PW conversion.

Temperature readings from the LGB traverses were not as widely available and were only found in the GL log books (both seasons) and digital meteorology files (1993/94 only). No temperature data were available at any of the ice-radar sites. Therefore temperature was assumed constant at the two sites (approximately 10 to 30 km distant) and the GL values used in all PW calculations. This assumption should be reasonable for the region of the survey and vertical/horizontal distance between sites. The temperature values were assumed to be accurate to better than $\pm$ 5°C. Errors in temperature of this magnitude will not significantly affect the PW estimates (see section 6.4.1).

8.4.3 LGB PW Results

The mean TZD estimates from the LGB surveys were extracted from the GAMIT solutions and converted to mean PW values for each observation session using the method and programs described in section 7.4.3. Results from these conversions were output as one file per survey season. An extract from the 1994/95 results is given in Table 8.1. The PW values estimated for each observation session are also depicted graphically in Figure 8.21.

As can be seen in Table 8.1 and Figure 8.21, some GPS observation sessions produced PW values that were negative. Most negative results are within 2σ of zero and therefore are statistically valid, however a few results are not. The presence of negative values is important and will be discussed further in section 8.4.3.1.

Table 8.1 - Excerpt from the 1994/95 LGB TZD to PW conversion (highlighted rows indicate negative WZD/PW results, * indicate pressure values from IR data)

Train	Time	Site	# Obs	DOY	TZD (mm)	σTZD (mm)	WZD (mm)	σWZD (mm)	PW (mm)	σPW (mm)	Press (hPa)	Temp (°C)
GL	pm	57	4	341	1624.7	2.3	0.8	3.2	0.1	0.5	714.3	-24
IR	pm	58	5	341	1614.7	1.9	-1.8	3.0	-0.3	0.4	711.0*	-24
GL	am	58	5	341	1630.9	1.8	8.1	2.9	1.2	0.4	713.7	-23
GL	pm	56	4	342	1636.0	2.4	4.8	3.3	0.7	0.5	717.5	-22
IR	pm	57	4	342	1613.6	2.0	-1.9	3.0	-0.3	0.4	710.6*	-22
GL	am	57	5	342	1631.9	2.0	10.2	3.0	1.5	0.4	713.3	-22
GL	pm	55	5	343	1631.0	2.2	9.2	3.2	1.3	0.5	713.4	-22
IR	pm	56	5	343	1624.3	2.0	3.7	3.0	0.5	0.4	712.9*	-22
GL	am	56	4	343	1640.7	1.8	13.2	2.9	1.9	0.4	715.9	-20

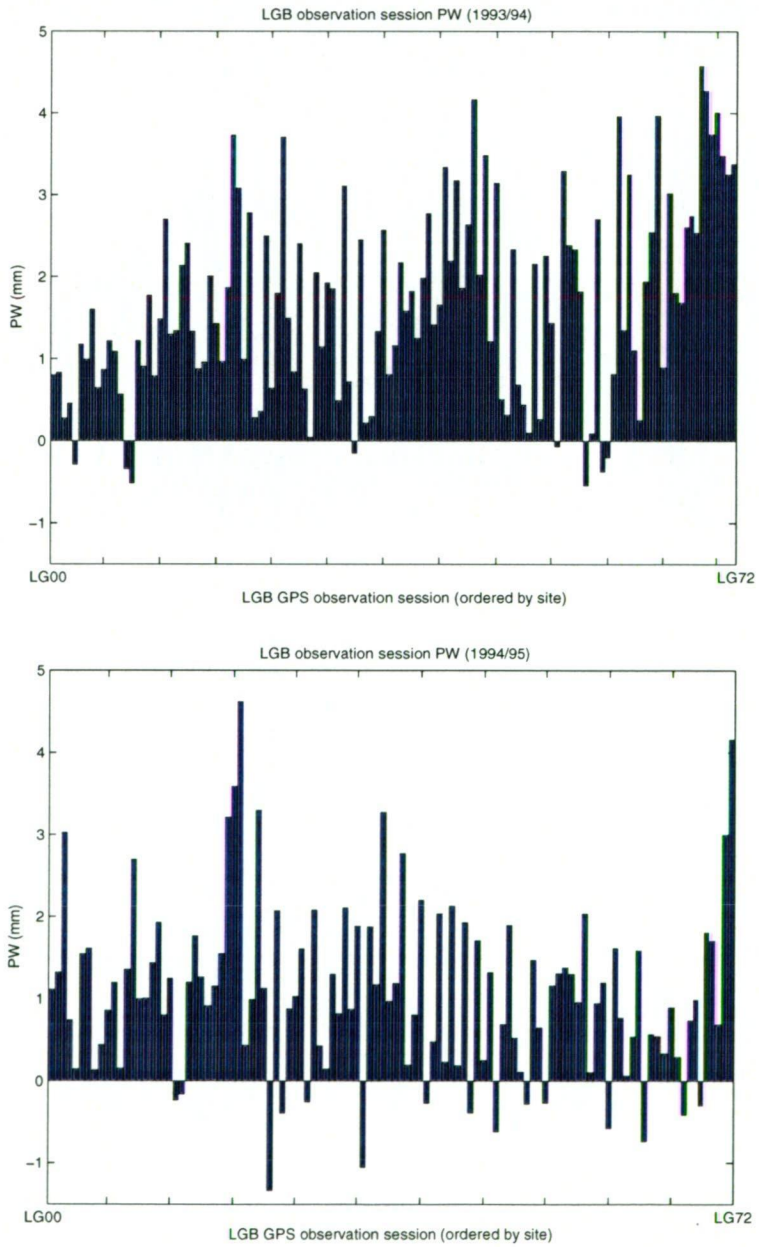

Figure 8.21 - GPS PW estimation for each LGB observation session

To test the consistency of the PW results, comparisons were made between the PW estimates for:

A - the same site on a given day (i.e., different antennas for the morning (GL) and evening (IR) sessions)

B - the same observation session on consecutive days (i.e., evening and morning results from the same 'overnight' (GL) occupation split into two sessions due to the 24 hour processing method)

C - consecutive sites during the same observation period (i.e., concurrent values at the IR site and the GL site - separated by approximately 30km)

D - consecutive days for the same time and site (i.e., GL evening session on day 1 and IR evening session on day 2)

The results of these tests are shown in Table 8.2. The comparisons in **A** indicate that for both seasons, the morning (GL) sessions recorded PW values approximately 2 mm higher than the evening session (IR) on the same day at the same site. The morning sessions generally had values between 2 - 4 mm while the evening values ranged from 0 - 2 mm. When comparing evening and morning values from the split overnight observation sessions, **B**, differences of approximately 0.8 mm (1994/95) and 1.9 mm (1993/94) in PW are observed with the morning sessions generally having a higher value. It is not known why there is a substantial difference between results for the two seasons in this comparison test as the processing was identical and pressure values should be more accurate in 1993/94.

Table 8.2 - GPS PW consistency tests - differences between GPS observation sessions (mm)

		A	B	C	D
1993/94	**Min**	0.8	1.0	0.0	0.1
	Max	3.0	3.1	1.7	1.4
	Mean	*2.1*	*1.9*	*0.5*	*0.6*
1994/95	**Min**	0.6	0.1	0.1	0.2
	Max	3.4	2.1	1.8	1.9
	Mean	*1.8*	*0.8*	*0.6*	*0.9*

The third comparison, **C**, displayed very good (mean difference 0.5 - 0.6 mm) similarities between the PW estimated at consecutive sites during the same observation period for all seasons. Neither antenna produced consistently higher or

lower values than the other. Testing of observations made at the same site on consecutive evenings (i.e., different antennas), **D**, showed that these results also compare to within approximately 0.6 - 0.9 mm.

The close comparisons found in **C** and **D** indicate that differences in PW caused by using two antennas are minimal. This result also suggests that in the other comparisons (morning vs evening - **A**: GL vs IR and **B**: GL vs GL), differences are more likely to be caused by discontinuities in the TZD estimation process rather than pressure errors or antenna variations. From these observations it is concluded that the gaps between observation sessions make a significant difference of the order of 1 - 2 mm in the estimated mean PW.

As there is no independent method for determining which is the correct PW value for any day or site, the values from the individual observation sessions were combined to produce mean daily values and uncertainties at each IMS. The daily values were then combined to obtain estimates of the mean PW for each site in each season (Tables 8.3 and 8.4). The resulting data sets contained significant outliers ($> 3\sigma$) that were removed or corrected. The final distribution of PW around the LGB traverse route for the 1993/94 and 1994/95 seasons is given in Figure 8.22 and Tables 8.3 and 8.4.

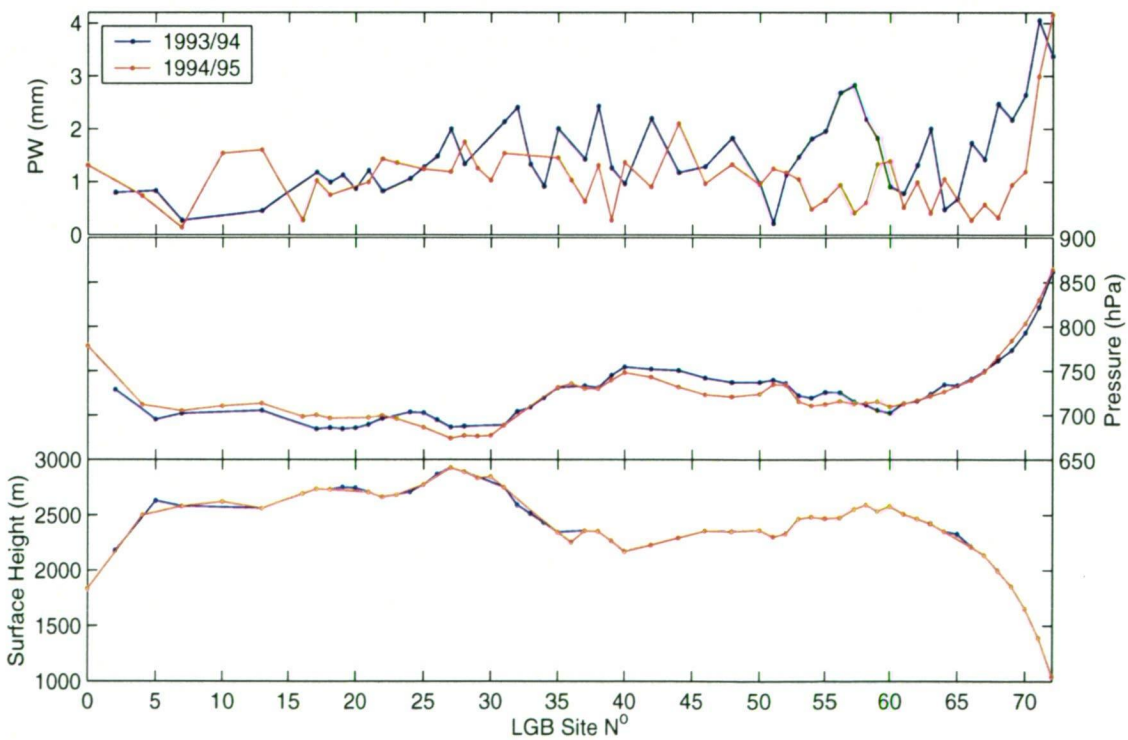

Figure 8.22 - PW, pressure and surface height values at the LGB traverse sites

Table 8.3 - PW results for the Lambert Glacier Basin traverse, summer 1993/94. (Dividing lines in the table represent the zone boundaries in section 8.4.4)

Site (LG)	PW (mm)	σPW (mm)	Pressure (hPa)	Latitude (°)	Longitude (°)	h (m)	H (m)	Distance from LG00 (km)
2	0.80	0.70	728.60	-69.2230	61.0953	2205.8	2177.5	63
5	0.83	0.83	695.11	-70.0673	61.1335	2652.8	2626.1	158
7	0.27	0.83	701.80	-70.6121	60.7835	2604.2	2579.0	221
13	0.45	0.76	705.25	-72.0915	58.8342	2581.5	2560.2	411
17	1.17	0.45	684.26	-73.0513	56.8381	2755.4	2735.1	538
18	0.99	0.43	685.84	-73.3148	56.4662	2749.8	2729.7	570
19	1.12	0.37	684.55	-73.5727	56.0698	2766.4	2746.8	601
20	0.87	0.53	685.48	-73.8318	55.6692	2759.2	2740.4	633
21	1.21	0.43	689.34	-74.0981	55.7887	2725.1	2706.9	662
22	0.82	0.30	696.27	-74.3649	55.9099	2681.1	2663.5	692
24	1.06	0.32	703.40	-74.8986	56.1717	2722.2	2706.0	753
25	1.28	0.31	702.50	-75.1645	56.3084	2788.8	2773.5	783
26	1.48	0.44	694.58	-75.4304	56.4498	2877.1	2862.5	813
27	2.00	0.31	686.19	-75.6973	56.5961	2940.7	2926.6	843
28	1.34	0.46	687.28	-75.8381	57.5276	2903.6	2890.3	873
31	2.13	0.47	688.80	-76.1056	60.5620	2760.8	2748.8	963
32	2.41	0.49	703.92	-76.0981	61.6806	2600.3	2588.0	993
33	1.33	0.57	708.72	-76.0849	62.7951	2523.1	2510.6	1023
34	0.91	0.38	719.36	-76.0665	63.9129	2442.9	2430.6	1053
35	2.00	0.48	730.84	-76.0436	65.0232	2355.1	2343.5	1083
37	1.43	0.41	732.89	-76.0765	66.1490	2366.6	2356.3	1134
38	2.43	0.22	730.97	-76.1364	66.8528	2362.6	2353.4	1154
39	1.26	0.31	744.82	-76.0234	67.4138	2275.3	2266.0	1174
40	0.96	0.26	754.25	-75.8603	68.2016	2180.2	2170.9	1202
42	2.20	0.28	751.70	-75.8580	69.2977	2236.6	2228.0	1232
44	1.18	0.28	750.54	-75.8554	70.4007	2302.5	2294.2	1262
46	1.29	0.21	741.83	-75.8527	71.4997	2363.5	2355.6	1292
48	1.82	0.27	737.10	-75.6620	72.2693	2359.7	2351.7	1322
50	0.97	0.32	737.15	-75.4709	73.0301	2370.8	2363.1	1352
51	0.22	0.42	739.70	-75.2789	73.7782	2312.3	2304.4	1382
52	1.12	0.28	735.78	-75.0874	74.5159	2341.6	2333.0	1412
53	1.47	0.19	722.12	-74.8964	75.2458	2475.3	2465.9	1442
54	1.81	0.28	719.48	-74.7327	75.5330	2493.2	2483.4	1463
55	1.95	0.32	725.83	-74.4794	75.8762	2480.3	2469.9	1493
56	2.68	0.32	725.50	-74.2595	76.1694	2488.3	2476.9	1519
57	2.82	0.27	714.96	-73.9721	76.5464	2566.4	2553.1	1553
58	2.18	0.29	711.18	-73.7193	76.8735	2606.3	2592.0	1583
59	1.82	0.29	705.53	-73.4520	76.7880	2549.2	2534.0	1613
60	0.91	0.26	702.12	-73.1914	77.0270	2594.3	2579.2	1643
61	0.78	0.26	713.52	-72.9312	77.2633	2525.1	2509.5	1673
62	1.32	0.25	715.88	-72.6713	77.4940	2482.9	2466.8	1703
63	2.00	0.22	723.59	-72.4107	77.7235	2438.7	2422.4	1733
64	0.48	0.29	734.37	-72.1506	77.9499	2366.5	2350.6	1763
65	0.68	0.30	733.54	-71.8808	77.9515	2341.2	2325.2	1793
66	1.73	0.41	740.81	-71.6206	77.7310	2230.0	2213.9	1823
67	1.42	0.33	750.03	-71.3607	77.5116	2151.7	2135.4	1853
68	2.47	0.29	761.33	-71.0955	77.2889	2013.1	1996.7	1884
69	2.17	0.42	773.38	-70.8353	77.0781	1871.4	1854.9	1914
70	2.64	0.33	792.90	-70.5759	76.8667	1669.1	1652.6	1944
71	4.05	0.29	821.55	-70.2591	76.6841	1406.2	1389.6	1980
72	3.37	0.37	861.52	-69.9211	76.4943	1057.3	1040.5	2018

Table 8.4 - PW results for the Lambert Glacier Basin traverse, summer 1994/95. (Dividing lines in the table represent the zone boundaries in section 8.4.4)

Site (LG)	PW (mm)	σPW (mm)	Pressure (hPa)	Latitude (°)	Longitude (°)	h (m)	H (m)	Distance from LG00 (km)
0	1.32	0.40	778.30	-68.6543	61.1201	1860.2	1831.9	0
4	0.74	0.39	712.12	-69.7859	61.1247	2526.2	2498.6	126
7	0.14	0.40	705.24	-70.6121	60.7836	2603.7	2578.5	221
10	1.54	0.39	710.52	-71.2862	59.2080	2644.1	2621.4	316
13	1.61	0.48	713.69	-72.0915	58.8346	2581.2	2559.9	411
16	0.28	0.25	698.85	-72.8084	57.3351	2712.9	2692.4	506
17	1.03	0.35	700.46	-73.0513	56.8384	2755.3	2734.9	538
18	0.75	0.31	696.74	-73.3148	56.4665	2749.5	2729.4	570
21	1.00	0.49	697.44	-74.0981	55.7890	2724.9	2706.7	662
22	1.44	0.67	699.74	-74.3649	55.9103	2680.7	2663.1	692
23	1.36	0.38	696.18	-74.6319	56.0399	2699.6	2682.5	723
25	1.24	0.43	686.46	-75.1644	56.3089	2788.5	2773.2	783
27	1.20	0.41	674.28	-75.6972	56.5964	2940.7	2926.5	843
28	1.76	0.50	677.17	-75.8380	57.5279	2903.5	2890.2	873
29	1.26	0.40	676.50	-75.9748	58.4769	2848.3	2835.7	903
30	1.03	0.27	677.31	-76.1081	59.4438	2857.3	2845.2	933
31	1.55	0.40	688.41	-76.1056	60.5622	2760.7	2748.7	963
35	1.46	0.23	731.61	-76.0433	65.0238	2354.8	2343.2	1083
36	1.04	0.33	735.72	-75.8736	65.4298	2266.8	2254.5	1105
37	0.63	0.25	729.93	-76.0764	66.1488	2366.4	2356.2	1134
38	1.32	0.26	729.94	-76.1363	66.8529	2362.4	2353.2	1154
39	0.28	0.33	739.49	-76.0232	67.4140	2275.1	2265.8	1174
40	1.38	0.30	748.32	-75.8602	68.2016	2179.9	2170.6	1202
42	0.91	0.29	743.16	-75.8578	69.2973	2236.3	2227.6	1232
44	2.11	0.25	731.83	-75.8551	70.4000	2302.3	2294.0	1262
46	0.97	0.48	723.33	-75.8525	71.4990	2363.2	2355.4	1292
48	1.33	0.30	721.19	-75.6616	72.2683	2359.1	2351.1	1322
50	0.95	0.28	724.00	-75.4707	73.0294	2370.4	2362.6	1352
51	1.25	0.30	735.02	-75.2787	73.7774	2311.9	2304.0	1382
52	1.18	0.32	734.06	-75.0874	74.5151	2341.3	2332.6	1412
53	1.05	0.30	715.81	-74.8964	75.2454	2475.1	2465.7	1442
54	0.49	0.26	711.04	-74.7327	75.5327	2493.0	2483.2	1463
55	0.66	0.31	712.53	-74.4793	75.8756	2480.1	2469.7	1493
56	0.95	0.28	715.94	-74.2595	76.1687	2488.1	2476.8	1519
57	0.42	0.28	713.12	-73.9721	76.5457	2566.2	2552.9	1553
58	0.61	0.31	713.66	-73.7193	76.8730	2606.1	2591.8	1583
59	1.34	0.34	715.55	-73.4520	76.7877	2549.0	2533.8	1613
60	1.40	0.29	709.87	-73.1914	77.0268	2594.2	2579.1	1643
61	0.53	0.32	712.92	-72.9312	77.2631	2524.7	2509.1	1673
62	1.00	0.28	716.92	-72.6712	77.4935	2482.5	2466.4	1703
63	0.41	0.34	721.56	-72.4106	77.7230	2438.3	2422.1	1733
64	1.06	0.31	726.64	-72.1505	77.9493	2366.2	2350.2	1763
66	0.28	0.34	739.39	-71.6205	77.7304	2229.9	2213.7	1823
67	0.58	0.28	748.84	-71.3606	77.5112	2151.5	2135.2	1853
68	0.33	0.28	766.37	-71.0954	77.2886	2012.3	1995.9	1884
69	0.94	0.29	784.30	-70.8352	77.0779	1870.8	1854.4	1914
70	1.19	0.36	803.66	-70.5757	76.8664	1668.5	1652.0	1944
71	3.00	0.55	830.29	-70.2587	76.6830	1405.2	1388.7	1980
72	4.16	0.47	864.46	-69.9209	76.4932	1055.8	1039.0	2018

These GPS PW results have not been corrected for seasonal effects due to the very small (approximately 0.1 - 0.2 mm) variation observed during the summer months in the 700 hPa models of annual PW from radiosonde soundings at Davis and Mawson (Figure 8.23). The NCEP mean monthly model data (section 8.3.3) also show PW variations above 700 hPa of less than 0.5 mm for the LGB traverse region from November - February. As there is no precise information on the seasonal fluctuation of PW at the LGB sites, these surrogate data are assumed to display the most likely PW trends. Therefore the LGB results given here are considered to represent true summer PW values, within the error bounds of the processing technique and not significantly affected by seasonal influences.

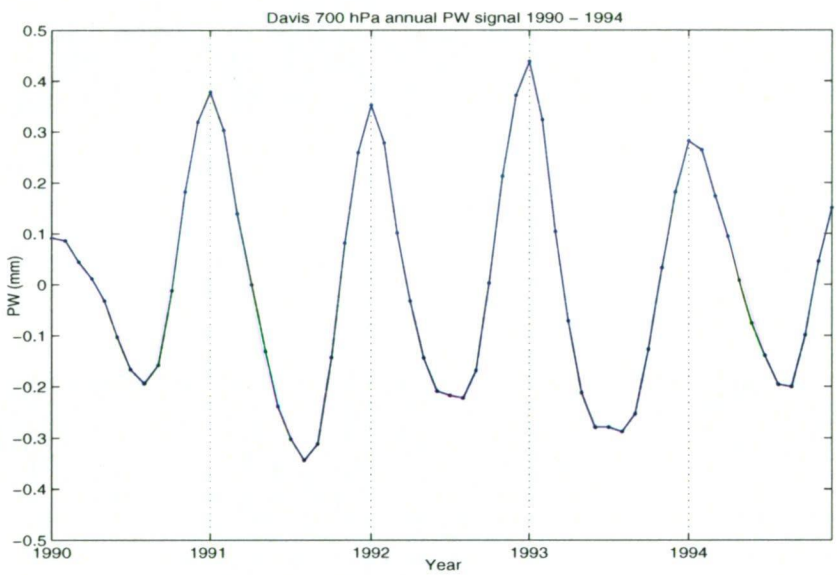

Figure 8.23 - 700 hPa annual model for mean monthly PW at Davis (derived from radiosonde data).

8.4.3.1 Negative PW results

Table 8.5 lists the GPS observation sessions when negative values for PW were obtained. The existence of negative values is important as in reality, such values are physically impossible.

The mean 2σ uncertainty for the PW data is approximately 1 mm and therefore, negative PW values lower than -1 mm indicate the presence of significant errors. Given the non-ideal input data for this study, it is not surprising that some negative values have been observed, there are most likely also a similar number of values which are too high although, as there is no upper bound on the PW values, these values cannot be easily identified other than in outlier detection.

Table 8.5 - Negative PW results. Highlighted rows indicate PW values that differ from zero by more than 2σ and are discussed in the text.

Session	IMS_Day	# Obs	TZD (mm)	σTZD (mm)	WZD (mm)	σWZD (mm)	PW (mm)	σPW (mm)	P (hPa)	T (°C)
1993/94										
IR_pm	23_340	4	1592.70	1.94	-3.62	2.99	-0.51	0.42	702.1	-26
IR_pm	50_011	4	1670.06	2.39	-1.02	3.30	-0.15	0.48	735.1	-16
IR_pm	65_036	5	1662.03	2.63	-1.38	3.48	-0.20	0.50	731.6	-18
IR_pm	16_330	5	1572.15	1.84	-2.02	2.92	-0.29	0.42	692.3	-23
GL_pm	23_339	3	1582.62	2.33	-2.42	3.26	-0.34	0.46	697.2	-26
GL_pm	63_031	4	1633.22	2.29	-0.45	3.23	-0.07	0.47	718.5	-20
GL_pm	64_034	4	1668.00	2.36	-3.78	3.28	-0.54	0.47	735.3	-21
GL_pm	65_035	4	1667.57	2.56	-2.61	3.42	-0.37	0.49	734.6	-23
1994/95										
IR_pm	69_325	4	1778.57	2.17	-2.06	3.14	-0.30	0.46	783.2	-18
IR_pm	62_333	4	1623.25	2.20	-4.07	3.16	-0.57	0.45	715.7	-28
IR_pm	58_341	5	1614.65	1.95	-1.85	2.99	-0.26	0.43	711.0	-24
IR_pm	57_342	4	1613.64	2.00	-1.93	3.03	-0.28	0.43	710.6	-23
IR_pm	55_344	5	1613.61	1.79	-4.35	2.89	-0.62	0.41	711.7	-26
IR_pm	50_351	6	1637.43	1.76	-1.86	2.87	-0.27	0.41	721.1	-21
IR_pm	42_361	6	1681.75	1.71	-7.28	2.84	-1.05	0.41	743.1	-20
IR_pm	38_364	5	1658.93	2.05	-1.75	3.06	-0.25	0.44	730.6	-20
IR_pm	36_003	3	1663.34	2.64	-9.30	3.48	-1.33	0.50	735.8	-22
GL_pm	66_327	3	1676.50	2.95	-5.11	3.72	-0.73	0.53	739.6	-22
GL_pm	54_344	4	1611.19	2.05	-2.73	3.06	-0.39	0.43	709.9	-26
GL_pm	37_364	5	1656.02	2.05	-2.71	3.06	-0.39	0.44	729.7	-20
GL_pm	26_016	3	1541.38	3.23	-1.65	3.95	-0.23	0.56	678.7	-24
GL_pm	26_017	5	1541.92	2.34	-1.11	3.26	-0.16	0.47	678.7	-24

The negative PW values must contain an error due to problems in the TZD estimation and/or the PW conversion. A negative WZD/PW value can only arise when the TZD estimate is too low and/or the HZD/pressure value is too high. It is likely in this study that the major errors leading to negative PW have been introduced by errors in the pressure values and/or the failure to remove unreliable TZD estimates during data manipulation (see sections 8.4.2.1 and 8.4.2.2).

Upon examination of the two-hourly TZD estimates for the negative PW occupations, it can be seen that in many cases, the last TZD estimate (end of session)

has a 1σ uncertainty of 5 mm or greater and a TZD value that does not concur with the other estimates in the same observation period. Examples of observation sessions in this category are shown in Figure 8.24.

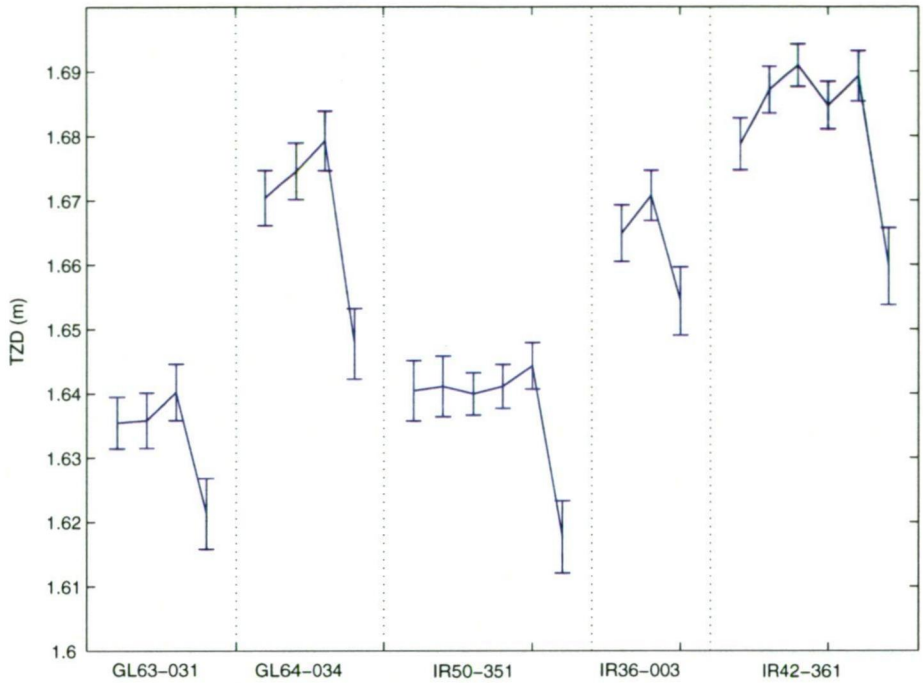

Figure 8.24 - Examples of TZD two-hourly estimates including unreliable boundary observations

All observation sessions that have PW values more than one standard deviation from zero (see Table 8.5) include an unreliable TZD boundary observation, as do several of the other negative sessions. Upon removal of these boundary values, these sessions return to a value that is generally positive, or if not, then it is within 1σ of zero.

The sessions with the greatest negative PW values, IR_42_361 and IR_36_003, include an end-of-session TZD estimate that is clearly not reliable (see Figure 8.24). Upon removal of the unreliable estimate for session IR_42_361, the mean PW returns a near-zero value (-0.4 mm). This result indicates that in this session there are other factors affecting the PW results, such as inaccurate pressure data or other TZD estimation errors. For session IR_36_003, there are only three TZD estimates, one of which does not appear to fit well and has a 1σ greater than 5 mm. However, in a set of only three data points, it is difficult to definitively single out the 'bad' value. Given the very low PW result, it is assumed that the lowest TZD value is contributing to the error. When this observation is removed, the mean PW for this session changes to -0.7 mm, which indicates the likely presence of residual errors from the input pressure data or the TZD estimation process.

Many of the negative PW results in Table 8.5 are also likely to be in part caused by inaccuracies in the pressure data. The pressures used for the IR observation sessions are especially uncertain as the values were derived from ice radar data and therefore may not reflect the actual mean pressure during the GPS observation period. For example, in session IR_69_325 the pressure obtained from the IR file and that calculated from the GL logbook differ by approximately 1 hPa with the IR value too high. On this day, the initial time/position in the ice radar data file did not agree well with the GPS occupation. Session GL_66_327 is another example of a PW result that is likely to have been affected by a significant pressure error. In this case, there was only one pressure value recorded during the observation period and therefore it is likely that this does not represent the mean value during this occupation.

8.4.4 LGB PW Zones

Having determined a mean PW value for each LGB IMS, it was decided to produce a broad-scale map of the spatial distribution of PW (in summer) along the traverse route. Such a map may facilitate identification of regional variations in PW at approximately 2500 m elevation around the basin. Any observed variations in PW can then be compared to other meteorological and glaciological data to investigate the presence of relationships between these parameters. A generalised PW map is also useful in providing a simple means of comparing the data from this study to model values for verification of model results.

To create the LGB PW map, it was assumed that at an approximately constant elevation and temperature, mean PW could be considered constant over distances of 150 - 250 kilometres[10]. Using this assumption, the LGB traverse was divided into nine zones, each with a length of approximately 200 km (see Figure 8.25). Mean PW values were then calculated for each zone (see Table 8.6 and Figure 8.26). The zones also relate approximately to the five accumulation regions defined by Higham *et al* (1997): *a)* the coastal regions (zones 1 and 9), *b)* the western basin (zones 2, 3 and 4), *c)* the southern region (zones 5 and 6) and *d)* the eastern basin (zones 7 and 8).

[10] Wolfe and Gutman (2000) state that moderate to strong correlation in PW is reasonable for sites separated by up to 800 km. Weather events such as storms and fronts will change this relationship but in general, for stable conditions this statement should be correct. Also the radiosonde analysis at Mawson and Davis and the NCEP data (sections 8.3.1 - 8.3.3) show long dominant length scales indicating that strong correlation is expected over distances of 200 - 600 km in this region.

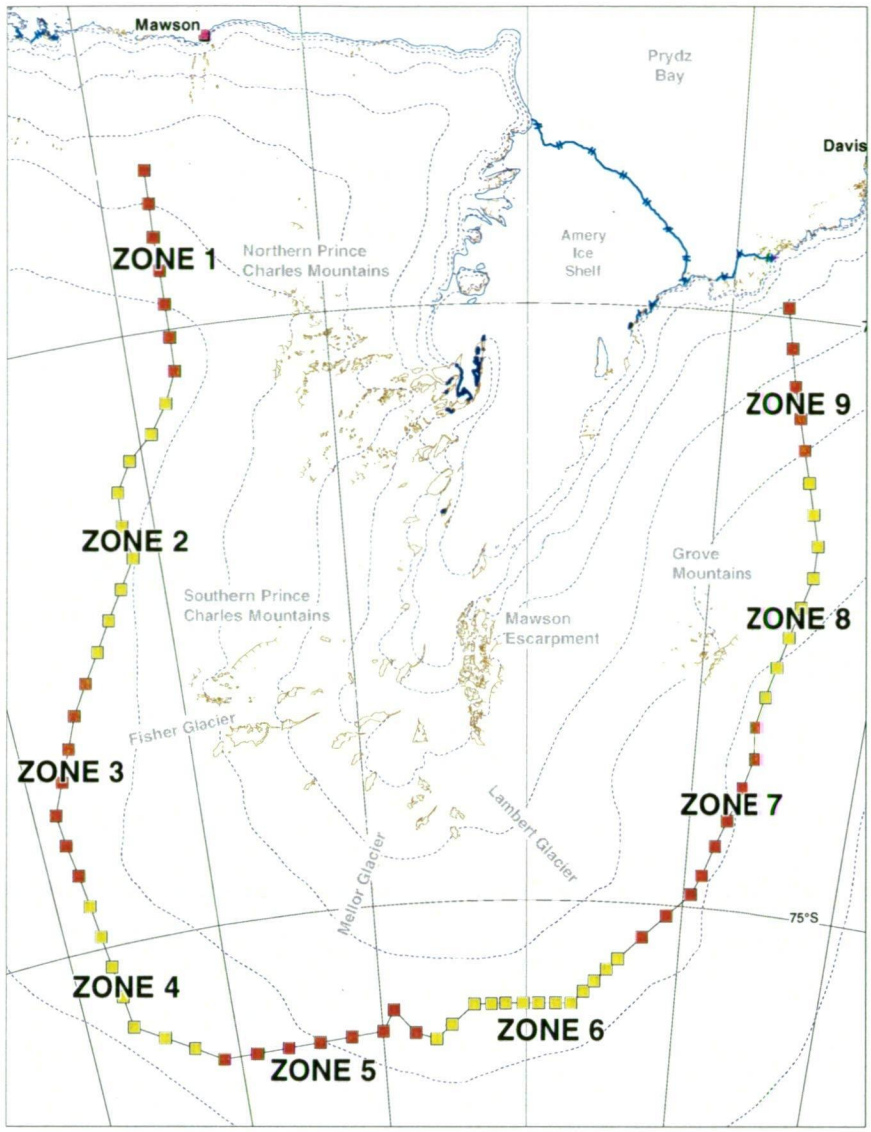

Figure 8.25 - Locations of the LGB PW zones

Table 8.6 - Mean PW values for the LGB zones

Zone	IMS	Mean PW 1993/94 (mm)	Mean PW 1994/95 (mm)
1	LG00 - LG06	0.8 ± 0.5	1.0 ± 0.3
2	LG07 - LG15	0.4 ± 0.6	1.1 ± 0.2
3	LG16 - LG22	1.0 ± 0.2	0.9 ± 0.2
4	LG23 - LG29	1.4 ± 0.2	1.4 ± 0.2
5	LG30 - LG37	1.7 ± 0.2	1.1 ± 0.1
6	LG38 - LG50	1.5 ± 0.1	1.2 ± 0.1
7	LG51 - LG59	1.8 ± 0.1	0.9 ± 0.1
8	LG60 - LG67	1.2 ± 0.1	0.8 ± 0.1
9	LG68 - LG72	2.9 ± 0.2	1.9 ± 0.2

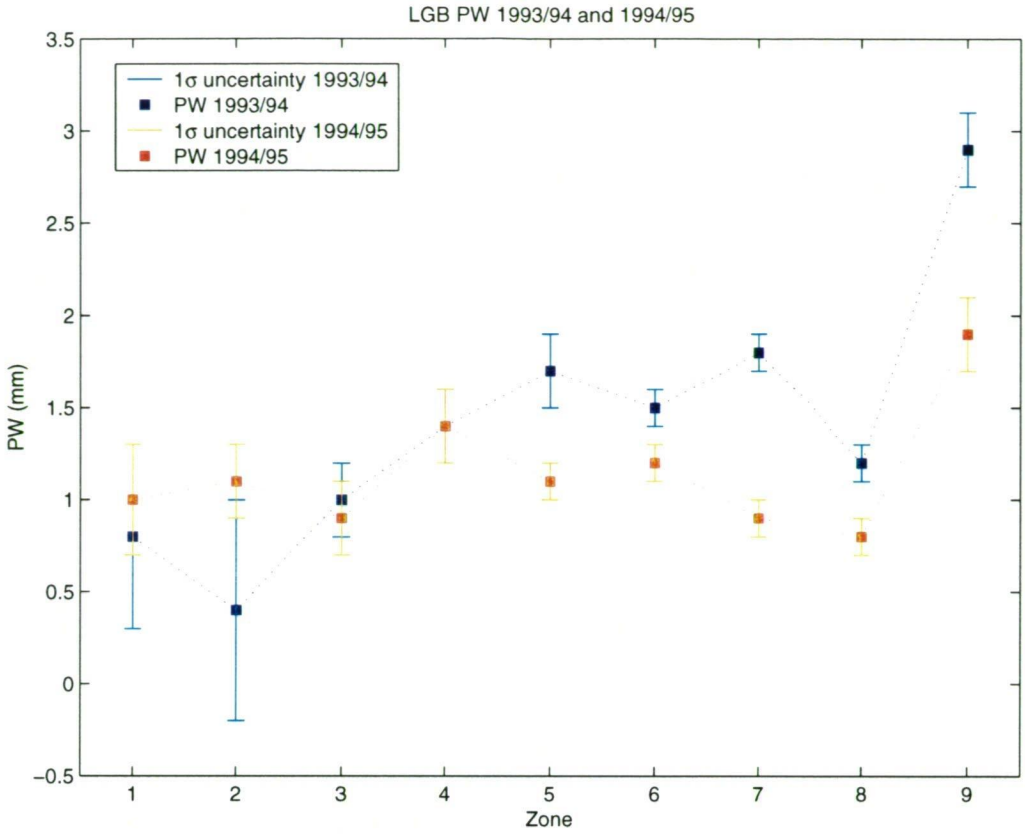

Figure 8.26 - Mean summer PW values for the LGB zones determined from analysis of GPS data (1993/94 and 1994/95).

8.4.4.1 Results

The meteorological patterns of the LGB region discussed in sections 8.2 and 8.3 indicate that PW should decrease with increasing distance inland and/or with elevation. From the model (NCEP) information (see section 8.3.3), it appears as though PW along the LGB traverse (i.e., above 700 hPa) only varies (spatially) by approximately 0.6 mm. There should also be a small variation in PW with time, peaking in December/January. The NCEP data and general circulation patterns of the region suggest that there should be slightly higher amounts of atmospheric PW in the eastern sector (i.e., zones 7, 8 and 9).

This predicted spatial pattern is not clearly seen in the data given in Table 8.6 and Figure 8.26. The PW values for most zones are close to 1.0 mm and the 1σ uncertainties indicate that there is little statistical difference in the PW results along most of the traverse. These results imply that adequate estimation of the small-scale spatial characteristics of PW along LGB traverse requires a higher level of precision from the GPS observations than is currently available. However, there are still other significant results that can be extracted from the GPS PW estimates.

The most significant feature in the GPS results is the high PW (2.9 and 1.9 mm) obtained for the eastern coastal zone (9). Zone 9 was expected to record the highest

PW levels due to its lower elevation and coastal location on the eastern side of the basin (i.e., a region where moist coastal air is advected onto the plateau). This result is therefore important in confirming that the GPS PW has adequately defined the major relative distribution between zones along the eastern side of the LGB traverse. However, zone 1 also represents coastal, lower elevation sites (in the west) and therefore would also be expected to have higher PW values than the more southern zones, although not as high as zone 9. In the GPS results, the PW for zone 1 is quite low (0.8 and 1.0 mm), and of a similar magnitude to the other western and southern zones. This may represent a 'real' result for the PW over zone 1 during the periods of the surveys indicating the strong influence of dry katabatic flow in this region. However it may also be due to a lack of reliable data in this zone (see Tables 8.3 and 8.4).

The results given in Table 8.6 and Figure 8.26 indicate higher PW values for the southern and eastern zones in 1993/94 than values in the same locations for 1994/95. This feature is not likely to be caused by the presence of larger errors in the estimation of PW in the first season as both sets of GPS data were processed in the same manner and have similar uncertainties for the input and output conversion parameters. It is more likely that the observed difference between seasons indicates a slight inter-annual variation in PW. Examination of the PW time series for Davis and Mawson (see Figure 8.7) also shows a slight reduction between the mean values for the summer months in 1993/94 and 1994/95. It is reasonable to expect that the PW in this region of the basin may have behaved similarly over this period.

The western LGB zones maintain consistent PW values between the two survey periods, within the 1σ uncertainty bounds. This suggests that the factors causing the observed variation in the southern and eastern zones do not have a similar influence on this side of the basin, possibly a reflection of the differences already known to exist between weather patterns on either side of the basin.

There is also potentially some seasonal variation exhibited in the LGB PW results where the lowest values are observed in November and the highest in December/January (see Table 8.7). However this result is not conclusive due to the magnitude of this possible monthly PW variation (0.2 - 0.7 mm) being similar to the uncertainties in the GPS results ($\pm$0.1 - $\pm$0.6 mm).

In summary, there is no definitive short-term temporal information available in these GPS PW results. However a significant variation between the PW results for the 1993/94 and 1994/95 traverse seasons has been identified across zones 5 - 9. The mean value of this variation is -0.6 mm. Short-term spatial variations at the LGB traverse sites are also too small to detect with current GPS capabilities, especially given the low GPS data quality and other inadequacies in the available data (e.g.,

pressure/temperature values, site occupation times). However, large-scale patterns in PW distribution are evident in the differences between coastal and inland zones in the east and between coastal zones on either side of the basin. Because no small-scale PW distribution information was obtained from the PW results, detailed comparisons to other LGB weather and accumulation data were not possible.

8.4.4.2 Comparison to NCEP values

Mean 700 hPa PW values corresponding to the time and locations of the LGB PW zone data were extracted from the NCEP information given in Figure 8.18. The GPS and NCEP PW values were then compared[11] to provide a validation of the amount of PW observed from each method (see Table 8.7). In making comparisons between these datasets it should be remembered that the NCEP data are monthly (grid-square) averages over several hundred kilometres whilst the GPS zone values are approximately two-weekly point values averaged over two-hundred kilometres.

Table 8.7 - NCEP and GPS mean PW values (mm) for the LGB zones

Zone	1993/94			1994/95		
	Month	NCEP	GPS	Month	NCEP	GPS
1	Nov	1.4	0.8	Feb	1.3	1.0
2	Nov	1.4	0.4	Feb	1.2	1.1
3	Nov/Dec	1.2	1.0	Jan	1.1	0.9
4	Dec	1.0	1.4	Jan	1.0	1.4
5	Dec	1.0	1.7	Jan	0.9	1.1
6	Dec/Jan	0.9	1.5	Dec	1.1	1.2
7	Jan	0.8	1.8	Dec	1.1	0.9
8	Jan/Feb	0.6	1.2	Nov	1.1	0.8

The results in Table 8.7 show that the values for the LGB zones determined by the GPS method are very close to the mean monthly values obtained from the NCEP reanalysis data. For 1993/94, the GPS and NCEP results compare to around 0.7 mm while for 1994/95, the comparisons are approximately within 0.3 mm. The differences in these comparison results for the two survey periods are most likely an indication that the unusual PW patterns seen in the monthly 1993/94 NCEP data have not been observed in the GPS measurements. This may be due to the GPS observations not coinciding with the timing of the strong influences that are known to be dominating the monthly models (see section 8.3.3) or due to some error in the magnitudes of the model PW data for these months (e.g., higher NCEP PW values

[11] Zone 9 is not included in this comparison as the sites in this zone are on a steep coastal slope (i.e., they have a range of elevations/surface pressures) and the GPS PW cannot therefore be compared to data relating to only one layer (e.g., 700 hPa) from the NCEP model.

are observed in the model data for the western LGB in November than in December 1994 and the opposite situation is suggested by the synoptic data at the time (see section 8.3.3)).

Global assimilation data (NCEP used here) provides the only readily available information for PW in this region. Therefore the close comparisons obtained between the GPS and NCEP PW data sets indicates that the GPS zone analysis has produced results of a realistic magnitude. From another perspective, it can be seen that the GPS PW estimates have provided ground truth information for the validation of NCEP data across a large section of the plateau region. This outcome suggests that future GPS measurements (especially from autonomous networks) operating in remote locations are capable of providing valuable PW data for the validation of climate model data.

8.4.5 Discussion

Current remote, ground-based meteorological data in the LGB are restricted to surface measurements from field parties and AWS. In this study, it has been demonstrated that the GPS meteorology technique can provide useful information regarding the amount and distribution of PW in dry, remote locations such as the LGB traverse line.

In regard to studying the input parameters for mass balance studies, the measurement of atmospheric water vapour is important because it represents the amount of potential precipitation if this air was cooled, raised or mixed. The results of this study suggest that a good indication of the amount of PW above the LGB traverse line during the summers of 1993/94 and 1994/95 has been achieved. These data represent the first ground based measurements of PW in this area.

As mentioned previously, the GPS and meteorological data that have been studied here were not collected with the intention of producing PW information and therefore did not result in the highest-quality PW results being obtained. However, the large number of PW values that were able to be determined along the traverse route allowed the estimation of reliable mean PW values for each site and for each of the nine zones. These mean results are sufficiently well defined to indicate the presence of approximately[12] 1 mm of PW above most of the traverse line (and 2 - 2.5 mm near LG68 - LG72) during the summer months, a range that compares well to model and expected values.

[12] As the GPS PW technique has previously been shown to produce results that contain biases of approximately 0 - +3 mm at three other sites in East Antarctica (see section 7.6.4), it is likely that these LGB PW values are also affected by some small amount of constant bias.

In this analysis, the spatial distribution of PW along the traverse route has generally not been observed due to the low amount of variation of this parameter in this region and the level of uncertainty in the PW estimates. The exception to this generalisation is zone 9, which has displayed high variation compared to the neighbouring zones. For GPS campaigns carried out at lower latitudes and elevations in the LGB, the detection of spatial patterns in PW should be achievable given the expected presence of higher amounts of PW in these regions that will most likely be above the noise level in the GPS PW estimates.

The application of the GPS meteorology technique in the LGB has also been successful in detecting a change in atmospheric PW over a one year period. This result indicates that the GPS meteorology technique is a very useful tool for the monitoring of PW variation in remote, dry locations.

The GPS meteorology technique offers a valuable, more efficient alternative to radiosondes for the monitoring and investigation of the distribution of atmospheric water vapour, especially in the spatial and temporal densification of PW observations. From the results of the analyses presented here, and with the current level of data collection and processing capabilities, the most appropriate application for a GPS meteorology project in the interior of Antarctica is in the monitoring of long-term changes in PW at a given site or, as shown here, over a given region. This application will produce reliable results if it is assumed that the PW bias at each GPS site is nearly constant over time. From the results of the case study presented in Chapter 7, this is a valid assumption. Although not studied here, due mainly to a lack of adequate meteorological and GPS data, short term fluctuations in PW (i.e., hourly, daily, weekly and monthly) over an individual site could also be monitored with a moderate level of absolute precision using the GPS technique. This application would provide valuable information regarding the movement of PW over remote areas.

8.4.5.1 Possible future applications for GPS meteorology in the LGB

The proven reliability of dedicated GPS meteorology stations (e.g., Coster *et al* (1996), Tregoning, Boers *et al* (1998) and Wolfe and Gutman (2000)) and the capability of measuring small amounts of PW accurately (Chapter 7) suggest that GPS could be used effectively in remote Antarctic regions to monitor PW above a site and/or across a region. If these observations are combined with surface meteorology measurements, satellite data and known circulation patterns, GPS measurements should provide new and useful detailed information regarding water transport and therefore precipitation and accumulation.

One important Antarctic application for the GPS PW technique would be in the monitoring of weather patterns experienced at a remote, plateau site. This type of application could provide valuable information on the presence and frequency of cyclonic systems penetrating into the interior as well as a measurement of seasonal variation in PW levels for validation of model estimates. Knowledge of the PW content of the air passing over a plateau site provides important information on the transport mechanisms and distribution of precipitation and accumulation that otherwise could not be monitored in detail. If a series of GPS meteorology stations were deployed, the passage of air masses over a given region could be observed which would assist in the understanding of spatial and temporal distributions of PW over the entire study area (e.g., Elgered *et al* (1997), Rocken, Van Hove *et al* (1997) and Wolfe and Gutman (2000)).

This development of a regional GPS network could (in the future) be incorporated into the current LGB AWS project[13] (Allison, 1998) (see Figure 8.27). The AWS

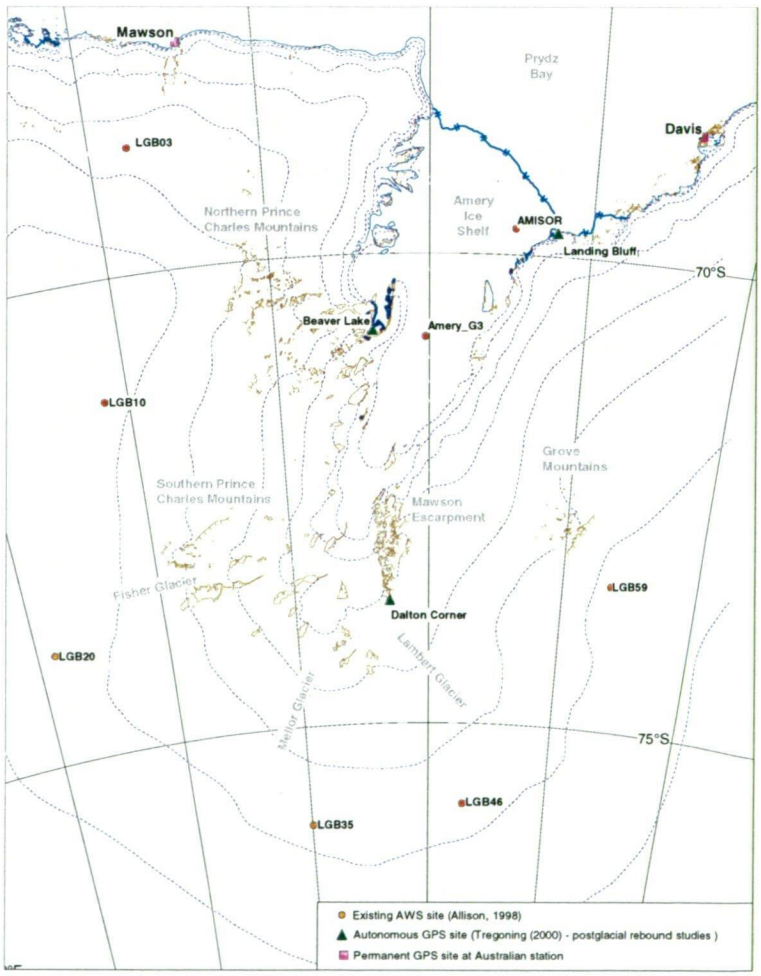

Figure 8.27 - Potential GPS PW network for the LGB incorporating current AWS and permanent GPS sites.

[13] Note that the implementation of such a network is reliant on a) the development of an efficient, autonomous GPS observation and data retrieval system and b) the ability to provide maintenance to such a system.

only provide information on the surface meteorology (up to 4 m) at each site and therefore the inclusion of GPS PW measurements would allow the corresponding atmospheric PW to be measured, providing insight into the characteristics of the air above the boundary layer. If a range of elevations and locations across the basin were sampled, a network of GPS/AWS meteorology sites could be used to achieve a greater understanding of the water vapour distribution pattern and transport mechanisms and hence the precipitation, accumulation and mass budget of the region.

Current permanent GPS sites, such as those used for glacial rebound studies (e.g., Tregoning (2000)) and those located at the Australian bases (i.e., the AUSLIG sites) should also be set up as GPS meteorology sites (see Figure 8.27). At a minimum, these sites would collect pressure and temperature data but ideally, would be co-located with a full AWS to provide air flow information. These permanent GPS sites would provide extremely valuable information on the short and long-term fluctuations in PW at a range of coastal and inland sites.

Outside of dedicated GPS meteorology campaigns/projects/sites, it is recommended that pressure and temperature information be collected whenever GPS observations are made over a substantial period (e.g., more than 24 hours). In this way, short-term information regarding PW magnitude and variation over the GPS site can be accessed in addition to the primary data from the survey. An example of this type of application is the Amery Ice Shelf Tidal Survey 2000/2001 (see section 3.3.3.5) where GPS data have been recorded over approximately eight weeks in a profile and one cross section on the ice shelf. These sites also collected temperature and (hourly) pressure data that will allow precise hourly estimates of PW to be extracted from the AIS data. These data cover a large latitudinal range over the ice shelf during this summer period, which should provide an excellent spatial and temporal description of PW movement over this region.

8.5 Chapter Summary

In this chapter, the general climatology and weather of the Antarctic and LGB was discussed followed by an analysis of radiosonde PW measurements at Mawson and Davis and the determination of GPS PW values for the interior of the LGB.

The Davis and Mawson radiosonde analysis showed a semi-annual oscillation in PW that agrees with the seasonal changes in temperature and pressure at these sites. Long-term PW fluctuations were also seen in the radiosonde data, some of which appeared to coincide with the movement of the ACW around the LGB coast.

Throughout the analysis, it was observed that Davis generally experienced more PW than Mawson. In regard to seasonal changes, it was noted (as expected) that summer months at both sites experience a different vertical distribution (i.e., greater lower atmospheric PW) than observed for other months. The autumn, winter and spring data generally displayed similar PW distributions to each other with the mean distribution reflecting low amounts of PW in both the upper and lower atmosphere.

GPS PW analysis from the 1993/94 and 1994/95 LGB traverse data commenced with the determination of GPS PW values for Davis and Mawson over the study period. These values were compared to radiosonde data to confirm the results observed at these sites in Chapter 7 and therefore validate the GPS meteorology method for the LGB study period/region. Following from this, the GAMIT TZD estimates for the LGB IMS were converted to mean daily PW values at each site using surface meteorological data. These PW values represent the first-ever ground-based estimates of water vapour in the interior of the LGB.

The LGB PW estimates from each survey season were then divided into nine zones to identify the mean PW over the major regions of the traverse route. These results did not allow observation of the spatial distribution of PW along the majority of the traverse line due to the levels of variation experienced in this region being lower than the noise levels of the PW results. However, the expected large difference between the eastern coastal region and the remainder of the traverse was identified in the GPS PW results. In terms of temporal change, the 1993/94 results for zones 5 to 8 (i.e., the southern and eastern basin) were found to be slightly higher than the 1994/95 values which concurs with the mean PW variation observed at Davis and Mawson over this period. In the western zones (1 - 4) there was no significant PW variation found between the two traverses, possibly reflecting the influence of different meteorological conditions within the LGB. Overall, these findings suggest that the GPS methodology used in this study is of sufficient quality to adequately detect inter-annual variation and large-scale spatial variances in PW for arid locations such as the LGB.

The results from the GPS analysis were also compared to NCEP model estimates. In these comparisons both data sets were found to display PW values of a similar magnitude above the LGB traverse line (i.e., approximately 1 mm). The GPS observations have therefore provided a validation of the NCEP model values.

From the results of this study, future theoretical applications of the GPS meteorology technique have been suggested. It is recommended that all long-term (greater than 24 hour) GPS occupations be accompanied by pressure, temperature, and wind velocity

observations. In combination, these observations will greatly assist in understanding the amount and transport of PW over important study regions. It is suggested that permanent GPS sites in Antarctica are especially useful for collecting GPS meteorology information and will provide excellent long term, seasonal and daily information on the PW near these locations.

In summary, the GPS meteorology method has been used to detect water vapour for the first time at dry and remote sites in the Antarctic interior. Future application of this technique in this region would provide valuable PW information for the determination and verification of atmospheric data for mass balance and climate studies.

Chapter 9

CONCLUSIONS

9.1 Overview

The work carried out in this thesis can be separated into two major sections, both of which have used high-level GPS processing techniques to extract information that is useful in terms of improving our understanding of parameters which affect the mass balance of the Lambert Glacier Drainage Basin.

The first section deals with the dynamics and topography of the ice surface near the 2500 m elevation contour while the second investigates the amount of water vapour in the atmosphere above this same region. In both cases, high-level GPS processing has been used to overcome deficiencies in the LGB GPS data and extract the most precise and complete set of results available from the LGB traverses. Within the two sections of the thesis there are also many smaller investigations that have produced new and/or improved insights into the parameters being studied.

The major results from this body of work are:

i) *GPS data from all five LGB traverses (i.e., 1989 - 1995) have been used to determine precise positions ($1\sigma < 5$ mm) and velocities (formal uncertainties of < 0.03 m/yr in the west and < 0.01 m/yr in the south and east) in a consistent reference frame (ITRF97). The velocity estimates also have directions that are consistent with the local topography at each of the IMS. In particular, results in the Western sector of the LGB traverse route have been greatly improved by the GPS processing methods adopted in this study.*

ii) *Surface ellipsoidal heights have been determined (with centimetre precision) for the IMS locations in the 1994/95 traverse. Unique height solutions have also been computed for each of the earlier traverse campaigns (generally with centimetre/decimetre precision, except for the 1989/90 results ($1\sigma > 1$ m)). These IMS height estimates along with the data from the LGB offset traverse and kinematic surveys have been used to calculate surface gradients over*

the entire western region (LG00 - LG35) and at selected points in the eastern sector (LG46, LG53, LG59, LG65, LG70).

iii) The velocities from i) were used for verification of a balance flux model. Comparisons between the GPS results and the best solution for the modelled balance velocities showed a general agreement of approximately 20%. Comparisons between the GPS velocities and the results of other model solutions provided an indication of the sensitivity of the modelling technique to the selection of input parameters. This analysis also confirmed that the ice flux across the traverse line (approximately 2500 m elevation) is most likely to be close to a state of balance.

iv) Significant elevation dependent errors were identified in the GPS data collected at Amundsen-Scott station. These large errors prevented the determination of an absolute error in the PW estimation, based on comparisons with an assumed zero-PW at this site.

v) GPS and radiosonde PW values were compared at Davis, Casey and Mawson. These comparisons showed constant biases that varied between sites from approximately 0 to +3 mm with wrms values of < 0.8 mm. These results provided validation for the process used in this study to determine mean daily PW values from GPS data under low PW conditions such as those found in Antarctica.

vi) Multi-period signals were identified within 11 years of PW data from radiosonde soundings at Mawson and Davis. Also, the time-series of PW data at Davis and Mawson stations showed almost identical characteristics indicating that the majority of PW transport at these sites is controlled by synoptic-scale meteorological events.

vii) Two sets of mean 'summer' PW values were obtained for the LGB IMS using the 1993/94 and 1994/95 GPS data providing the first-ever ground-based PW measurements in this region. These results showed variations in PW along the traverse route from 0.2 to 4 mm. These data also indicated a decrease in PW between 1993/94 and 1994/95 for the southern and eastern sections of the traverse.

viii) The PW values determined for the LGB sites were used to validate values from NCEP numerical modelling with both sets of data agreeing to better than 1 mm.

The most significant of these findings, in terms of current mass balance calculations (e.g., Fricker, Warner *et al* (2000) and Testut (2000)) are the well-determined directions and low level of uncertainty for the IMS velocity parameters. The velocity and elevation results presented here also provide the best possible data for the calibration/validation of numerical models and remotely sensed data and will be useful for future research in these areas.

The observation of PW at the LGB IMS, approximately 700 km inland from the coast, has shown that the GPS meteorology technique is capable of providing useful information under Antarctic conditions. The results presented here indicate that future studies using this technique will be able to accurately monitor the movement of PW above remote sites at a temporal resolution not available using any other method. The ability to determine PW values for inland sites is also important in terms of validating meteorological models and therefore improving model-based estimates of accumulation rates.

9.2 Glaciological Studies

9.2.1 Glaciological Results and Analysis (Chapter 5)

GAMIT/GLOBK/GLORG software was used to estimate and combine daily solutions for the GPS data from each LGB campaign and subsequently, combine all of the data from each of the LGB traverses to produce a set of IMS coordinate and velocity results in a consistent reference frame (ITRF97 at 1997.0).

The above processing resulted in the determination of the most precise set of position, height, surface slope and velocity results arising from the LGB traverse GPS data. In particular, the successful processing of the 1989 - 1993 GPS data resulted in significant improvements in the determination of coordinates and velocities (and their uncertainties) at the Western LGB traverse sites (i.e., LG00 to LG32).

9.2.1.1 Position

Horizontal positions for the LGB IMS were determined with varying precision, ranging from approximately 2.5 m in 1989/90 to 0.003 m in 1994/95. Precision of the ellipsoidal heights of the top of the IMS poles also varied between approximately 2.6 m and 0.01 m depending on the period of the survey. The conversion of the IMS pole heights to a surface value using fieldbook measurements resulted in the calculated surface ellipsoidal heights having additional uncertainties in the order of a few centimetres.

9.2.1.2 Velocity

Surface velocity values at the LGB traverse sites were estimated using all available IMS position data between 1989 and 1995. The majority of these velocity results have a mean formal uncertainty (1σ) of approximately 0.01 m/yr. For nine sites between LG00 and LG33, data were only collected during the 1989-1993 period and as such, the mean velocity uncertainty at these sites is approximately 0.3 m/yr. In terms of flow direction, significant improvements have been made when compared to known flow lines and topography, especially in regions of slow flow rates. It can be said that the LGB velocity values determined by this study are of a much higher quality than anticipated at the commencement of the traverse program. These new results allow improved estimates of the mass flux across the traverse route to be calculated and hence, more accurate analysis of the state of balance of this region (e.g., Fricker, Warner *et al* (2000) and Testut (2000)).

9.2.1.3 Surface slope

Detailed slope measurements from the LGB GPS observations have been presented here for the first time. The slope calculations for the western basin were determined using a TIN representation based on height results from static data collected along an offset line and the main traverse route. These results show a mean surface gradient in this region of 4 m/km with good definition of the large-scale surface topography. In the eastern basin, kinematic GPS data collected approximately 5 km up- and down-slope from five IMS were used to investigate local topography. The surface gradients observed with these kinematic GPS results ranged from 2 to 30 m/km. The slope values determined from this study were compared to ERS-1 radar altimeter DEM information (Fricker, Hyland *et al*, 2000) indicating that the DEM (with a resolution of 5 km) does provide a good representation of the surface gradients in all regions of the traverse route.

9.2.1.4 Comparisons

The position and velocity results determined in this study were compared to the initial results from the LGB traverses which had been obtained using commercial processing software (SKi) (Kiernan, 2001). These comparisons showed differences in flow rates that were generally less than 1.5 m/yr. For most sites east of LG16, differences were less than 0.5 m/yr. In general, variations in flow direction of 0.1° to 4° were observed between the two datasets in all regions of the traverse. Higher differences (up to 75°) were found in the region between LG00 and LG15 with the results of this study showing far better agreement with the local topography. In terms of ellipsoidal heights (solved directly from processing), the mean difference between

this study and those of Kiernan (2001) for the 1994/95 traverse is 0.3 m while for earlier years, the differences are around 1 - 2 m.

The most significant of improvements made in this study are the height and flow direction results. The increase in accuracy and precision of these parameters, in a consistent reference frame, is important for the validation of future elevation data and mass flux data (e.g., Wahr *et al* (2000) and Testut (2000)).

9.2.1.5 Validation of mass flux analysis

The velocity and elevation results at the LGB IMS from this study have been used as validation for remote sensing studies of ice sheet balance velocities (Testut, 2000) and DEM values (Fricker, Hyland *et al*, 2000). Additionally, these results will form an integral part in validation of future mass balance studies in the LGB region using GLAS (Brenner *et al*, 2000) and GRACE (Wahr *et al*, 2000) satellite data.

In this study, comparisons were made between balance velocities from the Testut-model and the GPS-derived values for the IMS. These comparisons revealed that regardless of which topographic or accumulation dataset is used as input, the largest errors in the modelled flow rates occur for the ice flowing into the major glaciers (i.e., the major region of mass flux). In general, it can be said that the modelling agrees well with the GPS results, with flow rate comparisons within 20% and excellent comparisons in the directions of the flows. A short study of the effects of varying the input data to the Testut-model suggested that the choice of DEM had less influence on the results than the selection of either observationally or meteorologically determined accumulation data.

9.2.1.6 Future recommendations

The final section of Chapter 5 investigated the level of precision achievable using multiple, short-term GPS occupations (i.e., helicopter-based fieldwork) within a single field season. From these investigations, it was found that for baselines of up to 700 km and sites moving between 17 and 59 m/yr, 2 - 4 hour occupations re-observed after approximately 40 days were adequate to provide velocities (with precisions of < 1 m/yr) at the 97% confidence level. The precision of the velocity results improved, as expected, with increased occupation times and longer reoccupation intervals. A strategy for providing high-accuracy ice velocity determination from single season, traverse-based GPS programs was also discussed, based on two traverse teams travelling with a separation of 14 days.

9.3 Meteorological Conclusions

9.3.1 Case-Study of PW Estimation in Antarctica (Chapter 7)

9.3.1.1 Elevation angle cut-off and coordinate constraints

The analysis of GPS PW estimates at DAV1, CAS1 and AMUN confirmed that the quality of the GPS installation is a major factor affecting the impact of elevation angle cut-off and coordinate constraints on the quality of the results.

When the elevation angle cut-off angle was changed from 15° to 10° at the AMUN site, significant variations in PW of 4 mm and 1 mm were observed in the presence of a rectangular dome and SCIGN dome respectively. At CAS1, testing with the same elevation cut-offs did not produce similar levels of variation, indicating a problem in the GPS PW estimation specific to the AMUN site.

The variation of coordinate constraints applied during least-squares processing resulted in a consistent variation in the DAV1 PW value but had little effect on the CAS1 results. The variations at DAV1 are thought to be caused by using constraints that were too close to the expected daily variation in height at this site. The low amount of variation seen in the CAS1 PW results indicated that the choice of either moderately-tight (50 mm) or loose (500 mm) constraints on well-known coordinates did not significantly affect the final PW value.

9.3.1.2 Testing of GPS PW at the South Pole

One of the major aims of this section of the thesis was to investigate the presence and magnitude of small errors in GPS-derived PW values by studying GPS results at a site with effectively zero PW. This investigation was not successful due to the noise in the GPS results at this site (as mentioned in 9.3.1.1).

The PW results determined for the AMUN site ranged from -1 to +3 mm and varied depending on the period in which the data were collected (i.e., either using a rectangular or SCIGN dome) and the elevation angle cut-off used in processing. The elevation dependency in the results using the SCIGN dome suggests that there are external influences affecting the data from this site or possibly inadequacies in the tropospheric mapping function at this location.

The only negative values determined in this study of PW at permanent Antarctic sites were observed at AMUN in 1998. These negative values were found to be caused by unmodelled variable path effects created by the rectangular shape of the antenna dome.

9.3.1.3 Testing of GPS PW in East Antarctica

The GPS-derived values of PW at the East Antarctic sites of DAV1, CAS1 and MAW1 mimic the radiosonde-derived values with seasonal biases of approximately 0 - +3 mm and a scatter about the bias of less than 0.8 mm (1σ). These values are consistent with results from other studies (e.g., Emardson *et al* (1998), Fang *et al* (1998) and Tregoning, Boers *et al* (1998)) and therefore indicate that standard GPS PW processing and conversion techniques are valid for Antarctic sites. A slight seasonal variation in the bias values at each site was also observed which is thought to be caused by variations in the radiosonde errors and/or station height fluctuations.

The biases observed between radiosonde and GPS estimates at DAV1, CAS1 and MAW1 are not consistent between sites, indicating the presence of site-specific effects in the data. These sites have the same GPS equipment configuration, are located at similar latitudes and use identical radiosonde equipment in similar climates. The only significant differences between the sites are the antenna mounting and local environment, which may explain some of the site dependency observed in the PW biases.

9.3.2 Radiosonde Analysis of PW in the LGB Region (Chapter 8)

Time-series analysis of radiosonde PW data at Davis and Mawson showed a strong annual peak in January and a smaller peak in June at both sites with Davis generally having higher values than Mawson. Frequency analysis of these data confirmed the presence of annual and semi annual oscillations in the PW signals that agree with the seasonal variations in temperature and pressure at these locations. Strong similarities between the PSD analysis at the two sites indicate that the transport of PW in this region is mostly due to synoptic-scale events. However, slight differences between the PW signals were also observed which are likely to be features of variations in the local environments.

Wavelet analysis was also carried out on the Davis and Mawson radiosonde PW data. This analysis displayed the annual and semi-annual information discussed above and also indicated the presence of a weak bi-annual signal and a possible 5 - 6 year signal in the PW at these sites. The 5 - 6 year PW signal is only just significant due to the limited (11-year) data span but appears to be correlated spatially and temporally with the movement of the Antarctic Circumpolar Wave (White and Peterson, 1996).

9.3.3 GPS Analysis of PW in the LGB Region (Chapter 8)

Mean PW values were estimated for all LGB sites occupied during the 1993/94 and 1994/95 summer traverses. The observed PW values ranged from 0.2 to 4.2 mm with a mean value of approx 1.6 mm and (1σ) uncertainties of approx 0.4 mm. Negative PW values were obtained for some individual GPS observation sessions, however, these were found to be caused by unreliable TZD estimates and/or errors in the pressure data.

The results of this study provide the first-ever ground-based measurements of PW in the LGB and also represent the first attempt to obtain GPS PW estimates using data collected on the East Antarctic ice-sheet. The standard of GPS and meteorological data available for this study limited the usefulness of the results. However, the values obtained for PW at the LGB sites appear to be within the current precision of the GPS meteorology technique (i.e., approximately 1 mm) given the comparisons to other PW data (e.g., Mawson and Davis radiosonde-derived PW above 700 hPa and NCEP atmospheric modelling) and assuming a minimum possible value of 0 mm in this region.

The PW values from the two traverses were divided into nine zones to allow spatial and temporal analysis of 'summer' PW levels across the LGB region. These analyses did not identify any small-scale spatial information regarding the distribution of PW along the traverse route due to the variation experienced in this region being less than the noise levels of the PW results. However, it was shown that the GPS results had correctly determined a significantly higher PW value for the eastern coastal zone than for the other regions. Short-term temporal variations could not be examined due to the small variation in amplitude of the PW signal during this period being similar to the precision of the GPS PW results. However, in terms of inter-annual variation, the GPS PW results show that 1993/94 PW values were consistently higher than those from 1994/95 for the eastern and southern zones. The western zones did not show the same inter-annual variation, which may be a factor of differences in the meteorological conditions on either side of the basin or a result of data limitations in this region.

The PW results from the GPS analysis were also compared to NCEP model estimates above 700 hPa. These comparisons showed that both datasets observe PW values of a similar magnitude above the LGB traverse line (i.e., better than 0.5 to 1 mm), thereby validating the NCEP data.

9.3.4 Future LGB GPS PW Studies (Chapter 8)

It has been shown that with current receiver technology and processing capabilities, temporal and spatial variation in PW at Antarctic sites can be observed using the GPS meteorology method. A dedicated PW study in the LGB should produce results similar to those above with a better temporal resolution of the PW movements.

Suggestions for possible future applications of the GPS meteorology technique in the LGB have been outlined, including the incorporation of the GPS meteorology technique into currently operating AWS and isostatic rebound projects. It is also recommended that the necessary surface meteorology observations (i.e., pressure and temperature) be collected during all long-term (i.e., > 24 hour) GPS occupations. If these recommended observations are collected, they have the potential to greatly assist in understanding the amount and transport of PW over the area.

9.4 Summary

In summary, this thesis has provided new, high-quality information regarding ice velocity, surface elevation, surface slope and precipitable water near the 2500 m elevation of the LGB. Obtaining this information from archived GPS data (1989-1995) required the application and manipulation of high-level processing techniques, including significant manual editing of the raw data and customisation of cleaning and processing parameters.

The determination of new values for the surface velocity at the LGB IMS provides the best possible information for mass flux calculations within the region. These results also provide data for comparison to, and validation of, modelled balance flux information as demonstrated in Chapter 5 of this thesis. The surface elevation and slope parameters determined here also provide useful ground-truth information for the validation of topographic models (also used in mass balance studies) from remotely sensed data. This application was also demonstrated in Chapter 5 of this thesis.

The determination of PW at the LGB IMS represents the first use of this technique in the Antarctic interior. The results of this study have shown the capability of this technique to identify spatial and temporal changes. These results were obtained using non-optimum data, however, they do suggest that future dedicated campaigns will be able to produce PW results of a much higher quality and resolution. GPS PW observations, especially if made over a network of sites, will provide useful

information for the validation of numerical modelling (e.g., Bromwich *et al* (1995) and Kalnay *et al* (1996)), the monitoring of PW fluctuations in interior regions and the provision of tropospheric corrections for SAR interferometry and altimetry studies (e.g., Williams *et al* (1998), Rignot and MacAyeal (1998) and Fricker, Hyland *et al* (2000)). It is concluded that the GPS meteorology technique is capable of providing an economical and efficient method of obtaining detailed, remote, ground-based water vapour information in Antarctica.

REFERENCES

Allison, I. (1979). The mass budget of the Lambert Glacier drainage basin, Antarctica. Journal of glaciology 22(87), 223-235.

Allison, I. (1991a). Ice in motion; mass and movement studies of Lambert-Amery basin. *ANARE News*(65), 4-5.

Allison, I. (1991b). The Lambert Glacier/Amery Ice Shelf study: 1988-1991. *Aurora. ANARE Club Journal* **10**(4), 22-25.

Allison, I. (1991c). World's largest glacial basin is focus of 1990-91 program. *ANARE News* (65), 3.

Allison, I. (1993). The Global Positioning System. *Aurora. ANARE Club Journal* **13**(2), 24-26.

Allison, I. (1995). Surveying the Amery Ice Shelf. *ANARE News* (Spring/Summer 1995-96), 12.

Allison, I. (1998). Surface climate of the interior of the Lambert Glacier Basin, Antarctica, from automatic weather station data. *Annals of Glaciology* **27**, 515-520.

Allison, I. (2001). Peephole through the ice: the AMISOR project. *Australian Antarctic Magazine* **1**(Autumn 2001), 20-21.

Allison, I., G. Wendler and U. Radok (1993). Climatology of the East Antarctic Ice Sheet (100degE to 140degE) derived from Automatic Weather Stations. *Journal of Geophysical Research* **98**(D5), 8815-8823.

Anderle, R.J. (1977). Stations in the TRANET Network. *Part1 National Geodetic Satellite Program (NASA SP365)*(eds), National Aeronautics and Space Administration, Washington D.C., 203-207.

Anthes, R.A., C. Rocken and Y.-H. Kuo (2000). Applications of COSMIC to meteorology and climate. *TAO* **11**(1), 115-156.

Aoki, S., T. Ozawa, K. Doi and K. Shibuya (2000). GPS observation of sea level variation in Lutzow-Holm Bay, Antarctica. *Geophysical Research Letters* **27**(15), 2285-2288.

Askne, J. and H. Nordius (1987). Estimation of tropospheric delay for microwaves from surface weather data. *Radio Science* **22**(3), 379-386.

Baby, H.B., P. Gole and J. Lavergnat (1988). A model for the tropospheric excess path length of radio waves from surface meteorological measurements. *Radio Science* **23**(B4), 1825-1828.

Bamber, J.L. (1994a). A digital elevation model of the Antarctic ice sheet derived from ERS-1 altimeter data and comparison with terrestrial measurements. *Annals of Glaciology* **20**, 48-53.

Bamber, J.L. (1994b). Ice sheet altimeter processing scheme. *International Journal of Remote Sensing* **15**, 925-938.

Bamber, J.L. and R. Bindschadler (1997). An improved elevation dataset for climate and ice-sheet modelling: validation with satellite imagery. *Annals of Glaciology* **25**, 439-444.

Bar-Sever, Y.E., P.M. Kroger and J.A. Borjesson (1998). Estimating horizontal gradients of tropospheric path delay with a single GPS receiver. *Journal of Geophysical Research* **103**(B3), 5019-5035.

Bentley, C.R. (1987). Antarctic ice streams: A review. *Journal of Geophysical Research* **92**(B9), 8843-8858.

Bentley, C.R. (1997). Rapid sea-level rise soon from West Antarctic Ice Sheet collapse. *Science* **275** (21 February), 1077-1078.

Bentley, C.R. and M.B. Giovinetto (1991). Mass balance of Antarctica and sea level change. *International Conference on the role of the Polar Regions in Global Change*, University of Alaska, Fairbanks, Alaska, USA, 481-488

Beutler, G., E. Brockmann, S. Fankhauser, W. Gurtner, J. Johnson, L. Mervart, M. Rothacher, S. Schaer, T. Springer and R. Weber (1996). Bernese GPS software Version 4.0. Documentation.

Beutler, G. and J. Kouba (1998). State of the IGS by the end of 1998. *IGS Workshop Proceedings:1998 Network Systems Workshop*, Pasadena, CA, USA., Jet Propulsion Laboratory, 3-17

Beutler, G., M. Rothacher, T. Springer, J. Kouba and R.E. Neilan (1998). The International GPS service (IGS): An interdisciplinary service in support of earth sciences. *32nd COSPAR Scientific Assembly*, Nagoya, Japan, July 12 - 19,

Bevis, M., S. Businger, T.A. Herring, C. Rocken, R.A. Anthes and R.H. Ware (1992). GPS meteorology: remote sensing of atmospheric water vapor using the Global Positioning System. *Journal of Geophysical Research* **97**(D14), 15,787-15,801.

Bevis, M., S. Businger, S. Chiswell, T.A. Herring, R.A. Anthes, C. Rocken and R.H. Ware (1994). GPS meteorology - mapping zenith wet delays onto precipitable water. *Journal of Applied Meteorology* **33**(3), 379-386.

Bindschadler, R., P. Vornberger, D. Blankenship, T. Scambos and R. Jacobel (1996). Surface velocity and mass balance of Ice Streams D and E, West Antarctica. *Journal of Glaciology* **42**(142), 461-475.

Boucher, C., Z. Altamimi and P. Sillard (1999). The 1997 International Terrestrial Reference Frame (ITRF97). IERS Technical Note 27, May 1999, Observatoire de Paris.

Bouin, M.N. and C. Vigny (2000). New constraints on Antarctic plate motion and deformation from GPS data. *Journal of Geophysical Research-Solid Earth* **105**(B12), 28279-28293.

Brenner, A.C., H.J. Zwally, C.R. Bentley, B.M. Csatho, D.J. Harding, M.A. Hofton, J. Minster, L. Roberts, J.L. Saba, R.H. Thomas and D. Yi (2000). Derivation of range and range distributions from laser pulse waveform analysis for surface elevations, roughness, slope and vegetation heights. Geoscience Laser Altimeter (GLAS). Algorithm Theoretical Basis Document, v3.0.

Bromwich, D.H. (1988). Snowfall in high southern latitudes. *Reviews of Geophysics* **26**(1), 149-168.

Bromwich, D.H., F.M. Robasky, R.I. Cullather and M.L. Vanwoert (1995). Atmospheric hydrologic cycle over the Southern Ocean and Antarctica from operational numerical analyses. *Monthly Weather Review* **123**(12), 3518-3538.

Bromwich, D.H. and T.R. Parish (1998). Antarctica: barometer of climate change. Report to the National Science Foundation from the Antarctic Meteorology Workshop. Madison, Wisconsin.

Bromwich, D.H. and T.R. Parish (1998). Meteorology of the Antarctic. *Meteorology of the Southern Hemisphere*. D.J. Karoly and D.G. Vincent (eds). Boston, Massachusetts, American Meteorological Society. **27(49)**, 175-200.

Brunner, F.K. and M. Gu (1991). An improved model for dual frequency ionospheric correction of GPS observations. *Manuscripta Geodetica* **16**(3), 205-214.

Brunner, F.K. and W.M. Welsch (1993). Effect of the troposphere on GPS measurements. *GPS World* **January**, 42-51.

Budd, W., I. Landon Smith and E. Wishart (1967). The Amery Ice Shelf. *The Physics of Snow and Ice. Proceedings: International Conference on Low Temperature Science*, Sapporo, Japan., Institute of Low Temperature Science, Hokkaido University, 447-467

Budd, W. and I.N. Smith (1982). Large-scale numerical modelling of the Antarctic ice sheet. *Annals of Glaciology* **3**, 42-49.

Budd, W.F. (1986). The Southern Hemisphere circulation of atmosphere, ocean and sea ice. *Second International Conference on Southern Hemisphere Meteorology*, Wellington, New Zealand, American Meteorological Society, Boston Massachusetts,

Budd, W.F. and I. Simmonds (1991). The impact of global warming on the antarctic mass balance and global sea level. *International Conference on the role of the polar regions in global change*, University of Alaska, Fairbanks U.S.A., 489-494

Budd, W.F., P.A. Reid and L.J. Minty (1995). Antarctic moisture flux and net accumulation from global atmospheric analyses. *Annals of Glaciology* **21**, 149-155.

Budd, W. and R.C. Warner (1996). A computer scheme for rapid calculations of balance-flux distributions. *Annals of Glaciology* **23**, 21-27.

Chen, G. and T.A. Herring (1997). Effects of atmospheric azimuthal asymmetry on the analysis of space geodetic data. *Journal of Geophysical Research* **102**(B9), 20489-20502.

Chen, X., R.A. Bindschadler and P.L. Vornberger (1996). Preliminary determination of ice flow velocity in West Antarctica using high precision GPS measurements. *ION, GPS-96, Sept 1996*, Kansas City, Missouri.

Chin, M. (1988). CIGNET report. *GPS Bulletin* **1**(1), 1.

Coleman, R., I. Allison, H.A. Fricker and J.B. Minster (2000). GLAS validation on the Amery Ice Shelf. *ASAC grant proposal 1263 - season 2000/01.*

Coleman, R., P. Morgan and L. Padman (2000). Amery Ice Shelf dynamics from GPS. *ASAC grant proposal 1120 - season 2000/01.*

Collins, J.P. and R.B. Langley (1998). The residual tropospheric propagation delay: how bad can it get? *11th International Technical Meeting of the Satellite Division of The Institute of Navigation (ION GPS-98)*, Nashville, Tennessee, U.S.A., September 1998, 729-738

Connolley, W.M. and J.C. King (1993). Atmospheric water-vapour transport to Antarctica inferred from radiosonde data. *Quarterly Journal of the Royal Meteorological Society* **119**(510), 325-342.

Coster, A.J., A.E. Niell, V.B. Mendes, P.C. Toor, R.B. Langley and C.A. Ruggles (1996). The Westford Water Vapor Experiment: use of GPS to determine total precipitable water vapor. *The 52nd Annual Meeting of The Institute of Navigation*, Cambridge, MA, June 1996, 529-538

Craven, M., I. Allison, R. Kiernan and M. Higham (1995). GPS applications in Antarctic glaciology. *Conference on Satellite Navigation Technology: 1995 and beyond, June 1995*, Brisbane, Australia, 1-8

Dach, R. and R. Dietrich (2000). Influence of the ocean loading effect on GPS derived precipitable water vapor. *Geophysical Research Letters* **27**(18), 2953-2958.

Dach, R. and R. Dietrich (2001). The ocean loading effect in the GPS analysis: a case study in the Antarctic Peninsula region. *Marine Geodesy* **24**, 13-25.

Davies, O.T. and P.A. Watson (1998). Comparison of integrated precipitable water vapour obtained by GPS and radiosondes. *Electronics Letters* **34**(7), 645-646.

Davis, J.L., T.A. Herring, I.I. Shapiro, A.E.E. Rogers and G. Elgered (1985). Geodesy by radio interferometry: effects of atmospheric modelling errors on estimates of baseline length. *Radio Science* **20**(6), 1593-1607.

Dietrich, R., R. Dach, G. Engelhardt, J. Ihde, W. Korth, H.-J. Kutterer, K. Lindner, M. Mayer, F. Menge, H. Miller, C. Muller, W. Niemeier, J. Perlt, M. Pohl, H. Salbach, H.-W. Schenke, T. Schone, G. Seeber, A. Veit and C. Volksen (2001). ITRF coordinates and plate velocities from repeated GPS campaigns in Antarctica - an analysis based on different individual solutions. *Journal of Geodesy* **74**, 756-766.

Doake, C.S.M., H.F.J. Corr, H. Rott, P. Skvarca and N.W. Young (1998). Breakup and conditions for stability of the Northern Larsen Ice Shelf, Antarctica. *Nature* **391**(6669), 778-780.

Dodson, A.H., P.J. Shardlow, L.C.M. Hubbard, G. Elgered and P.O.J. Jarlemark (1996). Wet tropospheric effects on precise relative GPS height determination. *Journal of Geodesy* **70**(4), 188-202.

Dodson, A.H. and H.C. Baker (1998). Accuracy of orbits for GPS atmospheric water vapor estimation. *Phys. Chem. Earth* **23**(1), 119 - 124.

Dong, D., T.A. Herring and R.W. King (1998). Estimating regional deformation from a combination of space and terrestrial geodetic data. *Journal of Geodesy* **72**(4), 200-214.

Dragert, H., T.S. James and A. Lambert (2000). Ocean loading corrections for continuous GPS: a case study at the Canadian coastal site Holberg. *Geophysical Research Letters* **27**(14), 2045-2048.

Drewry, D.J. (1983). The surface of the Antarctic Ice Sheet. Glaciological and Geophysical Folio, Scott Polar Research Institute.

Drewry, D.J. and E.M. Morris (1992). The response of large ice sheets to climatic change. *Antarctica and Environmental Change,*, Proceedings of a Royal Society Discussion, 20-21 May 1992, Royal Society, Clarendon Press, Oxford.

Duan, J.P., M. Bevis, P. Fang, Y. Bock, S. Chiswell, S. Businger, C. Rocken, F. Solheim, T. Van Hove, R. Ware, S. McClusky, T.A. Herring and R.W. King (1996). GPS meteorology - direct estimation of the absolute value of precipitable water. *Journal of Applied Meteorology* **35**(6), 830-838.

Elgered, G., J.L. Davis, T.A. Herring and I.I. Shapiro (1991). Geodesy by radio interferometry: water vapor radiometry for estimation of the wet delay. *Journal of Geophysical Research* **96**(B4), 6541-6555.

Elgered, G., J.M. Johansson, B.O. Ronnang and J.L. Davis (1997). Measuring regional atmospheric water vapor using the Swedish permanent GPS network. *Geophysical Research Letters* **24**(21), 2663-2666.

Elliott, W.P. and D.J. Gaffen (1991). On the utility of radiosonde humidity archives for climate studies. *Bulletin of the American Meteorological Society* **72**(10), 1507-1520.

Elliott, W.P., D.J. Gaffen, A.K. Betts, F.P. Bretherton, A. Del Genio, A. Gruber, R. Hoff, M.P. McCormick, E. Rasmusson, R.D. Rosen, E. Ruprecht, G. Stephens and G.M. Stokes (1995). Water Vapor in the Climate System. American Geophysical Union Special Report, December 1995. (www.agu.org/sci_soc/mockler.html)

Elosegui, P., J.L. Davis, L.P. Gradinarsky, G. Elgered, J.M. Johansson, D.A. Tahmoush and A. Rius (1999). Sensing atmospheric structure using small-scale space geodetic networks. *Geophysical Research Letters* **26**(16), 2445-2448.

Emardson, T.R., G. Elgered and J. Johansson (1998). Three months of continuous monitoring of atmospheric water vapor with a network of Global Positioning System receivers. *Journal of Geophysical Research* **103**(D2), 1807-1820.

Emardson, T.R., J. Johansson and G. Elgered (2000). The systematic behavior of water vapor estimates using four years of GPS observations. *IEEE Transactions on Geoscience & Remote Sensing* **38**(1 Part 1), 324-329.

Fang, P., M. Bevis, Y. Bock, S. Gutman and D. Wolfe (1998). GPS meteorology - reducing systematic errors in geodetic estimates for zenith delay. *Geophysical Research Letters* **25**(19), 3583-3586.

Feigl, K.L., D.C. Agnew, Y. Bock, D. Dong, A. Donnellan, B.H. Hager, T.A. Herring, D.D. Jackson, T.H. Jordan, R.W. King, S. Larsen, K.M. Larson, M.H. Murray, Z.K. Shen and F.H. Webb (1993). Space geodetic measurement of crustal deformation in central and southern California, 1984-1992. *Journal of Geophysical Research* **98**(B12), 21677-21712.

Ferland, R., J. Kouba and D. Hutchison (2000). Analysis methodology and recent results of the IGS network combination. *Earth Planets & Space* **52**(11), 953-957.

Foldvik, A., T. Gammelsrod, E. Nygaard and S. Osterhus (2001). Current measurements near Ronne Ice Shelf: implications for circulation and melting. *Journal of Geophysical Research* **106**(C3), 4463-4477.

Frezzotti, M., A. Capra and L. Vittuari (1998). Comparison between glacier ice velocities inferred from GPS and sequential satellite images. *Annals of Glaciology* **27**, 54 - 60.

Fricker, H.A., G. Hyland, R. Coleman and N. Young (2000). Digital elevation models for the Lambert Glacier-Amery Ice Shelf system, East Antarctica, from ERS-1 satellite radar altimetry. *Journal of Glaciology* **46**(155), 553 - 560.

Fricker, H.A., R.C. Warner and I. Allison (2000). Mass balance of the Lambert Glacier-Amery Ice Shelf system, East Antarctica: a comparison of computed balance fluxes and measured fluxes. *Journal of Glaciology* **46**(155), 561 - 570.

Fricker, H.A., I. Allison, M. Craven, G. Hyland, A. Ruddell, N. Young, R. Coleman, M. King, K. Krebs and S. Popov (2001). Redefinition of the grounding zone of Amery Ice Shelf, East Antarctica. *Journal of Geophysical Research* (submitted May 2001).

Fricker, H.A., S. Popov, I. Allison and N. Young (2001). Distribution of marine ice beneath the Amery Ice Shelf. *Geophysical Research Letters* **28**(11), 2241-2244.

Fricker, H.A., N. Young, I. Allison and R. Coleman (2001). Iceberg calving from the Amery Ice Shelf, East Antarctica. *Journal of Glaciology* **34**(submitted).

Gandolfi, S., M. Meneghel, M.C. Salvatore and L. Vittuari (1997). Kinematic global positioning system to monitor small Antarctic glaciers. *Annals of Glaciology* **24**, 326-330.

Giovinetto, M.B. and C.R. Bentley (1985). Surface balance in ice drainage systems of Antarctica. *Antarctic Journal of The United States* **20**(4), 6-13.

Gregorius, T. and G. Blewitt (1998). The effect of weather fronts on GPS measurements. *GPS World* **May 1998**, 52-60.

Gutman, S.I., R.B. Chadwick, D.E. Wolfe, A.M. Simon, T. VanHove and C. Rocken (1994). Toward an operational water vapour remote sensing system using GPS. *FSL Forum* **Sept, 1994**, 13-19.

Hamilton, G.S., I.M. Whillans and P. Morgan (1998). First point measurement of ice-sheet thickness change in Antarctica. *Journal of Glaciology* **27**, 125-129.

Hamilton, G.S. and I.M. Whillans (2000). Point measurements of mass balance of the Greenland Ice Sheet using precision vertical Global Positioning System (GPS) surveys. *Journal of Geophysical Research* **105**(B7), 16295-16301.

Hamley, T.C., I.N. Smith and N.W. Young (1985). Mass-balance and ice-flow-law parameters for East Antarctica. *Journal of Glaciology* **31**(109), 334-339.

Hasegawa, S. and D.P. Stokesbury (1975). Automatic digital microwave hygrometer. *Review of Scientific Instrumentation* **46**, 867-873.

Herring, T.A. (1992). Modelling atmospheric delays in the analysis of space geodetic data. *Symposium on refraction of transatmospheric signals in geodesy, Publications on Geodesy No 36*, Delft, Netherlands, Netherland Geodetic commission, 247

Herring, T.A. (1999a). Geodetic applications of GPS [Review]. *Proceedings of the IEEE* **87**(1), 92-110.

Herring, T. (1999b). Global Kalman filter VLBI and GPS analysis program. Massachusetts Institute of Technology. pp 85

Herzfeld, U.C., C.S. Lingle and L.-h. Lee (1993). Geostatistical evaluation of satellite radar altimetry for high-resolution mapping of Lambert Glacier, Antarctica. *Annals of Glaciology* **17**, 77-85.

Higham, M. (1993). 1500km Lambert traverse continues six-year program. *ANARE News*(74), 15.

Higham, M., M. Reynolds, Brocklesby and I. Allison (1995). Ice radar digital recording, data processing and results from the Lambert Glacier Basin traverses. *Terra Antarctica* **2**(1), 23-32.

Higham, M. and M. Craven (1997). Surface Mass Balance and Snow Surface Properties from the Lambert Glacier Basin Traverses 1990-94. Research Report, No. 9. Antarctic Cooperative Research Centre, University of Tasmania. Hobart, Australia. pp 129

Higham, M., M. Craven, A. Ruddell and I. Allison (1997). Snow-accumulation distribution in the interior of the Lambert Glacier basin, Antarctica. *Annals of Glaciology* **25**, 412 - 417.

Hill, R.J., R.S. Lawrence and J.T. Priestly (1982). Theoretical and calculational aspects of the radio refractive index of water. *Radio Science* **17**, 1251-1257.

Hinze, H. and G. Seeber (1988). Ice-motion determination by means of satellite positioning systems. *Annals of Glaciology* **11**, 36-41.

Hopfield, H.S. (1969). Two-quartic tropospheric refractivity profile for correcting satellite data. *Journal of Geophysical Research* **74**(18), 4487-4499.

Hulbe, C.L. and I.M. Whillans (1993). Stop-and-Go GPS in Antarctica. *Surveying and Land Information Systems* **53**(2), 151-158.

Hulbe, C.L. and I.M. Whillans (1994a). Evaluation of strain rates on Ice Stream B, Antarctica, obtained using GPS phase measurements. *Annals of Glaciology* **20**, 254-262.

Hulbe, C.L. and I.M. Whillans (1994b). Method for determining ice-thickness change at remote locations using GPS. *Annals of Glaciology* **20**, 263-268.

Ifadis, I.I. (1986). The atmospheric delay of radio waves: Modelling the elevation dependence on a global scale. Technical report 38L. Chalmers University of Technology. Goteborg, Sweden.

IPCC (1992). Climate Change 1992 : the supplementary report to the IPCC scientific assessment, Cambridge University Press. Cambridge, UK. pp xii, 200.

IPCC (1997). The Regional Impacts of Climate Change: An Assessment of Vulnerability. Special Report of IPCC Working group II, R.T.Watson, M.C.Zinyowera, R.H.Moss (Eds). Cambridge University Press, UK. pp 517

IPCC (2001). Climate Change 2001: Summary for Policy Makers. Contribution of Working Group I to the Third Assessment report of the Intergovernmental Panel on Climate Change, Cambridge University Press, UK. pp 20

Jacobs, S.S., H.H. Helmer, C.S.M. Doake, A. Jenkins and R.M. Frolich (1992). Melting of ice shelves and the mass balance of Antarctica. *Journal of Glaciology* **38**(130), 375-387.

Jaldehag, R.T.K., J.M. Johansson, J.L. Davis and P. Elosegui (1996). Geodesy using the Swedish permanent GPS network - effects of snow accumulation on estimates of site positions. *Geophysical Research Letters* **23**(13), 1601-1604.

Janes, H.W., R.B. Langley and S.P. Newby (1991). Analysis of tropospheric delay prediction models: comparisons with ray-tracing and implications for GPS relative positioning. *Bulletin Geodesique* **65**, 151-161.

Johansson, J.M., T.R. Emardson, P.O.J. Jarlemark, L.P. Gradinarsky and G. Elgered (1998). The atmospheric influence on the results from the Swedish GPS network. *Physics and Chem of the Earth* **23**(1), 107-112.

Johnston, G.M. (2000). GPS Heighting: The effect of the GPS antenna phase center variation on height determination. Unpublished Masters Thesis. University of Canberra, Canberra, Australia.

Kalnay, E., M. Kanamitsu, R. Kistler, W. Collins, D. Deaven, L. Gandin, M. Iredell, S. Saha, G. White, J. Woollen, Y. Zhu, A. Leetmaa, B. Reynolds, M. Chelliah, W. Ebisuzaki, W. Higgins, J. Janowiak, K.C. Mo, C. Ropelewski, J. Wang, R. Jenne and D. Joseph (1996). The NCEP/NCAR 40-year reanalysis project. *Bulletin of the American Meteorological Society* **77**(3), 437–472.

Kiernan, R. (1990). 1989-90 Lambert Glacier Basin Traverse. *ANARE News* (March 1990), 9-11.

Kiernan, R. (2001). Ice sheet surface velocities along the Lambert Glacier Basin traverse route. Research Report, No. 23. Antarctic Cooperative Research Centre, University of Tasmania. Hobart, Australia. pp 76

King, J.C. and J. Turner (1997). *Antarctic Meteorology and Climatology*. Cambridge, UK, Cambridge University Press.

King, M. (2001). The dynamics of the Amery Ice Shelf from a combination of terrestrial and space geodetic data. Unpublished PhD. Centre for Spatial Information Systems, School of Geography and Environmental Studies, University of Tasmania, Hobart. pp 350.

King, M., L.N. Nguyen, R. Coleman and P. Morgan (2000). Strategies for high precision processing of GPS measurements with application to the Amery Ice Shelf, East Antarctica. *GPS Solutions* **4**(1), 2-12.

King, R.W. and Y. Bock (1999). *Documentation for the GAMIT GPS analysis software*, Massachusetts Institute of Technology.

Komjathy, A. and R.B. Langley (1996). Improvement of a global ionospheric model to provide ionospheric range error corrections for single-frequency GPS users. *ION 52nd Annual Meeting*, Cambridge, MA, USA 19 - 21 June, 1996.

Kruse, L.P., B. Sierk, T. Springer and M. Cocard (1999). GPS-meteorology: impact of predicted orbits on precipitable water estimates. *Geophysical Research Letters* **26**(14), 2045-2048.

Langley, R.B. (1993). The GPS observables. *GPS World* **April**, 52-59.

Langley, R.B. (1996). GPS and the Neutral Atmosphere. *The Directions of GPS - University of New South Wales*, Sydney, Australia,

Lanyi, G. (1984). Tropospheric delay effects in radio interferometry. JPL Technical Report 42-78. Jet Propulsion Laboratory. Pasadena, CA. pp 152-159

Larson, K.M. and J. Freymueller (1995). Relative motions of the Australian, Pacific and Antarctic plates estimated by the Global Positioning System. *Geophysical Research Letters* **22**(1), 37-40.

Legresy, B. and F. Remy (1997). Altimetric observations of surface characteristics of the Antarctic ice sheet. *Journal of Glaciology* **43**(144), 265-275.

Leick, A. (1995). *GPS Satellite Surveying*. New York, John Wiley & Sons, Inc.

Lemoine, F.G., D.E. Smith, L. Kunz, R. Smith, E.C. Pavlis, N.K. Pavlis, S.M. Klosko, D.S. Chinn, M.H. Torrence, R.G. Williamson, C.M. Cox, K.E. Rachlin, Y.M. Wang, S.C. Kenyon, R. Salman, R. Trimmer, R.H. Rapp and R.S. Nerem (1997). The development of the NASA GSFC and NIMA joint geopotential model. *Gravity, Geoid and Marine Geodesy*, Springer, Berlin, Germany, 461-469

Liao, D.C. and H. Greiner-Mai (1999). A new ΔLOD series in monthly intervals (1892.0 - 1997.0) and its comparison with other geophysical results. *Journal of Geodesy* **73**, 466-477.

Lingle, C.S., L.H. Lee, H.J. Zwally, T.C. Seiss and E.M.e. Morris (1994). Recent elevation increase on Lambert Glacier, Antarctica, from orbit cross-over analysis of satellite-radar altimetry. *Annals of Glaciology* **20**, 26-32.

Lythe, M.B. and D.G. Vaughan (2001). BEDMAP: A new ice thickness and subglacial topographic model of Antarctica. *Journal of Geophysical Research* **106**(B6), 11335-11351.

MacMillan, D.S. (1995). Atmospheric gradients from Very Long Baseline Interferometry observations. *Geophysical Research Letters* **22**(9), 1041-1044.

Mader, G.L., M.S. Schenewerk, J.R. Ray, W.G. Kass, P.R. Spofford, R.L. Dulaney and D.G. Pursell (1994). GPS orbit and Earth Orientation Parameter production at NOAA for the International GPS service for Geodynamics for 1994. *IGS 1994 Annual Report*, IGS Central Bureau, 197-212

Mader, G.L. and J.R. MacKay (1997). Calibration of GPS antennas. *Proceedings of the 1996 Analysis Center Workshop, International GPS Service Central Bureau*, Jet Propulsion Lab, Pasadena, 81-105

Magnavox (1988). WM102 GPS Satellite Surveying Equipment Technical Reference Manual. Magnavox report R-7057, 60194A. Magnavox Advanced Products and Systems Company. Torrance, California, USA. pp 365

Manning, J. (2000). The SCAR geodetic infrastructure of Antarctica. *SCAR WG-GGI Meeting*, Tokyo, Japan,

Manning, J., P. Morgan and B. Murphy (1992). Antarctica - where is it, and where is it going? *The Australian Surveyor* **37**(1), 5-12.

Manson, R. (1995). GPS Processing Strategies for Antarctic Data. Unpublished Honours Thesis. Department of Surveying and Spatial Information Science, University of Tasmania, Hobart, Australia. pp 113.

Marini, J.W. (1972). Correction of satellite tracking data for an arbitrary tropospheric profile. *Radio Science* **7**(2), 223-231.

McDonald, J. and I.M. Whillans (1992). Search for temporal change in the velocity of Ice Stream B, West Antarctica. *Journal of Glaciology* **38**(128), 157-161.

McIntyre, N.F. (1985). A re-Assessment of the mass balance of the Lambert Glacier Drainage Basin, Antarctica. *Journal Of Glaciology* **31**(107), 34-38.

Meier, M.F. (1983). Snow and ice in a changing hydrological world. *Hydrological Sciences Journal* **28**(1), 3-22.

Meier, M.F. (1993). Ice, climate and sea level: do we know what is happening? *Ice in the climate system.* W.R. Peltier (eds). Berlin, Heidelberg, Springer-Verlag. **12**, 141-160.

Melbourne, W.G., S.S. Fisher, R.E. Neilan, T.P. Yunck, B. Engen, C. Reigber and S. Tatevjan (1991). The first GPS IERS and Geodynamics experiment - 1991. *Permanent Satellite Tracking Networks for Geodesy and Geodynamics*, Vienna, Austria, Springer-Verlag, 65 - 80

Melfi, S.H., D. Whiteman and R. Ferrare (1989). Observation of atmospheric fronts using Raman Lidar moisture measurements. *Journal of Applied Meteorology* **28**, 789-806.

Mendes, V.B. and R.B. Langley (1994). A comprehensive analysis of mapping functions used in modelling tropospheric propagation delay in space geodetic data. *KIS94, International Symposium on Kinematic Systems in Geodesy, Geomatics and Navigation*, Banff, 30 August - 2 September 1994, The University of Calgary, Calgary, Canada, 87-98

Mendes, V.B. and R.B. Langley (1995). Zenith wet tropospheric delay determination using prediction models: accuracy analysis. *Cartografia E Cadastro* **2**, 41-47.

Michel, G.W., M. Becker, D. Angermann, C. Reigber and E. Reinhart (2000). Crustal motion in E- and SE-Asia from GPS measurements. *Earth Planets Space* **52**(10), 713-720.

Morgan, P. (1994). The role of GPS in Antarctica. *FIG International Congress*, Melbourne, Australia, FIG,

Morgan, P. and R. Tiesler (1991). First epoch GPS baselines between Australia and Antarctica, January 1990. *Australian Journal of Geodesy, Photogrammetry and Surveying* **55**, 55-66.

Morgan, P., R. Tiesler, J. Manning, B. Murphy and M. Hendy (1992). The Scientific Committee for Antarctica GPS Project. *Australian National GPS Symposium, June 1992*, Sydney, Australia, University of NSW,

Morgan, P., Y. Bock, R. Coleman, P. Feng, D. Garrard, G. Johnston, G. Luton, B. McDowall, M. Pearse, C. Rizos and R. Tiesler (1996). A zero order GPS network for the Australian region. Unisurv Report, S-47. University of New South Wales. Sydney, NSW, Australia. pp 187

Morgan, V.I. and W.F. Budd (1975). Radio-echo sounding of the Lambert Glacier Basin. *Journal of Glaciology* **15**(73), 103-111.

Morgan, V.I. and T.H. Jacka (1979). Mass balance studies in East Antarctica. *Sea Level, Ice and Climatic Change (IAHS, Canberra Symposium, December 1979)*, Canberra, Australia, IAHS, 253-260

Morgan, V.I., T.H. Jacka and G.J. Akerman (1982). Outlet glacier and mass-budget studies in Enderby, Kemp and Mac. Robertson Lands, Antarctica. *Annals of Glaciology* **3**, 204-209.

Motoyama, H., H. Enomoto, T. Furukawa, K. Kamiyama, H. Shoji, T. Shiraiwa, K. Watanabe, K. Namasu and H. Ikeda (1995). Preliminary study of ice flow observations along traverse routes from coast to Dome Fuji, East Antarctica by differential GPS method. *Antarctic Record* **39**(2), 94-98.

Murphy, B., J. Manning and T. Morrison (1990). The transition to GPS: Australian experience in Antarctica with satellite positioning. *FIG: XIX International Congress*, Helsinki, Finland, FIG,

Naito, I., Y. Hatanaka, N. Mannoji, R. Ichikawa, S. Shimada, T. Yabuki, H. Tsuji and T. Tanaka (1998). Global Positioning System project to improve Japanese weather, earthquake predictions. *EOS Transactions* **79**(26), 301, 308, 311.

Niell, A.E. (1996). Global mapping functions for the atmosphere delay at radio wavelengths. *Journal of Geophysical Research* **101**(B2), 3227-3246.

Paterson, W.S.B. (1993). World sea level and the present mass balance of the Antarctic Ice Sheet. *Ice in the climate system.* W.R. Peltier (eds). Berlin, Heidelberg, Springer-Verlag. **12**, 131-140.

Phillips, H.A. (1999). Applications of ERS satellite radar altimetry in the Lambert Glacier-Amery Ice Shelf system, East Antarctica. Unpublished PhD Thesis. Institute of Antarctic and Southern Ocean Studies (IASOS), University of Tasmania, Hobart, Australia. pp 308.

Phillips, H.A., I. Allison, M. Craven, K. Krebs and P. Morgan (1996). Ice velocities and grounding line location in the Lambert - Amery system, East Antarctica. *Presented at the Western Pacific AGU Meeting, 23 - 27 July*, Brisbane, Australia,

Phillips, H.A., I. Allison, R. Coleman, G. Hyland, P. Morgan and N. Young (1998). Comparison of ERS satellite radar altimeter heights with GPS-derived heights on the Amery Ice Shelf, East Antarctica. *Annals of Glaciology* **27**, 19-24.

Piechocinska, J. and L. Sjoberg (1990). Some first experiences with the WM102 GPS receiver. *IAG Symposium 102 - Global Positioning Systems: An Overview*, Edinburgh, Scotland, August 7-8, 1989, Springer-Verlag,

Radok, U. (1985). The Antarctic ice. *Scientific American* **253**(2), 98-105.

Reid, P. (2000). Atmospheric Conditions Influencing Antarctic Ice Sheet Surface Mass Balance. Unpublished PhD Thesis. Institute of Antarctic and Southern Ocean Studies (IASOS), University of Tasmania, Australia, Hobart.

Reilinger, R.E., S.C. McClusky, M.B. Oral, R.W. King, M.N. Toksoz, A.A. Barka, I. Kinik, O. Lenk and I. Sanli (1997). Global Positioning System measurements of present-day crustal movements in the Arabia-Africa-Eurasia plate collision zone. *Journal of Geophysical Research* **102**(B5), 9983-9999.

Remy, F. and J. Minster (1997). Antarctica ice sheet curvature and its relation with ice flow and boundary conditions. *Geophysical Research Letters* **24**(9), 1039-1042.

Remy, F., P. Shaeffer and B. Legresy (1999). Ice flow physical processes derived from the ERS-1 high-resolution map of the Antarctic and Greenland ice sheets. *Geophysical Journal International* **139**, 645-656.

Rignot, E. and D.R. MacAyeal (1998). Ice-shelf dynamics near the front of the Filchner-Ronne Ice Shelf, Antarctica, revealed by SAR interferometry. *Journal of Glaciology* **44**(147), 405-418.

Rocken, C., R. Ware, T. Vanhove, F. Solheim, C. Alber and J. Johnson (1993). Sensing atmospheric water vapor with the Global Positioning System. *Geophysical Research Letters* **20**(23), 2631-2634.

Rocken, C., T. VanHove, J. Johnson, F.S. Solheim, R.H. Ware, M. Bevis, S. Chiswell and S. Businger (1995). GPS/STORM - GPS sensing of atmospheric water vapor for meteorology. *Journal of Atmospheric & Oceanic Technology* **12**(3), 468-478.

Rocken, C., F.S. Solheim, R.H. Ware, M. Exner, D. Martin and M. Rothacher (1995). Application of IGS data to GPS sensing of the atmosphere for weather and climate research. http://www.unavco.ucar.edu/science_tech/dev_test/publications/pots_pap/pots_pap.html

Rocken, C., R. Anthes, M. Exner, D. Hunt, S. Sokolovskiy, R. Ware, M. Gorbunov, W. Schreiner, D. Feng, B. Herman, Y.H. Kuo and X. Zou (1997). Analysis and validation of GPS/MET data in the neutral atmosphere. *Journal of Geophysical Research* **102**(D25), 29849-29866.

Rocken, C., T. Van Hove and R. Ware (1997). Near real-time GPS sensing of atmospheric water vapor. *Geophysical Research Letters* **24**(24), 3221-3224.

Rothacher, M., R. Weber, E. Brockmann, G. Beutler, L. Mervart, U. Wild, A. Wiget, C. Boucher, S. Botton and H. Seeger (1994). Annual Report 1994 of the CODE Processing Center of the IGS. *IGS 1994 Annual Report*, IGS Central Bureau, 139-163

Rothacher, M. and G. Beutler (1998). The role of GPS in the study of global change. *Chemistry and Physics of the Earth* **2**.

Saastamoinen, J. (1972). *Atmospheric Correction for the Troposphere and Stratosphere in Radio Ranging of Satellites*. The Use of Artificial Satellites for Geodesy, Geophysical Monograph Series. Washington DC, AGU. pp 247-251.

Saastamoinen, J. (1973). Contributions to the theory of atmospheric refraction. *Bulletin Géodésique* **107**(1), 13-34.

Santerre, R., I. Forgues, V.B. Mendes and R.B. Langley (1995). Comparison of tropospheric mapping functions: their effects on station coordinates. *IUGG XXI General Assembly, 2-14 July*, Boulder, Colorado, USA.,

Sauber, J., S. McClusky and R. King (1997). Relation of ongoing deformation rates to the subduction zone process in Southern Alaska. *Geophysical Research Letters* **24**(22), 2853-2856.

Scharroo, R. and P. Visser (1998). Precise orbit determination and gravity field improvement for the ERS satellites. *Journal of Geophysical Research-Oceans* **103**(C4), 8113-8127.

Scherneck, H.-G., J.M. Johansson, J.X. Mitrovica and J.L. Davis (1998). The BIFROST project: GPS determined 3-D displacement rates in Fennoscandia from 800 days of continuous observations in the SWEPOS network. *Tectonophysics* **294**, 305-321.

Seeber, G. (1993). *Satellite Geodesy*. Berlin, Walter de Gruyter.

Segall, P. and J.L. Davis (1997). GPS applications for geodynamics and earthquake studies [Review]. *Annual Review of Earth & Planetary Sciences* **25**, 301-336.

Seko, H., S. Shimada, H. Nakamura and T. Kato (2000). Three-dimensional distribution of water vapour estimated from tropospheric delay of GPS data in a mesoscale precipitation system of the Baiu front. *Earth, Planets and Space* **52**(11), 927-933.

Shabtaie, S., C.R. Bentley, R.A. Bindschadler and D.R. MacAyeal (1988). Mass-balance studies of Ice Streams A, B and C, West Antarctica, and possible surging behaviour of Ice Stream B. *Annals of Glaciology* **11**, 137-149.

Shardlow, P., J (1994). Propagation effects on precise GPS heighting. Unpublished PhD. Institute of Engineering Surveying and Space Geodesy, University of Nottingham, Nottingham, UK.

Shimizu, H., O. Watanabe, S. Kobayashi, T. Yamada, R. Naruse and Y. Ageta (1978). Glaciological aspects and mass budget of the ice sheet in Mizuho Plateau. *Memoirs of the National Institute of Polar Research, Tokyo*((Special Issue No. 7)), 264-274.

Shoji, Y., H. Nakamura, K. Aonashi, A. Ichiki and H. Seko (2000). Semi-diurnal and diurnal variation of errors in GPS precipitable water vapour at Tsukuba, Japan caused by site displacement due to ocean tidal loading. *Earth, Planets and Space* **52**(10), 685-690.

Sierk, B., B. Burki, H. Beckerross, S. Florek, R. Neubert, L.P. Kruse and H.G. Kahle (1997). Tropospheric water vapor derived from solar spectrometer, radiometer, and GPS measurements. *Journal of Geophysical Research* **102**(B10), 22411-22424.

Simons, W.J.F., B.A.C. Ambrosius, R. Noomen, D. Angermann, P. Wilson, M. Becker, E. Reinhart, A. Walpersdorf and C. Vigny (1999). Observing plate motions in SE Asia: geodetic results of the GEODYSSEA project. *Geophysical Research Letters* **26**(14), 2081-2084.

Smith, I.N., W.F. Budd and P. Reid (1998). Model estimates of Antarctic accumulation rates and their relationship to temperature changes. *Annals of Glaciology* **27**, 246-250.

Smith, T.L., S.G. Benjamin, B.E. Schwartz and S. Gutman (2000). Using GPS_IPW in a 4-D data assimilation system. *Earth, Planets and Space* **52**(11), 921-926.

Solheim, F.S., J. Vivekanandan, R.H. Ware and C. Rocken (1999). Propagation delays induced in GPS signals by dry air, water vapor, hydrometeors, and other particulates. *Journal of Geophysical Research* **104**(D8), 9663-9670.

Streten, N.A. (1990). A review of the climate of Mawson - a representative strong wind site in East Antarctica. *Antarctic Science* **2**(1), 79-89.

Stull, R.B. (1995). *Meteorology today for scientists and engineers - A technical companion book.* Minneapolis/St. Paul, West Publishing. pp 385.

Testut, L. (2000). Apport de la Topographie a L'Etude des Calottes Polaires. Unpublished PhD. Ecole Doctorale des Sciences de L'Univers, Universite Toulouse III - Paul Sabatier, Toulouse, France. pp 130.

Thayer, G.D. (1974). An improved equation for the radio refractive index of air. *Radio Science* **9**(10), 803-807.

Toh, H. and K. Shibuya, Eds. (1992). *Thinning Rate on Mizuho Plateau, East Antarctica, Determined by GPS Differential Positioning*. Recent Progress in Antarctic Earth Science, Terra Scientific Publishing Company, Tokyo. pp 579-583.

Tralli, D.M., T.H. Dixon and S.A. Stephens (1988). Effect of wet tropospheric path delays on estimation of geodetic baselines in the Gulf of California using the Global Positioning System. *Journal of Geophysical Research* **93**(B6), 6545-6557.

Tralli, D.M. and S.M. Lichten (1990). Stochastic estimation of tropospheric path delays in Global Positioning System geodetic measurements. *Bulletin Geodesique* **64**(2), 127-159.

Tregoning, P. (2000). The search for postglacial rebound near the Lambert Glacier, Antarctica. *Earth, Planets and Space* **52**(11), 1037-1042.

Tregoning, P., K. Lambeck, A. Stolz, P. Morgan, S.C. McClusky, P. Vanderbeek, H. McQueen, R.J. Jackson, R.P. Little, A. Laing and B. Murphy (1998). Estimation of current plate motions in Papua New Guinea from Global Positioning System observations. *Journal of Geophysical Research* **103**(B6), 12181-12203.

Tregoning, P., R. Boers, D. Obrien and M. Hendy (1998). Accuracy of absolute precipitable water vapor estimates from GPS observations. *Journal of Geophysical Research* **103**(D22), 28701-28710.

Tregoning, P., R.J. Jackson, H. McQueen, K. Lambeck, C. Stevens, R.P. Little, R. Curley and R. Rosa (1999). Motion of the South Bismarck plate, Papua New Guinea. *Geophysical Research Letters* **26**(23), 3517-3520.

UCAR (1999). SuomiNet: A Real-Time National GPS Network For Atmospheric Research And Education. University Corporation For Atmospheric Research.

van Dam, T.M. and J. Wahr (1998). Modeling environmental loading effects. *Physics and Chemistry of the Earth* **23**(9-10), 1077-1087.

van Dam, T.M., G. Blewitt and M.B. Heflin (1994). Atmospheric pressure loading effects on Global Positioning System coordinate determinations. *Journal of Geophysical Research* **99**(B12), 23939-23950.

Vaughan, D.G. (1994). Investigating tidal flexure on an ice shelf using kinematic GPS. *Annals of Glaciology* **20**, 372-376.

Vaughan, D.G., J.L. Bamber, M.B. Giovinetto, J. Russell and A.P.R. Cooper (1999). Reassessment of net surface mass balance in Antarctica. *Journal of Climate* **12**(4), 933-946.

Vijakumar, K. and K. Miyashita (2000). Regional network analysis of GPS data in the area of Kanto, central Japan. *Earth Planets Space* **52**(10), 971-974.

Wahr, J., D. Wingham and C. Bentley (2000). A method of combining ICESat and GRACE satellite data to constrain Antarctic mass balance. *Journal of Geophysical Research* **105**(B7), 16279-16294.

Ware, R., C. Rocken, F. Solheim, T. Vanhove, C. Alber and J. Johnson (1993). Pointed water vapor radiometer corrections for accurate Global Positioning System surveying. *Geophysical Research Letters* **20**(23), 2635-2638.

Ware, R., C. Alber, C. Rocken and F. Solheim (1997). Sensing integrated water vapor along GPS ray paths. *Geophysical Research Letters* **24**(4), 417-420.

Ware, R.H., D.W. Fulker, S.A. Stein, D.N. Anderson, S.K. Avery, R.D. Clark, K.K. Droegemeier, J.P. Kuettner, J.B. Minster and S. Sorooshian (2000). SuomiNet: A real-time national GPS network for atmospheric research and education [Review]. *Bulletin of the American Meteorological Society* **81**(4), 677-694.

Ware, R.H., D.W. Fulker, S.A. Stein, D.N. Anderson, S.K. Avery, R.D. Clark, K.K. Droegemeier, J.P. Kuettner, J.B. Minster and S. Sorooshian (2000). Real-time national GPS networks: Opportunities for atmospheric sensing. *Earth, Planets and Space* **52**(11), 901-905.

Watson, C. (1998). Australian Antarctic surveying and mapping. *Southern Exposure - the 39th Australian Surveyors Congress*, Launceston, Tasmania, 8 - 13 November, The Institution of Surveyors, Australia,

Weller, G. (1992). Antarctica and the detection of environmental change. *Antarctica and Environmental Change*, Proceedings of a Royal Society Discussion Meeting, 20 -21 May, Clarendon Press.

Whillans, I.M. (1992). Glaciology and Global Positioning System at Upstream B and from CASERTZ. *Antarctic Journal of the United States* **27**(5), 45-46.

Whillans, I.M., C.J. van der Veen and Y. Tseng (1990). Application of the Global Positioning System in Antarctica. *Antarctic Journal of the United States* **25**(2), 6-9.

Whillans, I.M. and C.J. Van Der Veen (1993). Controls on changes in the West Antarctic Ice Sheet. *Ice in the climate system.* W.R. Peltier (eds). Berlin, Heidelberg, Springer-Verlag. **12**, 48-54.

Whillans, I.M. and C.J. van der Veen (1993b). New and improved determinations of velocity of Ice Streams B and C, West Antarctica. *Journal of Glaciology* **39**(133), 483 - 490.

White, W.B. and R.G. Peterson (1996). An Antarctic circumpolar wave in surface pressure, wind, temperature and sea-ice extent. *Nature* **380**(6576), 699-702.

Williams, S., Y. Bock and P. Fang (1998). Integrated satellite interferometry - tropospheric noise, GPS estimates and implications for Interferometric Synthetic Aperture Radar products. *Journal of Geophysical Research-Solid Earth* **103**(B11), 27051-27067.

Wolfe, D.E. and S.I. Gutman (2000). Developing an operational, surface-based, GPS, water vapor observing system for NOAA: Network design and results. *Journal of Atmospheric & Oceanic Technology* **17**(4), 426-440.

Young, N. (1979a). Measured velocities of interior East Antarctica and the state of mass balance within the IAGP area. *Journal of Glaciology* **24**(90), 77-87.

Young, N.W. (1979b). Application of Doppler satellite observations to the study of ice flow in East Antarctica - problems peculiar to Doppler surveys in high latitudes. *Second International Geodetic Symposium on Satellite Doppler Positioning, Austin, Texas* **1**, 373-391.

Yuan, L.L., R.A. Anthes, R.H. Ware, C. Rocken, W.D. Bonner, M.G. Bevis and S. Businger (1993). Sensing climate change using the Global Positioning System. *Journal of Geophysical Research* **98**(D8), 14925-14937.

Zarraoa, N. and E. Sardon (1996). Test of GPS for permanent ionospheric TEC monitoring at high latitudes. *Annales Geophysicae-Atmospheres Hydrospheres & Space Sciences* **14**(1), 11-19.

Zwartz, D., P. Tregoning, K. Lambeck, P. Johnston and J. Stone (1999). Estimates of present-day glacial rebound in the Lambert Glacier region, Antarctica. *Geophysical Research Letters* **26**(10), 1461-1464.

APPENDIX - A

A.1 Discussion of the Method Used to Estimate Station Coordinate, Velocity and Precision Parameters Using GLOBK/GLORG

A.1.1 Transformation between reference frames

It is important to note that the GAMIT/GLOBK solutions are usually run in a "loose" constraint mode, which parallels a conventional free network adjustment. This means that internally the network is very strong and self-consistent (i.e., the network geometry), but externally quite weak (i.e., the reference frame). The external weakness is resolved at the very end of the solution process by rotating the "loose" solution onto a specified International Terrestrial Reference System. There are several reasons why this is done. Two important reasons are:

1. GAMIT operates in inertial space rather than terrestrial space. This frees the results from an explicit realisation of the Earth Orientation Parameter (EOP) matrix and allows satellite orbital information to be used in the combination of results.
2. Earth Orientation, that is consistent with the reference frame, can be resolved near the 1 mm level in position from the reference frame rotations. This is much more precise than can be realised by direct solution of the least squares transformation problem.

The connection between the 3x3 EOP matrix and the well-known 3x3 axial rotation matrix is readily shown in the following discussion.

The relationship between coordinates in an inertial and terrestrial reference frame is defined as:

$$X_{terrestrial} = S_{EOP} N P X_{inertial} \qquad (A.1)$$

where

$X_{terrestrial}$ represents a set of station coordinates in a terrestrial reference frame

S_{EOP} represents the 3x3 EOP matrix

N is the nutation matrix

P is the precession matrix

$X_{inertial}$ represents a set of station coordinates in an inertial reference frame

(Note: $NPX_{inertial}$ is equivalent to $X_{celestial}$)

Additionally, the EOP matrix possesses additive properties, such that $S_3 = S_1 + S_2$.

Now, the relationship between coordinates in two different terrestrial reference frames has the form:

$$X_1 = sRX^0 + \Delta X^0 \qquad (A.2)$$

where

X_1 represents a set of station coordinates in the observational system

X^0 represents the station coordinates in the reference system (e.g. ITRF)

s is a scalar that is often set to 1 and therefore discarded

R is the 3x3 axial rotation matrix

ΔX^0 represents the origin translations

Thus, the use of a rotation, R, from the reference system, X^0, to the observation system, X_1, is identical to the application of the EOP rotation from an inertial (or celestial) reference frame to a terrestrial reference frame. Therefore, like S_{EOP}, R also has additive properties.

In GLOBK we are dealing with both positions and linear velocities and each can have an independent relative base to the reference frame and therefore equation (A.2) needs to be re-written to include the velocity transformation. The full transformation from observational to reference system can thus be defined in matrix notation as:

$$\begin{bmatrix} x \\ y \\ z \\ v_x \\ v_y \\ v_z \end{bmatrix}_1 = \begin{bmatrix} s_X & 0 \\ 0 & s_V \end{bmatrix} \begin{bmatrix} R_X & 0 \\ 0 & R_V \end{bmatrix} \begin{bmatrix} x \\ y \\ z \\ v_x \\ v_y \\ v_z \end{bmatrix}^0 + \begin{bmatrix} \Delta x \\ \Delta y \\ \Delta z \\ \Delta v_x \\ \Delta v_y \\ \Delta v_z \end{bmatrix}^0 \qquad \text{(A.3)}$$

where

x_1, y_1, z_1	are the coordinates of the point in the observational system
$v_{x_1}, v_{y_1}, v_{z_1}$	are the velocity components at the point in the observational system
x^0, y^0, z^0	are the coordinates of the point in the reference system (e.g. ITRF)
v_x^0, v_y^0, v_z^0	are the velocity components at the point in the reference system (e.g. ITRF)
s_X and s_V	are the scalar values for the coordinate and velocity transformations respectively
R_X and R_V	are the 3x3 rotation matrices for the coordinate and velocity transformations respectively
$\Delta x^0, \Delta y^0, \Delta z^0$	are the coordinate translation parameters
$\Delta v_x^0, \Delta v_y^0, \Delta v_z^0$	are the velocity component translation parameters

Equation (A.3) represents the fourteen-parameter model used in GLOBK where the combined rotation matrix R is determined via the reference station coordinates.

A.1.2 GLOBK position and velocity estimation

There is no fundamental difference in the solution strategy for computing positions or positions and velocities. Both solution procedures use the same analysis structure, it is only the functional and stochastic models that differ. In the case of a positions-only solution, the secondary or updating model (discussed below, see equation(A.7)) does not include velocity terms and the stochastic model consists of first derivative

or velocity terms. In the case of a positions-and-velocities solution, the secondary model does contain the velocity terms and the stochastic models consist of second derivatives or accelerations for the coordinates and first derivatives for the velocity terms.

To illustrate the form of the equations that are used in GLOBK, it is best to consider a simplified example and link these equations to the published work of Dong *et al* (1998) on which GLOBK is based.

Consider firstly a case in which there are no reference frame rotations or episodic parameters. In this case, the state vector, X_i, contains only elements for position and velocity:

$$X_i = \left[x_i \; y_i \; z_i \; v_{x_i} \; v_{y_i} \; v_{z_i} \right]^T \tag{A.4}$$

Thus the primary model (a least-squares model to estimate parameters from the quasi-observation information), equivalent to equation (7) in Dong *et al* (1998), is:

$$AX_i = b_i + \varepsilon_i \tag{A.5}$$

or in matrix format:

$$\begin{bmatrix} 1 & 0 & 0 & 0 & 0 & 0 \\ 0 & 1 & 0 & 0 & 0 & 0 \\ 0 & 0 & 1 & 0 & 0 & 0 \end{bmatrix} \begin{bmatrix} x \\ y \\ z \\ v_x \\ v_y \\ v_z \end{bmatrix}_i = \begin{bmatrix} x^{q-obs} \\ y^{q-obs} \\ z^{q-obs} \end{bmatrix}_i + \begin{bmatrix} \varepsilon_1 \\ \varepsilon_2 \\ \varepsilon_3 \end{bmatrix}_i \tag{A.6}$$

where

$x_i^{q\text{-}obs}, y_i^{q-obs}, z_i^{q-obs}$	represent the coordinate quasi-observations for the station and epoch of investigation
$\varepsilon_1, \varepsilon_2, \varepsilon_3$	are the least-squares residuals

For a Kalman Filter, the necessary updating or secondary model which links the quasi-observations (i.e. is used to predict X_i from X_{i-1}) (equivalent to equation 8 in Dong *et al* (1998)) is:

$$X_i = MX_{i-1} + q_i \tag{A.7}$$

Assuming a constant velocity, the transition matrix for the secondary model is:

$$M = \begin{bmatrix} 1 & 0 & 0 & \Delta t & 0 & 0 \\ 0 & 1 & 0 & 0 & \Delta t & 0 \\ 0 & 0 & 1 & 0 & 0 & \Delta t \\ 0 & 0 & 0 & 1 & 0 & 0 \\ 0 & 0 & 0 & 0 & 1 & 0 \\ 0 & 0 & 0 & 0 & 0 & 1 \end{bmatrix} \tag{A.8}$$

where

Δt is the change in time between epochs i and i-1

The stochastic terms included in the second term on the right hand side of equation (A.7) are accelerations (in GLOBK, these are assumed to be random and can be set by the operator) represented by:

$$q = \begin{bmatrix} \frac{\Delta t^2}{2} & 0 & 0 \\ 0 & \frac{\Delta t^2}{2} & 0 \\ 0 & 0 & \frac{\Delta t^2}{2} \\ \Delta t & 0 & 0 \\ 0 & \Delta t & 0 \\ 0 & 0 & \Delta t \end{bmatrix} \begin{bmatrix} a_x \\ a_y \\ a_z \end{bmatrix} \tag{A.9}$$

where

a_x, a_y, a_z are the noise in each of the position and velocity components

The above represents the simplest example. An example that includes a rotation and translation will now be considered.

In this case the primary model will still be represented by equation (A.5) however, the state vector now includes rotation (α, β, γ) and translation (Δx, Δy, Δz) parameters and may be written as:

$$X_i = \left[x \; y \; z \; v_x \; v_y \; v_z \; \alpha \; \beta \; \gamma \; \Delta x \; \Delta y \; \Delta z \right]^T \tag{A.10}$$

The secondary model in this case is still defined by equation (A.7) however, the transition matrix, M, and the stochastic model, q, are now augmented by rotation and translation terms as identified below:

$$M = \begin{bmatrix}
1 & \gamma & -\beta & \Delta t & \gamma\Delta t & -\beta\Delta t & 0 & 0 & 0 & 1 & 0 & 0 \\
-\gamma & 1 & \alpha & -\gamma\Delta t & \Delta t & \alpha\Delta t & 0 & 0 & 0 & 0 & 1 & 0 \\
\beta & -\alpha & 1 & \beta\Delta t & -\alpha\Delta t & \Delta t & 0 & 0 & 0 & 0 & 0 & 1 \\
0 & 0 & 0 & 1 & \gamma & -\beta & 0 & 0 & 0 & 0 & 0 & 0 \\
0 & 0 & 0 & -\gamma & 1 & \alpha & 0 & 0 & 0 & 0 & 0 & 0 \\
0 & 0 & 0 & \beta & -\alpha & 1 & 0 & 0 & 0 & 0 & 0 & 0 \\
0 & 0 & 0 & 0 & 0 & 0 & 1 & 0 & 0 & 0 & 0 & 0 \\
0 & 0 & 0 & 0 & 0 & 0 & 0 & 1 & 0 & 0 & 0 & 0 \\
0 & 0 & 0 & 0 & 0 & 0 & 0 & 0 & 1 & 0 & 0 & 0 \\
0 & 0 & 0 & 0 & 0 & 0 & 0 & 0 & 0 & 1 & 0 & 0 \\
0 & 0 & 0 & 0 & 0 & 0 & 0 & 0 & 0 & 0 & 1 & 0 \\
0 & 0 & 0 & 0 & 0 & 0 & 0 & 0 & 0 & 0 & 0 & 1
\end{bmatrix} \qquad \text{(A.11)}$$

$$q = \begin{bmatrix}
\frac{\Delta t^2}{2} & 0 & 0 & 0 & 0 & 0 & 0 & 0 & 0 \\
0 & \frac{\Delta t^2}{2} & 0 & 0 & 0 & 0 & 0 & 0 & 0 \\
0 & 0 & \frac{\Delta t^2}{2} & 0 & 0 & 0 & 0 & 0 & 0 \\
\Delta t & 0 & 0 & 0 & 0 & 0 & 0 & 0 & 0 \\
0 & \Delta t & 0 & 0 & 0 & 0 & 0 & 0 & 0 \\
0 & 0 & \Delta t & 0 & 0 & 0 & 0 & 0 & 0 \\
0 & 0 & 0 & \Delta t & 0 & 0 & 0 & 0 & 0 \\
0 & 0 & 0 & 0 & \Delta t & 0 & 0 & 0 & 0 \\
0 & 0 & 0 & 0 & 0 & \Delta t & 0 & 0 & 0 \\
0 & 0 & 0 & 0 & 0 & 0 & \Delta t & 0 & 0 \\
0 & 0 & 0 & 0 & 0 & 0 & 0 & \Delta t & 0 \\
0 & 0 & 0 & 0 & 0 & 0 & 0 & 0 & \Delta t
\end{bmatrix}
\begin{bmatrix}
a_x \\ a_y \\ a_z \\ \dot{\alpha} \\ \dot{\beta} \\ \dot{\gamma} \\ \dot{\Delta x} \\ \dot{\Delta y} \\ \dot{\Delta z}
\end{bmatrix} \qquad \text{(A.12)}$$

It is this type of secondary or updating model (i.e. equations (A.10) to (A.12)) that is used in GLOBK analyses. The full secondary model employed within the GLOBK software is defined by equation (4) in Dong *et al* (1998).

The application of these matrices to the Kalman filter process within the GLOBK software is outlined in equations 10a to 15b in Dong *et al* (1998) and also discussed in Morgan *et al* (1996). The computation sequence described in Dong *et al* (1998) is also included here in the form of a flowchart (Figure 1). Within these equations, the procedure for the determination of the VCV information is also shown.

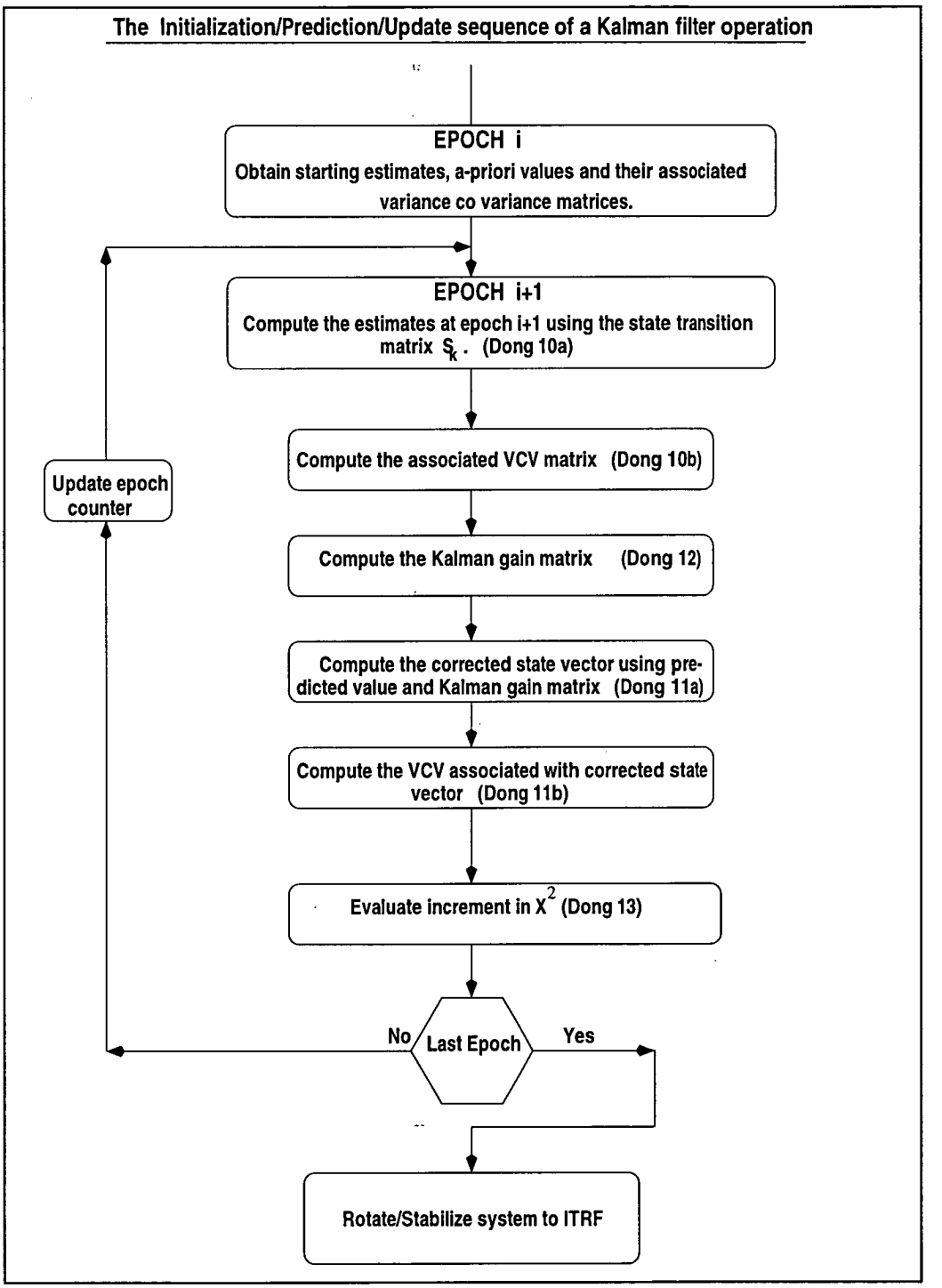

Figure 1 - Flowchart Describing GLOBK Kalman Filter Operation

In regard to the precisions of the final estimates, it has long been known (e.g. Feigl *et al* (1993) and Tregoning, Lambeck *et al* (1998)) that GAMIT/GLOBK, like most GPS processing software, overestimates precisions when correlated observations are present. In this study, high density, correlated data did not exist and the data, both raw and quasi-observational, could be deemed to be uncorrelated between each of the LGB traverses. Therefore the major concern in this study was not the between-epoch correlation but the relative strength of the solution and its relationship to the reference frame.

For the final LGB IMS velocity/position results, the scalar weighted sum of squared residuals, χ^2, was used to re-scale the posteriori uncertainty values. However, this χ^2 value was close to 1 (i.e., 1.147, see page 83 of the thesis) due to the correct assignment of the stochastic model and the re-weighting of the VCV associated with the quasi-observation data and the positions and parameters associated with the reference system (see page 82 of the thesis for an explanation of the re-weighting procedure). The correct values to be used in this procedure were determination by careful consideration of the incremental χ^2 statistic that is part of the GLOBK package (see equation 13 in Dong *et al* (1998)).

A.2 GAMIT Cleaning Parameters Used For the 1989 - 1993 LGB Campaigns

After running several 'test' solutions using data from the 1990/91 campaign, it was found that insufficient LGB data (in some cases, no data) were being maintained after cleaning using a standard command file. The command file was therefore edited using an iterative process on the test data. The result of this process was a series of commands that would allow sufficient LGB data to progress into the least-squares solution without degrading the estimated station coordinates. The final version of the cleaning command file used for the 1989 - 1993 processing is shown in Figure A.2.

```
## AUTCLN COMMAND FILE 89-93 ##
rng_jump_tol  100  0.95
clk_reset_tol  100
max_rclk_iterations  3
remove_bias  10  3  1800
allow_one_bg  yes
use_gamit_elev  yes
use_cview_edit  yes
remove_first_bias  yes
rcv_allan_sd  all  100
rng_noise  all  5000
rng_resid_tol  300  300
dd_return_size  10  10  5  10
trim_oneway  240  8  0.1  5
ion_jump_tol  all  240  6  2  6
site_params womb 10  10  1  1
site_params dove  10  10  1  1
```

Figure A.2 - Edited *AUTCLN* command file (*autcln.cmd*)

The most significant changes to the default *AUTCLN* commands were required in order to allow the GPS data series to have short continuous spans and large gaps. Additionally, changes were necessary to increase the level of acceptable ionospheric interference in the data. The important changes to the *AUTCLN* defaults are indicated (as red text) in Figure A.2 and a summary of the relevant command definitions from King and Bock (1999) is given below:

- *rng_resid_tol* - sets the tolerance for bad range residuals. The tolerances in Figure A.2 are set high to allow for poor orbit definition during these periods.

- *dd_return_size* - sets the amount of data to be used for cycle slip repair. The first three values in the command line represent the number of widelane estimates used in the one-way data (10), ionosphere free estimates used in the double-differences (10) and geometry free estimates used in one-way or double differences (5) (default values are 100 50 10 respectively). The fourth value specifies the maximum duration over which one-way data will be patched using the widelane and geometry free estimates (10 epochs). In Figure A.2, these values are all set low to allow cycle slip repair over very small segments of data and for data with high ionospheric noise levels.
- *trim_oneway* - defines the tolerance for removing small segments in the one-way data. When processing the GPS observations from the early LGB traverses it was found that even very small data segments are vital in obtaining a solution for site coordinates. Therefore, to retain the maximum amount of data in the solution, the fourth value in this command line (the number of epochs allowed after last bias flag) was set very low (5). To reduce the number of bias flags in the one-way data, a minimum time between biases of 240 seconds was set (default value is 120 secs).
- *ion_jump_tol* - sets the tolerances for cycle slip detection in the geometry free observable (LG). The first value indicates the maximum gap size (240 secs) over which the test for a data 'jump' will be carried out. The remaining values are a multiplier (6), the minimum change in the ionospheric delay (2 cycles) and the maximum change in the delay (6 cycles). The tolerance for detecting jumps in the LG observable will fall between the maximum and minimum values and is determined by applying the multiplier to the last observed change in the delay. In the LGB processing, the maximum gap was increased (default 30 secs) to allow testing over larger gaps and the maximum ionospheric change was increased (default 5) to allow larger jumps to pass through the cleaning process.
- *site_params* - sets the minimum elevation for data cleaning and *c-file* output (10° and 10° in this case) and the minimum signal to noise ratio for cleaning the L1 and L2 data. Inspection of *AUTCLN* summary files during sections of the 1990/91 processing indicated that the raw data at WOMB and DOVE were being totally rejected mainly due to high noise levels. In order to obtain coordinate solutions at these sites, it was necessary to invoke this command and allow the noisier data to be used in the solution.

A.3 GAMIT Processing Parameters Used For the 1989 - 1993 LGB Campaigns

The processing parameters used for the 1989 - 1993 data processing are documented in Figure A.3. The selected parameters included several important variations from the default (GAMIT v9.6) settings. The most significant change was the setting of very loose a priori constraints on the satellite parameters. This was done to account for the poorly defined orbits encountered at this time (especially in the Southern Hemisphere) by allowing new orbits that were consistent with the GPS data, to be solved for. Another important change in the solution parameters was the loosening of ionospheric constraints to provide better wide-lane ambiguity (bias) estimation. The constraint on the differential ionosphere at each epoch allows separation of this parameter from the wide-lane ambiguity (King and Bock, 1999). For the 1989 - 1993 LGB data processing, a constraint of 8 ppm was used as this is the recommended value for periods of high ionospheric activity (King and Bock, 1999). This level of constraint was found to be adequate for the solution of the LGB data.

```
Session Table     LGB    1989/90 - 1990/91
Processing Agency = TAS

Station Number =  *
Station Constraint = Y     ; Y/N
Satellite Number =  *
Satellite Constraint = Y   ; Y/N
all a  e  i  n  w  M  rad1 rad2 rad3 rad4 rad5 rad6 rad7 rad8 rad9
100  100  100  100  100  10  10  10  10  10  10  10  10  10

Type of analysis = 0-ITER       ; PREFIT/QUICK/0-ITER/1-ITER/2-ITER/
Data status = RAW               ; RAW/CLEAN
SOLVE-only = NO                 ; YES/NO
Choice of observable = LC      ; L1&L2/L1_ONLY/L2_ONLY/LC/LC_HELP
Choice of experiment = RELAX   ; BASELINE/RELAX/ORBIT/KINEMATIC

Ionospheric constraints =  0.0 mm + 8.00 ppm
Tropospheric constraints = NO           ; YES/NO
Zenith delay estimation = YES           ; YES/NO
Zenith model = PWL               ; PWL(piecewise linear)/CON(step)
Number zen = 13                  ; number of zenith-delay parameters
Zenith constraints = 0.500   ; zenith-delay a priori constraint in m
Zenith variation = 0.020 100.0   ; tau in m/sqrt(hr), hrs

Tide model = 3        ; Binary: 1 Earth, 2 freq-dep, 4 pole, 8 ocean
Earth rotation = 3    ; Binary 1=pole 2=UT1
Antenna model = NONE  ; NONE/ELEV/AZEL  default = NONE
Reference system for Orbit = ITR92       ; ITR92/ITR91/ITR90/WGS84
Inertial frame = J2000                   ; J2000/B1950
Radiation model for ARC = BERNE
Clean option = AUTCLN                   ; AUTCLN/SINCLN/DBLCLN
AUTCLN command file = autcln.cmd
Delete eclipse data = POST              ;ALL/POST
Estimate EOP = 15     ; Binary: 1 wob, 2 ut1, 4 wob_rate, 8 ut1_rate
Wobble constraint = 0.3   0.03    ; (arcsec, arcsec/day)
UT1 constraint = 0.00002  0.02    ; (sec, sec/day)
```

Figure A.3 - GAMIT processing options 1989/90 - 1992/93

A.4 GAMIT Processing Parameters Used For the 1993 - 1995 LGB Campaigns

```
Session Table  LGB  1993/94 - 1994/95
Processing Agency = TAS

Station Number = *
Satellite Number = *
Station Constraint = Y              ; Y/N
Satellite Constraint = Y            ; Y/N
all a e i n w M rad1 rad2 rad3 rad4 rad5 rad6 rad7 rad8 rad9;
0.1  0.1  0.1  0.1  0.1  0.1  10  10  0.1  0.1  0.1  0.1  0.1  0.1  0.1  0.1

Type of Analysis = 0-ITER           ; PREFIT / QUICK / 0-ITER/
                                      1-ITER/2-ITER
Choice of Observable = LC_ONLY      ;L1_SINGLE/L1&L2/L1_ONLY/
                                     L2_ONLY/LC_ONLY/
                                     L1,L2_INDEPEND./LC_HELP
Choice of Experiment = RELAX        ; BASELINE/RELAX./ORBIT
SOLVE-only = NO                     ; YES/NO
Data Status = RAW                   ; RAW/CLEAN

Inertial Frame = J2000              ; B1950/J2000
Radiation Model for ARC = BERNE     ; SPHRC/BERNE/SRDYB/SVBDY
Reference system for ARC = IGS92    ; WGS72/WGS84/MERIT/IGS92
                                     (default = IGS92)

Clean option = AUTCLN               ; AUTCLN/SINCLN/DBLCLN;
AUTCLN command file = autcln.cmd
AUTCLN postfit = NO                 ; YES/NO; default = NO
Delete eclipse data = POST          ; ALL/POST/NO; default POST
SCANDD control = FULL               ; BOTH/IFBAD/FIRST/FULL/NONE;

Ionospheric Constraints =  0.0 mm + 1.00 ppm

Elevation Cutoff = 15.              ; Conventional cutoff is 15.
Zenith Delay Estimation = YES       ; YES/NO  (default no)
Number Zen = 13                     ; number of zenith-delay
                                      parameters
Atmospheric gradients = NO          ; YES/NO  (default no)
Zenith Model = PWL                  ; PWL(piecewise linear)/CON(step)
Zenith Constraints = 0.50           ; zenith-delay a priori
                                      constraint in m
Zenith Variation = 0.02 100.        ; tau in m/sqrt(hr), hrs
                                      (default .02 100.)
Gradient Constraints = 0.03         ; gradient at 10° elevation in m
Tropospheric Constraints = NO       ; YES/NO

Yaw Model = YES          ; YES/NO  default = YES
Antenna model = NONE     ; NONE/ELEV/AZEL  default = NONE
Tide Model = 3         ; Binary: 1 earth, 2 freq-dep, 4 pole, 8 ocean
Earth Rotation = 3       ; Binary: 1=pole 2=UT1 default=3
Estimate EOP = 15      ; Binary: 1 wob, 2 ut1, 4 wob rate, 8 ut1 rate
Wobble Constraint = 3. 0.3     ; Default 3. (arcsec) 0.3 (arcsec/day)
UT1 Constraint = 0.00002 0.02  ; Default .00002 (sec) 0.02 (sec/day)
```

Figure A.4 - GAMIT processing options 1993/94 - 1994/95

A.5 Summary Information For the Multi-Season GLOBK/GLORG Solution of the LGB GPS Data (1989 - 1995)

```
 ++++++++++++++++++++++++++++++++++++
 + GLORG                Version 5.06S +
 ++++++++++++++++++++++++++++++++++++
 Stabilization with 50.0% constant,  50.0% site dependent weighting.
 Delete sites with   4.0-sigma condition.
 Height variance factor      10.00 Position,     10.00 Velocity
 Min dH sigma Position 0.0050 m;    Min Position RMS 0.0030 m
 Min dH sigma Velocity 0.0050 m/yr; Min Velocity RMS 0.0030 m/yr

============================================================
Starting stabilization iteration   4 seasons.gdl
For 9 sites in origin, min/max height sigma 19.30 27.64 mm;
Median 22.09 mm, Tol 5.00 mm seasons.gdl

 Position system stabilization results
 -------------------------------------
 X Rotation  (mas)    -1.33960 +-    0.25269 Iter  4 seasons.gdl
 Y Rotation  (mas)    -3.47025 +-    0.26929 Iter  4 seasons.gdl
 Z Rotation  (mas)    -3.63265 +-    0.28441 Iter  4 seasons.gdl
 X Translation (m)     0.12096 +-    0.00791 Iter  4 seasons.gdl
 Y Translation (m)    -0.09941 +-    0.00761 Iter  4 seasons.gdl
 Z Translation (m)    -0.08049 +-    0.00819 Iter  4 seasons.gdl
 Scale       (ppb)   -10.24823 +-    2.49489 Iter  4 seasons.gdl

Condition Sigmas used  0.000 0.000 0.000 0.000 0.000 0.000 0.000

Sites and relative sigmas used in stabilization
MADR_GPS   0.95  SANT_GPS   1.08  ALGO_GPS   0.92  YELL_GPS   0.93
KOKB_GPS   1.07  TIDB_GPS   1.02  YAR1_GPS   1.05  TROM_GPS   1.02
WETT_GPS   0.96

For 27 Position Iter 4 Pre RMS  0.1161 m; Post RMS  0.0149 m


For 9 sites in origin, min/max dh/dt  sigma 1.54 2.77 mm/yr;
Median  2.44 mm/yr, Tol  5.00 mm/yr seasons.gdl

 Velocity system stabilization results
 -------------------------------------
 X Rotate (mas/yr)    -0.00919 +-    0.06211 Iter  4 seasons.gdl
 Y Rotate (mas/yr)     0.19174 +-    0.06608 Iter  4 seasons.gdl
 Z Rotate (mas/yr)     0.13911 +-    0.06991 Iter  4 seasons.gdl
 X Trans    (m/yr)    -0.00179 +-    0.00194 Iter  4 seasons.gdl
 Y Trans    (m/yr)     0.00246 +-    0.00187 Iter  4 seasons.gdl
 Z Trans    (m/yr)    -0.01429 +-    0.00201 Iter  4 seasons.gdl
 Scale    (ppb/yr)    -0.37382 +-    0.61347 Iter  4 seasons.gdl

Condition Sigmas used  0.000 0.000 0.000 0.000 0.000 0.000 0.000

Sites and relative sigmas used in stabilization
MADR_GPS   0.95  SANT_GPS   1.07  ALGO_GPS   0.92  YELL_GPS   0.92
KOKB_GPS   1.08  TIDB_GPS   1.02
YAR1_GPS   1.04  TROM_GPS   1.03  WETT_GPS   0.96

For 27 Velocity Iter 4 Pre RMS 0.0070 m/yr; Post RMS 0.0037 m/yr
------------------------------------------------------------
```

```
 GLOBK Ver 5.06S, Global solution
------------------------------------------------------------
Solution commenced with: 1990/ 1/ 7 23:59 (1990.0192)
Solution ended with    : 1995/ 2/14 23:59 (1995.1233)
Solution refers to : 1990/ 2/ 3 11:59 (1990.0918)[Seconds tag 45.00]
Satellite IC epoch     : 1990/ 2/ 3 12: 0  0.00
GPS System Information : Time GPST Frame J2000 Precession IAU76
Radiation model BERNE
MODELS Used in Analysis: SD-WOB  SD-UT1  E-Tide  K1-Tide PoleTide
Run time               : 2001/ 8/15 10:27 27.00

There were 331 exps from 6 global files in the solution
There were 60725637 data used, 0 data not used and 60725637 total
There were 1260 global parameters estimated
There were 284 stations, 0 radio sources and 29 satellites

The  prefit chi**2 for    1530 input parameters is     1.147

 LIST file      : seasons.gdl
 COMMON file    : ./seasons_final_com.bin
 MARKOV file    : globk_8995.cmd
 GLORG CMD file : glorg.cmd
 APRIORI file   : ../tables_gps/89_95.apr
 APRIORI file   : ../tables_gps/sites.itrf96.peter
 APRIORI file   : ../tables_gps/lgb.apr
 APRIORI file   : ../tables_gps/sites.itrf97.apr
 APRIORI file   : ../tables_gps/89_95.apr (glorg)
 APRIORI file   : ../tables_gps/sites.itrf96.peter (glorg)
 APRIORI file   : ../tables_gps/sites.itrf97.apr (glorg)
 PMU file       : ../tables_gps/pmu_bull_b
 SVS EPHEM file : ../tables/svs_seasons.apr:A
 EARTHQUAKE file: ant90_95.fixer.GLX

 There were   35 site renames listed.  Renames used are:
 # Orig New Specific Period from -----> To Position change (m) Type
  3 LG26_GPS->LG26_BAD 1990/12/18 0:0 1991/ 3/ 1 0:0 0.0000 0.0000 0.0000 XYZ
  4 LG21_GPS->LG21_BAD 1990/12/18 0:0 1991/ 3/ 1 0:0 0.0000 0.0000 0.0000 XYZ
  5 LG19_GPS->LG19_BAD 1990/12/18 0:0 1991/ 3/ 1 0:0 0.0000 0.0000 0.0000 XYZ
  6 LG00_GPS->LG00_890 1989/12/ 1 0:0 1990/ 3/ 1 0:0 0.0000 0.0000 0.0000 XYZ
  7 LG00_GPS->LG00_901 1990/12/ 1 0:0 1991/ 3/ 1 0:0 0.0000 0.0000 0.0000 XYZ
  8 LG16_GPS->LG16_BAD 1990/12/ 1 0:0 1991/ 3/ 1 0:0 0.0000 0.0000 0.0000 XYZ
  9 ALBH_GPS->ALBH_923 1992/11/ 1 0:0 1993/ 3/ 1 0:0 0.0000 0.0000 0.0000 XYZ
 10 ONSA_GPS->ONSA_923 1992/11/ 1 0:0 1993/ 3/ 1 0:0 0.0000 0.0000 0.0000 XYZ
 11 STJO_GPS->STJO_923 1992/11/ 1 0:0 1993/ 3/ 1 0:0 0.0000 0.0000 0.0000 XYZ
 12 TAIW_GPS->TAIW_923 1992/11/ 1 0:0 1993/ 3/ 1 0:0 0.0000 0.0000 0.0000 XYZ
 13 LG00_GPS->LG00_GPS 1994/ 6/ 1 0:0 1995/ 4/ 1 0:0 0.0000 0.0000 -3.050 NEU
 14 LG01_GPS->LG01_GPS 1994/ 6/ 1 0:0 1995/ 4/ 1 0:0 0.0000 0.0000 -3.050 NEU
 15 LG10_GPS->LG10_GPS 1994/ 6/ 1 0:0 1995/ 4/ 1 0:0 0.0000 0.0000 -3.050 NEU
 16 LG19_GPS->LG19_GPS 1994/ 6/ 1 0:0 1995/ 4/ 1 0:0 0.0000 0.0000 -3.050 NEU
 17 LG20_GPS->LG20_GPS 1994/ 6/ 1 0:0 1995/ 4/ 1 0:0 0.0000 0.0000 -3.050 NEU
 20 DAVI_GPS->DAV1_GPS 1989/ 1/ 1 0:0 1990/ 3/ 1 0:0 0.0000 0.0000 0.0115 NEU
 25 NALL_GPS->NYAL_GPS 1900/ 1/ 1 1:0 2100/ 1/ 1 1:0 0.0000 0.0000 0.0000 XYZ
 32 USU3_GPS->USUD_GPS 1900/ 1/ 1 1:0 2100/ 1/ 1 1:0 0.0000 0.0000 0.0000 XYZ


EXPERIMENT LIST from ./seasons_final_srt.bin
 # Name                        SCALE   PPM  Forw Chi2 Back Chi2 Status
 1 glbf/LAMB_9495.GLX          2.000  0.000   0.000    -1.000    USED
 2 glbf/LAMB_9394.GLX          2.000  0.000   0.008    -1.000    USED
 3 glbf/LAMB_9293_noht.GLX     6.000  0.000   3.564    -1.000    USED
 4 glbf/LAMB_9091_noht.GLX     4.000  0.000   2.047    -1.000    USED
 5 glbf/LAMB_8990b_noht.GLX    4.000  0.000   0.211    -1.000    USED
 6 glbf/LAMB_8990_noht.GLX     4.000  0.000   1.162    -1.000    USED

------------------------------------------------------------
```

```
 Summary of Markov file globk_8995.cmd
------------------------------------------------------------------
 make_svs ../tables/svs_seasons.apr
 srt_dir -1
 eq_file ant90_95.fixer.GLX
*=========================
 com_file ./seasons_final_com.bin
 srt_file ./seasons_final_srt.bin
 sol_file ./seasons_final_sol.bin
*=========================
 apr_file ../tables_gps/89_95.apr
 apr_file ../tables_gps/sites.itrf96.peter
 apr_file ../tables_gps/lgb.apr
 apr_file ../tables_gps/sites.itrf97.apr
*=========================================
 in_pmu ../tables_gps/pmu_bull_b
 app_ptid all
 apr_wob   100 100 10 10   0   0  0  0
 apr_ut1   100  10   0.0   0.0   0.0  0.0
 mar_wob   36500  36500  365  365  0  0  0  0
 mar_ut1   36500  365  0  0 0  0
*=================================================
apr_neu   all    99.00   99.00   99.00  10   10   10
# Loose constraints on the LGB velocities
 apr_neu   lg00   99  99  99   50  50  50
 apr_neu   lg01   99  99  99   50  50  50
 apr_neu   lg02   99  99  99   50  50  50
 :
 :
 :
 apr_neu   lg71   99  99  99   50  50  50
 apr_neu   lg72   99  99  99   50  50  50
# No velocities for sites only observed in one season
 apr_neu   arex   99  99  99   0   0   0
 apr_neu   au13   99  99  99   0   0   0
 apr_neu   au39   99  99  99   0   0   0
 :
 :
 :
 apr_neu   wsam   99  99  99   0   0   0
 apr_neu   zimm   99  99  99   0   0   0
# Tighter constraints on core sites
 apr_neu   yar1    2.50   2.50   2.50  0.50   0.50   0.50
 apr_neu   tidb    2.50   2.50   2.50  0.50   0.50   0.50
 apr_neu   sant    2.50   2.50   2.50  0.50   0.50   0.50
 apr_neu   hart    2.50   2.50   2.50  0.50   0.50   0.50
 apr_neu   gold    2.50   2.50   2.50  0.50   0.50   0.50
 apr_neu   madr    2.50   2.50   2.50  0.50   0.50   0.50
 apr_neu   fair    2.50   2.50   2.50  0.50   0.50   0.50
 apr_neu   algo    2.50   2.50   2.50  0.50   0.50   0.50
 apr_neu   yell    2.50   2.50   2.50  0.50   0.50   0.50
 apr_neu   wett    2.50   2.50   2.50  0.50   0.50   0.50
 apr_neu   kosg    2.50   2.50   2.50  0.50   0.50   0.50
 apr_neu   trom    2.50   2.50   2.50  0.50   0.50   0.50
 apr_neu   kokb    2.50   2.50   2.50  0.50   0.50   0.50
*=======================================
 prt_opt   gdlf:psum:vsum:cmds
*=========================
 org_cmd glorg.cmd
 org_opt gdlf:cmds:blen:psum:vsum
 org_out seasons.org
*=========================
```

APPENDIX - B

Table B.1 - LGB Occupations Used in Velocity Calculations 1989 - 1995. Highlighted rows indicate IMS that were only occupied between 1989/90 and 1992/93.

LGBa				
Site	Nº Obs	First Obs (yr)	Last Obs (yr)	Period of Obs (yrs)
LG00	3	1993.10	1995.12	2.02
LG01	4	1990.12	1995.12	5.00
LG02	4	1990.12	1994.28	4.16
LG03	3	1990.12	1993.10	2.98
LG04	4	1990.09	1995.12	5.03
LG05	4	1990.09	1994.28	4.19
LG06	4	1990.09	1994.28	4.19
LG07	5	1990.09	1995.12	5.03
LG08	3	1990.09	1993.10	3.01
LG09	3	1990.09	1993.10	3.01
LG10	4	1990.09	1995.12	5.03
LG11	2	1991.13	1993.10	1.96
LG12	3	1990.09	1993.10	3.01
LG13	4	1991.13	1995.12	3.99
LG14	3	1990.09	1993.10	3.01
LG15	3	1990.09	1993.10	3.01
LG16	2	1994.28	1995.12	0.84
LG17	4	1990.09	1995.12	5.03
LG18	4	1990.09	1995.12	5.03
LG19	3	1990.09	1995.12	5.03
LG20	3	1991.13	1995.12	3.99
LG21	2	1994.28	1995.12	0.84
LG22	3	1991.13	1995.12	3.99
LG23	3	1991.13	1995.12	3.99
LG24	3	1991.13	1995.12	3.99
LG25	3	1991.13	1995.12	3.99
LG26	2	1994.28	1995.12	0.84
LG27	2	1994.28	1995.12	0.84
LG28	3	1991.13	1995.12	3.99
LG29	3	1991.13	1995.12	3.99
LG30	3	1991.13	1995.12	3.99
LG31	3	1991.13	1995.12	3.99
LG32	2	1991.13	1994.28	3.15
LG33	2	1991.13	1994.28	3.15

LGBb				
Site	Nº Obs	First Obs (yr)	Last Obs (yr)	Period of Obs (yrs)
LG34	2	1994.28	1995.12	0.84
LG35	2	1994.28	1995.12	0.84
LG36	2	1994.28	1995.12	0.84
LG37	2	1994.28	1995.12	0.84
LG38	2	1994.28	1995.12	0.84
LG39	2	1994.28	1995.12	0.84
LG40	2	1994.28	1995.12	0.84
LG41	2	1994.28	1995.12	0.84
LG42	2	1994.28	1995.12	0.84
LG43	2	1994.28	1995.12	0.84
LG44	2	1994.28	1995.12	0.84
LG45	2	1994.28	1995.12	0.84
LG46	2	1994.28	1995.12	0.84
LG47	2	1994.28	1995.12	0.84
LG48	2	1994.28	1995.12	0.84
LG49	2	1994.28	1995.12	0.84
LG50	2	1994.28	1995.12	0.84
LG51	2	1994.28	1995.12	0.84
LG52	2	1994.28	1995.12	0.84
LG53	2	1994.28	1995.12	0.84
LG54	2	1994.28	1995.12	0.84
LG55	2	1994.28	1995.12	0.84
LG56	2	1994.28	1995.12	0.84
LG57	2	1994.28	1995.12	0.84
LG58	2	1994.28	1995.12	0.84
LG59	2	1994.28	1995.12	0.84
LG60	2	1994.28	1995.12	0.84
LG61	2	1994.28	1995.12	0.84
LG62	2	1994.28	1995.12	0.84
LG63	2	1994.28	1995.12	0.84
LG64	2	1994.28	1995.12	0.84
LG65	2	1994.28	1995.12	0.84
LG66	2	1994.28	1995.12	0.84
LG67	2	1994.28	1995.12	0.84
LG68	2	1994.28	1995.12	0.84
LG69	2	1994.28	1995.12	0.84
LG70	2	1994.28	1995.12	0.84
LG71	2	1994.28	1995.12	0.84
LG72	2	1994.28	1995.12	0.84

Table B.2 - LGB IMS Accumulation Values - from the analysis of cane measurements presented in Higham and Craven (1997)

Site	Accumulation (m)						
	measured 89/90-90/91	measured 90/91-92/93	measured 92/93-93/94	measured 93/94-94/95	total 89/90-94/95	calculated 90/91-93/94	calculated 90/91-94/95
LG00	0.770	0.319	0.144	0.264	1.497		
LG01	0.571	0.183	-0.011	0.384	1.127		
LG02	0.518	0.100	-0.056	0.240	0.802		
LG03	0.328	0.010	0.034	0.024	0.396		
LG04	0.212	0.096	-0.078	0.073	0.303		
LG05	0.032	0.413	-0.011	0.145	0.579		
LG06	0.464	0.279	0.213	0.357	1.313		
LG07	0.243	0.250	0.314	0.375	1.182		
LG08	0.434	0.356	0.528	0.318	1.636		
LG09	0.541	0.327	0.203	0.180	1.251		
LG10	0.508	0.538	0.011	0.115	1.172		
LG11	0.384	0.191	0.237	0.133	0.945		
LG12	1.121	0.354	0.712	0.184	2.371		
LG13	0.726	0.220	0.000	0.335	1.281		
LG14	0.021	0.392	0.171	0.461	1.045		
LG15	0.396	0.124	-0.023	0.303	0.8		
LG16	0.289	0.191	0.513	0.102	1.095	0.840	0.942
LG17				-0.026		0.750	0.724
LG18				0.471		0.330	0.801
LG19				0.344		1.170	1.514
LG20				0.407		0.450	0.857
LG21				0.407		0.630	1.037
LG22				0.319		0.990	1.309
LG23				0.410		1.080	1.490
LG24				0.671		1.290	1.961
LG25				0.018		-0.060	-0.042
LG26				0.099		0.870	0.969
LG27				0.009		0.240	0.249
LG28				0.128		0.180	0.308
LG29				0.284		0.420	0.704
LG30				-0.046		0.090	0.044
LG31				0.056		0.360	0.416
LG32				0.187		0.330	0.517
LG33				-0.019		0.510	0.491
LG34				-0.028		0.690	0.662
LG35				0.010		0.300	0.310
LG36				-0.010			
LG37				0.258			
LG38				0.130			
LG39				0.050			

Site	Accumulation (m)						
	measured 89/90-90/91	measured 90/91-92/93	measured 92/93-93/94	measured 93/94-94/95	total 89/90-94/95	calculated 90/91-93/94	calculated 90/91-94/95
LG40				0.203			
LG41				0.020			
LG42				0.938			
LG43				0.143			
LG44				0.000			
LG45				-0.021			
LG46				0.168			
LG47				0.117			
LG48				0.011			
LG49				0.086			
LG50				0.054			
LG51				-0.022			
LG52				0.022			
LG53				0.308			
LG54				0.245			
LG55				0.223			
LG56				0.056			
LG57				0.000			
LG58				0.000			
LG59				0.281			
LG60				0.143			
LG61				0.431			
LG62				0.048			
LG63				0.000			
LG64				0.197			
LG65				0.324			
LG66				-0.038			
LG67				0.000			
LG68				0.280			
LG69				0.608			
LG70				0.597			
LG71				0.481			
LG72				0.700			

Table B.3 - Heights for the LGB IMS at epoch 1990.092
(h values refer to WGS84 ellipsoid; N values represent EGM96 separations.)

LGB Traverse 1989/90								
Site	**h sleeve (m)**	**sleeve-join (m)**	**h join (m)** (GLOBK)	**σh** (GLOBK)	**join-surface (m)**	**h surface (m)**	**N (m)**	**H surface (m)**
LG00^	1863.18	3.05	**1860.13**	3.61	1.55	**1858.58**	28.34	**1830.23**
LG01^	2028.40	3.05	**2025.35**	3.58	1.60	**2023.76**	28.19	**1995.57**
LG02^	2211.61	3.05	**2208.56**	4.32	2.00	**2206.56**	28.28	**2178.28**
LG03^	2359.29	3.05	**2356.24**	8.97	1.80	**2354.45**	28.16	**2326.28**
LG04	2529.95	3.05	**2526.90**	1.93	2.20	**2524.70**	27.63	**2497.07**
LG05	2656.46	3.05	**2653.41**	1.82	2.00	**2651.41**	26.74	**2624.67**
LG06	2640.49	3.05	**2637.44**	2.04	1.85	**2635.59**	25.74	**2609.85**
LG07	2608.49	3.05	**2605.44**	1.91	1.85	**2603.59**	25.15	**2578.44**
LG08	2604.46	3.05	**2601.41**	2.43	2.05	**2599.37**	24.51	**2574.85**
LG09	2640.04	3.05	**2636.99**	2.30	1.95	**2635.04**	23.79	**2611.25**
LG10	2645.78	3.05	**2642.73**	3.08	1.80	**2640.93**	22.69	**2618.24**
LG12	2534.90	3.05	**2531.85**	2.83	1.85	**2530.00**	21.33	**2508.67**
LG14	2640.83	3.05	**2637.78**	3.68	1.85	**2635.94**	21.04	**2614.89**
LG15	2721.02	3.05	**2717.97**	4.50	1.65	**2716.32**	20.68	**2695.63**
LG17	2759.42	3.05	**2756.37**	2.65	1.80	**2754.57**	20.38	**2734.18**
LG18	2753.57	3.05	**2750.52**	2.23	1.90	**2748.62**	20.10	**2728.52**
LG19	2770.35	3.05	**2767.30**	2.11	1.75	**2765.55**	19.52	**2746.03**

^ Heights referred to Epoch 1990.119

Table B.4 - Heights for the LGB IMS at epoch 1991.133
(h values refer to WGS84 ellipsoid; N values represent EGM96 separations.)

LGB Traverse 1990/91								
Site	**h sleeve (m)**	**sleeve-join (m)**	**h join (m)** (GLOBK)	**σh** (GLOBK)	**join-surface (m)**	**h surface (m)**	**N (m)**	**H surface (m)**
LG00	1861.78	3.05	**1858.73**	0.06	0.93	**1857.80**	28.35	**1829.45**
LG01	2026.58	3.05	**2023.53**	0.06	1.12	**2022.41**	28.19	**1994.22**
LG02	2209.47	3.05	**2206.42**	0.09	1.71	**2204.71**	28.28	**2176.43**
LG03	2357.47	3.05	**2354.42**	0.09	1.60	**2352.82**	28.16	**2324.66**
LG04	2529.50	3.05	**2526.45**	0.21	2.10	**2524.35**	27.63	**2496.71**
LG05	2656.44	3.05	**2653.39**	0.18	1.37	**2652.02**	26.75	**2625.27**
LG06	2639.99	3.05	**2636.94**	0.08	1.37	**2635.57**	25.74	**2609.83**
LG07	2608.14	3.05	**2605.09**	0.11	1.43	**2603.66**	25.15	**2578.50**
LG08	2603.82	3.05	**2600.77**	0.09	1.50	**2599.27**	24.51	**2574.76**
LG09	2639.81	3.05	**2636.76**	0.05	1.47	**2635.29**	23.79	**2611.50**
LG10	2645.47	3.05	**2642.42**	0.04	1.10	**2641.32**	22.69	**2618.63**
LG11	2611.39	3.05	**2608.34**	0.20	1.38	**2606.96**	21.75	**2585.20**
LG12	2532.05	3.05	**2529.00**	0.05	1.16	**2527.84**	21.33	**2506.50**
LG13	2585.25	3.05	**2582.20**	0.04	1.58	**2580.62**	21.32	**2559.29**
LG14	2639.43	3.05	**2636.38**	0.05	1.42	**2634.96**	21.04	**2613.92**
LG15	2723.00	3.05	**2719.95**	0.04	1.10	**2718.85**	20.69	**2698.16**
LG16	2717.00	3.05	**2713.95**	0.04	1.42	**2712.53**	20.49	**2692.04**
LG17	2759.16	3.05	**2756.11**	0.09	1.30	**2754.81**	20.39	**2734.42**
LG18	2753.79	3.05	**2750.74**	0.09	1.87	**2748.87**	20.11	**2728.77**
LG19				0.65	1.63			
LG20	2764.29	3.05	**2761.24**	0.51	1.00	**2760.24**	18.82	**2741.42**
LG21	2732.19	3.05	**2729.14**	0.62	1.85	**2727.29**	18.15	**2709.13**
LG22	2686.11	3.05	**2683.06**	0.72	1.88	**2681.18**	17.64	**2663.54**
LG23	2704.21	3.05	**2701.16**	3.02	1.58	**2699.58**	17.06	**2682.52**
LG24	2721.11	3.05	**2718.06**	1.15	2.30	**2715.76**	16.23	**2699.53**
LG25	2792.46	3.05	**2789.41**	0.27	2.05	**2787.36**	15.31	**2772.05**
LG26					2.15			
LG27					1.93			
LG28					2.10			
LG29	2850.56	3.05	**2847.51**	1.22	1.97	**2845.54**	12.64	**2832.89**
LG30	2860.44	3.05	**2857.39**	0.82	1.47	**2855.92**	12.07	**2843.85**
LG31	2762.83	3.05	**2759.78**	1.22	1.61	**2758.17**	12.03	**2746.13**
LG32	2604.63	3.05	**2601.58**	1.02	1.67	**2599.91**	12.29	**2587.61**
LG33	2528.26	3.05	**2525.21**	0.91	1.62	**2523.59**	12.51	**2511.08**
LG34					1.88			
LG35					1.55			

Table B.5 - Heights for the LGB IMS at epoch 1993.097
(h values refer to WGS84 ellipsoid; N values represent EGM96 separations.)

LGB Traverse 1992/93								
Site	**h sleeve (m)**	**sleeve-join (m)**	**h join (m)** (GLOBK)	**σh** (GLOBK)	**join-surface (m)**	**h surface (m)**	**N (m)**	**H surface (m)**
LG00	1860.97	3.05	**1857.92**	0.29	0.27	**1857.65**	28.35	**1829.30**
LG01	2025.84	3.05	**2022.79**	0.49	0.66	**2022.13**	28.19	**1993.94**
LG02	2208.75	3.05	**2205.70**	0.42	1.56	**2204.14**	28.28	**2175.87**
LG03	2357.20	3.05	**2354.15**	0.53	1.30	**2352.85**	28.16	**2324.70**
LG04	2529.64	3.05	**2526.59**	0.28	1.50	**2525.09**	27.63	**2497.46**
LG05	2655.92	3.05	**2652.87**	0.25	0.85	**2652.02**	26.75	**2625.27**
LG06	2639.26	3.05	**2636.21**	0.26	0.88	**2635.33**	25.74	**2609.59**
LG07	2607.34	3.05	**2604.29**	0.64	0.93	**2603.36**	25.15	**2578.21**
LG08	2603.04	3.05	**2599.99**	0.68	0.78	**2599.21**	24.51	**2574.69**
LG09	2639.19	3.05	**2636.14**	0.28	0.93	**2635.21**	23.79	**2611.42**
LG10	2645.03	3.05	**2641.98**	0.39	0.68	**2641.30**	22.69	**2618.60**
LG11	2610.52	3.05	**2607.47**	0.94	0.85	**2606.62**	21.75	**2584.86**
LG12	2530.67	3.05	**2527.62**	0.72	0.47	**2527.15**	21.33	**2505.81**
LG13	2584.86	3.05	**2581.81**	0.39	1.15	**2580.66**	21.32	**2559.34**
LG14	2639.17	3.05	**2636.12**	0.68	0.49	**2635.63**	21.04	**2614.59**
LG15	2722.05	3.05	**2719.00**	1.23	0.88	**2718.12**	20.69	**2697.43**

Table B.6 - Heights for the LGB IMS at epoch 1994.281
(h values refer to WGS84 ellipsoid; N values represent EGM96 separations.)

LGB Traverse 1993/94						
Site	**h sleeve/join (m)** (GLOBK)	**σh (m)** (GLOBK)	**join-surface (m)**	**h surface (m)**	**N (m)**	**H surface (m)**
LG00	**1858.09**	0.02	0.13	**1857.96**	28.35	**1829.61**
LG02	**2205.30**	0.03	1.62	**2203.68**	28.28	**2175.40**
LG05	**2652.34**	0.03	0.86	**2651.48**	26.75	**2624.73**
LG06	**2635.49**	0.03	0.67	**2634.82**	25.74	**2609.08**
LG07	**2603.89**	0.03	0.62	**2603.28**	25.15	**2578.12**
LG13	**2581.20**	0.02	1.15	**2580.05**	21.32	**2558.72**
LG16	**2713.01**	0.01	0.58	**2712.43**	20.49	**2691.94**
LG17	**2755.37**	0.01	0.55	**2754.82**	20.39	**2734.43**
LG18	**2749.69**	0.01	1.54	**2748.15**	20.10	**2728.04**
LG19	**2767.04**	0.01	0.46	**2766.58**	19.53	**2747.06**
LG20	**2759.88**	0.01	0.55	**2759.33**	18.82	**2740.51**
LG21	**2725.05**	0.01	1.22	**2723.83**	18.15	**2705.68**
LG22	**2680.99**	0.01	0.89	**2680.10**	17.64	**2662.46**
LG23	**2699.89**	0.01	0.50	**2699.39**	17.06	**2682.33**
LG24	**2722.15**	0.01	1.01	**2721.14**	16.23	**2704.90**
LG25	**2788.70**	0.01	2.11	**2786.59**	15.31	**2771.28**
LG26	**2877.11**	0.01	1.28	**2875.83**	14.62	**2861.21**
LG27	**2940.73**	0.01	1.69	**2939.04**	14.14	**2924.90**
LG28	**2903.54**	0.01	1.92	**2901.62**	13.29	**2888.34**
LG29	**2848.47**	0.01	1.55	**2846.92**	12.64	**2834.28**
LG30	**2857.32**	0.01	1.38	**2855.94**	12.07	**2843.87**
LG31	**2760.81**	0.01	1.25	**2759.56**	12.03	**2747.53**
LG32	**2599.91**	0.01	1.34	**2598.57**	12.29	**2586.27**
LG33	**2522.59**	0.01	1.11	**2521.48**	12.51	**2508.97**
LG34	**2442.77**	0.01	1.19	**2441.58**	12.29	**2429.29**
LG35	**2355.00**	0.00	1.25	**2353.75**	11.61	**2342.14**
LG36	**2267.12**	0.00	1.69	**2265.43**	12.24	**2253.19**
LG37	**2366.53**	0.01	1.96	**2364.57**	10.26	**2354.31**
LG38	**2362.58**	0.00	1.83	**2360.75**	9.22	**2351.53**
LG39	**2275.26**	0.01	1.95	**2273.31**	9.29	**2264.01**
LG40	**2180.12**	0.01	2.00	**2178.12**	9.27	**2168.85**
LG41	**2228.86**	0.11	1.62	**2227.24**	8.86	**2218.39**
LG42	**2236.53**	0.01	2.14	**2234.39**	8.64	**2225.76**
LG43	**2259.99**	0.04	1.94	**2258.05**	8.46	**2249.59**
LG44	**2302.46**	0.01	1.70	**2300.76**	8.31	**2292.45**
LG45	**2350.10**	0.04	1.48	**2348.62**	8.08	**2340.54**
LG46	**2363.39**	0.00	1.57	**2361.82**	7.83	**2353.99**
LG47	**2358.25**	0.03	2.12	**2356.13**	7.93	**2348.21**
LG48	**2359.50**	0.01	1.61	**2357.89**	7.91	**2349.97**
LG49	**2329.57**	0.04	1.39	**2328.19**	7.83	**2320.36**

LGB Traverse 1993/94						
Site	**h sleeve/join (m)** (GLOBK)	**σh (m)** (GLOBK)	**join-surface (m)**	**h surface (m)**	**N (m)**	**H surface (m)**
LG50	**2370.69**	0.01	1.85	**2368.83**	7.75	**2361.09**
LG51	**2312.17**	0.01	1.58	**2310.59**	7.92	**2302.67**
LG52	**2341.52**	0.01	1.62	**2339.90**	8.65	**2331.25**
LG53	**2475.27**	0.00	1.91	**2473.36**	9.42	**2463.94**
LG54	**2493.15**	0.01	1.75	**2491.41**	9.81	**2481.60**
LG55	**2480.23**	0.01	2.22	**2478.01**	10.36	**2467.65**
LG56	**2488.23**	0.01	1.86	**2486.37**	11.38	**2475.00**
LG57	**2566.32**	0.01	1.80	**2564.52**	13.28	**2551.23**
LG58	**2606.24**	0.01	1.30	**2604.94**	14.30	**2590.64**
LG59	**2549.17**	0.00	1.48	**2547.68**	15.18	**2532.50**
LG60	**2594.31**	0.01	2.14	**2592.17**	15.11	**2577.06**
LG61	**2524.94**	0.01	2.03	**2522.91**	15.56	**2507.35**
LG62	**2482.83**	0.01	1.65	**2481.18**	16.15	**2465.03**
LG63	**2438.57**	0.01	1.40	**2437.17**	16.21	**2420.95**
LG64	**2366.44**	0.01	1.40	**2365.05**	15.97	**2349.08**
LG65	**2341.08**	0.01	1.72	**2339.36**	15.95	**2323.41**
LG66	**2229.98**	0.01	1.36	**2228.62**	16.13	**2212.49**
LG67	**2151.66**	0.01	1.20	**2150.46**	16.33	**2134.14**
LG68	**2012.88**	0.00	1.28	**2011.60**	16.40	**1995.20**
LG69	**1871.21**	0.01	1.91	**1869.30**	16.40	**1852.90**
LG70	**1668.91**	0.01	1.90	**1667.01**	16.44	**1650.57**
LG71	**1405.91**	0.01	1.68	**1404.23**	16.58	**1387.65**
LG72	**1056.90**	0.01	1.70	**1055.20**	16.78	**1038.42**

Table B.7 - Calculated Slopes Between the LGB Traverse and Offset Traverse Lines for the Western LGB.

Slope	Magnitude (m/km)	Azimuth (°)	Triangle
S2	4	17	LG28 OS06 LG27
S3	4	14	OS06 OS07 LG27
S4	4	20	LG29 OS06 LG28
S5	3	6	LG30 OS05 LG29
S6	4	18	LG31 OS04 LG30
S7	4	37	LG32 OS03 LG31
S8	4	15	LG33 OS02 LG32
S9	3	10	LG34 OS01 LG33
S10	3	7	OS01 OS02 LG33
S11	3	11	LG35 OS01 LG34
S12	4	19	LG32 OS02 OS03
S13	4	37	LG31 OS03 OS04
S14	4	14	LG30 OS04 OS05
S15	3	13	LG29 OS05 OS06
S17	3	15	LG24 LG25 OS08
S19	4	16	LG26 OS07 OS08
S20	5	46	LG22 LG23 OS09
S21	5	43	LG23 LG24 OS09
S22	4	21	LG24 OS08 OS09
S23	5	47	LG22 OS09 OS10
S24	5	110	LG21 LG22 OS11
S26	7	118	LG20 LG21 OS12
S28	8	108	LG20 OS12 OS15
S29	7	131	OS16 LG20 OS15
S30	7	140	OS16 OS17 LG20
S33	7	133	LG18 LG19 OS18
S35	6	129	LG16 LG17 W030
S37	6	125	W125 LG16 W030
S38	6	117	LG13 LG14 W125
S41	5	134	LG10 LG11 W210
S42	5	134	LG11 LG13 W210
S44	5	142	W230 W270 LG10
S46	7	143	W310 LG08 LG09
S48	3	39	LG07 W310 W350
S49	2	7	LG03 LG04 W380
S50	2	7	LG04 LG05 W380
S52	3	39	LG07 W350 W380

Table B.8 - Comparison of Surface Height (H) Results for the LGB Traverse IMS: this study (RH) vs Kiernan (2001) (RK). (Note: 1990/91 height results are given for sites LG00 to LG35 in Kiernan (2001), therefore the 1990/91 results from this study are also presented for these sites - grey text)

Site	Surface H (m)		
	RH	RK	Diff
LG00	1829.45	1829.4	0.05
LG01	1994.22	1994.8	-0.58
LG02^	2176.43	2179.8	-3.37
LG03^	2324.66	2328.1	-3.44
LG04	2496.71	2496.1	0.61
LG05^	2625.27	2628.5	-3.23
LG06^	2609.83	2612.5	-2.67
LG07	2578.50	2576.2	2.30
LG08^	2574.76	2574.8	-0.04
LG09^	2611.50	2610.0	1.50
LG10	2618.63	2618.2	0.43
LG11^	2585.20	2582.0	3.20
LG12^	2506.50	2503.8	2.70
LG13	2559.29	2555.5	3.79
LG14^	2613.92	2612.0	1.92
LG15^	2698.16	2696.3	1.86
LG16	2692.04	2689.3	2.74
LG17	2734.42	2732.7	1.72
LG18	2728.77	2726.8	1.97
LG19			
LG20	2741.42	2740.9	0.52
LG21	2709.13	2703.3	5.83
LG22	2663.54	2660.8	2.74
LG23	2682.52	2680.1	2.42
LG24	2699.53	2703.2	-3.67
LG25	2772.05	2771.1	0.95
LG26			
LG27			
LG28			
LG29	2832.89	2832.3	0.59
LG30	2843.85	2841.8	2.05
LG31	2746.13	2745.7	0.43
LG32	2587.61	2585.0	2.61
LG33	2511.08	2507.9	3.18
LG34			
LG35			
LG36	2252.76	2250.4	2.36

Site	Surface H (m)		
	RH	RK	Diff
LG37	2354.43	2350.2	4.23
LG38	2351.45	2346.1	5.35
LG39	2263.85	2259.1	4.75
LG40	2168.79	2164.6	4.19
LG41	2218.31	2213	5.31
LG42	2226.37	2221.8	4.57
LG43	2249.60	2245	4.60
LG44	2292.30	2287.9	4.40
LG45	2340.43	2336	4.43
LG46	2353.96	2349.6	4.36
LG47	2348.24	2344.1	4.14
LG48	2349.48	2345.5	3.98
LG49	2320.00	2315.9	4.10
LG50	2360.76	2356.5	4.26
LG51	2302.30	2299.3	3.00
LG52	2331.00	2329.1	1.90
LG53	2464.03	2463.4	0.63
LG54	2481.68	2481	0.68
LG55	2467.66	2467.6	0.06
LG56	2474.94	2476	-1.06
LG57	2551.09	2553.8	-2.71
LG58	2590.53	2594.2	-3.67
LG59	2532.59	2536.7	-4.11
LG60	2577.10	2580.5	-3.40
LG61	2507.44	2510.9	-3.46
LG62	2464.75	2468.3	-3.55
LG63	2420.68	2423.7	-3.02
LG64	2348.97	2351.4	-2.43
LG65	2323.50	2325.3	-1.80
LG66	2212.30	2213.7	-1.40
LG67	2133.98	2135.1	-1.12
LG68	1994.85	1996.2	-1.35
LG69	1853.08	1853.8	-0.72
LG70	1650.65	1651	-0.35
LG71	1387.37	1387.4	-0.03
LG72	1037.84	1037.7	0.14

grey text = results from 1990/91 traverse
black text = results from 1994/95 traverse

APPENDIX - C

C.1 GAMIT Command File Used For Processing The GPS Data For The PW Case Study At Permanent Antarctic Sites

```
Session Table for regional + global analysis
------------------------------------
      Analysis
Processing Agency = TAS          ;
Station Number = *               ;
Station Constraint = Y           ;
Satellite Number =  *            ;
Satellite Constraint = Y         ;
all a    e    i    n    w    M    rad1 rad2 rad3 rad4 rad5 rad6 rad7 rad8 rad9
  0.01 0.01 0.01 0.01 0.01 0.01 0.01 0.01 .01  .01  .01  .01  .01  .01  .01
## These values are tight and are acceptable for IGS orbits (post 1994)
Type of Analysis = 0-ITER        ;
Data Status = RAW                ;
Choice of Observable = LC_ONLY   ;
Choice of Experiment = RELAX.    ;
      Atmospherics
Zenith Delay Estimation = YES    ;
Number Zen = 13                  ;
Zenith Constraints = 0.50        ;
Zenith Model = PWL               ;
Zenith Variation = 0.02 100.     ;
Atmospheric gradients = NO       ;
Gradient Constraints = 0.01      ;
       Orbit Parameters
Initial ARC = YES                ;
Final ARC = NO                   ;
Yaw Model = YES                  ;
Delete eclipse data = POST       ;
Update T/L files = L_ONLY        ;
Inertial frame = J2000           ;
Radiation Model for ARC = BERNE  ;
      Cleaning
AUTCLN Command File = autcln.cmd ;
AUTCLN Postfit = NO              ;
Use N-file = NO                  ;
Delete AUTCLN input C-files = YES ;
      Modelling
Earth Rotation = 7  (pole, ut1 and ray model)      ;
Tide Model = 3      (earth and frequency-dependant);
Antenna Model = ELEVATION   (IGS model)                ;
      Solving
Estimate EOP = 15   (wobble, ut1, wobble rate and ut1 rate);
Wobble Con = 0.01 0.01           ;
UT1 Con = 0.00001 0.01           ;
Decimation Factor = 1            ;
```

C.2 Pressure Correction (Hypsometric Equation)

In order to convert from GPS TZD to PW values, it is necessary to have a measure of the surface pressure at the GPS antenna site. In many cases, pressure may not be measured directly at the GPS antenna and therefore, it must be corrected relative to the difference in height between the barometer and antenna before PW conversion. This correction is performed using the hypsometric equation (C.1).

Pressure Correction (Stull, 1995)

$$p_{GPS} = p_s \cdot \exp\left(\frac{-a\Delta H}{T_s}\right) \qquad \text{(C.1)}$$

where:

p_s = pressure at sensor (hPa)

p_{GPS} = pressure at GPS antenna (hPa)

$$a = \frac{g}{R_d} = \frac{9.81}{287.053} = 0.0342 \ (Km^{-1})$$

g = gravitational acceleration

R_d = gas constant for dry air

$\Delta H = \mathrm{H_{GPS}} - \mathrm{H_{sensor}} \ (m)$

T_s = surface temperature (K)

Equation (C.2) gives an expression for the standard deviation of GPS pressure (derived from equation (C.1)). The accompanying examples ({1} and {2}) indicate that uncertainty in the measured pressure at the meteorological sensor will translate into an uncertainty of almost the same magnitude in the determination of pressure at the GPS antenna. It can also be seen from the examples that uncertainty in the height difference (ΔH) between the barometer and GPS antenna may be significant in terms of the final precision of the GPS pressure if ΔH has a value of more than a few metres. The significance of the uncertainty in ΔH is dependant on the pressure value at the site (refer to (C.2) and examples {1} and {2}). For example, an uncertainty in ΔH of approximately 1-3 m will introduce a 0.12 - 0.37 hPa uncertainty in the

calculated pressure for sites with high pressure values (e.g., 980 hPa), while the same ΔH uncertainty will contribute 0.09 - 0.26 hPa to the pressure uncertainty at sites with lower pressure readings (e.g., 700 hPa). From equation (C.2) it can be seen that errors in the temperature measurements are generally do not have a significant influence on the uncertainty in the GPS pressure calculation.

Uncertainty in Corrected Pressure

$$\sigma_{P_{GPS}} = \sqrt{\left(\exp\left(\frac{-a\Delta H}{T_k}\right)\right)^2 \sigma_{P_s}^2 + \left(\left(\frac{-ap_s}{T_k}\right)\exp\left(\frac{-a\Delta H}{T_k}\right)\right)^2 \sigma_{\Delta H}^2 + \left(\left(\frac{a\Delta H p_s}{T_k^2}\right)\exp\left(\frac{-a\Delta H}{T_k}\right)\right)^2 \sigma_{T_k}^2} \qquad \text{(C.2)}$$

Example {1}

$$\sigma_{P_{GPS}} = \sqrt{0.9975\sigma_{P_s}^2 + 0.01502\sigma_{\Delta H}^2 + 0.00002\sigma_{T_k}^2}$$

$for\ p_s = 980$ hPa

$\Delta H = 10$ m

$T_k = 273.16K$

$a = 0.0342$ Km^{-1}

Example {2}

$$\sigma_{P_{GPS}} = \sqrt{0.9975\sigma_{P_s}^2 + 0.00766\sigma_{\Delta H}^2 + 0.00001\sigma_{T_k}^2}$$

$for\ p_s = 700$ hPa

$\Delta H = 10$ m

$T_k = 273.16K$

$a = 0.0342$ Km^{-1}

C.3 GPS TZD to PW Conversion Program

```
%M-file to calculate wet delay from GAMIT q-file values
%
%Requires setup file with strict formatting
%Setup file contains links to: gps_wv file, met_data file,
geodetic_coords file and pressure_sensor_ht file
%
% gps_wv format:            [delay sigma]
% surface met data format: [doy press temp]
% coordinates format:       [site lat lon ht] <- decimal degrees, ht
km
% sensor ht format:         [site ht_diff] <- gps-barometer (usually
+ve)
%%%%%%%%%%%%%%%%%%%%%%%%%%%%%%%%%%%%%%%%%%%%%%%%%%%%%%%%%%%%%%%%%%%
clear infile outfile lg yr doy gps met llh pht process

% Enter setup details

infile = input('Enter name of Setup file:    ','s');
outfile = input('Enter name of Output file:    ','s');
limit = input('Enter cut-off sigma for input TZD (m):   ');

[lg,yr,doy,gps,met,llh,pht] = textread(infile,'%d %d %d %s %s %s
%s', 'headerlines',1,'commentstyle','matlab');

gps = char(gps);
met = char(met);
llh = char(llh);
pht = char(pht);

% Enter Header of Output file

fid = fopen(outfile,'a+');

fprintf(fid, ' [input file => %s  ]\n [processed  => %s ]\n',
infile, datestr(now));
fprintf(fid,'\n-----------------------------------------');
fprintf(fid, '\n\nPrecipitable Water Results Using TZD Values From
GAMIT Processing  \n');
fprintf(fid,'\n-----------------------------------------');
fprintf(fid,'\n\nCut-off GAMIT sigma => %6.4f\n\n',limit);
fprintf(fid, '\ncol 1  Site No');
fprintf(fid, '\ncol 2  Year');
fprintf(fid, '\ncol 3  Day of Year & Processing Option');
fprintf(fid, '\ncol 4  Total Zenith Delay (TZD) in mm from GAMIT');
fprintf(fid, '\ncol 5  TZD (1 sigma) uncertainty in mm from GAMIT');
fprintf(fid, '\ncol 6  Hydrostatic zenith delay (HZD) in mm ');
fprintf(fid, '\ncol 7  HZD (1 sigma) uncertainty in mm (assumed
pressure uncertainty of 0.3hPa ');
fprintf(fid, '\ncol 8  Wet Zenith Delay (WZD) in mm (TZD - HZD) ');
fprintf(fid, '\ncol 9  WZD (1 sigma) uncertainty in mm');
fprintf(fid, '\ncol 10 Precipitable Water (PW) in mm');
fprintf(fid, '\ncol 11 PW (1 sigma) uncertainty in mm ');
fprintf(fid, '\ncol 12 Pressure at GPS (hPa)');
fprintf(fid, '\ncol 13 Ground temperature at met station (degC)');
fprintf(fid, '\ncol 14 GPS Latitude (geodetic, decimal degrees)');
fprintf(fid, '\ncol 15 GPS Height (km)');
```

```
fprintf(fid,'----------------------------------------\n\n');


%%%%%%%%%%%%%%%%%%%%%%%%%%%%%%%%%%%%%%%%%%%%%%%%%%%%%%%%%%%%%%%%%%%%%%%%%%%%
% Load data files and variables

[m,n] = size(lg);
row = 1;

for row = 1:m;

clear data data2 aws coords dh site date1 date2

data = load(gps(row,:));
aws = load(met(row,:));
coords = load(llh(row,:));
dh = load(pht(row,:));

site = lg(row,:);
date1 = yr(row,:);
date2 = doy(row,:);

option = gps(row,16:19);

% Remove bad data

[m,n] = size(data);
i = 1;
j = 1;

for i = 1:m
 x = data(i,2);
  if x <= limit
    data2(j,1) = data(i,1);
    data2(j,2) = data(i,2);
    j = j + 1;
  end
 end

% Create daily average tzd and precision matrices

clear avzd saaszd precision

yep = exist('data2','var');

 if yep == 1
  i = 1;
  prec = 0;
  nobs = size(data2);
  saaszd = mean(data2(:,1));
   for i = 1:nobs(1,1)
     prec = prec + data2(i,2)^2;
   end
  precision = (sqrt(prec))/nobs(1,1);
  else
  nobs = 0;
  saaszd = 0;
  precision = 0;
 end

% Input site coordinates

clear lat phi H m n w x
```

```
 [m,n] = size(coords);
 x = 1;
 for x = 1:m
  w = coords(x,1);
   if w == site;
    lat = coords(x,2);
    phi = lat*pi/180;
    H = coords(x,4);
   end
 end

% Find pressure and temp for given doy

clear d p temp

[m,n] = size(aws);
x = 1;

if site < 73
  for x = 1:m
   d = aws(x,1);
   s = aws(x,2);
   if d == date2 & s == site
    p = aws(x,3);
    temp = aws(x,4);
    break
   end
  end
else
  for x = 1:m
   d = aws(x,1);
   if d == date2
    p = aws(x,2);
    temp = aws(x,3);
    break
   end
  end
end

% Adjust Pressure for Height Diff

clear Tk x p2

a = 0.0342;
Tk = temp + 273.16;

[m,n] = size(dh);
x = 1;

for x = 1:m
  w = dh(x,1);
  if w == site
    p2 = p * exp(-a*dh(x,2)/Tk);
    break
  else
    p2 = p;
  end
end


% Calculate Wet Delay and Precision (1-sigma) assuming a 0.3 hPa
error in pressure.
```

```
clear ffun dryzd wetzd

ffun = (1 - 0.266E-02 * cos(2 * phi) - 0.28E-03 * H);
dryzd = 0.2277E-02 * p2/ffun;
dzdprecision = 0.002277*0.3;

wetzd = saaszd - dryzd;
wzdprecision = sqrt(precision^2 + dzdprecision^2);

% Calculate Tm and K

clear Tm Ts K

if temp > 30
 K = 1/6.5;
else
 Ts = temp + 273.16;
 Tm = 70.2 +0.72*Ts;
 K = 10E6/((3.739E5/Tm + 22.1)*46150);
%NOTE: k values from Bevis et al(1994)
 kprec = (2/100)*K;
%NOTE: k precision 2% from Bevis et al(1992)
end

% Calculate GPS Precipitable Water (mm)

clear PW pwprecision

PW = 1000*(K * wetzd);
PWprecision = 1000*sqrt(K^2*wzdprecision^2 + wetzd^2*kprec^2);
% NOTE: *1000 to convert to mm

% Write output matrix and text file

clear out
xxx = 1;

out(xxx,1) = site;
out(xxx,2) = date1;
out(xxx,3) = date2;
out(xxx,4) = saaszd*1000;
out(xxx,5) = precision*1000;
out(xxx,6) = dryzd*1000;
out(xxx,7) = dzdprecision*1000;
out(xxx,8) = wetzd*1000;
out(xxx,9) = wzdprecision*1000;
out(xxx,10) = PW;
out(xxx,11) = PWprecision;
out(xxx,12) = p2;
out(xxx,13) = temp;
out(xxx,14) = lat;
out(xxx,15) = H;

fprintf(fid, '%3.0f 19%-2.0f %3.0f', out(1,1:3));
fprintf(fid, '%c',option);
fprintf(fid, ' tzd:%7.4f +/- %6.4f dzd:%7.4f +/- %6.4f wzd:%7.4f +/-
%6.4f PW:%7.4f +/- %6.4f %5.2f %4.1f %4.2f %4.2f\n', out(1,4:15));

end  %for row = 1:m

fclose(fid);
```

C.4 Winter 1998 Coordinate Results (see Chapter 7)

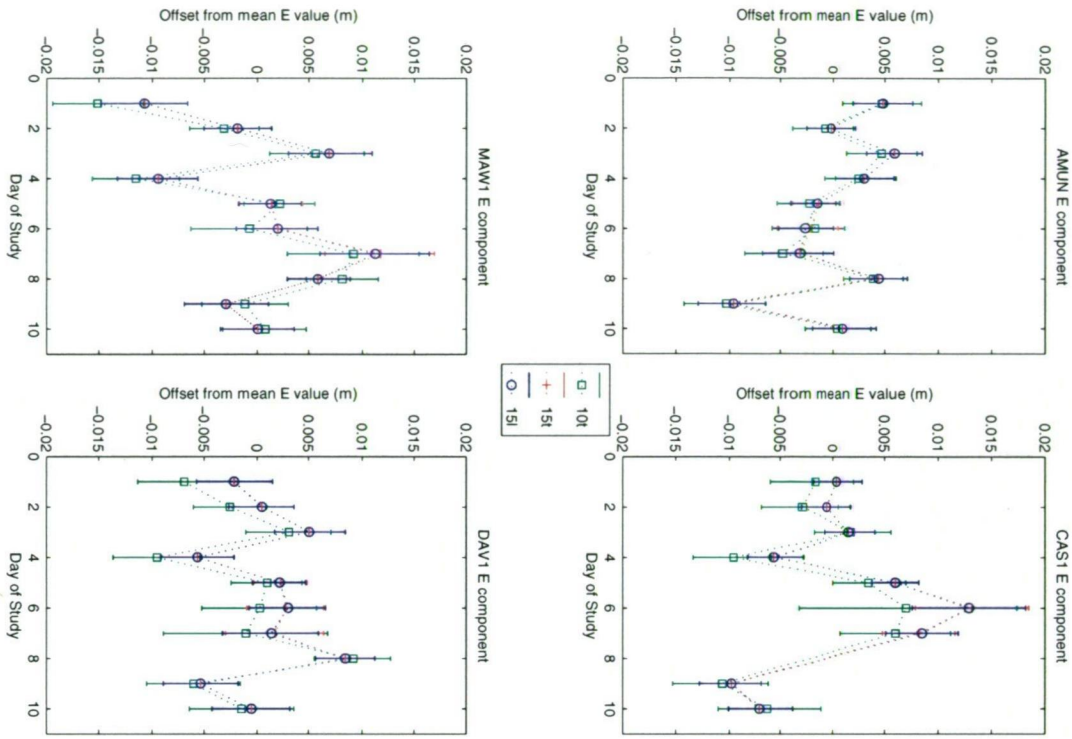

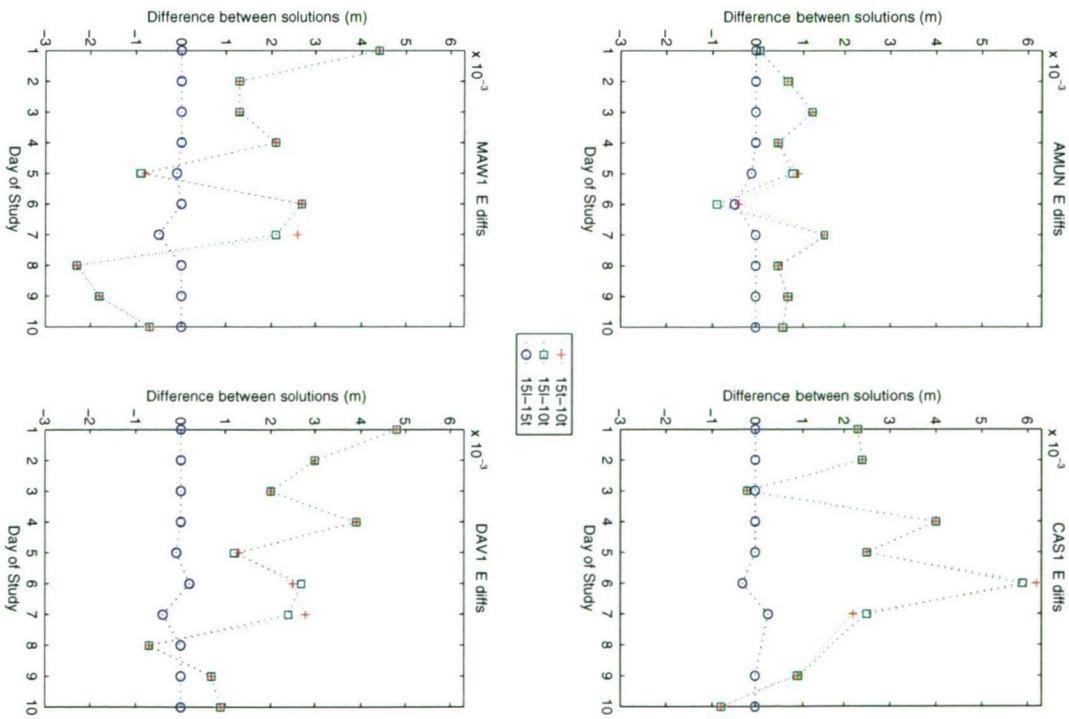

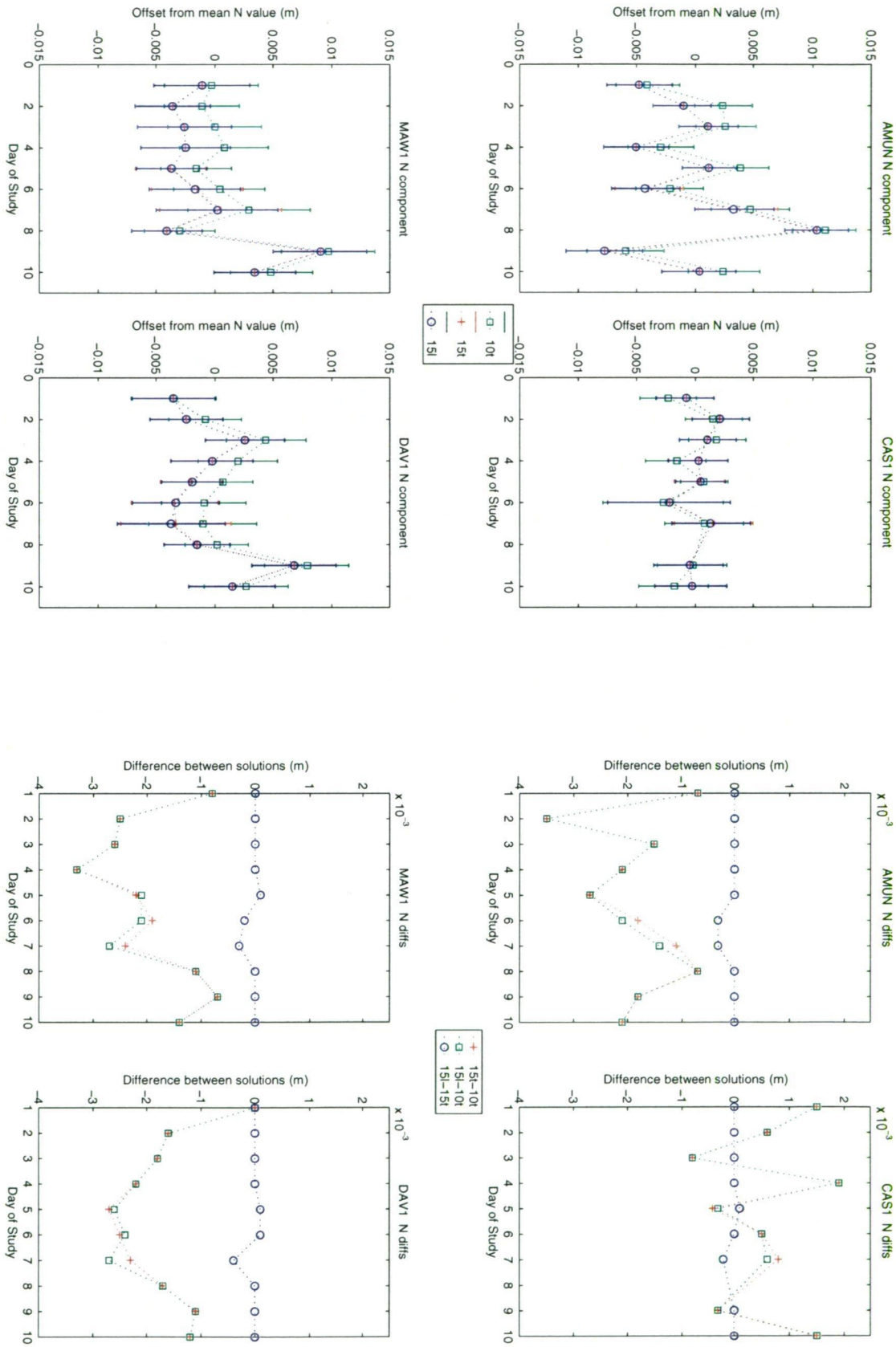
AMUN N component
CAS1 N component
MAW1 N component
DAV1 N component
Offset from mean N value (m)
Day of Study
10t
15t
15l
AMUN N diffs
CAS1 N diffs
MAW1 N diffs
DAV1 N diffs
Difference between solutions (m)
15t–10t
15l–10t
15l–15t
x 10^-3

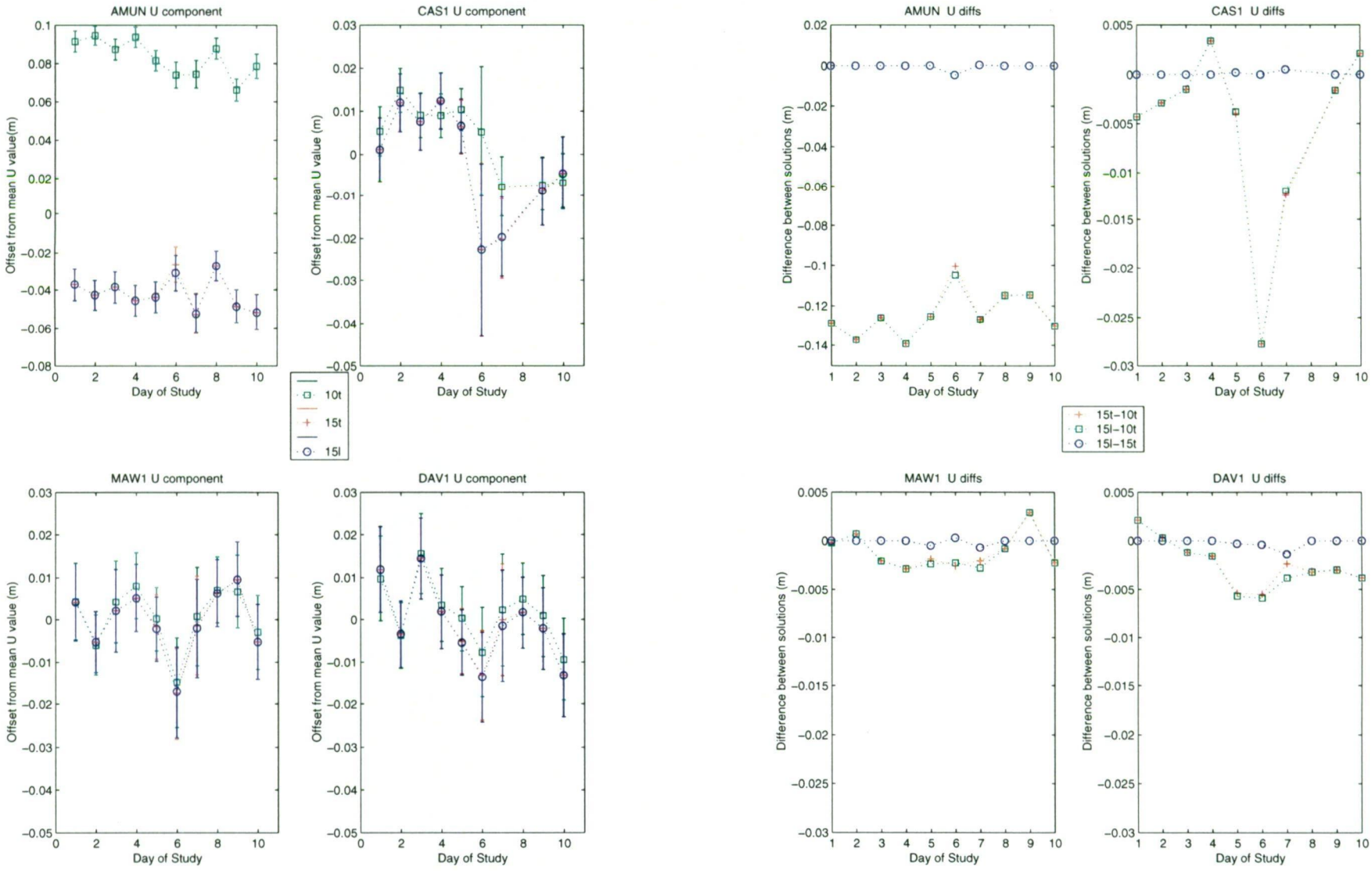
AMUN U component
CAS1 U component
MAW1 U component
DAV1 U component
Offset from mean U value(m)
Offset from mean U value (m)
Day of Study
10t
15t
15l
AMUN U diffs
CAS1 U diffs
MAW1 U diffs
DAV1 U diffs
Difference between solutions (m)
15t−10t
15l−10t
15l−15t

C.5 Summer 1999 Coordinate Results (see Chapter 7)

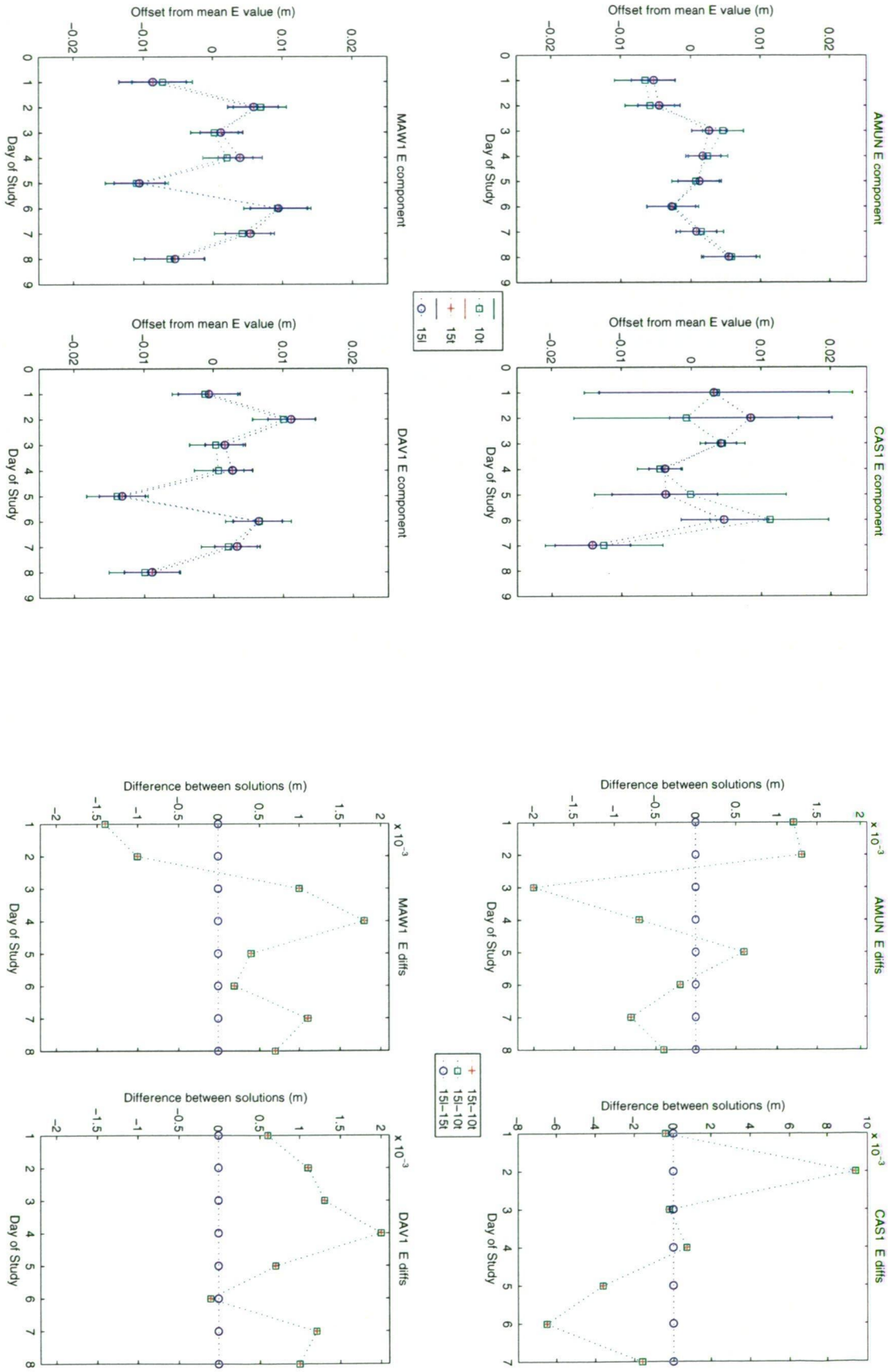

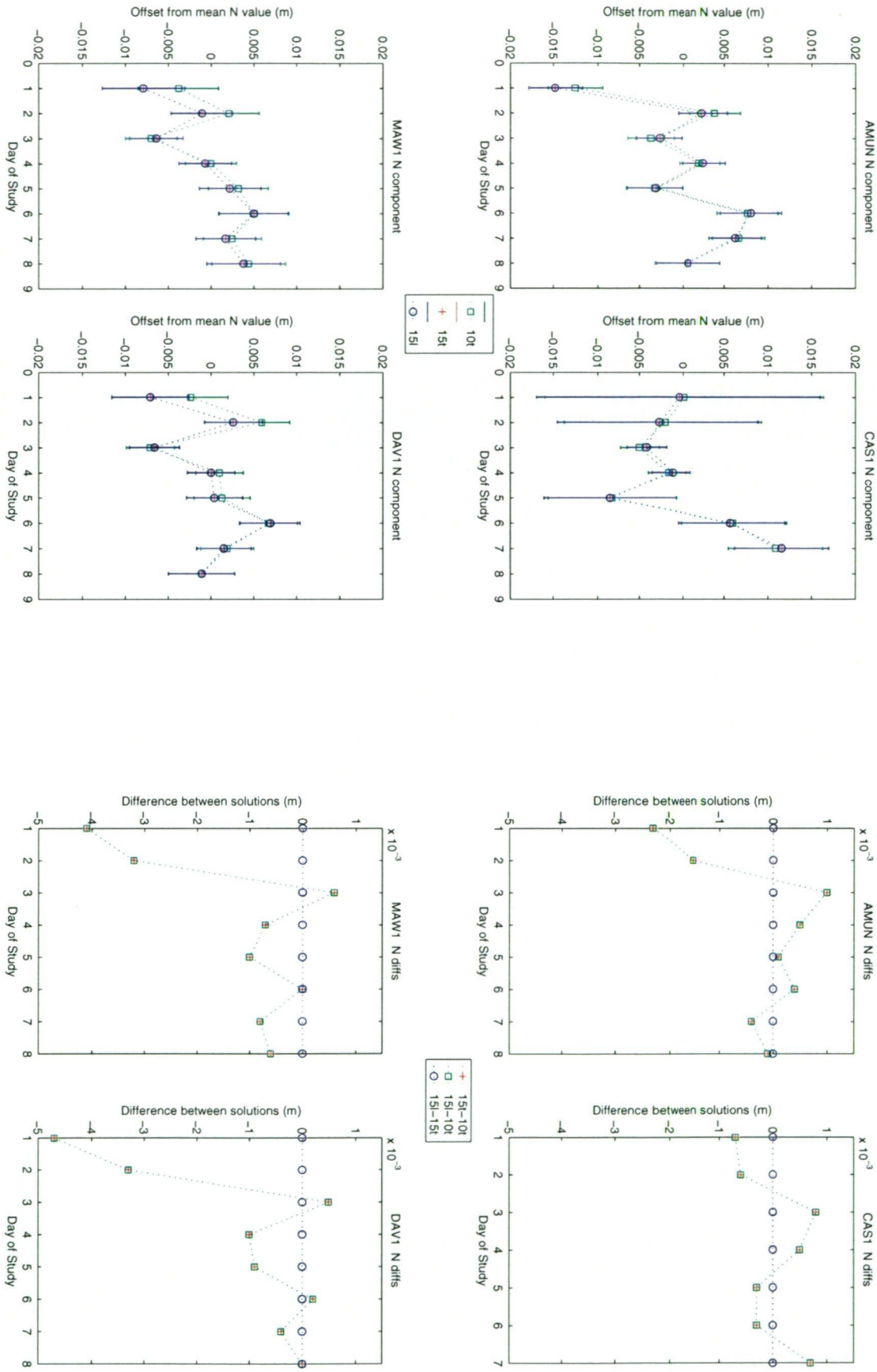
AMUN N component
CAS1 N component
MAW1 N component
DAV1 N component
Offset from mean N value (m)
Day of Study
10t
15t
15l
AMUN N diffs
CAS1 N diffs
MAW1 N diffs
DAV1 N diffs
Difference between solutions (m)
x 10^-3
15t−10t
15l−10t
15l−15t

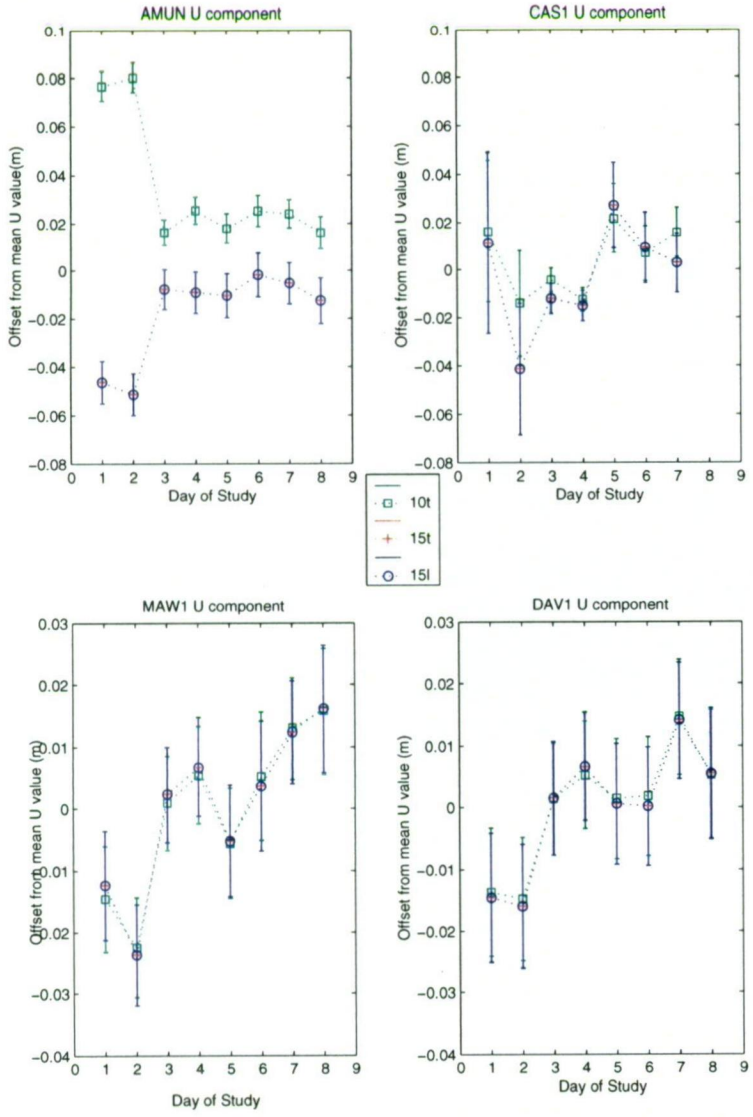
AMUN U component
CAS1 U component
MAW1 U component
DAV1 U component
Offset from mean U value(m)
Offset from mean U value (m)
Day of Study
10t
15t
15l

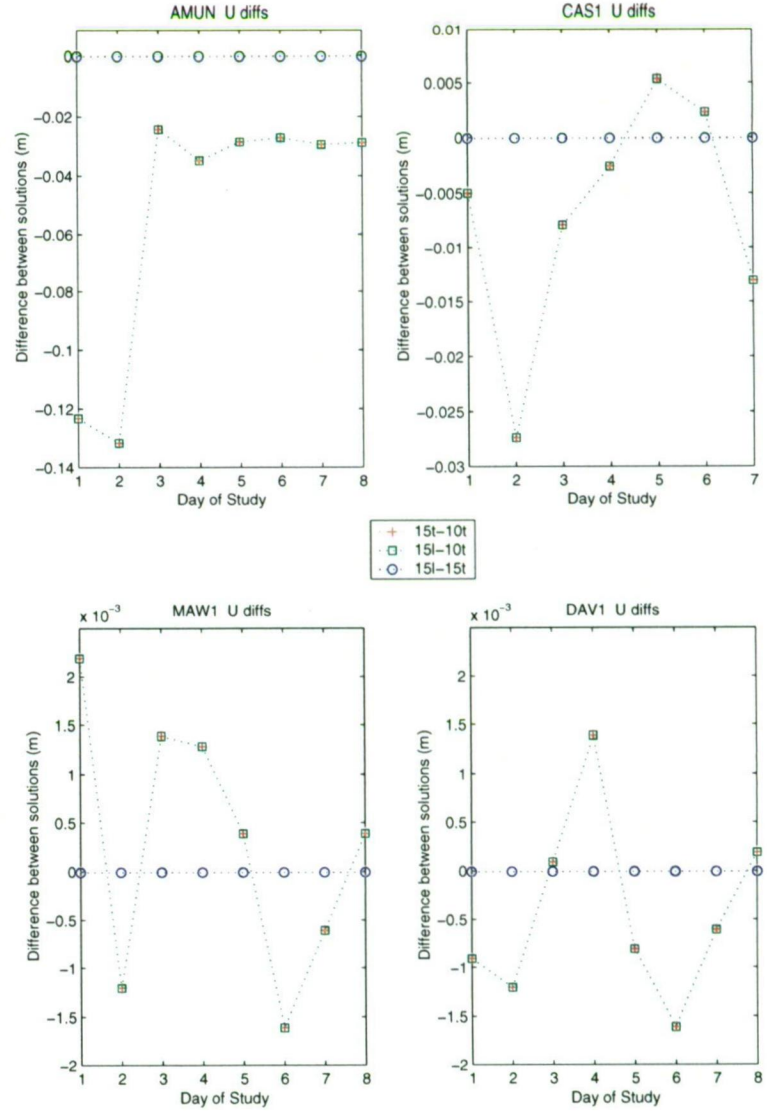
AMUN U diffs
CAS1 U diffs
MAW1 U diffs
DAV1 U diffs
Difference between solutions (m)
Day of Study
15t–10t
15l–10t
15l–15t

APPENDIX - D

D.1 Radiosonde Analysis

To define the characteristics of regions above and below the line representing the least-squares fit to the 700 hPa versus surface PW data (see section 8.3.2.1), atmospheric profile of eight randomly selected radiosonde soundings were plotted (T vs P diagrams). This appendix gives more detailed information regarding the T vs P diagrams and analysis of the information they contain.

The selected soundings represent each of the three major regions of the 700 hPa vs surface PW plot (i.e. below the line, on the line and above the line) and provide a range of examples within each region. The values and plot locations of each of the example soundings are given in Figure D.1 and Table D.1 while Table D.2 contains a summary description of each T vs P diagram.

Table D.1 - Radiosonde Sounding Case Studies

Sounding	Year-Day [Season]	Surface PW (mm)	700 hPa PW (mm)	Characteristic
A (★)	1999-323 [Summer]	2.91	0.31	Excess Surface PW
B (▼)	1996-242 [Winter]	3.24	0.60	On Model
C (▲)	1995-001 [Summer]	4.38	0.37	Excess Surface PW
D (■)	1993-186 [Winter]	1.90	0.51	On Model
E (●)	1999-060 [Summer]	5.49	1.15	On Model
F (◆)	1995-130 [Winter]	2.55	1.14	Excess 700 hPa PW
G (▶)	1995-321 [Summer]	6.48	1.04	Excess Surface PW
H (✸)	1998-323 [Summer]	5.55	1.53	Excess 700 hPa PW

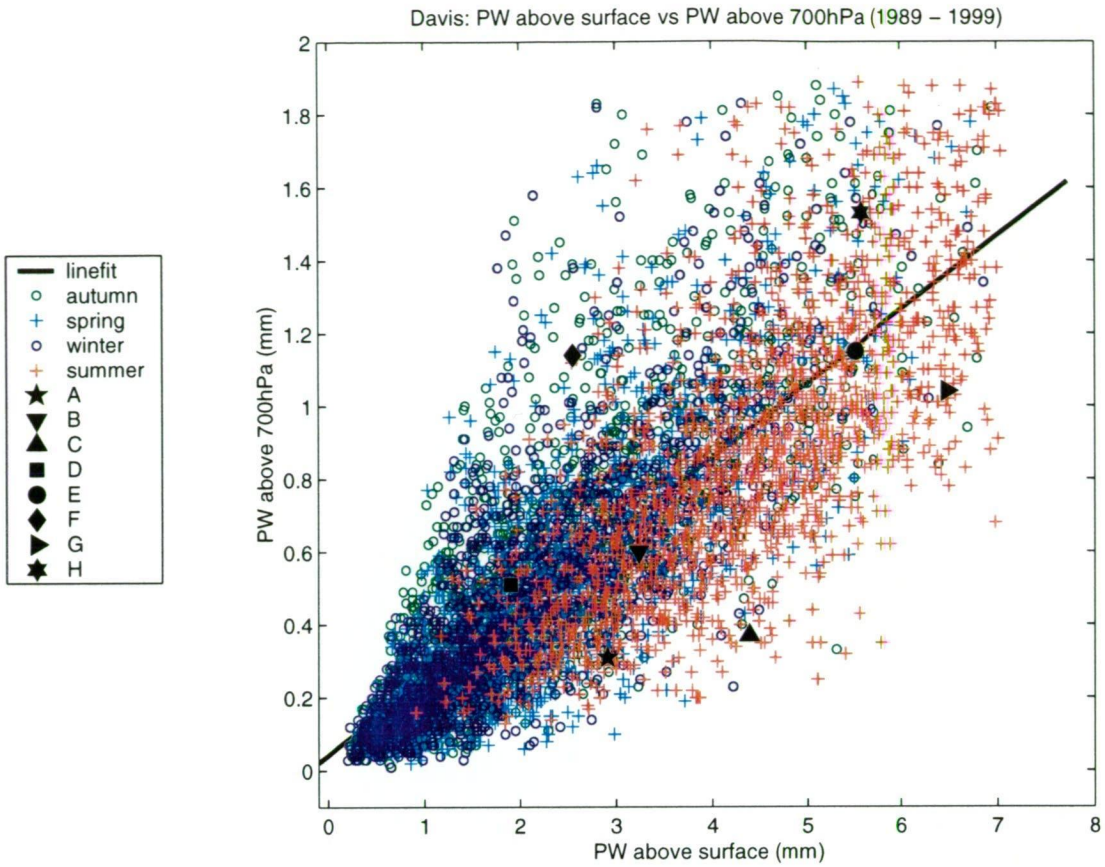

Figure D.1 - Davis surface vs 700 hPa PW plot showing location of the soundings in Table D.1

Days A, C and G were selected as typical summer observations with high moisture in the lower atmosphere. In the T vs P plots, A and C show descending, dry upper air which is depleted of PW while G has a similar plot but indicates a deeper, moist lower layer reflected in the higher surface PW value. Soundings on or very close to the model were represented by days B, D and E. The T vs P diagrams on these days indicate relatively stable, well mixed profiles through the atmosphere which therefore should represent the average atmospheric structure at Davis and Mawson. The soundings on days F and H were selected for their very high 700 hPa PW values. The atmospheric profiles on these two days indicate excess moisture in the upper layers due to frontal inversions, with cooler, drier air in the surface layers below. Soundings with PW values close to the line of best fit or with excess PW in the upper atmosphere occur during both winter and summer while excess surface PW is observed to be a mostly summer phenomenon.

Table D.2 - Descriptions of Soundings depicted in the T vs P plots

HIGH SURFACE MOISTURE (BELOW LINE)
A - has subsiding dry warm air above ~750 hPa (inversion at this point) and colder, moist air in the lower layers. Temperatures follow a saturated adiabat indicating a frontal air mass. Almost all of the moisture is below 700 and is likely to be precipitated if the air column rises or cools.
C - is a dry air column from top to bottom. Slight surface inversion due to cooling indicates calm air conditions with little mixing. A slight subsidence inversion above 700 hPa indicates sinking air. No precipitation likely.
G - shows warm, moist air in the lower layers with little mixing. At around 750 hPa there is a small temperature inversion but some moisture is observed up to approximately 620 hPa. Above this level there is little moisture.
STABLE MOISTURE PROFILE (NEAR LINE)
B - is a dry air column from top to bottom. Slight surface inversion due to cooling indicates calm air conditions with little mixing. A slight subsidence inversion above 700 hPa indicates sinking air. No precipitation likely.
D - has a very strong surface cooling effect and generally quite cold temperatures. The air in the column is well mixed and does not appear to hold much moisture.
E - here we have a turbulent mixing layer between the surface and approximately 800 hPa. Above this mixed layer the moisture content of the air layers is more stable and appears to be reasonably saturated.
HIGH UPPER LEVEL MOISTURE (ABOVE LINE)
F - has cold dry air in the lower layers with a deep frontal inversion at approximately 850 hPa. Above approximately 800 hPa the air is warmer, quite moist and stable.
H - shows a frontal inversion below 700 hPa with warm dry air at the surface. Above 700 hPa the air is quite stable and moist.

D.2 Logbook Meteorological Data From The 1994/95 LGB Traverse

LGB Traverse 1994/95

Weather Information From Logbook

(D = Digiquartz Barometer A = Analog Barometer)

Site	DOY	UT	Temp (Dry)	Temp (Wet)	Press (D)	Press (A)	Cloud	Other
72	317	0.00	-10.8		860.5		8/8 stratus	5m drift
71		19.30	-19.6		830.0		clear	
70	318	21.05	-22.4	-21.9	801.2	799.6	-	
70	319	3.00					clear	strong drift
70		11.15	-14.0		802.0		clear	
70	321	4.30	-16.4	-16.6	806.4		clear	strong drift
70	323	4.00	-18.7	-18.4	800.3		clear	
70		11.00					2/8 cirro stratus	
70	324	7.55	-14.7	-15.1	804.8	803.4	2/8 cirrus/cirro stratus	
69		14.00	-20.2		783.8		7/8 alt.strat	
69	325	7.35	-15.6	-15.9	784.9	782.6	4/8 strat.cum	
68		18.00	-25.2	-24.4	768.6	765.7	clear	
68	326	9.00	-15.7	-16.2	765.3	762.7	clear	
67		17.30	-24.1	-23.4	749.8	747.0	clear	
67	327	5.00	-19.5	-19.5	748.2	745.4	1/8 cir.strat	
66		17.20	-24.3	-23.7	740.2	737.2	-	strong drift
66	328	8.30	-18.7	-18.1	738.6	734.6	8/8 cir.strat	
65		16.45	-24.6	-23.9	728.5		4/8 cir.strat	
65	329	17.00	-25.1	-24.5	728.2		1/8 cir.strat	drift
65	330	6.45	-21.2	-21.2	728.4		" " " "	
64		20.40	-31.1	-30.5	725.3	721.7	" " " "	
64	331	4.00					8/8 cir.strat	
64		6.45	-24.7	-23.0	725.6	722.6	3/8 cir.strat	
64		10.20	-22.8	-20.9	726.4	722.8	-	light snow
63		18.05	-30.7	-28.9	720.3	717.0	clear	
63		22.00	-30.8		721.2		6/8 cir.strat	
63	332	2.30	-27.1		721.0		clear	
62		17.00	-25.7	-26.2	717.5	714.2	6/8 alt.strat	
62	333	6.15	-22.0		716.6		clear	
61		17.45	-28.9	-28.4	710.7	707.2	clear	
61	334	3.00	-26.5		710.5		clear	
60		17.10	-27.3		708.2	704.5	6/8 cir.strat	
60	335	6.00	-22.4		710.3		3/8 cir.strat	
59		17.30	-24.8	-23.9	715.4	711.8	4/8 cir.strat	
59	336	7.00	-20.7		715.1		6/8 cir.strat	
59		8.50	-19.9		715.5		5/8.	

59		10.30					-	light snow/ice
59		17.30	-24.6		716.8		7/8 alt.strat	
59	337	7.00	-19.2		719.6		8/8 cir.strat	light snowfall overnight
59		12.15	-18.5		721.3		" " " "	
59		23.40	-21.4		723.5		" " " "	
59	338	8.00	-17.0		724.9		1/8 cir.strat	
59		12.55	-17.5		725.5		" " " "	
59		16.25	-22.3		725.3		8/8 alt.strat	
59		23.15	-24.0		725.0		" " " "	
59	339	8.25	-18.0		723.0		8/8.	
59		15.30	-19.6		720.5		8/8 alt.strat	
59		20.35	-22.0		720.4		" " " "	
59		23.00	-23.1		720.4		6/8.	
59	340	7.30	-18.5		720.2		3/8 cir.strat	
59		10.10	-18.8		720.4		2/8 cir.strat	
58		18.15	-25.9	-24.7	715.1	711.8	clear	
58		23.20	-27.3		714.2		clear	
58	341	6.30	-20.3		712.8		clear	
57		17.30	-23.1	-22.4	714.3	710.6	clear	
57		23.20	-24.8		713.8		clear	
57	342	6.15	-19.3		712.3		1/8 cir.strat	
56		17.40	-21.6	-21.1	717.8		" " " "	
56		23.05	-23.7		716.8		" " " "	
56	343	6.50	-17.6	-17.9	714.5		clear	
55		16.40	-20.3	-20.0	713.7	710.2	clear	
55	344	0.40	-24.8		712.6		clear	
54		16.40	-23.4	-22.8	709.7	706.3	clear	
54		22.00	-27.6		709.7		clear	
54	345	6.30	-22.2		711.3		clear	strong drift
53		16.05	-22.4	-21.8	715.2	711.7	clear	
53	346	7.00	-19.9	-19.9	715.9		1/8 cir.strat	strong drift
53		12.15	-18.1		715.8		-	
53	347	4.45	-21.6		714.9		clear	
53		7.00	-15.6	-15.4	713.4		8/8 cir.strat	strong drift
53		11.20	-13.2		714.8		8/8.	light snow
53		14.30	-14.3		716.0		6/8.	
53		22.00	-20.2		718.0		6/8 cir.strat	
53	348	6.30	-15.0		718.8		8/8 cir.strat	ground drift
53		10.15	-14.1		720.0		" " " "	
53		17.05	-14.3		720.9		8/8 cir.strat	
52		23.25	-17.4	-17.4	733.9	730.8	8/8 cir.strat	
52	349	7.45	-13.5		733.6		1/8 cir.strat	
52		11.15	-12.4		733.6		" " " "	
51		19.00	-19.3	-19.3	737.2	734.0	3/8 cir.strat	
51	350	6.00	-14.6		736.3		2/8 cir.strat	
51		10.00	-12.2		735.6		3/8 cir.strat	

50		16.40	-17.5	-17.8	727.7	724.3	2/8 cirrus	
50	351	6.00	-14.8		722.6		5/8 cir.strat	
50		8.50	-13.5		721.5		" " " "	
49		13.20	-14.1		723.9		" " " "	
48		18.10	-20.6	-20.1	720.2	716.6	2/8 cirrus	
48		22.20	-22.0		720.1		5/8 cirrus	
48	352	7.00	-15.9		720.9		8/8 stratus	
46		17.55	-18.3	-17.4	722.3	718.8	8/8 cir.strat	
46	353	1.20	-20.2		723.9		-	
46		15.30	-17.6		726.2		8/8 cir.strat	snow falling
46		17.30	-18.8		726.5		8/8 cir.strat	
46		20.15	-18.9		727.4		8/8 cir.strat	
46	354	7.00	-18.6		728.5		8/8 cir.strat	
46		11.30	-17.9		728.6		" " " "	
46		15.00	-18.4		728.8		" " " "	
46		18.00	-19.0		729.0		" " " "	
46		22.00	-19.0		729.0		" " " "	
46	355	7.25	-18.0		729.4		" " " "	blowing snow
46		11.45	-17.1		728.7		" " " "	
46		14.50	-16.9		727.5		" " " "	
46	356	9.15	-16.0		726.0		1/8 cir.strat	
46		15.00	-15.7		725.6		clear	
46		23.20	-24.4		726.1		clear	
46	357	8.40	-14.6	-14.7	725.8	721.3	6/8 cir.strat	
45		12.45	-14.6	-14.1	726.0	723.1	7/8 cir.strat	
44		17.50	-18.4	-17.0	730.0	726.5	6/8 cir.strat	
44		20.45	-21.3		729.9		" " " "	
44	358	8.55	-15.5		729.2		" " " "	
44	359	0.25	-19.7		730.2		-	
44		5.30	-16.0		729.2		4/8 cir.strat	
44		11.30	-13.7		728.8		" " " "	
44		22.30	-18.2		733.7		8/8 cir.strat	
44	360	7.15	-14.1		736.8		3/8 cir.strat	
43		13.05	-14.4	-13.4	740.7	738.0	clear	
42		17.45	-18.3	-18.0	742.6	739.7	clear	
42		23.40	-20.9		743.2		clear	
42	361	7.15	-13.1		742.8		clear	
41		12.25	-13.3	-12.6	743.1	740.1	clear	
40		17.00	-18.3	-17.3	747.5	744.3	clear	
40		23.15	-21.4		747.8		1/8 cir.strat	
40	362	7.00	-14.9		748.6		3/8 cir.strat	
39		16.30	-17.0		740.1		clear	
39		21.45	-20.8		740.0		clear	
38	363	15.40	-17.7	-18.1	728.5	725.2	clear	
38		21.35	-23.9		729.7		4/8 alt.strat	
38	364	7.00	-15.8		731.0		1/8 cir.strat	
37		14.15	-16.5	-16.1	730.0	726.9	clear	
37		22.40	-23.4		728.9		clear	
37	365	9.00	-16.5		728.9		clear	
37		12.00	-15.7		728.8		clear	
37		16.40	-20.6		728.3		clear	

37	1	13.20	-16.5		730.1		clear	
37		20.15	-24.1		730.3		clear	
37	2	7.15	-19.6		731.2		clear	
36		20.00	-24.2		736.7		clear	
36		23.25	-25.7		736.2		clear	
36	3	8.00	-17.3		734.5		clear	
35		15.10	-19.1	-19.4	726.9	723.5	clear	
35	4	0.15	-24.7		727.5		clear	
35		7.20	-19.2		728.0		clear	
35		10.15	-17.6		728.6		clear	
35		14.50	-16.4		729.7		clear	
35		18.20	-23.0		730.1		1/8.	
35		21.30	-24.9		730.4		" " " "	
35	5	9.00	-16.9		731.5		8/8.	
35		12.10	-17.9		731.6		8/8 cir.strat	
35		17.30	-19.5		731.8		" " " "	light snow
35	6	8.20	-17.1		732.0		clear	
35		14.30	-17.0		732.4		4/8 cirrus	
35		15.40						heavy snow shower
35	7	8.10	-14.0		735.4		8/8.	light snow
35		16.10	-13.5		736.9		" " " "	light snow
35		22.35	-16.5		739.5		2/8 cir.strat	light snow
35	8	8.00	-9.9		742.0		8/8 cir.strat	
35		11.55	-8.4	-8.6	741.8	738.8	" " " "	
34		19.10	-14.8	-14.5	732.5	729.0	" " " "	light snow
34		23.40	-16.3		731.2		" " " "	
34	9	8.35	-12.2		727.6		" " " "	light snow
31	11	1.00	-21.3	-20.7	688.5	684.5	" " " "	
31		13.15	-17.1		687.9		7/8 cir.strat	
30		21.00	-28.5	-27.4	678.9	674.4	3/8 cir.strat	
30	12	1.10	-26.6		679.0		2/8 cirrus	
30		8.55	-17.6		679.8		clear	
30		16.00	-23.1		678.4		3/8 cir.strat	
30		18.40	-26.0	-23.0	677.5		7/8 cirrus	
30		20.00					8/8.	fog
30		22.50	-25.1		676.7		8/8.	fog
30	13	9.35	-23.1		675.0		4/8.	
29		20.15	-28.1	-27.5	674.6	670.6	8/8 cirrus	
29	14	9.00	-20.8		676.6		8/8 cir.strat	
29		12.00	-20.5		677.6		" " " "	
28		20.50	-24.5	-24.1	675.2	670.9	5/8 cir.strat	
28	15	9.20	-20.0		677.9		4/8 cir.strat	
28		11.30	-20.2		677.9		2/8 cir.strat	
27		19.20	-26.9	-26.3	674.5	670.0	6/8 cir.strat	
27	16	9.15	-24.2		673.6		8/8 cir.strat	
26		19.00	-23.8	-23.0	679.0	674.8	" " " "	

26	17	8.50	-23.4		677.9		6/8 cir.strat	
25		18.10	-28.5	-27.8	685.2	681.0	4/8 cir.strat	
25	18	8.55	-22.7		686.4		3/8 cir.strat	
25		11.10	-21.5		687.2		8/8 cir.strat	
24		19.00	-30.1	-27.4	694.5	690.5	1/8.	
23	19	20.00	-29.9	-29.0	697.9	693.9	clear	
23	20	8.50	-23.1		694.9		clear	
23		11.00	-22.3		694.8		clear	
22		18.10	-28.3	-27.7	697.4	693.4	clear	
22	21	8.35	-24.9		701.5		clear	
21		18.40	-31.1	-30.1	698.4	694.4	clear	
21	22	9.15	-22.4		696.0		clear	
20	27	8.50	-24.6		691.2		clear	
20		12.40	-24.9		691.0		clear	
19		20.15	-37.3	-35.7	689.3	684.6	clear	
19	28	9.15	-21.7		690.5		8/8 cir.strat	
18		17.50	-33.6	-32.0	694.1	690.0	4/8 cir.strat	
18	29	8.35	-25.2		698.9		1/8 cir.strat	
17		20.00	-37.5	-36.6	701.0	696.7	clear	
17	30	9.05	-26.7		699.9		clear	
17		11.15	-27.4		699.6		clear	
16		19.10	-34.8	-33.5	701.9	697.7	clear	
16	31	6.30	-29.3		698.3		clear	
16		19.30	-34.4		696.4		clear	
16	32	4.00	-31.9		696.5		clear	light drift
16		8.25	-26.3		697.2		clear	
16		17.30	-31.0		699.4		2/8 cir.strat	
16	33	0.40	-36.2		701.8		clear	
13	34	13.30	-20.6	-20.2	714.0	710.1	7/8 cir.strat	
13	35	1.25	-26.8		712.7		2/8 cir.strat	
10	36	12.15	-18.5	-18.5	710.9	707.2	clear	
10	37	2.30	-27.1		710.0		clear	
10		6.00	-21.9		709.8		clear	
10		14.00	-20.6		709.0		clear	
10	38	1.00	-27.0		707.2		1/8 cir.strat	
7	39	14.00	-22.1	-21.3	703.8	699.9	1/8 cir.strat	
7	40	1.10	-32.4		706.0		" " " "	
4	41	12.00	-21.0	-20.5	711.6	707.9	2/8 cir.strat	
4	42	3.45	-25.7		712.1		clear	blowing snow
1	43	11.40	-6.7	-5.7	763.9	760.9	4/8 cir.strat	
1		12.30					8/8 cir.strat	light snow
1	44	1.00	-20.1		761.9		" " " "	blowing snow
1		2.10	-19.6		762.6		" " " "	blowing snow
0		12.45	-18.3		778.9		" " " "	blowing snow
0	45	1.30	-23.3		778.5		4/8 cir.strat	
0		8.00	-17.1		777.6		2/8 cir.strat	
0	46	1.10	-28.0		777.2		clear	